THE JOURNAL OF PHYSICAL CHEMISTRY

VOLUME 67, NUMBER 4 APRIL, 1963

NOTES

COMMUNICATION TO THE EDITOR

AUTHOR INDEX

THE JOURNAL OF
PHYSICAL CHEMISTRY

(Registered in U. S. Patent Office)

VOLUME 67, NUMBER 4 APRIL 15, 1963

IONIC ASSOCIATION IN AQUEOUS SOLUTIONS OF THIONINE

BY G. R. HAUGEN AND E. R. HARDWICK

Department of Chemistry, University of California, Los Angeles, California

Received April 25, 1962

The associative tendencies of thionine ions in electrolyte solutions have been investigated by means of optical and solubility behavior. The data indicate dimerization in very dilute solutions followed by higher polymerization as the dye concentration is increased. Gegenions play an important role, especially in the early stages.

Introduction

The well known tendency of certain dye ions to associate in aqueous solution has been investigated previously through a number of experimental approaches. It is interesting that while the formation of micelles seems to offer the best interpretation of the conductivity, osmotic pressure, and diffusion rate experiments,[1] the Beer law deviation data, even for identical systems, have been explained in terms only of dimerization.[2-4]

We find also that previous optical studies have been made in the absence of detailed knowledge of the far from insignificant participation of anions in the polymerization process.

Correct interpretation of spectrophotometric data in dye solutions is currently of significant importance because of the many kinetic studies which rest experimentally on the measurement of optical density; however, existing reports of Beer law studies virtually ignore association beyond the dimer. This is not surprising, since the interpretation of Beer law deviation is fairly insensitive to the assumed degree of association.

Primarily to facilitate the processing of our own and other kinetic data, we have made a reinterpretation of the optical behavior of the much studied thionine.[1-3] An explicit mathematical expression for such a process must contain the extinction coefficient of the associated species, the extinction coefficient of the monomeric species, the average degree of association, and the equilibrium constants for the various associative steps. The only one of these parameters which may be measured directly is the extinction coefficient of the monomeric dye, which is taken by extrapolating the Beer law plots to zero concentration. The other parameters are determined indirectly either by fitting the data to some model or by making certain simplifying assumptions. Relying mainly on spectrophotometry and the methods of quantitative analysis, we have investigated the solubility and the associative behavior of thionine in the presence of various other ions and have attempted to fit the data to an association model. The results are discussed along with our findings related to dye purification as given in the experimental section.

Experimental

A. Reagents, Instruments, and Glassware.—What we refer to as thionine is the hydrochloride salt THCl or its cation, TH^+. Because of the small dissociation constant of TH^+, the concentration of non-protonated dye, T, is in most cases negligible.

Our starting material was the commercial dyestuff as marketed by Allied Chemical and Dye Corp. at about 90% purity. All other reagents were standard C.P. grade.

It is well known that thionine solutions sometimes change their titer over a period of time by precipitating out on the walls of glass vessels.[5] Apparently this effect is due to contaminants on the surface of the glass, for we found that solutions stored in glass previously cleaned by hydrogen fluoride followed with distilled water were stable at all dye concentrations and acidities in either Pyrex or soft glass.[6] The concentrated dye still adsorbed, however, on *ground* glass surfaces. All the dye solutions were stable to air oxidation and thermal decomposition, although the concentrated solutions were extremely sensitive to salting out caused by contamination with electrolytes.

Absorption spectra were taken at 25° on a Cary 14 spectrophotometer. The effect of fluorescence on the absorption measurements was checked by interchanging the light source and detector so as to place the monochrometer between the detector and the sample. The spectra were independent of this change.

The solubility of the dye was measured by equilibrating an excess of the solids with various supporting electrolyte solutions for 24 hr. at 50° followed by a second 24 hr. period of equilibration at 25°. The solutions then were filtered and the filtrate was diluted and analyzed spectrophotometrically.

B. Purification of Thionine.—Most of the experiments described were made with samples of dye which had been recrystallized three times from solutions of 50% water–ethanol. Well formed crystals of the dye chloride were obtained when hot concentrated solutions were slowly cooled to 0°.

For purposes of determining an accurate extinction coefficient,

(1) (a) C. Robinson and H. E. Garrett, *Trans. Faraday Soc.*, **35**, 771 (1939); (b) C. Robinson and J. W. Selby, *ibid.*, **35**, 780 (1939); (c) C. Robinson, *ibid.*, **31**, 245 (1935); (d) E. Valko. *ibid.*, **31**, 230 (1936).

(2) (a) W. E. Speas, *Phys. Rev.*, **31**, 569 (1928); (b) G. Körtum, *Z. Physik. Chem.*, **B30**, 317 (1935); **B33**, 1 (1936); **B34**, 255 (1936); **B31**, 137 (1935); **B33**, 243 (1936).

(3) E. Rabinowitch and L. F. Epstein, *J. Am. Chem. Soc.*, **63**, 69 (1941).

(4) J. Lavorel, *J. Phys. Chem.*, **61**, 1600 (1957).

(5) F. Epstein, F. Karush, and E. Rabinowitch, *J. Opt. Soc. Am.*, **31**, 77 (1941).

(6) The stability of the dye solutions in vessels washed with dilute hydrogen fluoride apparently is due either to removal of contaminants or to conditioning of the glass surface.

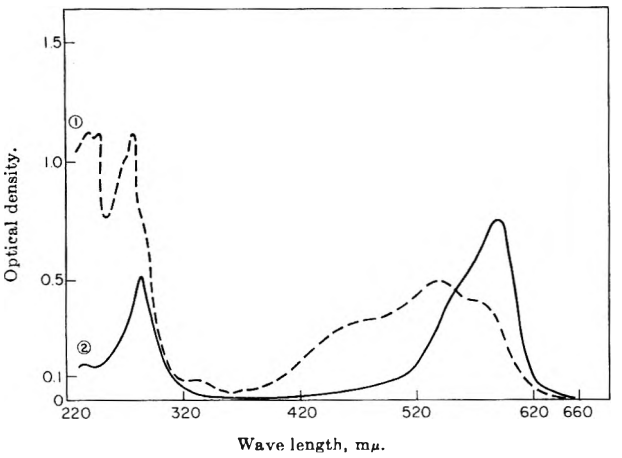

Fig. 1.—Absorption spectra of thionine and of pink impurity: solid curve, $T_0 = 1.48 \times 10^{-5} M$, $[H_2SO_4] = 0.1 N$; dashed curve, pink impurity at unknown concentration, $[H_2SO_4] = 0.1 N$.

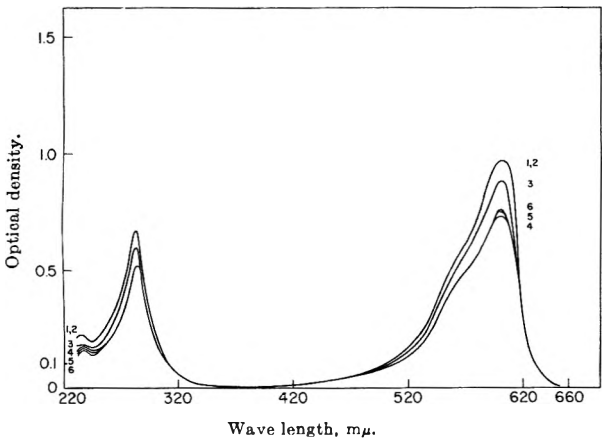

Fig. 2.—Absorption spectra of various dye solutions: curve 1, $T_0 = 1.85 \times 10^{-6} M$, [KCl] = 1.0, 10-cm. cell; curve 2, $T_0 = 1.85 \times 10^{-6} M$, $[H_2SO_4] = 0.05$, 10-cm. cell; curve 3, $T_0 = 1.85 \times 10^{-6} M$, 10-cm. cell; curve 4, $T_0 = 1.48 \times 10^{-5} M$, [KCl] = 1.0, 1.0-cm. cell; curve 5, $T_0 = 1.48 \times 10^{-5} M$, 1.0 cm. cell; curve 6, $T_4 = 1.48 \times 10^{-5} M$, $[H_2SO_4] = 0.05$, 1.0-cm. cell.

we took extreme care in preparing samples of dye at known concentrations. The two most important sources of error in preparation of standard solutions lay in the determination of the exact amount of dye used and in the difficulty of assuring complete solution of the solid salt. To this end, samples were dried at 100° to constant weight, and only well formed crystals were used. The solid was dissolved in hot water (50–60°) with constant stirring for several hours. After the solution was cooled, it was filtered to make sure that no solid material remained. For extinction coefficient measurements, only very dilute solutions prepared in this way were used.

To check the efficiency of fractional crystallization, methanol solutions of the dye were chromatographed on a silica gel column. Although the dye was irreversibly absorbed, a small amount of pink impurity, Fig. 1, passed through. The impurity is easily obtained and optically characterized as thionol, but we have not yet obtained what we consider to be a completely reliable sample of *solid* thionine, thus our *extinction coefficient* values may still contain an error of a few per cent. In a further report, we hope to give a value based on direct measurement of a dye sample purified by one or more stages of liquid–liquid extraction between recrystallization steps.

C. The Spectrum of Thionine.—Determinations of the absorption and fluorescence spectra of thionine do not depend on knowledge of exact concentrations, thus are not subject to the difficulties caused by reducing the samples to dryness. The spectral data given in Fig. 2 are taken from solution samples which show no impurity on chromatography through SiO_2.

Thionine absorption spectra display a shoulder at about 560 mμ on the short wave length side of the main 600 mμ peak. Since this inflection occurs even at very low concentrations, is found in solvents which preclude dimerization, and occurs with mirror symmetry in the fluorescence, we follow Lewis[7] in ascribing it to a vibrational band. If this assignment is correct, it should reasonably be expected that the action spectrum for photobleaching would also show a shoulder. Although Hardwick's rough measurements[8] indicate a symmetrical action spectrum, another, more recent, qualitative experiment by Miller[9] gives a curve which seems to match the absorption spectrum.

Results and Discussion

A. Dye–Dye Interactions Creating Soluble Polymeric Species.—Our results indicate that many of the large observed Beer law deviations in thionine solutions are indeed due, as previously found,[1,3] to ionic interactions, but that these are not simple dimerizations or even the formation of uncomplicated higher polymers. The presence and the nature of anionic species plays a large role in dye cation interaction and must significantly affect the interpretation of association processes. Rabinowitch,[3] who measured Beer law deviations in thionine solutions of molar concentrations 2.5×10^{-6} to 2.5×10^{-3} at pH 3.5, was able to fit his data to a simple dimer model. A more general model must include provision for anionic effects and for participation of higher polymers.

1. Cation–Anion Pairs.—The significance of pairing of dye cations with anions may be assessed by an experiment in which the concentration of anions is held constant while the dye cation concentration is changed. Such an experiment shows, Fig. 3, that strong Beer law deviations occur, for instance, in a dye chloride solution when $[Cl^-]$ is held constant through addition of supporting salts, *e.g.*, KCl. The simple ion pair association model allows no such deviations, since the apparent extinction coefficient E (the ratio of the optical density to the nominal dye concentration) should be invariant under these conditions. This follows from eq. 1 which is derived from stoichiometry and equilibrium conditions.

$$E \equiv \frac{\text{O.D.}}{[T]_0} = \frac{\varkappa_{TH^+} + K_1[Cl^-]\varkappa_{THCl}}{1 + K_1[Cl^-]} \qquad (1)$$

where $K_1 \equiv [THCl]/[TH^+][Cl^-]$, the equilibrium constant for ion pair formation, $[T]_0$ represents total dye concentration, $\varkappa_{TH^+}$ is the extinction coefficient of the monomer, *i.e.*, the ratio of the optical density to monomer concentration in a cell of unit length, and $\varkappa_{THCl}$ is similarly defined for the ion pair.

Although these considerations demonstrate that Beer law deviations are not due to ion pairing, they do not necessarily preclude the existence of such pairs.

2. Dependence of Dye–Dye Interactions on Anion Concentration. a. Chloride Systems.—Figure 3 shows clearly the strong dependence of the degree of dye association on $[Cl^-]$.[10] Since ion pairing as such is not responsible for the observed Beer law deviations in chloride systems, this behavior must occur through the effect of the anions on a cation association process.

(7) G. N. Lewis and co-workers, *J. Am. Chem. Soc.*, **65**, 1150 (1943).
(8) R. Hardwick, *ibid.*, **80**, 5667 (1958).
(9) Leroy Miller, private communication.
(10) On the basis of two spectrophotometric tracings, Rabinowitch reported *independence* of the degree of association on anion concentration. The concentration of his pure dye solution was such, however, that considerable salting out must have occurred on the addition of Cl^- (*cf.* section B1). The resulting decrease in dye concentration would have favored dissociation while the presence of the anion would encourage association. The two effects seem essentially to have cancelled each other.

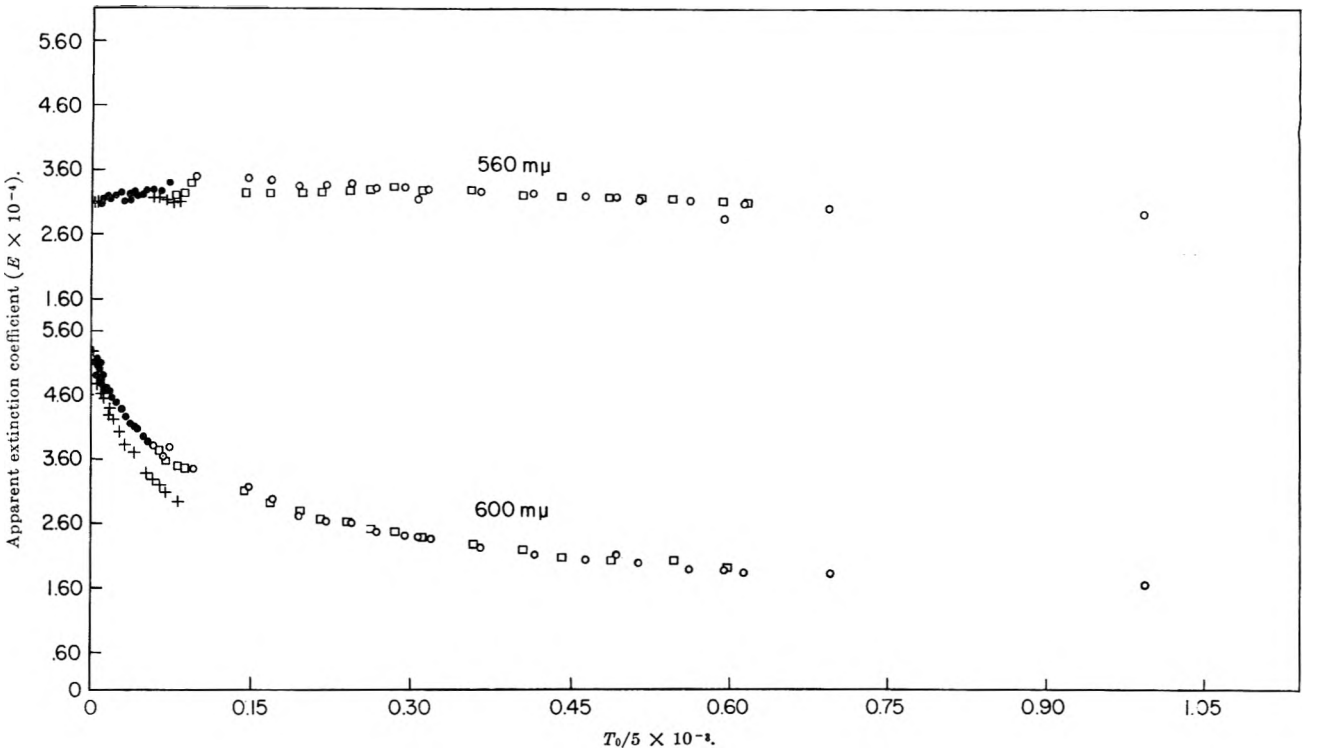

Fig. 3.—Dependence of apparent extinction coefficient on dye concentration: dye–H_2SO_4, pH 3.5 □; pure dye, pH 7.0 ○; Dye–KCl, [KCl] = 0.064 M +. Following systems all represented by ●: pure dye, pH 7.0; dye–H_2SO_4, pH 3.5; dye–H_2SO_4, pH 2.8; dye–KCl, [KCl] = 0.0041 M.

Several possibilities may be considered for a first association step

$$2THCl \rightarrow (TH)_2Cl_2 \qquad (2a)$$

$$2THCl \rightarrow (TH)_2Cl^+ + Cl^- \qquad (2b)$$

$$2THCl \rightarrow (TH)_2{}^{++} + 2Cl^- \qquad (2c)$$

$$2TH^+ + 2Cl^- \rightarrow (TH)_2Cl_2 \qquad (2d)$$

$$2TH^+ + Cl^- \rightarrow (TH)_2Cl^+ \qquad (2e)$$

If association is to be enhanced through increase in [Cl^-], the process cannot be 2a, 2b, or 2c, since these give either the wrong dependence on [Cl^-] or no dependence at all. The solubility requirements discussed in section B1 rule out (2d), leaving (2e) as a reasonable choice.

For a system in which the dye exists only as the monomeric species TH^+ or as the dimer $(TH)_2Cl^+$ (*cf.* eq. 2e), the equilibrium constant for dimerization is

$$K_2 = \frac{[(TH)_2Cl^+]}{[TH^+]^2[Cl^-]} \qquad (3)$$

and the apparent extinction coefficient

$$E = \alpha\kappa_{TH^+} + {}^1/_2(1 - \alpha)\kappa_{(TH)_2Cl^+} \qquad (4)$$

where α is the fraction of monomeric dye

$$\alpha = \frac{[TH^+]}{[T]_0}$$

Invoking stoichiometry, we may write eq. 3 in terms of $[T]_0$ and α

$$2K_2[T]_0[Cl]\alpha + \alpha - 1 = 0 \qquad (5)$$

from which an approximate α may be substituted into eq. 4. The resulting expression imposes the requirement of linear dependence of the limiting slope of the Beer law plots on [Cl^-]

$$\lim_{T_0 \to 0} \left[\frac{dE}{d[T]_0}\right] \approx 2K_2[Cl^-]\{{}^1/_2\kappa_{(TH)_2Cl^+} - \kappa_{TH^+}\} \qquad (6)$$

We have made E *vs.* $[T]_0$ measurements for several solutions containing added KCl from 0 to 2.2 M (for two examples of the original data, see Fig. 3) and find that the linearity requirement of eq. 6 is satisfied, Fig. 4, within the large experimental errors that arise at extremely low concentrations. The approximate value of K_2 obtained from this plot agrees roughly with that discussed below.

Our value for κ_{TH^+} as obtained from extrapolating the Beer law plots to zero dye concentration is 5.7 × 10^4 at 600 mμ. This may be compared with the value obtained by Rabinowitch of 5.6 × 10^4. In certain systems, the molar extinction coefficients are dependent on the total ionic strength of the medium; however, in the present case, as seen in Fig. 2 and 3, the *limit* was independent of ionic strength.

b. Association Constant and Extinction Coefficient of the Dimer in Chloride Systems.—From eq. 4, it may be seen that the quantity $(E - \alpha\kappa_{TH^+})$ is linearly dependent on α with slope ${}^1/_2\kappa_{(TH)_2Cl^+}$. If K_2 is known, it is possible to calculate α at various $[T_0]$ and [Cl^-] and make the indicated plot to determine the extinction coefficient of the dimer. Since K_2 is not directly measurable, however, various values must be assumed and the resulting $(E - \alpha\kappa_{TH^+})$ *vs.* α plots studied in order to estimate $\kappa_{(TH)_2Cl^+}$.

As might be expected, after curve fitting of this kind we found that the *slope* of the plot, Fig. 5, is relatively insensitive to the assumed values of K_2. The *degree of linearity*, however, does depend slightly on K_2, our best fit indicating an order of magnitude value, $K_2 \sim 4 \times 10^5$. The dimer extinction coefficient,

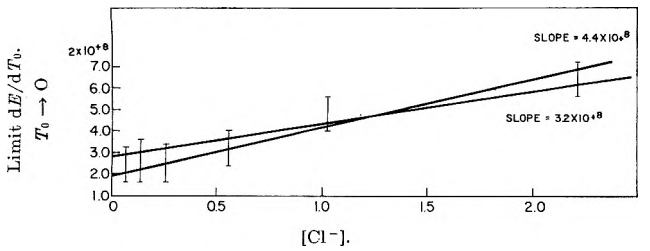

Fig. 4.—Dependence of dye association on chloride ion concentration in dilute dye solutions.

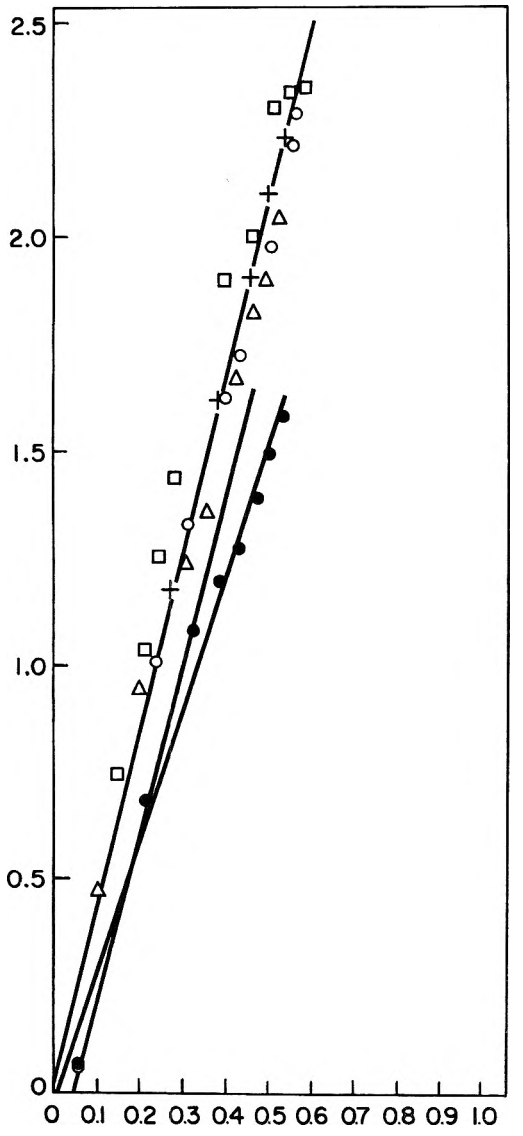

Fig. 5.—Test of dimer at low concentrations: dye–KCl, [KCl] = 2.22 M □; dye–KCl, [KCl] = 1.03 M +; dye–KCl, [KCl] = 0.554 M ○; dye–KCl, [KCl] = 0.256 M △; dye–KCl, [KCl] = 0.139 M ●.

$\kappa_{(TH)_2Cl^+}$, lies between 8 and 10 × 10^4 at 600 mμ, considerably less than twice that of the monomer, 2 × 5.7 × 10^4.

The behavior of the system at 560 mμ is interesting. At this wave length, Beer's law is obeyed over a large range of T_0; thus the absorption *per dye cation* must be essentially unchanged regardless of the degree of association. For instance, the molar extinction coefficient of the dimer is evidently twice that of the monomer at this wave length, *viz.*, 2 × 3.2 × 10^4. Unfortunately this coincidence provides no additional approach to the problem, for it gives only the trivial concentration information, T_0, which is already known from solution preparation data.

The spectrum of the dimer can be obtained by repeating this analysis at other wave lengths. The dimer spectrum differs from that of the monomer only between the wave lengths 570 to 610 mμ, the maximum deviation occurring at 600 mμ. This is a surprising result if compared with those from the concentrated dye solutions, where the absorption peak is shifted towards the blue.

c. Sulfate Systems.—Although the data of dye–chloride systems are subject to fairly straightforward interpretation, dye–sulfate systems are not well behaved. To begin with, the sulfate salt cannot be purified well by fractional crystallization, since its crystals are not well formed. Moreover, where the E *vs.* T_0 plots of chloride systems are linear at low T_0, those taken with sulfate as the predominant anion are S shaped, Fig. 6, indicating complicated associative behavior. The limiting κ_{TH^+} does, however, correspond to that of the chloride system, 5.7 × 10^4.

For the purpose of relating our measurements to those of various earlier papers, we have taken data in a few sulfate systems, but we cannot yet claim to make detailed interpretations of these.

3. Association beyond the Dimer.—The classical conductivity, osmotic pressure, and diffusion rate measurements of Connan, Robinson, Valko,[1] and others have led to the conclusion that dye anions of certain species associate to form large polymers which in many cases may include significant numbers of gegenions. We do not attempt to construct an explicit mathematical model of the detailed contribution of counter ions in dye aggregates, but we present experimental evidence which indicates the presence of large soluble aggregates in thionine solutions of $>10^{-4}$.

i. The dimer absorption peak as calculated from the degree of association in the presence of KCl lies at 600 mμ, but in very concentrated solutions the maximum falls at 560 mμ, suggesting that another species is predominant at these concentrations, Fig. 7.

ii. It is a characteristic of micelle formation that the concentration of the unassociated species can be increased up to the point where condensation begins, but afterwards will remain relatively constant. By making calculations based on the somewhat shaky assumptions discussed below, we have estimated the monomer concentration as a function of $[T]_0$. Figure 8 shows the monotonic increase of such a plot up to $\approx 10^{-4}$ mole/l., but beyond this, through a factor of only two in dye concentration, the curve levels out and the monomer concentration thenceforth remains roughly constant. The worth of this calculation rests on the spectral assumptions discussed in the footnote.[11]

(11) If the 560 mμ peak of the polymer can be assumed to be symmetric (and careful study of the spectral curves at very high concentrations leads us to believe that this is so), the monomer concentrations may be determined by a Beer law calculation made at 600 mμ after correction for the polymer absorption. The correction is made simply by taking the 600 mμ polymer absorption to be the same as that at an equal distance on the opposite side of the 560 mμ peak, *i.e.*, at 520 mμ, where monomer absorption is negligible. When correction is subtracted away, the resulting absorption at 600 mμ, representing primarily monomer, indicates the concentration behavior indicated in Fig. 8. A quasi justification for the spectral assumption may be made if the average *degree* of polymerization is assumed to be constant in the concentrated dye solutions. The optical density difference,

Since these are slightly dubious, we are unable to offer the findings as firm evidence of condensation phenomena, although we are quite pleased with the appearance of the plot.

For these reasons, then, we believe that thionine in concentrated solutions occurs mainly as a polymer. Rough calculations lead up to estimate an average degree of association of at least 5–10 units. The structure of the polymer unit might reasonably be assumed to be $(TH)_nCl_{n-m}^{+n-m}$ in chloride solutions.[12]

Tobolsky and Eisenberg's[14] model for equilibrium polymerization may be used to give at least a feeling for the influence of anions. If it is assumed that the polymer is $(TH)_n^{n+}$ (*i.e.*, no gegenions) and that all the association constants are equal, the number average of monomer units in all polymers, P, is given by

$$P^2 = T_0K_2 \qquad (7)$$

from which $P = 1$ at $T_0 \sim 2 \times 10^{-6}$; $P = 10$ at $T_0 - 2 \times 10^{-4}$.

If the high values of the association constants depend, however, on the presence of a counterion, then for the chloride system, taking the polymer as $(TH)_nCl_{n-1}^{+}$

$$P^2 = \sim T_0[Cl^-]K_2 \qquad (8)$$

This indicates *no* polymerization for pure thionine chloride solutions at any attainable concentration, a finding that disagrees with all of our experimental results.

The conclusions to be reached are fairly obvious. Tobolsky's equation does not apply to simple dimers and trimers (nor was it intended to do so). For the higher polymers which seem to exist in concentrated solutions, gegenion participation must be fairly small unless excess supporting salts are added. In this case, polymerization may be enhanced and the proportion of counterions raised. These assumptions are reasonable and seem to fit our experimental facts. The existence of the very impressive salting out effects essentially require, of course, that the micelles incorporate counterions when plentiful.

4. Influence of Protons on Dye Association.—To assess the effect of proton concentration on the associative behavior of thionine, we have made E *vs.* T_0

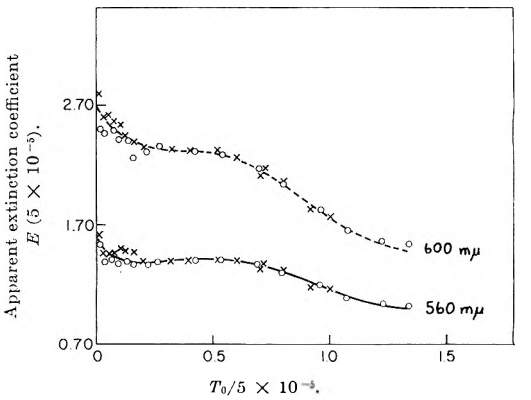

Fig. 6.—Dependence of apparent extinction coefficient on dye concentration in two solutions at different pH: upper curve, 600 mμ; lower curve, 560 mμ. Added $[K_2SO_4] = 0.05$ all solutions; $[H_2SO_4] = 1.6 \times 10^{-4}$ 0; $[H_2SO_4] = 5.0 \times 10^{-3}$ x.

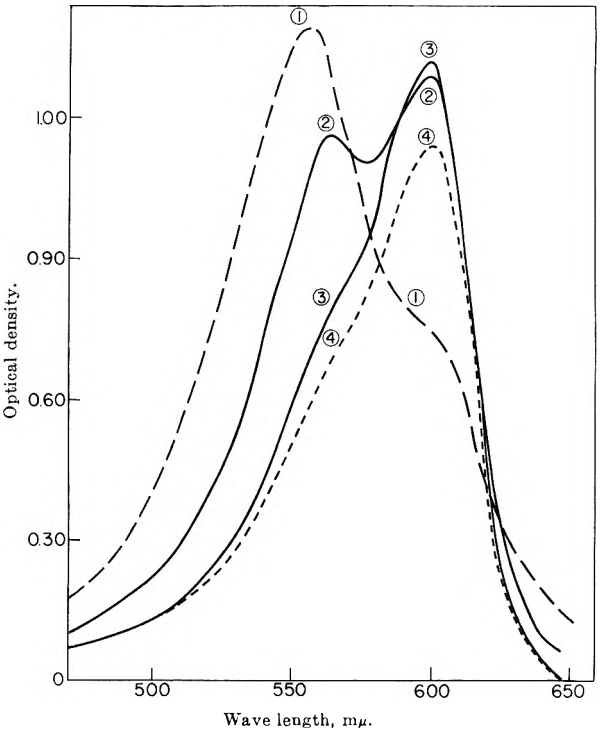

Fig. 7.—Absorption spectra of pure dye solutions at various concentrations: curve 1, $T_0 = 4.98 \times 10^{-3} M$, 0.01 cm. cell; curve 2, $T_0 = 3.40 \times 10^{-4} M$, 0.1 cm. cell; curve 3, $T_0 = 2.94 \times 10^{-6} M$, 10.0 cm. cell; curve 4, $T_0 = 2.95 \times 10^{-7} M$, 10.0 cm. cell.

measurements in systems to which various amounts of acid have been added. Sulfuric acid was chosen because of its earlier wide use in kinetic experiments with thionine.

Figure 3 comprises plots of E *vs.* T_0 at 600 and 560 mμ for systems at pH 7, 3.5, and 2.8. It may be seen that the points taken at lower pH fall on the curve drawn for the pure dye solution, indeed the data match so well at low T_0 that the points coincide.

A further experiment taken at pH 1 gave data which deviate slightly from the other curves; however, this almost negligible difference can be accounted for by the increase in sulfate ion concentration. Data taken for K_2SO_4 systems show similar effects (Fig. 6).

The non-dependence of association on $[H]^+$ over a range of 10^6 rules out such mechanisms as

$$2TH^+ \rightarrow T_2H^+ + H^+,$$

$$T_2H^+ + TH^+ \rightarrow T_3H_2^+ + H^+ \ldots$$

O.D. (600 mμ) − O.D. (520 mμ), is simply ΔO.D. = $k_1[TH^+] + k_2T_0$, where k_1 and k_2 are constants. The difference, ΔO.D., is independent of the total concentration only when k_2 is zero and the monomer concentration is simultaneously constant. The vanishing of the constant k_2 can be shown to be equivalent to the spectral assumption stated above.

(12) The chloride data indicate that the early stages of association require the incorporation of a gegenion. Evidently the weak forces which are responsible for dimerization cannot alone counteract the internal electrostatic repulsion of the two cations, but the introduction of an anion reduces this without destroying internal resonance.

A likely possibility for the structure of an associated species is the sandwich structure, which has been shown by theoretical and experimental investigations[4,13] to lead to splitting of the absorption band of the monomer, producing an allowed transition on the short wave length side and a forbidden transition on the long wave length side of the original monomer peak. We have observed what may be such a phenomenon, however, only in solutions at high dye concentration. For these, there is a very strong peak at 560 mμ and the indication of a small peak at about 650 mμ as hinted by the strong concentration dependence of the absorption tail, Fig. 7. In the concentration region where the dimer model holds we find no splitting; the dimer absorbs at the same wave length as the monomer. This implies an intrinsic difference between the structure of the dimer and of higher polymers; thus we are inclined to favor a dimer which does not necessarily have its transition dipole oriented parallel or antiparallel as required by the sandwich structure which may characterize the higher polymers.

(13) (a) G. Levinson, W. Simpson, and W. Curtis, *J. Am. Chem. Soc.*, **79**, 4314 (1957); (b) T. Förster, "Fluoreszenz Organischer Verbindungen," Van Denhoeck and Ruprecht, Gottingen, 1951.

(14) A. V. Tobolsky and A. Eisenberg, *J. Am. Chem. Soc.*, **82**, 289 (1960).

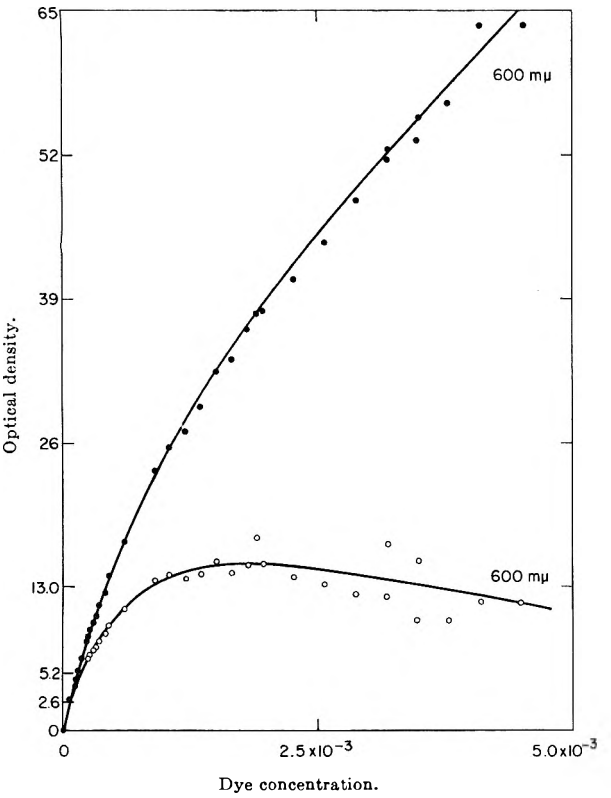

Fig. 8.—Absorption intensity of pure solutions: upper curve, total measured density of solution; lower curve, estimated optical density of monomer alone.

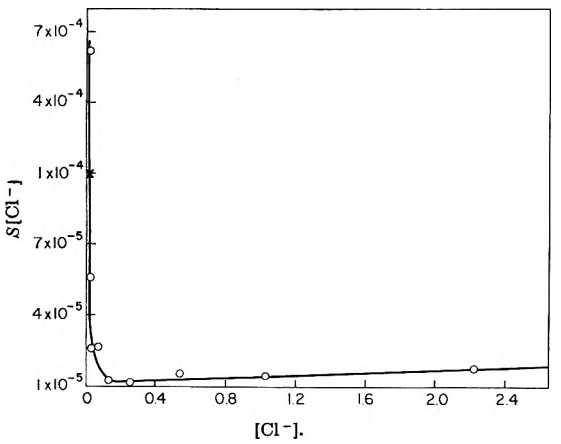

Fig. 9.—Solubility of thionine as a function of chloride ion concentration. (Note: in abscissa, [C$^-$] designates total concentration, *i.e.*, S + [K$^+$] where [K$^+$] gives amount of added KCl and S gives contribution of dye salt.)

or

$$2TH^+ \rightarrow T_2 + 2H^+, \text{ etc.} \qquad (9)$$

In pure dye solutions at extremely low concentrations, the apparent extinction coefficient at 600 mμ seems to decrease slightly, *i.e*, the E *vs.* T_0 plot has a small but noticeable downturn below $T_0 \sim 2 \times 10^{-6}$. The effect, which disappears with addition of small amounts of KCl or K_2SO_4 or with traces of acid, may be caused by the dissociation, $TH^+ \rightarrow T + H^+$, resulting in the substitution of less intensely colored T for TH$^+$. The addition of protons would, of course, diminish this dissociation through the common ion effect. Other anions might remove TH$^+$ from solution (as THCl for example), thus repress the dissociation.

B. Solubility and Solubility Product.—Since precipitation of the dye might reasonably be expected to be a process related to other associative phenomena, we have extended the models into this region and have taken and analyzed solubility data.

1. Chloride Systems.—Defining the solubility product in the usual way, $K_{sp} \equiv [TH^+][Cl^-]$ and the total concentration of soluble dye species as S, we find for the simple non-associative case, rewriting the solubility product

$$S[Cl^-] = K_{sp} \qquad (10)$$

This equation predicts independence of the function S[Cl] from [Cl$^-$]; however the relation as such is not useful because the absorption measurements indicate that in every case significant association occurs before saturation. It is interesting, however, to compare the prediction with the experimental data of Table I.

TABLE I

SOLUBILITY OF THIONINE IN VARIOUS SOLUTIONS

Solubility of dye, M	Concn. of KCl added, M	Concn. of H_2SO_4 added
	(1) Chloride salt	
2.49×10^{-2}	0	0
2.96×10^{-3}	0.016	0
8.59×10^{-4}	.0296	0
4.10×10^{-4}	.0641	0
9.34×10^{-5}	.139	0
4.63×10^{-5}	.256	0
2.84×10^{-5}	.554	0
1.42×10^{-5}	1.03	0
7.81×10^{-6}	2.22	0
2.99×10^{-3}	0	1.58×10^{-4}
2.14×10^{-4}	0	8.50×10^{-4}
5.21×10^{-5}	0	5.0×10^{-2}
	(2) Sulfate salt	
4.14×10^{-4}	0	0

These data are plotted in Fig. 9 as S[Cl$^-$] *vs.* [Cl$^-$]. At chloride concentrations greater than ~0.2 molar, the curve behaves nearly as required, having only a small slope which may be attributed to changes in ionic activity. At lower [Cl$^-$] (*i.e.*, high dye concentration) however, the data misbehave and the curve becomes nearly vertical.

If we attempt to prevent this catastrophic misfit by resorting to the dimer model previously used, we find that

$$S[Cl^-] = K_{sp} + 2K_2K_{sp}^2 \qquad (11)$$

a function once more independent of [Cl$^-$]. Even if chloride ion concentration is now calculated on the basis of added chloride (as KCl) plus the contribution from the dye itself, *i.e.*, [Cl$^-$] = [K$^+$] + [TH$^+$] + [(TH)$_2$Cl$^+$] + ... the shape of the curve is altered only slightly through a small change in the calculated S[Cl] (marked X on the curve) for the datum corresponding to pure dye. In the other data, added chloride far exceeds any contribution by the dye salt.

Equation 1 can be employed, however, to estimate the solubility product, which takes the value $K_{sp} \sim 3 \times 10^{-6}$ if the data of Table I and $K_2 \sim 4 \times 10^{+5}$ are used.

For purposes of discussion we again adopt the model of the polymer containing $n - 1$ chloride ions. Tobolsky's approach when applied to this model leads essentially to result

$$S[Cl] = K_{sp} + K_2K_{sp}^2P^2 \qquad (12)$$

where once more (*cf.* section A3) the assumption $K_3 = K_4 \ldots . K_n$ is invoked.

Although eq. 12 rests on somewhat dubious approximations, it leads to the entirely reasonable conclusion that the solubility of the dye evidently is enhanced as the extent of polymerization increases and that this effect is the cause of the very high dye solubility at low $[Cl^-]$. However, it is not possible to determine by these methods how many Cl are included in the polymer. Judging by the appearance of the curve $S[Cl^-]$ *vs.* $[Cl^-]$ in Fig. 9, however, polymerization is encouraged at fairly low $[Cl^-]$. Evidently, as anions become more plentiful, the tendency to form the insoluble uncharged species containing relatively more Cl^- overtakes the polymerization process and the dye salts out.

If each polymer unit is singly charged entity, the total concentration of all such units in a solution of pure THCl must be equal to the concentration of anions, $[Cl^-]$. The solubility, *i.e.*, the total number of dye ions (associated and otherwise) in a saturated solution of pure dye, then, is the average degree of polymerization multiplied by the number of polymers, or $P[Cl^-] = S$. This relation may be used with eq. 12 and the values of K_2, K_{sp}, and S for pure dye to estimate a minimum value, $P = 6$, under these circumstances. If, as the case seems to be, fewer anions are included in the polymers, P must be correspondingly larger.

2. **Sulfate Systems.**—We are unable to give quantitative data on the dependence of $S[SO_4^{-2}]^{1/2}$ on $[SO_4^{-2}]^{1/2}$ in analogy to the chloride data since we were not able to prepare acceptable crystals of $(TH)_2SO_4$. The solubility of the chloride salt in sulfate systems, of course, has no direct bearing on the question since the composition of the solid phase is not determined in such systems.

We report the solubility of crude $(TH)_2SO_4$ in Table I.

Acknowledgments.—We gratefully acknowledge the full support of this research by the Air Force Office of Scientific Research under Contract Af 19(604)-6643.

STABILIZATION OF WATER-IN-OIL EMULSIONS BY SOLID PARTICLES[1]

By E. H. Lucassen-Reynders and M. van den Tempel

Unilever Research Laboratory, Vlaardingen, Netherlands

Received May 12, 1962

Emulsions of water in paraffin oil can be stabilized by crystals of glycerol tristearate, provided that small amounts of surface-active agents are also present. Both oil- and water-soluble surfactants can be used, in concentrations which have no appreciable stabilizing power in the absence of tristearate crystals. The contact angle of water and paraffin oil against tristearate crystals was found to be unaffected by the addition of surfactants. The increased stabilizing power in the presence of surfactants is due to a decreased interaction of the tristearate crystals, which allows the crystals to reach the surface of the water droplets before an appreciable amount of coalescence has occurred. The effect of surfactants on the interaction energy of the crystals is investigated by means of steady-state viscosity measurements at very low shear rates. The interaction energy is decreased by about 1 kT unit at shear rates of the order of 0.001 sec.$^{-1}$, by adding a surfactant to the dispersion of crystals in oil. The estimated effect of the decreased interaction energy on the emulsion stability is in agreement with experimental results.

Introduction

Emulsions may be stabilized by solid particles if (i) the contact angle between the two liquids and the particle surface has a value which favors adsorption of the particle at the liquid–liquid interface[2] and (ii) the particles are in a state of incipient flocculation.[3,4] This behavior usually is explained by considering that a dense layer of solid particles at the oil–water interface is required for stability.

The relation between emulsion stability and contact angle has been investigated in emulsions containing water, benzene, and barium sulfate as solid particles.[5] It was shown that the contact angle in this system can be varied by adding surface-active materials, and this affects the stability of the emulsions formed. On the other hand, in the system containing triglyceride crystals, paraffin oil and water the contact angle is not affected by the addition of surface active materials,[6] even though this results in a considerably increased emulsion stability. The value of the contact angle (measured in the water phase with Bartell's method) is 110°, and this accounts for the high stability of the water-in-oil emulsions compared with the stability of inverse type emulsions.[2b]

In the present paper it is shown that the effect of surfactants in this system is due to a decreased interaction between the triglyceride crystals, as found by rheological measurements on their suspensions in paraffin oil.

Experimental

Materials.—Glyceryl tristearate was produced by recrystallizing fully hydrogenated linseed oil from acetone until the melting point exceeded 71°. Crystals with an average diameter of about 10^{-5} cm. were obtained by rapid crystallization of a hot, 25% solution in paraffin oil. After recrystallization had been allowed to proceed for at least several days, the plastic mass was diluted with paraffin oil to a concentration of 1% by weight. The following surfactants were added in the oil used for diluting: glyceryl α-monoöleate (purity 98% by weight as determined by oxidation with periodic acid; iodine value 71.5; melting point

(1) The contents of this paper have been presented by M. vdT. at the 142nd National Meeting of the American Chemical Society in Atlantic City, September 9–14, 1962; they are part of a thesis of E. L., prepared under the supervision of Prof. Dr. J. Th. G. Overbeek of Utrecht University.

(2) (a) S. U. Pickering, *J. Chem. Soc.*, **91**, 2001 (1907); (b) J. L. van der Minne, "Over Emulsies," Thesis, Amsterdam, 1928.

(3) T. R. Briggs, *Ind. Eng. Chem.*, **13**, 1008 (1921).

(4) M. van der Waarden, *Kolloid-Z.*, **156**, 116 (1958).

(5) J. H. Schulman and J. Leja, *Trans. Faraday Soc.*, **50**, 598 (1954).

(6) E. H. Lucassen-Reynders, paper submitted for publication in *J. Phys. Chem.*

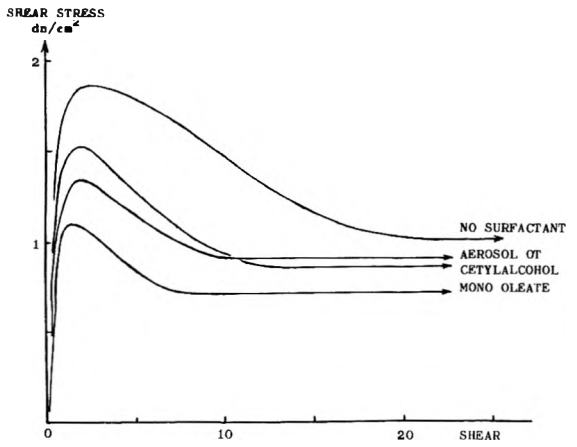

Fig. 1.—Effect of surfactants on the stress–shear curve of a 1% glyceryl tristearate suspension in paraffin oil, at a shear rate of 0.00767 sec.$^{-1}$. Surfactant concentrations are given in the text.

35°); sodium diethyl hexyl sulfosuccinate (Aerosol OT; from American Cyanamid Co.); cetyl alcohol (purity 92% by weight as determined by gas chromatography, the residue consisting of higher and lower homologs). In one single case (the stability measurement with Aerosol OT) the surfactant was added to the water phase.

The paraffin oil was a water-white, medical grade having a density of 0.864 g. cm.$^{-3}$ and a viscosity of 0.76 poise, both at 20°. Its surface tension against water was not affected by purification with alumina; this shows the absence of surface-active impurities.

Emulsion stability was found from the change in reflectance of the coagulating emulsions, containing a water-soluble dye in the interior of the droplets. The amount of light of a suitable wave length reflected from the upper surface of such emulsions is a simple function of the specific interfacial area, as has been shown empirically by Lloyd[7]

$$\log R = b \log A + c \qquad (1)$$

R being the percentage of normally incident light reflected from the emulsion under an angle of about 10°; A is the area of interface per unit volume of the emulsion, and b and c are constants not depending on A.

This equation can be transformed easily into a relation between reflectance and time in cases where the coagulation follows a first-order reaction mechanism,[8] with probability of coalescence K (in sec.$^{-1}$)

$$\log R = \frac{bK}{3.2{,}30} t + \text{constant} \qquad (2)$$

Thus the probability of coalescence K can be found from the slope of the log reflectance–time plot. Knowledge of the additional constant is not necessary. The constant b, however, has to be known; its value was evaluated from the reflectances of a coarse and a fine emulsion with identical composition and a mixture of these two, as suggested by Lloyd.

The accuracy and reproducibility of the values of b obtained in this way were not better than by a factor of about 2, and hence the uncertainty in the value of K is of the same magnitude. Since the addition of surfactant results in changes of K with several orders of magnitude, the measurement is considered sufficiently accurate for the purpose of the present investigation.

Table I shows the results of stability measurements on emulsions of water (20% by volume) in paraffin oil which contained 1% by weight of glyceryl tristearate crystals, upon addition of various amounts of surfactants.

Surfactant concentrations refer to the phase in which the surfactant had been dissolved: oil for the first two materials, and water for Aerosol OT.

A coalescence rate of about 0.01 sec.$^{-1}$, as found in the emulsion containing only tristearate and no surfactant, indicates that the emulsion is completely broken in less than 10 min. In emulsions containing only surfactants but no tristearate, breaking occurred at the same high rate.

Table I

Influence of Surfactants on the Stabilization of Emulsions of Water in Paraffin Oil by Glyceryl Tristearate Crystals

Surfactant	Concn., 10^{-6} moles cm.$^{-3}$	Probability of coalescence of emulsion, sec.$^{-1}$
None	...	$\sim 10 \times 10^{-3}$
Glyceryl monooleate	1	2×10^{-3}
	2.5	0.01×10^{-3}
Cetyl alcohol	5	0.3×10^{-3}
	25	0.08×10^{-5}
Aerosol OT	10	0.04×10^{-3}

Flocculation of fat crystals dispersed in oil was investigated by means of steady-state viscosity measurements at very low shear rates. A concentric cylinder instrument was used in which the outer cylinder (internal diameter 3.15 cm.) is slowly rotated at a constant, low speed. The inner cylinder (diameter 2.80 cm., height 8.58 cm.) is freely suspended from a torsion wire. The surfaces of the cylinders are provided with vertical grooves of triangular cross-section and a depth of 0.1 mm. Rotation of the inner cylinder is recorded by means of an optical lever. The cylinders are carefully aligned and centered before a measurement starts; the error due to imperfect adjustment could be made smaller than about 10%, which is small compared with the effects to be measured. The instrument is permanently held at 20.0°. The range of shear rates that can be covered with this instrument extends from about 1 sec.$^{-1}$ to about 10^{-5} sec.$^{-1}$. At these low speeds, transient effects can be measured in the beginning of an experiment. A plot of the shear stress in the sample as a function of the shear generally will show a maximum stress at shear values of the order of unity (*cf.* Fig. 1). At higher shear values, the stress drops to a stationary value, which measures the steady-state viscosity. Stress–shear curves of this type generally have been found for disperse systems at sufficiently low shear rates.[9] The discussion of the present paper is restricted to the behavior in the steady state.

For measurements at shear rates in excess of 50 sec.$^{-1}$, a cone-and-plate instrument (Ferranti–Shirley) was used.

In the dilute suspensions (1% by weight of glyceryl tristearate), no sedimentation could be observed even after storage periods of several weeks. At shear rates exceeding 100 sec.$^{-1}$, the suspensions showed newtonian behavior with a viscosity coefficient of 0.95 poise, both in the absence and presence of surfactants.

In performing a measurement at low shear rate, the suspension was thoroughly stirred before being poured into the viscometer. The measurement was started about 1 hr. after assembling and adjustment of the instrument had been completed.

Typical stress–shear curves are shown in Fig. 1. Steady-state viscosities obtained from these curves have been assembled in Fig. 2. Altogether, four different dispersions were made without surfactant, using two different batches of tristearate crystals. The steady-state viscosities of these dispersions varied over a range indicated by the height of the vertical lines in Fig. 2. Surfactants investigated were glycerol monooleate, Aerosol OT, and cetyl alcohol, in concentrations of, respectively, 2.5, 10, and 10 μmoles/cm.^{3} of oil. The results collected in Fig. 2 show that, at shear rates less than about 0.1 sec.$^{-1}$, the steady-state viscosities of the dispersions containing surfactant are significantly lower than those of the dispersions without surfactant.

Results obtained with dispersions that had been carefully dried or to which 1% of water had been added, did not differ significantly from those shown in Fig. 2.

Discussion

(a) **Flocculation of Solid Particles.**—Dispersed triglyceride crystals in oil are always flocculated to a high degree, because attractive forces prevail at all distances between the particles. The absence of sedimentation in the quiescent, dilute dispersions shows that the tri-

(7) N. E. Lloyd, *J. Colloid Sci.*, **19**, 441 (1959).

(8) M. van den Tempel, *Proc. 2nd Intern. Congr. Surface Activity*, London, I, 1957, p. 439.

(9) A. A. Trapeznikov and V. A. Fedotova, *Proc. Akad. Sci. U.S.S.R.*, **81**, 1101 (1951).

glyceride crystals are flocculated to form a three-dimensional network sufficiently strong to withstand the action of gravity. In more concentrated suspensions the strength of this network has been measured[10]; the average energy content of the bonds between consecutive particles in the network was estimated at about 40 kT units. Addition of surfactant causes a reduced interaction energy between the particles in the network and this results in a decreased viscosity as shown in Fig. 2.

The presence of the crystal network in the dilute suspensions, and the effect of surfactants on the strength of the network, can easily be demonstrated by observing the movements of water droplets through a layer of the suspension. In a suspension containing surfactant, a water droplet of 0.3 cm. diameter falls regularly at a velocity of the order of 1 cm./min. In the absence of surfactant, a droplet is trapped in the upper layer of the suspension where it may remain stationary for very long periods. A more quantitative estimate of the effect of surfactants on the strength of the crystal network can be made as follows.

The network is considered to consist of an assembly of branched and interlinked chains, each chain consisting of a linear arrangement of solid particles. The distance between consecutive particles in a chain is small compared with the average particle diameter. The properties of the network are described by the free energy (ΔG) of the interparticle bonds and by the number (n) of bonds per cm. chain length, or alternatively, by the number (N) of chains cutting through 1 cm.^{2} cross-section. In a steady-state viscosity measurement at a shear rate D, the stress supported by the network is $S = \eta D$. The average load upon each interparticle bond is S/N and the rate of breaking of bonds is given by reaction rate theory as

$$-\frac{1}{N}\frac{dN}{dt} = A' \exp\left(-\frac{\Delta G}{kT}\right) \sinh\left(\frac{\lambda S}{NkT}\right) \quad (3)$$

A' is a proportionality constant which need not be specified and λ measures the distance over which the particles must be moved apart to break the bond. The shear rate is proportional to the rate of breaking of bonds

$$D = n\lambda A' \exp\left(-\frac{\Delta G}{kT}\right) \sinh\left(\frac{\lambda S}{NkT}\right) \quad (4)$$

In comparing the behavior of two dispersions at the same shear rate, it will now be assumed that any difference in viscosity (and hence in S) is due to different values of the bond energy ΔG, whereas variations in the values of λ and n (or of N) are negligible. Under these conditions eq. 4 may be considered as a relation giving the stress S as a function of the bond energy ΔG, and in which all the other parameters are constant. It is then easily derived that

$$\left.\begin{aligned} \frac{d}{d \ln S}\left(\frac{\Delta G}{kT}\right) &= \frac{x}{\tanh x} \\ \text{where} \qquad x &= \frac{\lambda S}{NkT} \end{aligned}\right\} \quad (5)$$

(10) M. van den Tempel, *J. Colloid Sci.*, **16**, 284 (1961).

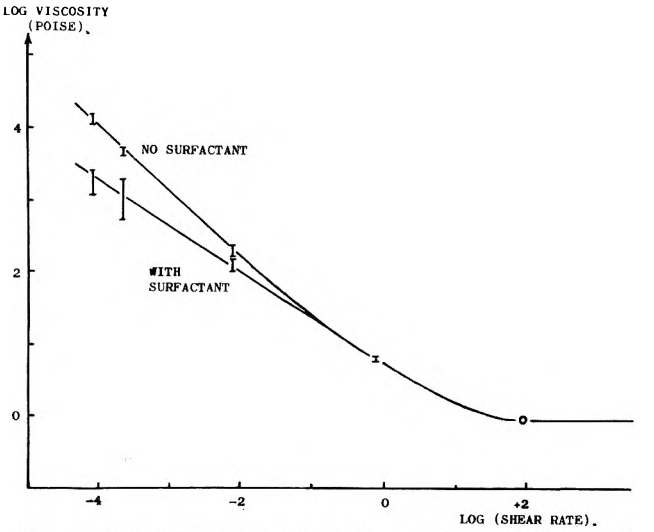

Fig. 2.—Effect of shear rate on the steady-state viscosity of 1% glyceryl tristearate suspensions in paraffin oil, with and without surfactants (concentrations given in the text).

Under the conditions used in the present investigation, the value of $x \ll 1$ and hence $x/\tanh x \cong 1$. The result is, at constant rate of shear

$$\frac{d}{d \ln \eta}\left(\frac{\Delta G}{kT}\right) \cong 1 \quad (6)$$

Application of this equation to the results shown in Fig. 2 indicates that the average bond energy is decreased with an amount of about 1 kT unit at a shear rate of 10^{-3} sec.$^{-1}$, if surfactant is added to the dispersion. At higher shear rates the effect becomes smaller, and the energy difference increases to about 1.75 kT units at a shear rate of 10^{-4} sec.$^{-1}$.

An explanation for such an effect of surfactants on the interaction energy of flocculated solid particles has been proposed by Vold,[11] who investigated the influence of long-chain alcohols on the subsidence rate of jelled lithium stearate suspensions in heptane. An increased rate of subsidence on addition of surfactant was attributed to a decreased van der Waals attraction energy of the solid particles, and this was assumed to result from an increased average interparticle distance in the presence of surfactant. An estimation of the magnitude of this effect resulted in an interaction energy decreasing by 1 kT unit if the interparticle distance was increased with a few Å. The distance between flocculated tristearate crystals in oil had been estimated at about 10 Å.[10] and a slight change in this average interparticle distance would evidently result in appreciable changes of the interaction energy. The effect of shear rate on the magnitude of the energy decrease may be explained by the presence of a distribution of bond energies in the actual network.

(b) **Emulsion Stability.**—Only a rough estimate, based on a simplified model, can be given for the influence of the flocculation of the solid particles on the stability of the emulsion. The solid particles must assemble at the surface of a water droplet in order to prevent coalescence of the droplet with a neighboring one. Free diffusion of solid particles to the water droplets, however, is prevented by the presence of a network between the solid particles. It will first be

(11) M. J. Vold, *ibid.*, **16**, 1 (1961); M. J. Vold and D. V. Rathnamma, *J. Phys. Chem.*, **64**, 1619 (1960).

shown that this network is formed almost instantaneously, before any appreciable coalescence of water droplets could have occurred. Immediately after emulsification has ceased, a more or less random distribution of water droplets and solid particles is present. Since repulsive forces are absent, flocculation proceeds at a rate given by Smoluchowski's theory for rapid flocculation. The time required for one-half of the particles to be flocculated is, then, $3\eta_0/8kTn_0$, if η_0 is the viscosity of the medium and n_0 is the initial particle concentration. The number of solid particles in the system must always be much higher than that of the water droplets, because it is desired that ultimately every water droplet is covered by solid particles. Under the conditions of the present investigation, the number of tristearate crystals is about 1000 times the number of water droplets in the emulsion. Flocculation of one-half of the solid particles requires about 1 sec., whereas the half-life time for the water droplets would be about 1000 sec. This means that the network of the solid particles is formed almost instantaneously, and before any appreciable coalescence of water droplets has occurred. In the time available before the water droplets have approached each other, the surrounding solid particles must be released from the network and adsorb at the droplet surface. The energy content of the bonds in the solid network may therefore be considered as an energy barrier preventing diffusion of the solid particles to the interface. If the energy barrier (ΔG) is sufficiently low, surface coverage of the water droplets will be nearly complete before flocculation of the droplets becomes appreciable. At higher values of ΔG, only a fraction of all the available solid particles has been adsorbed at the droplet surface, in the available time. This fraction depends upon the interparticle bond strength by a relation of the form

$$\text{fraction} \sim \exp\left(\frac{-\Delta G}{kT}\right) \qquad (7)$$

Now compare two emulsions, differing only in the strength of the bonds between solid particles by an amount (gkT). The fraction of the particles adsorbed, at any time before coalescence becomes appreciable, will differ by a factor of e^g in these emulsions. It is not known how the free energy barrier preventing coalescence depends upon the number of solid particles adsorbed at the droplet surface, but for small variations in surface coverage it probably may be assumed that the height of this free energy barrier, ΔF, increases in proportion with the fraction of the particles adsorbed. The use of the symbols G and F is not meant to define these energies as a Gibbs function and a Helmholtz function, respectively; they only distinguish the free energy of the interparticle bonds and the free energy barrier against coalescence. Since the rate of coalescence (K) is again an exponential function of ΔF, the stability ratio of the emulsions is approximately

$$\ln \frac{K_1}{K_2} = \frac{\Delta F_1}{kT}(e^g - 1)$$

This shows that considerable differences in stability against coalescence may result from minor variations in the interparticle bond energy. In fact, a difference in bond energy of 1 kT unit (*i.e.*, $g = 1$) already would result in a stability ratio of 1000 if $\Delta F_1/kT = 4$.

The results of this investigation show that the stabilizing action of solid particles is sensitive to small changes in the interaction energy of these particles. In a completely flocculated system with strong interparticle bonds no emulsion can be formed. On the other hand, in a completely deflocculated (*i.e.*, stable) suspension emulsification is promoted by adding weak flocculating agents.[2a] It appears that partial flocculation, *i.e.*, moderately prevalent attraction between the solid particles, is necessary for emulsion stabilization. From this point of view, it is concluded that flocculation in a dispersion of tristearate crystals in paraffin oil is already too far advanced, and emulsification is promoted by agents which reduce flocculation.

The theory developed for the effect of these agents does not pretend to explain why prevalent attraction between the solid particles is necessary at all; it only accounts for the effect of too high an attraction energy.

Acknowledgment.—The authors are indebted to Mr. L. L. Hoekstra, who carried out the viscosity measurements.

POLAROGRAPHY OF CARBONYL COMPOUNDS. IV. MULTIPLE DERIVATIVES OF BENZALDEHYDE AND ACETOPHENONE

BY WILLIAM R. CROWELL AND DALE M. COULSON[1]

Chemistry Department of the University of California at Los Angeles and the Stanford Research Institute, Menlo Park, Calif.

Received May 25, 1962

Two types of empirical equations described in Part III of this series are used to test new data obtained from polarograms of multiple substituted compounds of benzaldehyde and acetophenone in 50% dioxane buffer solutions. Experimental values of $E^0_{1/2}$ are compared with those predicted by these equations employing the structural parameters previously obtained with the unsubstituted and monosubstituted compounds.

In parts I and II,[2] the relation between pH and half-wave potentials of certain carbonyl compounds was discussed. It was demonstrated that there was no significant effect of ionic strength on half-wave potentials. However, undesirable solvent effects had been observed and 50% dioxane–50% water was chosen as the solvent in order to minimize activity and solubility effects. A more complete discussion of these problems is given in part I of this series of papers.

It is well known that the solubility of large organic molecules is limited in water and in highly aqueous

(1) Stanford Research Institute, Menlo Park, California.

(2) (a) D. M. Coulson and W. R. Crowell, *J. Am. Chem. Soc.*, **74**, 1290 (1952); (b) D. M. Coulson and W. R. Crowell, *ibid.*, **74**, 1294 (1952).

systems. Notwithstanding, a considerable amount of work continues to be done with solvents that are not well suited for studying the effect of organic structures on half-wave potentials due to specific solvent effects. Any attempt to relate structure to half-wave potentials in these solvent systems must first take into account the specific solvent effects. The work of Elving and Leone[3,4] in 9.5 and 19% ethanol and that of Suzuki and Elving[5] in 9.5 to 38% ethanol bear out the earlier findings of the authors[2,6] that undesirable kinetic effects can be avoided by using a suitable solvent system. It was shown in part I that for the one-electron reduction of certain carbonyl compounds in acid solutions that $E_{1/2}$ is a linear function of pH as indicated in equation 1

$$E_{1/2} = E^0_{1/2} - \mathrm{pH}(B) \qquad (1)$$

where $E^0_{1/2}$ is the half-wave potential at zero pH and B is the slope of the $E_{1/2}$ *vs.* pH plot. Since then most investigators of the polarography of aldehydes and ketones have assumed equation 1 to be valid. This slope is usually approximately 0.06 volt per pH unit and the electrode reaction has been assumed to be

$$\mathrm{RCHO} + \mathrm{H^+} + \mathrm{e^-} \rightleftarrows \mathrm{R\dot{C}HOH} \qquad (2)$$

In parts II and III, using semi-empirical relationships, three types of empirical equations were derived expressing the relation between structures and half-wave potentials at zero pH. The first type was based on a reinterpretation of the zero order linear combination of atomic orbitals–molecular orbital theories of Scrocco and Cappellina[7] and of Schmid and Heilbronner,[8] the second was based on Pacault and Pointeau's equation for the free electron gas model,[9] and the third was based on Hammett's $\rho\sigma$ equation. The agreement between experimental results and those predicted by these equations was reasonably satisfactory.

The purpose of the present work is to test the application of two of the three types of equations to multiple derivatives of benzaldehyde and acetophenone, using the previously studied individual substituents and their structural constants. The types of compounds considered include the 3,4- series, the 3,5 series, the 3,4,5 series, and others such as the 2,3, 2,4, and 2,5.

Benzophenones were not included in this study because steric hindrance adds another structural parameter that must be included in the interpretation of results.

Experimental

All polarograms were obtained by use of the same recording polarograph as that employed in previous work by essentially the same procedures. In the pH measurements a Model G or Model H Beckman meter was used. The reference half-cell was a saturated calomel electrode and all measurements were made in a thermostat regulated at 25.0 ± 0.1°. The dropping mercury electrodes used in these studies had drop times of 3.25 to 4.71 seconds and the mass of mercury per second ranged from 1.77 to 2.33 mg. per second.

The 50% dioxane buffer solutions were prepared by adding the dioxane solutions to an equal volume of an aqueous solution 0.2 *f* in potassium chloride, 0.2 *f* in acetic acid, and 0.2 *f* in orthophosphoric acid to which had been added sufficient concentrated sodium hydroxide solution to produce the pH desired after the addition of the dioxane solution. In most of the solutions the pH's were in the region between 2.2 to and including 3.3 in steps of approximately 0.2 resulting in $E^0_{1/2}$ values reliable to approximately 3 mv. The dioxane was refluxed over sodium at least 12 hours and stored over sodium shavings. The purity of the dioxane was always checked by running polarograms on the buffer solutions before addition of the aldehyde or ketone.

The aldehydes and ketones were either freshly distilled or recrystallized, or, if necessary, recrystallized after vacuum sublimation before each run. Compounds commercially unavailable were prepared by student assistants using standard methods or those described in the literature.

Results

Half-wave potentials at a pH of zero, $E^0_{1/2}$, at 25° in 50% dioxane solutions for several multiple derivatives of benzaldehyde and acetophenone are shown in column 4 of Table I and the corresponding slopes are shown in column 3. These data were obtained by extrapolating a plot of $E_{1/2}$ *vs.* pH for each compound in the same manner as those for the individual substituents in part III. Each compound in Table I had a diffusion current constant that ranged from 1 to 2 and the concentrations were all in the range of 0.4 to 0.8 mmole per liter.

TABLE I

POLAROGRAPHIC RESULTS OF MULTIPLE DERIVATIVES OF BENZALDEHYDE AND ACETOPHENONE AND PREDICTED HALF-WAVE POTENTIALS

Compound	3,4 Subst.	Slope V/pH unit	$E^0_{1/2}$, v. *vs.* S.C.E. Expt.	Eq. 3 or 4 (M.O.)	Eq. 5 or 6 (free-electron-gas)	Diffusion current constants
Aldehyde	Br, Br	0.062	0.708	0.723	0.722	1.36
Ketone		.063	.852	.846	.845	2.12
Aldehyde	Cl, Cl	.063	.736	.740	.744	1.91
Ketone		.061	.870	.863	.867	1.50
Aldehyde	CH_3, CH_3	.063	.904	.908	.906	0.83
Ketone		.059	1.038	1.031	1.029	1.51
Aldehyde	CH_3O, CH_3O	.063	0.942	0.937	0.933	1.04
Ketone		.060	1.052	1.060	1.056	1.71
Aldehyde	OH, OH	.060	0.990	0.993	0.991	1.47
Ketone		.059	1.107	1.116	1.114	1.84
Aldehyde	CH_3O, OH	.062	0.972	0.960	0.959	1.47
Ketone		.063	1.081	1.083	1.082	2.28
Aldehyde	Cl, OH	.064	0.930	0.890	0.899	1.36
Ketone		.060	1.046	1.013	1.022	1.63
Aldehyde	OH, Cl	.065	0.822	0.811	0.809	1.81
	3,5 Subst.					
Aldehyde	Br, Br	0.057	0.678	0.694	0.692	1.26
Ketone		.060	.802	.817	.815	1.13
Aldehyde	Cl, Cl	.058	.711	.728	.738	1.08
Aldehyde	CH_3, CH_3	.059	.887	.899	.898	1.28
Aldehyde	CH_3O, CH_3O	.063	.834	.829	.828	1.07
	3,4,5 Subst.					
Aldehyde	CH_3O, CH_3O, CH_3O	0.058	0.884	0.915	0.908	1.21
Ketone		.064	0.994	1.038	1.031	1.45
Aldehyde	Cl, Cl, Cl	.063	0.668	0.684	0.690	1.01
Ketone	OH, OH, OH	.066	1.080	1.125	1.119	1.77
	Miscellaneous subst.					
Aldehyde	2OH, 4OH	0.058	1.070	1.065	1.062	1.77
Aldehyde	2OH, 5Cl	.061	0.829	0.845	0.851	1.27
Aldehyde	$2CH_3O$, $3CH_3O$	.063	0.823	0.824	0.817	1.28

LCAO–MO Equations.—Equations 3 and 4 derived in part III are those based on our application of zero-order linear combination of atomic orbitals–molecular orbital theories in showing the relationship between $E^0_{1/2}$, expressed in volts, and the structural parameters,

(3) P. J. Elving and J. T. Leone, *J. Am. Chem. Soc.*, **80**, 1021 (1958).
(4) P. J. Elving and J. T. Leone, *ibid.*, **82**, 5076 (1960).
(5) M. Suzuki and P. J. Elving, *J. Phys. Chem.*, **65**, 391 (1961).
(6) D. M. Coulson, W. R. Crowell, and S. K. Tendick, *J. Am. Chem. Soc.*, **79**, 1354 (1957).
(7) F. Scrocco and F. Cappellina, *Boll. Sci. fac. chim. ind. Bologna*, **12**, 101 (1954).
(8) R. W. Schmid and E. Heilbronner, *Helv. Chim. Acta*, **37**, 1453 (1954).
(9) A. Pacault and R. Pointeau, *Compt. rend.*, **236**, 2060 (1953).

Z_i, of the benzaldehyde and acetophenone compounds involved in reaction 2. In these equations

$$E^0_{1/2}\ (\text{benzaldehyde}) = +0.060 - \frac{4.421}{\Sigma_i Z_i} \quad (3)$$

$$E^0_{1/2}\ (\text{acetophenone}) = -0.063 - \frac{4.421}{\Sigma_i Z_i} \quad (4)$$

$\Sigma_i Z_i$ is equal to 4.767, the sum of the parameters for the unsubstituted compound, plus the sum of the structural parameters of the substituents in the substituted compound undergoing reduction. The substituent parameters are listed in Table II which is a duplicate of Table IV in part III with the exceptions that the *m*-methylbenzaldehyde parameter has been added and the parameter of *m*-chloroacetophenone has been replaced by a redetermined value.

TABLE II

EMPIRICAL STRUCTURAL PARAMETERS FOR SUBSTITUENTS ON THE BENZENE RING OF BENZALDEHYDES AND ACETOPHENONES DERIVED FROM THE LCAO–MO EQUATIONS AND FROM THE PACAULT–POINTEAU EQUATIONS

	Constant Z_i					
	LCAO–MO			Pacault–Pointeau		
Substituent	Benzaldehyde	Acetophenone	Average	Benzaldehyde	Acetophenone	Average
m-Br	0.572	0.521	0.547	0.283	0.260	0.272
m-Cl	.386	.452	.419	.196	.183	.190
p-Br	.303	.344	.324	.154	.174	.164
p-Cl	.326	.356	.341	.165	.179	.172
m-CH_3O	.118	.086	.102	.063	.048	.056
m-OH	− .018	− .049	− .034	− .001	− .017	− .009
m-CH_3	− .064	− .094	− .079	− .027	− .040	− .034
p-CH_3	− .099	− .143	− .121	− .042	− .063	− .052
p-CH_3O	− .451	− .417	− .434	− .215	− .196	− .205
p-OH	− .561	− .508	− .535	− .269	− .253	− .261
o-OH	− .247	− .355	− .301	− .115	− .168	− .141
o-CH_3O	.098	.167	.132	.053	.113	.083

The substituent constants were averaged for each substituent on the corresponding benzaldehyde and acetophenone in order to get the "best" value for predicting half-wave potentials. As data for other compounds containing these same substituents become available, the "best" values of substituent constants will undoubtedly require revision to include the new data. The effect of averaging several datum points for each substituent is to make the average deviations between experimental and predicted half-wave potentials as small as possible. Substituent constants from individual compounds were included rather than averages, only, to make it possible for others to recognize any sources of error in the original data based on later experimental work.

Using equations 3 or 4 and the proper average parameters listed in Table II, the predicted $E^0_{1/2}$'s were calculated and recorded in column 5 of Table I. The experimental values are listed in column 4 of Table I.

Free Electron Gas Model Equations.—In part III we tested our data with the following Pacault and Pointeau equations for a free electron gas model. For substituted benzaldehydes

$$E^0_{1/2} = 4.866 - 19.06\left[\frac{j+2}{2j+3.506}\right]^2 \quad (5)$$

and for substituted acetophenones

$$E^0_{1/2} = 4.743 - 19.06\left[\frac{j+2}{2j+3.506}\right]^2 \quad (6)$$

The value of j was calculated for each unsubstituted and monosubstituted compound, using the experimental $E^0_{1/2}$. From these values the constant Z_i for each substituent was assumed to be equal to the j of the compound of that substituent minus 0.789 the j of the unsubstituted compound. The j of the multiple substituted compound then is equal to 0.789 plus the sum of the Z_i's of the substituents involved, or

$$j = 0.789 + \Sigma_i Z_i \quad (7)$$

Selecting the proper average parameters from Table II, equation 5 or 6 was then used to calculate the predicted $E^0_{1/2}$'s shown in column 6 of Table I.

Discussion

In part III of this series the derivation of a LCAO-MO method of relating polarographic half-wave potentials and structures for conjugated aldehydes and ketones was dealt with in some detail. Because of the complexity of the calculations involved in the rigorous treatment of the theoretical equations, empirical relations which are similar to the theoretical equations but much simpler to use were developed and used to relate molecular structures and polarographic potentials. We felt that our approach to this problem is justified because it shows that as molecules become more complex the effect of adding an additional structural group diminishes in a predictable and reasonable manner. This is demonstrated in equations 3 and 4 which show an inverse relationship between polarographic potentials and linearly additive structural parameters, Z_i. In the limiting case where ΣZ_i is large, the predicted $E^0_{1/2}$ value is finite and approaches a limiting value. In this case, the addition of substituents with small Z_i values would have no significant effect on the polarographic potential. On the other hand, groups with small substituent constants have significant effects in simple molecules. Because of this feature of diminishing effects as molecules get more complex it is possible to deal successfully with multiple substituents without modifying the constants in equations 3 and 4.

The agreement between experimental and predicted half-wave potentials for 3,4-disubstituted benzaldehydes and acetophenones is satisfactory. The only serious discrepancies were for the 3-chloro, 4-hydroxy compounds. In these cases, it is possible that direct interaction between the hydrogen of the 4-hydroxy group and the 3-chloro group results in a suppression of the electron releasing effect of the chloro group. In the cases of the 3,5-disubstituted compounds and of the 3,4,5-trisubstituted compounds, there appears to be a slight reinforcement of effects over those predicted by our equations. This effect is small and relatively insignificant in using half-wave potentials as a means of determining the types of structures that may be present in unknown compounds. The deviations were greatest for compounds containing the 4-hydroxy substituent.

Acknowledgments.—The authors wish to thank Doctors Theodore A. Geissman and Kenneth Conrow for their most helpful advice during the progress of this investigation, and to express their appreciation to Leonard Slevin, Marie Salvinger, William Flaschenreim, and especially Joseph Behar for their able assistance in the experimental work.

CYANOCARBON CHEMISTRY. XXIII. THE IONIZATION BEHAVIOR OF CYANOCARBON ACIDS

BY RICHARD H. BOYD[1]

Contribution No. 769 from the Central Research Department, Experimental Station, E. I. du Pont de Nemours and Company, Wilmington, Delaware

Received June 4, 1962

The reversible protonations of a number of cyanocarbon anions have been studied spectroscopically in sulfuric and perchloric acid solutions. An indicator acidity function, H_-, based on this protonation can be set up for acid solutions up to ~12 M and pK_a's of the cyanocarbon acids determined. The H_- function is very similar to H_0 (based on protonation of neutral bases) showing differences at lower concentrations (5 M or less) expected on the basis of charge type and above 5 M it tends to parallel H_0. The strengths of the cyanocarbon acids can be correlated with the favorability of resonance structures of the anions and resonance possibilities in the protonated form. The positions of protonation for many of the acids can be inferred from the ultraviolet spectra. The stronger cyanocarbon acids form solid dihydrates which are ionized as shown by the ultraviolet spectra.

Introduction

A number of organic molecules highly substituted with cyano groups exhibit acidic properties. The remarkable strengths of several of these acids and their utility in studying acid solutions have been briefly reported.[2] Specifically, their reversible protonation in solutions of strong acids can be detected spectroscopically. Thus, the behavior of cyanocarbon acids as indicators can be used to determine their own acid strengths (pK_a) and to set up an acidity scale based on the protonation of anions. The Hammett acidity function, H_0, is based on protonation of neutral bases and is defined according to

$$H^+ + B \rightleftharpoons BH^+ \text{ and}$$

$$H_0 \equiv pK_B + \log \frac{C_B}{C_{BH^+}} = -\log a_{H^+} - \log \frac{f_B}{f_{BH^+}} \quad (1)$$

where C_B and C_{BH^+} are indicator concentrations, a_{H^+} refers to the hydrogen ion activity, and f_B and f_{BH^+} are molar activity coefficients for the indicator.[3] A similar function can be defined for the protonation of anions

$$H^+ + A^- \rightleftharpoons HA$$

$$H_- \equiv pK_a + \log \frac{C_{A^-}}{C_{HA}} = -\log a_{H^+} - \log \frac{f_{A^-}}{f_{HA}} \quad (2)$$

Such a scale should have important implications in the study of concentrated acid solutions, but in the past it has not been possible to set one up due to the lack of suitable indicators. The cyanocarbon acids appear to fulfill this need up to acid concentrations equivalent to approximately 80% sulfuric acid. The present paper presents in detail the study of the protonation of cyanocarbon acids and some additional observations concerning their properties. Some measurements on picric acid are also reported for comparison.

Measurements were largely made in perchloric and sulfuric acid solutions, but some measurements on *p*-(tricyanovinyl)-phenyldicyanomethane and picric acid were also made in hydrochloric acid. A number of the cyanocarbon acids reacted irreversibly with the latter, so it was not used extensively.

(1) Department of Chemistry, Utah State University, Logan, Utah.

(2) R. H. Boyd, *J. Am. Chem. Soc.*, **83**, 4288 (1961).

(3) (a) L. P. Hammett and A. J. Deyrup, *ibid.*, **54**, 2721 (1932); (b) M. A. Paul and F. A. Long, *Chem. Rev.*, **57**, 1 (1957).

Experimental Details

Tetramethylammonium *p*-(tricyanovinyl)-phenyldicyanomethanide was prepared by the method of Williams[4] and was used at a final concentration of 1.58×10^{-4} M in the acid solutions. Sodium methyldicyanoacetate was made according to the directions of Arndt, *et al.*,[5] and used at a concentration of 1.09×10^{-3} M. Sodium 1,1,2,6,7,7-hexacyano-1,3,5-heptatrienide was made by potentiometric titration with 0.1 N NaOH of a solution of the free acid made by ion exchange from the ammonium salt. The latter was made by the method of Wiley, *et al.*[6] A final concentration of 5.37×10^{-5} M was used. Potassium tricyanomethanide (cyanoform) made by the method of Trofimenko, *et al.*,[7] was used at a concentration of 2.82×10^{-4} M. Sodium bis-(tricyanovinyl)-amine (sodium 1,1,2,4,5,5-hexacyano-3-azapentadienide) and sodium 1,1,2,3,3-pentacyanopropenide were prepared by ion exchange and titration from the tetramethylammonium salts made by the methods of Middleton, *et al.*[8] They were used at concentrations of 2.66×10^{-4} M and 4.20×10^{-4}, respectively. Sodium hexacyanoisobutylenediide (sodium 2-dicyanomethylene-1,1,3,3-tetracyanopropanediide) was prepared by the method of ref. 8 and was used at a concentration of 3.60×10^{-4} M. Sodium 1,1,3,3-tetracyanopropene[9] was a laboratory sample and used at 4.0×10^{-4} M.

Hydrates of the cyanocarbon acids were made by rapidly evaporating under vacuum, stirred solutions of the free acids made by ion exchange. A water bath starting at room temperature was used to prevent the solutions from freezing. Final bath temperatures of 10–15° were obtained. The hydrates are not very stable at room temperature as judged by color formation but may be stored at Dry Ice temperature.

Picric acid was Matheson Coleman and Bell reagent grade and was used at 9.75×10^{-4} M.

Most of the solutions of the indicators (salts of cyanocarbon acids) in sulfuric and perchloric acids were made up by pipetting given amounts of indicator stock solution (aqueous) into the acid solutions. The acid solutions were made up by mixing known volumes of acid (sulfuric acid was Du Pont Reagent Grade, approximately 95%, and perchloric acid was Eastman White Label, approximately 70%) with known volumes of water. The final volumes and compositions were computed from I.C.T. density data.[10] Solutions with hydrochloric acid (Du Pont Reagent Grade) (and also tetramethylammonium *p*-(tricyanovinyl)-phenyldicyanomethanide in perchloric acid) were made up to constant total volume in volumetric flasks.

All spectra with the exception of cyanoform solutions were taken with a Cary Model 11 recording spectrophotometer (Applied Physics Corporation) with a thermostated cell holder. The temperature of the water circulating in the walls of the

(4) J. K. Williams, *J. Am. Chem. Soc.*, **84**, 3478 (1962).

(5) F. Arndt, H. Scholz, and E. Frobel, *Ann.*, **521**, 95 (1935).

(6) D. W. Wiley, J. K. Williams, and B. C. McKusick, *J. Am. Chem. Soc.*, **84**, 2216 (1962).

(7) S. Trofimenko, E. L. Little, Jr., and H. F. Mower, *J. Org. Chem.*, **27**, 433 (1962).

(8) W. J. Middleton, E. L. Little, D. D. Coffman, and V. A. Engelhardt, *J. Am. Chem. Soc.*, **80**, 2795 (1958).

(9) Y. Urushibara, *Bull. Chem. Japan*, **3**, 278 (1927); *Chem. Abstr.*, **22**, 579 (1928).

(10) "International Critical Tables," Vol. III, McGraw-Hill Book Co., New York, N. Y., 1st Ed., 1928, p. 51.

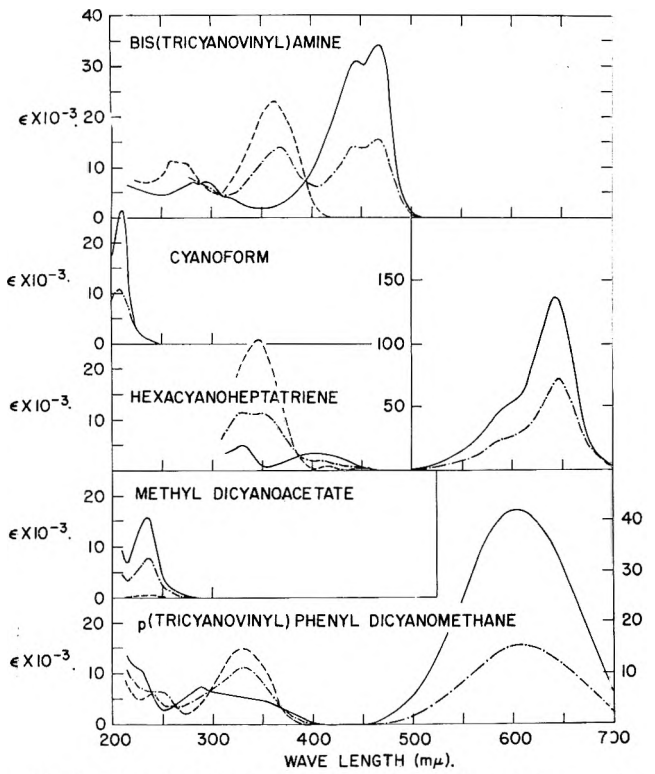

Fig. 1.—Spectra of cyanocarbon acids: full curve (———) is anionic form in water; dashed curve (– – –) is undissociated form in sulfuric acid solution of high concentration; dashed-dot curve (–·–·–) shows anionic form in equilibrium with undissociated form in sulfuric acid of intermediate concentration.

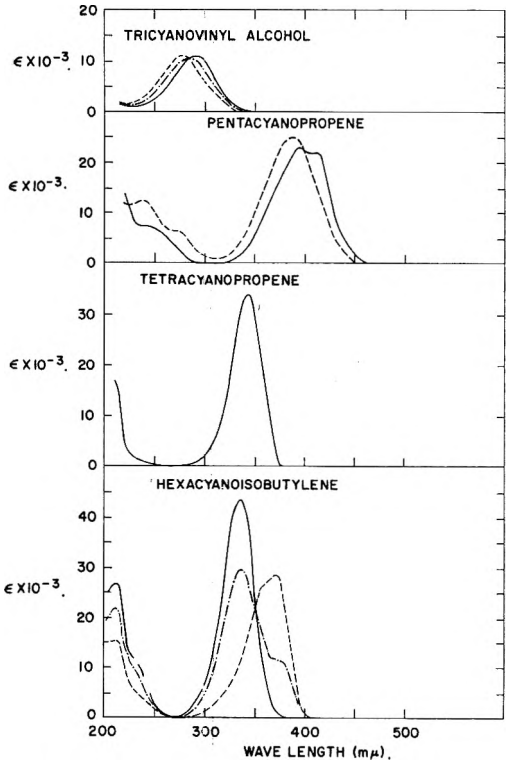

Fig. 2.—Spectra of cyanocarbon acids: full curve (———) is anionic form in water; dashed curve (– – –) is undissociated form in sulfuric acid solution of high concentration; dashed-dot curve (–·–·–) shows anionic form in equilibrium with undissociated form in sulfuric acid of intermediate concentration. For pentacyanopropene the dashed curve is for the sodium salt dissolved in anhydrous sulfuric acid. It may still be in the anionic form.

holder was held at 25.0 ± 0.1°. Measurements with a thermocouple indicated that the inside temperature was within 0.5° of this. The spectra of the cyanoform solutions were made with a Cary Model 14 spectrophotometer without temperature control. The latter instrument has better response near 2100 Å. where the cyanoform anion absorbs.

The time after adding the indicator to the acid solution was kept at a minimum in order to avoid any hydrolysis; 10–20 minutes was usually allowed for temperature equilibration in the cell holder. Methyldicyanoacetate was the most sensitive to hydrolysis but with a 10-minute equilibration period no appreciable loss of indicator took place. Calibrated quartz absorption cells (Aminco) were used; 1 or 2 mm. cells were used for solutions of the free anions, and the less acidic solutions. Cells up to 5 cm. were used to measure small amounts of the anions in the more acid solutions and also small amounts of the protonated forms in the less acid solutions.

The spectra were all taken with an empty reference cell compartment. A blank with each cell with water was run for each series of measurements on an indicator. Blanks with the acid solutions gave the same results as with water.

Spectra of solid hydrates of the cyanocarbon acids were taken in KBr pellets in a Cary Model 14 spectrophotometer.

Anhydrous solvents were prepared by drying in a molecular sieve column (Linde 5A).

Results

1. Spectral Changes on Protonation.—The general features of the spectral changes that take place on protonation are shown in Fig. 1 and 2. The absorptions are generally intense, well resolved, and relatively free from medium effects. All of the protonation effects were accurately reversible upon dilution. There is a slight shift of the anion peak toward longer wave length with increasing acid concentration. This shift appears to be greatest in going from pure water to acid concentrations of several molar, and of less importance above that. The optical densities were usually taken at λ_{max} rather than at a fixed wave length but for most of the cases the particular method makes little difference. The method of calculation of the indicator ratio, $R = C_{A^-}/C_{HA}$, is outlined below for each of the systems. The indicator ratio when measurements on the anion peak alone are used is given by equation 3

$$R = \frac{D - D^0_{HA}}{D^0_{A^-} - D} \qquad (3)$$

where D is the optical density at the anion peak, $D^0_{A^-}$ is the optical density of a solution when all of the indicator is in the anion form and D^0_{HA} is the density at the anion peak when all of the indicator is in the acid form. If both the anion and acid form peaks are used together to calculate R, the equation derived below is used. The optical density at λ_{max} (anion) is

$$D_2 = D_{2,A^-} + D_{2,HA}$$

and the optical density at λ_{max} (protonated form) is

$$D_1 = D_{1,HA} + D_{1,A^-}$$

If D_1 and D_2 in pure water are D^0_{1,A^-} and D^0_{2,A^-} if D_1 and and D_2 are $D^0_{1,HA}$ and $D^0_{2,HA}$ in very concentrated acid, then

$$R = C_{A^-}/C_{HA} = \frac{D_2D^0_{1,HA} - D_1D^0_{2,HA}}{D_1D^0_{2,A^-} - D_2D^0_{1,A^-}} \qquad (4)$$

The optical densities used in the calculations are all corrected for any change in volume on mixing. Although salts of the acids were actually used, they are designated below as the acid itself.

***p*-(Tricyanovinyl)-phenyldicyanomethane.**—R was calculated from the anion peak with $D^0_{HA} = 0$ in eq. 3.

The peak due to the acidic form (332 mμ) is overlapped by anion absorption but calculations were made using the peak to show that it gives the same results as the anion peak but with less accuracy and sensitivity. After this acid is completely converted to the protonated form, no further change in the spectrum (other than a minor shift to longer wave lengths) occurs up to 11 M acid concentration.

Methyldicyanoacetate.—R was calculated from the anion peak with a small correction from D^0_{HA} (eq. 3) (= $0.0123D^0_{A^-}$ ($HClO_4$) and = $0.0150D^0_{A^-}$ (H_2SO_4)).

Hexacyanoheptatriene.—The anion peak was used with $D^0_{HA} = 0$ in eq. 3. Calculations were also made with the acid form peak to show that they give the same results.

Cyanoform.—Only the anion peak is observable and eq. 3 with $D^0_{HA} = 0$ is used.

Bis-(tricyanovinyl)-amine.—A well defined isosbestic point is observed for this compound. Both the acid and anion form peaks were used to calculate R from eq. 4 with $D^0_{2,HA} = 0$ and $D^0_{1A} = 0.106D^0_{1,HA}$ (H_2SO_4) and $0.107D^0_{1,HA}$ ($HClO_4$). Using only the anion peak leads to the same results, but the range of R values measurable is restricted. For the three highest acid concentrations eq. 3, $D^0_{HA} = 0$, was used.

Hexacyanoisobutylene.—A well defined isosbestic point is observed here. Peaks due to $A^=$ and HA^- are both observable and both were used to calculate

$$R = \frac{C_{A^-}}{C_{HA^=}}$$

from the appropriate adaptation of eq. 4. No change in the spectrum corresponding to further protonation (to H_2A) was observed up to 11 M perchloric acid or ~85% sulfuric acid. Above 90% sulfuric acid irreversible, time dependent changes in the spectrum took place indicating a chemical attack, probably by hydrolysis of the cyano groups.

Pentacyanopropene and Tetracyanopropene.—No changes in the spectra are noted up to 11 M perchloric acid or ~85% sulfuric acid. Above 90% sulfuric acid irreversible time dependent changes in the spectrum took place, probably due to hydrolysis of cyano groups. In anhydrous sulfuric acid sodium pentacyanopropenide is more stable again and can be recovered by dilution before decomposition. Its spectrum is reversibly modified (see Fig. 2) but not as much as expected for protonation and the free anion may exist even in this strong acid medium.

Tricyanovinyl Alcohol.—This acid apparently undergoes protonation in the range 7–10 M, but the anion and protonated form peaks were not well resolved. The acid concentration at which the anion and protonated form were at equal concentration could be located fairly well and a pK_a was calculated from this single point ($pK_a = H_-$ when $\log C_{A^-}/C_{AH} = 0$).

Picric Acid.—This acid is not ideal for quantitative work since there is a serious overlap of the spectrum of the protonated form with that of the free anion. In order to extend the measurements to higher acid concentrations, optical densities away from λ_{max} (anion) have to be used. This is not too satisfactory since the solvent shift has a rather important effect then. R was calculated from eq. 3 from optical densities at several longer wave lengths and extrapolated to λ_{max}.

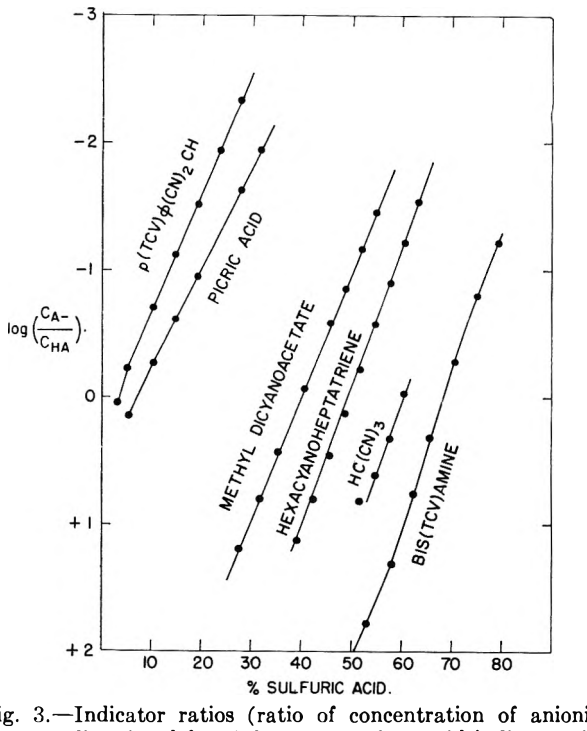

Fig. 3.—Indicator ratios (ratio of concentration of anionic form to undissociated form) for cyanocarbon acid indicators in sulfuric acid solution.

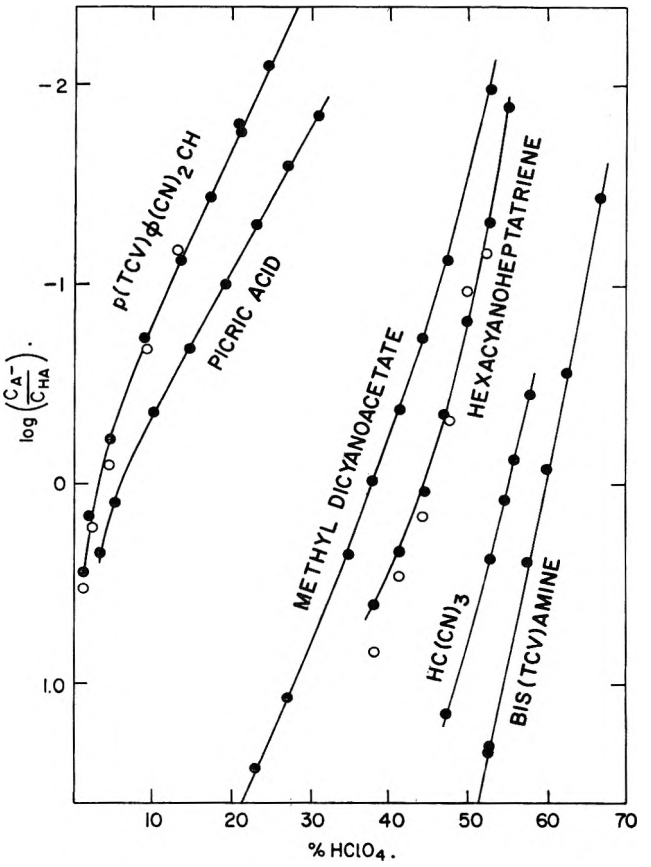

Fig. 4.—Indicator ratios (ratio of concentration of anionic form to undissociated form) for cyanocarbon acid indicators in perchloric acid solution. Open circles are ratios determined from the absorption of the protonated form rather than the anion.

2. Indicator Behavior and an H_- Acidity Function.—Values of log R *vs.* acid concentration are listed in Table I. In indicator studies it is customary to display log R plotted *vs.* acid concentration. Figures 3 and 4 show such plots for sulfuric and perchloric acids. Two criteria

for a meaningful indicator acidity function that are often used are the requirements that such plots as above by parallel for different indicators at the same acid concentration and the pK_a values obtained from the vertical displacements of these curves should be independent of the acid solution they are measured in. The first of these requirements seems to be accurately fulfilled for the indicators studied. The pK_a values determined are listed in Table II. The stronger acids are determined relative to methyl dicyanoacetate which in turn is relative to *p*-(tricyanovinyl)-phenyldicyanomethane. The pK_a determination of the latter is discussed below. The agreement of pK_a's is not quite as good as has been reported[3b] for some of the Hammett indicators but is considered to be satisfactory with perhaps the exception of hexacyanoheptatriene. Tricyanovinyl alcohol was subject to difficulties (see preceding section). The picric acid slope agrees approximately with the others, the agreement being better when density data at λ_{max} is used, but the measurements cannot be extended as far.[11] The rather few Hammett indicators that have been widely studied have been selected from a large number of similar molecules. The useful cyanocarbon indicators are not yet very numerous and are not particularly closely matched in molecular structure and size.

The determination of the pK_a of *p*-(tricyanovinyl)-phenyldicyanomethane by extrapolation of the log of the equilibrium quotient *vs.* concentration to zero concentration requires some care. Such extrapolations for

TABLE I

PROTONATION RATIOS FOR CYANOCARBON ACIDS

25°, $R = C_A^-/C_{HA}$

Molar	Concn., %	Log R	Molar	Concn., %	Log R
Sulfuric Acid					
p-(Tricyanovinyl)-phenyldicyanomethane			Hexacyanoheptatriene		
0.326	3.14	+0.043	5.13	39.0	1.127
0.546	5.19	−0.222	5.71	42.4	0.800
1.098	10.11	−0.705	6.30	45.7	0.463
1.662	14.84	−1.132	6.89	48.9	0.130
2.23	19.29	−1.518	7.47	51.9	−0.214
2.80	23.58	−1.944	8.06	54.9	−0.566
3.38	27.7	−2.336	8.67	57.8	−0.900
			9.25	60.5	−1.223
			9.85	63.2	−1.539
Methyl dicyanoacetate			Cyanoform		
3.38	27.7	1.191	7.47	51.9	0.816
3.96	31.6	0.800	8.06	54.9	0.612
4.55	35.4	0.429	8.67	57.8	0.330
5.41	40.7	−0.070	9.25	60.5	−0.031
6.30	45.7	−0.581			
6.89	48.9	−0.856			
7.47	51.9	−1.169			
8.06	54.9	−1.456			
			Picric acid		
Bis-(tricyanovinyl)-amine			0.326	3.14	0.41
7.64	52.8	1.787	0.546	5.19	0.17
8.67	57.8	1.307	1.098	10.11	−0.27
9.67	62.4	0.760	1.662	14.84	−0.61
10.44	65.7	0.316	2.23	19.29	−0.96
11.59	70.5	−0.284	2.80	23.58	−1.29
12.72	75.0	−0.810	3.38	27.7	−1.63
13.90	79.3	−1.220	3.96	31.6	−1.95
Perchloric Acid					
p-(Tricyanovinyl)-phenyldicyanomethane			Hexacyanoheptatriene		
0.118	1.18	0.438	4.79	38.0	0.599
0.236	2.35	0.160	5.34	41.3	0.330
0.473	4.65	−0.234	5.87	44.3	0.024
0.946	9.11	−0.743	6.41	47.3	−0.353
1.419	13.36	−1.115	6.93	50.0	−0.819
1.891	17.40	−1.443	7.49	52.8	−1.322
2.36	21.1	−1.765	8.02	55.3	−1.881
2.36	21.1	−1.807			
2.84	24.8	−2.10			
Methyl dicyanoacetate			Cyanoform		
2.64	23.3	1.415	6.41	47.3	1.143
3.18	27.3	1.066	7.49	52.8	0.373
4.26	34.6	0.345	7.86	54.5	0.075
4.79	38.0	−0.028	8.19	56.0	−0.135
5.34	41.3	−0.376	8.57	57.8	−0.414
5.87	41.3	−0.750			
6.41	47.3	−1.128			
7.49	52.8	−1.996			
			Picric acid		
Bis-(tricyanovinyl)-amine			run 1		
7.49	52.8	1.338	0.321	3.18	0.34
7.49	52.8	1.306	0.530	5.21	0.07
8.57	57.8	0.380	1.062	10.18	−0.37
9.12	60.2	−0.078	1.585	14.81	−0.70
9.68	62.5	−0.567	2.11	19.20	−1.01
10.71	66.7	−1.440	2.64	23.3	−1.31
			3.18	27.3	−1.59
			3.72	31.0	−1.86
			run 2		
			0.118	1.18	0.79
			0.236	2.35	0.50
			0.473	4.65	0.15
			0.709	6.89	−0.08
			1.655	15.28	−0.73
Hydrochloric Acid					
p-(Tricyanovinyl)-phenyldicyanomethane			Picric acid		
0.0596	0.751		0.108		0.84
0.119	0.525		0.215		0.60
0.238	0.243		0.323		0.44
0.477	−0.100		0.538		0.20
0.954	−0.542		1.075		−0.16
1.430	−0.876		1.613		−0.45
1.907	−1.167				
2.38	−1.442				

TABLE II

IONIZATION CONSTANTS OF CYANOCARBON ACIDS, 25°

Cyanocarbon acid	pK_a $HClO_4$	pK_a H_2SO_4	λ_{max} (mμ) for longest wave band: Free anion	λ_{max} (mμ) for longest wave band: Protonated form
p-(Tricyanovinyl)-phenyldicyanomethane	0.60	...	607	332
Methyl dicyanoacetate	−2.78	−2.93	235	<200
Hexacyanoheptatriene	−3.55	−3.90	645	347
Cyanoform	−5.13	−5.00	210	<200
Tricyanovinyl alcohol	−5.3	−5.0	295	275
Bis-(tricyanovinyl)-amine	−6.07	−5.98	467	366
Tetracyanopropene	< −8		344	?
Pentacyanopropene	< −8.5	...	395	?
Hexacyanoisobutylene	pK_1 < −8.5	...	370	?
	pK_2 (2.5)[a]	...	336	370

[a] From a crude extrapolation of $-H_0 + \log (C_A/C_{HA})$ and $-H^- + \log (C_A/C_{HA}^-)$ to zero concentration of $HClO_4$ and H_2SO_4. The value given here is preferred to that of reference 2.

(11) Data for picric acid in sulfuric acid in fair agreement with this have been reported; N. C. Deno, H. J. Peterson, and E. Saeber, *J. Phys. Chem.*, **65**, 199 (1961).

the Hammett indicators are linear and present no problem. Because of the different charge types, such plots for anionic bases are not linear and show a minimum characteristic of the mean activity coefficient of a 1–1 electrolyte (see Fig. 5). The pK_a can be determined to a few hundredths of a logarithmic unit by assuming that between the minimum in-(log $C_{H^+} + R$) (~0.2 M acid) and zero concentration, $f_{\pm(H^+,A^-)}$ for the indicator is given by various modified Debye–Hückel equations[12] or that $f_{\pm(H^+,A^-)}$ follows the measured $f_\pm$ of the acid solution itself.[13] The activity coefficient of the neutral form of the indicator should be close to one in the neighborhood of 0.2 M acid.[14] Measurements on picric acid are also shown in Fig. 5, which indicate $pK_a = 0.25$. A value for its pK_a of 0.04 has been reported[15] based on assuming H_- is approaching H_0 in this region. This leads to a small error for the above reasons.

Smoothed values of $H-$ calculated from eq. 2 have been previously reported.[2] The value of pK_a determined in a given acid was used in the calculation of $H-$ in that acid.

3. Hexacyanoisobutylene.—A rough value of pK_a for this dibasic acid was determined by using H_0 or H_- as an extrapolation function. For instance, if

$$-H_0 + \log \frac{C_{A^-}}{C_{HA^-}} = -pK_a + \log \frac{f_B}{f_{BH^+}} \frac{f_{AH^-}}{f_{A^-}} \quad (5)$$

and

$$-H_- + \log \frac{C_{A^-}}{C_{HA^-}} = -pK_a + \log \frac{f_{A^-}}{f_{AH}} \frac{f_{AH^-}}{f_{A^-}} \quad (6)$$

are plotted *vs.* concentration, the intercept at $c = 0$ gives $-pK_a$. The variation in this quantity with concentration is much less than that of the equilibrium quotient. See Fig. 6 and the next section for further discussion.

Discussion

1. Strengths of Cyanocarbon Acids.—The remarkable strength of these acids is due to resonance stabilization in the anion that is not possible in the protonated form. Resonance structures for several of the anions have been discussed before.[8]

Simplified LCAO–MO calculations[16] predict rather large resonance energies for the anions.[17] We wish here only to propose a qualitative criterion for a cyanocarbon being a relatively strong acid, *i.e.*, with $pK_a \sim 0$ or less. If the structure

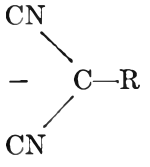

I

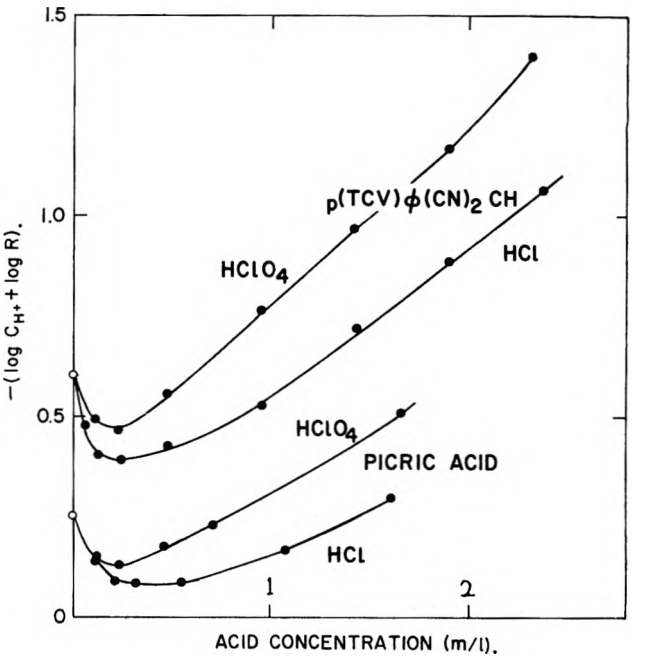

Fig. 5.—Equilibrium quotient (log $C_{H^+}C_{A^-}/C_{HA}$ = log C_H + log R) plotted against acid concentration for *p*-(tricyanovinyl)-phenyldicyanomethane and picric acid in sulfuric and perchloric acids.

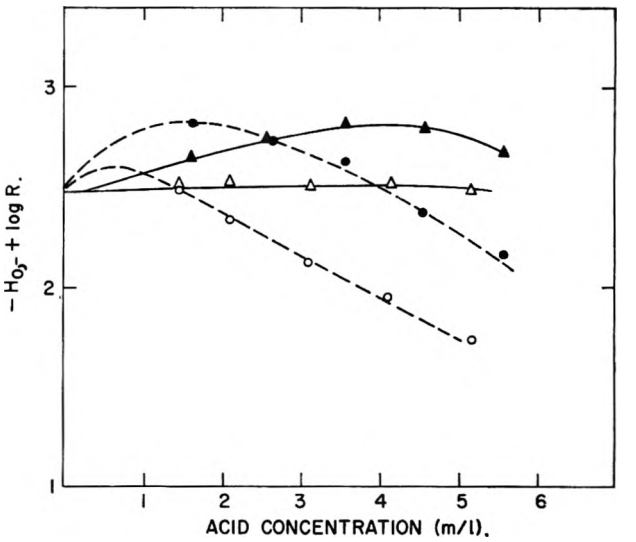

Fig. 6.—Determination of pK_2 of hexacyanoisobutylene by using H_0 and H_- as extrapolation functions. Solid lines (triangles) are $-H_- + \log R$, while the dashed lines (circles) are $-H_0 + \log R$. Open circles and triangles are measurements in $HClO_4$, closed in H_2SO_4.

is present[18] and can resonate through conjugation with with the R group, that is, if the structure

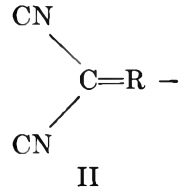

II

(12) See, for instance, R. A. Robinson and R. H. Stokes, "Electrolyte Solutions," Chap. 9, Academic Press, New York, N.Y., 2nd Ed., 1959.

(13) R. A. Robinson and R. H. Stokes, ref. 12, Appendix 8, 10.

(14) F. A. Long and W. F. McDevit, *Chem. Rev.*, **51**, 119 (1952).

(15) J. E. B. Randles and J. M. Tedder, *J. Chem. Soc.*, 1218 (1955).

(16) R. H. Boyd, *J. Phys. Chem.*, **65**, 1834 (1961).

(17) Of the order of 3–5 β when compared to localized bonds in the protonated form, where β is the carbon–carbon resonance integral. The relative order of resonance energies in different anions does not follow the relative order of pK_a. Perhaps allowance for resonance in the protonated forms would improve the correlation.

(18) The relatively great stability of structure I is related to the electronegativity of the cyano group and includes contributions from such structures as

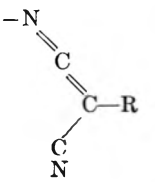

is also a good resonance structure, then the acid will be a relatively strong acid. All of the acids studied here fulfill this criterion. The dicyanomethyl group (I) alone imparts considerable acidity to a hydrogen attached to it but is insufficient to result in a strong acid (see malononitrile in Table III).

The situation where I and II are identical should be particularly favorable. The simplest of such structures, pentacyanopropene, tetracyanopropene, and monoprotonated hexacyanoisobutylene are exceptionally strong acids. For hexacyanoheptatriene the structures are identical, but it is not as strong as the previous three acids. This may well be attributable to greater stability of the protonated form due to conjugated double bonds. In *p*-(tricyanovinyl)-phenyldicyanomethane both forms are like I but are non-equivalent, the quinoid structure may be of relatively high energy, there may also be considerable resonance stabilization in the protonated form, and this acid is not as strong as the others.

Methyl dicyanoacetate and tricyanovinyl alcohol are further examples where structure II is favorable but probably not as much so as I so that they are strong acids but not as strong as pentacyanopropenide. Cyanoform is a special case where structure II reduces to one of three structures with the charge on the cyano group.[18] The effect of cyano groups on acidity in these structures s summarized in Table III.

TABLE III

EFFECT OF CYANO GROUPS ON ACIDITY

Compound	Acidity (pK_a)
CH_4	~58[a]; chemically very inert
CH_3CN	Chemically slightly acidic
$CH_2(CN)_2$	11.19[b]
$CHBr(CN)_2$	~5[b]
$CH(CN)_3$	−5.1
$CH_3CO_2CH_3$	Hydrogens chemically unreactive
$CH_2CNCO_2C_2H_5$	>9[b]
$CHBrCNCO_2C_2H_5$	~6
$CH(CN)_2CO_2CH_3$	−2.9

[a] R. P. Bell (ref. 25). [b] R. G. Pearson and R. L. Dillon, *J. Am. Chem. Soc.*, **75**, 2439 (1953).

2. **Nature of Protonated Species.**—The positions of protonation of several of the cyanocarbon acids are indicated by the spectra. The protonated forms of cyanoform and methyl dicyanoacetate are transparent down to 200 mμ. For the former, this is consistent with protonation on the central carbon as it would be expected to give the spectrum of independent cyano groups which are transparent to 200 mμ. However, Trofimenko[19a] has prepared solid dicyanoketenimine (the nitrogen protonated form of cyanoform). Its ultraviolet spectrum is unknown so that we cannot say which is the stable form in aqueous solution.[19b] Methyl dicyanoacetate appears to protonate on the α-carbon rather than on the carbonyl oxygen, since cyano groups and the ester group are transparent to 200 mμ. The presence of a dicyanovinyl group in an oxygen protonated form would be expected to have an ultraviolet absorption above 200 mμ.[20]

Tricyanovinyl alcohol protonates on the oxygen as evidenced by the similarity of the protonated form and the anion.

p-(Tricyanovinyl)-phenyldicyanomethane probably protonates on the methyl carbon since the quinoid structure resulting from protonation on the tricyanovinyl group carbon would probably be less stable. Also, the ultraviolet spectrum is similar to phenyltricyanoethylene[21] (λ_{max} 332 mμ, ϵ 15.3 × 10^3 (aqueous acid) *vs.* λ_{max} 343 mμ, ϵ 16.6 × 10^3 (chloroform); whereas 7,7-8,8-tetracyanoquinodimethane has λ_{max} 395, ϵ 63,600.[22] A terminal skeletal carbon atom is probably the site of protonation in hexacyanoheptatriene since three conjugated skeletal double bonds would probably be required to give absorption at as long wave length as that found experimentally (λ_{max} 347 mμ). Bis-(tricyanovinyl)-amine has the possibility of protonation on either a terminal skeletal carbon or the amine nitrogen. We are unable to decide from the spectrum which possibility occurs.

The structure of hexacyanoisobutylene suggests that the first protonation takes place on a methyl carbon of a dicyanomethyl group. The ultraviolet spectrum is consistent with this, since it would be expected to resemble those of the tetra- and pentacyanopropenide anions (see Table II and Fig. 2) which it does.

It has been assumed in all the foregoing discussion that the cyanocarbons are protonated only once to a neutral species. It is appropriate to digress here for a discussion of this assumption. The abundance of cyano groups presents the possibility of further protonation on nitrogen. However, the cyano group is known to be very weakly basic and such protonation seems unlikely. In fact, simple nitriles are only partially protonated even in 100% sulfuric acid.[23] The acid-catalyzed hydrolysis of nitriles probably involves protonation of the nitrogen as the first step. In our work, the onset of hydrolysis limits the usable concentration range (< 80–85% sulfuric acid). However, since the rate of hydrolysis, when it first becomes noticeable, is a rapidly increasing function of acid concentration, the relative number of protonated cyano groups is probably extremely small over the acid concentration range where measurements were made. More direct evidence comes from the spectra themselves. For *p*-(tricyanovinyl)-phenyldicyanomethane the protonated form can be measured with sufficient accuracy to show that the protonation equilibrium involves only two spectral species all the way up to ~10 *M* acid concentration. Thus, if multiple protonation takes place it would have to do so in a single step. This is clearly not the case for *p*-(tricyanovinyl)-phenyldicyanomethane as may be inferred from Fig. 4 (and also potentiometric titration). Hexacyanoheptatriene and bis-(tricyanovinyl)-amine also show the presence of only two species from their spectra (unless, of course, the multiply protonated species has the same spectrum as the neutral species, which seems unlikely).

3. **H_- Acidity Function.**—H_- and H_0 are plotted against molarity for sulfuric and perchloric acids in Fig. 7 (these functions have previously been presented in tabular form[1]). Below about 5 *M*, H_- shows be-

(19) (a) S. Trofimenko, private communication. (b) Several known ketenimines absorb in the 220–240 mμ region (G. Dijkstra and H. J. Backer, *Rec. trav. chim.*, **73**, 575 (1954)). We are indebted to Dr. B. C. McKusick of this Laboratory for pointing this out.

(20) C. E. Looney and J. R. Downing, *J. Am. Chem. Soc.*, **80**, 284 (1958).

(21) G. N. Sausen, V. A. Engelhardt, and W. J. Middleton, *ibid.*, **80**, 2815 (1958).

(22) D. S. Acker, R. J. Harder, W. R. Hertler, W. Mahler, L. R. Melby, R. E. Benson, and W. E. Mochel, *ibid.*, **82**, 6408 (1960).

(23) M. Liler and Dj. Kosanovic, *J. Chem. Soc.*, 1084 (1958).

havior compared to H_0 that might be expected on the basis of the charge types involved. The difference between H_- and H_0 is given by

$$(-H_-) - (-H_0) = \log \frac{f_{BH^+} f_{A^-}}{f_B f_{HA}} \qquad (7)$$

This difference is also plotted in Fig. 7.

The variation of neutral molecule activity coefficients (f_B, f_{HA}) with acid concentration is probably relatively modest.[14] They perhaps increase from one as the acid concentration increases and then decrease again in very concentrated solution (above 5 M). The total variation in log f is probably only several tenths.

The observed difference (Fig. 7) is typical of log $f_\pm$ variation with ionic strength up to about 5 M; that is, decreasing to a minimum and then increasing. Above 5 M there does not seem to be appropriate data available on activity coefficients of dilute salts in concentrated acids for comparison. It is tempting to suppose that f_{A^-}/f_{BH^+} and f_B/f_{BH^+} become nearly constant, the rapid increase of either acidity function along being largely due to the hydrogen ion. This increase, in turn, is related to its hydration and the availability of water as discussed by Bell and Bascombe[24,25] and by Wyatt.[26] If this is so, then the reason for the quite different behavior of an acidity function such as J_0,[3] *i.e.*, for

$$ROH + H^+ = R^+ + H_2O$$

$$J_0 \equiv pK_{a\,ROH} - \log \frac{C_{R^+}}{C_{ROH}} \qquad (8)$$

remains obscure. Further studies on the behavior of activity coefficients of appropriate indicator molecules in acid solution are clearly called for.

4. Hexacyanoisobutylene.—The second ionization of this acid is remarkably strong. Its pK_a of ~ -2.5 compares to 2.0 for sulfuric acid. This extreme ease of ionization to $A^=$ is the result of the great resonance stabilization of the anion and the extent of charge delocalization over such a large molecule.

The spectra of the two forms $A^=$ and HA^- are interesting in that the singly protonated form absorbs at longer wave length than the free anion. This is in contrast, of course, to the monovalent cyanocarbon acids, but is consistent with the predictions of simple Hückel M. O. theory[27] and also the discussion of Looney and Downing.[20]

The correlation of the species concentrations $A^=$ and HA^- with H_0 or H_- (see Fig. 6) is interesting. From eq. 5, in less concentrated solutions we would expect f_{BH^+} and f_{HA^-} to cancel approximately and the variation of f_B to be small so that f_{A^-} would be the major influence on the variation of the left hand side of eq. 5 with concentration. Furthermore, f_{A^-} probably decreases with increasing concentration passes through a minimum and then increases. Therefore, the left hand side of eq. 5 would be increasing and then decreasing with increasing concentration. In Fig. 6 it is seen that only the region of decrease is observed experimentally, but a maximum in the curve is inferred by comparison with the H_- extrapolation. From eq. 6 it is seen that the major contribution to the variation of $-H_- + \log (C_{A^-}/C_{HA^-})$ with concentration would be $f_{A^-} f_{HA^-}/f_{A^-}$. The charge effect should partially cancel and the left hand side of (6) should probably vary less than that in (5). Figure 6 bears this out. Over-all, then, this protonation appears to correlate in the expected manner with H_0 and H_-. Thus, it appears further confirmed that even drastic changes in the charge type of the base while presenting quantitative differences results in rather similar protonation behavior in acid solutions.

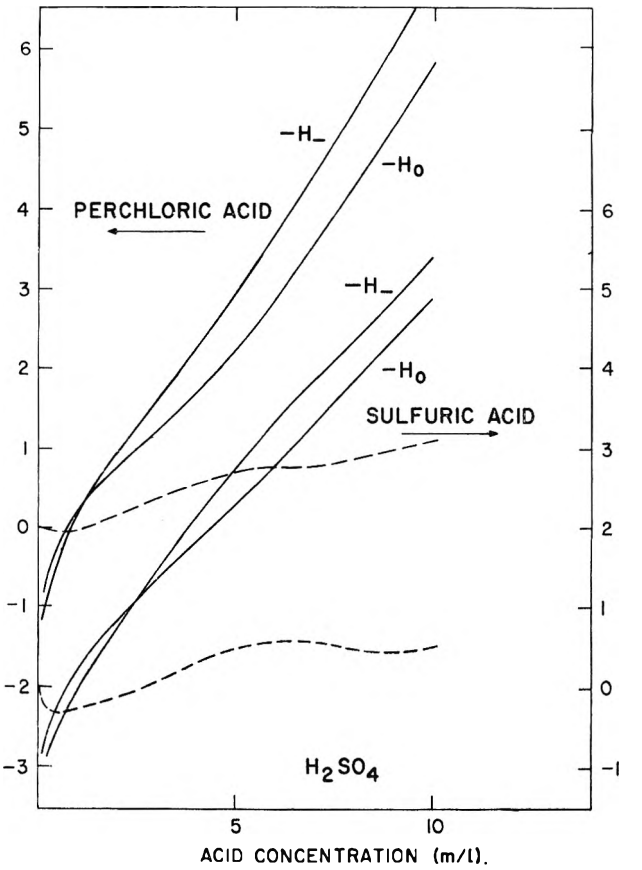

Fig. 7.—H_0 and H_- acidity functions plotted against acid concentration. For perchloric acid, the scale is on left and for sulfuric acid the scale is on the right. Dashed curves are the differences $(-H_-) - (-H_0)$ for the two acids.

5. Cyanocarbon Acid Hydrates.—Dihydrates of pentacyanopropene and bis-(tricyanovinyl)-amine have previously been reported.[8] In addition, cyanoform, tricyanovinyl alcohol, and methyl dicyanoacetate also were found to form dihydrates. These are relatively unstable and upon further dehydration decompose apparently by some kind of addition or polymerization. The characteristic intense anion absorption was found in the ultraviolet visible spectra of pentacyanopropene and bis-(tricyanovinyl)-amine solid dihydrates showing that they are ionized in the solid state. This is consistent with the behavior of other acid hydrates. Nitric acid, which is much weaker (pK_a = −1.6), is ionized in the solid hydrate.[28] The weakest of the cyanocarbon acids studied here, *p*-(tricyanovinyl)-phenyldicyanomethane appears to be un-ionized in the solid and undergoes a striking change from a white solid to an intense blue color upon solution.

(24) R. P. Bell and K. N. Bascombe, *Discussions Faraday Soc.*, **34**, 158 (1957).

(25) R. P. Bell, "The Proton in Chemistry," Cornell University Press, Ithaca, N. Y., 1959, Chap. VI.

(26) P. A. H. Wyatt, *Discussions Faraday Soc.*, **34**, 162 (1957).

(27) We are indebted to Dr. R. E. Merrifield of this Laboratory for pointing this out.

(28) Reference 25, Chapter III.

Hexacyanoisobutylene forms a solid hydrate corresponding to 5 or 6 molecules of water. The ultraviolet spectrum of this hydrate also showed the characteristic anion absorption indicating that it is completely ionized in the solid state.

6. Solutions of Cyanocarbon Salts in Anhydrous Acid Solutions.—Sodium salts of pentacyanopropene are soluble in a number of organic solvents and permit some interesting observations with anhydrous acid solutions. The sodium salt of pentacyanopropene when dissolved in an anhydrous solution of hydrochloric acid or *p*-toluenesulfonic acid in tetrahydrofuran (THF) will not precipitate sodium chloride or sodium *p*-toluenesulfonate. The latter are insoluble in this solvent. Furthermore, an equimolar mixture of hydrochloric acid and sodium pentacyanopropenide in THF will precipitate sodium chloride when an equivalent amount of water is injected into it. However, none is precipitated when several equivalent amounts of methanol are added. One interpretation is that the acids exist in this solvent in un-ionized forms which do not ionize at a fast enough rate to allow the precipitation. Addition of water results in hydronium ion–anion ion pair formation which will exchange ions with the sodium pentacyanopropenide ion pair and results in precipitation. Methanol apparently under these conditions is a weaker base than water and does not result in ionization of the acid.

Acknowledgments.—The author is greatly indebted to several colleagues in this Laboratory, especially Drs. E. L. Little, J. K. Williams, D. W. Wiley, and S. Trofimenko, for suggesting particular cyanocarbon acids and for preparing samples. He is also grateful to Professor C. Gardner Swain of the Massachusetts Institute of Technology for his encouragement.

THE EQUILIBRIUM CONTROLLED REDUCTION OF URANIUM CHLORIDE BY MOLTEN ALUMINUM IN A FUSED SALT SOLVENT

By R. H. Moore,[1] J. R. Morrey,[1] and E. E. Voiland[1]

Heavy Element Chemistry, Hanford Atomic Products Operation, General Electric Co., Richland, Washington

Received June 12, 1962

In connection with studies of fuel element processing, it has been found that reduction of UCl_3 by Al from solutions in molten $AlCl_3$–KCl mixtures is an equilibrium controlled reaction dependent upon the $AlCl_3$/KCl ratio. Uranium reduction is a maximum at an $AlCl_3$/KCl ratio of about unity. A simple model is proposed to explain this behavior which permits satisfactory interpretation of the reaction mechanism in terms of chloride ion concentration and complex ion formation. It is concluded that activity coefficients are constant over the range of variables studied and, very probably, in the salt phase are unity, if the species can be defined.

Introduction

Molten potassium chloride–aluminum chloride mixtures are interesting solvents for study of reactions involving reduction of solute metal chlorides by molten aluminum. The reactions occur in an almost completely immiscible two-phase system, *e.g.*

$$MCl_3 + Al \rightleftharpoons M + AlCl_3 \quad (1)$$

(Salt phase) (Metal phase) (Metal phase) (Salt phase)

It is of interest that constituents from each of these solvent phases play an active role in the reaction.

It was observed that the actinide elements distributed themselves between the two phases. UCl_3, for example, underwent appreciable reduction although the standard free energy change for the reaction was calculated to be 40 ± 6.0 kcal./mole at 1000°K.[2] The extent of reduction despite the large positive ΔF_0 for the reaction suggested that this system was highly non-ideal and merited detailed study. The effects of composition and temperature changes on the equilibrium distribution of uranium between the salt and metal phases are reported here.

Experimental

In general the procedure for studying this equilibrium was to combine the reactants at the desired temperature for a time sufficient to ensure attainment of equilibrium, quench to halt the reaction and freeze the equilibrium, separate the phases mechanically, and analyze samples for the constituents of interest. For most of this work the materials were equilibrated in evacuated Vycor ampoules. The constituents: vacuum-melted potassium chloride, vacuum-resublimed aluminum chloride, uranium metal of 99.9% purity, and aluminum metal of 99.99% purity were handled and weighed in a drybox containing an argon atmosphere (zirconium gettered). After being filled, the ampoules were evacuated, sealed off, and the contents cautiously warmed with a small flame until the aluminum chloride and potassium chloride had reacted. (During this step, since the temperature is below the melting point of aluminum, most of the uranium metal reacts to form UCl_3). When it was desired to approach the equilibrium from the other direction, a uranium–aluminum alloy was substituted for the elemental constituents. The ampoules were equilibrated in a horizontal tube furnace which was rocked gently to continuously agitate the contents. After 60 min. at a constant reaction temperature, the samples were quenched, the bulbs broken, and samples taken for chemical analysis.

A slight variation in procedure was employed in measurements at temperatures above 725°. Vycor bulbs containing a graphite liner were used to eliminate side reactions resulting from corrosion of the Vycor bulb by the metal phase. These were essentially static equilibrations. This variation completely eliminated corrosion effects which were of concern at higher temperatures.

At 725° at which most of this work was done, the metal phase was only 35–40° above its freezing point. Upon immersing the tube or ampoule in water, no more than a few seconds elapsed before the metal phase froze. This appeared to completely arrest the reaction. Solidification of the salt phase followed within 30–40 sec.

In all cases a salt to metal phase weight ratio of approximately two to one was maintained. The metal phase ranged in weight from 6 to 10 g.

Results and Discussion

The results of measurements of the distribution of uranium between the salt and metal phases, at 725°, are shown in the second column of Table I. The

(1) General Electric Company, Richland, Washington. Work performed under Contract No. AT(45-1)-1350 for the U.S. Atomic Energy Commission.

(2) J. R. Morrey and R. H. Moore, *J. Phys. Chem.*, **66**, 748 (1963).

TABLE I

DISTRIBUTION DATA AND CALCULATED EQUILIBRIUM CONSTANTS ($AlCl_3/KCl < 1$)

$AlCl_3/KCl$	D (exptl.)	K_5' (React. 5)	K_6' (React. 6)	K_7' (React. 7)
0.39	0.14	0.0025	0.008	0.03
.48	.22	.0035	.013	.05
.59	.36	.0044	.022	.11
.69	.68	.0057	.037	.24
.79	1.23	.0054	.051	.49
.90	4.0	.0045	.090	1.80
.95	6.8	.0020	.081	3.20
1.0	10.2			5.1
Mean value		0.0040 ± 0.0011	0.043 ± 0.027	1.4 ± 1.5
		0.0047 ± 0.0006[a]		

[a] Excludes first and last values.

distribution coefficient, D, is defined simply as

$$D = \frac{(X_U)_m}{(X_U)_s} \qquad (2)$$

where $(X_U)_m$ and $(X_U)_s$ are the concentrations of uranium in the metal and salt phases, respectively, in mole fraction units. The data in Tables I and II illustrate the dependence of D on the mole ratio, Al/K, of aluminum and potassium in the salt phase.

TABLE II

DISTRIBUTION DATA AND CALCULATED EQUILIBRIUM CONSTANTS ($AlCl_3/KCl > 1$)

$AlCl_3/KCl$	D (exptl.)	K_8'
1.05	3.8	0.20
1.10	3.3	.37
1.18	0.7	.15
1.20	0.7	.17
1.29	1.05	.43
1.48	0.32	.30
1.66	.28	.54
1.70	.27	.63
1.87	.13	.86
1.90	.23	2.1
Mean value		0.35 ± 0.14[a]

[a] Excludes last two data.

Equation 1 is an oversimplification of this system, since it does not take into account the presence of KCl which, the data show, is obviously important. It is instructive, however, to explore the relationship between D and the equilibrium constant for reaction 1, K, where

$$K = \frac{a_U a_{AlCl_3}}{a_{UCl_3} a_{Al}} = \frac{X_U X_{AlCl_3}}{X_{UCl_3} X_{Al}} \cdot \frac{f_U f_{AlCl_3}}{f_{UCl_3} f_{Al}} \qquad (3)$$

In eq. 3, the a's are activities, the X's indicate mole fractions, and the f's are activity coefficients. In this work, X_U was always low, < 0.025 mole fraction. The activity of aluminum may therefore be approximated as unity if pure aluminum is chosen as the standard state. As a result of this choice, the activity coefficient for uranium will approach a limiting value, f_U^0, consistent with Henry's law. Since this is closely approached, eq. 3 reduces to

$$K' = DX_{AlCl_3} \frac{f_{AlCl_3}}{f_{UCl_3}} \qquad (4)$$

Equation 4 reveals that deviations from ideal behavior occur primarily as a result of the concentration dependence of the activity coefficients of $AlCl_3$ and UCl_3.

Whenever it is necessary to consider large deviations from unity in the values of activity coefficients, it is pertinent to consider the possibility of complex ion formation. In the presence of the chloride ion donor, KCl, variations in f_{AlCl_3} and f_{UCl_3} (eq. 4) may, in fact, result from formation of ions such as $Al_2Cl_7^-$ and $AlCl_4^-$, in the case of $AlCl_3$, and UCl_6^{-3}, UCl_5^{-2}, and UCl_4^- in the case of UCl_3.[3]

With the assumption of complex ion formation, equation 1 is no longer appropriate. In the region where there is an excess of chloride ion, *i.e.*, where $R = Al/K < 1.0$, equation 1 becomes

$$UCl_6^{-3} + Al \rightleftarrows AlCl_4^- + U + 2Cl^- \qquad (5)$$

$$\text{or } UCl_5^{-2} + Al \rightleftarrows AlCl_4^- + U + Cl^- \qquad (6)$$

$$\text{or } UCl_4^- + Al \rightleftarrows AlCl_4^- + U \qquad (7)$$

In a region where the system is deficient in chloride ion, there will be a competition between $AlCl_3$ and UCl_3 for the available chloride ion. If it is postulated that the complexes of $AlCl_3$ are formed preferentially, eq. 1 becomes

$$AlCl_4^- + UCl_3 + Al \rightleftarrows U + Al_2Cl_7^- \qquad (8)$$

Reactions 5 through 8 contain species which are indeterminate from these experiments. Only the cations have been determined by chemical analysis. Thus it is not possible to distinguish $AlCl_3$ from $AlCl_4^-$ or UCl_3 from UCl_6^{-3}, etc. However, in both of the above cases, *i.e.*, for Al/K being either greater or less than one, the number of ions in the salt phase (neglecting the uranium) is twice the number of KCl molecules. Thus, in equilibrium considerations mole fractions have been calculated on the basis of a total salt composition equal to twice the number of moles of KCl initially added.

The equilibrium constant for reaction 5 can be written

$$K_5' = \frac{X_{AlCl_4^-} X_U X^2_{Cl^-}}{X_{UCl_6^{-3}} X_{Al}} \qquad (9)$$

where the X's are mole fractions and activity coefficients are unity or constant. Assuming all the uranium in the salt phase is present as UCl_6^{-3} leads to

$$K_5' = D \frac{X_{AlCl_4^-} X^2_{Cl^-}}{X_{Al}} \qquad (10)$$

where D has the same significance as in eq. 2. As the mole fraction of Al is greater than 0.99 in all experiments, it may be considered unity, and

$$K_5' = DX_{AlCl_4^-} X^2_{Cl^-} \qquad (11)$$

The prime emphasizes that the constant is not the thermodynamic equilibrium constant, but is related to it by a constant factor.

The values for $X_{AlCl_4^-}$ and X_{Cl^-} can be determined from R and the assumption previously made for defining mole fractions. In this system essentially all the $AlCl_3$ will be converted to $AlCl_4^-$, hence to a very close approximation

(3) Because of a coördination number of six, the uranium ions may be solvated.

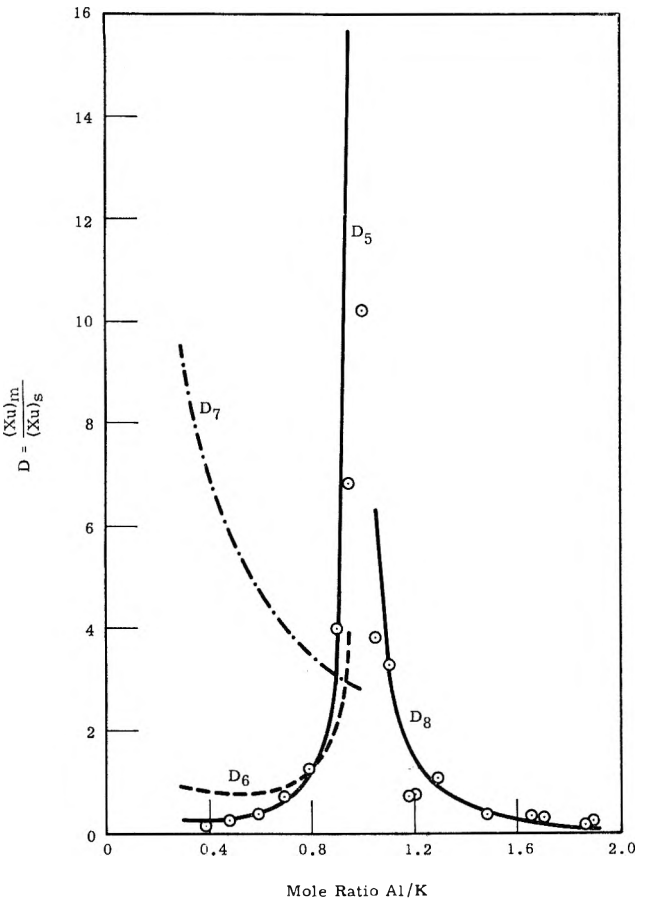

Fig. 1.—Comparison of observed and calculated distribution coefficients.

$$AlCl_4^- = AlCl_3^0$$

and

$$Cl^- = KCl^0 - AlCl_3^0$$

R can be closely approximated from the initial quantities of KCl (KCl^0) and $AlCl_3$ ($AlCl_3^0$), the latter corrected for partial reaction with U metal. Thus

$$R = \frac{AlCl_3^0}{KCl^0}$$

$$X_{AlCl_4^-} = \frac{R}{2} \qquad (12)$$

and

$$X_{Cl^-} = \frac{1 - R}{2} \qquad (13)$$

Equation 12 is valid for values of R of unity and less since the ratio $AlCl_4^-/AlCl_3$ is always large over this range. On the other hand, it is evident that eq. 13 fails when $R = 1$ since X_{Cl^-} becomes zero. Where X_{Cl^-} has finite values, *i.e.*, where $R < 1.0$, eq. 13 may be expected to hold.

Substituting from (12) and (13) into (11)

$$K_5' = \frac{D}{8} \times R(1 - R)^2 \qquad (14)$$

and

$$D_5 = \frac{8K_5'}{R(1 - R)^2} \qquad (14a)$$

where D_5 is the calculated distribution coefficient. Equation 14 permits evaluation of the equilibrium constant for reaction 5, the results appearing in Table I for the range $R = 0.39$ to $R = 0.95$. The values of K_5' are relatively constant.

In similar fashion, the expressions for the equilibrium constants for reactions 6 and 7 were derived as functions of R

$$K_6' = D\frac{R(1 - R)}{4} \qquad (15)$$

$$K_7' = D\frac{R}{2} \qquad (16)$$

The values for K_6' and K_7' also are shown in Table I and it can readily be seen that in both cases the values are not constant but increase with increasing R; particularly is this so for K_7'. The data of Table I therefore suggest that reaction 5 is the correct reaction to describe the equilibrium in this system when the $AlCl_3$/KCl ratio is less than unity.

Using as the value of K_5', 0.0047, values for the distribution coefficient were calculated from eq. 14a for the range $R = 0.3$ to $R = 0.95$. These values are plotted in Fig. 1, as the solid line. Similarly D_6 and D_7, the calculated distribution coefficients corresponding to the average values of K_6' and K_7' also were determined and are plotted in Fig. 1 as dashed and dotted curves, respectively. Although D_6 varies with R in superficially the same way as D_5, the correspondence with the experimental data is not nearly as good. Since D_6 is directly proportional to K_6', no change in the curvature of the D_6 *vs.* R plot can be accomplished by varying K_6' as this will only shift the curve relative to the ordinate by a constant factor. Quite obviously the distribution coefficients calculated on the basis of reaction 7 do not agree at all with the experimental data, thus ruling out the existence of UCl_4^- under these conditions.

On the $AlCl_3$-rich side of Fig. 1, $R > 1.0$, and the system is deficient in chloride ion. If it is assumed that $AlCl_3$ is complexed more extensively than UCl_3, then equation 8 applies. Here

$$K_8' = \frac{X_U X_{Al_2Cl_7^-}}{X_{AlCl_4^-} X_{UCl_3} X_{Al}} \qquad (17)$$

and

$$K_8' = D\frac{X_{Al_2Cl_7^-}}{X_{AlCl_4^-}} \qquad (18)$$

In the concentration range defined by $1 < R < 2$, it is assumed that $AlCl_3$ in excess of the stoichiometric ratio to form $KAlCl_4$ forms $Al_2Cl_7^-$. Thus, in a system prepared from R moles of $AlCl_3$ and one gram-ion of chloride, $AlCl_4^-$ and $Al_2Cl_7^-$ will form according to the equation

$$R\,AlCl_3 + Cl^- = (R - 1)\,Al_2Cl_7^- + (2 - R)\,AlCl_4^- \qquad (19)$$

and

$$\frac{X_{Al_2Cl_7^-}}{X_{AlCl_4^-}} = \frac{(R - 1)}{(2 - R)} \qquad (20)$$

Substituting into eq. 18 results in

$$K_8' = D\frac{(R-1)}{(2-R)} \qquad (21)$$

and

$$D_8 = K_8'\frac{(2-R)}{(R-1)} \qquad (22)$$

The equilibrium constants calculated from eq. 21 are shown in Table II. The values are reasonably constant with the exception of those at high values of R. Omitting values at $R = 1.87$ and $R = 1.90$, where dissociation of the species $Al_2Cl_7^-$ into $AlCl_3$ and Cl^- may be causing the deviation, an average $K_8' = 0.35$ results. D_8 calculated for the range $R = 1.05$–1.90 is plotted in Fig. 1 as the solid curve. The agreement with experimental values (open circles) is shown to be excellent. It should be remarked that eq. 21 is not valid for $R = 1$ or $R = 2$, since the assumptions underlying eq. 19 do not provide for the presence of equilibrium concentrations of $Al_2Cl_7^-$ or $AlCl_4^-$, respectively, at these values. However, it is believed that the expression is valid over quite a large range between $R = 1$ and $R = 2$.

In summary, the system has been divided into KCl-rich and KCl-deficient regions. In the former, eq. 5 has been shown to yield the best fit with the experimental data. The assumption of the UCl_6^{-3} species is supported by observations of the spectra of these molten salts.[2] Further, the postulate of the $AlCl_4^-$ species is supported by calculations of Kryagova[4] and by X-ray studies of Baenziger.[5]

On moving to the $AlCl_3$-rich region the absorption spectrum, typical of UCl_6^{-3} is no longer observed.[2] This is consistent with the postulate of a changed reaction mechanism, *i.e.*, reaction 8.

No data are available for the region of Al/K mole ratios > 2.0. Extension of the theory outlined here leads to the prediction that the extent of UCl_3 reduction will fall sharply as the activity of $AlCl_3$ increases beyond $R = 2$. Unfortunately, the most interesting region (around $R = 1$) is the most difficult to study. Since D rises so rapidly as R approaches unity (essentially as $1/(1-R)^2$ on the KCl-rich side and as $1/(R-1)$ for the $AlCl_3$-rich system), R must be determined with great precision for the plot to be meaningful. In this study, the precision of R was ± 0.03 hence great uncertainty exists for the points around $R = 1$.

Measurements as a Function of Temperature.—The results of measurements at temperatures above 725° are shown in Table III. These data show that the reaction is essentially temperature independent until a temperature of 905° is attained. At this temperature, it was found that recoveries of aluminum as metal (alloy) tended to be low, whereas recoveries of aluminum in the salt phase were correspondingly high. This effect is attributed to the onset of the reaction

$$AlCl_3 + 2Al \xrightarrow{905°} 3AlCl \qquad (23)$$

TABLE III

THE TEMPERATURE DEPENDENCE OF REACTION 5

Al recovery, %	U recovery, %	KCl recovery, %	$AlCl_3$ recovery, %	Final Al/K	Uranium distribution, D	Temp., °C.
...	...	...	...	0.73	1.02[a]	725
99.1	101.7	98.5	103.0	.73	1.19	775
99.0	100.5	99.0	102.0	.72	0.91	825
99.3	100.6	95.6	97.9	.72	1.14	825
99.3	101.0	96.2	100.1	.73	0.84	875
98.3	97.8	97.9	101.3	.73	1.28	875
89.6	96.4	95.6	143.6	1.05	0.63	905
94.2	99.1	97.3	105.2	0.76	0.75	905

[a] From data in Fig. 1.

Upon quenching, the AlCl formed as a result of the above reaction disproportionated, *i.e.*, reaction 23 reverses. The finely divided aluminum produced did not have time to coalesce and re-enter the bulk metal phase. This aluminum was consequently analyzed as part of the salt phase and was counted as $AlCl_3$. An apparent high Al/K mole ratio resulted. The actual effect of reaction 23, however, was to consume $AlCl_3$, lowering the Al/K mole ratio, with resulting reduction in D.

Conclusions

By the simple expedient of changing the Al/K mole ratio, marked changes in the extent of reduction of uranium chloride by aluminum have been demonstrated.

The simple treatment presented in this paper provides an explanation for the experimental data which is based on the assumption that changes in the activities of reactants in the salt phase can be accounted for largely by formation of complex ion species. The corollary is that the activity coefficients of the species are either unity or constant.

Acknowledgments.—The authors wish to express their appreciation to Mr. Wayne L. Delvin of the Analytical Laboratories Operation for his invaluable assistance in this work.

(4) I. A. I. Kryagova, *Zh. Priklad. Khim.*, **21**, 561 (1948).
(5) N. C. Baenziger, *Acta Cryst.*, **4**, 216 (1951).

THERMODYNAMIC EVIDENCE FOR COMPLEX FORMATION BY ACTINIDE ELEMENTS IN FUSED KCl–$AlCl_3$ SOLVENTS[1]

BY J. R. MORREY AND R. H. MOORE

Hanford Laboratories, General Electric Company, Richland, Washington

Received June 12, 1962

Previously reported experimental measurements of the equilibrium $UCl_3(l) + Al(l) \rightleftarrows {}^1/_2\ Al_2Cl_6\ (l)$, which was carried out in the solvent KCl–$AlCl_3$, have been explained by a model involving the complex ions $Al_2Cl_7^-$, $AlCl_4^-$, and UCl_6^{-3}. Calculations made by a high speed computer have proven the sufficiency of the model and have provided the appropriate formation constants. Models involving anionic complexes other than $UCl_6^{=}$ were rejected because they could not adequately reproduce the data. Analysis of less complete data for the reduction of thorium, protactinium, neptunium and plutonium chlorides shows that a model involving the same aluminum species and complex actinide species describes the experimental results.

Introduction

A perusal of the literature on the thermodynamics and structure of fused-salt systems reveals two rather remarkable generalizations: (1) the majority of systems studied behave either ideally, provided the species are correctly designated, or obey Henry's law[2,3]; (2) stable complex ions are frequently formed.[2,4] In this Laboratory it has been shown spectrophotometrically that both U(III) and U(IV) form different complexes in different fused media[5]; complex formation is markedly dependent on the solvent. For example, the tendency of U(IV) to complex in CsCl–$CsAlCl_4$ or KCl–$KAlCl_4$ is appreciably greater than in pure molten CsCl. Furthermore, the tendency to complex in CsCl is greater than in KCl and still greater than in NaCl. Although the species most prevalent in NaCl cannot yet be characterized, general considerations suggest that it is UCl_4, whereas that most prevalent in CsCl is UCl_6^{-2}. Complex formation by U(IV) and U(III) follow the same trends although U(IV) complexes more effectively than does U(III). Both oxidation states show remarkable spectral changes in KCl–$AlCl_3$ as the potassium chloride to aluminum chloride mole ratio is varied near the ratio [K]/[Al] = 1. Spectrophotometric observations in pure molten alkali halides are consistent with e.m.f. data for U(III) in fused LiCl–KCl and NaCl–KCl solvents.[6] When combined with other data,[7] e.m.f. measurements predict only a small negative free energy change which can be attributed to complexing, *viz.*

$$\text{solvent} + UCl_3(l)\ \text{pure} \xrightarrow{450^\circ} UCl_3 \left[\begin{array}{c} X = 1\ \text{in} \\ \text{LiCl–KCl} \\ \text{or} \\ \text{NaCl–KCl} \end{array}\right];$$

$$\Delta F^0 = -4.9 \pm 1.5\ \text{kcal.}$$

This equation represents the partial molar free energy of mixing to a hypothetical standard state where the solution contains a unit mole fraction of the salt, but in all other respects exhibits the thermodynamic properties of an ideal dilute solution of the complexed uranium.[8]

This paper presents thermodynamic evidence of strong complex formation by U(III) in KCl–$AlCl_3$ where the mole ratio [K]/[Al] is greater than unity, thereby drawing attention to the fact that large differences in chloride "activities" in LiCl–KCl and KCl–$AlCl_3$ solvents exist. The experimental data and procedure have been reported previously.[9] This is an attempt to provide further theoretical significance to these data, to ascertain the associated thermodynamic constants, and to provide evidence for the existence of strong complexes in KCl–$AlCl_3$.

Discussion

Uranium.—Careful evaluation of the free energies of formation of liquid aluminum chloride and uranium chloride using the data summarized in Table I, in accordance with standard thermodynamic procedure, shows that the equilibrium in reaction 1 should lie far to the left at 1000°K.

$$UCl_3(l) + Al(l) \rightleftarrows {}^1/_2Al_2Cl_6(l) + U(l);\ \Delta F_{1000}{}^0 = +41.2 \pm 3.1\ \text{kcal.} \quad (1)$$

However, in the presence of molten potassium chloride, appreciable reduction of uranium occurs, the extent of which depends on the potassium chloride to aluminum chloride mole ratio. Furthermore, in regions where [K]/[Al] approaches unity the reduction of uranium approaches a maximum.

The fact that these experiments could be carried out in sealed ampules without bursting the container provides sufficient proof that an exceedingly stable complex of aluminum chloride with potassium chloride is formed upon fusion. The additional fact that the vapor pressure of aluminum chloride was not sufficient to burst the bulb, even when [K]/[Al] was less than unity, requires that more than one mole of aluminum chloride ($AlCl_3$) be stabilized by one mole of chloride

(1) Work performed under Contract No. AT(45-1)-1350 for the U. S. Atomic Energy Commission.

(2) S. Senderoff, G. W. Mellors, and R. I. Bretz, *J. Electrochem. Soc.*, **108**, 93 (1961).

(3) M. S. Zakharevskiĭ and T. V. Permyakova, *Zh. Obshcheĭ Khim.*, **26**, 2947 (1956); S. N. Flengas and T. R. Ingraham, *Can. J. Chem.*, **36**, 1662 (1958); H. A. Laitinen and C. H. Liu, *J. Am. Chem. Soc.*, **80**, 1015 (1958).

(4) D. M. Gruen and R. L. McBeth, *J. Inorg. Nucl. Chem.*, **9**, 290 (1959); *J. Phys. Chem.*, **63**, 393 (1959); L. A. Tsiovkina and M. V. Smirnov, *Zh. Neorgan. Khim.*, **4**, 158 (1959); B. R. Sundheim and G. Harrington, *J. Chem. Phys.*, **31**, 700 (1959); C. M. Cook, Jr., *J. Am. Chem. Soc.*, **81**, 535 (1959); G. Harrington, *Dissertation Abstr.*, **20**, 114 (1959).

(5) J. R. Morrey, *Inorg. Chem.*, 2, 163 (1963).

(6) D. M. Gruen and R. A. Osteryoung, *Ann. N. Y. Acad. Sci.*, **79**, 897 (1960); D. Inman, G. J. Hills, L. Young, and J. O'M. Bockris, *Trans. Faraday Soc.*, **55**, 1904 (1959); *Ann. N. Y. Acad. Sci.*, **79**, 803 (1960); D. Inman and J. O'M. Bockris, *Can. J. Chem.*, **39**, 1161 (1961); B. A. Partridge, *J. Inorg. Nucl. Chem.*, **19**, 379 (1961); S. N. Flengas, *Can. J. Chem.*, **39**, 773 (1961).

(7) W. Hamer, M. Malmberg, and B. Rubin, *J. Electrochem. Soc.*, **103**, 8 (1956); see also Table I.

(8) Some previous authors have neglected to separate the free energy of melting of UCl_3 at 450° from that attributed to complex formation in making calculations of the type indicated above. This led to the conclusion that uranium trichloride does not complex. However, when melting is taken into account, this conclusion no longer holds. The result presented above is an average calculated from data by Gruen and Osteryoung; Inman, Hills, *et al.*; Inman and Bockris; and Flengas.

(9) R. H. Moore, J. R. Morrey, and E. E. Voiland, *J. Phys. Chem.*, **67**, 744 (1963).

TABLE I

THERMODYNAMIC DATA USED IN THE CALCULATION OF $\Delta F^0_{1000°K}$ FOR $UCl_3(l) + Al(l) \rightarrow {}^1/_2\ Al_2Cl_6(l) + U(l)$

	Al	U	Al_2Cl_6	UCl_3
$\Delta H_{f,298}$ (s), kcal./mole	0	0	$-337.2 \pm .6$	$-212.2 \pm .5$
S^0_{298} (s), cal./mole deg.	$6.77 \pm .01$	$12.03 \pm .03$	53.4 ± 2.0	38.5 ± 1.2
$(H_{1000}(l) - H_{298}(s))$, kcal./mole	$7.33 \pm .02$	$11.22 \pm .01$	58.0 ± 1.9	26.0 ± 2.0
$S^0_{1000}(l)$, cal./mole deg.	$17.52 \pm .02$	$26.20 \pm .04$	159.8 ± 2.6	79.3 ± 1.5
$(F^0_{1000}(l) - H_{298}(s))$, kcal./mole	$-10.19 \pm .03$	$-14.98 \pm .04$	-101.8 ± 4.6	-53.3 ± 2.0
Ref.	10–12	11, 13, 14	11, 14–17	11, 13, 14, 18

ion. With no such stabilization, the vapor pressure would have been about 10^5 atmospheres. It therefore seemed necessary to attribute the reduction of uranium to the remarkable stability of aluminum chloride complexes. Furthermore, it appeared necessary to attribute the maximum reduction at [K]/[Al] = 1 to competitive complex equilibria, analogous in some respects to the titration of a mixture of a dibasic acid and a weaker polybasic acid present in much smaller concentration with a base

$$Cl^- + Al_2Cl_6 \rightleftarrows Al_2Cl_7^-;\ K_2 \qquad (2)$$

$$Cl^- + Al_2Cl_7^- \rightleftarrows 2AlCl_4^-;\ K_3 \qquad (3)$$

$$mCl^- + UCl_3 \rightleftarrows UCl_{3+m}^{-m};\ K_4 \qquad (4)$$

Hence, it was postulated that the neutralization of the weaker Lewis acid, UCl_3, would begin when stoichiometry was approached, [K]/[Al] → 1. Reactions 2 and 3 would drive reaction 1 to the right, but reaction 4 would drive it to the left.

Since experimentally the mole fraction of aluminum in the metal phase was nearly unity, the equilibrium of reaction 1 would be governed by the ratio of free aluminum chloride to free uranium chloride providing the model was appropriate. By defining $P_{Al} = -\log (X_{\text{free } Al_2Cl_6})^{1/2}$ and $P_U = -(X_{\text{free } UCl_3})$ we could measure the extent of reaction 1 by the difference ${}^1/_2P_{Al} - P_U$ as illustrated in Fig. 1. If ΔP, the difference between titration curves, were large, the equilibrium of reaction 1 would be far to the right.

The equilibrium constants for equations 1–4 can be written in terms of activities

$$\frac{(a_{Al_2Cl_6})^{1/2} \cdot a_U}{a_{UCl_3} \cdot a_{Al}} = K_1 \qquad (5)$$

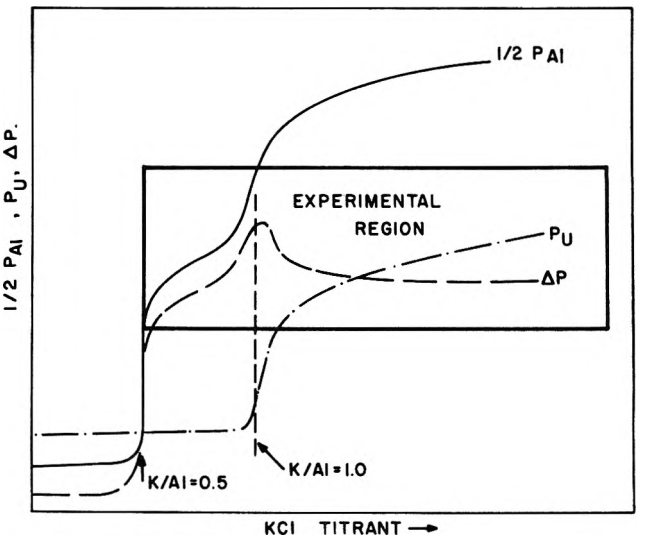

Fig. 1.—Titration curves of the Lewis acids Al_2Cl_6, $Al_2Cl_7^-$, and UCl_3 by chloride ions.

$$\frac{a_{Al_2Cl_7^-}}{a_{Al_2Cl_6} \cdot a_{Cl^-}} = K_2 \qquad (6)$$

$$\frac{(a_{AlCl_4^-})^2}{a_{Al_2Cl_7^-} \cdot a_{Cl^-}} = K_3 \qquad (7)$$

$$\frac{a_{UCl_{m+3}-m}}{a_{UCl_3} \cdot (a_{Cl^-})^m} = K_4 \qquad (8)$$

The originally proposed model assumed ideality of all species in solution, thus allowing the replacement of activities by mole fractions. However, it was later shown by Yonco, Johnson, and Cafasso[19] that the activity coefficient of uranium in molten aluminum is about 1.4×10^{-3} at 725° and is reasonably constant over the range of concentrations encompassed in our study. It could therefore be absorbed into K_1 to form K_1'

$$\frac{(X_{Al_2Cl_6})^{1/2} X_U}{X_{UCl_3} X_{Al}} = K_1' \cong K_1/1.4 \times 10^{-3} \qquad 5a)$$

The model for which calculations in this paper were made assumed the salt to be Raoultian and the actinide metal to obey Henry's law. The species in pure liquid aluminum chloride was assumed to be Al_2Cl_6 in agreement with X-ray studies of Harris, *et al.*[20] Postulation of the tetrahedral species, $AlCl_4^-$, also is supported by calculations of Kryagova[21] and X-ray studies of Baenziger.[22]

(10) W. F. Giauque and P. F. Meads, *J. Am. Chem. Soc.*, **63**, 1897 (1941).
(11) K. K. Kelley, U. S. Bur. Mines Bull. No. 584, 1960.
(12) D. R. Stull and G. C. Sinke, "The Thermodynamic Properties of the Elements," American Chemical Soc., Washington, D. C., 1956.
(13) G. N. Lewis and G. E. Gibson, *J. Am. Chem. Soc.*, **39**, 2554 (1917); W. M. Jones, J. Gordon, and E. A. Long, *J. Chem. Phys.*, **20**, 695 (1952); D. C. Ginnings and R. J. Corruccini, *J. Res. Natl. Bur. Std.*, **39**, 309 (1947); G. E. Moore and K. K. Kelley, *J. Am. Chem. Soc.*, **69**, 2105 (1947); J. M. North, Atomic Energy Research Estab. (Gt. Brit.), M/R 1016 (1956).
(14) F. D. Rossini, D. D. Wagman, W. H. Evans, S. Levine, and I. Jaffe, Natl. Bur. Standards (U. S.) Circ. No. 500 (1952).
(15) H. Villa, *J. Soc. Chem. Ind.* (London), **69**, Suppl. No. 1, S9 (1950).
(16) G. C. Sinke and D. R. Stull, "J.A.N.A.F. Interim Thermochemical Table," Vol. 1, Thermal Laboratory, Dow Chemical Co., 1960; D. R. Stull, private communication.
(17) J. P. Coughlin, *J. Phys. Chem.*, **62**, 419 (1958); W. A. Roth and A. Buchner, *Z. Elektrochem.*, **40**, 87 (1934); W. Fischer, *Z. anorg. allgem. Chem.*, **200**, 332 (1931); T. Takahashi, *J. Chem. Soc. Japan, Ind. Chem. Sect.*, **57**, 337 (1954).
(18) G. E. MacWood, "Thermodynamic Properties of Uranium Compounds," Report No. MDDC-657, Manhattan Project (1946); C. H. Barkelew, Report R.L. 4.6.906, Lawrence Radiation Laboratories, Jan. 18, 1945; G. E. MacWood, Report R.L. 4.7.600, Lawrence Radiation Laboratories, Aug. 9, 1944; W. Biltz and C. Fendius, *Z. anorg. allgem. Chem.*, **176**, 49 (1928); Heat of fusion estimated as 10.7 ± 2.0 kcal. at 1115°K. by the authors.
(19) F. Cafasso, private communication. See also AEC Research and Development Reports, ANL 5996 and ANL 6101 (1959).
(20) R. L. Harris, R. E. Wood, and H. L. Ritter, *J. Am. Chem. Soc.*, **73**, 3151 (1951).
(21) A. I. Kryagova, *J. Gen. Chem. USSR*, **17**, 421 (1947); *Zh. Priklad. Khim.* **21**, 561 (1948).
(22) N. C. Baenziger, *Acta Cryst.*, **4**, 216 (1951).

In order to test the model, we made some preliminary calculations using reasonable values for K_2, K_3, K_4 and m. It was readily apparent that the species UCl_4^-, *i.e.*, $m = 1$, could not be made to produce a maximum ΔP at $[K]/[Al] \simeq 1$. In order for this to occur, K_3 would have to be large enough to cause the titration of $Al_2Cl_7^-$ before UCl_3. Yet upon titration of UCl_3, its concentration would need to diminish more rapidly than that of Al_2Cl_6 with further addition of chloride in order to successfully shift equilibrium 1 back to the left. This is impossible.

Larger values of m provided some promise that the experimental data could be reproduced with a proper choice of K_2, K_3, K_4. Since the region of primary interest occurred where conventional approximations could not be successfully made, and an optimum set of the three constants K_2, K_3, K_4 would have to be obtained by successive choices, the problem lent itself well to use of a digital computer—an I.B.M. 7090. "Fortran" language was used. Combinations of equilibrium constants between the limits

$$10^3 \leq K_2 \leq 10^{20}$$
$$10^{-4} \leq K_3 \leq 10^{10}$$
$$10^{-4} \leq K_4 \leq 10^{10}$$

were used and "best fits" were determined for each combination. Analyses revealed that there was an optimum set for each value of m. (The computer could make calculations for 125 sets in 2 minutes, a task requiring approximately 700 to 1500 man days with a conventional calculator.)

Mathematical Development.—The material-balance equations consistent with eq. 5a, and 6–8 are

$$A/N = 2X_{Al_2Cl_6} + 2X_{Al_2Cl_7^-} + X_{AlCl_4^-} \quad (9)$$

$$B/N = X_{UCl_3} + X_{UCl_{m+3}^{-m}} \quad (10)$$

and

$$C/N = X_{Cl^-} + mX_{UCl_{m+3}^{-m}} + X_{Al_2Cl_7^-} + X_{AlCl_4^-} \quad (11)$$

where A, B, and C, respectively, represent the gram atoms of aluminum, uranium, and potassium in the salt phase and N represents the total number of moles of the various species. The species considered for the model were K^+, Cl^-, Al_2Cl_6, $Al_2Cl_7^-$, $AlCl_4^-$, UCl_3 and UCl_{3+m}^{m-}. It was unnecessary to include intermediate uranium species since the concentration of uranium in the salt in all cases was so small that a slight excess of potassium chloride was sufficient to form the highest stable complex. Clearly, the data are not accurate enough to provide any additional information on intermediate complexes.

The function ΔP can be calculated in two independent ways, either from concentrations in the metal phase, which are purely experimental values, or from concentrations in the salt phase, calculated by consideration of the model. From eq. 5a

$$\Delta P_{exp} = \log\left[\frac{X_{UCl_3}}{(X_{Al_2Cl_6})^{1/2}}\right] = \log\left[\frac{D}{EK_1'}\right] \quad (12)$$

where D and E are the atom fractions of uranium and aluminum, respectively, in the metal phase. In order to calculate ΔP_{theor} from the salt phase data, it is necessary to obtain the mole fraction of free Al_2Cl_6, $X_{Al_2Cl_6}$, hereafter simply designated x, from equations of the model. In order to do this, however, it is necessary to also determine the mole fraction of free chloride ion, X_{Cl^-}, hereafter designated y, simultaneously by the iterative process outlined below.

Since the total number of moles of species, N, is given by

$$N = N(X_{K^+} + x + y + X_{Al_2Cl_7^-} + X_{AlCl_4^-} + X_{UCl_3} + X_{UCl_{m+3}^{-m}}) \quad (13)$$

it can be expressed in terms of x, y, and the equilibrium constants by combining eq. 13 with eq. 6, 9, 10, and 11 to form 14

$$N = (A + B + C)/(1 - y + x + K_2xy) \quad (14)$$

Substituting N into eq. 9, along with eq. 6 and 7, and solving for y leads to an expression in terms of the equilibrium constants and x

$$y = [Q(1 + x) - 2x]/[K_2x(2 - Q) + R\sqrt{x} + Q] \quad (15)$$

where $Q = A/(A + B + C)$ and $R = \sqrt{K_2K_3}$. In like manner, substitution of N into eq. 11, with eq. 6–8 and 10, produces a solution for x in terms of the constants and y

$$x = \left[\frac{-b + \sqrt{b^2 - 4ac}}{2a}\right]^2 \quad (16)$$

where

$$a = K_2y + (1 + K_2y)\left[\frac{mVK_4y^m}{1 + K_4y^m} - T\right],\ T = C/(A + B + C),\ V = B/(A + B + C),\ b = Ry,\ \text{and}\ c = y - (1 - y)\,[T - mVk_4y^m/(1 + K_4y^m)]$$

Equations 15 and 16 can be solved simultaneously by an iterative process. This is accomplished by first placing the limits $L < x < H$ on x. A minimum value $x_0 = L$ is then placed into eq. 15 to solve for y. This value for y then is used in eq. 16 to solve for a new x, called x_0'. If $x_0' < x_0$ then x_0 is multiplied by a factor greater than unity and the cycle is repeated with a new x_1 in eq. 15. This process is repeated until $x_i < x_i'$. When this occurs, x_i becomes the upper limit and x_{i-1}, the lower limit. A new value $x_{i+1} = (x_i + x_{i-1})/2$ is calculated and the cycle is repeated, each time testing to determine whether $x_{i+n} < x_{i+n}'$ or $x_{i+n}' < x_{i+n}$. If the former case holds, the upper limit becomes $H = x_{i+n}$ and the lower limits remains fixed. If the latter case holds, $L = x_{i+n}$ and H remains fixed. The test is then made to determine whether $H < 1.01L$. If so, then $x_f = (H + L)/2$ and a similar test is made on y. In this fashion both x and y are determined to within 1% of the correct values.

From (8), (10), and (14), the mole fraction of UCl_3 can be obtained. Thus a theroetical ΔP, which is a function of the constants and measurable concentrations in the salt phase, is derived (eq. 17).

TABLE II

"BEST" EQUILIBRIUM CONSTANTS FOR THE MODEL PROPOSED

	M	K_1	K_2	K_3	K_4	γ_U	Variance	Sd[a]
a	2	1.82×19^{-9}	4.2×10^{14}	1.0×10^4	5.6×10^4	1.4×10^{-3}	1.349	0.270
b	3	1.25×10^{-6}	3.2×10^{14}	1.0×10^4	3.2×10^5	1	0.645	0.161
c	3	1.25×10^{-6}	1.3×10^8	2.0×10^3	9.0×10^4	1.4×10^{-3}	.524	.145
d	3	1.82×10^{-9}	5.9×10^{13}	1.7×10^3	6.6×10^4	1.4×10^{-3}	.632	.159
e	4	1.82×10^{-9}	1.7×10^{13}	2.9×10^2	1.1×10^6	1.4×10^{-3}	.964	.197

[a] $Sd = \sqrt{Var/(n-1)}$, where n represents the number of data.

$$\Delta P_{theor} = \log \left[\frac{V(1 - y + x + K_2xy)}{x^{1/2}(1 + K_4y^m)} \right] \quad (17)$$

The variance

$$Var = (\Delta P_{theor} - \Delta P_{exp})^2 \quad (18)$$

becomes a measure of applicability of the theory.

Results

The constants which produced the least variance, thus the best statistical fit for the data, are given in Table II. Row b represents the first attempt to find a self-consistent set of constants before the activity coefficient of uranium in aluminum was known. Row c represents the recalculation taking this into account. However, recent measurements on the third law entropy of solid aluminum chloride[16] required K_1 to be revised. An estimated value of S_{298}^0 previously generally used was found to be high by 10 e.u. Thus rows a, d, and e were calculated. They are believed to be the most accurate. Previous calculations were included to show that variations of γ_U or K_1 (hence K_3) are, for the most part, reflected in K_2; K_3 does not vary by more than a factor of about 8 and K_4 remains remarkably constant. It is thus concluded that, although there is an uncertainty of about 3 kcal. in eq. 1, K_4 must be close to 7×10^4. Furthermore, models containing UCl_5^{-2} and UCl_7^{-4} as the ultimate complexes can be ruled out by statistical considerations. Figure 2 represents the data for rows a, d, and e.

If reliance can be placed on the measurement at [K]/[Al] = 0.527, it appears that chloride ion can appreciably lower the activity of Al_2Cl_6, even in the region [K]/[Al] < 0.5, but the lack of data in this region discourages further discussion.

Other Actinides.—Limited experiments on thorium, protactinium, neptunium and plutonium chlorides in KCl–$AlCl_3$ have been reported.[23] Although these data are not as precise as those involving uranium, it is still evident that a maximum distribution into the aluminum metal phase occurs near [K]/[Al] = 1. An attempt has therefore been made to describe these systems with the model already presented, where now the actinide in question replaces the uranium. Since the equilibrium constants K_2 and K_3 refer to aluminum species, they should not vary from one actinide system to another. Thus, having been determined in the uranium system for which the most accurate and complete data are available, they were held constant ($K_2 = 5.9 \times 10^{13}$, $K_3 = 1.7 \times 10^3$).

Whereas the experiments involving uranium were performed in sealed vessels, this was not so for the other actinides. These experiments were performed in glove boxes where sealed reaction vessels were considered hazardous. As a result, it was necessary to chemically analyze the salt phase for the potassium to aluminum ratio, a procedure not necessary in the uranium experiments because the carefully weighed quantities had no chance to vaporize and escape from the reaction vessel. There are further complications because there is evidence that the aluminum metal reacted to some extent with the quartz vessel, producing a salt-soluble aluminum oxide, probably diaspore, which was inactive in the distribution reactions but analyzed as aluminum in the salt phase, producing a bias. Although an attempt was made to compensate for this bias in the theoretical treatment, the net effect is a rather serious uncertainty in the potassium to aluminum ratio.

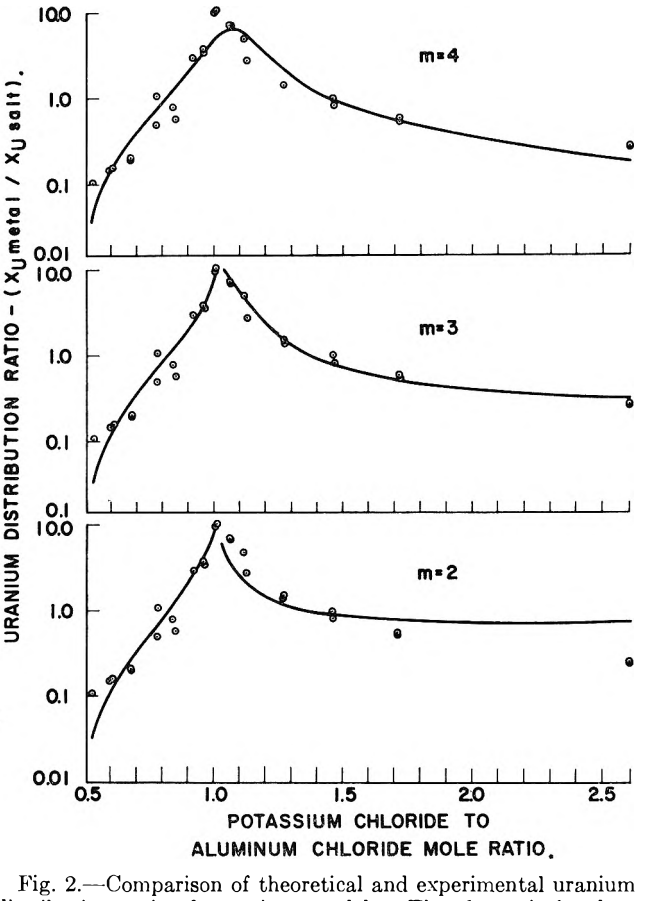

Fig. 2.—Comparison of theoretical and experimental uranium distribution ratios for various models. The theoretical values are represented by the solid lines.

Unfortunately, with the exception of UCl_3 and $PuCl_3$, the free energies of formation of the actinide trichlorides, have not been experimentally determined and only the activity coefficient of uranium in liquid aluminum is available. Therefore K_1 cannot be independently

(23) R. H. Moore and W. L. Lyon, A.E.C. Research and Development Report HW-59147, October 20, 1959.

TABLE IV

SUMMARY OF EQUILIBRIUM DATA

	K_1	K_2	K_3	K_4	K_5	K_8	K_5[a]	K_8[a]
Thorium	2.3×10^{-8}	5.9×10^{13}	1.7×10^{3}	3.3×10^{5}	2.2×10^{-5}	4.3×10^{-3}	4.2×10^{-5}	5.6×10^{-3}
Protactinium	5.7×10^{-6}	5.9×10^{13}	1.7×10^{3}	2.1×10^{5}	5.7×10^{-3}	0.11	9.3×10^{-3}	.....
							$0.4 \pm 0.1 \times 10^{-2}$	0.35 ± 0.14
Uranium	1.3×10^{-6}	5.9×10^{13}	1.7×10^{3}	6.6×10^{4}	0.63×10^{-2}	0.24		
Plutonium	1.0×10^{-8}	5.9×10^{13}	1.7×10^{3}	5.8×10^{4}	5.4×10^{-5}	1.9×10^{-3}	4.4×10^{-6}	2.1×10^{-3}

[a] Calculated from equations defined in ref. 9.

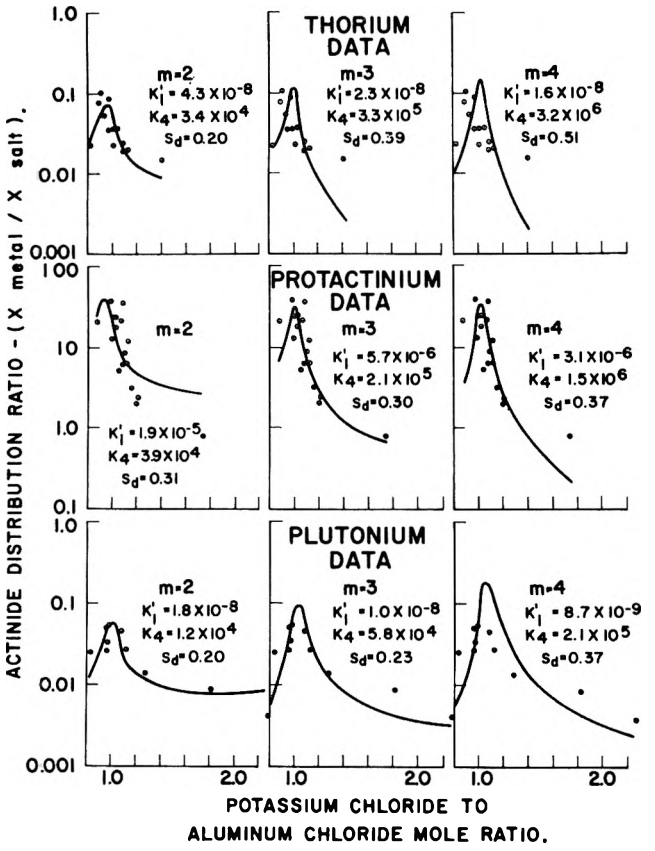

Fig. 3.—Theoretical and experimental actinide distribution ratios for various models. The theoretical values are represented by the solid lines.

calculated. However, by assuming Henry's law to be valid, we have grouped the activity coefficient into K_1 to form a new constant: $K_1' = K_1/\gamma_M$. The constants K_1' and K_4 were then determined simultaneously on the computer. This procedure only allowed two parameters to vary whereas that for uranium allowed three.

Because of uncertainties in the data, it was impossible to ascertain from this study which of the three species, MCl_5^{-2}, MCl_6^{-3}, MCl_7^{-4}, would best fit. However, the important conclusion was that the general postulated mechanism describes the experimental data within experimental error, but in doing so requires all of the formation constants for the actinide complexes to be about 10^4–10^5. Results are illustrated in Fig. 3.

Two constants which are directly comparable to K_5 and K_8 of part I[9] can be calculated from K_1', K_2, K_3, K_4 as

$$K_5 = \frac{K_1'}{K_4}\sqrt{K_2K_3} \qquad (19)$$

$$K_8 = K_1'\sqrt{\frac{K_2}{K_3}}$$

Comparisons are made in Table IV between the approximate method of part I and the results obtained by the statistical approach outlined in Part II. The general agreement points out the consistency of the two approaches. The main advantage of the latter approach is the determination of individual constants.

NUCLEAR MAGNETIC RESONANCE SPECTRA OF SOME SUBSTITUTED METHANES

BY S. G. FRANKISS

The University Chemical Laboratory, Lensfield Road, Cambridge, England

Received July 16, 1962

The n.m.r. spectra of eleven substituted methanes have been studied. Deviations of up to 20% from the J_{CH}(CHXYZ) additivity relationship have been observed with highly electronegative substitutents containing lone pairs of electrons on the atom bound to the ^{13}C atom. A linear relationship between the ^{13}C isotopic chemical shift $\Delta\phi(^{13}C-^{12}C)$ and J_{CF} has been observed in both saturated and unsaturated systems.

This n.m.r. study of substituted methanes, which was initiated as a corollary to an investigation of SiH systems, has produced several observations of considerable theoretical interest. Highly electronegative substitutents with lone pairs of electrons on the atom bound to ^{13}C atom show deviations of up to 20% from the J_{CH}(CHXYZ) additivity relation.[1] In the fluorine resonance spectrum the isotopic chemical shift between fluorine bound to ^{13}C, on the one hand, and ^{12}C, on the other, $\Delta\phi(^{13}C-^{12}C)$ increases approximately linearly with the directly bound ^{13}C–F coupling constant both in saturated and in unsaturated systems. A concentration dependent HF coupling constant is reported.

(1) E. R. Malinowski, *J. Am. Chem. Soc.*, **83**, 4479 (1961).

Experiments and Results

All the alkoxy methanes are commercially available compounds and were purified by fractional distillation. The fluoro- and nitromethanes and N,N,N′,N′-tetramethylmethanediamine were prepared by standard methods; the fluoromethanes were purified by low temperature fractional distillation, purity being checked by measurements of vapor pressure and molecular weight.

TABLE I

CHEMICAL SHIFTS AND COUPLING CONSTANTS IN SOME SUBSTITUTED METHANES

Molecule	τ^0, p.p.m.	ϕ, p.p.m.	J_{HF}, c.p.s.	J_{CH}, c.p.s.	J_{CF}, c.p.s.	$\Delta\phi(^{13}C-^{12}C)$, p.p.m.	$\Delta\tau(^{13}C-^{12}C)$, p.p.m.	CH dilution shift, c.p.s.
CH_3F	5.90 ± 0.01	271.9 ± 1.7	46.36 ± 0.10	149.1 ± 0.2	157.5 ± 0.2	0.072 ± 0.007	0.003 ± 0.002 (5)	−1.4 ± 0.3
CH_2F_2	4.55 ± .01	143.4 ± 1.5	50.22 ± .10	184.5 ± .4	234.8 ± .6	.115 ± .010	.002 ± .005	−2.8 ± .5
CHF_3	3.75 ± .01	78.6 ± 0.7	79.72 ± .07[a]	239.1 ± .2	274.3 ± .1	.126 ± .003	.003 ± .005	−0.9 ± .4
CF_4	...	63.4 ± .3	...	...	259.2 ± .3	.118 ± .003	...	...

Molecule	τ^0CH_3, p.p.m.	J_{CH}, c.p.s.	J_{CH_3}, c.p.s.	$\Delta\tau CH(^{13}C-^{12}C)$, p.p.m.	$\Delta\tau CH_3(^{13}C-^{12}C)$, p.p.m.	CH dilution shift, c.p.s.	CH_3 dilution shift, c.p.s.
$(CH_3)_2O$	6.793 ± 0.003	139.6 ± 0.4	...	0.006 (5) ± 0.005	...	−0.3 ± 0.2	...
$CH_2(OMe)_2$	5.560 ± .005	6.800 ± .006	161.8 ± .3	141.5 ± .3	.007 ± .004	0.004 (5) ± 0.003	−1.9 ± .3	−2.8 ± 0.4
$CH_2(OEt)_2$[b]	5.452 ± .003	8.87 ± .01	161.1 ± .1	126.0 ± .3	.004 ± .002	.000 (2) ± .006	−1.0 ± .2	−0.3 ± .5
$CH(OEt)_3$[c]	4.967 ± .005	8.87 ± .01	185.1 ± .4	125.4 ± 1.0	.003 ± .004	[d]	−1.2 ± .5	−0.0 (3) ± .5
$CH_3(NMe_2)_2$	7.418 ± .004	7.852 ± .003	136.6 ± .2	132.5 ± .2	.004 ± .002	.002 (5) ± .003	+0.1 ± .2	−0.0 (5) ± .2

Molecule	τ^0, p.p.m.	J_{CH}, c.p.s.	$\Delta\tau(^{13}C-^{12}C)$, p.p.m.	CH dilution shift, c.p.s.
CH_3NO_2	5.95 ± 0.02	146.7 ± 0.2	0.005 ± 0.003	−12 ± 1
$CH_2(NO_2)_2$[e]	4.03 ± .05	169.4 ± .8	[d]	[d]
$CH(NO_2)_3$	2.81 ± .08	195.8 ± .3	0.005 ± 0.004	−24 ± 2

τ^0 are τ values extrapolated to infinite dilution in cyclohexane or tetramethylsilane. [a] For pure liquid CHF_3. $J_{HF}(CHF_3)$ for 5% solution in cyclohexane, 79.23 ± 0.10 c.p.s. [b] τ^0CH_3, 6.48 ± 0.01 p.p.m. J_{CH_3}, 140.5 ± 1.0 c.p.s.; CH_2 dilution shift, 0.01 ± 0.02 c.p.s.; J_{vic}^{HH}, 7.07 ± 0.05 c.p.s. [c] τ^0CH_2, 6.47 ± 0.01; CH_2 dilution shift, −0.4 ± 0.5 c.p.s.; J_{vic}^{HH}, 7.11 ± 0.07 c.p.s. [d] Not measured. [e] Measured in Et_2O solution with TMS as internal standard.

The n.m.r. spectra were recorded using a Varian Associates V4300B Spectrometer operating at 40 Mc./sec., with sample spinning, flux stabilization and a K-3519 Field Homogeneity Control System; measurements were made using sidebands generated by a Muirhead-Wigan D695A decade oscillator, samples being held in 5 mm. o.d. Pyrex tubing. Proton resonances were measured using cyclohexane (for fluoromethanes) or tetramethylsilane (for all other compounds) as solvent and internal standard. Fluorine resonances were measured using solutions in trichlorofluoromethane. For each compound at least two solutions of known concentration (*ca.* 95 and 5% by liquid volume) were studied.

Each measurement given in Table I is the average of at least eight separate determinations; and the error quoted consists of the calculated mean error plus, for τ values and dilution shifts, an estimated extrapolation error. The proton chemical shifts τ_H^0 were obtained by extrapolation to infinite dilution. As the fluorine dilution shifts of all the fluoromethanes were less than the mean errors in the fluorine chemical shifts no extrapolations were made and the ϕ values in Table I are the means of measurements in concentrated and dilute solutions. The ^{13}C isotopic chemical shifts $\Delta\phi(^{13}C-^{12}C)$ and $\Delta\tau(^{13}C-^{12}C)$, and the directly bound $^{13}C-H$ and $^{13}C-F$ coupling constants (J_{CH} and J_{CF}, respectively) were measured in 95% solution. The dilution shift is $\Delta(\nu_1 - \nu_0)$ c.p.s., where ν_1 is the extrapolated chemical shift of the pure solute and ν_0 the solute shift extrapolated to infinite dilution. The values of the coupling constants J_{HF} and J_{vic}^{HH} in Table I are the averages of measurements in dilute and concentrated solutions, except for $J_{HF}(CHF_3)$, which was concentration dependent.

Discussion

The $^{13}C-H$ spin spin coupling constants (J_{CH}) in fluoro-derivatives of methane, and to a lesser extent in alkoxy- and chloro-derivatives show large deviations from the simple additivity relation observed[1] for many other substituted methanes (Table II). While J_{CH} in the nitromethanes and N,N,N′,N′-tetramethylmethanediamine are closely additive. Thus deviations from additivity are found with highly electronegative substituents that have lone pair electrons on the atom bound to the ^{13}C atom.

TABLE II

DEVIATIONS (ΔJ) FROM ADDITIVITY OF THE $^{13}C-H$ COUPLING CONSTANTS OBSERVED IN DI- AND TRISUBSTITUTED METHANES

CH_nX_{4-n}	J_{CH} (obsd.), c.p.s.	J_{CH} (add), c.p.s.	ΔJ[a], c.p.s.
$CH_2(NMe_2)_2$	136.6	137	0
$CH_2(OEt)_2$	161.1	155	6
$CH_2(NO_2)_2$	169.4	169	0
CH_2Cl_2	178[4]	175	3
CH_2F_2	184.5	173	12
$CH(OEt)_3$	185.2	170	15
$CH(NO_2)_3$	195.8	191	5
$CHCl_3$	209[4]	200	9
CHF_3	239.1	197	42

[a] $\Delta J = J_{CH}^{(obs)} - J_{CH}^{(add)}$.

A semi-empirical interpretation of the $J_{CH}(CHXYZ)$ additivity effect has been developed[2] in which changes in J_{CH} are dominated by changes of the s character of the carbon hybrid orbital involved in the C–H bond (α^2_H). It was shown[2] that the square of the C–H bond normalization constant η^2 (λ_{CH}, α_H, Z_{eff}) is constant to within about 5%, where λ_{CH} is a parameter related to the C–H bond polarity[2,3] and Z_{eff} is the effective nuclear charge for the 2s and 2p electrons of carbon. Now it is unlikely that these positive deviations

(2) C. S. Juan and H. S. Gutowsky, *J. Am. Chem. Soc.*, **84**, 307 (1962), and *J. Chem. Phys.*, **37**, 2198 (1962). I am indebted to the authors for communicating results to me prior to publication.

(3) M. Karplus and D. M. Grant, *Proc. Natl. Acad. Sci. U.S.*, **45**, 1269 (1959).

of J_{CH} from additivity can be attributed solely to increases in η^2, even though the anomalous substituents are very electronegative; the NO_2 group has a larger Taft σ^* value than F or OR,[4] and the small range of proton chemical shifts for the fluoromethanes and alkoxymethanes, $CH(OR)_{4-n}$ (n = 1 to 3) indicates that there are no unexpectedly large changes in λ_{CH}. The perturbation by fluoro or alkoxy substituents of the carbon 2s orbital between the four bonds is thus dependent on the other substituents, strongly suggesting that interactions between lone pair electrons of fluorine or oxygen and other substituents are important. Such interactions have previously been invoked to explain the anomalously low nuclear quadrupole resonance frequency of ^{35}Cl in chlorofluoromethanes and α-chloroethers, for which overlap between the p orbitals on the fluorine or oxygen atom and the C-Cl bond was considered.[5,6] We hope to study the n.m.r. spectra of these compounds and to estimate the effect of this interaction of J_{CH}. Meanwhile, we note that the ratio of ΔJ values (Table II) for CHX_3 and CH_2X_2 (X = Cl, OR, F) is approximately 3:1 which is the ratio of the number of (X, C–X) interaction terms in these compounds.

Consideration of this interaction, in valence bond terms, by contributions to the ground state of the molecule of structures such as

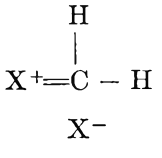

can lead to a qualitative understanding of the positive deviation of J_{CH} from additivity. If we suppose that η^2 remains approximately constant (the effect on η^2 of the decrease of Z_{eff} for the 2p and 2s electrons of carbon being largely cancelled by the decrease in λ_{CH}) then the increase in the s character of the carbon hybrid orbital should cause an increase in J_{CH}. There is also the possibility of π contributions to the coupling.

In the halosilanes, however, reduction of bond polarity can occur through (p → d)π bonding without appreciably changing the silicon sp hybridization, though d hybridization might make a significant contribution to the σ-orbitals of the monosubstituted derivatives. In this respect we note that a graph of $J_{CH}(CH_3X)$ against $J_{SiH}(SiH_3X)$ gives a smooth curve for most substituents except X = NR_2, OR, and F, which are those most likely to be involved in (p → d)π bonding.[7] This observation, taken with the deviations from additivity of J_{CH} in the fluoromethanes and the small range of proton chemical shifts observed in SiH compounds (τ $SiH_{4-n}F_n$ actually increases with n),[8] suggests that the importance of inductive effects in the interpretation of J_{SiH} may have been over-emphasized.[2]

$\tau CH_{4-n}X_n$ (n = 0 to 3) decreases almost linearly with increasing n when X = Cl and Br.[9] In contrast to this, when X = F and OR there is such a marked increase in slope with increasing n that the proton resonances of both CHF_3 and $CH(OEt)_3$ are to high field of $CHBr_3$, $CHCl_3$, and $CH(NO_2)_3$. Though these changes in chemical shifts are consistent with a reduction of the carbon electronegativity through lone pair interactions, no definite conclusions on this point can be drawn until the magnitude of the shieldings due to magnetic anisotropy of the halogens are more clearly known. If, however, it is assumed that when the magnetic anisotropy of X is insignificant τ_{CH_3X} is linearly related to the electronegativity of X, the low field shifts due to the magnetic anisotropy of the halogens are 1.0 and 0.7 p.p.m. for X = I and Cl, respectively.[10] As $\tau_{CH_2I_2} - \tau_{CHI_3} = 1.0$ this correction, though perhaps slightly too large, is of the correct order of magnitude. Thus if the halogen magnetic anisotropy in $CHCl_3$ deshields the proton by 2 p.p.m., the "corrected" proton chemical shift is $\tau = 4.7$, which is to high field of CHF_3 but still to low field of $CH(OEt)_3$.

A very approximate additivity relationship has been observed for $J_{CF}(CHXYZ)$ using contributions according to the equation $J_{CF}(CHXYZ) = \zeta_x + \zeta_y + \zeta_z$.[11] The fluoromethanes, however, show large deviations from this relationship as ζ_H decreases markedly with increasing n for $CF_{4-n}H_n$; and $J_{CF}(CH_3F)$ is exceptionally small.

We have observed that the $F(^{13}C-^{12}C)$ isotopic chemical shift in the fluoromethanes increases linearly with J_{CF} according to the equation[12]

$$\Delta\phi(^{13}C-^{12}C) = +0.001 + 4.62 \times 10^{-4} J_{CF} \quad (1)$$

The deviations of $\Delta\phi(^{13}C-^{12}C)_{obs}$ from this line, which passes very close to the origin are less than the mean errors of $\Delta\phi(^{13}C-^{12}C)_{obs}$. The fluorine resonance spectra of twenty-two other saturated compounds containing CF groups bound to C, N, P, As, O, S, Se, F, Cl, Br, I, and Hg atoms have recently been studied[13]; when the values for the twenty-six compounds are plotted in this form a least square fit gives[12]

$$\Delta\phi(^{13}C-^{12}C) = 0.007 + 4.36.10^{-4} J_{CF} \quad (2)$$

Twenty-two of the plots lie within ±0.012 p.p.m. of this line, with an average magnitude of deviation of 0.005 p.p.m. (Table III); while $(CF_3)_2Hg$, $(CF_3)_2AsCl$,

TABLE III

SOME VALUES OF J_{CF} AND $\Delta\phi(^{13}C-^{12}C)$ FOR F BOUND TO sp^3 HYBRIDIZED ^{13}C

Molecule	J_{CF}	$\Delta\phi(^{13}C-^{12}C)_{obs}$	$\Delta\phi(^{13}C-^{12}C)_{calc}$[a]
CH_3F	157.5	0.072 ± 0.007	0.076
CH_2F_2	234.8	0.115 ± .010	.109
CF_4	259.2	0.118 ± .003	.120
CHF_3	274.3	0.126 ± .003	.127
CF_3CCl_3[14]	282.5	.131 ± .002	.130
CF_3CO_2H[14]	283.2	.129 ± .002	.130
$(CF_3)_2S$	309.4[11]	.148[13]	.142
$^{13}CF_3SCFS$[15]	312.4	.141 ± .003	.143
$(CF_3)_2Se$	331.3[11]	.145[13]	.151
CF_3I[10]	344.8	.149	.157
CF_2Br_2	357.0[11]	.168[13]	.163

[a] Calculated from J_{CF} using equation 2.

(4) N. Muller and D. E. Pritchard, *J. Chem. Phys.*, **31**, 1471 (1959).
(5) R. W. Taft, Jr., *J. Am. Chem. Soc.*, **75**, 4231 (1953).
(6) E. A. C. Lucken, *J. Chem. Soc.*, 2954 (1959).
(7) D. P. Craig, A. Maccoll, R. S. Nyholm, L. E. Orgel, and L. E. Sutton, *ibid.*, 332 (1954).
(8) E. A. V. Ebsworth and J. J. Turner, to be published.
(9) A. A. Bothner-By and C. Naar-Colin, *J. Am. Chem. Soc.*, **80**, 1728 (1958).
(10) H. Spiesecke and W. G. Schneider, *J. Chem. Phys.*, **35**, 722 (1961).
(11) R. K. Harris, *J. Phys. Chem.*, **66**, 768 (1962).
(12) Equations 1, 2, and 3 were determined by regression analysis of $\Delta\phi(^{13}C-^{12}C)$ on J_{CF} using the method of least squares.
(13) R. K. Harris, to be published.
(14) G. V. D. Tiers, *J. Phys. Soc. Japan*, **15**, 354 (1960).
(15) A. J. Downs, to be published.

$CFBr_3$, and $CFCl_3$ show large deviations (between 0.018 and 0.040 p.p.m.). Thus equation 2 holds approximately for molecules that contain only 1st row elements and hydrogen, or less than three 2nd row elements directly bound to the ^{13}C atom.

A linear relationship between $\Delta\phi(^{13}C-^{12}C)$ and J_{CF} has also been found for fluorine bound to an unsaturated (sp^2) ^{13}C atom. The equation of this line,[12] which is significantly displaced from that given by equation 2 towards larger J_{CF} is

$$\Delta\phi(^{13}C-^{12}C) = -0.039 + 5.04.10^{-4}J_{CF} \quad (3)$$

The maximum deviation of $\Delta\phi(^{13}C-^{12}C)_{obs}$ from this line is 0.005 p.p.m., which is close to the quoted errors (Table IV).

Finally we report that J_{HF} in CHF_3 is concentration dependent. J_{HF} in a 5% solution of CHF_3 in cyclohexane is 79.23 ± 0.10 c.p.s. and this is 0.49 ± 0.17 c.p.s. less than in pure liquid CHF_3.

TABLE IV

J_{CF} AND $\Delta\phi(^{13}C-^{12}C)$ FOR F BOUND TO sp^2 HYBRIDIZED ^{13}C

Molecule	J_{CF}	$\Delta\phi(^{13}C-^{12}C)_{obs}$	$\Delta\phi(^{13}C-^{12}C)_{calc}$[a]
$CF_2:CCl_2$[14]	288.9	0.103 ± 0.002	0.107
$CFCl:CCl_2$[14]	303.1	.112 ± .002	.114
COF_2[15]	308.35	.121 ± .003	.116
CSF_2[15]	366.0	.143 ± .004	.145
$CF_3S:^{13}CFS$[15]	395	0.16 ± .05	.160

[a] Calculated from J_{CF} using equation 3.

Acknowledgment.—The author is very grateful to Dr. E. A. V. Ebsworth for helpful discussions; to the Department of Scientific and Industrial Research, for a maintenance grant; and to the Wellcome Trustees, who lent the Varian Spectrometer to the Department.

THE SOLUBILITY OF NAPHTHALENE IN SUPERCRITICAL ETHANE

BY G. S. A. VAN WELIE AND G. A. M. DIEPEN

Laboratory of General and Inorganic Chemistry, Julianalaan 136, Delft, Holland

Received July 17, 1962

Unlike Prins, we found, in measuring the P–T projection of the system ethane–naphthalene, no temperature minimum on the three phase curve solid naphthalene–liquid–gas. It follows that there is no essential difference in phase-behavior between the systems ethane–naphthalene and ethylene–naphthalene. Together with the P–T projection we have measured some P–T cross-sections at constant composition of the binary mixture. The first critical end-point is situated at 51.5 atm. and 36.8°, the second critical end-point, with a composition of approximately 19.5 mole %, was found at 122.5 atm. and 56.6°.

Introduction

For binary systems, characterized by metastable immiscibility of the liquid phase and intersection of the three phase line solid–liquid–gas and the critical curve it is usual to draw the P–T projection of the three phase curve S_BL_2G with a negative slope dP/dT.

According to measurements taken by Prins,[1] the system ethane–naphthalene should belong to this type, with the difference that whereas at lower pressures the S_BL_2G-curve has a negative slope, the curve passes a temperature minimum, to end finally into the second critical end-point with a positive slope dP/dT.

This would lead, as a consequence, to a T-x projection as given in Fig. 1. From 0, the triple point of naphthalene, the gas- and liquid branch of the S_BL_2G-equilibrium move to lower naphthalene-compositions and lower temperatures. The gas phase in equilibrium with the liquid phase will always be richer in the most volatile component. As a result the gas branch will move at smaller x-values than the corresponding liquid branch. It follows from the P–T projection of the S_B–L_2–G equilibrium that both branches pass a minimum temperature and move to higher temperatures, their x-values steadily coming closer. Finally, at the temperature of the second critical end-point, the gas- and liquid branch will merge smoothly into each other. The composition of the two phases will then be equal and the slope of the T–x projection, dT/dx, becomes zero.

Figures 2 and 3 are P–x cross-sections, through Fig. 1, respectively, for a temperature below the critical end-point and the temperature of this point.

(1) A. Prins, *Verslag Akad. Wetenschappen Amsterdam*, **23**, 1037 (1915).

From Fig. 3 the conclusion must be drawn that in the vicinity of the second critical end-point the solubility of solid naphthalene in the fluid phase falls sharply if the pressure is increased at constant temperature. In other words: at the temperature of the second critical end-point the system ethane–naphthalene should demonstrate a behavior just opposite to that of the system ethylene–naphthalene.[2]

We have measured some P–T cross-sections at constant composition to investigate this phenomenon quantitatively.

Since our results did not show any substantial difference with those of the system ethylene–naphthalene, we were compelled to reinvestigate the P–T projection of the system ethane–naphthalene according to Prins.

Experimental Procedure

For all data given in this communication use was made of the Cailletet-apparatus. The technique of measuring P–T cross-sections and determining the equilibrium conditions for three phase coexistence has been described earlier.[2]

The ethane is a research grade-product of Phillips Petroleum Co. with a purity of 99.99 mole %. Our naphthalene had a melting point of 80.25°.

Determination of P–T Cross-sections at Constant Composition.—After some orientation we succeeded in establishing the composition of the second critical end-point: approximately 19.5 mole % $C_{10}H_8$. The point was found at 122.5 atm. and 56.6°.

In its vicinity we have measured some P–T cross-

(2) G. S. A. van Welie and G. A. M. Diepen, *Rec. trav. chim.*, **80**, 659 (1961).

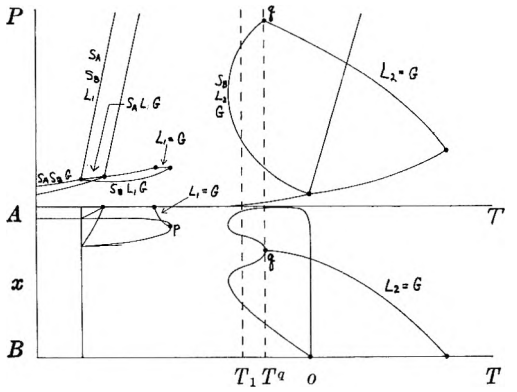

Fig. 1.—P–T and T–x projection of a binary system in which the three phase curve S_B, L_2, G passes a temperature minimum and ends into a second critical end point.

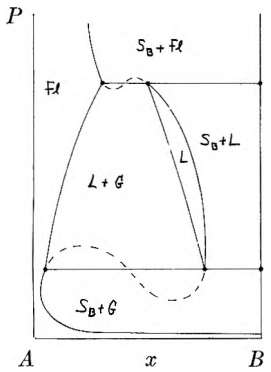

Fig. 2.—P–x section through Fig. 1 for $T = T_1$.

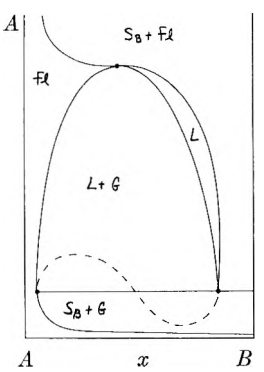

Fig. 3.—P–x section through Fig. 1 for $T = T_q$.

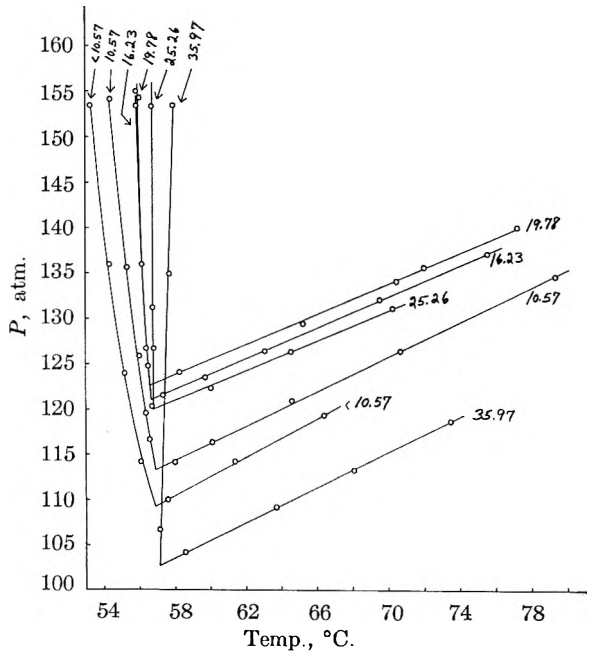

Fig. 4.—The system ethane–naphthalene. P–T measurements for various constant compositions (in mole %).

sections. The data are listed in Table I and set out in Fig. 4.

It appeared from visual observations that a composition of 19.78 mole % is very close to the critical composition. Consequently the L_2G-boundary curve for this composition may be supposed to coincide with the curve $L_2 = G$.

It should be clear that in the P–T projection (Fig. 5) the second critical end-point may be considered as a limit case in which the S_B–Fl-equilibrium becomes identical with the S_BL_2G-equilibrium. Hence the corresponding equilibrium curves should have equal slopes at critical end-point conditions.

TABLE I

THE SYSTEM ETHANE–NAPHTHALENE P–x SECTION AT VARIOUS CONSTANT COMPOSITIONS

x < 10.57 mole % $C_{10}H_8$		10.57 mole % $C_{10}H_8$		16.23 mole % $C_{10}H_8$	
P, atm.	t, °C.	P, atm.	t, °C.	P, atm.	t, °C.
S_B–Fl		S_B–Fl		S_B–Fl	
153.5	53.30	154.1	54.40	193.8	55.50
136.0	54.35	135.6	55.35	153.4	55.90
124.0	55.20	125.9	56.05	136.0	56.20
114.2	56.10	116.7	56.60	124.8	56.55
L–G		L–G		L–G	
Liquid vanishing points		Liquid vanishing points		Liquid vanishing points	
119.3	66.40	134.4	79.30	134.9	83.20
114.2	61.40	126.3	70.70	136.9	75.55
110.0	57.60	120.9	64.60	132.0	69.60
		116.4	60.15	126.4	63.10
		114.1	58.00	123.5	59.75
				121.5	57.35
19.78 mole % $C_{10}H_8$		25.26 mole % $C_{10}H_8$		35.97 mole % $C_{10}H_8$	
P, atm.	t, °C.	P, atm.	t, °C.	P, atm.	t, °C.
S_B–Fl		S_B–Fl		S_B–Fl	
155.0	55.90	169.6	56.80	153.4	57.95
154.3	56.05	153.3	56.75	134.9	57.70
136.0	56.25	131.2	56.75	106.7	57.15
126.7	56.45	121.4	56.85		
		Gas vanishing points		Gas vanishing points	
L_2 = G		L–G		L–G	
139.8	77.25	131.0	70.30	118.6	73.50
135.5	72.00	126.3	64.55	113.2	68.10
134.0	70.50	122.3	60.05	109.2	63.75
129.4	65.25	120.3	56.75	104.2	58.60
124.1	58.35	119.6	56.40		

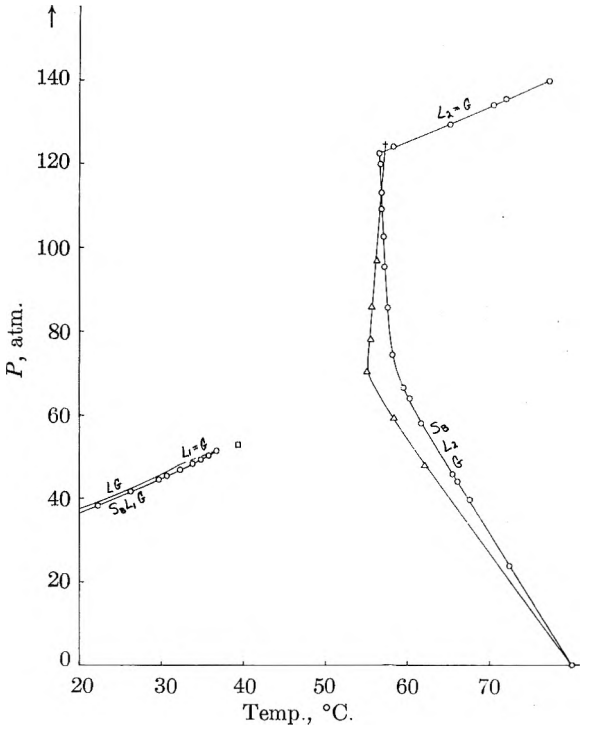

Fig. 5.—The system ethane–naphthalene. P–T projection of the three phase curve S_B, L, G: □, first critical end-point according to Prins; +, second critical end-point according to Prins; △, three-phase curve, solid naphthalene–liquid–gas according to Prins; ○, own measurement.

It follows from Fig. 4 that the slope of the S_B–Fl-equilibrium for the critical composition (19.78 mole %) is negative. This experimental result excludes the occurrence of a temperature minimum on the S_BL_2G curve and so we are justified in concluding that there is no essential difference in phase behavior between the system ethane–naphthalene and the system ethylene–naphthalene.

Determination of the Three Phase Curve S_B–L–G.— From direct measurements of the three phase equilibrium and the P–T measurements described above, we have constructed the three phase curve, as represented in Fig. 5. The data are listed in Table II.[3] The liquid–gas equilibrium of ethane is given in Fig. 5 from literature data.[4,5]

Figure 5 shows that the first critical end-point is situated at 51.5 atm. and 36.8°. The rise in critical temperature is 4.6°, and not 7.2° as found Ada Prins.

This increase is considerably lower in the system ethylene–naphthalene (1.5°)[6,7] which points to a greater solubility of naphthalene in ethane, at least for conditions close to the first critical end-point.

Figure 5 demonstrates at the same time the remarkable fact that contrary to Prins' findings, there is no temperature minimum.

Table II

The System Ethane–Naphthalene P–T Projection of the Three Phase Curve S_B, L, G.

P, atm.	t, °C.	P, atm.	t, °C.
		Second critical end-point	
		122.5	56.6
S_B, L_1, G		S_B, L_2, G	
38.3	22.25	122.6	56.60
41.7	26.25	121.1	56.70
44.5	29.65	120.0	56.80
45.4	30.65	113.2	56.90
46.9	32.25	109.2	56.90
47.8	33.30	102.8	57.15
48.3	33.80	95.5	57.20
49.3	34.80	85.8	57.60
50.2	35.60	74.5	58.20
50.3	35.80	66.6	59.55
50.6	36.00	64.1	60.30
50.9	36.30	58.0	61.70
51.1	36.50	45.8	65.50
First critical end-point		44.0	66.10
51.5	36.8	39.7	67.60
		23.8	72.40

As a result we may conclude that the systems ethane–naphthalene and ethylene–naphthalene are similar in their phase behavior.

Meanwhile we discovered a system, that does show a temperature minimum, *viz.*, the system methane–naphthalene,[8] about which another communication has appeared.

(3) L_2=G data (for a composition of 19.78 mole %) are given in Table I

(4) J. A. Beattie, G. J. Su, and G. L. Simard, *J. Am. Chem. Soc.*, **61**, 924 (1939).

(5) J. A. Beattie, C. Hadlock and W. Poffenberger, *J. Chem. Phys.*, **3**, 93 (1935).

(6) G. A. M. Diepen and F. E. C. Scheffer, *J. Am. Chem. Soc.*, **70**, 4085 (1948).

(7) G. A. M. Diepen and F. E. C. Scheffer, *J. Phys. Chem.*, **57**, 575 (1953).

(8) Y. van Hest, Thesis, Delft, 1962

RATE DEPENDENCE OF THE STOICHIOMETRY OF FORMIC ACID VAPOR PHOTOLYSIS

By Peter E. Yankwich and Edward F. Steigelmann

Noyes Laboratory of Chemistry, University of Illinois, Urbana, Illinois

Received July 23, 1962

Formic acid vapor was photolyzed at 304.8°K. and a total pressure of 26.3 mm. in an end-illuminated tubular vessel; a high pressure mercury arc lamp was used. The photolysis rate was varied from 0.187–59.0 × 10^{-9} mole per sec., and the degree of decomposition was limited to 1%. Over the rate range studied, the mole fraction of carbon dioxide in the product fell from 0.53 to 0.38. Analysis of the data in terms of a model suggested by the work of R. M. Noyes showed that this mole fraction should be a linear function of the inverse one-fourth power of the intensity of illumination (as measured by the rate of appearance of products). Within modest experimental errors, the results obtained are in fair agreement with the predictions of this simple treatment.

Introduction

One of the first investigations of the photochemical decomposition of formic acid was that of Berthelot and Gaudechon,[1] who reported the products of the decomposition of the liquid to be carbon dioxide, carbon monoxide, hydrogen, and a small amount of methane. Later, Ramsperger and Porter[2] found that formic acid vapor decomposed photochemically into two different product sets: carbon dioxide and hydrogen, and carbon monoxide and water, the yields of each set being 36 and 64%, respectively. Herr and Noyes[3] found that the quantum yield for the vapor photolysis was slightly less than unity and that the amount of hydrogen formed was somewhat smaller than the amount of carbon dioxide.

The studies of Gorin and Taylor[4] revealed the quantum yield to be unity at three different wave lengths (2540, 2100, and 1900 Å.) and independent of temperature and pressure. They found the dimer to decompose exclusively to carbon dioxide and hydrogen, while the monomer formed both product sets; tests with parahydrogen for the presence of hydrogen atoms in the decomposition were negative. Using the antimony mirror technique, Burton[5] also was unable to detect the presence of free radicals in the decomposition.

(1) D. Berthelot and H. Gaudechon, *Compt. rend.*, **151**, 478 (1910).

(2) H. C. Ramsperger and C. W. Porter, *J. Am. Chem. Soc.*, **48**, 1268 (1926).

(3) W. N. Herr and W. A. Noyes, Jr., *ibid.*, **50**, 2345 (1928).

(4) E. Gorin and H. S. Taylor, *J. Am. Chem. Soc.*, **56**, 2042 (1934).

(5) M. Burton, *ibid.*, **58**, 1655 (1936).

Using spectrometric techniques, Terenin and Nuejmin[6] studied the photochemical decomposition of formic acid vapor in the Schumann ultraviolet and discovered the presence of OH radicals. They postulated that excited formic acid split into two radicals, HCO and OH; the dissociation thresholds for this reaction were quoted to be 182 kcal. mole^{-1} and 1560 Å. Using scavengers and deuterated formic acid (DCOOH which photodecomposed to yield H_2, D_2, and HD), Gorden and Ausloos[7] showed the existence of free radicals in the formic acid photodecomposition; above 200°, a chain mechanism component was found. Cundall and Milne[8] irradiated formic acid in the presence of *cis*-butene-2 and found evidence for an excited triplet formic acid state.

The results of these different investigations of the formic acid vapor photolysis exhibited a variety of ratios of carbon dioxide to carbon monoxide product under comparable conditions of wave length, temperature, and pressure. In none of these experiments was much attention paid to the possible influence of the *rate* of photolysis on the stoichiometry of the decomposition. The research reported here was undertaken to explore the dependence of the stoichiometry on the rate of the photodecomposition in order to provide further understanding of the decomposition mechanism.

Experimental

Reagent.—Since vapor phase chromatographic analysis revealed minor impurities other than water in Baker's 98–100% reagent grade formic acid, this material was purified before use by the following procedure. Several freezings with liquid nitrogen or carbon dioxide–ethanol slush were each followed by pumping and subsequent thawing of the solid formic acid under vacuum. After the last of these treatments, the stopcock to the pumps was left open and a trap between the frozen formic acid and the pumps was cooled to −78°; pumping was continued and purified formic acid (which had no contaminant detectable by gas chromatography) was distilled in this trap.

Apparatus.—The light source used was a high pressure mercury arc lamp (Hanovia Model L). The reactor, of 4100-ml. volume, was made from a 91 cm. section of 80 mm. i.d. Pyrex tubing by sealing one end; on the other was a 40 mm. O-ring joint (Corning Glass Co.). A 6 mm. right angle vacuum stopcock was attached to the side of the reactor about 7.5 cm. below the O-ring joint. A quartz window (Amersil, Inc.) was held in place on the Neoprene O-ring by air pressure upon evacuation of the reactor.

Temperature control was maintained during the irradiation by placing the reactor completely inside a furnace which was made from 112 cm. section of 84 mm. i.d. aluminum tubing with a 13 mm. wall. Several layers of asbestos paper covered the tube over which were wound four individual heaters, each heating 28 cm. length of the furnace. Power to each heater was controlled by a 2.5 amp. Variac, the four being connected in series to the output of a 10 amp. Variac. Power to the latter was controlled by a thermistor-actuated relay, which operated on an a.c. bridge principle, using a thyrotron circuit, and which maintained a furnace temperature (between 20 and 80°) constant to less than 0.1° when the appropriate thermistor was used. To measure the furnace temperature, a thermometer graduated to 0.1° was inserted through the furnace wall to the interior. Fine adjustments were made on the 2.5 amp. Variacs to reduce the adjacent section temperature differences, measured with differential thermocouples imbedded in the middle of each section, to less than 0.1°.

To permit study of the intensity dependence of the stoichiometry of the decomposition, a set of diaphragms was constructed from 8 cm. square metal plates in which single circular holes were made ranging in diameter from 0.6 to 5 cm. Irradiation time was adjusted appropriately for each diaphragm area to limit decomposition to 1% in each experiment.

(6) A. Terenin and H. Nuejmin, *J. Chem. Phys.*, **3**, 436 (1935).
(7) R. Gorden and P. Ausloos, *J. Phys. Chem.*, **65**, 1033 (1961).
(8) R. B. Cundall and D. G. Milne, *J. Am. Chem. Soc.*, **83**, 3903 (1961).

Procedure.—Before irradiation, the reactor and the quartz window were cleaned with hot Alconox solution and rinsed exhaustively with distilled water. Then, the window was attached and the reactor evacuated for 12 hours before filling. (The pumping system consisted of a Welch Duo-Seal pump and a Consolidated Vacuum Corp. oil diffusion pump. Two liquid nitrogen traps were kept between the outgassing reactor and the rest of the vacuum system to prevent contamination of the reactor by mercury or other vapors.) Charging was accomplished by expanding into the reactor a sample of purified formic acid which had been measured with a micropipet. Twenty minutes were allowed for thermal equilibration of the reactor in the furnace and warming of the lamp before the irradiation was started. During the irradiation, a diaphragm was placed immediately before the quartz window with the lamp removed 15 cm. from it.

An automatic Toepler pump was used to pull the irradiated gases through two U-traps, the first at −78° and the second at liquid nitrogen temperature; these served to collect the formic acid, water, and much of the carbon dioxide. The remainder of the gas was exhausted into a storage vessel until the reactor was empty; then the uncondensed gases were cycled through the liquid nitrogen trap to assure collection of the remaining carbon dioxide. After manometric quantity determination of the noncondensable gases, they were cycled repeatedly through a furnace packed with copper oxide wire to convert the carbon monoxide to carbon dioxide and the hydrogen to water, and then through a liquid nitrogen trap to condense the combusted products. Both carbon dioxide samples were purified by three distillations between −110° (liquid nitrogen–ethanol) and liquid nitrogen temperature and were measured in calibrated mercury manometer. All the decomposition products except water were determined quantitatively.

Results

All experiments were conducted with the same initial amount of formic acid and at the same irradiation temperature. The only experimental parameter varied was the rate of reaction, this variation being accomplished with the different sized diaphragms. The results of these experiments with 0.00928 mole (0.35 ml.) of formic acid, yielding a total pressure of 26.3 mm. at the irradiation temperature of 304.8°K. (mole fraction monomer = 0.322), are given in Table I. *Rate* is

TABLE I

DEPENDENCE OF STOICHIOMETRY UPON RATE OF PHOTOLYSIS

Rate, moles sec.$^{-1}$ × 10^3	$f(CO_2)$	$r(H_2)$
0.187	0.529	0.86
0.217	.518	..
0.322	.520	..
0.958	.482	0.78
1.45	.466	..
1.68	.474	..
3.05	.429	..
3.75	.444	..
6.17	.407	..
7.13	.399	..
8.73	.420	0.89
14.1	.401	..
15.0	.378	..
16.4	.388	..
21.6	.389	..
33.9	.379	..
49.2	.383	0.76
51.7	.374	..
59.0	.379	..

defined as the total number of moles of carbon dioxide plus carbon monoxide products divided by the irradiation time in sec., $f(CO_2)$ is the mole fraction of the carbon product appearing as carbon dioxide, and $r(H_2)$ is the ratio of the number of moles of hydrogen

to carbon dioxide. As zero rate is approached, $f(CO_2)$ increases sharply; and, as found previously by Herr and Noyes,[3] $r(H_2)$ is slightly less than unity.

Gorden and Ausloos[7] have shown that oxygen is an effective radical scavenger in the photodecomposition of formic acid and causes a low hydrogen yield in the decomposition. The decreases of $r(H_2)$ from the expected value of unity probably can be attributed to scavenging by small amounts of air in the reactor.

Discussion

The dependence of $f(CO_2)$ upon rate of reaction indicates that more than one process is occurring in the photodecomposition. It is possible that the method used to alter the rate might cause the effect observed. If the beam of light were parallel, the same concentration of excited species or radicals would be produced in the beam regardless of its cross sectional area, absorption effects being neglected. If this were the case, use of a different diaphragm would change the ratio of the cross sectional area to the circumference of the beam; the occurrence of two types of reaction, one within the light path and one without, could account for the observed dependence of $f(CO_2)$ on rate.

However, the beam from the high pressure arc lamp is divergent. In fact, even when the smallest diaphragm is used, only a small fraction of the total reactor volume is dark, and throughout the reactor the intensity of illumination is moderately uniform; the non-uniformity is caused by the divergent nature of the beam and by attentuation due to absorption by formic acid. As a first approximation, this non-uniformity will be neglected, and the rate experiments will be considered as carried out under conditions of uniform illumination throughout the reactor. The effects of the non-uniformity will be discussed below.

Since the dependence of the stoichiometry on the rate of photolysis might be due to a combination of thermal and photochemical components of the decomposition, the thermal decomposition was examined. While the thermal reaction does occur, with $f(CO_2)$ equal to about 0.87, its rate of 5.5×10^{-12} mole sec.$^{-1}$ is equivalent to only 3% of the photochemical rate at the *lowest* rate of photolysis investigated, and, therefore, was neglected.

Although the existence of radicals in the photochemical decomposition of formic acid vapor has been demonstrated previously, there is little or no evidence for a chain reaction under the conditions employed in this investigation.[8] A possible explanation for the observed rate dependence of the stoichiometry is found in the type of mechanism discussed by Noyes,[9] consisting of a second-order homogeneous termination of radicals in the gas phase in competition with a first-order heterogeneous reaction at the walls of the reactor,[10] a different product split being associated with each process.

A number of different radical pairs can be produced upon excitation of the monomer or the dimer, and, to maintain generality, R will refer to any radical. Consider the following termination reactions

$$R + R' \longrightarrow f_h \qquad (1)$$

$$R + \text{wall} \longrightarrow f_w \qquad (2)$$

(9) R. M. Noyes, *J. Am. Chem. Soc.*, **73**, 3039 (1951).
(10) K. E. Shuler and K. J. Laidler, *J. Chem. Phys.*, **17**, 1212 (1949).

The symbols f_w and f_h represent the distributions of products which are formed from the wall and homogeneous terminations, respectively. These distributions can include species which are stable at room temperature as well as free radicals; but since the only measurement made of such a distribution is $f(CO_2)$, f_w and f_h are effectively the values of $f(CO_2)$ for the wall and homogeneous terminations, respectively.

Since one of the proposed components of the detailed decomposition mechanism is heterogeneous termination of radicals at the wall, diffusion of radicals to the wall must be considered. Fick's second law of diffusion provides a mathematical expression for the concentration of radicals R as a function of time and position within the reactor

$$D\nabla^2 R + Q - k_h R^2 = \partial R/\partial t \qquad (3)$$

where D is the mean diffusion coefficient of radicals in the formic acid medium, Q the rate of production of radicals per cc., and k_h the second-order rate constant for vapor phase termination. If a steady-state concentration of radicals is achieved in an interval short compared with the duration of the irradiation, R the radical concentration is independent of time, and equation 3 becomes

$$D\nabla^2 R + Q - k_h R^2 = 0 \qquad (4)$$

Noyes[9] has considered the solution of equation 4 subject to the boundary condition that the wall–radical recombination coefficient is unity, and the following discussion is based on his work.

Even after assuming the diffusion coefficient and rate of radical production to be constant, the reactor spherical, and only one radical species to be present, Noyes found that explicit solution of equation 4 was not possible. However, he pointed out that the walls tended to remove radicals from a shell of thickness $0.9(D^2/k_hQ)^{1/4}$ cm. next to the wall of the reactor.

In order to evaluate the competition between homogeneous and wall terminations, we make the following additional assumptions: (1) that the rate of diffusion of radicals is small compared to the rates of the other processes, (2) that within the shell defined by the Noyes approximation all products formed are characteristic of the heterogeneous process, and (3) that throughout the rest of the vessel termination occurs homogeneously. Since the Noyes approximation assumes uniform light absorption, the fraction of products produced by the wall process is the same as the fraction of the reactor volume contained within the shell next to the wall.

Because the shell for the wall reaction is thin (a few mm. thick at the most, *vide infra*), the results obtained for a spherical reactor can be extended to the case of a tubular reactor without serious additional approximation. For a tubular reactor of radius r and length h, the shell volume is approximately

$$V = 1.8\pi rh(D^2/k_hQ)^{1/4} \qquad (5)$$

The fraction ϕ of radicals terminating at the wall (*i.e.*, the fraction of the total reactor volume contained within the shell next to the wall) is

$$\phi = \frac{1.8}{r}\left[\frac{D^2}{k_hQ}\right]^{1/4} \qquad (6)$$

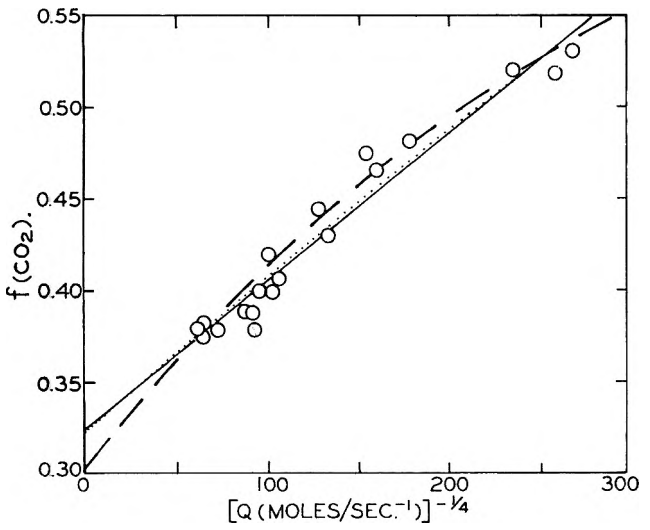

Fig. 1.—Effect of photolysis rate on product composition. $f(CO_2)$ = mole fraction of carbon dioxide in carbon-containing products; Q = intensity of illumination (expressed in terms of rate of decomposition in moles/sec^{-1}).

and

$$f(CO_2) = \phi f_w + (1 - \phi) f_h \qquad (7)$$

which can be rearranged to

$$f(CO_2) = \phi(f_w - f_h) + f_h \qquad (8)$$

Since ϕ is a function of the rate of photolysis, it is convenient to introduce a quantity B, defined as

$$B = \phi(f_w - f_h)Q^{1/4} \qquad (9)$$

for a tubular reactor

$$B = \frac{1.8(f_w - f_h)}{r}\left[\frac{D^2}{k_h}\right]^{1/4} \qquad (10)$$

Substitution of eq. 9 into eq. 8 yields

$$f(CO_2) = BQ^{-1/4} + f_h \qquad (11)$$

a plot of $f(CO_2)$ *vs.* $Q^{-1/4}$ should be linear with slope B, and its intercept at $Q = \infty$ should be f_h. Such a plot for the data of Table I is shown in Fig. 1.

The straight line in Fig. 1 was obtained by least-squares fitting of the experimental points; the r.m.s. deviation of the points from the line is 0.011 in the $f(CO_2)$ direction. An imprecision of this magnitude is about that associated with an individual determination of $f(CO_2)$; within this modest experimental error, the experimental results conform satisfactorily to a relation of the form of eq. 11.

The slope of the line in Fig. 1, which may be taken as B_{exp}, is 7.95×10^{-4} (moles sec.$^{-1}$)$^{1/4}$. It is of interest to compare B_{exp} with a B_{calc} obtained from simple considerations.

If the "hard-sphere approximation" is assumed, the mean diffusion coefficient for the radicals in the formic acid vapor is

$$D = \frac{3}{8n\sigma_{RF}^2}\left[\frac{RT}{2\pi}\left(\frac{1}{M_R} + \frac{1}{M_F}\right)\right]^{1/2} \qquad (12)$$

where n is the number of molecules per cc., σ_{RF} the formic acid–radical collision diameter (estimated to be 4.8×10^{-8} cm.), and M_R and M_F are the mean molecular weights of the radicals (taken as 23) and the formic acid vapor, respectively. The value of M_F is taken as the number average

$$M_F = 92/(1 + \alpha) \qquad (13a)$$

where α is the degree of dissociation of the dimer. These estimates lead to the value $D = 9.42$ cm.^{2} sec.$^{-1}$.

The homogeneous rate constant k_h can be calculated from collision theory

$$k_h = 4\sigma_{RR}^2 (\pi RT/M_R)^{1/2} \exp(-E/RT) \qquad (13b)$$

We assume zero activation energy for radical recombination and take 3.5×10^{-8} cm. for σ_{RR}; then, $k_h = 2.88 \times 10^{-10}$ cm.^{3} molecule^{-1} sec.$^{-1}$.

Substitution of the calculated values of D and k_h and the value $r = 4.0$ cm. into eq. 10 yields

$$B_{calc} = 5.50 \times 10^{-4}(f_w - f_h) \qquad (14)$$

We take the value $f_h = 0.325$ from Fig. 1; f_w is not obtained so easily. It can be assumed that f_w is the low Q limit of $f(CO_2)$; but, the slope near $Q = 0$ of a plot of $f(CO_2)$ is so large that reliable extrapolation is not possible. The minimum value of f_w is estimated to be 0.60, while the maximum is unity. Thus, we have $B_{calc}(min) = 1.51 \times 10^{-4}$ and $B_{calc}(max) = 3.71 \times 10^{-4}$, which are to be compared with $B_{exp} = 7.95 \times 10^{-4}$, all of these quantities being expressed in the units (moles sec.$^{-1}$)$^{1/4}$. In view of the highly approximate nature of the treatment developed above, and of the sensitivity of B_{calc} to the values assumed for the collision diameters, this is fair agreement between calculated and experimental values of B.

The Noyes approximation was developed originally for a spherical reactor and is applicable (to either a tubular or a spherical vessel) only when the shell thickness is small in comparison to the reactor dimensions. The largest shell thickness in the present experiments occurs at the lowest rate of irradiation, and is about a centimeter; the mean shell thickness over the whole range of irradiation rates is about 2 mm. We believe that these shell thicknesses are sufficiently small that the Noyes approximation may be assumed except, perhaps, at the very lowest values of Q.

Figure 1 indicates that $f(CO_2)$ is a linear function of $Q^{-1/4}$ within the experimental imprecision, as predicted for a uniformly illuminated reactor. Though Q was varied by a factor of 315, the range of $Q^{1/4}$ encompasses only a factor of 4.2, so modest deviations from actual linearity of the plot in Fig. 1 would be difficult to establish. A detailed analysis of the effects of absorption and radiation polychromaticity shows that important effects on $f(CO_2)$ attributable to these sources would lead to a dependence other than on $Q^{1/4}$; apparently, the corrections for polychromaticity and non-uniformity of illumination are small.

More Complex Models.—In the derivation of eq. 11 it was assumed that product formation occurred *via* a pair of types of competitive radical termination processes. It is possible that the actual mechanism of the photolysis involves the admixture of other routes to the products. In this section we give preliminary attention to such possibilities.

Suppose that the fraction of the carbon-containing products produced *via* an alternate path is α; there will be an f_α characteristic of that path, and we can write

$$f(CO_2) = (1 - \alpha)\,[\phi(f_w - f_h) + f_h] + \alpha f_\alpha \qquad (8')$$

$$= (1 - \alpha)BQ^{-1/4} + [(1 - \alpha)f_h + \alpha f_\alpha] \qquad (15)$$

Provided both α and f_α are independent of Q, eq. 15 has the same dependence on Q as eq. 11, and a plot such as that in Fig. 1 will be linear and not necessarily indicative of the occurrence of the "α" process. Changes of reaction conditions which result in suppression of the "α" process will, however, provide information from which one can obtain both α and f_α.

Gorden and Ausloos[7] have concluded that near room temperature the direct rearrangement of formic acid into product pairs

$$\mathrm{HCOOH} \rightarrow \left\{ \begin{array}{l} \mathrm{CO_2 + H_2} \\ \mathrm{CO + H_2O} \end{array} \right\} (r, f_r) \qquad (16)$$

accounts for only a few per cent of the yield of products. (It was for this reason that this mode of reaction was not considered earlier in this Discussion.) The value, f_r, of $f(CO_2)$ characteristic of this route to the products is certainly independent of Q and of all other experimental variables but wave length, with the possible exception of secondary effects arising in the monomer–dimer equilibrium. The value, r, of the fraction of the product yield produced by these rearrangement processes is also independent of Q, being determined by the comparative *rearrangement* and *radical-pair formation* reaction probabilities. We would expect that a plot of $f(CO_2)$ *vs.* $Q^{-1/4}$ for the *radical termination plus direct rearrangement* mechanism would be linear; however, if the latter component were very important, r nearly unity, the line could lie so close to the horizontal that the contribution of radical termination would be masked. Since the slope of such a linear plot depends also upon the factor $(f_w - f_h)$, the large slope observed in this investigation may be taken as confirmation of the conclusion of Gorden and Ausloos that direct rearrangement is a path of small importance in the production of products.

Another family of unimolecular processes yielding product species are those which occur subsequent to the formation of radical pairs in the dissociations

$$\mathrm{HCOOH} \rightarrow \left\{ \begin{array}{l} \mathrm{H + COOH} \\ \mathrm{HCO + OH} \\ \mathrm{HCOO + H} \end{array} \right\} \qquad (17)$$

following light absorption, such as

$$\left. \begin{array}{l} \mathrm{COOH} \rightarrow \left\{ \begin{array}{l} \mathrm{CO + OH} \\ \mathrm{CO_2 + H} \end{array} \right. \\ \mathrm{HCO} \rightarrow \mathrm{CO + H} \\ \mathrm{HCOO} \rightarrow \left\{ \begin{array}{l} \mathrm{CO_2 + H} \\ \mathrm{O + HCO \rightarrow H + CO} \end{array} \right. \end{array} \right\} (u, f_u) \qquad (18)$$

Each of the reactions listed in eq. 18 which forms a product molecule yields another radical also; that is, these unimolecular processes do not change the numerical population of the radicals importantly, though they alter its character. This change in the character of the radical population affects the calculated average values of D and k_h, but does not in any other new respect alter the application of the Noyes approximation to the situation at hand.

It seems simplest, in treating the complexities introduced by the occurrence of unimolecular radical decompositions in the gas phase, to retain the "single radical" notion of the Noyes approximation. Let k_u be a mean specific rate constant for unimolecular generation of products in the gas phase, defined subject to those limitations[9] of the Noyes approximation operating for k_h, D, etc. In general, f_u is a function of the composition of the population of radicals "available" for unimolecular decomposition in the photochemical steady state; in turn, this composition depends upon k_u, k_h, D, and Q as does the value of u, the fraction of the yield due to unimolecular decompositions of radical intermediates.

Since the relative importance of the radical *termination* processes increases more rapidly than first-order with respect to R, the steady-state concentration of the radicals, u will decrease with increasing Q. If $k_u \gg k_h R$, the effect of increasing Q (over a range similar to that covered in the experiments described herein) is slight and $f(CO_2) \cong f_u$, here virtually a constant, at any Q. The contribution of f_w to $f(CO_2)$ is vanishingly small under these conditions. If $k_u \ll k_h R$, unimolecular decomposition is unimportant in competition with wall and gas phase radical terminations, and the dependence of $f(CO_2)$ on Q is as shown in eq. 11.

The case where $k_u \approx k_h R$ is much more complicated. For convenience, we shall assume that f_u is constant, as f_h and f_w have been assumed to be, although all three are likely slowly—varying functions of Q, as are k_u, k_h, and D; further, we shall limit our discussion to the situation exemplified by the plot in Fig. 1, where $(f_w, f_u) > f_h$. In this example, u falls as Q increases; the slope of the plot of $f(CO_2)$ *vs.* $Q^{-1/4}$ increases with rising Q, resulting in a curve concave somewhat downward in the region of $Q^{-1/4} = 0$.

Examination of a data plot of the type of Fig. 1, but one without any smooth curves on it, leads to the conclusion that a quite resonable curve through the experimental points would be one such as that formed by the long dashes in Fig. 1; this curve will be designated Case II, the linear fit Case I. Case III is represented by the dotted curve in the figure; the latter is a "barely non-linear function" type of curve. In order to compare the physical models which underlie these three Cases, some reasonable, but arbitrary, parameter selections have been made: (a) $f_u = f_h + 0.100$, and (b) $u = 0$ when $Q = \infty$. The results of calculations made with the appropriate form of eq. 15 are shown in Table II. It is seen that demonstrated

TABLE II

FRACTION u, OF TOTAL PRODUCT YIELD RESULTING FROM UNIMOLECULAR GAS-PHASE RADICAL DECOMPOSITIONS

			$Q^{-1/4}$ (mole/sec.$^{-1}$)$^{-1/4}$			
Case	$B_{exp} \cdot 10^4$	u_{calc}	0	100	200	300
I	7.95		0[a]	0	0	0
II	12.13		0[a]	(0.2)[b]	0.35	0.41
III	8.69		0[a]	(0.06)	0.11	0.21

[a] These values are assumed. [b] Values in parentheses have associated with them calculation errors of magnitudes similar to their own.

curvature of a plot such as that in Fig. 1 implies the occurrence, in the mix of reactions leading to products,

of at least one process whose α value depends upon Q—in the present example, one or a group of unimolecular gas phase decompositions of radical intermediates competitive with radical termination processes.

Before this conclusion is accepted, it is important that some additional information concerning this (these) unimolecular reaction(s) be developed. Let us assume, for the sakes of argument and some crude computations, that k_h is sufficiently large that, under conditions of illumination like those employed in the experiments described above, ϕ (the fraction of radicals terminating at the wall) may be neglected; further, assume that k_h has no associated activation energy, and so has a high value such as that calculated above, eq. 13: $k_h = 2.88 \times 10^{-10}$ cm.^{3} molecule^{-1} sec.$^{-1}$ = 1.73×10^{14} cm.^{3} mole^{-1} sec.$^{-1}$. When $u = 0.5$, the steady-state condition is equivalent to the approximation

$$k_u R + k_h R^2 = 2k_h R^2 = Q \qquad (19)$$

from this equality, k_u, and the known range of Q, we calculate $R = (1.2 - 20.4) \times 10^{-14}$ mole cm.$^{-3}$. The corresponding range of k_u is (2.0 − 35.2) sec.$^{-1}$; this is the specific rate constant for a relatively slow unimolecular reaction—certainly, it is much too low to be characteristic of the decompositions of *excited* radicals.

Additional complexity of the photolysis mechanism can be considered in terms of equations similar to those derived above. Mention will be made here of only one other possibility: that in which just one of the reactions in eq. 18, say COOH → CO_2 + H, occurs when the radicals are hyperthermal, while the others may or may not be effective competitors with the earlier described radical termination processes. In such a situation, provided f_w and f_h differ significantly, the character of the plot of $f(CO_2)$ *vs.* $Q^{-1/4}$ depends upon the relation of $k_h R$ to the mean k_u for the *non-hyperthermal* unimolecular decompositions exactly as discussed at length above, because αf_α for the hyperthermal reaction is independent of Q. Polychromaticity and nonuniformity of illumination seem to be much more attractive explanations of the possible deviation from linearity of the plot in Fig. 1 than the assumption of slow unimolecular radical decomposition processes.

Acknowledgments—This research was sponsored by the U. S. Atomic Energy Commission. We are indebted to Professors Aron Kuppermann and R. Linn Belford for helpful interest and discussion, and to a referee for his suggestion that we consider our original neglect of unimolecular reactions in the gas phase.

A THERMODYNAMIC STUDY OF THE THORIUM–OXYGEN SYSTEM AT HIGH TEMPERATURES[1]

BY R. J. ACKERMANN, E. G. RAUH, R. J. THORN

Argonne National Laboratory, Argonne, Illinois

AND M. C. CANNON

Department of Chemistry, Utah State University, Logan, Utah

Received August 8, 1962

The evaporation behavior of the thorium–oxygen system in the temperature range 2000–3000°K. has been studied. The results of the effusion measurements of the dioxide phase and liquid metal–dioxide mixtures and a mass spectrometric investigation of the former have been combined to yield an internally consistent set of thermodynamic data for the system. The solid dioxide evaporates congruently at all temperatures. Above 2800°K. there is a measurable but thermodynamically insignificant substoichiometry, $ThO_{1.998}$. The "effective" pressure based on the assumption that the vapor is comprised entirely of dioxide molecules is given by the equation $\log p_e$ (atm.) = (8.26 ± 0.13) − (3.55 ± 0.03)$10^4/T$. The average heat and entropy of sublimation of the solid dioxide to ThO_2(g) are 158.7 ± 2.5 kcal. mole^{-1} and 35.3 ± 1.0 e.u., respectively, and the respective values for the reaction ThO_2(s) = ThO(g) + O(g) are 347.0 ± 3.1 kcal. mole^{-1} and 76.9 ± 1.4 e.u. The standard free energies of formation of the gaseous thorium oxides are $\Delta F_f^0(ThO_2) = -138{,}600 + 11.4T$ (2000–3000°K.) and $\Delta F_f^0(ThO) = -10{,}300 - 14.4T$ (2000–3000°K.). Upper limits to the dissociation energies at absolute zero of ThO_2(g) and ThO(g) are $D_0(ThO_2) \leq 16.3$ e.v. and $D_0(ThO) \leq 8.3$ e.v. The reaction occurring in thoriated tungsten filaments is discussed.

Introduction

Although thorium is generally considered to be the first member of the 5f "actinide" series, the high temperature chemical behavior of its oxides closely parallels that of the oxides of the group IV transition metals, zirconium and hafnium, in that the +4 valence state in the solid and both +4 and +2 states in the vapor exhibit paramount stability. This similar behavior is perhaps to be expected since the electronic configuration $nd^2\ (n+1)s^2$ is common to all three metals. Because of the refractory nature of thorium dioxide, vaporization studies utilizing the effusion method are a convenient means of obtaining chemical bond energies and, more importantly in a thermodynamic sense, the standard free energies of formation of the gaseous molecules which exist at high temperatures. Previous determinations[2-4] of the vapor pressure of ThO_2 have been critically reviewed[5] and appear to be in error because of inaccurate measurement of the temperature, reduction of the sample by the effusion cell, and nonequilibrium conditions resulting from too little sample. Darnell, *et al.*,[6] report the vapor pressure of thorium

(1) Based on work performed under the auspices of the U. S. Atomic Energy Commission.

(2) E. Shapiro, *J. Am. Chem. Soc.*, **74**, 5233 (1952).

(3) M. Hoch and H. L. Johnston, *ibid.*, **76**, 4833 (1954).

(4) R. J. Ackermann and R. J. Thorn, "Vaporization Properties of Thoria," 133rd National Meeting of the American Chemical Society, San Francisco, Calif., 1958.

(5) R. J. Ackermann and R. J. Thorn, Ch. 2 of "Progress in Ceramic Science," Pergamon Press, Oxford, 1961.

metal and the effect of oxygen contamination thereon from which the dissociation energy of ThO(g), 8.5 e.v., was estimated. More recently, Darnell and McCollum[7] have measured effusion rates for both solid dioxide and mixtures of metal and dioxide. In the case of the dioxide the method of determining the effusion rates over a 300° temperature range yielded data which when treated in accordance with the second law of thermodynamics resulted in a precision of ±5 kcal. mole^{-1} in the heat of sublimation. An attempt to increase the precision in the heat of sublimation by a third law treatment of the data is precluded since there are no reliable free energy functions for the gaseous thorium oxides. In the case of the mixtures the monoxide was shown mass spectrometrically to be the principal gaseous species, but since the solubility of the dioxide in liquid thorium was found to be rather extensive and significantly temperature-dependent, the activities of the components in the condensed phases cannot be accurately obtained by the assumption of Raoult's law and hence an accurate evaluation of the thermodynamic properties of the gaseous monoxide is not possible.

The experimental goals of the present investigation were these:

(1) To measure more precisely the effusion rate of thorium-containing species from solid dioxide over a large range of temperature in order to minimize the effect of experimental errors in the subsequent treatment of the data by means of the second law of thermodynamics.

(2) To measure the effusion rate of gaseous monoxide from a metal–dioxide mixture under experimental conditions where the solubility of the dioxide in the liquid metal is minimized and practically insignificant.

(3) To examine mass spectrometrically the composition of the vapor and the temperature dependence of the predominant species in equilibrium with the dioxide phase.

(4) To demonstrate that the dioxide phase evaporates congruently and essentially stoichiometrically.

From these measurements it will be possible to derive the standard free energies of formation and dissociation energies for ThO(g) and ThO_2(g) and to demonstrate the extent of reduction of thoria by tungsten in a discussion of the reaction occurring in thoriated tungsten filaments. It will be shown that tungsten does not significantly reduce thoria at high temperatures and it is suggested that carbon is present in tungsten filaments as an impurity and accounts for the reduction of thoria and the evaporation behavior observed by previous investigators.

Experimental Methods and Apparatus

A variety of experimental adaptations of the effusion method were utilized in the present investigation in order to minimize systematic errors. Basically, the effusion method allows one to calculate the vapor pressure p of a condensed phase from the measured mole effusion rate z (moles cm.$^{-2}$ sec.$^{-1}$) of the vapor having a molecular weight M and an absolute temperature T *via* the equation

$$p = Z(2\pi MRT)^{1/2} \qquad (1)$$

All effusion cells used in the present investigation were made of tungsten. Temperature measurements were carried out by means of a calibrated optical pyrometer[8] and it is believed that the absolute accuracy of these measurements is within 10° over the range of the present investigation. All temperatures reported herein correspond to the cavity of the effusion cell and have been corrected for an interposed window and prism. The samples of thorium and thorium dioxide were 99.9% pure as established by spectroscopic analysis. Mass spectrometric analysis confirmed that any volatile impurities were less than 1% of the thorium-containing vapor species. Subsequent to the evaporation studies spectroscopic analysis showed that the dioxide samples contained less than 1% tungsten.

The mass effusion rate of ThO_2 from a tungsten cell was measured in a collection-type apparatus essentially the same as described previously.[9] The amount of thorium collected on the plates was determined by neutron activation analysis shown by the scheme

$$Th^{232}(n,\gamma)\ Th^{233} \xrightarrow{23.3m\ \beta^-} Pa^{233} \xrightarrow{27.4d\ \beta^-} U^{233}$$
$$Pa^{233} \xrightarrow{313\ kev.\ \gamma}$$

The condensation plates were 0.75 in. in diameter and 0.005 in. thick and were made from Corning's ultrasonic grade of fused silica which contains less than a few parts per million total impurities. After exposure in the vapor pressure apparatus a series of the plates containing unknown amounts of thorium were packaged for thermal neutron irradiation by separating the targets with fused silica annuli and by interspersing plates containing known amounts of thorium as standards. The standard plates were prepared by transferring to the plate with a micropipet a volume of an aqueous solution of known concentration of thorium and then evaporating to dryness in a desiccator. In general, for plates containing of the order of 10^{-7} g. 2-hr. irradiations were sufficient to produce reliably measurable amounts of Pa^{233}. The amount of Th^{232} present on the plates was then determined by quantitatively counting the 313 kev. γ[10] of Pa^{233} by means of a γ-ray spectrometer. The plates with known amounts of Th^{232} provided the necessary relationship between counts per minute and weight of Th^{232}. It also was possible to utilize the 98.4 kev. K_α X-ray[11] of U^{233} which is emitted simultaneously with the 313 kev. γ of Pa^{233}.

The total mass effusion rate of thorium dioxide and of mixtures of thorium metal and dioxide were measured over a relatively short range of temperature by means of the vacuum balance and effusion cell assembly similar to that previously described.[12] Relative rates of evaporation of ThO_2 and ThO were measured by means of a Bendix Model 12-101 time-of-flight mass spectrometer. The tungsten effusion cell assembly and the operational characteristics of the instrument have been described previously.[12]

Results

Three series of collector plates were exposed to the vapor effusing from tungsten effusion cells containing approximately 0.5 g. of ThO_2 and these plates along with standard plates subsequently were analyzed for thorium by neutron activation analysis. The results in order of exposure of one of these series, which is typical of all the measurements, are given in Table I. The weight of ThO_2 on each plate determined by activation analysis is given in column 2. The "effective" pressure given in column 5 was calculated from eq. 1 in which $Z = (W/Mat)\ [(d^2 + r^2)/r^2]$, $M = 264$ based on the assumption that the vapor was comprised en-

(6) A. J. Darnell, W. A. McCollum, and T. A. Milne, *J. Phys. Chem.*, **64**, 341 (1960).

(7) A. J. Darnell and W. A. McCollum, NAA-SR-6498, September 15, 1961.

(8) F. Hoffmann and C. Tingwaldt, "Optische Pyrometrie," Edwards Bros., Inc., Ann Arbor, Mich., 1944. See also Natl. Bur. Standards (U. S.) Tech. New Bull. 43 (6), 114 (1959).

(9) R. J. Ackermann, P. W. Gilles, and R. J. Thorn, *J. Chem. Phys.*, **25**, 1089 (1956).

(10) D. Strominger, J. M. Hollander, and G. T. Seaborg, *Rev. Mod. Phys.*, **30**, 814 (1958).

(11) C. E. Crouthamel, "Applied Gamma-Ray Spectroscopy," Pergamon Press, Oxford, 1960.

(12) R. J. Ackermann and E. G. Rauh, *J. Chem. Phys.*, **36**, 448 (1962).

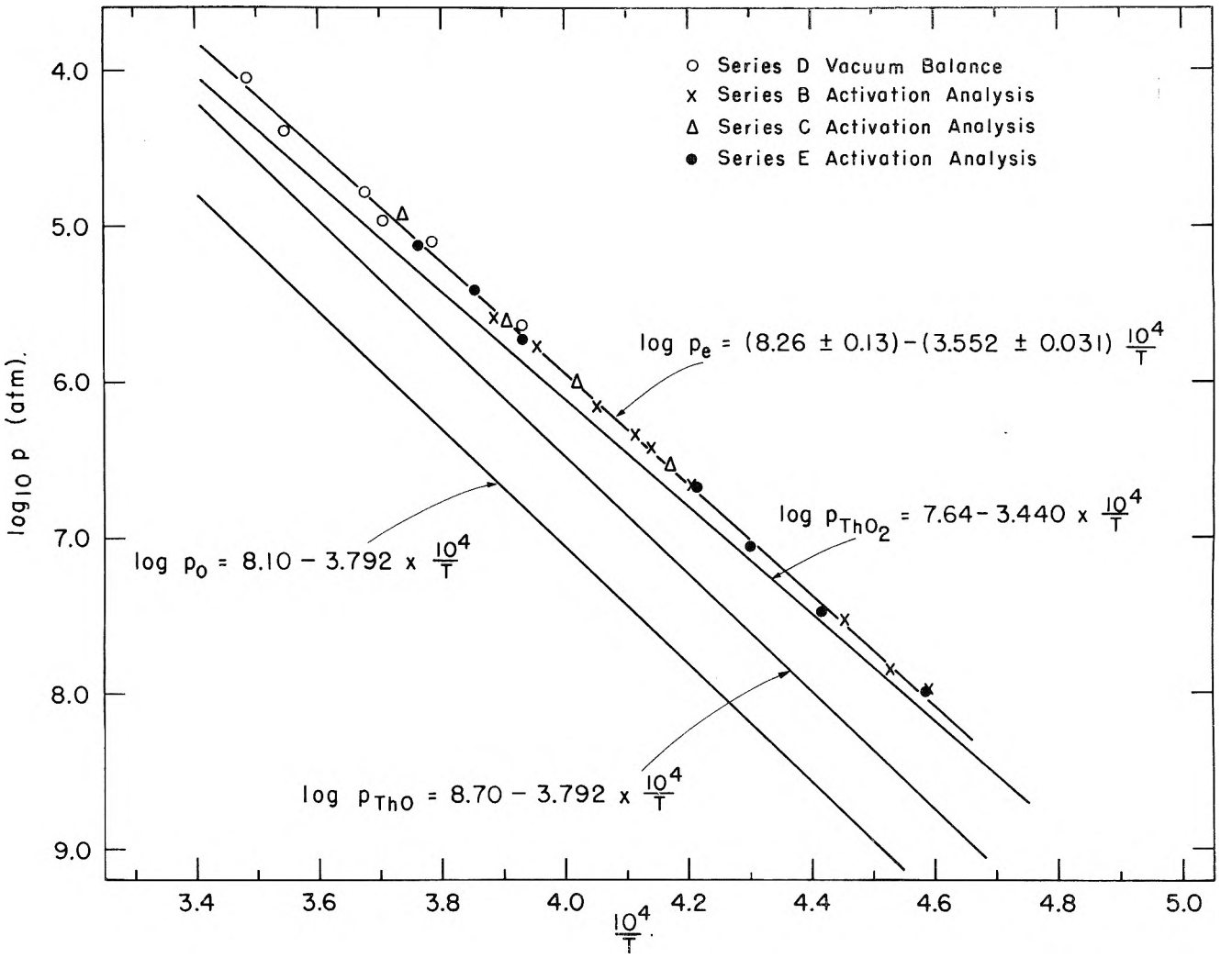

Fig. 1. —The temperature-dependence of the "effective" pressure and the partial pressures of predominant vapor species in equilibrium with solid thorium dioxide.

tirely of $ThO_2(g)$, and a, r, and d have the values given in Table I.

The total mass effusion rate of ThO_2 from a tungsten effusion cell containing a channel orifice (diameter = 0.158 cm., length = 0.299 cm.) was determined by means of the vacuum balance.[12] The dimensions of the orifice necessitated the use of a Clausing factor,[13] $K = 0.417$. The resulting data are shown in the order of determination in Table II-A. The weight losses of the empty tungsten effusion cell were determined at six arbitrary temperatures over the range of the effusion measurements and the particular weight loss at a chosen temperature then was calculated from a least squares equation. The calculated weight loss at each temperature is shown in column 2, and in column 3 is given the corresponding net weight loss of ThO_2. The "effective" pressures were calculated from eq. 1 in which $Z = 1.04W/MKat$. The factor of 1.04 was necessary to correct the observed weight losses for the fraction of the effusate that condensed on the support rods and hence was not weighed by the balance. The results of all measurements of the effusion rate of ThO_2 are shown in Fig. 1. If one calculates an effective pressure p_e by assuming the vapor to be comprised entirely of dioxide molecules, the experimental data can be represented by the equation

$$\log p_e \text{ (atm.)} = (8.26 \pm 0.13) - (3.55 \pm 0.03)10^4/T \quad (2)$$

A limited investigation of the effusion rate of ThO(g)

Table I

The Effusion Rate of ThO_2: Series E with Standard Plates

Counts/min.[a] 313 kev. γ Pa^{233}	ThO_2, g.	T, °K.	t, sec.	− log p_e, atm.
683	5.72×10^{-7}	2326	3600	7.064
6981	5.84×10^{-6}	2233	900	5.418
1007	8.43×10^{-7}	2374	2700	6.766
627	5.25×10^{-7}	2264	8400	7.475
4704	3.94×10^{-6}	2543	1200	5.731
257	2.15×10^{-7}	2180	10800	7.980
8967	7.50×10^{-6}	2661	600	5.138
		Counts/ min./10^{-6} g.		
4034	3.42×10^{-6}	1180		
14276	1.21×10^{-5}	1179		
1715	1.43×10^{-6}	1204		Standard
17397	1.43×10^{-5}	1221		plates
16972	1.43×10^{-5}	1191		
		Av. = 1195 ± 8		

Orifice area (a) = 8.04×10^{-3} cm.^{2}
Effective target radius (r) = 0.960 cm.
Orifice-to-target distance (d) = 7.746 cm.

[a] Corrected for background count of the silica targets, which is 39 ± 1 counts/min.

(13) S. Dushman, "Scientific Foundations of Vacuum Techniques," John Wiley and Sons, New York, N. Y., 1949.

from a mixture of liquid metal and solid dioxide was carried out. The tungsten effusion cell, similar to that

TABLE II

A. THE EFFUSION RATE OF ThO_2: SERIES D—VACUUM BALANCE

T, °K.	$W \times 10^3$ (empty cell)	$W \times 10^3$, g. ThO_2	t, sec.	$-\log p_e$, atm.
2642	0.4	2.2	2520	5.101
2720	0.7	3.2	1800	4.785
2822	0.9	3.1	720	4.393
2694	1.0	4.3	3660	4.967
2871	1.4	5.6	600	4.053
2544	0.5	3.1	12120	5.642

B. THE EFFUSION RATE OF Th–ThO_2: SERIES F—VACUUM BALANCE

	$W \times 10^3$, g. ThO	t, sec.	$-\log p_{ThO}$,[a] atm.
2337	5.2	2700	4.614
2381	2.5	900	4.451
2369	3.0	1200	4.498
2366	3.0	1200	4.498
2362	2.7	1200	4.544

[a] Uncorrected for the non-unit activity of liquid thorium.

described in a previous study,[12] (orifice diameter = 0.139 cm., length = 0.38 cm.) contained a thoria cup into which approximately 1 g. of thorium metal was added. The present authors have observed, as have Darnell and McCollum,[7] that liquid thorium is difficult to contain in the effusion cell. After several hours at high temperature the liquid is able to "dissolve" through the thoria cup, wet the tungsten, and then creep out of the cell through the orifice. When the metal is first melted it does not wet the thoria as evidenced by its pronounced convex meniscus. However, after a few hours time the meniscus becomes concave as a result of the change in physical properties of the metal phase as it slowly dissolves thoria. It therefore is difficult to determine reliably the heat of sublimation for the process

$$\text{Th(l, activity} < 1) + ThO_2(s) \longrightarrow 2ThO(g) \quad (3)$$

in which the activity is both time and temperature dependent. However, if the measurements are confined to sufficiently short time intervals during which the meniscus of the metal phase always remains convex, measurements of limited success can be achieved. The results are given in Table II-B. Samples of thorium metal that had been heated in a thoria cup at 2370°K. for 30 min. and had retained a convex meniscus upon cooling contained 0.395 and 0.380 weight % oxygen or an average of 2.8 mole % ThO_2 as determined by the method of Smiley.[14] Several samples (of the order of 5 g.) of the fragments of the thoria cups that were used to contain the liquid thorium were heated in air at 1000° in an attempt to measure deviation from ideal stoichiometry of the dioxide phase. Since no measurable weight increases ($>2 \times 10^{-4}$ g.) were observed one concludes that the dioxide phase did not dissolve a significant amount of the liquid metal and that the stoichiometric composition was maintained throughout the effusion measurements. Since the vapor pressures of thorium metal[6] and dioxide are sufficiently small at 2370°K., the weight losses given in

(14) W. G. Smiley, *Anal. Chem.*, **27**, 1098 (1955).

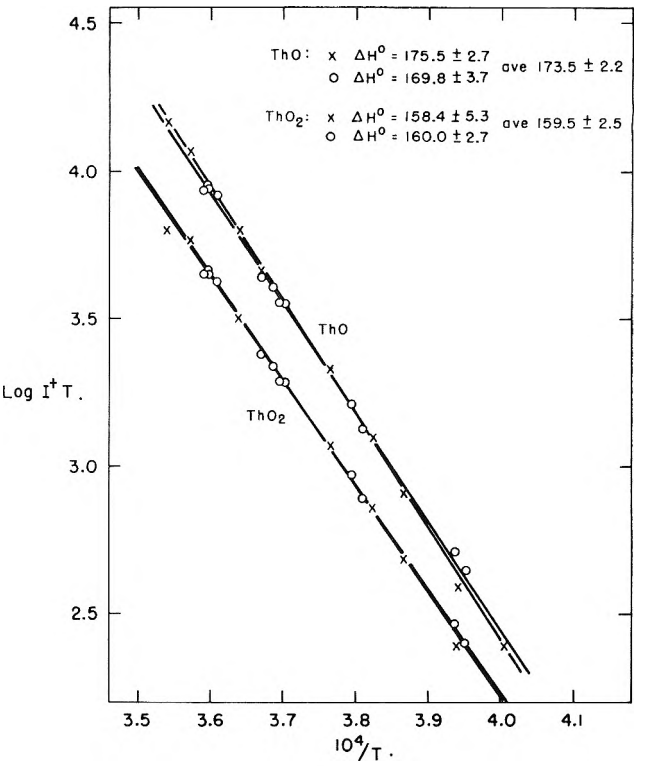

Fig. 2.—Mass spectrometric measurement of the temperature-dependence of ThO^+ and ThO_2^+ in equilibrium with solid thorium dioxide (30 e.v. ionizing electrons.)

Table II-B correspond essentially to the pressures of gaseous monoxide calculated from eq. 1. If Raoult's law is assumed, the liquid thorium phase in eq. 3 has an activity of 0.97 based on the concentration of dissolved thoria. Therefore, the monoxide pressures given in Table II-B essentially correspond to a liquid metal with an activity 0.97 and a dioxide phase at unit activity.

The mass spectrometric examination of the vapor effusing from a tungsten cell containing thoria established that both ThO_2(g) and ThO(g) are of comparable importance. The dependence of the respective intensities on the absolute temperature is shown in Fig. 2 for 30 e.v. ionizing electrons. For the purpose of plotting, the data of different runs were normalized at $10^4/T = 3.750$. The heats of sublimation 173.5 ± 2.2 and 159.5 ± 2.5 kcal. mole^{-1} for ThO(g) and ThO_2(g), respectively, were shown to be essentially independent of the ionizing electron voltage within experimental error for 25, 30, 35, and 50 e.v. electrons. Ion currents of Th^+ also were observed but were severely dependent on the electron energy and hence appeared to have resulted from fragmentation of the ThO_2 and ThO by the ionizing electrons. Subsequent thermodynamic calculation will confirm this observation. There was no evidence of volatile tungsten oxides such as WO, WO_2, WO_3, or polymers thereof. The limit of detection of such species is approximately 1/100 the ThO^+ intensity. The failure to observe such gaseous reduction products is concordant with previous observations[15] of the lack of reduction of ThO_2 by tungsten. However, other investigators,[2,16] have reported the significant reduction of ThO_2 in tungsten filaments to yield gaseous reduction products. The cause and

(15) R. J. Ackermann and R. J. Thorn, Argonne National Laboratory Report, ANL-5824, January, 1958.

(16) P. Schneider, *J. Chem. Phys.*, **28**, 675 (1958).

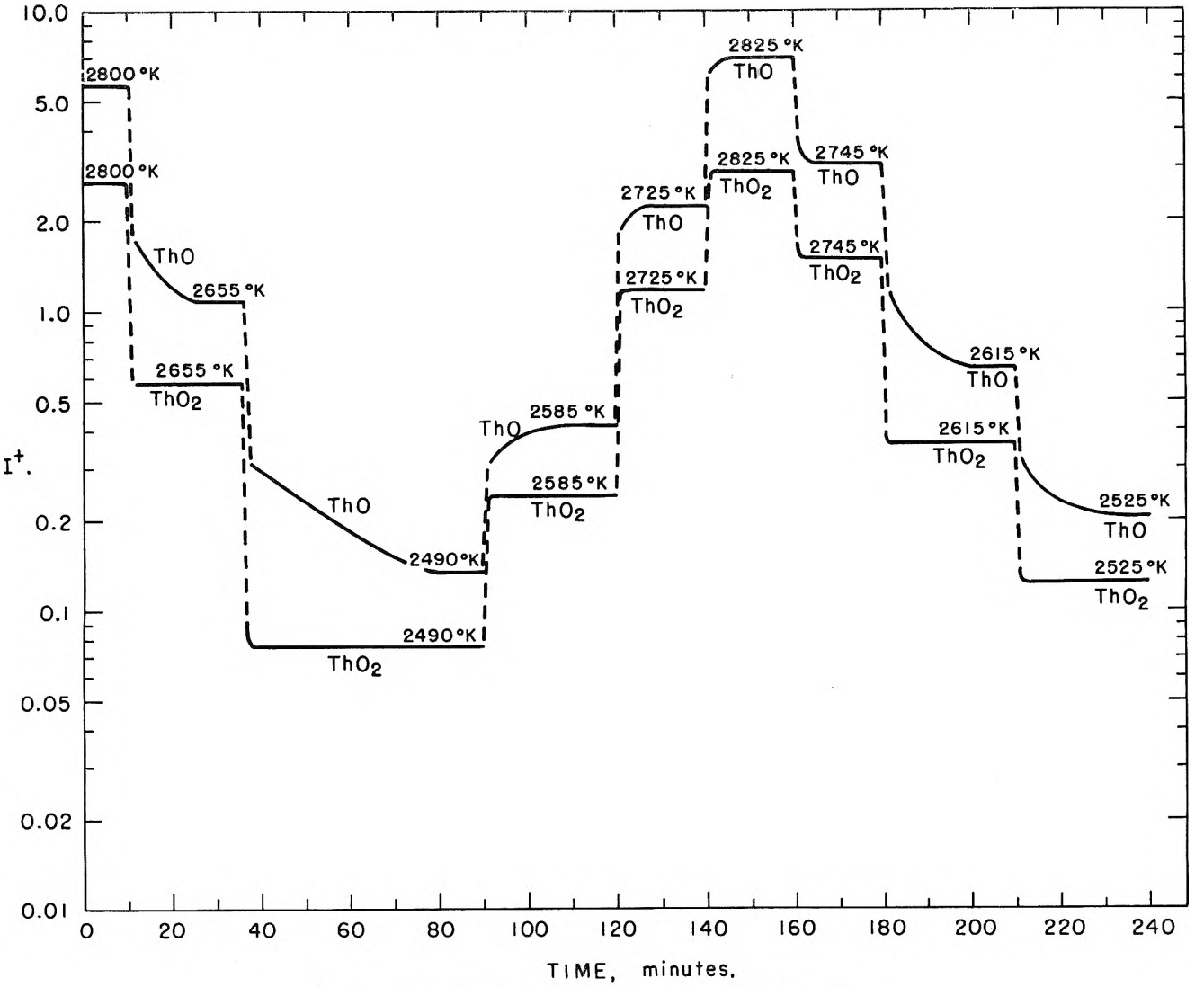

Fig. 3.—Time and temperature dependence of ThO_2^+ and ThO^+.

extent of the observed reduction will be discussed in some detail later.

Some evidence has been found for a slight deviation from stoichiometry of ThO_2 samples heated *in vacuo*. All of the residues from the evaporation studies acquired a medium gray color but rapidly reverted to the original white color when heated in air to 1200°K. Both materials had the fluorite cubic structure and lattice parameters identical within the error of measurement, *i.e.*, $a_0 = 5.5973 \pm 0.0003$ Å. Several 5-g. samples were heated *in vacuo* and analyzed by determining the weight gain when heated in air at 1200°K. Thoria which had been heated to 2800°K. was found to have the composition $ThO_{1.998}$, whereas no measurable deviation from stoichiometry was observed in samples heated to temperatures below 2600°K.

It was possible to demonstrate the effect of slight substoichiometry and the change of composition with temperature by the mass spectrometric observations shown in Fig. 3. The ThO_2^+ and ThO^+ ion currents were recorded simultaneously and continuously as the temperature of the cell was varied. The temperature of the cell could be changed from an initial value to within a few degrees of a final value in less than 1 min. In all cases the ThO_2^+ reached a constant value within 2 min. or essentially as soon as the temperature attained the final value. On the other hand the ThO^+ did not come to equilibrium immediately but decreased toward a constant value when the temperature was lowered and increased when the final temperature was higher than the initial. The rate of approach to the equilibrium value was considerably more rapid at higher temperatures and for smaller temperature increments. All of these observations appear to be correlated with the previously described composition change occurring in the sample which influences essentially only the gaseous monoxide. Since both species ultimately reached steady-state values, the solid phase must evaporate congruently, and in view of the very small substoichiometry actually detected, it will be considered to evaporate stoichiometrically.

Thermodynamics of the Thorium–Oxygen System

Using the heat capacity data of Southard[17] and Hoch and Johnston[18] for ThO_2(s), the heat capacity data of Stull and Sinke[19] for liquid thorium and diatomic oxygen, the heat of formation[20] of ThO_2(s), $\Delta H^0_{298} = -293.2 \pm 0.4$ kcal. mole^{-1}, and the absolute entropy,[21] S^0_{298}

(17) J. C. Southard, *J. Am. Chem. Soc.*, **63**, 3142 (1941).

(18) M. Hoch and H. L. Johnston, *J. Phys. Chem.*, **65**,1184 (1961).

(19) D. R. Stull and G. C. Sinke, "Thermodynamic Properties of the Elements," American Chemical Society, Washington, D. C., 1956.

(20) E. J. Huber, Jr., C. E. Holley, Jr., and E. H. Meierkord, *J. Am. Chem. Soc.*, **74**, 3406 (1952).

(21) D. W. Osborne and E. F. Westrum, Jr., *J. Chem. Phys.*, **21**, 1884 (1953).

= 15.59 e.u., one obtains for the standard free energy of formation of ThO_2(s) the equation

$$\Delta F_f^0(ThO_2,s) = -296{,}000 + 46.38T \text{ (2000–3000°K.)} \quad (4)$$

Based on the mass spectrometric identification of vapor species and the congruency of evaporation of the stoichiometric ThO_2(s), there are two principal evaporation processes, namely

$$ThO_2(s) \longrightarrow ThO_2(g) \quad (5)$$

and

$$ThO_2(s) \longrightarrow ThO(g) + O(g) \quad (6)$$

The importance of each process can be ascertained in the following manner. The standard free energy change for reaction 3 can be evaluated from the pressure of ThO(g) at 2369°K. (Table II-B) corrected for the assumed activity of liquid thorium, 0.97. When this quantity is combined with the standard free energy of formation of ThO_2(s) (eq. 4) and the standard free energy of formation of atomic oxygen,[19] one obtains the standard free energy for eq. 6, $\Delta F^0_{2369} = 164.9$ kcal. Combining this value with the average heat of sublimation of ThO(g) corresponding to eq. 6 reported in Fig. 2 one obtains for reaction 6 the standard free energy

$$\Delta F_6^0 = 347{,}000 - 76.9T \quad (7)$$

Since it has been established that the dioxide phase evaporates essentially *via* reactions 5 and 6, it necessarily follows that the mole effusion rate of ThO(g) equals that of atomic oxygen. Therefore, $p_0 = (16/248.12)^{1/2} p_{ThO}$, which fact when combined with eq. 7 yields the partial pressures of monoxide and atomic oxygen

$$\log p_{ThO} \text{ (atm.)} = 8.70 - 3.79 \times 10^4/T \quad (8)$$

and

$$\log p_O \text{ (atm.)} = 8.10 - 3.79 \times 10^4/T \quad (9)$$

It can be easily shown that the "effective" pressure given by eq. 2 is related to the partial pressures of the dioxide and monoxide *via* the relationship

$$p_e = p_{ThO_2} + (264.12/248.12)^{1/2} p_{ThO} \quad (10)$$

from which one can obtain the partial pressure of the gaseous dioxide

$$\log p_{ThO_2} \text{ (atm.)} = 7.64 - 3.44 \times 10^4/T \quad (11)$$

which is shown in Fig. 1. The heat of sublimation corresponding to reaction 5 is 157.4 ± 2.5 kcal. mole^{-1} and is in concordance with the mass spectrometric value of 159.5 ± 2.5 shown in Fig. 2, which fact illustrates the internal consistency of the mass effusion and the mass spectrometric measurements.

It is interesting to note that the internal consistency demonstrated by the two kinds of measurements allows the evaluation of the ratio of the ionization efficiencies of ThO(g) and ThO_2(g) of 3.5 to 1.

By combining eq. 7 and eq. 4 with the standard free energy of formation of atomic oxygen,[19] one obtains for the standard free energy of formation of gaseous thorium monoxide the equation

$$\Delta F_f^0(ThO,g) = -10{,}300 - 14.4T \text{ (2000–3000°K.)} \quad (12)$$

The combination of eq. 4 and 11 yields for the standard free energy of formation of gaseous thorium dioxide the equation

$$\Delta F_f^0(ThO_2,g) = -138{,}600 + 11.4T \text{ (2000–3000°K.)} \quad (13)$$

The estimation of the dissociation energies of ThO(g) and ThO_2(g) at absolute zero can be accomplished by means of the molecular constants and thermodynamic functions given in Table III. The respective values of the dissociation energy, 8.3 and 16.3 e.v., shown in Table III-A represent upper limits since the electronic states of the molecules are unknown. For the case of ThO(g) the calculated values of the absolute entropy at 2000 and 3000°K. are 3 and 5 e.u., respectively, less than those evaluated from the measured entropy of formation and the absolute entropies of liquid thorium and atomic oxygen. This discrepancy between the calculated and measured entropies probably reflects to some extent the existence of unknown low-lying electronic states. The vibrational constants for ThO(g) were estimated from the valence-bond model described by Herzberg.[22]

Discussion

The over-all agreement between the mass effusion rates of thoria reported herein (eq. 2) and those reported by Darnell and McCollum[7] [log p(atm.) = (8.16 ± 0.47) − (35,500 ± 1100)/T] is quite consistent within the precision of the respective measurements. The heat of formation and dissociation energy of ThO(g) given in Table III are in agreement with the values (−8.0 kcal. and 8.5 e.v., respectively) reported by Darnell, *et al.*[6]

The extent of reduction of ThO_2 by tungsten has been a subject of considerable discussion. The presence of approximately 1% thoria in tungsten filaments has been shown to produce electron emission which is orders of magnitude greater than that of a pure tungsten filament. The increased emission generally is ascribed to a layer of thorium atoms adsorbed on the surface of the tungsten filament, and this layer of thorium atoms is said to result from the reduction of ThO_2 to metallic thorium by the tungsten and the subsequent diffusion of the metal to the surface,[23,24] Shapiro[2] has reported relatively large losses of tungsten from filaments at temperatures above 2400°K. which cannot be attributed to the vapor pressure of pure tungsten. It was concluded that the loss of tungsten results from the reduction of ThO_2 by tungsten to produce volatile oxides of tungsten. Measurements of the evaporation rate of thorium-bearing species from thoriated tungsten filaments both carbonized and non-carbonized have been reported recently by Schneider,[16] who has demonstrated that heating at 2150°K. for 5 min. causes an appreciable fraction of the thoria content of the filament to be reduced to metal without producing appreciable evaporation of the metal. It is, however, significant to note

(22) G. Herzberg, "Infrared and Raman Spectra of Polyatomic Molecules," D. Van Nostrand, New York, N. Y., 1945.
(23) I. Langmiur, *Phys. Rev.*, **22**, 357 (1923).
(24) C. J. Smithells, *J. Chem. Soc.*, **121**, 2236 (1922).

Table III

A. Molecular Constants and Thermodynamic Properties of Gaseous Thorium Oxides

Property	ThO(g)	ThO_2(g)	References: ThO	References: ThO_2
Interatomic distance, Å.	1.93	~1.9	6	Estimated
Vibrational constant(s), cm.$^{-1}$	740	715,305(2), 763	[a]	Estimated
Electronic ground state	($^3\pi$)	($^1\Sigma$)	[a]	Assumed
Heat of formation, cal. (2000–3000°K.)	−10,300	−138,600	Eq. 12	Eq. 13
Entropy of formation, e.u. (2000–3000°K.)	+14.4	−11.4	Eq. 12	Eq. 13
Dissociation energy (0°K.), e.v.	≤8.3	≤16.3		

B. Thermodynamic Functions for ThO(g), ThO_2(g), and ThO_2(s)

	ThO(g)[b]		ThO_2(g)[b]		ThO_2(s)[c]	
T, °K.	$H_T^0 - H_0^0$, kcal.	$-(F^0 - H_0^0)$, kcal.	$H_T^0 - H_0^0$, kcal.	$-(F_T^0 - H_0^0)$, kcal.	$H_T^0 - H_0^0$, kcal.	$-(F_T^0 - H_0^0)$, kcal.
2000	17.5	134.4	26.8	145.2	34.4	65.5
2200	19.5	149.7	29.8	162.5	38.7	75.2
2400	21.4	165.2	32.8	180.1	43.0	85.7
2600	23.3	181.0	35.8	198.0	47.5	96.6
2800	25.2	196.9	38.7	216.1	52.1	107.9
3000	27.1	212.9	41.7	234.4	56.7	119.5

[a] S. Krishnamurty, *Proc. Phys. Soc.* (London), **A64**, 852 (1951). [b] Calculated from the data given in Table III-A. Low lying electronic states are unknown and may contribute substantially to these values. [c] Calculated from data given in ref. 17, footnote a, and J. L. Margrave, paper in "Proceedings of the Symposium on High Temperature—A Tool for the Future," Stanford Research Institute, Menlo Park, Calif., 1956, p. 103.

Table IV

Reduction and Evaporation of Thoria at 2550°K.

Reaction	Pressure, atm.	Wt. loss, g./min.[a]	Ref.
(1) Reduction obsd. by Schneider		~1.4×10^{-2}	16
(2) ThO_2(s) → vapor	$p_e = 2.2 \times 10^{-6}$	1.7×10^{-4}	eq. 2
(3) ThO_2(s) + W(s) → Th(l) + WO_2(g)[b]	$p_{WO_2} = 2.5 \times 10^{-15}$	...	5 and eq. 4
(4) ThO_2(s) + W(s) → Th(g) + WO_2(g)[b]	$p_{Th} \cong p_{WO_2} = 1.15 \times 10^{-10}$	8.2×10^{-9}	5, 6, and eq. 4
(5) 2ThO_2(s) + W(s) → 2ThO(g) + WO_2(g)[b]	$p_{ThO} \cong 2p_{WO_2} = 7.1 \times 10^{-8}$	5.3×10^{-6}	5 and eq. 4 and 12
(6) ThO_2(s) + 2C(s) → Th(l) + 2CO(g)	$p_{CO} = 0.18$	...	*c* and eq. 4
(7) Th(l) → Th(g)	$p_{Th} = 5.0 \times 10^{-6}$	3.6×10^{-4}	6
(8) ThO_2(s) + Th(l) → 2ThO(g)	$p_{ThO} = 2.6 \times 10^{-4}$	2.0×10^{-2}	eq. 4 and 12

[a] The weight losses of thorium were calculated from eq. 1 and the assumption that the effective evaporating area is the surface area of the filament (≅ 4.7 cm.^{2}) multiplied by the fraction of ThO_2 contained in the filament (0.0189). Even if this latter factor is omitted the conclusions reached are unaltered. [b] Calculations involving WO(g) and WO_3(g) yield similar conclusions. [c] J. P. Coughlin, Bur. Mines Bulletin No. 542, 1954.

that all of the thoria could not be reduced, but only a fraction thereof. At approximately 2550°K. it is possible to evaporate all of the thorium metal (or reduction product) in less than 1 min. In attempting to explain this behavior, it is instructive to compare the evaporation rates for non-carbonized filaments with those calculated for possible reactions occurring in the filament. In order to make these calculations it is necessary to recall certain features of the filaments employed by Schneider. Each filament weighed approximately 1.5 g. and initially contained 1.89% ThO_2 by weight and 0.20% thorium by weight or 2.8×10^{-2} g. of ThO_2 and 3×10^{-3} g. of thorium. From an inspection of the experimental diode employed by Schneider it is reasonable to assume that at least half of the length of the filament attains the uniform reaction temperature. However, in the present discussion the calculations can be simplified if it is assumed that the entire filament (0.06 cm. diameter, 25.0 cm. long) attains the reaction temperature since at most an error of a factor of two is involved, which is insignificant for the present purpose. At 2550°K. (see Fig. 2, ref. 16) about half of the initial amount of ThO_2 is reduced to thorium metal or a volatile species all of which evaporates from the filament in less than 1 min. The results of the calculations of various reduction and evaporation processes are shown in Table IV. Clearly there is no reduction process involving tungsten metal that is capable of producing thorium metal or a volatile species containing thorium which can account for the extent of reduction and subsequent evaporation observed by Schneider. An explanation of Schneider's observations, therefore, demands the presence of a reducing agent in the filament which is capable of reducing thoria to thorium metal at temperatures greater than approximately 2000°K. Reaction 6 in Table IV demonstrates that carbon is quite capable of reducing thoria to thorium metal. Furthermore, it also has been demonstrated by Schlier[25] that carbon is a common impurity in tungsten filaments. According to his measurements a large amount of carbon monoxide is produced when an emitting tungsten filament is heated in an oxygen atmosphere of the order of 10^{-7} mm. Actually there are few, if any, reducing agents in addi-

(25) R. E. Schlier, *J. Appl. Phys.*, **29**, 1162 (1958).

tion to carbon capable of reducing thoria at high temperatures. It appears, therefore, to be a necessary conclusion that the filaments employed by Schneider contained a carbon impurity sufficient to reduce some of the thoria according to reaction 6 followed by the subsequent evaporation of gaseous monoxide *via* reaction 8. Only these two of the proposed reactions are capable of explaining quantitatively the extent of reduction and subsequent loss in weight observed by Schneider[16] if the carbon content of the filaments was of the order 0.05–0.1% by weight. This value is in reasonable agreement with the findings of Schlier.[25]

Since it has been shown that the extent of reduction of thoria by tungsten is indeed small, the previous discussion suggests that a carbon impurity in tungsten filaments is implicated in the production of thorium metal which is necessary for the enhancement of the electron emission of thoriated filaments.

DETERMINATION OF ACIDITY OF SOLID CATALYSTS BY AMMONIA CHEMISORPTION

By Yutaka Kubokawa[1]

Department of Applied Chemistry, University of Osaka Prefecture, Sakai, Osaka, Japan

Received August 27, 1962

The determination of the strength of acid sites on silica–alumina and alumina catalysts has been carried out by measuring the rate of desorption of ammonia chemisorbed on the catalysts. The activation energy of desorption is increased with decreasing amount adsorbed from 10 to 50 kcal./mole on the silica–alumina, indicating the heterogeneous nature of the distribution of acid sites. The acid strength of the alumina is found to be comparable to that of the silica–alumina. The energy distribution of acid sites on silica–alumina determined by the desorption method is markedly different from that obtained by the indicator method proposed by Benesi. The reason for such discrepancy is discussed.

Introduction

In view of the importance of acidic catalysts in the petroleum industry, a considerable amount of research on measurements of the acidity of solid catalysts has been carried out by various workers. The most general method seems to be the titration of solid catalysts in a non-aqueous medium with amines as proposed by Tamele.[2a] Benesi[2b] expanded this method to make it possible to determine the acid strength distribution using a complete set of available Hammett indicators. As pointed out by Benesi, such a method is based upon some assumptions and it also has a number of limitations in its actual application.

For measuring surface acidity, the investigation of the chemisorption of a basic gas such as ammonia at elevated temperatures seems to be very promising. Most of these studies are at present restricted to measurements of the amount adsorbed at a particular temperature.[3] If, however, the energy values of ammonia chemisorption were determined over a wide range of coverage, the information concerning the acid strength distribution would be much improved. At present, the only work along these lines seems to be that of Zettlemoyer, *et al.*,[4] who have determined the acid strength distribution from heat of immersion measurements.

In previous work[5] it has been shown that measurement of the desorption rate can give the energy relation for chemisorption on oxide catalysts over a wide range of coverage. It therefore has been undertaken to investigate the rate of desorption of ammonia chemisorbed on solid acid catalysts such as silica–alumina and alumina.

Experimental

Materials.—The silica–alumina catalyst containing 13% alumina was obtained from the Shokubaikasei Co. The alumina used in this work was the material for chromatographic use manufactured by the Wako Junyaku Kogyo Co. The impregnation of the catalysts with sodium hydroxide was carried out as follows: a solution containing the desired amount of sodium hydroxide was added to the catalysts, dried at 100°, and sintered at 400°. The final catalysts contained 3 mmoles of NaOH/g. By a similar impregnation procedure, sulfuric acid was mounted on pure silica gel for chromatographic use obtained from Mallinckrodt Chemical Works. The acid concentration was 1 meq./g. Ammonia was obtained from the thermal decomposition of ammonium chloride and purified by fractional distillation. Prior to the chemisorption experiments, the silica–alumina and alumina catalysts were evacuated at 500° for 12 hr., and the sulfuric acid mounted on silica gel at 250° for 8 hr. The surface areas determined by BET method using nitrogen adsorption were 448 $m.^2/g.$ for the silica–alumina and 190 $m.^2/g.$ for the alumina catalysts.

Apparatus and Procedure.—The amount adsorbed was determined by using a conventional constant volume apparatus. The method for measuring the rate of desorption has been described in the previous paper,[5] and will be repeated here only in outline. The chemisorbed gas was desorbed by making use of a mercury diffusion pump and the desorbed gas was collected in a McLeod gage whose pressure was followed at definite intervals. It was confirmed that the observed rate of desorption is unaffected by the reverse process, *i.e.*, readsorption. The activation energy of desorption was determined as follows. The temperature was lowered abruptly during the desorption experiment and the rates before the temperature drop were extrapolated to those for the smaller amounts adsorbed when the measurements were carried out after the temperature drop. Thus, the rates at the two temperatures corresponded to the same amount adsorbed and, the activation energy of desorption could be obtained.

Results and Discussion

Acid Strength Distribution by Desorption Method.—After ammonia was allowed to adsorb at about 250°, the temperature of the specimen was raised from −50° to 450° in stages, at each of which the activation energy of desorption was determined in the manner given

(1) Department of Chemistry, The Johns Hopkins University, Baltimore 18, Md.

(2)(a) M. W. Tamele, *Discussions Faraday Soc.*, **8**, 270 (1950); (b) H. A. Benesi, *J. Am. Chem. Soc.*, **78**, 5490 (1956); *J. Phys. Chem.*, **61**, 970 (1957).

(3) G. A. Mills, E. R. Boedecker, and A. G. Oblad, *J. Am. Chem. Soc.*, **72**, 1554 (1950).

(4)(a) J. J. Chessick and A. C. Zettlemoyer, *J. Phys. Chem.*, **62**, 1217 (1958); **64**, 1131 (1960); (b) A. Clark, V. C. F. Holm, and D. M. Blackburn have recently determined the energy values of ammonia chemisorption on silica–alumina catalysts from adsorption equilibrium measurements (*J. Catalysis*, **1**, 244 (1962)).

(5) Y. Kubokawa, *Bull. Chem. Soc. Japan*, **33**, 546, 550, 555, 739, 747, 936 (1960).

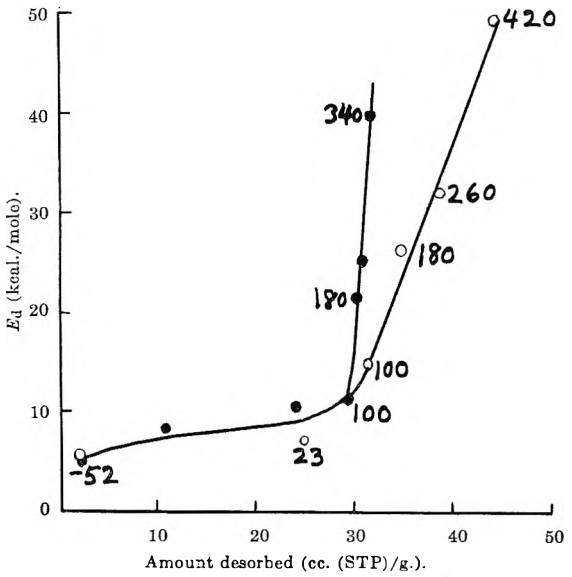

Fig. 1.—Activation energy of desorption of ammonia adsorbed on silica–alumina; —●—, NaOH impregnated; the amount adsorbed at room temperature and about 10 mm. before desorption decreased from 50.51 to 37.16 cc. after NaOH treatment. Figures indicate the temperature of desorption.

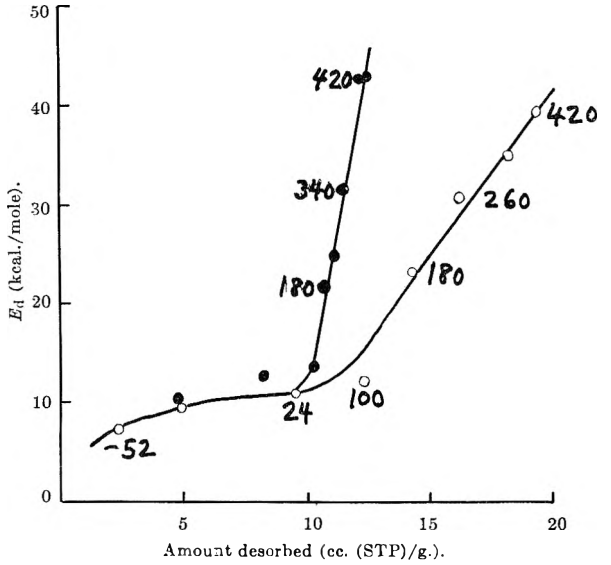

Fig. 2.—Activation energy of desorption of ammonia adsorbed on alumina; —●—, NaOH impregnated; the amount adsorbed at room temperature and about 10 mm. before desorption decreased from 22.26 to 12.57 cc. after NaOH treatment.

above, *i.e.*, by observing the rate change caused by an abrupt temperature drop during the desorption experiment. The results are shown in Fig. 1, which also contains the results of similar experiments with the catalyst impregnated with sodium hydroxide. It is seen that the curve of E_d (activation energy of desorption) against the desorbed amount is composed of two parts, one corresponding to the desorption below room temperature with E_d lower than 10 kcal./mole and the other to the desorption with higher values of E_d. For the former, the impregnation of the catalyst with sodium hydroxide has little or no effect on the amount adsorbed or on the value of E_d, whereas for the latter, the impregnation reduces markedly the amount adsorbed to about 20% of the original value. This suggests that the former is mainly associated with a physical adsorption and the latter with a chemisorption on the acid sites. It may therefore be concluded that a marked change in E_d with

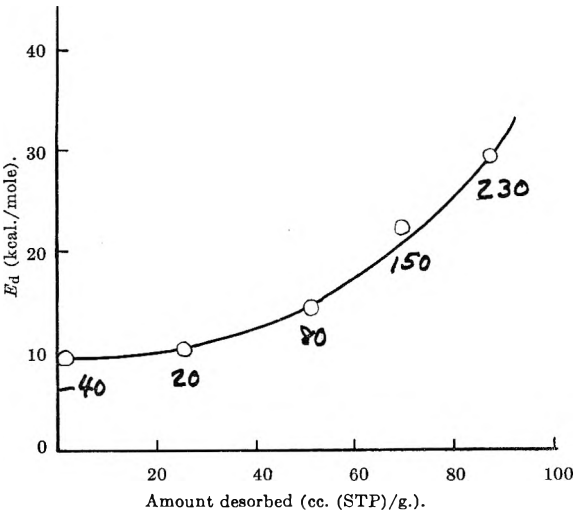

Fig. 3.—Activation energy of desorption of ammonia adsorbed on sulfuric acid mounted on silica gel; the amount adsorbed at room temperature and about 10 mm. Hg before desorption was 96.5 cc.

decreasing amount adsorbed as represented in Fig. 1 indicates the heterogeneous nature of the strengths of the acid sites and also that the energy distribution of acid sites can be obtained approximately from such plots of E_d against the amount adsorbed.[6,7] Similar experiments were carried out with the alumina catalyst. The results are shown in Fig. 2. It is seen that the acid strength of the alumina is comparable to that of the silica–alumina catalyst.

For comparison, the surface acidity of sulfuric acid mounted on pure silica gel was measured in a similar manner with the result shown in Fig. 3. It may be assumed that the desorption with E_d higher than 10 kcal./mole is associated with the acid sites produced by sulfuric acid, since all the ammonia adsorbed on non-mounted silica gel can be desorbed with E_d lower than that value. From a comparison of Fig. 1–3, it is concluded that the acid strength of alumina as well as of silica–alumina is higher than that of sulfuric acid mounted on silica gel. Such high acid strengths also have been reported by Benesi[2] using the indicator method.

Comparison of Desorption and Indicator Method.—The acidity measurements by the butylamine titration method have been carried out with the same catalysts in a manner similar to that described by Benesi. The results are represented in Table I. Although a complete set of Hammett indicators has not been used in the pres-

TABLE I

ACIDITY OF SOLID ACID CATALYSTS BY AMINE TITRATION (MEQ./G.)

Indicator	pK_a	Silica–alumina	Alumina
Dimethyl yellow	3.3	0.48	0.28
Dicinnamalacetone	−3.0	.43	.25
Benzalacetophenone	−5.6	.43	.23

(6) Strictly speaking, the values of E_d can be used as a measure of the strengths of the acid sites only in the cases where the E_d values are equal to the heats of adsorption. Even if they are different, however, such a treatment still may be correct in an approximate sense, since there seems to be little or no doubt that the heat of adsorption varies in parallel with the E_d value.

(7) According to the current physical model for the acid sites on silica–alumina, the total amount of acid sites is only a fraction of the total sites. It may therefore be allowed to assume that such a marked variation in E_d is attributed to a heterogeneity of the surface rather than interaction between chemisorbed molecules or induced heterogeneity.

ent work, the results obtained are in qualitative agreement with those of Benesi, apart from the high acid strength observed with the alumina. By means of the indicator method, Ballou, *et al.*,[8] also have found that alumina has high acid strength only when the adsorbed water vapor is completely eliminated. Such a high acid strength of alumina would be expected from the results of the desorption method described above, but there seems to be some disagreement between the conclusions obtained from the desorption and indicator methods. From the result in Table I, it is concluded that almost all of the acid sites on silica–alumina are very strong, since essentially the same acidity value has been obtained at different pK_a values. On the other hand, the desorption method indicates the presence of weak as well as strong acid sites on silica–alumina as seen in Fig. 1. The reason for such discrepancy is not apparent. It is a well known fact that the Benesi method is based upon the following assumption: the acid strength on solid catalyst can be discussed in terms of the H_0 function or pK_a value of indicators, both referring to homogeneous media, in spite of the fact that the acidity is determined from the color change of the indicator adsorbed on solid catalysts. Further work is necessary to check whether such an assumption is indeed true.

(8) E. V. Ballou, R. T. Barth, and R. A. Flinn, *J. Phys. Chem.*, **65**, 1639 (1961).

Acknowledgments.—It is a pleasure for the author to acknowledge Professor P. H. Emmett of Johns Hopkins University and Professor O. Toyama of University of Osaka Prefecture, to whom he is indebted for valuable discussion and encouragement in this work. The author also wishes to thank Mr. K. Togano and Mr. S. Kobayashi for their assistance.

FOILS OF POLYSTYRENESULFONIC ACID AND ITS SALTS. VIII. LOW-TEMPERATURE INVESTIGATION OF THE INFRARED CONTINUOUS ABSORPTION SPECTRUM OF AQUEOUS ACID SOLUTIONS

BY G. ZUNDEL AND G.-M. SCHWAB

Institute for Physical Chemistry, the University, Munich, Germany

Received August 27, 1962

In studying aqueous acid solutions, a continuous absorption spectrum is observed in the infrared. The present work discusses the question of whether this continuous absorption is connected with thermal vibrations in the hydrate complexes, or whether the high exchange probability of the excess proton in these hydrate complexes is a necessary condition for the existence of the absorption continuum. To decide this, we investigated polystyrenesulfonic acid at 90°K. by infrared spectroscopy. It was found that the continuous absorption is at least as strong at 90°K. as at 298°K. From this it follows that the continuous absorption has no connection with the thermal vibrations in the complexes. Finally, the high exchange probability of the excess proton is discussed as a cause for the existence of the continuum.

Continuous absorption has been observed in the infrared spectra of aqueous acid solutions, for the first time in the higher frequency regions as early as 1933 by Suhrmann and Breyer[1] and later by Meerlender[2]; in the lower frequency regions it was observed by Falk and Giguère[3] and by Ackermann[4] and later discussed by Wicke, Eigen and Ackermann,[5] Eigen and de Maeyer[6] and Ackermann.[4]

We have investigated this continuum more closely in polystyrenesulfonic acid foils[7] and have shown the following: The polystyrenesulfonic acid foils contain according to the degree of hydration $-SO_3^-H_3O^+$, respectively more strongly hydrated complexes as, for instance, $-SO_3^-H_7O_3^+$. In these complexes, the proton is largely free movable. Therefore, it is best described in proton boundary structures as done in Fig. 1 for the $-SO_3^-H_7O_3^+$ complex.

The present study clarifies the temperature dependence of the absorption continuum. In order to make understandable the question answered by the present experiments we shall discuss first two alternative hypotheses.

The Origin of the Absorption Continuum.—It is possible to imagine two ways in which the continuum could be produced.

First Possibility.—Between the oxygen atom of "H_2O" and that of "H_3O^+" in the hydrate complex is a potential with a small barrier. This potential barrier has to be small for the reason that the proton frequently changes from one position to the other. We may now suppose that the height and breadth of such a small potential barrier are particularly strongly affected by the thermal vibrational and rotary motions of the molecules in these complexes. The changes of the barrier effected by thermal motions could then be large in comparison with the height and breadth of the barrier at low temperatures. A model which makes this conceivable as a cause for the continuum was discussed by us in ref. 7.

Second Possibility.—The absorption continuum is caused by the high exchange probability of the excess proton within the complexes (see below).

The low-temperature test permits of a decision between these two possibilities.

The Experiments and their Results

We investigated[8a] two polystyrenesulfonic acid foils,[8b] one 5% cross-linked[8c] (Fig. 2) and one 10%

(1) R. Suhrmann and F. Breyer, *Z. physik. Chem.*, **B23**, 193 (1933).
(2) G. Meerlender, Dissertation (R. Suhrmann), Braunschweig, 1959.
(3) M. Falk and P. A. Giguère, *Can. J. Chem.*, **35**, 1195 (1957).
(4) Th. Ackermann, *Z. physik. Chem.* (Frankfurt), **27**, 253 (1961).
(5) E. Wicke, M. Eigen, and Th. Ackermann, *Z. physik. Chem.* (Frankfurt), **1**, 340 (1954).
(6) M. Eigen and L. de Maeyer, *Proc. Roy. Soc.* (London), **A247**, 505 (1958).
(7) G. Zundel, H. Noller, and G.-M. Schwab, *Z. Elektrochem.*, **66**, 129 (1962).

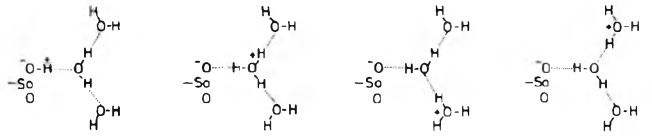

Fig. 1.—Boundary structures of the excess proton in the $-SO_3^-H_7O_3^+$-complex.

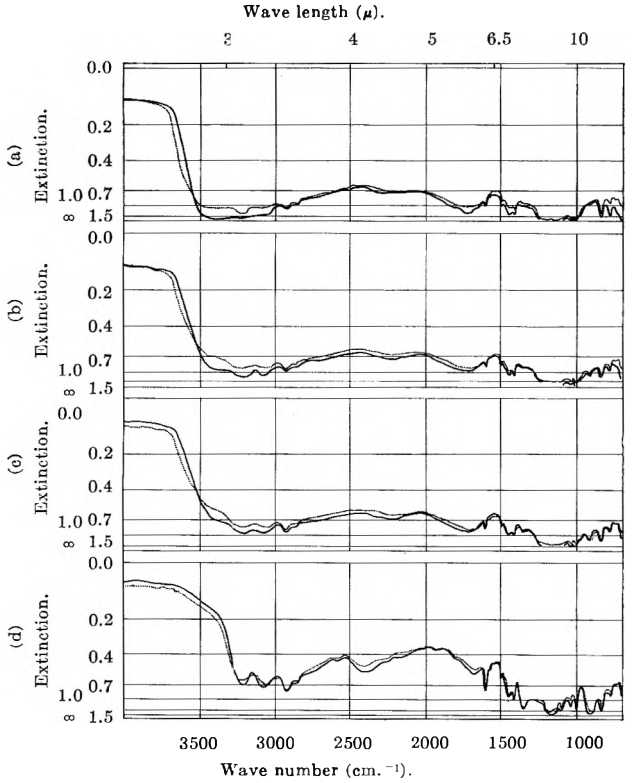

Fig. 2.—Infrared spectra of a 5% cross-linked polystyrene sulfonic acid foil: broken curve, spectrum at 298°K.; continuous curve, spectrum at 90°K. Relative humidity of the air in contact with the foil: (a) 33%, (b) 11%, (c) 7%, (d) approx. 0.1%.

cross-linked (Fig. 3), each sulfonated for 5 days. The 5% cross-linked one was naturally much more strongly sulfonated within the 5 days than the 10% cross-linked one. The 5% cross-linked one was tested with relative humidities of the air in contact with the sample of 33, 22.5, 11, 7, and approximately 0.1% (Fig. 2). The 10% cross-linked foil was tested with relative humidities of 71, 33, and 11%, as well as after three days' drying over P_2O_5 (Fig. 3). All measurements in each of these series were made on one and the same sample. The spectrum drawn with a broken line is in each case that at 298°K., that with a continuous line is that after instantaneous cooling of the sample to 90°K.

The spectra as shown in Fig. 2 and 3 will supply the following findings. The continuous absorption is at least as strong after cooling the specimen from 298° to 90°K. (comparison of the broken and continuous curves in each case). This holds for the 5% cross-linked, strongly sulfonated sample (Fig. 2) as well as for the 10% cross-linked one. Further, this result is independent of the moisture content of the specimen.

(8) (a) All measurements were made with the IR-Spectrophotometer, model 221 with grating, of the firm Bodenseewerke Perkin–Elmer G.m.b.H., Überlingen, Germany. It is intended to publish details of the method, in particular the container used, in the "Zeitschrift für Chemie-Ingenieur-Technik." (b) For methods of preparation see: G. Zundel, H. Noller, and G.-M. Schwab, *Z. Naturforschung*, **16b**, 716 (1961). (c) By per cent-cross-linking is understood the weight-percentage of divinylbenzene added in polymerization.

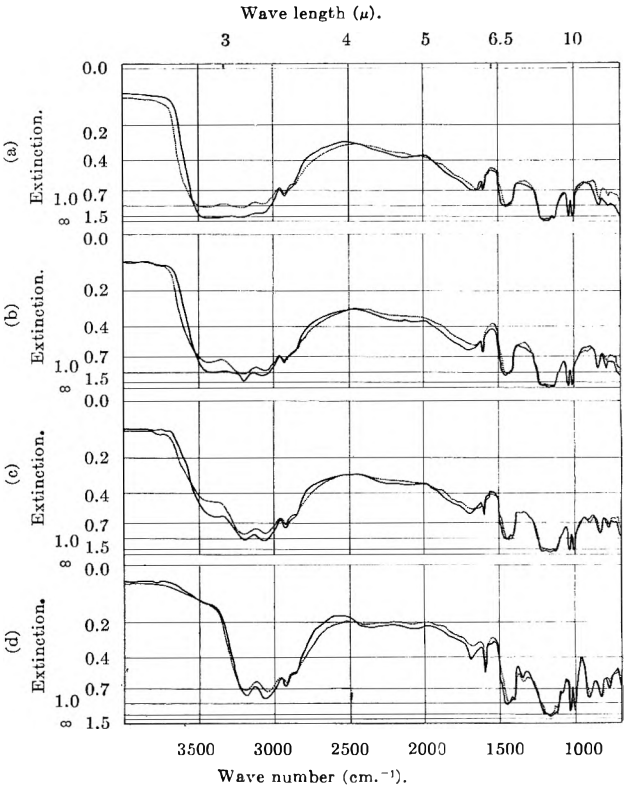

Fig. 3.—Infrared spectra of a 10% cross-linked polystyrene sulfonic acid foil: broken curve, spectrum at 298°K.; continuou curve, spectrum at 90°K. Relative humidity of the air in contact with the foil: (a) 71%, (b) 33%, (c) 11%, (d) after 3 davs' drying over P_2O_5.

The possibility is not ruled out that the intensity of the continuous absorption is even slightly increased by cooling (see in particular Fig. 2).

With the 10% cross-linked, weakly sulfonated sample, it is nevertheless observed that the absorption on the sides of the OH-bands decreases as a result of cooling. This presents the illusory appearance of a decrease of the continuous absorption here on cooling. It is nevertheless observed that the maximum extinction of the OH-bands increases considerably on cooling. This shows that this decrease of extinction on the sides of the bands is caused by a sharpening of the bands with decrease of temperature. This is naturally due to increasing restriction of thermal vibrations in these complexes on cooling the sample. The same change with temperature decrease can also be observed occasionally on other bands, however not so distinctly.

Discussion of Results

This experimental result is decisive: the thermal vibrational and rotary motions are not effective as a cause of continuous absorption. In this case the production of continuous absorption by the large exchange probability of the protons in the complexes must be discussed.

If the lifetime of a state decreases, the associated band becomes broader. Meerlender[2] has discussed his results from this standpoint. In our work, however, we do not observe broadened bands, but an absorption continuum as shown by the experimental results.

We consider it probable that, besides the fast proton transfer, coupling of the individual complexes with one another is necessary for the production of continuous absorption. The transfer of a proton within a complex presumably leads to variations of the field in the im-

mediate neighborhood of this complex. A coupling of the individual complexes could be effected by these fields. This has to be clarified later on.

Nevertheless, the present work has shown clearly that the fast proton transfers within the hydrate complexes are a necessary condition for the existence of absorption continuum. Thus, *vice-versa*, an absorption continuum with corresponding properties[7] can be regarded as a criterium for such fast proton transfers.

Acknowledgment.—We thank Dr. E. Weidemann of the Institute for Theoretical Physics of the University of Munich for many long discussions and valuable suggestions as well as for carrying out interesting calculations. We are indebted to Dr. Th. Ackermann of the Institute for Physical Chemistry of the University of Muenster, Westphalia, and Dr. M. Eigen of the Max Planck Institute for Physical Chemistry, Goettingen, for helpful discussions. We are further particularly indebted to the Deutsche Forschungsgemeinschaft for supporting this work.

RADIATION EFFECTS ON *p*- AND *n*-TYPE CATALYSTS USED IN THE THERMAL DISSOCIATION OF ETHYL ALCOHOL

BY MATTEO DONATO

Mines Branch, Department of Mines and Technical Surveys, Ottawa, Ont., Canada

Received August 28, 1962

The dissociation of anhydrous ethyl alcohol has been studied over the temperature range 330–430° with the employment of catalysts that had been exposed to a range of estimated "integrated" neutron doses of up to 96.6×10^{18} n./cm.^{2}. The catalysts are ZnO, an *n*-type semiconductor, prepared by decomposition of the carbonate, and Cr_2O_3, a *p*-type semiconductor, prepared by dehydration of the hydroxide. Measurable changes in yield and decomposition mechanism have been observed as compared with the unirradiated catalysts. The variation in the behavior of the catalysts has been related to the various neutron doses received and the results are discussed in the framework of the electronic theory of catalysis on semiconductors.

Introduction

In recent years, there has been an increasing interest in the effect of nuclear radiation on solid inorganic catalysts. This is due to the fact that catalytic behavior is strongly dependent on the structure and energy conditions of the catalyst and its structure may be modified under nuclear irradiation.[1-4] The object of the present paper is to discuss the behavior, as catalysts, of ZnO, an *n*-type semiconductor, and Cr_2O_3, a *p*-type semiconductor, before and after irradiation in the Chalk River reactor. Studies have been made of the well-known thermal dissociation reaction of ethyl alcohol that proceeds along two paths

$$\mathrm{R{-}CH_2OH} \begin{cases} \longrightarrow \mathrm{RCHO + H_2} & \text{hydrogenation} \\ \longrightarrow \mathrm{C_2H_4 + H_2O} & \text{dehydration} \end{cases}$$

The particular reaction path taken is determined at the first stage of reaction, the adsorption of the alcohol molecule, and depends on the particular bond broken in the molecule, the OH or C–OH bond; this in turn depends on the nature of the catalyst. With ZnO and Cr_2O_3 catalysts both reactions occur.

It is well known that the reactor irradiation of a solid semiconductor can generally produce the following effects: (a) direct ionization; (b) change in the degree of disorder in the lattice of the solid irradiated; and (c) nuclear reaction in the solid. Each of these effects produces a variation in the number of free carriers in the solid. The first effect is only a temporary effect. The second one can be removed by heating the sample at a high temperature. The third one, which leads to the production of impurities of different chemical character in the lattice of the solid, is a permanent effect and irreversible.

In the last twenty years many authors, such as Hauffe,[5] Schwab,[6] Garner,[7] Wolkenstein,[8] and others have developed an electronic theory of catalysis on semiconductors. According to this theory the nature of the substrate bonding determines the transfer of electrons from the adsorbed molecule to the unfilled electronic levels in the solid catalyst or from a solid with an excess of electrons to the adsorbed molecule. The well-known catalytic activity of the transition metals is thus correlated with their unfilled d-bands, and the different activities of *n*- and *p*-type semiconductors with their capability to donate or accept electrons, respectively.[9,10]

The relative activity of the catalyst, in this case for dehydration or dehydrogenation, depends on the position of the Fermi level. The lowering of the Fermi level retards dehydrogenation and accelerates dehydration.[8] In this framework, the gamma and neutron irradiation of a solid catalyst would be expected to alter its catalytic activity because the products of irradiation include trapped electrons and holes (in non-metals), displaced atoms, and impurities of a different chemical nature, due to the neutron-induced transmutations, all of which influence the electronic structure of the solid catalyst and hence its ability to interchange electrons with the adsorbed molecules on the surface.

Apparatus and Procedure.—The reaction, the decomposition of the ethyl alcohol, was observed at atmospheric pressure and at

(1) I. I. Barry, "Report to the International Congress on Catalysis," Paris, July 1960.

(2) T. Brown and I. Maxim, *Nature*, **192**, 598 (1961).

(3) R. H. Bragg, F. L. Morritz, R. Holtzman, P. Y. Feng, and F. Pizzarello, Wright Air Development Center, Technical Report 59, 986 (1959).

(4) H. W. Kohn, G. E. Moore, and E. H. Taylor, Oak Ridge National Laboratory, Progress Report 2589, 17 (1958).

(5) K. Hauffe, "Semiconductor Surface Physics," University of Pennsylvania Press, 1957.

(6) G. M. Schwab, ref. 5.

(7) W. E. Garner, "Chemistry of the Solid State," Butterworths, London, 1955.

(8) F. F. Wolkenstein, *Advances in Catalysis*, **12**, 121 (1960).

(9) S. Z. Roginsky, O. V. Krylov, and E. A. Fokina, *Bull. Acad. Sci. USSR, Div. Chem. Sci.*, 442 (1952).

(10) W. E. Garner, *Advances in Catalysis*, **9**, 169 (1957).

TABLE I

ANALYSIS OF CATALYSTS[a]

Catalyst	Surface area, m.²/g.	Elements, % Si	Mg	Fe	Cu	Ca	Al	Mn	Pb	Cd	B
ZnO	23.7	0.02	0.005	0.004	0.002	n.d.	n.d.	n.d.	n.d.	0.08	n.d.
Cr_2O_3	19.8	0.07	0.009	0.01	0.01	n.d.	n.d.	n.d.	n.d.	n.d.	n.d.

[a] n.d. = not detected.

TABLE II

(a) MAXIMUM FLUX AND (b) INTEGRATED NEUTRON DOSES[a]

Catalyst	Weight, g.	I	II	III	IV	V
ZnO	0.4	(a) not irradiated	2.3×10^{13}	3.9×10^{13}	4.6×10^{13}	4.8×10^{13}
		(b) not irradiated	13.9×10^{18}	23.3×10^{18}	59.6×10^{18}	96.6×10^{18}
Cr_2O_3	0.2	(a) not irradiated	3.3×10^{13}	5.8×10^{13}		
		(b) not irradiated	20×10^{18}	34.8×10^{18}		

[a] Fluxes in neutrons/cm.² sec.; neutron doses in neutrons/cm.².

temperatures within the range 330–390° for ZnO and 370–430° for Cr_2O_3. The experiments were carried out in a continuous flow reactor made of Vycor quartz glass.

The apparatus used in the present study consisted of an alcohol feeding system, a vaporizing unit, a reactor, an ethanol recovery system and a gas measuring device. The ethanol feed system consisted of a Milton-Roy "Minipump" that ensured a constant, slow rate of gas flow. A water condenser and a Dry Ice–acetone trap in series were used to condense the liquid products. The volume of the gaseous products was measured with a gas volumeter. The composition of the gas mixture was determined by means of a temperature-controlled chromatographic system. The samples of gas were introduced by means of a gas sampling valve which provided a convenient and highly reproducible system for sampling gas streams. A portion of the gas stream to be analyzed was allowed to flow continually through the valve. The temperature of the catalyst bed during the reaction was measured and recorded by a chromel–alumel thermocouple placed in the reactor thermocouple well. Control of the reactor temperature was maintained by adjusting the voltage to the reactor heating coil.

Preparation of Catalysts.—The zinc oxide catalysts were prepared by ignition of $ZnCO_3$ at 450° in air for 3 hr. The resulting powder was pressed into pellets and the latter were then crushed in order to have granules in the size range of 20–28 mesh. The amount of catalyst used in each test was 0.4 g. The surface area was 23.7 m.²/g.

The chromic oxide catalysts were prepared by precipitation of the hydroxide from a solution of the nitrate using ammonium hydroxide as the precipitating agent. The reagents used were highly pure Mallinckrodt "Transistar" products. The precipitate was then washed, filtered, and dried. The dry hydroxide was then ground and heated at 450° for 3 hr. in air. The dry Cr_2O_3 was pressed into pellets that were then granulated and screened to yield a 20–28 mesh product. The amount of Cr_2O_3 used in each test was 0.2 g. The surface area was 19.8 m.²/g.

The alcohol feed for both series of catalyst tests was 0.204 ml./min. Properties of the alcohol used are: refractive index $n^{25}D$ 1.3600, specific gravity G^{20}_{20} 0.7955, G^{20}_{4} 0.7914, water = 0.10% v./v., b.p. 78.2°. Four samples of ZnO and two samples of Cr_2O_3 were irradiated in the Chalk River reactor at various estimated integrated neutron doses up to 10^{20} n./cm.² at a maximum flux of 5.8×10^{13} n./cm.² sec. The estimated gamma flux was 1×10^{8} roentgens per hour.

The spectrographic analyses for the ZnO and Cr_2O_3 catalysts are presented in Table I.

The reactor irradiation conditions are presented in Table II.

The experimental variables determined consisted of feed rate, reaction time, temperature, and amount of gas evolved (hydrogen and ethylene).

From these results, the behavior of the catalyst, the reaction rates, and the percentage of conversion at various temperatures were calculated and curves of percentage conversion *vs.* temperature were plotted. Before and after each series of runs the reactor was flushed with dried argon to ensure that no air or moisture was present. The surface areas of the samples were not redetermined after irradiation, both because of handling problems presented by the high levels of radioactivity and because more even heating of the powder would be expected in a reactor than under electron bombardment[11] and hence less surface spalling.

Experimental Results

After irradiation the zinc oxide catalysts presented a yellow-brown color, whereas the green chromia catalysts did not show any change in color.

In the case of ZnO, the initial experiments indicated that on a fresh catalyst surface the activity of the irradiated catalyst was lower than on the non-irradiated one, but when the catalyst was aged by use at 390° for a few days the radioactive catalysts were more active and the ratio H_2/C_2H_4, which was changing during the first runs, reached a constant value. The reaction rate at a temperature of 390° for normal and irradiated, stabilized catalysts was found to increase with neutron dose. Figure 1 compares the proportion of hydrogen and ethylene evolved for normal and irradiated catalysts as a function of temperature. Figures 2a and 2b report the per cent conversion to hydrogen and ethylene and Fig. 2c the total conversion *vs.* the integrated neutron doses that the catalysts received, over the range of temperatures studied. It is evident that the nuclear irradiation significantly affects the reaction paths and the effect increases with irradiation times or integrated neutron doses of the solid catalyst, to reach an asymptotic value of the ratio H_2/C_2H_4.

The exposure to neutron and gamma irradiation of the Cr_2O_3 catalysts did not produce any shifting in the reaction path of the catalyst (Fig. 3 and 4) and resulted in a decrease in the activity of the two chromic oxide catalysts, as seen in Fig. 4. Such behavior of the chromic oxide catalysts was expected. The neutron irradiation of Cr_2O_3 does not result in any nuclear transmutation such as to create significant impurities of different chemical character in the specimen and the only nuclear reaction of interest is

$$Cr^{50} + n_0^1 \longrightarrow Cr^{51} + \gamma$$

Chromium-51 decays by K-capture with a 27.8 day half-life to vanadium-51, which is stable. The tests described here were done before there was any appreciable decay of chromium-51.

Discussion of Results

The neutron irradiation of ZnO results in nuclear transmutations in the solid, which lead to the produc-

(11) E. A. Mason, R. C. Reid, and N. J. Stevens, "The effect of electron irradiation prior to reaction on the activity of a semiconductor catalyst," U. S. AEC Report NYO-9217 (1961).

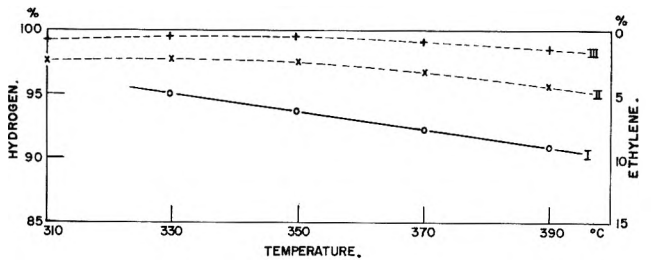

Fig. 1.—Behavior of zinc oxide catalysts at various temperatures: ethyl alcohol feed = 0.204 ml./min.; catalyst—ZnO type A, 0.4 g., 20–28 mesh; normal catalyst —O—; irradiated catalysts II - × -, integrated neutron dose 13.9 × 10^{18} n./cm.^{2}; III - + -, integrated neutron dose 23.3 × 10^{18} n./cm.^{2}.

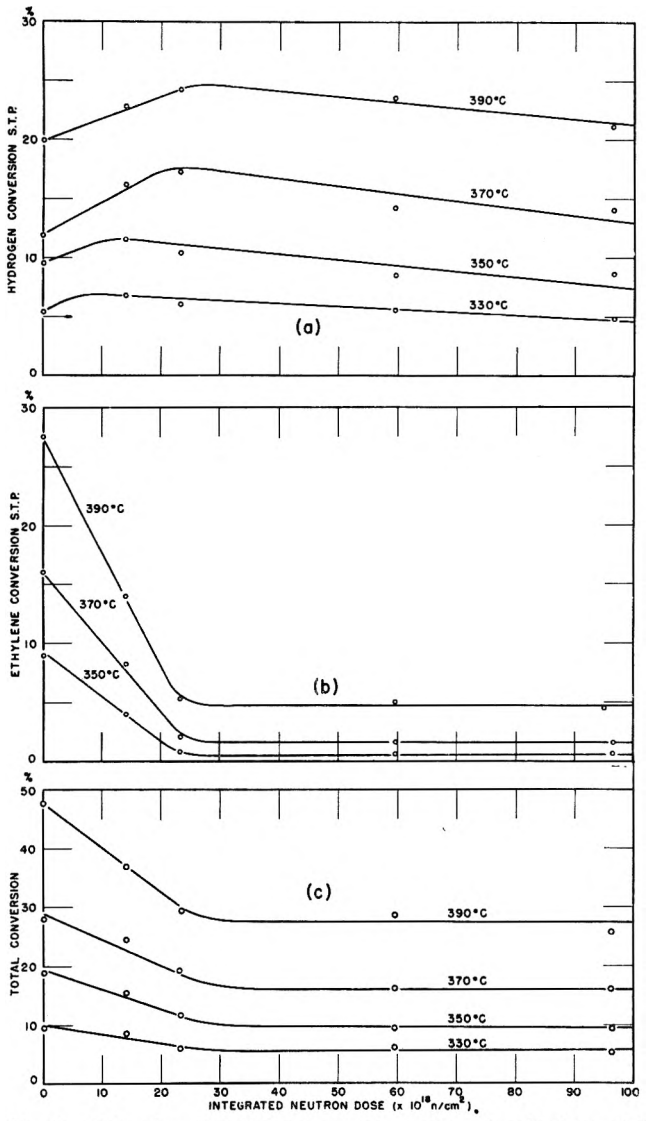

Fig. 2.—Behavior of ZnO catalyst after neutron irradiation: (a) hydrogen yield; (b) ethylene yield; (c) total conversion.

tion of impurities (mainly gallium-69) of different chemical character in the specimen, and obviously this is an irreversible process. In the case of ZnO it is evident that a higher Fermi level has been obtained in the irradiated catalysts compared with the non-irradiated one and this leads to an increase in the hydrogen/ethylene ratio in the reaction products. There is also an increase in the dehydrogenation activity of the same catalysts, which seems to be a function of the estimated integrated neutron dose of the catalysts (Fig. 1) or of the amount of gallium-69 created.

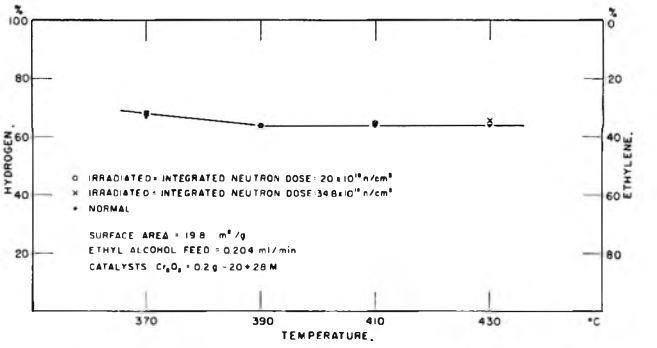

Fig. 3.—Behavior of Cr_2O_3 catalysts at various temperatures.

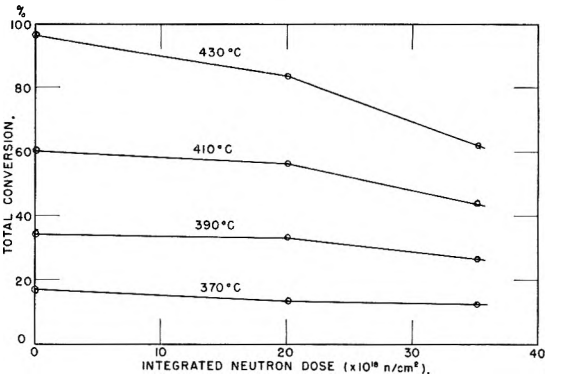

Fig. 4.—Total conversion at various integrated neutron doses—Cr_2O_3 catalyst.

The natural abundance of zinc-68 is 18.75% in the zinc element, its neutron cross-section is 1.06 barn and the half-life of zinc-69 is 52 min.[12] Because of this short half-life, creation of gallium is practically complete by the time of receipt of the irradiated sample. An approximate calculation of the amount of gallium-69 created by nuclear transmutation of zinc-68 in the catalyst samples used is given in Table III.

TABLE III

PRODUCTION OF Ga-69 IN IRRADIATED ZnO[a]

Catalyst:ZnO	Integrated neutron dose, n./cm.^{2}	Ga-69, p.p.m.
I	0	0
II	13.9 × 10^{18}	2.64
III	23.3 × 10^{18}	4.84
IV	59.6 × 10^{18}	12.2
V	96.6 × 10^{18}	22.0

[a] Gallium is a donor impurity in ZnO.

For the zinc oxide catalysts the amount of copper produced by transmutation of the isotope zinc-64 is of the order of 0.5–2 p.p.m., about $^1/_{20}$ of the amount of copper initially present as an impurity in the non-irradiated catalyst; it becomes appreciable (12 p.p.m.) for the highest neutron dose and after a long period of decay (catalyst V). Copper is an acceptor impurity if present as Cu^{++}, a donor if present as Cu atom, while the Cu^+ ion possesses a closed electron shell.[8]

Conclusions

For an *n*-type semiconductor it has been found by Wagner,[13] Hauffe,[14] Schwab, and others[15] that the charge carrier concentration can be raised by incorporat-

(12) D. J. Hughes and R. B. Schwartz, Neutron Cross Section, Brookhaven Natl. Lab. Report B.N.L. 325 (1958).

(13) C. Wagner and K. Hauffe, *Z. Elektrochem.*, **45**, 403 (1949); **44**, 172 (1938).

(14) K. Hauffe, R. Glang, and H. J. Engell, *Z. physik. Chem.*, **201**, 223 (1962).

(15) G. M. Schwab and J. Block, *J. chim. phys.*, **51**, 664 (1954).

ing small amounts, ~0.01% of impurities. Addition of oxides of trivalent metals, *e.g.*, Al_2O_3, Ga_2O_3, causes an increase, whereas oxides of monovalent metals cause a decrease, in the concentration of charge carriers. In irradiated zinc oxide both zinc and oxygen vacancies, as well as interstitial zinc atoms, are produced. Interstitial oxygen atoms are unlikely in stabilized ZnO and the displaced oxygen atoms probably go to vacancies or grain boundaries to be freed later. The nuclear reaction

$$Zn^{68}(n,\gamma)Zn^{69} \xrightarrow{\beta} Ga^{69}$$

appears to be responsible for the amount of gallium present. In the range of temperatures investigated so far, it is believed that the lattice defects introduced by γ-ray and neutron irradiation are removed slowly and this could explain the aging period during which the catalysts present a lower activity and a lower H_2/C_2H_4 ratio compared with the non-irradiated one. It may be mentioned that Kohn, Moore and Taylor[4] had shown that irradiation effects are relatively stable in refractory oxides. The decrease in catalytic activity of the chromic oxides as a result of both gamma and neutron irradiation may be attributed to the decrease in the number of conduction-band electrons by the creation of chromium in interstitial positions that are not completely annihilated in the temperature range and in the time these catalysts were used.

This work has indicated a method for introducing controlled amounts of impurities into catalysts by neutron irradiation that may have important practical applications.

Acknowledgments.—The author wishes to express his appreciation to Dr. G. G. Eichholz for his helpful suggestions during this work and to all members of the Physics and Radiotracer Subdivision of the Mineral Sciences Division for advice and assistance. Thanks are also due to Mr. R. G. Draper for his help in analysis of the gas mixtures used in the calibration of the chromatographic equipment, to Dr. A. H. Gillieson for the spectrographic analyses of the catalysts, and to Mr. H. J. Mullington of Eldorado Mining and Refining Ltd. for the surface area determination of the catalysts.

This work was done during a two-year tenure of a Postdoctorate Fellowship of the National Research Council of Canada, which is gratefully acknowledged.

SOLUBILITIES OF WATER IN SEVERAL NORMAL ALKANES FROM C_7 TO C_{16}[1]

BY PAUL SCHATZBERG

U. S. Naval Engineering Experiment Station, Annapolis, Maryland

Received August 30, 1962

The solubilities of water in several *n*-alkanes from C_7 to C_{16} have been determined at 25 and 40°. When expressed on a weight basis the solubilities show an inverse relationship to solvent molecular weight and, when expressed as mole fraction, a direct relationship. The solubilities have been correlated with the solvent properties, solubility parameter and surface tension.

Knowledge of water solubilities in pure hydrocarbon liquids and the effect of increasing molecular weight on these solubilities is necessary to understand the chemical and physical effects of water in hydrocarbon liquids, such as jet fuels and lubricating oils. The most extensive determinations of water solubilities in hydrocarbon liquids are found in the work of Black, Joris, and Taylor.[2] Using tritium oxide as a tracer, they determined water solubilities at several temperatures for various hydrocarbons from C_4 to C_8. These included normal and branched-chain alkanes, alkenes, cyclohexane, and benzene. Although a number of other investigators using different methods have determined water solubilities in hydrocarbons, no such data are available beyond octane. In addition, the data of Black, Joris, and Taylor for the normal alkanes from C_4 to C_8, when expressed on a weight basis, indicate increasing water solubilities with increasing molecular weights; these solubilities are much higher than those found in kerosene fuels of greater chain length (12 to 13 carbon atoms), as pointed out by Davies.[3] Further, the data of Griswold and Kash[4] for straight-run petroleum fractions show solubilities expressed on a weight basis which decrease with increasing molecular weight of the hydrocarbon, a trend directly opposite to that shown by the data of Black, Joris, and Taylor. In an attempt to resolve these disagreements and provide data beyond octane, the solubilities of water in several normal alkanes from C_7 to C_{16} were determined at 25 and 40°.

(1) The opinions expressed in this paper are those of the author and are not to be construed as official or reflecting the views of the Department of the Navy or naval services at large.

(2) C. Black, G. G. Joris, and H. S. Taylor, *J. Chem. Phys.*, **16**, 537 (1948).

(3) P. L. Davies, "Fourth World Petroleum Congress Section V/E," 1955, p. 427.

(4) J. Griswold and J. E. Kash, *Ind. Eng. Chem.*, **34**, 804 (1942).

Experimental

Apparatus and Procedure.—The hydrocarbons were saturated by storing them over a layer of distilled and deionized water in 4-oz. brown glass bottles without any agitation. The bottles were sealed with tightly fitting serum caps and completely submerged in a water-bath maintained within ±0.02° of the saturation temperature for 7 days. This is referred to as the static water saturation method. The storage period of 7 days was based on experience with kerosene fuels. It was found that the dissolved water content of these fuels contacting liquid water without agitation became constant after 3 to 4 days. Thus, a storage period of 7 days was considered more than adequate for this method. At the end of 7 days, each bottle was raised out of the bath sufficiently to expose the serum cap, which was rinsed with acetone and thoroughly dried. A hypodermic syringe pierced the serum cap and was pushed approximately $^2/_3$ of the way down into the hydrocarbon liquid. A small hypodermic needle also pierced the cap. Air pressure through the small needle quickly forced a 20-ml. sample into the syringe.

A dynamic water saturation procedure was used for two of the hydrocarbons in order to compare two different methods of saturation. In this method saturation was achieved by passing moist air through the hydrocarbon. Filtered air at a flow rate of approximately 20 ml./min. was passed through a water saturator

and from there through a hydrocarbon saturator. Both saturators were submerged in the same water-bath at the conditions previously stated. Saturation time was approximately 16 hr. An Aminco-Dunmore conducting-film sensor, situated in the top of the hydrocarbon saturator, measured the relative humidity of the exit air. When a constant reading of 97 to 99% relative humidity was obtained, a 20-ml. sample was quickly removed. This was done by attaching a syringe to a hypodermic needle situated in the hydrocarbon saturator and closing off the air exit, so that the moist air flow forced the hydrocarbon into the syringe.

Sampling and transfer to the water analysis apparatus in both saturation methods were achieved in less than 30 sec. All sampling equipment surfaces were rendered hydrophobic with a silicone compound (Clay-Adams) to minimize any water loss.

Water content in the hydrocarbons was determined by the Karl Fischer method. Stabilized Karl Fischer reagent (Fischer Scientific Co.) diluted to a titer of 1.0 to 1.3 mg. water/ml. was used to titrate hydrocarbon water content directly in the presence of methanol to a "dead-stop" end-point, using a Beckman KF3 automatic titrimeter with a 5-ml. microburet. Reagent titer was accurately determined before each separate hydrocarbon analysis by using distilled water introduced into the titration chamber from a weighed microliter syringe.

The solubility of water in benzene at 20° was determined for comparison of the saturation and analysis methods with those of other investigators.

Materials.—Table I lists the hydrocarbons, sources of supply, and grades. All hydrocarbons (except benzene) were passed repeatedly through a 4-ft. column of silica gel (Davison No. 12) until essentially no absorption occurred in the spectral range of 220 to 340 mμ as measured by a Beckman DK2 ratio recording spectrophotometer. This assured that contamination by aromatics, which exhibit a much higher affinity for water than the alkanes, was eliminated. The silica gel treatment also served to remove small amounts of polar materials which exhibit a very high affinity for water. The most probable impurities are branched-chain and cyclic isomers in the same boiling range. The effect of such impurities on the water solubilities was considered negligible. The *n*-heptane was doubly distilled before treatment with silica gel. The refractive indices of the purified solvents agreed with the literature values[6] within 0.7 part per 10^4 or better.

TABLE I

HYDROCARBON SOURCES AND GRADES[a]

n-Heptane	EOC
n-Nonane	PP, research grade, 99.69 mole %
n-Decane	PP, research grade, 99.43 mole %
n-Undecane	PP, research grade, 99.33 mole %
n-Dodecane	PP, pure grade, 99+ mole %
n-Tridecane	PP, research grade, 99.73 mole %
n-Tetradecane	PP, pure grade, 99+ mole %
n-Hexadecane	HW, ASTM normal cetane
Benzene	MCB, chromatoquality reagent, 99+ mole %

[a] EOC, Eastman Organic Chemicals; PP, Phillips Petroleum Co.; HW, Humphrey–Wilkinson, Inc.; MCB, Matheson, Coleman and Bell.

Experimental Results

Results of the water solubility determinations at 25 and 40° are recorded in Table II.

Each value reported is the mean of two to four determinations. The deviations from the mean ranged from 0 to 6% for the 25° data and from 0 to 2% for the 40° data. Data other than the experimental data, also recorded in Table II, will be discussed subsequently. Results of water solubility determinations for *n*-nonane and *n*-decane at 25° by the dynamic water saturation method were 81 and 71 p.p.m. by weight, respectively, comparing well with the corresponding results obtained by the static water saturation method (Table II).

(5) F. D. Rossini, K. S. Pitzer, R. L. Arnett, R. M. Braun, and G. C. Pimentel, "Selected Values of Physical and Thermodynamic Properties of Hydrocarbons and Related Compounds," Carnegie Press, Pittsburgh, Pa., 1953.

It is seen from Table II that the water solubilities expressed by weight decrease gradually with increasing alkane chain length. The opposite trend is noted when the solubilities are expressed as mole fraction. The water solubilities found compare favorably with those of kerosene fuels having equivalent chain lengths. Disagreement exists, however, with the water solubilities found by Black, Joris, and Taylor.[2] For *n*-heptane at 25°, they found 151 p.p.m. against 91 in this work; their data from C_4 to C_8 showed a direct relationship between dissolved water by weight and alkane molecular weight, while in this work the reverse was found for C_7 to C_{16}.

Results of the water solubility determinations for benzene at 20° are recorded in Table III, along with the methods and results of other investigators for comparison. Excluding the low result of Black, Joris, and Taylor,[2] the average solubility of the values in Table III is 545 ppm, which differs from the value found in this work by 2%. It can be concluded, therefore, that the saturation and analysis methods used in this investigation are comparable to those used by other investigators.

Discussion

Hildebrand[6] has derived an equation to describe the mixing of components of different internal pressures and volumes

$$RT \ln (\alpha_2/x_2) = V_2(\phi_1)^2(\delta_2 - \delta_1)^2 \qquad (1)$$

where α = activity, V = molal volume, δ = solubility parameter, ϕ = volume fraction, and x = mole fraction. Subscripts 1 and 2 refer to the hydrocarbon solvent and water solute, respectively. The following simplifying assumptions can be applied: $\alpha_2 = 1$, and, since the water concentration is very small compared to the hydrocarbon concentration, ϕ_1 is very nearly unity. Thus, eq. 1 becomes

$$\ln x_2 = \frac{-V_2}{RT}(\delta_2 - \delta_1)^2 \qquad (2)$$

Values of δ_2 and δ_1 were calculated from the Hildebrand relation

$$\delta = [(\Delta H_v - RT)/V]^{1/2} \qquad (3)$$

Values of the heats of vaporization, ΔH_v^{25}, for the alkanes were obtained from the literature,[5] while values of ΔH_v^{40} were calculated from

$$\Delta H_v^{40} = \Delta H_v^{25} - \Delta C_p(313 - 298) \qquad (4)$$

where ΔC_p is the difference between the heat capacity of the liquid and that of the gaseous hydrocarbon.

Calculated water solubilities shown in Table II were obtained from eq. 2. Figure 1 shows the least squares straight lines through the experimental plot of log water solubility against alkane molecular weight. It is seen that the water solubilities are inversely proportional to molecular weight when expressed on a weight basis and directly proportional when expressed as mole fraction. Figure 2 shows the least squares straight lines through the experimental plot of log x_2 against $(\delta_2 - \delta_1)$,[2] as expected from eq. 2. With the exception of *n*-heptane, the experimental and calculated

(6) J. H. Hildebrand and R. L. Scott, "Solubility of Non-electrolytes," Reinhold Publ. Corp., New York, N. Y., 1950.

TABLE II

SOLUBILITIES OF WATER IN NORMAL ALKANES

	P.p.m. by wt.				Mole fraction × 10^4									
	Exptl.		Calcd.[a]		Exptl.		Calcd.		Exptl./calcd.		δ_1[b]		$(\delta_2 - \delta_1)^2$	
Temp., °C.	25	40	25	40	25	40	25	40	25	40	25	40	25	40
Heptane	91		74		5.1		4.2		1.2		7.43		255	
Nonane	79		72		5.6		5.2		1.1		7.65		248	
Decane	72	136	70	111	5.7	10.7	5.6	8.8	1.0	1.2	7.72	7.60	246	241
Undecane	69	130	69	109	6.0	11.3	6.0	9.4	1.0	1.2	7.80	7.68	243	239
Dodecane	65	127	66	104	6.1	12.0	6.2	9.8	1.0	1.2	7.84	7.72	242	238
Tridecane	60	123	64	100	6.1	12.6	6.5	10.2	0.9	1.2	7.89	7.77	241	236
Tetradecane		114		96		12.6		10.6		1.2		7.81		235
Hexadecane	54	104	58	91	6.8	13.1	7.3	11.4	0.9	1.2	8.01	7.89	237	232

[a] Based on the Hildebrand equation presented in the Discussion. [b] δ is the solubility parameter in the Hildebrand equation.

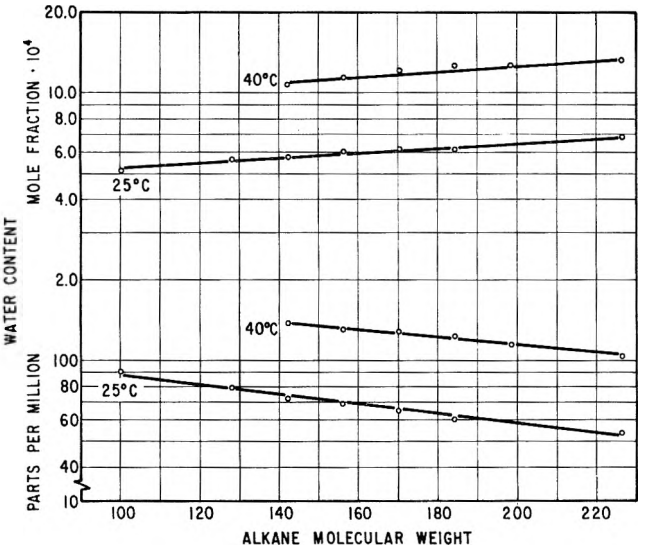

Fig. 1.—Alkane water solubilities and molecular weights.

TABLE III

SOLUBILITY OF WATER IN BENZENE AT 20°

Ref.	Saturation method	Analysis method	Results p.p.m. by wt.
2	Water vapor	DTO tracer	430
7	Shaking with water and storage	Karl Fischer	530
8	Water vapor	HTO tracer	520
9	Shaking with water and heating	Cloud point	570
10	Shaking with water and heating	Cloud point	530
11	Shaking with water, cooling, and standing	Gasometric with CaH_2	573
This work	Storage with water	Karl Fischer	532 ± 3

water solubilities at 25° show remarkably close agreement, as seen from their ratios recorded in Table II. This must be regarded as fortuitous, since eq. 2 involves several simplifying assumptions and neglects a correction for the entropy of mixing molecules of different size. Inclusion into eq. 2 of a correction for entropy of mixing results in calculated water solubilities which are from three to six times larger than the experimental solubilities.

(7) T. I. Berkenheim, *Zavodskaya Lab.*, **10**, 592 (1941).
(8) B. D. Caddock and P. L. Davies, *J. Inst. Petrol.*, **46**, 391 (1960).
(9) L. A. K. Staveley, J. H. E. Jeffes, and J. A. E. Moy, *Trans. Faraday Soc.*, **39**, 5 (1943).
(10) D. N. Tarasenkov and E. N. Polzhintzeva, *Zh. Obshch. Khim.*, **1**, 71 (1931).
(11) C. K. Rosenbaum and J. H. Walton, *J. Am. Chem. Soc.*, **52**, 3568 (1930).

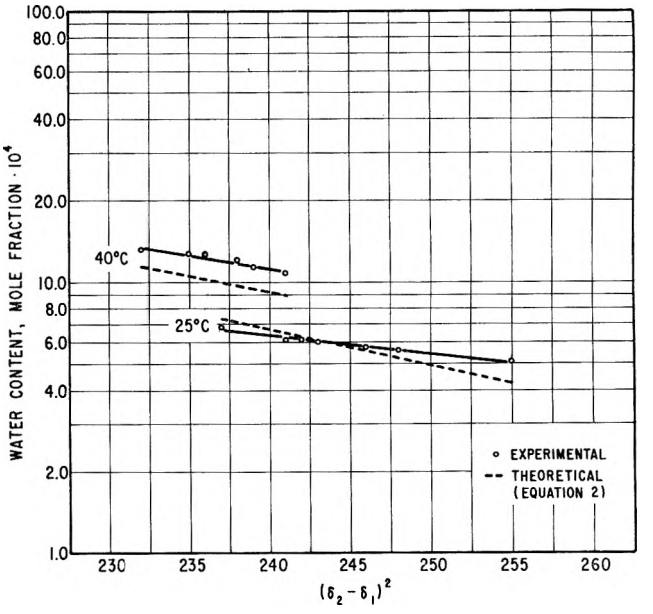

Fig. 2.—Alkane water solubilities *vs.* $(\delta_2 - \delta_1)^2$.

Uhlig[12] describes the energy change in placing a gas molecule of radius R into a solvent as consisting of the work to produce a spherical cavity of radius r in the solvent and the interaction energy between solute and solvent molecules. Based on this description and applying the Maxwell–Boltzmann distribution theory, he derived the equation

$$\log B = -\frac{4\pi r^2\sigma}{2.303kT} + \frac{E}{2.303kT} \qquad (5)$$

where B = Ostwald solubility coefficient, r = radius of the gas molecule, σ = the solvent surface tension, E = the interaction energy between solute and solvent, and k = the Boltzmann constant.

For those gases which have small interaction with solvent molecules, E is small. Considering the dissolved water as a gas, E should remain nearly constant in the homologous series of solvents used, since the water molecule would always be in an environment of $-CH_2$ and $-CH_3$ groups. Consequently, the logarithm of the Ostwald solubility coefficient for water when plotted against n-alkane surface tension should produce a straight line. This is seen in the least squares straight lines shown in Fig. 3. The efficiency of fit, standard deviation, slope, and intercept for each line are recorded in Table IV.

Based on eq. 5, the slopes and intercepts were used to calculate the radius of the water molecule and the

(12) H. H. Uhlig, *J. Phys. Chem.*, **41**, 1215 (1937).

TABLE IV
LEAST SQUARES DATA

Temp., °C.	Efficiency of fit, %	Standard dev. × 10^4	Slope	Intercept
25	96	1.78	−0.0248	−0.5734
40	90	1.42	−0.0232	−0.3384

solute–solvent interaction energy. For the 25 and 40° data, respectively, the water radii calculated were 1.37 and 1.36 Å., while the interaction energies were −782 and −485 cal./mole. Although literature values for the radius of the water molecule range from 1 to 3 Å., depending on the assumptions made, some of these are very close to the values determined in this work: 1.25,[13] 1.32,[13] 1.39,[14] and 1.44.[13] The negative interaction energies can be interpreted, according to Uhlig,[12] as an absorption of energy by the system as water dissolves, which is indicative of a low solubility. The negative interaction energies account in part, according to Le Chatelier's rule, for the increase in solubility of water with increasing temperature.

Conclusions

Results of water solubilities in normal alkanes from C_7 to C_{16} show a gradual decrease with increasing molecular weight, when the solubilities are expressed on a weight basis; when expressed on a mole fraction basis, the reverse trend occurs. The experimental water solubilities agree well with two different theoretical treatments.

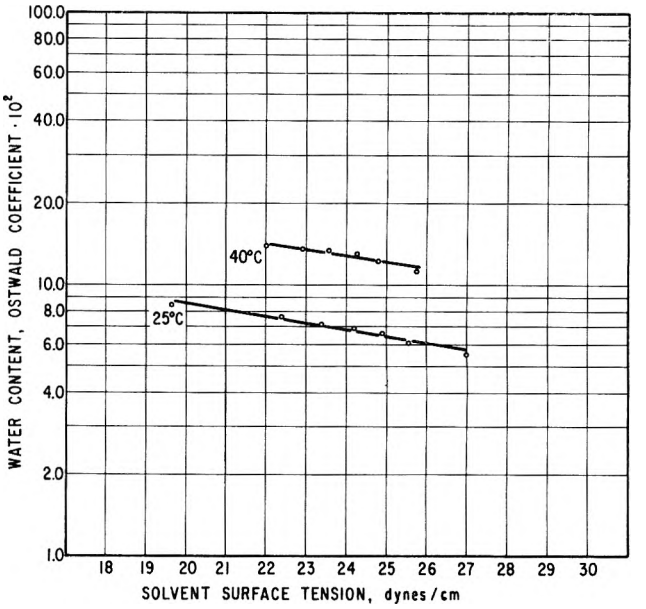

Fig. 3.—Alkane water solubilities and surface tensions.

(13) N. E. Dorsey, "Properties of Ordinary Water Substance," ACS Monograph, Reinhold Publ. Corp., New York, N. Y., 1940.
(14) C. J. F. Böttcher, *Rec. trav. chim.* (Rotterdam), **65**, 14 (1946).

ACID–BASE EQUILIBRIA IN CONCENTRATED SALT SOLUTIONS. II. CHARGED CARBOXYLATE BASES IN DILUTE ACID SOLUTIONS[1]

BY JAMES S. DWYER AND DONALD ROSENTHAL[2]

Department of Chemistry, The University of Chicago, Chicago, Illinois

Received September 5, 1962

$pH_{G.E.}$ − pMH is shown to be a constant for a given salt solution in slightly acidified 1 to 8 *M* LiCl. ($pH_{G.E.}$ is the pH measured using a cell with a glass indicator electrode and a saturated calomel reference electrode. pMH = −log total strong acid concentration.) Values of $pH_{G.E.}$ − pMH are reported. In dilute acid solutions of acetate or formate ion $K_{BH} = ([B^-][H^+]/[BH])Q_{BH}$ where K_{BH} is the thermodynamic acid dissociation constant of the acid (BH), and Q_{BH} is a constant for a particular base, B^-, and a particular salt solution. The values of $pH_{G.E.}$ calculated using this equation are in good agreement with the experimental values. Values of $\log Q_{BH}$ are reported for acetic acid in 1–8 *M* LiCl. It is shown that calculated values of $\log Q_{BH}$ using the equation $\log Q_{BH} = -(\sqrt{M}/1 + A\sqrt{M}) + BM$ do not differ significantly from the experimental values. Calculated and experimental Q_{BH} values are compared with published results for dilute LiCl solutions.

Introduction

In a previous study[3] $pH_{G.E.}$ − pMH was shown to be a constant for dilute acid solutions in 4 and 8 *M* LiCl, 6 *M* $NaClO_4$, 6 *M* $NaNO_3$, and 4*M* $CaCl_2$. ($pH_{G.E.}$ is the pH measured using a cell with a glass indicator electrode and a saturated calomel reference electrode and pMH is −logarithm of the total molar concentration of strong acid.) Further, it was found that the quantitative aspects of equilibrium between a weak uncharged base, B, and its conjugate acid, BH^+, in such solutions can be accounted for using the equation

$$K_{BH^+} = ([B][\text{total strong acid concn.}]/[BH^+])Q_{BH^+} \quad (1)$$

where K_{BH^+} is the thermodynamic molar acid dissociation constant and Q_{BH^+} depends upon the nature and concentration of salt and the nature of the base, B. Apparently, the various factors[4–11] which are important in concentrated salt solutions can be satisfactorily incorporated into the Q_{BH^+} term.

(1) Taken in part from the Ph.D. research of James S. Dwyer. This work was supported by research grants from the U. S. Public Health Service (RG-9583 and RG-8069).
(2) To whom inquiries should be directed at Clarkson College of Technology, Potsdam, New York.
(3) D. Rosenthal and J. S. Dwyer, *J. Phys. Chem.*, **66**, 2687 (1962).
(4) H. S. Harned and B. B. Owen, "The Physical Chemistry of Electrolytic Solutions," Reinhold Publ. Corp., New York, N. Y., 1958, pp. 509–547.
(5) H. S. Frank, *et al.*, *J. Chem. Phys.*, **13**, 507 (1945); *Ann. Rev. Phys. Chem.*, **5**, 43 (1954). R. W. Gurney, "Ionic Processes in Solution," McGraw-Hill Book Co., Inc., New York, N. Y., pp. 248–260.
(6) J. B. Hasted, *et al.*, *J. Chem. Phys.*, **16**, 1 (1948); **29**, 17 (1959).
(7) (a) R. A. Robinson and R. H. Stokes, "Electrolyte Solutions," Butterworths Publications Ltd., London, 1959, p. 62; (b) E. Glueckauf in "The Structure of Electrolyte Solutions," W. J. Hamer (editor), John Wiley and Sons, Inc., New York, N. Y., 1959, pp. 97–112.
(8) J. Beck, *Physik. Z.*, **40**, 474 (1939); G. W. Brady, *J. Chem. Phys.*, **28**, 464 (1958); H. S. Frank and P. T. Thompson in ref. 7b, pp. 113–134.
(9) Ref. 4, pp. 514, 634–643.
(10) E. Grunwald, G. Baughman, and G. Kohnstam, *J. Am. Chem. Soc.*, **82**, 5801 (1960).
(11) J. N. Brönsted, *Trans. Faraday Soc.*, **23**, 430 (1927); G. Scatchard in ref. 7b, pp. 9–18.

TABLE I

COMPARISON OF CALCULATED AND EXPERIMENTAL VALUES OF $pH_{G.E.}$ OBTAINED IN THE NEUTRALIZATION OF 0.03 *M* NaAc

% Neutralized	4 *M* LiCl Exptl.	4 *M* LiCl Calcd.	8 *M* LiCl Exptl.	8 *M* LiCl Calcd.	6 *M* $NaClO_4$ Exptl.	6 *M* $NaClO_4$ Calcd.	6 *M* $NaNO_3$ Exptl.	6 *M* $NaNO_3$ Calcd.	4 *M* $CaCl_2$ Exptl.	4 *M* $CaCl_2$ Calcd.
10	4.76	4.76	4.01	4.04	4.95	4.94	5.31	5.33	3.58	3.56
20	4.42	4.41	3.69	3.68	4.58	4.58	4.98	4.97	3.21	3.21
50	3.80	3.81	3.07	3.08	3.98	3.98	4.38	4.37	2.59	2.61
90	2.88	2.88	2.13	2.13	3.02	3.03	3.41	3.43	1.73	1.69
100	2.22	2.21	1.28	1.16	1.93	1.84	2.54	2.54	1.22	1.09
110	1.57	1.57	0.23	0.22	0.71	0.68	1.70	1.70	0.52	0.52
120	1.28	1.29	<0	− .08	.35	.38	1.41	1.40	0.17	0.25
140	0.99	0.99	<0	− .37	.07	.08	1.11	1.10	<0	−0.05
pMH − $pH_{G.E.}$	0.93		2.30		1.84		0.817		1.97[c]	
log Q_{HAc}[a,b]	− .015		0.625		0.066		.0432		0.181	
S.D. log Q_{HAc}	.007		0.0059		0.0047		.0075		0.011	
K_{HAc}/Q_{HAc}	1.91×10^{-5}		4.15×10^{-6}		1.50×10^{-6}		6.47×10^{-6}		2.655×10^{-5}	

[a] $pK_{HAc} = 4.757$, R. A. Robinson and R. H. Stokes, "Electrolyte Solutions," Butterworths Publications Ltd., London, 1959, p. 517, 30. [b] Log Q_{HAc} values represent an average obtained from the 10–90% neutralized points, except that the following points were not used in computing the average: 4 *M* LiCl, 10 and 90%; 8 *M* LiCl, 10%; 6 *M* $NaNO_3$, 90%; 4 *M* $CaCl_2$, 90%. [c] Preliminary results obtained with a purer grade of $CaCl_2$ indicate there may be some systematic variation in pMH − $pH_{G.E.}$ with pMH.

The present study indicates that results obtained for negatively charged carboxylate bases can be explained satisfactorily by the equation

$$K_{BH} = ([B^-][\text{total strong acid}]/[BH])Q_{BH} \quad (2)$$

which is identical to eq. 1 except that BH refers to an uncharged acid. The nature of Q_{BH} is examined and Q_{BH} values are compared with published results for the more dilute salt solutions.

Experimental Details

Except where specifically noted below, experimental details were the same as described previously.[3]

Reagents.—Reagent grade glacial acetic and formic acids were used.

Solutions.—All solutions used in this study were prepared from standardized stock solutions. Acetate and formate was added as acetic and formic acid. The appropriate amount of sodium hydroxide was added to give less than 100% neutralized NaAc or NaFo solutions. Hydrochloric acid was added to give greater than 100% neutralized solutions. Each solution was prepared and used at 25 ± 0.5°. Final concentrations with respect to each of the salts were 3.995 and 7.990 *M* LiCl, 5.987 *M* $NaClO_4$, 5.989 *M* $NaNO_3$, and 4.013 *M* $CaCl_2$ for Table I; 3.997 and 7.995 *M* LiCl in Table II. Separate solutions were prepared for each of the per cent neutralized points.

Potentiometric Measurements.—$pH_{G.E.}$ measurements were made with a Beckman model G or GS pH meter using the General Purpose Glass Electrode (shielded, 5 inch) and the Fiber Type Calomel Electrode (5 inch). The pH meter was standardized and checked using the reference solutions: 0.1 *M* HCl (pH 1.10), 0.05 *M* KH phthalate (4.01), and 0.025 *M* KH_2PO_4, 0.025 *M* Na_2HPO_4 (6.86).

Results

The results of $pH_{G.E.}$ measurements obtained in the neutralization of sodium acetate are presented in Table I. An estimate of K_{BH}/Q_{BH} can be obtained from the $pH_{G.E.}$ measurements in the buffer region. pMH was calculated using the previously determined[3] pMH − $pH_{G.E.}$ values. $[BH]/[B^-]$ was calculated. $\text{Log}(K_{BH}/Q_{BH})$ was then calculated for each salt solution using the logarithmic form of eq. 2.

$$-\log(K_{BH}/Q_{BH}) = \text{pMH} + \log([BH]/[B^-]) \quad (3)$$

The calculated $pH_{G.E.}$ presented in Table I were obtained using this estimate of K_{BH}/Q_{BH} in eq. 2. The differences between calculated and experimental values are comparable to the error in the $pH_{G.E.}$ measurements except at the 100% point and for some of the $CaCl_2$ results. At or near the 100% point, solutions are poorly buffered and $pH_{G.E.}$ values are significantly affected by acidic or basic impurities or small errors in the preparation of solutions. The basic impurities known[3] to be present were neglected (assumed to be negligibly weak bases) in making the calculations. Better agreement at the 100% neutralized point in 4 and 8 *M* LiCl and 6 *M* $NaClO_4$ could be obtained by postulating that the impurity had finite basic strength. The large amount of impurity in the $CaCl_2$ solution and its variability with time is believed to account, at least in part, for the somewhat larger discrepancies between calculated and experimental $CaCl_2$ results.

If eq. 2 is valid pMH and $pH_{G.E.}$ should be constant for an *x M* HAc − *x M* Ac^- buffer in a given salt solution, provided the concentration of buffer is small compared to the concentration of salt. Measurements were made in 4 and 8 *M* LiCl solutions over a tenfold range of buffer concentrations and $pH_{G.E.}$ was indeed constant (*x* = 0.1 to 0.01, $pH_{G.E.}$ 3.80 in 4 *M* LiCl and from 3.07 to 3.06 in 8 *M* LiCl).

Experimental and calculated $pH_{G.E.}$ results obtained for the neutralization of sodium formate are presented in Table II. The differences between calculated and experimental results are comparable to the error in the glass electrode measurements. Thus, the results for both sodium acetate and sodium formate were consistent with eq. 2.

Values of pMH − $pH_{G.E.}$ for dilute HCl solutions and log Q_{BH} values for acetic acid in 1 to 8 *M* LiCl are presented in Table III. Each value represents the pooled best estimate taking into consideration the results of all pertinent experiments. At least five independent measurements of pMH − $pH_{G.E.}$ and of log Q_{BH} were made in 4 and 8 *M* LiCl. Two measurements were made in each of the other solutions. The values given in columns four and five were calculated using the expression

$$\log Q_{BH} = -\frac{\sqrt{M}}{1 + A\sqrt{M}} + BM \quad (4)$$

where *M* is the molarity of salt (equal to the molar ionic strength). In column 5, *A* was assumed to be equal to 1 and the least squares value of *B* was employed. The least squares value of *B* was calculated for various values of *A*. The results presented in column 4 are for that value of *A* and *B* which gives a

TABLE II

COMPARISON OF CALCULATED AND EXPERIMENTAL VALUES OF $pH_{G.E.}$ OBTAINED IN THE NEUTRALIZATION OF 0.03 *M* SODIUM FORMATE

% Neutralized	H_2O Exptl.	H_2O Calcd.	4 *M* LiCl Exptl.	4 *M* LiCl Calcd.	8 *M* LiCl Exptl.	8 *M* LiCl Calcd.
10.19	4.61	4.62	3.64	3.64	2.71	2.72
20.25	4.28	4.28	3.30	3.30	2.36	2.37
50.12	3.70	3.70	2.69	2.71	1.78	1.78
80.09	3.16	3.16	2.16	2.16	1.20	1.20
90.04	2.93	2.93	1.93	1.93	0.94	0.91
100.00	2.66	2.65	1.67	1.66	.55	.51
110	2.40	2.39	1.42	1.42	.13	.14
120	2.22	2.20	1.23	1.23	<0	− .10
140	1.96	1.95	0.97	0.97	<0	− .39
$pMH - pH_{G.E.}$	$\log f_i$[c]		0.93		2.30	
$\log Q_{HF_0}$[b]	$2 \log f_i$		-0.11_5		0.33_7	
S.D.$_{\log Q_{HF_0}}$			0.0046		0.009	
K_{HF_0}/Q_{HF_0}	$1.82_8 \times 10^{-4}/f_i^2$		2.38×10^{-4}		$8.39_5 \times 10^{-5}$	

[a] Calculated using the expression $\log f_i = -0.5I^{1/2}/(1 + I^{1/2}) + 0.2I$ (see R. A. Robinson in "The Structure of Electrolyte Solutions," W. J. Hamer (editor), John Wiley and Sons, Inc., New York, N. Y., 1959, p. 257). [b] An average pK_{HF}° of 3.734 was obtained from the 10.19–90.04% neutralized $pH_{G.E.}$ measurement ($n = 5$, $S.D._{\bar{x}} = 0.0025$). The literature value of 3.739 was used in the calculations. (R. A. Robinson and R. H. Stokes, "Electrolyte Solutions," Butterworths Publications, Ltd., London, 1959, pp. 519, 523, 5230.) The $\log Q_{HF_0}$ values represent an average obtained from the 10.19–90.04% neutralized $pH_{G.E.}$ measurements ($n = 5$).

best fit, *i.e.*, a minimum sum of squared deviations (SSD) between the calculated and experimental $\log Q_{BH}$ and a minimum SD_B (calculated as above). The differences between the calculated and experimental $\log Q_{BH}$ values are not very much greater than the uncertainty in the experimental values themselves.

Discussion

The measured $pH_{G.E.}$ values are in good agreement with values calculated assuming eq. 2 is valid. This suggests[3] the situation in concentrated salt solutions is formally similar to the situation in water, *i.e.*, the pH determining equilibrium is

$$BH \rightleftharpoons B^- + H^+$$

and

$$Q_{BH} = f_B \cdot f_{H^+}/f_{BH} \qquad (5)$$

where f is a molar activity coefficient. Combining equation 5 with equation 4

$$\log Q_{BH} = \log (f_B \cdot f_{H^+}/f_{BH}) = -\frac{\sqrt{M}}{1 + A\sqrt{M}} + BM \qquad (6)$$

This equation, 6, has been shown to be consistent with the $\log Q_{BH}$ results obtained for acetic acid (see Table III). Activity coefficient data for undissociated acetic acid in 0–1.5 *M* LiCl are available[12] and conform to the equation

$$\log f_{BH} = B'M \qquad (7)[13]$$

where $B' = 0.08_5$. If it is assumed eq. 7 applies to 0–8 *M* LiCl solutions[13]

$$\log f_B \cdot f_{H^+} = -\frac{\sqrt{M}}{1 + A\sqrt{M}} + (B + B')M \qquad (8)$$

(12) J. N. Sugden, *J. Chem. Soc.*, 177 (1926).

(13) M. Randall and C. F. Failey, *Chem. Rev.*, **4**, 300 (1927); F. A. Long and W. F. McDevit, *ibid.*, **51**, 119 (1952).

TABLE III

COMPARISON OF EXPERIMENTAL AND CALCULATED LOG Q_{BH} VALUES FOR ACETIC ACID

LiCl, *M*	$pMH - pH_{G.E.}$	Log Q_{BH} exptl.	Calcd. log Q_{BH} using eq. 4, $A = 0.917$, $B = 0.1759$	Calcd. log Q_{BH} using eq. 4, $A = 1$, $B = 0.1684$
1.00	0.12	−0.32	-0.34_6	-0.33_2
2.00	.35$_5$	− .27	− .26$_4$	− .24$_9$
3.00	.64	− .14$_5$	− .14$_2$	− .12$_9$
4.00	.93$_5$	− .02	− .00$_2$	.00$_7$
5.00	1.25	.13$_5$	.14$_6$	.15$_1$
6.00	1.61	.32$_5$	.30$_1$	.30$_0$
7.00	1.95	.45	.45$_9$	.45$_3$
8.00	2.30	.62$_5$	.62$_0$	.60$_8$
		$S.D_B$[a]	.001$_1$	.0014
		SSD[b]	.001854	.002716

[a] Calculated assuming no error in the estimate of *A*. [b] Sum of $[(\log Q_{BH}(\text{calcd.}) - \log Q_{BH}(\text{exptl.})]^2$.

From the results of the calculations of Table III where *A* is 1, $B + B'$ is 0.253 and where *A* is 0.917, $B + B'$ is 0.261.

Equation 8 resembles the expression which is applicable in dilute aqueous solutions.[14] Even the values of *A* and *B* are similar.[14,15] Consideration of the dilute solution expression[14] suggests that including an additional term in eq. 4 and 8 (which converts activity coefficients from the mole fraction to the molar scale)[14] might result in a better fit to the experimental data. However, this modified form of eq. 4 did not give a significantly better fit. (Least squares *A*, *B*, SSD were, respectively, 0.934, 0.1806, 0.001798; and 1, 0.1747, 0.002334.)

TABLE IV

COMPARISON OF CALCULATED AND EXPERIMENTAL VALUES OF LOG Q_{BH} FOR ACETIC ACID IN LiCl

LiCl, moles/l.	Values of log Q_{BH}: Experimental, H and H[a]	Experimental, K and E[b]	Experimental, E[c]	Experimental, This study	Calcd. eq. 4, $A = 0.917$, $B = 0.1759$	Calcd. eq. 4, $A = 1$, $B = 0.1684$
0.02	−0.116				−0.12	−0.12
.03	− .136				− .14	− .14
.05	− .165	−0.177			− .18	− .17
.06	− .176				− .19	− .19
.10	− .208	− .256			− .23	− .22
.20	− .252	− .273			− .28	− .27$_5$
.30	− .277	− .287			− .31	− .30
.40	− .292	− .321			− .33	− .32
.50	− .301	− .317	−0.311		− .34	− .33
.60	− .308	− .315			− .35	− .33$_5$
.70	− .311	− .313			− .35	− .34
.80	− .313	− .311			− .35	− .34
.90	− .313	− .317			− .35	− .33$_5$
1.00	− .312	− .315	− .312	−0.32	− .35	− .33
1.50	− .297	− .309			− .31	− .30
2.00	− .271	− .261	− .242	− .27	− .26	− .25
2.50		− .183			− .21	− .19
3.00		− .168	− .140	− .14$_5$	− .14	− .13

[a] Obtained from the data of Harned and Hickey, ref. 16, by conversion to the molar scale and interpolation. [b] Kilpatrick and Eanes, ref. 17. [c] Ellila, ref. 18.

Experimental values of $\log Q_{BH}$ for acetic acid in more dilute LiCl solutions have been reported by others.[16–18] The results obtained in 1, 2, and 3 *M* LiCl are in good agreement with the values obtained in the present study. Table IV presents a comparison of these results with $\log Q_{BH}$ values obtained using eq. 4 and the least squares values for *A* and *B* of Table III.

(14) Reference 7a, pp. 229–232, 236, 30–32.

(15) Reference 4, p. 736.

(16) H. S. Harned and F. C. Hickey, *J. Am. Chem. Soc.*, **59**, 2303 (1937).

(17) M. Kilpatrick and R. D. Eanes, *ibid.*, **75**, 586 (1953).

(18) A. Ellila, Ann. *Acad. Sci. Fennicae, Ser. A, II Chem.*, No. 51 (1953).

In most instances the difference between calculated and experimental results is within a few hundredths of a unit and in no instance do they differ by more than 0.04.

The substitution of n log a_w for the BM term in eq. 4 led to a poorer fit of the experimental data. The addition of an n log a_w term did not result in a significantly better fit. This is unlike the situation for uncharged bases.[19]

The log Q_{BH} values obtained for formic and acetic acids in LiCl are different (see Tables I and II). These results indicate that, if an acidity function, H_-[20]

$$H_- = pK_{BH} - \log \frac{[BH]}{[B^-]} = -\log [H^+] \frac{f_{H^+} f_{B^-}}{f_{BH}} = -\log [H^+] - \log Q_{BH} \quad (9)$$

is defined in terms of a particular indicator or series of indicators for LiCl solutions, the degree of protonation cannot be calculated directly from H_- measurements using eq. 9. The difference between the log Q_{BH} values for the H_- indicator and the acid in the particular LiCl solution also must be known.[3] If an H_- scale is to be defined for LiCl solutions, the indicators used must more closely resemble each other than do formic and acetic acids.[3,20]

(19) D. Rosenthal and J. S. Dwyer, *Can. J. Chem.*, **41**, 80 (1963); K. N. Bascombe and R. P. Bell, *Discussions Faraday Soc.*, **24**, 158 (1957).

(20) M. A. Paul and F. A. Long, *Chem. Rev.*, **57**, 1 (1957).

THE THERMAL DENATURATION AND AGGREGATION OF OVALBUMIN

BY JOHN HOLME

Miami Valley Laboratories, The Procter and Gamble Company, Cincinnati 39, Ohio

Received September 12, 1962

The techniques of optical rotation, viscosity, ultracentrifugation, electrophoresis, and solubility have been used to study the effect of heat treatment on the properties of ovalbumin in aqueous solutions of pH 5.5, 7.0, and 8.5. The results have been considered as they relate to the possible sequence of events in any denaturation experiment; native ⇄ denatured → aggregated. The monomeric form of the protein which remains after heating has been characterized by viscosity and sedimentation measurements and has been found to be hydrodynamically equivalent to the native protein. No evidence for the existence of a denatured monomeric form of ovalbumin in heated solutions has been found. Aggregation of the protein has been found to be rapid and extensive with heating over this pH range. The sedimentation constants of the aggregated form were dependent upon the pH (decreasing with increase in pH) and the ionic strength (decreasing with salt concentration) at which the aggregate was formed. The aggregation of the protein gave rise to increases in viscosity and turbidity which were also dependent upon pH (increasing less at higher pH). The aggregated protein had an electrophoretic mobility at pH 7.0 and 8.5 greater than that of the original protein.

Introduction

The denaturation of ovalbumin has been studied by many workers utilizing many physical techniques.[1-9] In general, these reports indicate that denaturation, defined here as an "intramolecular configurational change" in accord with present views,[10] does occur prior to aggregation of the protein. This conclusion has been given for the urea denaturation of ovalbumin by Frensdorff, *et al.*,[3] and Steven and Tristram.[11]

Many proteins show an increase in levorotation when they are exposed to certain environmental conditions. Based upon the relation of a change in this property to the helix-coil transformation found for certain synthetic polyamino acids,[12] the technique of optical rotation is commonly employed to study protein denaturation. However, recent work by a number of people[13-17] has pointed out the difficulties in assigning a change in rotation to a particular physical change in the protein and at this time it appears that much more work is required before the complete significance of rotational changes can be known.

The very marked tendency of ovalbumin to aggregate under denaturing conditions has been recognized by viscosity[18] and light scattering measurements.[19] Since changes in viscosity can arise from aggregation reactions, it would appear necessary that the absence of *any* aggregation must be shown before a change in viscosity can be related to an intramolecular change in the protein molecule itself.

In order to determine whether a solution of ovalbumin contains native, denatured, and aggregated protein as a result of any given heating experiment, a systematic study was undertaken of changes in optical rotation, viscosity, solubility, ultracentrifugal sedimentation, and electrophoretic properties which accompany heat treatment of ovalbumin under a number of conditions. It was hoped that the process of "denaturation" could be described in such a way that kinetic and thermodynamic treatment of clearly distinguishable features—

(1) H. A. Barker, *J. Biol. Chem.*, **103**, 1 (1933).
(2) R. B. Simpson and W. Kauzmann, *J. Am. Chem. Soc.*, **75**, 5139 (1953).
(3) H. K. Frensdorff, M. T. Watson, and W. Kauzmann, *ibid.*, **75**, 5157 (1953).
(4) J. Schellman, R. B. Simpson, and W. Kauzmann, *ibid.*, **75**, 5152 (1953).
(5) A. S. Tsiperovich, *Ukr. Biochem. Zh.*, **21**, 44 (1949).
(6) C. F. C. MacPherson and M. Heidelberger, *J. Am. Chem. Soc.*, **67**, 574 (1945).
(7) A. Rothen, *Ann. N. Y. Acad. Sci.*, **43**, 229 (1942).
(8) N. F. Burk and D. M. Greenberg, *J. Biol. Chem.*, **87**, 197 (1930).
(9) F. Haurowitz, F. DiMoia, and S. Tekman, *J. Am. Chem. Soc.*, **74**, 2265 (1952).
(10) W. Kauzmann, *Advan. Protein Chem.*, **14**, 1 (1959).
(11) F. S. Steven and G. R. Tristram, *Biochem. J.*, **73**, 86 (1959).
(12) J. T. Yang and P. Doty, *J. Am. Chem. Soc.*, **79**, 761 (1957).
(13) G. D. Fasman and E. R. Blout, *ibid.*, **82**, 2262 (1960).
(14) E. R. Blout, *Proc. Fourth Intern. Cong. Biochem.*, **8**, 37 (1960).
(15) G. E. Perlmann, *ibid.*, **8**, 32 (1960).
(16) C. Tanford, P. K. De, and U. G. Taggart, *J. Am. Chem. Soc.*, **82**, 6028 (1960).
(17) A. Todd, "A Laboratory Manual of Analytical Methods of Protein Chemistry," Vol. 2, edited by P. Alexander and R. J. Block, Pergamon Press, Oxford, 1960, p. 245.
(18) C. F. C. MacPherson, M. Heidelberger, and D. N. Moore, *J. Am. Chem. Soc.*, **67**, 578 (1945).
(19) J. F. Foster and R. C. Rhees, *Arch. Biochem. Biophys.*, **40**, 437 (1952).

intramolecular configurational changes and aggregation—could be made.

Experimental

1. **Preparation of Protein Solutions.**—Crystalline lyophilized ovalbumin[20] was used throughout. Reagent grade chemicals were used for the preparation of buffer solutions. Protein solutions were prepared by addition of ovalbumin to the required volume of buffer. Water solutions of protein were prepared in a similar way with adjustment of the pH to the desired value by addition of hydrochloric acid or sodium hydroxide. Since solution of ovalbumin is incomplete and some "surface denatured" material is formed, all solutions were clarified by centrifugation prior to use.

Protein concentrations were determined from semimicro Kjeldahl nitrogen analyses (% N × 6.3).

2. **Heat Treatment.**—Protein solutions were divided into 15 or 20-ml. samples, contained in stoppered test tubes, and immersed in a water bath maintained at the desired temperature. At intervals of time ranging up to 150 minutes, a tube was removed and cooled rapidly in ice.

3. **Viscosity.**—The cooled solutions were equilibrated in a 30° bath for times of 30 to 120 minutes prior to measurement of viscosities. Flow times of all solutions were determined in an Ostwald–Fenske viscometer (100 bore—flow time for phosphate buffer, 59.4 seconds) at 30 ± 0.2°. Kinetic energy corrections were small and not applied. Since all solutions were clarified prior to heating and care was taken to prevent "surface denaturation" during handling, particulate matter offered no problem except at pH 5.5. Here, the particulate material formed during heating was removed prior to measurement of viscosity. The very viscous gel-like systems produced at the higher temperatures showed less reproducible values than the solutions treated at lower temperatures. Reduced viscosities were calculated from flow times relative to the buffer control. Throughout this paper, reduced and intrinsic viscosities will be expressed in units of (g. per 100 ml.)$^{-1}$.

Following the determination of viscosity, aliquots of the solutions were removed for nitrogen analysis, optical rotation, electrophoresis and sedimentation measurements.

4. **Optical Rotation.**—Optical rotations were determined at 5461 Å. in a one decimeter cell with a Rudolph precision polarimeter at room temperature (25–27°). If the turbidity of a solution was sufficient to prevent measurement of optical rotation, the sample was first clarified by centrifugation and analyzed again for nitrogen content. The unheated solutions containing 1.8% protein gave an average specific rotation of −36 ± 2°.

5. **Ultracentrifugation.**—Sedimentation velocity runs were made in a Spinco Model E ultracentrifuge (at 59,780 r.p.m. unless otherwise stated) maintained at a constant temperature of about 20° by a Spinco temperature control unit. Areas of peaks were determined with a planimeter from tracings of the fivefold enlarged plates, and corrected for radial dilution. The Johnston–Ogston effects were found to be negligible. Sedimentation rates, S, were corrected for viscosity and density according to the equation

$$S_{20,w} = (S_t)\left(\frac{\eta_t^{\text{solvent}}}{\eta_{20}^{\text{water}}}\right)\left(\frac{[1 - \bar{v}\rho]_{20,w}}{[1 - \bar{v}\rho]}\right)$$

A value of 0.749 cc./g. was used for v.

6. **Electrophoresis.**—Protein solutions were subjected to electrophoresis at 1° in a Perkin–Elmer Model 38A apparatus.

Results

Heat Treatment in Phosphate Buffer, pH 7.0.—The increases in reduced viscosity which occur upon heat treatment of 1.8% ovalbumin in phosphate buffer, pH 7.0, are shown in Fig. 1. Stiff, slightly turbid gels result at the temperatures of 73 and 75°. The turbidity in certain cases rendered optical rotation measurements impossible, so that clarification of these particular solutions was carried out by centrifugation prior to determination of rotation. This clarification procedure yielded firm gel-like residues and clear supernatants of much lower reduced viscosity. Table I lists the

(20) Worthington Biochemical Corporation, Freehold, New Jersey; lot No. 551 used throughout.

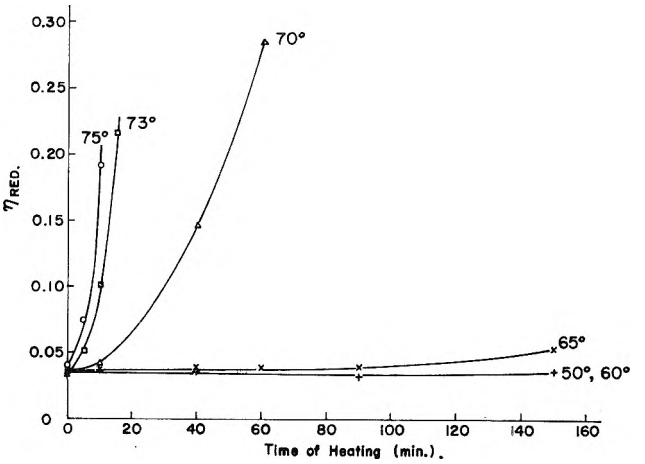

Fig. 1.—The effect of heat treatment on reduced viscosity of 1.8% ovalbumin in phosphate buffer, pH 7.0, 0.1 ionic strength.

TABLE I

EFFECT OF CLARIFICATION ON PROTEIN CONCENTRATION AND VISCOSITY OF OVALBUMIN SOLUTIONS HEATED IN PHOSPHATE BUFFER, pH 7.0

Heat treatment	% Protein		η_{red}	
	Original	Clarified	Original	Clarified
70°— 90 min.	1.80	1.51	0.324	0.072
150 min.	1.80	1.32	0.892	.057
73°— 30 min.	1.80	1.26	1.250	.077
40 min.	1.80	1.07	3.15	.065
60 min.	1.80	0.82	15.32	.051

changes in protein concentration and viscosity which occurred upon clarification. The ovalbumin remaining in solution shows viscosity behavior not greatly different from that of the native protein. The intrinsic viscosities of the protein remaining in the clear supernatants obtained from solutions heated at various temperatures are shown in Table II. The small increases in

TABLE II

EFFECT OF HEAT TREATMENT IN PHOSPHATE BUFFER, pH 7.0, ON INTRINSIC VISCOSITY OF OVALBUMIN

Sample	$[\eta]$
Native	0.040
150 min. at 60°	.041
150 min. at 62°	.040
150 min. at 65°	.050[a]
150 min. at 70°—clarified	.061[a]

[a] Shown to be polydisperse by ultracentrifugation.

$[\eta]$ noted after heating at 65 and 70° might suggest that the molecules had undergone a shape change during heating. Ultracentrifugation of these same solutions, however, revealed the presence of 5–10% of material which was much *faster* sedimenting than monomeric protein. Hence, the increased viscosity cannot be assigned to a configurational change. In those cases where no aggregate was seen, no increase in intrinsic viscosity was noted.

The specific levorotation of ovalbumin was increased only slightly (from a value of −36 to −41°) after heating for times from 60 to 150 min. at temperatures of 50, 60, 65, and 70°. A value for $[\alpha]$ of −43° was obtained for the protein after heating for 40 and 60 min. at 73° or 30 min. at 75°. The solutions which received heat treatments for times equal to or longer than 40 min. at 70°, 30 min. at 73°, and 20 min. at 75° required clari-

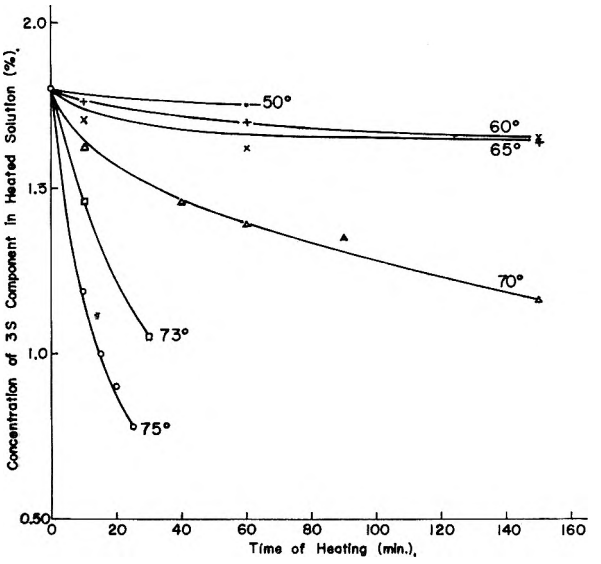

Fig. 2.—The effect of heat treatment on the concentration of monomeric (3S) ovalbumin in phosphate buffer.

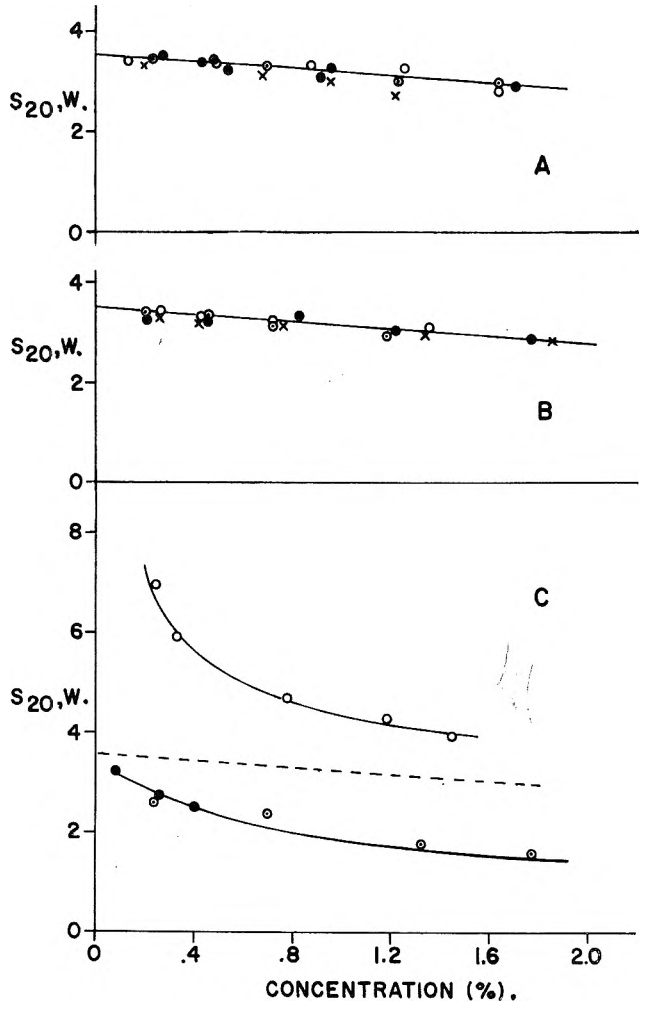

Fig. 3.—Concentration dependence of $S_{20,w}$ for native and heated ovalbumin. (A) Ovalbumin in phosphate buffer, pH 7.0; native (●); 3S component after 3 hours at 60° (⊙); 3S component after 3 hours at 65° (○); 3S component after 3 hours at 70°—clarified (×). (B) Ovalbumin in acetate buffer, pH 5.5; native (○); 3S component after 2.5 hours at 55° in acetate, pH 5.5 (●); native ovalbumin in veronal buffer, pH 8.5 (×); 3S component after 2.5 hours at 60° in veronal, pH 8.5 (⊙). (C) Ovalbumin in water, pH 7.0; native (⊙); 2S component after 2.5 hours at 75° (●); 4S component after 2.5 hours at 75° (○); native ovalbumin in phosphate buffer, pH 7.0 (- - - -).

fication before the optical rotations could be measured. These small increases in levorotation would not suggest very extensive changes in the configuration of the protein molecule.

Ultracentrifugation of the heated solutions revealed the continuous formation of aggregated ovalbumin during heating, this aggregate having a sedimentation rate of $\geqslant$ 40S. The remaining protein was a 3S component. The areas of the 3S peaks were measured and the concentrations of 3S material in the solutions were calculated using a value of 0.001865 for the specific refractive index increment of the protein at 5461 Å.[21] Figure 2 shows the concentration of monomer (3S) as a function of time of heating at the various temperatures. No material of sedimentation rate lower than 3S was seen in any of the heated solutions. The concentration of the 3S component in each solution was next plotted against the measured sedimentation rate. Figure 3a shows the concentration dependence of the sedimentation constants of native ovalbumin and the 3S material in a number of heated solutions. The data clearly indicate that this hydrodynamic property, $S_{20,w}^0$, is unaltered by heating. The relation between $S_{20,w}$ and concentration is given by $S_{20,w} = S_{20,w}^0 - kc$. Here $k = 0.35$ and $S_{20,w}^0 = 3.53$.

The results obtained after heating in phosphate buffer, pH 7.0, suggest that if irreversible denaturation (an intramolecular configurational change) occurs, it is not extensive since the intrinsic viscosity and intrinsic sedimentation constant of the monomer are apparently unchanged. The optical rotation reveals the only evidence of denaturation and amounts to only about a 7° increase in levorotation.

Effect of Protein Concentration at pH 7.0.—The changes in viscosity and sedimentation behavior following heat treatment of 1% solutions of the protein revealed similar results to those noted at the higher protein concentration. The increases in viscosity were less, as one would expect, and the rate of disappearance of monomer was slower. The aggregate produced had a sedimentation constant of $\geqslant$40S. Changes in optical rotation were very small and of rather poor precision, making them of questionable significance.

Effect of pH.—Similar heat treatment of 1.8% solutions was carried out in acetate buffer, pH 5.5, and veronal buffer, pH 8.5, both of 0.1 ionic strength. The rate of aggregation was greater in both cases than at pH 7.0, as is shown in Fig. 4. The changes in viscosity and levorotation which occurred at pH's 8.5 and 5.5 are shown in Fig. 5. A marked difference in physical form exists between solutions heated at pH's 5.5 and 8.5, however. At pH 5.5 heating leads to rapid development of turbidity and actual precipitation of the protein. This precipitate can be readily removed by centrifugation and the clarified solution shows only slight increases in levorotation ($\sim$ 7–10°) and viscosity (η_{red} increases from 0.035 to 0.048 (g./100 ml.)$^{-1}$ after 150 min. at 70°). The solution clarified after heating 150 min. at 55° (5–10% aggregate produced) contains essentially only 3S material and the concentration dependence of $S_{20,w}$ for this 3S component is identical with that of native ovalbumin, as shown in Fig. 3b. Here, $S_{20,w}^0 = 3.44$ and $k = 0.30$.

(21) G. E. Perlmann and L. G. Longsworth, *J. Am. Chem. Soc.*, **70**, 2719 (1948).

At pH 8.5 marked increases in levorotation and viscosity are produced with but very slight turbidity development. Ultracentrifugation of solutions heated at 65° at pH 8.5 revealed the presence of two components, 3S and 20S. The dependence upon concentration of the $S_{20,w}$ of the 3S component remaining after heating for 150 min. at 60° was identical with that of native protein as shown in Fig. 3b. Here, $S_{20,w}{}^0 = 3.39$ and $k = 0.31$.

Heat Treatment in Water, pH 7.0.—Heat treatment of 1.8% ovalbumin solutions in water, pH 7.0, produced the changes in viscosity and levorotation shown in Fig. 6. At 70° and 75° the viscosities of heated solutions are much less than those obtained in pH 7.0 buffer. The changes in $[\alpha]$, however, are much greater than those seen at 70 and 75° in buffer. These results would suggest greater denaturation but less aggregation under such conditions if optical rotation and viscosity were valid means for determining the presence of a denatured species. The ultracentrifuge revealed a single 2S peak for native ovalbumin in water, pH 7.0; a 2S peak for solutions heated at 65°; and two peaks, 2S and 4S, after heating at 70 and 75°. Figure 7 reveals that the rate of disappearance of the monomeric protein is somewhat slower in water than in buffer solution, pH 7.0. Figure 3c reveals the concentration dependence of $S_{20,w}$ for native ovalbumin in water, pH 7.0, along with the corresponding data for the monomer remaining in selected heated solutions. After dialysis against phosphate buffer, pH 7.0, the 2S component possessed a rate of sedimentation equal to that of the native protein in the same buffer. Figure 3c also shows the plot of $S_{20,w}$ *vs.* concentration for the 4S component. Here the sharp upward curve at low concentrations reveals the marked effect of absence of electrolyte. This 4S component had a $S_{20,w}$ in phosphate buffer, pH 7.0, of 13, indicating that it is a fairly large aggregate although not as large as those produced in the buffered systems. The results show that the monomer remaining after heating in water is also similar in sedimentation behavior to the native protein.

Effect of Heat Treatment on Electrophoretic Behavior.—Electrophoretic examination was made of several of the ovalbumin solutions heated in buffers at pH 7.0 and 8.5. A new, faster-moving electrophoretic component was continuously produced by heating at both conditions of pH. The fast peak had a mobility of about 2 units greater than the original protein when heated at pH 8.5. The mobility difference produced by heating at pH 7.0 was too small (0.5–1.0 unit) to effect complete resolution of the peaks.

In order to determine whether this faster component represented aggregated ovalbumin or a denatured monomer, heated solutions were centrifuged under conditions calculated to remove aggregate with minimal removal of monomeric protein. Typical results are shown in Fig. 8. Here, electrophoretic patterns are shown of the original protein and of solutions heated 30 min. at 73° in phosphate, pH 7.0, and 120 min. at 65° in veronal, pH 8.5, before and after centrifugation. These and many other unreported examples show that removal of aggregate (proved by ultracentrifugal examination) was accompanied by removal of the fast electrophoretic component. These results lead to the conclusion that no monomeric form different from the native in electrophoretic properties is present in the heated solutions.

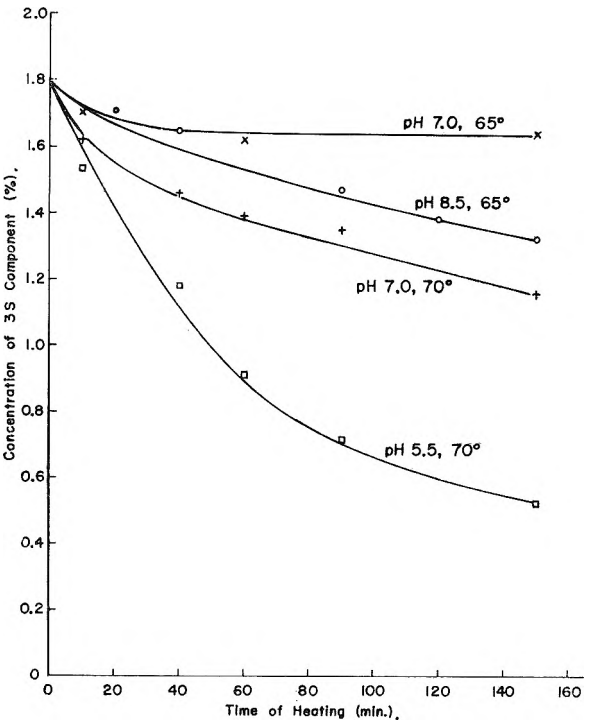

Fig. 4.—The effect of heat treatment on the concentration of monomeric (3S) ovalbumin in 0.1 ionic strength buffers.

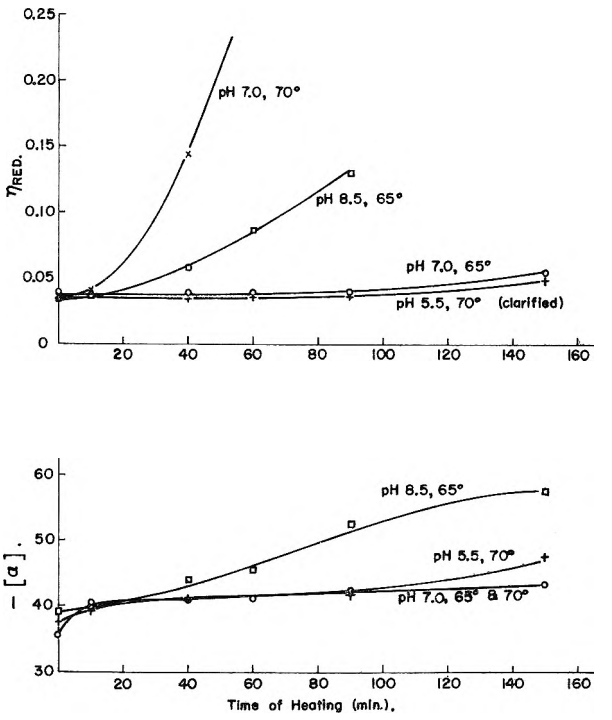

Fig. 5.—The effect of heat treatment on reduced viscosity and optical rotation of ovalbumin in 0.1 ionic strength buffers. Concentration of 1.8% ovalbumin.

Effect of Removal of Aggregate on Other Solution Properties.—Experiments described in the preceding sections have shown that the removal of aggregate (by centrifugation) lowers the viscosities of heated solutions to values comparable to those of the unheated samples and quantitatively removes the fast electrophoretic peak. Table III indicates the effects of removal of the aggregated protein on these and additional properties of heated protein solutions. It is evident

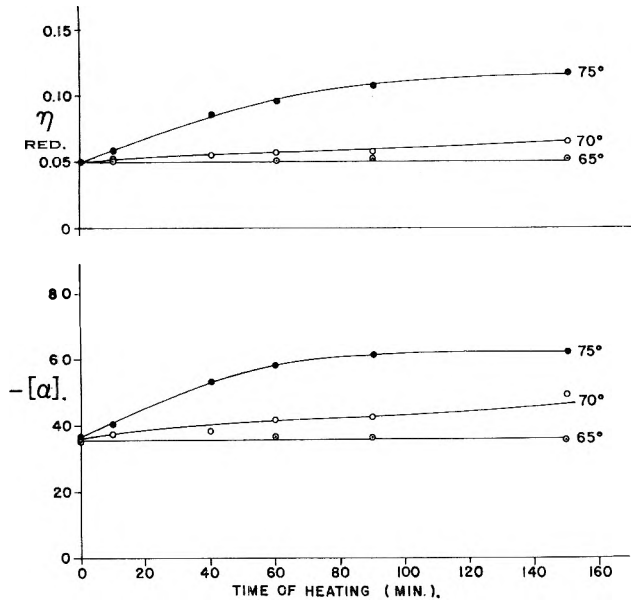

Fig. 6.—The effect of heat treatment on reduced viscosity and optical rotation of 1.8% ovalbumin in water, pH 7.0.

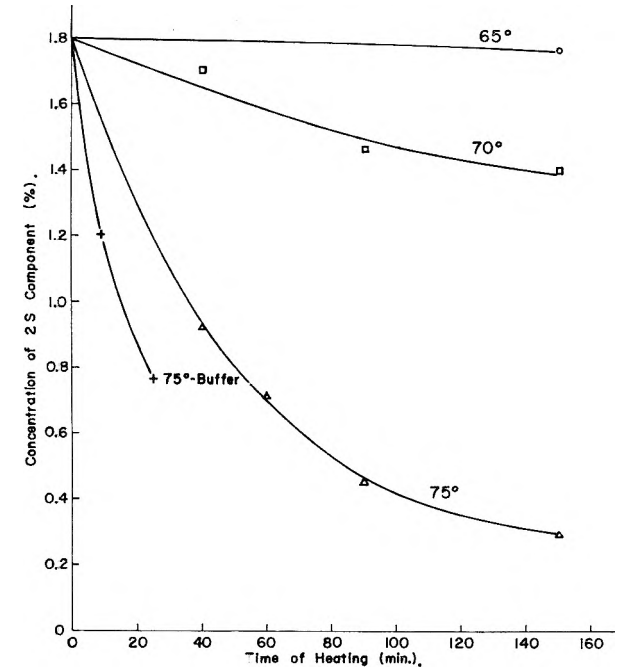

Fig. 7.—The effect of heat treatment on the concentration of monomeric (2S) ovalbumin in water, pH 7.0.

TABLE III

EFFECT OF REMOVAL OF AGGREGATE ON PROPERTIES OF HEATED OVALBUMIN SOLUTIONS

Sample	Protein concn.[a]	[α]	η_{red}	No. of components EL	UC
A. Phosphate buffer, pH 7.0					
Unheated	1.8%	−35.5°	0.036	1	1
Heated 90 min. at 70°[b]	1.8	(−43)	very high	(2)	2
Up to speed 40,000 r.p.m.	1.1	−33.6	0.044	1	1
30 min. at 40,000 r.p.m.	1.1	−34.5	0.036	1	1
120 min. at 40,000 r.p.m.	1.1	−27.1	0.036	1	1
B. Veronal buffer, pH 8.5					
Unheated	1.7%[c]	−39.0°	0.035	1	1
Heated 2 hr. at 65°	1.7	−53.4	0.317	2	2
15 min. at 40,000 r.p.m.	1.4	−45.9	0.293	2	2
150 min. at 40,000 r.p.m.	1.2	−40.2	0.053	1	1

[a] Kjeldahl nitrogen × 6.3. [b] Solution too turbid to measure α or see peaks in electrophoresis. [c] Protein concentration calculated from area of sedimentation peaks.

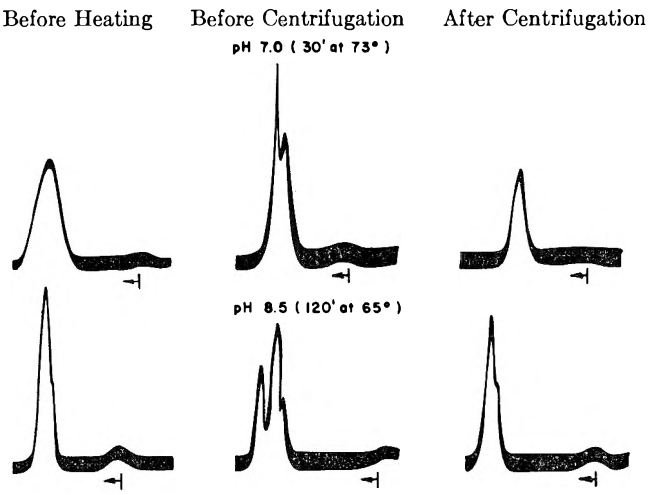

Fig. 8.—Descending electrophoretic patterns of heated ovalbumin solutions before and after removal of aggregated protein by centrifugation.

that all molecular properties measured here return to values not greatly unlike those of the native protein when the aggregated protein is removed. The fact that the optical rotation also returns to values near the original is consistent with the idea that the properties of the aggregate might determine those properties of the solutions which have been chosen as criteria for denaturation (intramolecular change) of the protein.

Additional Tests for the Presence of a Denaturated Monomeric Component. a. Tests for Reversible Denaturation.—Optical rotation measurements of 1.8% ovalbumin in phosphate, pH 7.0, and veronal, pH 8.5, were made during heating at 60, 65, and 70° for times up to 150 min. and during subsequent cooling to room temperature (cooling was allowed to occur slowly in some cases, rapidly in others). No evidence was found that the optical rotations while the solutions were hot exceeded those values reported earlier which were measured at room temperature, indicating the absence of a reversible effect.

The viscosity of a 2% ovalbumin solution was determined during heating at 60° for times up to 150 min. No indication was found that the reduced viscosity exceeded the values reported earlier for cooled solutions, thus failing to support a reversible denaturation step.

b. Insolubility of the Isoelectric Point.—Since irreversibly denatured proteins are commonly understood to be insoluble under isoelectric conditions, a number of experiments were performed in which solutions heated in phosphate buffer, pH 7.0, and veronal buffer, pH 8.5, were dialyzed against water and 0.3 *M* sodium chloride solutions or acetate buffer, pH 5.5. The amount of protein which precipitated was determined from nitrogen analyses and the final supernatants were examined by ultracentrifugation. In all cases the loss of protein by such precipitation treatments and the decrease in area of sedimenting peaks were equal (within 5–10%) to the amount of aggregated protein known exist in the heated solutions. The heating conditions examined in such a manner included 2 and 3 hr. at 65°, 2 hr. at 70°, and 2 hr. at 75°. An additional fractional precipitation experiment was performed in which a solution heated 3 hours at 65° in phosphate buffer, pH 7.0, was dialyzed against water, then 0.3 *M* NaCl, clarified and analyzed for protein concentration. This supernatant was then treated with additional

quantities of sodium chloride to give concentrations up to 1.74 *M*. No precipitation other than at 0.3 *M* sodium chloride was encountered until a concentration of 1.74 *M* salt was reached. Since native ovalbumin acted similarly at the high concentration of salt, no peculiar properties of the heated protein were recognized.

Discussion

A denatured protein is one in which the three-dimensional configuration of the molecule is considered to be different from that of the native form; generally the denatured state is believed to be a state of less order. The process of denaturation is one during which this change in configuration occurs and leads to a form of the protein which *may* then aggregate. In order to characterize the nature of the configurational change it is essential that the denatured form of the protein be isolated. The properties of this molecule must then be such as to explain the changes in solution properties one sees during the denaturation process which produced this species.

The present study has included the application of a number of physical techniques to follow the thermal denaturation and aggregation of ovalbumin. Changes in properties commonly associated with the formation of a denatured protein such as optical rotation, viscosity, electrophoretic mobility and solubility have been measured. It has been found that aggregation of the protein occurs simultaneously with changes in these properties making it difficult to assign these changes to an intramolecular process. Heat treated solutions which contain aggregated protein have been subjected to centrifugation to remove the aggregate. The properties of viscosity, optical rotation, sedimentation rate, electrophoretic mobility and solubility of the monomeric form of ovalbumin remaining in the solutions have been found to be essentially the same as those of the native protein. These observations have led to the conclusion that ovalbumin molecules of significantly different configuration than native do not exist in the heated solutions.

Other workers have reported denatured forms of proteins possessing unchanged hydrodynamic properties. Saenko[22] and Strachitskii and Furfarova[23] reported this for ovalbumin and serum albumin based on viscosity measurements. Connell[24] has reported a denatured monomeric form of cod myosin which cannot be distinguished ultracentrifugally from the native form. The heat treatment of thyroglobulin[25] and bovine serum albumin[26] leads to formation of monomeric denatured forms which have the same sedimentation properties as the native molecules. In the last mentioned case the denatured species was recognized by insolubility at high salt concentrations at the isoelectric pH after 2 minutes of heating at 65° in phosphate buffer, pH 7, 0.2 ionic strength. No evidence of such a form of ovalbumin was found in the present work.

The literature does not reveal many examples of unequivocal proof of the existence of monomeric denatured form of protein possessing markedly different hydrodynamic properties. Configurational changes are induced in certain proteins at certain pH values which do result in changes in sedimentation and viscosity. Charlwood and Ens have reported this for BSA, HSA, and horse serum albumin in the pH range 3–5[27] and Pedersen[28] has reported the effect of pH in the range of 6–8 on the sedimentation of β-lactoglobulin. Arachin is denatured to a species which is slower sedimenting and of greater reduced viscosity by alkali and 4 *M* guanidine hydrochloride.[29] Alexander and Hamilton[30] found a form of BSA which was not different in molecular weight but lower in sedimentation constant than native, which was produced by limited radiation. This form was not found in heat denaturation work, however. Jirgensons[31] reports an unchanged molecular weight but increased intrinsic viscosity upon exposure of γ-globulin to heat in the presence of 3 *M* guanidine·HCNS. *p*-Dioxane profoundly enhances the expansion of the BSA molecule in acid media as measured by sedimentation and viscosity.[32]

Some proteins appear to dissociate under denaturing conditions or in solution of extremes of pH, for example, catalase,[33] β-lactoglobulin,[34] and thyroglobulin.[35] There are many other instances where the presence of aggregated forms of protein present difficulties in interpretation of denaturation results. Cohn and Kesslinger[36] point this out in a study of the reversible inactivation of chymotrypsin; RNase was aggregated in ethylene glycol[37]; and the many references to sulfhydryl induced aggregation in heat and urea denaturation[38–40] are well known.

Since the heated solutions in the present study contain only aggregated and native ovalbumin molecu'es, the conversion of an intermediate "denatured" species to aggregate must be very rapid. This situation makes it virtually impossible to assign any characteristics to the denatured form. The only evidence found in this work for a denaturation process is the increase in levorotation. This fact alone does not aid in describing the type of configurational change involved nor the extent of this change. Generally, the extent of "unfolding," for example, would be taken to be small since the increases in levorotation are small. However, since aggregation is occurring and since this process could yield rotational changes too[41] (generally decreasing levorotation), the net change in optical rotation observed is an average of these different processes and does not predict the importance of either alone. It is also possible that configurational changes in the monomers occur as a result of aggregation or as a result of the tendency of the protein to aggregate. The newly-

(22) T. V. Saenko, *Ukr. Biokhim. Zh.*, **24**, 196 (1952).
(23) K. I. Strachitskii and H. F. Furfarova, *Biokhimiya*, **18**, 2235 (1953).
(24) J. J. Connell, *Biochem. J.*, **75**, 520 (1960).
(25) H. P. Lundgren and J. W. Williams, *J. Phys. Chem.*, **43**, 989 (1939).
(26) R. C. Warner and M. Levy, *J. Am. Chem. Soc.*, **80**, 5735 (1958).
(27) P. A. Charlwood and A. Ens, *Can. J. Chem.*, **35**, 99 (1957).
(28) K. O. Pedersen, *Biochem. J.*, **30**, 961 (1936).
(29) W. E. F. Naismith and R. K. Williams, *J. Polymer Sci.*, **26**, 199 (1957).
(30) P. Alexander and L. D. G. Hamilton, *Arch. Biochem. Biophys.*, **88**, 128 (1960).
(31) B. Jirgensons, "Natural Organic Macromolecules," Pergamon Press, New York, N. Y., 1962, p. 196.
(32) K. E. Van Holde and S. F. Sun, *J. Am. Chem. Soc.*, **84**, 66 (1962).
(33) T. Samejima and K. Shibata, *Arch. Biochem. Biophys.*, **93**, 407 (1961).
(34) L. M. Gilbert and G. A. Gilbert, *Nature*, **192**, 1181 (1961).
(35) H. Edelhoch and H. Metzger, *J. Am. Chem. Soc.*, **83**, 1428 (1961).
(36) M. Cohn and S. Kesslinger, *J. Biol. Chem.*, **235**, 1365 (1960).
(37) H. J. Sage and S. J. Singer, *Biochemistry*, **1**, 305 (1962).
(38) V. D. Hospelhorn and E. V. Jensen, *J. Am. Chem. Soc.*, **76**, 2830 (1954).
(39) I. M. Kolthoff, A. Anastasi, and B. H. Tan, *ibid.*, **82**, 4147 (1960).
(40) V. D. Hospelhorn, B. Cross, and E. V. Jensen, *ibid.*, **76**, 2827 (1954).
(41) W. B. Neely, *ibid.*, **82**, 4354 (1960).

linked monomers may alter their shape to achieve a more stable arrangement with their neighbors. This whole question becomes, "is the aggregate made up of native or denatured molecules?" This is an old question and one which is very difficult to answer.

The present work has revealed the value of using ultracentrifugation along with *any other* technique for studying protein denaturation. The recognition of the aggregate in the heated solutions, particularly during the early stages of heating and with solutions in which very little turbidity (veronal, pH 8.5) or no turbidity (water, pH 7) arose has prevented the assignment of changes in such properties as viscosity, optical rotation, solubility and electrophoretic mobility to the formation of a new monomeric species. This technique is proving of real value too in work with other proteins and with other denaturing agents than heat. It may be that rather subtle configurational changes are involved in the actual "denaturation" of ovalbumin and that aggregation follows rapidly leading to the actual species which others have pictured as the one of different intramolecular configuration.

Acknowledgments.—The author wishes to acknowledge the valuable technical assistance which Mr. Walter Gagen and Mr. James Smith provided to the experimental portion of this study.

KINETICS OF THE LOW PRESSURE NITROUS OXIDE DECOMPOSITION ON A PLATINUM FILAMENT[1]

BY JOHN P. REDMOND

Applied Physics Laboratory, The Johns Hopkins University, Silver Spring, Maryland

Received September 13, 1962

The decomposition of nitrous oxide on a platinum filament has been investigated over a pressure range of 0.02 to 4.0 mm. and a temperature range of 545 to 820°. The reaction kinetics have been found to fit the Langmuir–Hinshelwood equation for a unimolecular decomposition with poisoning by atomic oxygen. The apparent activation energy is 32 ± 1 kcal./mole. Added oxygen has the same poisoning effect on the reaction rate as the product oxygen. Nitric oxide is produced in small amounts during the decomposition at the higher pressures. However, neither nitric oxide nor nitrogen has been found to poison the reaction.

Introduction

Hinshelwood and Pritchard[2] investigated the catalytic decomposition of nitrous oxide on platinum in the pressure region from 50 to 400 mm. and found the reaction velocity (r) to be represented by the equation

$$r = k[N_2O]/(1 + b[O_2]) \qquad (1)$$

where b is a constant. This reaction is a classical example of Langmuir–Hinshelwood kinetics for a unimolecular surface reaction with poisoning by a product.[3] However, this kinetic expression does not hold at low pressures (<1 mm.), and there is some uncertainty as to what is the correct rate equation for the low pressure decomposition on platinum. Cassel and Glückauf[4] have proposed the equation

$$r = k[N_2O](1 + b[O_2]^{1/2})/(1 + b'[O_2]^{1/2}) \qquad (2)$$

Also, Van Praagh and Topley[5] have studied the kinetics in the low pressure region and reported that the reaction rate was variable. More recently, Miyazaki[6] investigated the decomposition kinetics between 0 and 270 mm. and found the relationship

$$r = k[N_2O]/(1 + b[N_2O])(1 + b'[O_2]) \qquad (3)$$

The decomposition of nitrous oxide has been reviewed by Laidler[7] and he considers the above rate expressions as special cases of the Langmuir–Hinshelwood general expression.

In addition to the confusion in kinetics, there is also some question as to the nature of the adsorbed oxygen and the effect of added oxygen. The theoretical rate equation employed by Hinshelwood and Pritchard was derived on the basis of molecular oxygen adsorption, but Schwab and Eberle[8a] and Steacie and McCubbin[8b] have reported that the product oxygen was adsorbed as atoms. This atomic adsorption is in agreement with the low pressure kinetics of Cassel and Glückauf. In addition, Steacie and McCubbin have studied the effect of added oxygen on the reaction rate. They applied their rate data to eq. 1 and found that added oxygen lowered the rate constant (k) but did not enter into the $b[O_2]$ term. They concluded, therefore, that the product oxygen was adsorbed as atoms but that added oxygen was adsorbed as molecules. Yet the chemisorption of oxygen on metals is generally considered to result in oxygen atoms bound to the surface.[9]

Because of the conflicting kinetic interpretations of the reaction rate, a re-investigation of the decomposition may help to clarify the situation. This investigation has been aided by better vacuum and analytical techniques not available to the early workers, and the experimentally determined rate equation has been applied to some of the more recently developed kinetic theories based on adsorption isotherms other than Langmuir's.[10,11] The results of this study may be important to programs employing the nitrous oxide decomposition reaction to correlate the catalytic and electronic properties of solids.[12]

(1) This work supported by Bureau of Naval Weapons, Department of the Navy, under NOw 62-0604-e.

(2) C. N. Hinshelwood and C. R. Pritchard, *J. Chem. Soc.*, **127**, 327 (1925).

(3) C. N. Hinshelwood, "Kinetics of Chemical Change," Oxford University Press, New York, N. Y., 1940, p. 192.

(4) H. Cassel and E. Glückauf, *Z. physik. Chem.*, **B9**, 427 (1930).

(5) G. Van Praagh and B. Topley, *Trans. Faraday Soc.*, **27**, 312 (1931).

(6) S. J. Miyazaki, *J. Chem. Soc. Japan*, **72**, 723 (1951).

(7) K. J. Laidler, "Catalysis," Vol. I, edited by P. H. Emmett, Reinhold Publ. Corp., New York, N. Y., 1954, Chap. 4.

(8) (a) G. M. Schwab and B. Eberle, *Z. physik. Chem.*, **B19**, 102 (1931); (b) E. W. Steacie and J. McCubbin, *J. Chem. Phys.*, **2**, 585 (1934).

(9) B. M. W. Trapnell, "Chemisorption," Butterworth Scientific Publications, London, 1955, p. 180.

(10) M. Temkin and V. Pyzhev, *Acta Physicochim. URSS*, **12**, 237 (1940).

(11) T. Kann, *J. Phys. Chem.*, **60**, 1083 (1956).

(12) R. M. Dell, F. S. Stone, and P. F. Tiley, *Trans. Faraday Soc.*, **49**, 201 (1953).

Experimental

Apparatus.—The experimental set-up shown in Fig. 1 consists of a glass apparatus connected directly to a Westinghouse Type LV mass spectrometer. The apparatus has two sections. The first is designed to purify and store gases employed in the reaction study and in the mass spectrometer calibration. The second section is designed to carry out the reaction study. The volume of the reactor is 1.17 liters. The reactor flask contains two tungsten lead-throughs to which a spiraled platinum filament is spot-welded. A side arm connects the flask to a one-liter per sec. VacIon pump which is capable of producing a vacuum of 1×10^{-8} mm. Also the side arm is connected to the mass spectrometer by a glass leak with an orifice diameter of 0.0025 cm. Hoke diaphragm type metal valves are used in this section. The reactor and the intervening tubing to the mass spectrometer are wrapped with heating tape to provide a moderate bake-out of 150°.

The filament's temperature above 700° is measured by a disappearing filament optical pyrometer. The emissivity of the wire and the reflectivity and absorptivity of the glass are taken into account in computing the true temperature from the measured brightness temperature. The filament's resistance is measured by making it one branch of a Wheatstone bridge, and a temperature-resistance calibration curve is made. During a run the filament temperature is automatically controlled to prevent temperature drift due to changes in the thermal conductivity of the gas mixture. This is accomplished by controlling the current in the bridge circuit through a series transistor regulator. The control signal for the regulator is provided by amplifying and phase detecting a small 2 kilocycle modulation superimposed upon the bridge circuit.

The mass spectrometer has been modified to include a peak selector which consecutively monitors four independent preselected mass numbers during a two-minute time cycle. The peak height for each mass number can be attenuated by an appropriate scale factor in order to record the signal.

The gases used in this investigation, N_2O, O_2, N_2, and NO, were commercially available. They were further purified by freezing out the impurities in liquid nitrogen or Dry Ice cold traps. The gases were analyzed by the mass spectrometer. Nitrous oxide was repeatedly distilled between liquid nitrogen and Dry Ice traps to remove almost all impurities. However, analysis indicated that water vapor and oxygen were present in the range of 100 and 30 p.p.m., respectively. Nitrogen and nitric oxide also may have been present in low concentrations, but the cracking pattern of nitrous oxide interferred with their determination. The gas purities of oxygen and nitrogen used in this study were in the order of 99%. The nitric oxide analysis showed approximately 4% nitrogen present as an impurity.

The platinum filament obtained from Engelhard Industries was 3.3×10^{-2} cm. in diameter and had a calculated surface area of 2.6 cm.^{2}.

Results and Discussion

Kinetics.—A typical graph of the experimental data for a decomposition run is shown in Fig. 2 where the decrease of nitrous oxide pressure with time is plotted. The reaction rates (dP_{N_2O}/dt) are obtained from Fig. 2 by drawing tangents to the curve; these tangents are drawn with the aid of a prism.[13] By plotting the reaction rate against various concentration functions, it is possible to determine the form of the kinetic rate equation. In Fig. 3, the rates are plotted against $P_{N_2O}/(1 + P_{O_2}^{1/2})$ for a series of runs at different temperatures and a nitrous oxide pressure of ~100 μ. Shortly after the reaction begins, the $P_{O_2}^{1/2}$ term in the denominator becomes greater than unity, and the approximate form of the rate equation is

$$-\frac{dP_{N_2O}}{dt} = k\frac{P_{N_2O}}{P_{O_2}^{1/2}} \qquad (4)$$

where k is an apparent rate constant. In Fig. 3, the curves are fairly linear with the exception of the points near the start of the run where the reaction rates and concentration functions are largest. The slopes of

(13) V. L. Frampton, *Science*, **107**, 323 (1948).

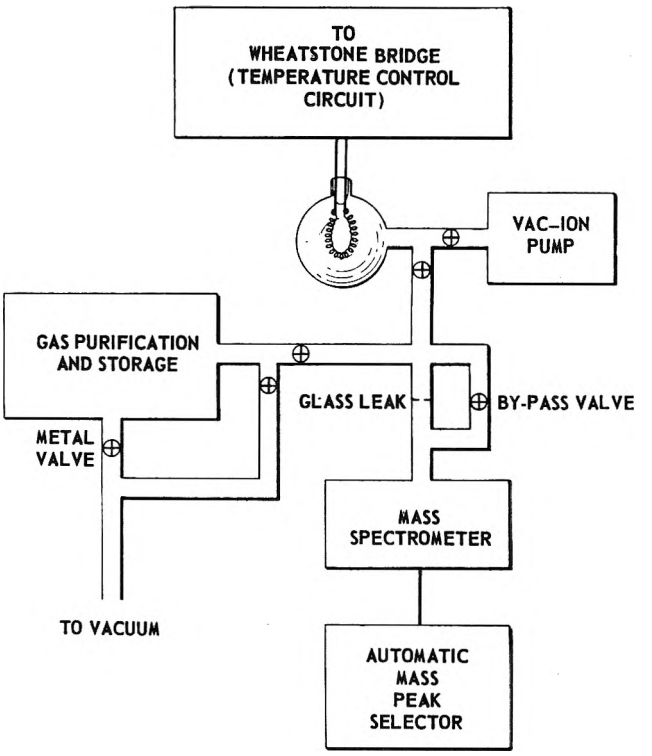

Fig. 1.—Schematic diagram of the experimental apparatus.

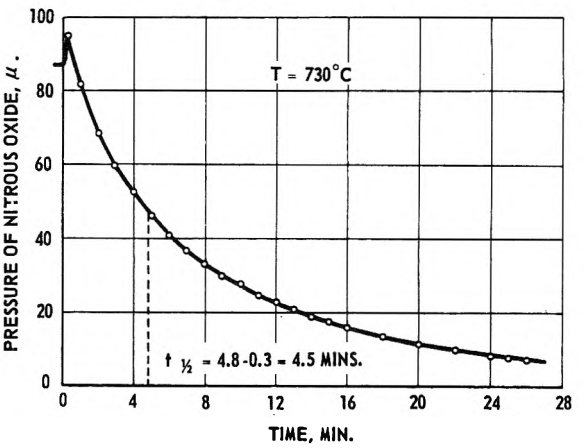

Fig. 2.—Typical nitrous oxide decomposition run. The time for the filament to attain reaction temperature is 0.3 min., during which time the pressure increases from 88 to 95 μ.

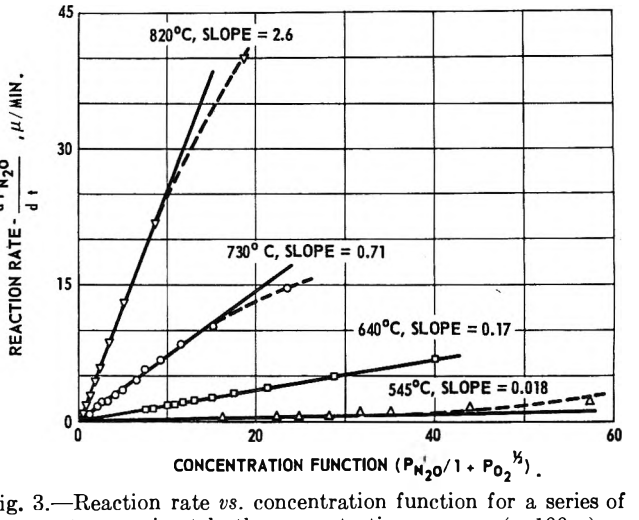

Fig. 3.—Reaction rate *vs.* concentration function for a series of runs at approximately the same starting pressure (~100 μ).

these curves are equal to the apparent rate constant. In Table I, the apparent rate constants are listed for a series of runs at different temperatures. A factor of 3.66×10^4 is used to convert the units of the apparent rate constant from $\mu^{1/2}$ min.$^{-1}$ to (molecules/cc.)$^{1/2}$ sec.$^{-1}$ cm.$^{-2}$, which is the rate constant per unit area of catalyst.

TABLE I

APPARENT RATE CONSTANT AND HALF-LIFE VALUES AT VARIOUS TEMPERATURES AND PRESSURES

T, °C.	P_{N_2O}, μ	$t_{1/2}$, min.	$k \times 10^{-4}$, (molecules/cc.)$^{1/2}$ sec.$^{-1}$ cm.$^{-2}$
545	94	..	0.065
	118	..	.070
590	158	74	.183
640	21.4	9.7	.62
	41.1	11.5	.70
	89.6	18.7	.56
	103.5	19.7	.59
	111	21.2	.60
	336	31	.62
	570	37.3	.70
730	30	2.9	2.7
	38.5	2.7	2.8
	91	5.5	2.1
	95	4.5	2.6
	102	4.8	2.5
	109	5.7	2.1
	174	6.0	2.5
	540	7.9	3.2
	970	10.5	3.8
	1450	10.9	4.0
	2970	15.0	4.6
	2970	14.7	5.1
	4200	17.5	4.9
820	118.5	1.4	9.5
	860	3.0	11.6
	1325	3.3	14.4
	2200	5.0	14.0

The rate expression (eq. 4) is similar to the Langmuir–Hinshelwood kinetic equation for a unimolecular decomposition with strong poisoning by the product.[3] Recently a number of other kinetic equations have been developed which are similar to Langmuir–Hinshelwood kinetics and may be applicable to nitrous oxide decomposition kinetics. Temkin and Pyzhev[10] have derived a rate equation for the ammonia decomposition based on the Elovich equation and the Temkin isotherm, and Kann[11] has interpreted a number of catalytic reactions based on the Freundlich isotherm.

If the rate controlling step is the adsorption of nitrous oxide which is represented by the Elovich equation, and if the surface coverage is primarily due to oxygen which obeys the Temkin isotherm, the resulting kinetic equation is

$$r = k \frac{P_{N_2O}}{(AP_{O_2})^{\alpha/\sigma}} \qquad (5)$$

where A is a constant, α and σ are proportionality constants relating the variation of activation energy for nitrous oxide adsorption and the heat of oxygen adsorption with coverage, respectively.

The ratio of α/σ is less than 1/2 since the variation of the heat of oxygen adsorption (σ) with coverage on platinum is large[14] while the activation energy for nitrous oxide adsorption based on Hirschfelder rules[15] is small. Consequently, α would be small, and the ratio of α/σ would be less than a half in contradiction to the experimentally determined value of one-half for the power dependence on oxygen.

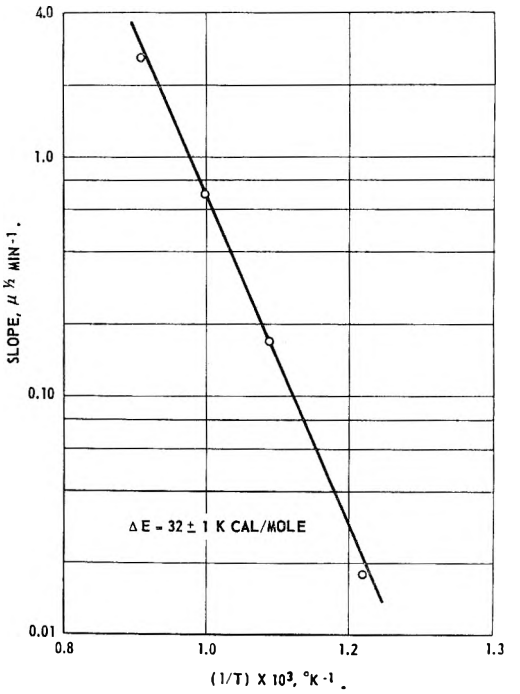

Fig. 4.—Arrhenius plot; slopes in Fig. 3 are taken as the rate constants.

The rate equation for the nitrous oxide decomposition based on Kann's assumptions is

$$r = k \frac{(P_{N_2O})^{\beta/n}}{(P_{O_2}^{1/2})^{\beta'/n'}} \qquad (6)$$

where $1/n$ and $1/n'$ are the fractional power of the pressure for the Freundlich isotherms for nitrous oxide and oxygen adsorption, respectively, and β and β' are the power exponents for the kinetic equations for the nitrous oxide surface reaction and the oxygen desorption, respectively. Since $n = \alpha + \beta$ where α is the power exponent for the adsorption kinetic equation, it is not likely that $\beta/n = \beta'/n' = 1$. Therefore the kinetics based on either the Temkin or the Freundlich isotherm do not apply to the nitrous oxide decomposition.

The Langmuir–Hinshelwood kinetic equation for the decomposition (with weak nitrous oxide adsorption) is

$$\frac{dP_{N_2O}}{dt} = \frac{k_0 K_1 P_{N_2O}}{1 + K_2 P_{O_2}^{1/2}} \qquad (7)$$

where k_0 equals the true rate constant, K_1 and K_2 are the adsorption equilibrium constants for nitrous oxide and oxygen, respectively. Setting K_2 equal to unity, the above equation reduces to the form which is plotted in Fig. 3. As mentioned earlier, the slopes of the linear portion of the curves in Fig. 3 are equal to the apparent rate constant. An Arrhenius activation energy is obtained by plotting the logarithm of these slopes against the reciprocal of the temperature; this is shown in Fig. 4. The apparent activation energy is 32 ± 1 kcal./mole which is in good agreement with the values reported by previous workers. Hinshelwood and Prit-

(14) G. B. Taylor, G. B. Kistiakowsky, and J. H. Perry, *J. Phys. Chem.*, **31**, 799 (1930).

(15) J. Hirschfelder, *J. Chem. Phys.*, **9**, 645 (1941).

chard[2] reported a value of 32.5 kcal./mole and Miyazaki[6] reported a value of 31.8 kcal./mole. Since the apparent rate constant (k) equals k_0K_1/K_2, the apparent activation energy is given by the relationship

$$\Delta E_{app} = \Delta E_{true} - \lambda_1 + \lambda_2 \qquad (8)$$

where λ_1 and λ_2 are the heats of adsorption for nitrous oxide and oxygen, respectively.

If K_2 is an equilibrium constant, its value will vary with temperature and cannot be set equal to unity at all temperatures as is done in Fig. 3. This is the reason why the initial points do not fall on the curve in the above figure. According to eq. 4, once the reaction gets underway, any variation in K_2 is hidden in the apparent rate constant. The evaluation of K_2 and its temperature dependence would aid in the establishment of the correct kinetic mechanism, but it is not possible to evaluate K_2 from the differential rate equation because the $K_2P_{O_2}^{1/2}$ term exceeds unity except at the very beginning of a run. During this initial period the experimental error is largely due to a pressure rise caused by the heating of the filament. However, it is possible to evaluate K_2 by integrating eq. 7 and substituting in the values at the half-life. Integration of eq. 7 produces the equation

$$\ln (a/(a-x)) - K_2\sqrt{2x} + K_2\sqrt{\frac{a}{2}}\ln\left(\frac{\sqrt{a}+\sqrt{x}}{\sqrt{a}-\sqrt{x}}\right) = k_0K_1t \qquad (9)$$

where (a) equals the starting pressure of nitrous oxide and (x) corresponds to the pressure of nitrous oxide which has decomposed. At the half-life ($t_{1/2}$), $x = a/2$ and the above equation reduces to

$$\frac{0.696}{k_0K_1} + \frac{0.246\ K_2}{k_0K_1}\sqrt{a} = t_{1/2} \qquad (10)$$

The values of k_0K_1 and K_2 may be obtained from the intercept and slope of a plot of the above equation. The half-life values listed in Table I are plotted against the square root of the initial nitrous oxide pressure at three different temperatures in Fig. 5. The curves are fairly linear, substantiating the integrated half-life equation. In Table II, the slopes and intercepts are listed along with the corresponding values of K_2 and k_0K_1. When plotting the data according to eq. 7, the actual value of K_2 is evident only at the start of a run. During this initial period, however, the reaction rate is largest and most difficult to measure accurately. A comparison of the rate data when plotted according to the concentration function ($P_{N_2O}/1 + K_2P_{O_2}^{1/2}$) for different values of K_2 is shown in Fig. 6. The upper curve corresponds to an assumed value of K_2 equal to 1.0 $\mu^{-1/2}$ in the concentration function, and the lower curve corresponds to a K_2 value of 0.29 $\mu^{-1/2}$. This K_2 value is obtained from Table II at 730°. In Fig. 6, the first point falls on the predicted curve when the K_2 value is taken from Table II. The slope of the upper curve is equal to the apparent rate constant, while the slope of the lower curve is equal to k_0K_1.

A semilogarithmic plot of K_2 *vs.* the reciprocal of the temperature gives a value of approximately 18 kcal./mole for the heat of adsorption of oxygen on platinum. Based on the heat of oxygen adsorption measurements

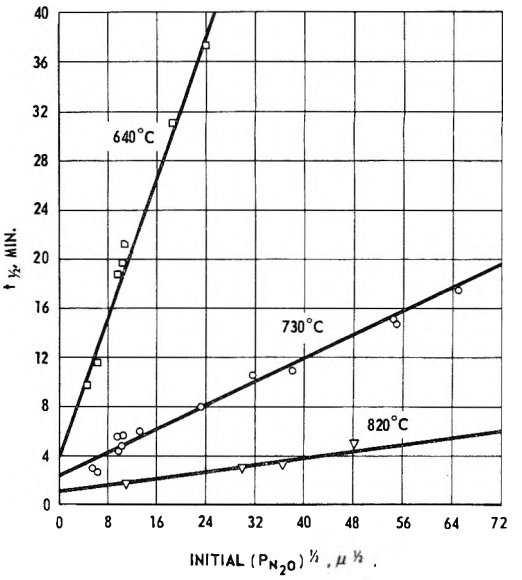

Fig. 5—Half-life *vs.* square root of nitrous oxide starting pressure.

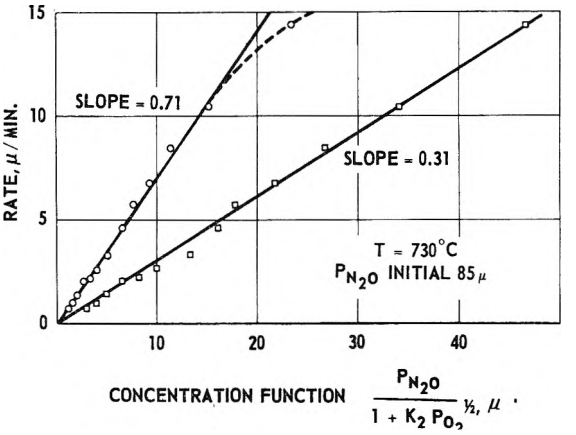

Fig. 6.—Reaction rate *vs.* concentration function: the upper curve corresponds to a K_2 value of 1.0 $\mu^{-1/2}$ in the concentration function, while the K_2 value for the lower curve is 0.29 $\mu^{-1/2}$.

TABLE II

EVALUATION OF CONSTANTS IN EQ. 10

T, °C.	Slope	Intercept	K_2, $\mu^{-1/2}$	k_0K_1, min.$^{-1}$	k_0K_1/K_2,[a] $\mu^{1/2}$ min.$^{-1}$
545[b]	...	...	3.0	0.062	0.02
595[b]	...	...	1.5	.08	0.05
640	1.45	4.0	1.03	.17	0.17
730	0.246	2.4	0.29	.29	1.0
820	0.062	1.0	0.17	.70	4.1

[a] k_0K_1/K_2 equals the apparent rate constant. [b] The half-life data are not sufficient to plot. The value of k_0K_1 is obtained from eq. 7 by empirically adjusting K_2 to give a linear plot of the data including the initial points.

with coverage by Brennan, *et al.*,[16] a value of 18 kcal./mole indicates that the platinum surface is nearly covered during a run, and according to eq. 7, the oxygen is adsorbed as atoms, which is in agreement with Harano,[17] who has studied the release of oxygen atoms from a platinum surface treated with nitrous oxide.

If the platinum filament's active surface is nearly saturated, this covered surface would be consistent with Langmuir–Hinshelwood kinetics in two respects. First, a heavily covered platinum surface is not likely to have a large energy variation with a change in coverage;

(16) D. Brennan, D. O. Hayward, and B. M. W. Trapnell, *Proc. Roy. Soc.* (London), **256**, 81 (1960).

(17) Y. Harano, *Nippon Kayaku Zasshi*, **82**, 22 (1961).

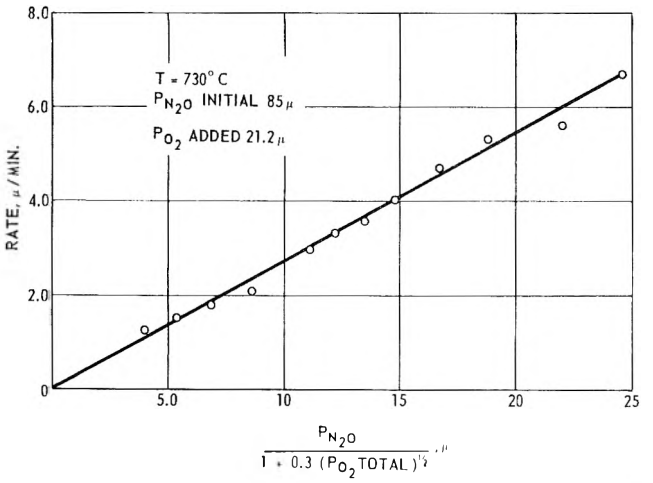

Fig. 7.—Reaction rate *vs.* concentration function where P_{O_2} total equals the sum of added and product oxygen.

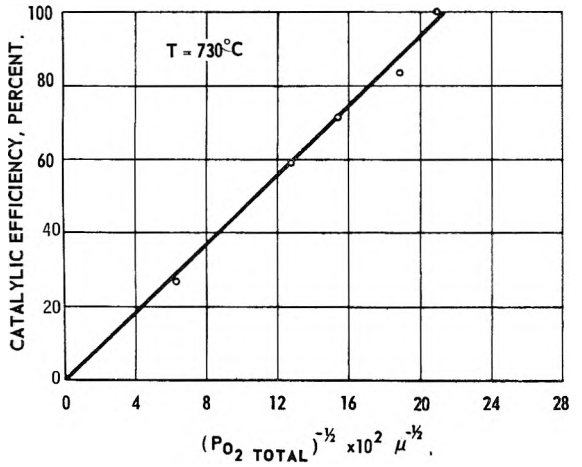

Fig. 8.—Variation of catalytic efficiency with added oxygen for a series of runs at approximately the same nitrous oxide starting pressure (~90 μ).

Langmuir–Hinshelwood kinetics are based on the assumption that the energy terms do not vary with coverage. Second, the rate equation indicates that the reaction is poisoned by oxygen atoms, which again suggests that a large number of the sites must be covered.

It is of general interest to calculate the apparent rate constant from the transition state theory and to compare it with the experimental value; this will aid in checking the proposed reaction kinetics. The apparent rate constant in terms of partition functions for the case of unimolecular reaction with strong poisoning is given below[18]

$$k_{app} = \frac{k_0 K_1}{K_2} = \frac{L k_B T}{h} \frac{f_{\neq} F_{gp}^{1/2}}{f_{ap} F_g} e^{-E_{app}/RT}$$

where L equals the number of sites per square centimeter and is taken as 10^{15} sites/cm.^{2}, k_B is Boltzmann's constant and h is Planck's constant, and $f_{\neq}$, F_{gp}, f_{ap}, and F_g represent the partition functions for the activated complex, oxygen, adsorbed oxygen atoms, and nitrous oxide. The values for f_{ap} and $f_{\neq}$ are assumed equal to unity or to each other. The calculated value for f_{gp} at room temperature is 0.645×10^{28}, and the value of f_g at room temperature is calculated to be equal to 15.4×10^{28}. The vibrational contributions to the nitrous oxide partition function are neglected.

(18) B. M. W. Trapnell, "Chemisorption," Butterworth Scientific Publications, London, 1955, Chapter 5.

The respective partition function values are substituted into the above equation, and the apparent rate constant is calculated to be equal to 1.2×10^6 (molecules/cc.)$^{1/2}$ sec.$^{-1}$ cm.$^{-2}$. The experimentally determined rate constant is $\sim 3 \times 10^4$ (molecules/cc.)$^{1/2}$ sec.$^{-1}$ cm.$^{-2}$ for a reactor volume of 1.17 liters. Normalizing this rate constant to a 1 cc. reactor volume, the experimental value is $\sim 3.5 \times 10^7$ (molecules/cc.)$^{1/2}$ sec.$^{-1}$ cm.$^{-2}$, which is in fair agreement with the calculated rate constant.

A reaction mechanism consistent with the proposed kinetics is

$$N_2O + S \underset{k'_1}{\overset{k_1}{\rightleftarrows}} N_2O \text{ ads}$$

$$N_2O \text{ ads} \xrightarrow{k_0} N_2 + O \text{ ads}$$

$$O \text{ ads} \underset{k_2}{\overset{k'_2}{\rightleftarrows}} (1/2)O_2 + S$$

where the slow step is assumed to be the decomposition of the adsorbed nitrous oxide complex. However the proposed kinetics would be in agreement also with the adsorption of nitrous oxide or the dissociative chemisorption of nitrous oxide as the slow step. The rate-determining step cannot be established from the kinetic study alone, since the nitrous oxide adsorption equilibrium constant, K_1, cannot be separated out in the rate equation. Values for K_1 or λ_1, the heat of adsorption for nitrous oxide on platinum, were not found in a literature survey. Therefore the determination of the slow step in the reaction mechanism must wait upon an adsorption isotherm study.

There is one ambiguity in the postulated reaction kinetics, and that is the variation of the apparent rate constant with pressure. In Table I it is evident that the rate constants at 730 and 820° are increasing with pressure. The rate constant increases by a factor of two over a pressure range that varies by a factor of a hundred. However, no explanation for this ambiguity has been established. It may be due to an experimental effect; for example, the thermal conductivity of a gas varies with pressure over this region. It could also be due to the energy terms in the rate constant; over a wide pressure range these energy terms may vary slightly. Hinshelwood and Pritchard[2] reported that the apparent activation energy varied with pressure in their study, and they concluded that they were operating in different θ regions.

Added Oxygen.—As mentioned in the Introduction, the oxygen effect has been investigated by the early workers. There is general consensus that added oxygen retards the reaction, but there is disagreement as to whether its effectiveness as a poison is the same as that of the product oxygen. This investigation has found no difference between poisoning by added oxygen or product oxygen. This is shown by the linear plot of eq. 7 in Fig. 7, where the $(P_{O_2}$ total$)^{1/2}$ term includes the added oxygen and the oxygen formed as a reaction product. Table III lists the apparent rate constants and the variation of $t_{1/2}$ with added oxygen. It is possible to evaluate the effect of added oxygen on the

TABLE III

THE EFFECT OF AN ADDED GAS ON THE TIME IT TAKES 50% OF THE NITROUS OXIDE TO DECOMPOSE AT 730°

P_{N_2O}, μ	P_{O_2} added, μ	$k_{app} \times 10^{-4}$, (molecules/cc.)$^{1/2}$ / sec. cm.^{2}	$t_{1/2}$, min.	Catalytic efficiency, %
93[a]	0	2.4	5.0	100
79	8	2.3	6.0	83.4
85	21	2.6	7.0	71.5
93	38	2.4	8.5	58.8
98	230	2.3	19.0	26.3
105	70 μ of NO	2.1	5.7	
108	150 μ of N_2	2.2	5.4	

[a] Average value of 2 runs.

rate equation by a comparison of the half-life times. The ratio of the half-lives is called the catalytic efficiency, and the relationship between the oxygen pressure and the catalytic efficiency is shown below

$$\text{catalytic efficiency} = \frac{(t_{1/2})'}{t_{1/2}} = \frac{(P_{O_2}{}^{1/2})'}{(P_{O_2\text{total}})^{1/2}}$$

where $(t_{1/2})'$ represents the half-life value for the case of no added oxygen and $(P_{O_2}\ \text{total})^{1/2}$ represents the sum of pressures for added oxygen and product oxygen. A plot of catalytic efficiency *vs.* $(P_{O_2}\ \text{total})^{-1/2}$ is shown in Fig. 8. The curve is linear and has the predicted slope and intercept. Thus the reaction rate is inversely proportional to the square root of the total oxygen pressure and is independent of the oxygen source.

Added Nitrogen and Nitric Oxide.—The effect of added nitrogen and added nitric oxide on the decomposition has been investigated and the results are listed also in Table III. Within experimental error, the half-life values indicate that the added gases do not poison the reaction. Nitric oxide at the temperature and pressure range investigated does not decompose or react with the product oxygen.

When studying the nitrous oxide decomposition at pressures greater than 1 mm., small amounts of nitric oxide are detected among the reaction products. The nitric oxide generally represents less than one per cent of the reaction products. It is not certain whether any nitric oxide is formed during the low pressure runs, since the quantity formed is too small to be accurately determined. No efforts have been made to establish the mechanism of nitric oxide formation, but its presence at high pressures indicates that the surface reactions may be more complicated than the kinetic equation suggests.

Conclusion

The low pressure nitrous oxide decomposition kinetics are compatible with the following Langmuir–Hinshelwood equation

$$-\frac{dP_{N_2O}}{dt} = \frac{k_0K_1P_{N_2O}}{1 + K_2P_{O_2}{}^{1/2}}$$

The apparent energy of activation is 32 ± 1 kcal./mole, which is in good agreement with previous literature values. The oxygen adsorption equilibrium constant has been evaluated at various temperatures, and the heat of oxygen adsorption is determined to be approximately 18 kcal./mole. This low heat of adsorption is indicative of a high degree of surface coverage based on the work of Brennan, *et al.*[16] The rate equation indicates that the reaction is poisoned by oxygen atoms, and it has been found that the added oxygen has the same poisoning effect as the oxygen produced by the reaction. Nitrogen and nitric oxide do not poison the reaction. However, nitric oxide is produced in small amounts during the decomposition, which indicates that the over-all reaction mechanism is not as straightforward as the kinetics suggest.

Acknowledgment—The author wishes to thank Dr. S. N. Foner and Mr. R. L. Hudson for their coöperation during the entire course of this investigation.

THE HEATS OF FORMATION OF TANTALUM CARBIDES[1]

BY ELMER J. HUBER, JR., EARL L. HEAD, CHARLES E. HOLLEY, JR., AND ALLEN L. BOWMAN

University of California, Los Alamos Scientific Laboratory, Los Alamos, New Mexico

Received September 14, 1962

Heats of combustion in an oxygen bomb calorimeter have been measured for tantalum metal and a series of tantalum carbides, TaC_x, where x varied from 0.485 to 0.998. Heats of formation were calculated. The values found for the heats of formation of Ta_2C, TaC, and Ta_2O_5 were −47.2 ± 3.4, −34.6 ± 0.9, and −487.7 ± 0.9 kcal./mole, respectively.

Introduction

The tantalum carbides, like those of the other transition metals, are finding increasing use in the field of high temperature technology. Thermochemical data for these compounds are sparse and need to be confirmed. In addition, the variation of these properties with composition must be considered important.

Measured values of the heat of formation of TaC vary, according to McKenna,[2] Humphrey,[3] and Sanz,[4] from −38 and −38.5 kcal./mole to −58.1 kcal./mole (corrected to the modern value for Ta_2O_5). The heat of formation of the TaC phase has been reported[5] as varying from −18.7 kcal./mole at $TaC_{.60}$ to −31.7 kcal./mole at $TaC_{0.90}$. The heat of formation of Ta_2C was found to be −34 kcal./mole.[5]

This paper describes the determination of the heat evolved from the combustion of weighed samples of

(1) This work was done under the auspices of the Atomic Energy Commission.

(2) P. M. McKenna, *Ind. Eng. Chem.*, **28**, 767 (1936).

(3) G. L. Humphrey, *J. Am. Chem. Soc.*, **76**, 978 (1954).

(4) M. C. Sanz, North American Aviation, Inc., Report AL-203, May, 1947.

(5) V. I. Smirnova and B. F. Ormont, *Dokl. Akad. Nauk SSSR*, **100**, 127 (1955); *Zh. Fiz. Khim.*, **30**, 1327 (1956).

TaC_x, where x varies from 0.485 to 0.998. The method, using a bomb calorimeter at a known initial pressure of oxygen, has been described.[6] The energy equivalent of the calorimeter was 9988.0 ± 3.3 j./deg. as determined by the combustion of standard benzoic acid.

Preparation and Analysis of the Tantalum Carbides.—The analyses of the tantalum carbides and tantalum metal are given in Table I. The tantalum was in sheet form, 0.015 in. thick. The carbides were powdered. These materials were prepared by the direct reaction of Fansteel high-purity tantalum powder and spectroscopic grade Madagascar flake graphite. The thoroughly mixed powders were heated inductively in 25-g. batches in graphite crucibles at 1850°, under vacuum of 10^{-5} mm., for six 1.5-hour periods, with material ground to a powder after each heating.[7] The samples were analyzed for tantalum and total carbon by combustion, and for free carbon by a chemical method.[8] The samples were analyzed for nitrogen by a modified Winkler procedure. The sample is dissolved in hot H_2SO_4–K_2SO_4, then made strongly alkaline with KOH, and the ammonia is steam-distilled into boric acid, which is titrated with HCl. The samples were analyzed for hydrogen by burning at 1000° in a stream of oxygen and weighing the water absorbed in $Mg(ClO_4)_2$, and analyzed for oxygen by vacuum extraction.[9] Niobium and tungsten were found by spectroscopic analysis. No iron was found. The estimated uncertainty in the C:Ta ratio is ±0.005.

Combustion of the Tantalum Carbides.—Each sample, including the tantalum metal, was burned in oxygen at 25 atm. pressure on sintered disks of Ta_2O_5. Ignition was made by passing an electrical current through a 10 mil diameter tantalum fuse wire. No oxygen pickup was observed under the oxygen pressure in a

TABLE I

ANALYSES OF TANTALUM CARBIDES AND METAL, WEIGHT %

x in TaC_x	Ta	C, total	C, free	N	O	H	Nb	W
Metal	99.80	0.00	..	0.012	0.027	0.004	...	0.15
0.485	96.78	3.10	..	...	.023	.002	0.085	.02
.724	95.23	4.57	0.12	...	.017	.013	.04	.01
.749	95.16	4.71	..	.018	.016	.018	.07	.01
.802	94.89	5.03	..	.006	.008	.008	.04	.01
.821	94.73	5.14	..	.010	.015	.029	.06	.01
.838	94.67	5.26	..	.005	.008	.004	.04	.01
.904	94.28	5.64	..	.018	.010	...	.04	.01
.936	94.08	5.85	..	...	.003	.016	.04	.01
.958	93.88	5.94	..	.014	.012	.029	.12	.01
.982	93.85	6.10	..	.021	.005	...	.04	.01
.998	93.73	6.19	..	.005	.008	.012	.04	.01

TABLE II

THE HEATS OF COMBUSTION OF Ta AND TaC_x

Mass burned, g.	Wt. Ta fuse wire, mg.	Wt. Ta_2O_5, g.	Energy equiv., j./°, total	ΔT, °K.	Energy: From firing, j.	Energy: From TaC_x, j./g.	Dev. from mean
Ta Metal							
2.0356		26.1	10008.4	1.1421	14.1	5608.4	3.1
2.3208		72.8	10022.6	1.3017	9.5	5617.4	12.1
1.9303		49.3	10015.4	1.0884	11.2	5641.4	36.1
2.2373		50.1	10015.7	1.2512	9.9	5596.8	8.5
2.3033		50.7	10015.9	1.2861	9.6	5588.4	16.9
2.2885		50.0	10015.6	1.2748	10.1	5574.7	30.6
2.1006		49.0	10015.3	1.1757	11.5	5600.1	5.2
2.0540		48.8	10015.3	1.1503	9.7	5604.1	1.2
2.1437		48.3	10015.1	1.2032	10.1	5616.5	11.2
2.1031		48.3	10015.1	1.1803	10.6	5615.6	10.3
1.8553		48.3	10015.1	1.0389	10.6	5602.4	2.9
2.3860		48.6	10015.2	1.3345	9.6	5597.5	7.8
					Av.	5605.3	12.2
					Stand. dev.		4.8

TABLE II (*Continued*)

Mass burned, g.	Wt. Ta fuse wire, mg.	Wt. Ta_2O_5, g.	Energy equiv., j./°, total	ΔT, °K.	Energy: From firing, j.	Energy: From TaC_x, j./g.	Dev. from mean
$TaC_{0.485}$							
2.0630	62.31	29.0	10009.2	1.2695	12.2	5983.3	24.6
1.9811	59.79	29.0	10009.2	1.2000	11.2	5887.1	71.6
1.9412	60.87	29.2	10009.3	1.1986	10.6	5998.1	39.4
1.9936	61.69	29.1	10009.3	1.2159	9.9	5925.4	33.3
1.9407	60.35	28.8	10009.2	1.2056	10.4	6037.4	78.7
1.9691	61.13	29.3	10009.3	1.1981	10.3	5910.1	48.6
1.9786	59.47	29.1	10009.3	1.2210	11.8	6001.5	42.8
1.9238	63.06	28.0	10008.9	1.1760	13.1	5926.9	31.8
					Av.	5958.7	46.4
					Stand. dev.		18.8
$TaC_{0.724}$							
1.7597	56.35	24.8	10008.1	1.1446	15.5	6320.6	26.8
1.7356	59.32	24.0	10007.8	1.1252	14.1	6287.5	6.3
1.7733	57.75	24.3	10007.9	1.1542	13.9	6322.6	28.8
1.7709	55.94	24.7	10008.0	1.1518	14.0	6323.4	29.6
1.7162	57.87	24.5	10008.0	1.1114	14.1	6283.0	10.8
1.7312	58.08	24.5	10008.0	1.1139	13.7	6242.5	51.3
1.7206	58.22	24.5	10008.0	1.1219	15.3	6326.2	32.4
1.8624	56.20	24.1	10007.9	1.1952	14.6	6244.8	49.0
					Av.	6293.8	29.4
					Stand. dev.		12.4
$TaC_{0.749}$							
1.7181	62.85	25.3	10008.2	1.1149	15.1	6279.6	18.0
1.7512	60.25	24.8	10008.1	1.1287	15.6	6247.8	13.8
1.7640	62.39	25.2	10008.2	1.1401	15.5	6260.4	1.2
1.7323	61.86	25.4	10008.2	1.1210	13.6	6267.5	5.9
1.7796	60.43	25.2	10008.2	1.1479	13.2	6256.9	4.7
1.7700	59.78	25.0	10008.1	1.1408	11.5	6253.7	7.9
1.7862	60.21	25.2	10008.2	1.1516	15.0	6254.2	7.4
1.7921	61.20	24.7	10008.0	1.1591	13.9	6272.9	11.3
					Av.	6261.6	8.8
					Stand. dev.		3.8
$TaC_{0.802}$							
1.7836	60.48	23.5	10007.7	1.1677	14.8	6352.6	57.0
1.7966	58.82	23.6	10007.7	1.1620	13.5	6280.8	14.8
1.7469	56.77	23.9	10007.8	1.1314	14.6	6290.2	5.4
1.6683	61.98	23.7	10007.7	1.0806	15.4	6263.7	31.9
1.7737	57.83	23.6	10007.7	1.1506	15.8	6299.5	3.9
1.7056	58.02	24.7	10008.0	1.1122	16.3	6324.9	29.3
1.2361	58.14	23.8	10007.8	0.8072	15.5	6257.8	37.8
					Av.	6295.6	25.7
					Stand. dev.		12.7
$TaC_{0.821}$							
1.7512	60.09	24.9	10008.1	1.1474	13.0	6356.7	11.2
1.7348	59.54	25.0	10008.1	1.1354	12.8	6349.4	18.5
1.7501	61.14	24.8	10008.1	1.1510	12.3	6378.3	10.4
1.7499	59.42	25.3	10008.2	1.1507	12.6	6382.7	14.8
1.7677	60.55	25.5	10008.3	1.1638	9.0	6391.2	23.3
1.7106	60.36	25.2	10008.2	1.1172	10.3	6331.6	36.3
1.7002	60.81	24.9	10008.1	1.1261	11.2	6420.7	52.8
1.8111	67.67	25.4	10008.2	1.1854	13.6	6332.6	35.3
					Av.	6367.9	25.3
					Stand. dev.		10.9
$TaC_{0.838}$							
1.7395	58.95	29.3	10009.4	1.1408	14.3	6365.3	4.3
1.7510	53.99	29.3	10009.4	1.1463	13.6	6371.3	10.3
1.7742	56.63	29.5	10009.5	1.1596	14.1	6354.4	6.6
1.7413	55.71	28.6	10009.2	1.1390	14.5	6358.6	2.4
1.7543	56.22	23.5	10007.7	1.1472	12.6	6356.7	4.3
1.7845	57.96	23.6	10007.7	1.1688	14.8	6363.5	2.5

(6) E. J. Huber, Jr., C. O. Matthews, and C. E. Holley, Jr., *J. Am. Chem. Soc.*, **77**, 6493 (1955).

(7) A. L. Bowman, *J. Phys. Chem.*, **65**, 1596 (1961).

(8) O. H. Kriege, Los Alamos Scientific Laboratory Report LA-2306, March, 1959.

(9) W. R. Hansen and M. W. Mallett, *Anal. Chem.*, **29**, 1868 (1957).

TABLE II (*Continued*)

Mass. burned, g.	Wt. Ta fuse wire, mg.	Wt. Ta_2O_5, g.	Energy equiv., j./°, total	ΔT, °K.	Energy From firing, j.	Energy From TaC_x, j./g.	Dev. from mean
1.7883	55.87	23.5	10007.7	1.1685	12.6	6356.1	4.9
1.7180	60.12	22.6	10007.4	1.1274	13.7	6462.0	1.0
					Av.	6361.0	4.5
					Stand. dev.		2.0
				$TaC_{0.904}$			
1.7503	59.34	24.0	10007.8	1.1636	16.8	6452.7	14.3
1.7543	49.88	29.4	10009.5	1.1590	15.7	6443.8	5.4
1.7014	57.37	29.6	10009.5	1.1256	13.4	6424.2	14.2
1.7257	61.35	29.4	10009.5	1.1487	12.5	6455.2	16.8
1.7583	57.20	29.2	10009.4	1.1660	14.4	6446.2	7.8
1.7432	59.69	29.0	10009.3	1.1596	14.9	6456.9	18.5
1.7882	58.00	28.8	10009.3	1.1837	14.2	6435.0	3.4
					Av.	6444.9	9.0
					Stand. dev.		4.5
				$TaC_{0.936}$			
1.7258	56.33	24.8	10008.1	1.1530	15.3	6493.6	41.0
1.7703	58.61	25.1	10008.2	1.1768	16.0	6457.4	4.8
1.7726	57.73	24.4	10007.9	1.1735	17.2	6432.3	20.3
1.7523	58.55	24.2	10007.9	1.1529	14.8	6387.9	64.7
1.7358	62.72	23.4	10007.6	1.1601	16.3	6475.5	22.9
1.7940	61.15	24.8	10008.2	1.1850	15.3	6410.3	42.3
1.6983	59.12	24.1	10007.9	1.1355	16.3	6485.7	33.1
1.7056	59.65	24.1	10007.9	1.1391	15.0	6478.1	25.5
					Av.	6452.6	31.8
					Stand. dev.		13.6
				$TaC_{0.958}$			
1.7176	67.74	25.2	10008.2	1.1574	10.0	6516.1	23.2
1.7443	60.96	25.3	10008.2	1.1721	12.5	6521.1	18.2
1.7080	63.10	25.0	10008.1	1.1519	13.2	6533.8	5.5
1.7434	63.05	24.7	10008.0	1.1632	11.4	6467.1	72.2
1.7546	63.50	24.9	10008.1	1.1853	9.2	6551.7	12.4
1.7844	62.10	24.7	10008.1	1.2168	8.8	6623.7	84.4
1.8527	62.67	24.7	10008.1	1.2582	9.1	6601.2	61.9
1.6747	66.10	25.0	10008.1	1.1259	10.3	6500.0	39.3
					Av.	6539.3	39.6
					Stand. dev.		18.3
				$TaC_{0.982}$			
1.5093	54.08	52.3	10016.5	1.0169	15.3	6536.7	4.9
1.5019	56.90	51.4	10016.2	1.0155	15.4	6548.8	7.2
1.6488	57.04	51.6	10016.2	1.1100	14.7	6539.3	2.3
1.6509	48.93	52.2	10016.4	1.1098	14.4	6557.8	16.2
1.7121	51.82	52.0	10016.4	1.1509	14.4	6554.3	12.7
1.7290	58.06	51.8	10016.4	1.1641	15.1	6546.0	4.4
1.7079	58.71	26.8	10008.7	1.1466	15.3	6516.8	24.8
1.7485	56.69	26.9	10008.8	1.1747	15.1	6533.0	8.6
					Av.	6541.6	10.1
					Stand. dev.		4.6
				$TaC_{0.998}$			
1.7209	60.46	25.6	10008.3	1.1594	14.1	6536.7	11.6
1.7727	57.78	25.7	10008.4	1.1898	13.9	6526.0	22.3
1.7584	56.30	25.7	10008.4	1.1875	13.4	6571.0	22.7
1.7598	59.83	26.0	10008.5	1.1906	13.9	6571.9	23.6
1.7784	59.53	25.8	10008.5	1.1984	13.3	6548.4	0.1
1.7662	58.81	25.7	10008.4	1.1810	14.7	6496.4	51.9
1.8017	56.29	25.9	10008.5	1.2190	14.8	6587.4	39.1
					Av.	6548.3	24.5
					Stand. dev.		11.9

1-hour period. The average initial temperature was 24.9° and the average temperature rise 1.1512°.

Each solid combustion product was heated to constant weight in oxygen at 1000° to determine the amount of unburned material. Any CO_2 evolved was weighed. From the change in weight of the sample and the amount of CO_2 evolved, it was possible to calculate how much CO_2 was adsorbed, and how much came from unburned carbide. Combustion varied from 94.83 to 100% of completion but was usually greater than 99%.

Only the high temperature form of Ta_2O_5 was found in the combustion products. Its specific heat was taken as 0.305 j./g./deg. From seven to eight runs were made on each material (twelve on the metal). They are summarized in Table II.

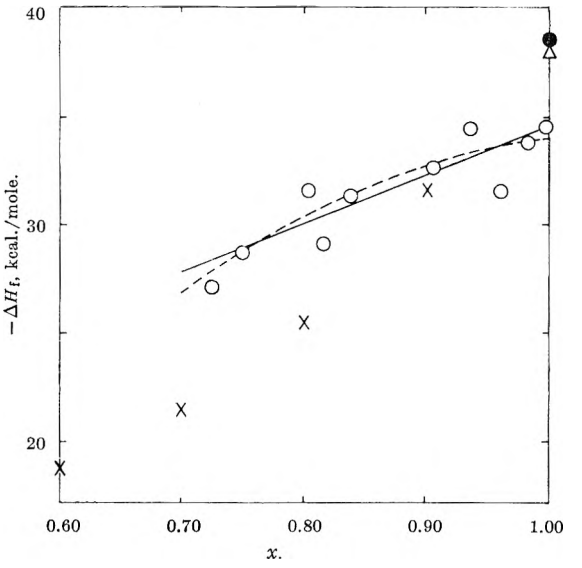

Fig. 1.—Variation of heat of formation of TaC_x with x: O, this work; ×, Smirnova and Ormont; ●, Humphrey; Δ, McKenna.

Results and Discussion

The measured heats of combustion were corrected by assuming that (1) nitrogen was present as TaN which burned to Ta_2O_5 and NO_2 with a heat of 3800 j./g.; (2) oxygen was present as Ta_2O_5; (3) hydrogen was combined as TaH which evolved 5400 j./g.; (4) free carbon gave 33,000 j./g.; and (5) niobium and tungsten burned with heats of 10,195 and 4545 j./g., respectively. The atomic weight of tantalum was taken as 180.95.

The values for the heats of formation of the tantalum carbides were calculated by the same method as that used for the niobium carbides.[10]

The corrected heats of combustion, the amount of correction given as percentage of the measured heat of combustion, and the calculated heats of formation for each composition are given in Table III. The uncertainties attached to the ΔH values include the uncertainties in the determination of the energy equivalent of the calorimeter, the calorimetric measurements, and the value for the heat of formation of Ta_2O_5 (all expressed as twice the standard deviation), plus an estimated uncertainty in the correction for impurities, combined according to standard methods for the propagation of errors.

The value obtained here for the heat of formation of Ta_2O_5, $\Delta H^0_{298} = -487.7 \pm 0.9$ kcal./mole, agrees within experimental error with the value obtained by Humphrey,[3] which is -489.0 ± 0.5 kcal./mole (he reported -488.8 on the basis of the atomic weight of tantalum as 180.88). The weighted mean of these two values is $\Delta H^0_{298} = -488.7 \pm 0.4$ kcal./mole. In calculating the heats of formation of the carbides, this was used as the best value presently available for the heat of formation of Ta_2O_5.

(10) E. J. Huber, Jr., *et al.*, *J. Phys. Chem.*, **65**, 1846 (1961).

TABLE III
HEATS OF COMBUSTION AND HEATS OF FORMATION OF TANTALUM CARBIDES

x, in TaC_x	Heat of combustion cor. for impurities, cal./g.	% change from uncor. value	Heat of formation, $-\Delta H_f$, kcal./mole
Metal	1343	+0.25	487.7 ± 0.9 (for Ta_2O_5)
0.485	1426	+ .12	22.9 ± 1.7
.724	1498	− .41	27.1 ± 1.3
.749	1500	+ .22	28.7 ± 0.5
.802	1506	+ .08	31.5 ± 1.2
.821	1526	+ .28	29.0 ± 1.1
.838	1521	+ .05	31.3 ± 0.5
.904	1543	+ .14	32.2 ± 0.6
.936	1544	+ .12	34.4 ± 1.3
.958	1567	+ .29	31.5 ± 1.7
.982	1565	+ .10	33.8 ± 0.6
.998	1567	+ .12	34.6 ± 1.2
1.00 (TaC, linear extrapolation)	..	....	34.6 ± 0.9

The values for the heats of formation for the ten compositions in the homogeneous phase region[7,11] were fitted to both a quadratic and a linear equation by the method of least squares by means of an IBM 704 computer. Each value was weighted inversely proportional to the square of its uncertainty. The resulting equations are

$$\Delta H = 22.81 - 103.78x + 46.88x^2$$

$$\Delta H = -11.92 - 22.67x$$

When these equations are extrapolated to $x = 1$, the values for the heat of formation of stoichiometric TaC are found to be -34.1 ± 1.2 and -34.6 ± 0.9 kcal./mole, respectively. There is no statistically significant difference between the quality of the fit of the two curves to the experimental data.

The calculated values of ΔH for the TaC phase are plotted as a function of composition in Fig. 1. The values of McKenna,[2] Humphrey,[3] and Smirnova and Ormont[5] are shown for comparison. If it is assumed that the samples of Humphrey were actually $TaC_{0.95}$ + 0.05 mole free carbon, then his data lead to a heat of formation of −33.8 kcal./mole for $TaC_{0.95}$, in excellent agreement with the present work. Such a free carbon content has been observed in commercial tantalum carbide samples. A similar argument could be applied to the data to McKenna.[2]

Since most of the samples of Smirnova and Ormont[5] appear to be inhomogeneous, and since their lattice parameter–composition data are seriously in error,[7,12] no correlation should be expected between their calculated heats of formation and the present work.

The range of homogeneity of the Ta_2C phase is very narrow at the temperature of preparation of the samples (1850°)[11,13]; hence, the heat of formation per mole of carbon should be expected to be nearly constant. Thus the heat of formation of Ta_2C may be taken as -47.2 ± 3.4 kcal./mole by linear extrapolation.

Acknowledgments.—Valuable assistance was rendered by F. H. Ellinger, X-ray analysis; H. M. Burnett, spectrochemical analysis; and G. C. Heasley, chemical analysis. Thanks are due R. K. Zeigler for programming the data for the IBM 704 computer.

(11) F. H. Ellinger, *Trans. Am. Soc. Metals*, **31**, 89 (1943).

(12) R. Lesser and G. Brauer, *Z. Metallk.*, **49**, 622 (1958).

(13) A. L. Bowman, to be published.

THE MOLYBDENUM–ZIRCONIUM–CARBON SYSTEM[1]

BY T. C. WALLACE, C. P. GUTIERREZ, AND P. L. STONE

University of California, Los Alamos Scientific Laboratory, Los Alamos, New Mexico

Received September 15, 1962

The approximate phase boundaries of the solid portion of the 2100° isothermal section of the Mo–Zr–C system were determined by chemical and X-ray techniques. Two of the more interesting features are: (1) an extensive horn shaped solid solution region formed between ZrC and Mo_3C_2 that extends from the Zr–C boundary to $Mo_{0.58}Zr_{0.02}C_{0.40}$; and (2) the highest carbide of the Mo–C system, Mo_3C_2 (a_0 = 3.010 ± 0.002, c_0 = 14.62 ± 0.01 Å.) lies at 38 at. % C. ΔF_f^0 of $MoC_{0.61}$ ($\sim 1/3$ Mo_3C_2) is estimated to be −2.6 ± 1.5 kcal./mole. In addition, the phases in equilibrium in the low-carbon portion of the 1500° isothermal section were established, and melting temperatures were determined along the Mo–C boundary and in the high-carbon (C > 50 at. %) portion of the ternary.

Introduction

Increasing interest has been shown in recent years in the refractory metal carbides for use as high temperature materials. The binary systems of these metals with carbon have been extensively studied and recently have been critically reviewed[2]; however, very little research has been reported on ternary systems consisting of two transition metals and carbon. In the Zr–Mo–C ternary, the Zr–C[3] and Zr–Mo[4–6] boundary systems are well known. The Mo–C[7–11] boundary system has been investigated by a number of workers, but until recently there has been little agreement about the composition and structure of the higher carbide. Apparently, the only work on the ternary is that of Nowotny and Kieffer,[12] who studied

(1) Work performed under the auspices of the U. S. Atomic Energy Commission.

(2) E. K. Storms, "A Critical Review of Refractories. Part I. Selected Properties of Group 4a, -5a, and -6a Carbides," Los Alamos Scientific Laboratory Report LAMS-2674, Feb. 1, 1962.

(3) J. D. Farr, *J. Phys. Chem.*, in press.

(4) P. Duwez and C. B. Jordan, *J. Am. Chem. Soc.*, **73**, 5509 (1951).

(5) R. F. Domagala, D. J. McPherson, and M. Hansen, *Trans. Am. Inst. Mining, Met. Petrol. Engrs.*, **197**, 73 (1953).

(6) E. Pipitz and R. Kieffer, *Z. Metallk.*, **46**, 187 (1955).

(7) W. P. Sykes, K. R. Van Horn, and C. M. Tucker, *Trans. Am. Inst. Mining, Met. Petrol. Engrs.*, **117**, 173 (1935).

(8) W. Few and G. Manning, *ibid.*, **194**, 271 (1952).

(9) H. Nowotny, E. Parthé, R. Kieffer, and F. Benesovsky, *Monatsh. Chem.*, **85**, 255 (1954).

(10) E. Rudy, F. Benesovsky, and K. Sedlatschek, *ibid.*, **92**, 841 (1961).

(11) E. Rudy, El. Rudy, and F. Benesovsky, *Planseeber. Pulvermet.*, **10**, 42 (1962).

the ZrC–Mo_2C section, and Umanski,[13,14] who studied the ZrC–MoC section.

This work was concerned with three areas of the Mo–Zr–C ternary: (1) establishment of the approximate solid-phase boundaries in the 2100° isothermal section; (2) determination of the phases in equilibrium in the low-carbon Zr–Mo portion of the 1500° isothermal section; and (3) determination of some melting temperatures in the γ + C region and along the Mo–C boundary.

Experimental

Starting materials were reactor grade zirconium sponge from Wah Chang Corporation, high-purity molybdenum rod, and National Carbon spectrographic grade carbon rod. The chemical purity of the zirconium was 99.9%, and spectrochemical analysis showed that the major metal impurities were Al, Si, Ca, Ti, V, Co, Ni, Mo, and Hf, each of which was present in quantities of less than 100 p.p.m. The chemical purity of the molybdenum was 99.8%, and the major metal impurities were found to be W < 0.1%, Ta < 300 p.p.m., and Fe < 200 p.p.m. The spectrochemical analysis of the carbon rod indicated that B, Mg, and Na, were present in quantities of less than 50 p.p.m., while chemical analysis showed O_2, N_2, H_2, and H_2O to be present in quantities of 0.68, 0.17, 0.15, and 0.08 wt. %, respectively.

The samples were prepared by arc-melting the components on a water-cooled copper hearth in an atmosphere of purified helium, using a carbon electrode. Five to ten gram portions of the pulverized melt (−325 mesh) were pressed, without binder, in a $^3/_8$ in. steel die at 100,000 p.s.i. A 0.040 by $^3/_8$ in. hole was drilled in the top of the cylinder to give blackbody conditions for pyrometric temperature measurements.

The heating was done inductively with an eddy-current concentrator, which has been described previously in detail.[15] The eddy-current concentrator was contained in a vacuum system capable of maintaining pressures of 10^{-5} torr or lower. Those samples which were not to be in equilibrium with carbon were supported on a molybdenum tripod, whereas samples containing free carbon were heated in graphite crucibles. After the pressure had been reduced to less than 10^{-4} torr, the temperature was slowly raised to the appropriate value and maintained there. During most of the heatings, the pressure was below 10^{-5} torr. After they were heated, the samples were cooled by radiation, and dropped to 900° in about 1 min. Samples were heated for 15–30 hr., cooled, pulverized to −325 mesh powder, re-pressed, and heated for an additional 15–30 hr.

After the final heating, the samples were again pulverized to −325 mesh powder, an X-ray powder pattern was taken, and the remaining material was analyzed separately for Zr, Mo, total C, and free C.[16] The sum of the percentages of the individual analyses of all the samples lay within the interval 99.3–100.2%. The X-ray powder patterns were made in a 114.6 mm. Debye–Scherrer camera, using nickel-filtered copper radiation. Lattice parameters were obtained from the back-reflection lines by applying the least-squares extrapolation of Cohen[17] as modified by Hess[18] and calculating the results on an IBM 704 computer. Standard deviations were calculated for each lattice-parameter. These deviations were less than ±0.003 Å. in the cubic phases (α-Mo, γ, and σ), less than ±0.005 in the β-phase and less than ±0.005 for a_0 and ±0.02 for c_0 in the γ'-phase.

Table I gives the analytical chemical composition of the annealed samples, number of phases that were found by X-ray techniques to be present, and the lattice parameters of these phases when they were present in sufficient quantity to show lines in the back-reflection region. The standard deviations are not presented.

(12) H. Nowotny and R. Kieffer, *Metallforschung*, **2**, 257 (1947).

(13) Ya. S. Umanski, *Izvest. Sektora Fiz. Khim. Anal. Inst. Obshchei Neorg. Khim. Akad. Nauk SSSR*, **16**, No. 1, 127 (1943).

(14) Ya. S. Umanski and G. V. Samsonov, "Hard Alloys of the Refractory Metals," Metallurgical Publishing House, Moscow, 1957 (in Russian).

(15) J. M. Leitnaker, M. G. Bowman, and P. Gilles, *J. Electrochem. Soc.*, **108**, 568 (1961).

(16) O. H. Kriege, "The Analysis of Refractory Borides, Carbides, Nitrides and Silicides," Los Alamos Scientific Laboratory Report LA-2306, March, 1959.

(17) M. U. Cohen, *Rev. Sci. Instr.*, **6**, 68 (1935); *Z. Krist.*, **94A**, 288 and 306 (1936).

(18) J. B. Hess, *Acta Cryst.*, **4**, 209 (1951).

TABLE I: ANALYTICAL AND X-RAY DATA OF SAMPLES ANNEALED AT 2100 AND 1500°

Compn. by chemical analysis	No. of phases	Phases present by X-ray and lattice parameters, Å.[a]
		2100° data
Mo	1	α-Mo a_0 = 3.147
$Mo_{0.76}C_{0.25}$	2	α-Mo (3.147 + β (2.993, 4.724)
$Mo_{0.71}C_{0.29}$	2	α-Mo + β (2.994, 4.722)
$Mo_{0.69}C_{0.31}$	1	β, a_0 = 2.994, c_0 = 4.725
$Mo_{0.68}C_{0.32}$	1	β, a_0 = 3.000, c_0 = 4.727
$Mo_{0.67}C_{0.33}$	1	β, a_0 = 3.015, c_0 = 4.739
$Mo_{0.63}C_{0.37}$	2	β + γ' (3.012, 14.62)
$Mo_{0.62}C_{0.38}$	1	γ', a_0 = 3.008, c_0 = 14.63
$Mo_{0.60}C_{0.40}$	2	C + γ' (3.008, 14.62)
$Mo_{0.57}C_{0.43}$	2	C + γ' (3.011, 14.63)
$Mo_{0.54}C_{0.46}$	2	C + γ' (3.009, 14.62)
$Mo_{0.50}C_{0.50}$	2	C + γ' (3.009, 14.62)
$Mo_{0.96}Zr_{0.01}C_{0.03}$	3	α-Mo (3.147) + β + γ
$Mo_{0.93}Zr_{0.04}C_{0.03}$	2	α-Mo (3.151) + γ
$Mo_{0.90}Zr_{0.07}C_{0.03}$	2	α-Mo (3.159) + γ
$Mo_{0.74}Zr_{0.14}C_{0.12}$	2	α-Mo (3.150) + γ (4.672)
$Mo_{0.70}Zr_{0.17}C_{0.13}$	2	α-Mo (3.151) + γ (4.682)
$Mo_{0.52}Zr_{0.22}C_{0.26}$	3	α-Mo (3.148) + β + γ (4.649)
$Mo_{0.52}Zr_{0.26}C_{0.22}$	2	α-Mo (3.149) + γ (4.669)
$Mo_{0.45}Zr_{0.31}C_{0.24}$	2	α-Mo (3.154) + γ (4.684)
$Mo_{0.67}Zr_{0.03}C_{0.30}$	2	α-Mo + β (3.002, 4.751)
$Mo_{0.65}Zr_{0.02}C_{0.33}$	1	β, a_0 = 3.010, c_0 = 4.747
$Mo_{0.64}Zr_{0.03}C_{0.33}$	2	β (3.009, 4.746) + γ
$Mo_{0.62}Zr_{0.05}C_{0.33}$	3	α-Mo + β (3.002, 4.754) + γ
$Mo_{0.60}Zr_{0.07}C_{0.33}$	3	α-Mo + β (3.002, 4.753) + γ
$Mo_{0.61}Zr_{0.02}C_{0.37}$	3	β + γ + γ'
$Mo_{0.57}Zr_{0.06}C_{0.37}$	2	β (3.015, 4.759) + γ (4.492)
$Mo_{0.59}Zr_{0.03}C_{0.38}$	2	γ (4.267) + γ' (3.017, 14.66)
$Mo_{0.58}Zr_{0.01}C_{0.41}$	3	C + γ (4.267) + γ'
$Mo_{0.57}Zr_{0.02}C_{0.41}$	2	C + γ (4.282)
$Mo_{0.56}Zr_{0.03}C_{0.41}$	2	C + γ (4.287)
$Mo_{0.55}Zr_{0.03}C_{0.42}$	2	C + γ (4.285)
$Mo_{0.53}Zr_{0.06}C_{0.41}$	2	γ (4.305) + γ'
$Mo_{0.50}Zr_{0.09}C_{0.41}$	2	β + γ (4.362)
$Mo_{0.497}Zr_{0.005}C_{0.498}$	3	C + γ (4.261) + γ' (3.012, 14.63)
$Mo_{0.47}Zr_{0.03}C_{0.50}$	2	C + γ (4.293)
$Mo_{0.46}Zr_{0.03}C_{0.51}$	2	C + γ (4.295)
$Mo_{0.43}Zr_{0.06}C_{0.51}$	2	C + γ (4.329)
$Mo_{0.46}Zr_{0.08}C_{0.46}$	2	C + γ (4.348)
$Mo_{0.52}Zr_{0.10}C_{0.38}$	2	β (3.018, 4.758) + γ (4.523)
$Mo_{0.46}Zr_{0.15}C_{0.39}$	2	β (3.005, 4.749) + γ (4.635)
$Mo_{0.38}Zr_{0.24}C_{0.38}$	3	α-Mo (3.148) + β (3.002, 4.754) + γ (4.651)
$Mo_{0.34}Zr_{0.18}C_{0.48}$	2	C + γ (4.455)
$Mo_{0.31}Zr_{0.32}C_{0.37}$	3	α-Mo (3.147) + β (3.001, 4.756) + γ (4.652)
$Mo_{0.28}Zr_{0.28}C_{0.44}$	2	β (3.011, 4.758) + γ (4.576)
$Mo_{0.28}Zr_{0.25}C_{0.47}$	1	γ, a_0 = 4.510
$Mo_{0.26}Zr_{0.26}C_{0.48}$	2	C + γ (4.517)
$Mo_{0.20}Zr_{0.32}C_{0.48}$	1	γ, a_0 = 4.557
$Mo_{0.14}Zr_{0.39}C_{0.47}$	2	β + γ (4.613)
$Mo_{0.13}Zr_{0.45}C_{0.42}$	2	α-Mo (3.162) + γ (4.687)
$Mo_{0.13}Zr_{0.39}C_{0.48}$	1	γ, a_0 = 4.606
$Mo_{0.11}Zr_{0.61}C_{0.28}$	2	α-Mo + γ (4.696)
$Mo_{0.09}Zr_{0.41}C_{0.50}$	2	C + γ (4.624)
$Mo_{0.09}Zr_{0.42}C_{0.49}$	1	γ, a_0 = 4.623
$Mo_{0.07}Zr_{0.48}C_{0.45}$	2	α-Mo + γ (4.680)
$Mo_{0.06}Zr_{0.46}C_{0.48}$	1	γ, a_0 = 4.660
$Mo_{0.03}Zr_{0.54}C_{0.43}$	2	α-Mo + γ (4.692)
$Mo_{0.03}Zr_{0.49}C_{0.48}$	1	γ, a_0 = 4.676
$Zr_{0.55}C_{0.45}$	1	γ, a_0 = 4.698
$Zr_{0.51}C_{0.49}$	1	γ, a_0 = 4.699
		1500° data
$Mo_{0.80}Zr_{0.15}C_{0.05}$	2	α-Mo (3.173) + γ
$Mo_{0.59}Zr_{0.30}C_{0.11}$	3	α-Mo (3.175) + γ (4.692) + σ (7.583)
$Mo_{0.44}Zr_{0.44}C_{0.12}$	2	γ (4.689) + σ (7.604)
$Mo_{0.34}Zr_{0.50}C_{0.16}$	2	γ (4.690) + σ (7.608)
$Mo_{0.20}Zr_{0.64}C_{0.16}$	3	γ (4.690) + σ (7.608) + β-Zr
$Mo_{0.16}Zr_{0.74}C_{0.11}$	2	γ (4.691) + β-Zr
$Mo_{0.09}Zr_{0.84}C_{0.07}$	2	γ (4.688) + β-Zr
$Mo_{0.43}Zr_{0.36}C_{0.21}$	3	γ (4.690) + σ (7.586) + α-Mo (3.175)
$Mo_{0.40}Zr_{0.40}C_{0.20}$	3	γ (4.688) + σ (7.582) + α-Mo (3.174)
$Mo_{0.35}Zr_{0.40}C_{0.25}$	3	γ (4.690) + σ (7.588) + α-Mo (3.175)
$Mo_{0.13}Zr_{0.54}C_{0.33}$	2	γ (4.688) + σ (7.592)
$Mo_{0.04}Zr_{0.65}C_{0.31}$	3	β-Zr + γ (4.690) + σ
$Mo_{0.09}Zr_{0.54}C_{0.37}$	3	γ (4.689) + σ + α-Mo
$Mo_{0.05}Zr_{0.59}C_{0.36}$	2	γ (4.686) + σ (7.605)
$Mo_{0.07}Zr_{0.64}C_{0.29}$	2	γ (4.698) + α-Mo
$Mo_{0.04}Zr_{0.57}C_{0.39}$	2	γ (4.690) + σ
$Zr_{0.58}C_{0.42}$	1	γ, a_0 = 4.699
$Zr_{0.60}C_{0.40}$	1	γ, a_0 = 4.693
$Zr_{0.61}C_{0.36}$	1	γ, a_0 = 4.689
$Zr_{0.67}C_{0.33}$	2	α-Zr + γ (4.689)

[a] The free carbon was determined by chemical analysis.

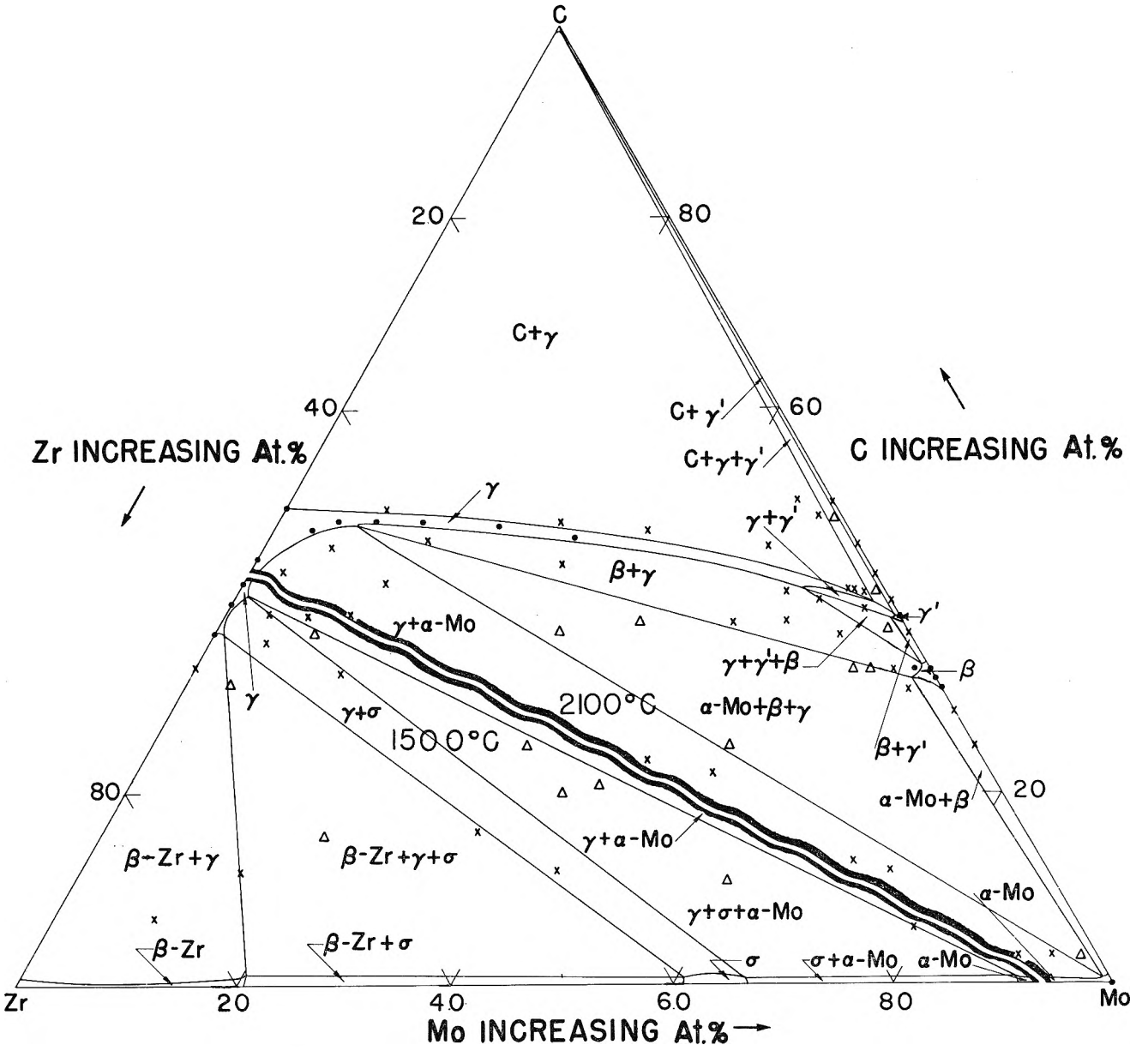

Fig. 1.—Isothermal sections at 1500 (lower left portion) and 2100° (upper right portion): ●, single phased; ×, two-phased; △, three-phased points.

Melting temperatures were determined by two methods. Method 1: The temperature of the sample was slowly raised (10–20°/min.) until the blackbody hole filled with liquid. Ordinarily this occurred over a 10° temperature interval. The determination was made under an atmosphere of helium to prevent composition shifts. Method 2: A thermal arrest apparatus[19] was used to determine the solidification temperature. Briefly, the method consists of taking light from a blackbody hole in a sample or crucible and focusing it on a photomultiplier tube connected to the y-axis of a time-sweep oscilloscope. Abrupt changes in the smoothly changing slope of the display trace as the sample cools indicate a heat effect that would normally be present during a phase change. With proper calibration, it is then possible to ascertain the temperature at which the transition took place. Again the determination was made in a helium atmosphere.

Temperature measurements were made with a Pyro Micro-Optical pyrometer that had been compared with a standard pyrometer calibrated at the National Bureau of Standards. In addition, the pyrometer and optical system were calibrated against the melting points of Co(1495°), Pt (1773°), Rh (1964°), Nb (2468°), Mo (2620°), Ta (2996°), and W (3410°). The purity of these metals was better than 99%.

Results and Discussion

2100° Isothermal Section.—The upper left- and right-hand portions of Fig. 1 show the solid phase field distribution that was found at 2100°. The γ-phase (ZrC solid solution), γ'-phase (Mo_3C_2), β-phase (Mo_2C), α-Mo-phase and some thermodynamic estimations will be discussed below.

α-Mo-Phase.—The solubility of carbon in molybdenum[8] is quite low (approximately 0.16 at. % with a_0 = 3.148 Å.) at 2200°, whereas the solubility of zirconium at 1000° is reported[6] to be about 7 at. %. The lattice parameters of the α-Mo phase in samples $Mo_{0.75}C_{0.25}$, $Mo_{0.96}Zr_{0.01}C_{0.03}$, $Mo_{0.93}Zr_{0.04}C_{0.03}$, and $Mo_{0.90}Zr_{0.07}C_{0.03}$ were 3.147, 3.147, 3.151, and 3.159 Å., respectively. The low carbon content of the last three samples and the variation of the lattice parameter with zirconium content seem to indicate that the solubility of carbon is quite small in the α-Mo (Zr) region. From considerations of the Mo–Zr boundary system[5,6] the α-Mo (Zr) phase must pass into a two phase region (liquid + solid) with increasing Zr. However, all the samples examined in the α-Mo + γ region showed no signs of melting, hence the multiphased regions containing liquid must lie to the left of those samples studied.

(19) G. N. Rupert, to be published.

β-Phase.—The β-phase has the hexagonal Mo_2C crystal structure. On the basis of variation of lattice parameter with composition, the β-phase has an appproximate range of homogeneity lying between 30.8 and 33.3 at. % C, which is in agreement with previous work.[7] There appears to be a slight solubility of the γ-phase in the β-phase, which extends the β-phase slightly into the interior of the ternary. The exact location of the interior boundary of the β-phase as determined by X-ray techniques is limited by the amount of the new phase that has to be present to show in the diffraction pattern (2–10 at. %). The variation of the lattice parameters along the 33.3 at. % C line indicates that the *c*-axis is expanding and the *a*-axis is shrinking with increase of Zr. From consideration of the lattice parameter variation, it would appear that probably less than 3 at. % γ-phase is dissolved by the β-phase.

γ′-Phase.—In older investigations reviewed by Storms,[2] a compound, MoC, is described; but there is little agreement as to its crystal structure and composition. The various structures reported appear to be related to the method of preparation. Nowotny and co-workers[9] were the first investigators to solve successfully the complex crystal structure of the compound. They reported that two higher carbide phases were probably present; a complex hexagonal structure (D_{6h}^4-type, a_0 = 3.01 Å., c_0 = 14.61 Å.) and a face-centered cubic structure (a_0 = 4.28 Å.). Unfortunately, there were no chemical analyses given for the compounds. Recently Rudy and co-workers[11] have reported that the cubic structure (a_0 = 4.281 Å.) is a high temperature modification of the hexagonal structure (a_0 = 3.013, c_0 = 14.64 Å.). They were able to prepare the cubic modification by very rapid quench from the molten state. The composition of the cubic and hexagonal modifications was found[10,11] to lie within the range from 40.0 to 40.8 at. % C and they assigned a formula of Mo_3C_2.

The higher carbide phase that we found was successfully indexed with the hexagonal structure (D_{6h}^4), however we were unable to prepare the pure cubic modification. Along the Mo–C boundary, the lattice parameters of the γ′-phase were the same within experimental error in the β + γ′, γ′, and γ′ + C regions, with the average value of all determinations being a_0 = 3.010 ± 0.002 Å. and c_0 = 14.63 ± 0.01 Å. The back-reflection lines of the γ′-phase were always somewhat diffuse. Analysis of arc-melted samples with 43, 46, and 50 at. % C showed the combined carbon to be 40.8 ± 0.5 at. %, which is in agreement with Rudy and co-workers.[10,11] However, the analysis of samples annealed at 2100° with 40, 43, 46, and 50 at. % C showed combined carbon to be 38.2 ± 0.5 at. %. Hence, with increase in temperature (2100° to melting temperature), the carbon-rich phase boundary would appear to move toward higher carbon. Since the sample $Mo_{0.63}C_{0.37}$ showed the β-phase and γ′-phase to be present, the homogeneity range of Mo_3C_2 must be quite narrow at 2100° and lies at approximately 38 at. % C. The presence of significantly larger lattice parameters (3.017 Å., 14.66 Å.) in the sample $Mo_{0.59}Zr_{0.03}C_{0.38}$ indicates a slight solubility of the γ-phase in the γ′-phase.

γ-Phase.—The γ-phase crystallizes in the NaCl type tructure. Along the Zr–C boundary, the γ-phase extends from approximately 35.5–50.0 at. % C, with the lattice parameter remaining essentially constant over the interval 37.5–50.0 at. % C (4.699 ± 0.002 Å.) and decreasing to 4.691 ± 0.001 Å. at the lower limit.[3]

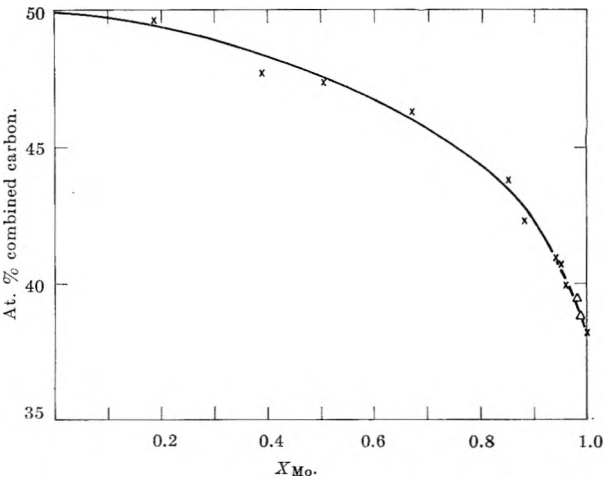

Fig. 2.—Variation of the at. % of combined carbon to the molar ratio, X_{Mo}, of Mo to total metal: ×, two-phased (γ + C); Δ, three-phased (γ + γ′ + C).

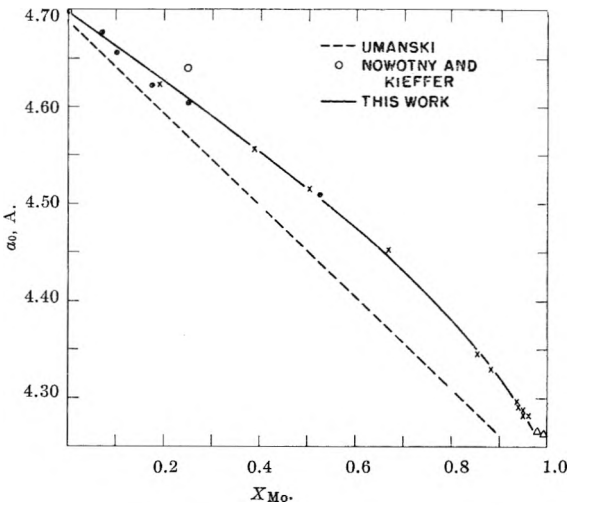

Fig. 3.—Variation of the lattice parameter of the face-centered cubic γ-phase with the molar ratio, X_{Mo}, of Mo to total metal: ●, single-phased (γ); ×, two-phased (γ + C); Δ, three-phased (γ + γ′ + C).

The carbon-rich side of the γ-phase was determined by chemical analyses. Figure 2 shows the variation of combined carbon with the molar ratio, X_{Mo}, of Mo to total metal. The samples for $X_{Mo} < 0.96$ were two-phased, C + γ, and established the phase boundary, whereas for $0.96 < X_{Mo} < 1$, they were three-phase, C + γ + γ′. The samples with $X_{Mo} > 0.9$ showed a higher combined carbon content for the arc-melted samples than for the annealed samples, indicating the C + γ-phase boundary moves to higher carbon with increase in temperature. The relative intensity of the γ′-phase (in the sample $Mo_{0.497}Zr_{0.005}Mo_{0.498}$) to the γ-phase was much less in the arc melted sample than the annealed sample, indicating that a continuous solid solution series might be formed between ZrC and Mo_3C_2 near the melting temperature (2580°).

Figure 3 shows the variation of the lattice parameter of the γ-phase with X_{Mo}. The intersection of this curve with the three-phased curve indicates the carbon-rich side of the γ-phase extends to X_{Mo} = 0.97 ± 0.01. In conjunction with Fig. 2, the composition of the end-

point on the carbon-rich side would be approximately $Mo_{0.58}Zr_{0.02}C_{0.40}$. The carbon-deficient side of the molybdenum-rich γ-phase has a range of composition that is in equilibrium with the γ'-phase (see Fig. 1). The lattice parameters of the single-phase and two-phase points that make up Fig. 3 generally lie on the same curve, indicating that the lattice parameter is constant across the γ-phase for fixed X_{Mo}, at least for the $0.15 < X_{Mo} < 0.55$ region. The width of the γ-phase for $X_{Mo} > 0.1$ is generally of the order of 2–3 at. % C.

Umanski[13,14] prepared a series of samples by heating mixtures of ZrC and MoC at 1700–2000° for 10–12 hr. His lattice parameter curve *vs.* composition is shown on Fig. 3. There are three possible reasons why his curve lies below that of the current work. First of all, the lattice parameter of his ZrC (4.687 Å.) indicates oxygen contamination, and consequently one would expect lower lattice parameters. Secondly, he notes that the system was slow to come to equilibrium. The present investigation confirms this observation. A few samples were prepared by mixing powders of ZrC and MoC (Mo_2C + C) and heating them at 2100°. In contrast to the situation when arc-melted mixtures were used, the powder mixtures took 80–100 hr. to come to equilibrium, as evidenced by sharp lines in the back-reflection region. Our higher values may be due to the sharper lines obtained. Thirdly, his annealing temperature may have been nearer 1700° than 2000° and his values represent a different equilibrium condition than that at 2100°.

Nowotny and Kieffer[12] heated one set of mixtures of ZrC and Mo_2C together for 2 hr. at 1600° and another set of mixtures for 5 min. at 2100°. They show a sample of composition $Mo_{0.13}Zr_{0.40}C_{0.47}$ (2100°) to be single phased, however the lattice parameter of the sample as shown on Fig. 3 lies considerably above our curve. However, by using the tie line passing through the point to roughly locate the γ-phase composition, the parameter (4.643 Å.) is found to agree with this work, if one assumes it was two-phased. The present work shows that approximately 9 mole % Mo_2C is soluble in ZrC at 2100° as compared to 15 mole % found by Nowotny and Kieffer.

Estimation of the Free Energy of Formation of Mo_3C_2.—Recently, Rudy[20] has derived some thermodynamic equations for the appearance of multiple phase equilibria. To apply the equations to experimental data, one must assume that the solid solution regions are ideal and that as the phase boundaries of single phase regions extend across the ternary diagram, they are parallel to one of the sides. Even with such assumptions the ΔF_f^0 derived is reasonable and in agreement with values derived from other systems.

Rudy's method can be applied to the data in the α-Mo + γ region to obtain an estimate of the ΔF_f^0 of Mo_3C_2, where Mo_3C_2 is considered to be a defect structure of the form $MoC_{0.61}$. The energy values are expressed as kcal./mole. The equation of interest is

$$\Delta F_f^0(MoC_{0.61}) - \Delta F_f^0(ZrC_{0.92}) = RT \ln \frac{x_{Mo}\, x_{ZrC_{0.92}}}{x_{Zr}\, x_{MoC_{0.61}}} = RT \ln K$$

(20) E. Rudy, *Planseeber. Pulvermet.*, **10**, 32 (1962).

where

$x_{MoC_{0.61}}$ = mole fraction of $MoC_{0.61}$ in the γ solid soln.

$x_{ZrC_{0.92}} = 1 - x_{MoC_{0.61}}$ = mole fraction of $ZrC_{0.92}$ in the γ solid soln.

x_{Mo} = mole fraction of Mo in the α-Mo solid soln.

$x_{Zr} = 1 - x_{Mo}$ = mole fraction of Zr in the α-Mo solid soln.

and the carbon content is expressed as the mole ratio of C to metal. In the region where we have equilibrium data, the carbon deficient boundary of the γ-phase varies from 46 to 48 at. % C and 2 to 7 at. % Mo. The center of this region lies at $Mo_{0.045}Zr_{0.485}C_{0.470}$ and can be prepared from a mixture of $ZrC_{0.92}$ and $MoC_{0.61}$. Further, the approximation is made that any composition in the area of interest along the carbon deficient boundary can be prepared from mixtures of $MoC_{0.61}$ and $ZrC_{0.92}$. Thus, knowing the end points of a tie line passing through a point in the γ + α-Mo region, and $\Delta F_f^0(ZrC_{0.92})$, one can estimate $\Delta F_f^0(MoC_{0.61})$.

The values of $x_{MoC_{0.61}}$ and $x_{ZrC_{0.92}}$ were obtained from Fig. 3, and those of x_{Mo} and x_{Zr} from a straight line drawn through $a_0 = 3.147$ Å. for Mo and $a_0 = 3.175$ Å. for $Mo_{0.93}Zr_{0.07}$. Table III summarizes the data. From the evaluation of the RT ln K term we obtain $\Delta F_f^0{}_{MoC_{0.61}} - \Delta F_f^0{}_{ZrC_{0.92}} = 35.8$ kcal. From the JANAF tables[21] we estimate $\Delta F_f^0(ZrC_{1.0}) = -40.3 < \Delta F_f^0(ZrC_{0.92}) < -36.4 = 0.92\Delta H_f^0(ZrC_{1.0}) - T\Delta S$. Therefore, $-4.5 < \Delta F_f^0(MoC_{0.61}) < -0.6$.

This value can be compared to a similar analysis made by Rudy and co-workers[10] in the Nb–Mo–C system at 1850°. They expressed their results as $\Delta F_f^0(MoC_{1-x}) - \Delta F_f^0(NbC_{1-x}) = 19$–$22$ and used a value of -28 for $\Delta F_f^0(NbC_{1-x})$ to obtain $-9 < \Delta F_f^0(MoC_{1-x}) < -6$. However, the value of -28 kcal. of ΔF_f^0 of NbC_{1-x} is really the value one expects for $NbC_{1.0}$. It appears more reasonable, perhaps, to represent the equilibrium along their γ-phase boundary [(Nb, Mo)$C_{0.72}$] as a mixture of $NbC_{0.75}$ and $MoC_{0.61}$. With this treatment, one has $\Delta F_f^0(MoC_{0.61}) - \Delta F_f^0(NbC_{0.75}) = 19$–$22$. Using the heat of combustion data of Huber and co-workers[22] and the high temperature heat capacity data of Gel'd and Kusenko,[23] we find $\Delta F_f^0(NbC_{0.75}) = -23$ kcal. Therefore, in the Nb–Mo–C system one has $-4 < \Delta F_f^0(MoC_{0.61}) < -1$, which is in fair agreement with results obtained from the Zr–Mo–C system. Further, we have found that $MoC_{0.61}$ decomposes to $MoC_{0.5}(Mo_2C)$ and C at 1450 ± 100°. Using a value of $\Delta F_f^0(Mo_2C) = -6.7$,[24] one obtains $\Delta F_f^0(MoC_{0.61}) = -3.3$. From these three systems we estimate that $\Delta F_f^0(MoC_{0.61}) = -2.6 \pm 1.5$ kcal./mole for the temperature range of 1450 to 2100°.

Consistent ΔF_f^0 values can be obtained from ternary phase diagrams by the application of Rudy's equations combined with appropriate corrections for the variation of ΔF_f^0 with composition over existing homogeneity ranges.

1500° Isothermal Section.—The data on the 1500° isothermal section lies in the zirconium-rich corner and

(21) The Dow Chemical Company, Thermal Laboratory, "JANAF Thermochemical Data, Zirconium Carbide," March 31, 1962.

(22) E. Huber, E. Head, C. Holley, E. Storms, and N. Krikorian, *J. Phys. Chem.*, **65**, 1846 (1961).

(23) P. Gel'd and F. Kusenko, *Izvest. Akad. Nauk. SSSR Otd. Tekh. Nauk. Met. i Toplivo*, 79 (1960).

(24) O. Kubaschewski and E. Evans, "Metallurgical Thermochemistry," Pergamon Press Ltd., London, 1958, p. 335.

along the Zr–Mo boundary (Fig. 1). No new ternary compounds were found. There are four solid single-phase regions: a solid solution, α-Mo of Zr and C in Mo; a solid solution, β-Zr of Mo and C in Zr, the γ-phase, and the compound $ZrMo_2(\sigma)$. In addition to the single-phase regions, the following two-phase and three-phase regions were found: α-Mo + γ, α-Mo + σ; β-Zr + γ; β-Zr + σ; γ + σ; α-Mo + γ + σ; and α-Mo + β-Zr + σ. The α-Mo phase was found to dissolve approximately 7 at. % Zr, but apparently very little C. The maximum lattice parameter (3.175 Å.) for the α-Mo-phase occurred in the three-phase region α-Mo + γ + σ. The β-Zr dissolves approximately 21 at. % Mo, but the X-ray patterns of this phase were always diffuse. Along the Zr–C boundary, α-Zr is detected in the X-ray patterns of the quenched samples. However, since the α to β transformation of Zr occurs at 862°, it appears β-Zr is present at 1500° and transforms to α-Zr on cooling. The phases found at the various compositions are in general agreement with the lower limit of the γ-phase at $Zr_{0.64}C_{0.36}$. The lattice parameter of the σ-phase is 7.608 Å. in the β-Zr + γ + σ region, and 7.583 Å. in the α-Mo + γ + σ region. These two values are in agreement with previously reported lattice parameters[4,5] which indicate $ZrMo_2$ has a range of homogeneity (~9 at. % Zr).

Melting Temperatures.—The work of Nowotny and co-workers[9] had indicated a maximum (2650°) in the melting temperature at approximately 50 at. % C. This is in contradiction to the present work, which finds that the higher phase exists in the neighborhood of 38 at. % C. This apparent conflict led to the determination of the melting temperature *vs.* composition shown in Table II. The value of the melting temperature (2440 ± 30°) of the sample $Mo_{0.66}C_{0.34}$ is in fair agreement with that reported by Nadler and Kempter[25] (2410 ± 15°) for $Mo_{0.67}C_{0.33}$. For 38–51 at. % C, the melting temperatures are the same (2580 ± 30°) within experimental error, and no apparent maximum was observed at 50 at. % C.

TABLE II

MELTING TEMPERATURES

Compn. by chemical analysis	Free carbon	Method	Melting temp. °C.
$Mo_{0.66}C_{0.34}$	No	1	2440 ± 30
$Mo_{0.63}C_{0.37}$	No	1	2460 ± 30
$Mo_{0.62}C_{0.38}$	No	1	2590 ± 30
$Mo_{0.59}C_{0.41}$	Yes	1	2580 ± 30
$Mo_{0.57}C_{0.43}$	Yes	1	2570 ± 30
$Mo_{0.55}C_{0.45}$	Yes	1	2580 ± 30
$Mo_{0.49}C_{0.51}$	Yes	2	2575 ± 30
$Mo_{0.52}Zr_{0.02}C_{0.46}$	Yes	1	2590 ± 30
$Mo_{0.38}Zr_{0.05}C_{0.57}$	Yes	2	2640 ± 30
$Mo_{0.27}Zr_{0.10}C_{0.63}$	Yes	2	2720 ± 30
$Mo_{0.18}Zr_{0.16}C_{0.66}$	Yes	2	2819 ± 30
$Mo_{0.08}Zr_{0.23}C_{0.69}$	Yes	2	2840 ± 30
$Zr_{0.28}C_{0.72}$	Yes	2	2870 ± 30

TABLE III

EQUILIBRIUM MOLE FRACTIONS IN THE γ + α-Mo REGION

Composition	x_{Mo}	$x_{MoC_{0.61}}$	K
$Mo_{0.53}Zr_{0.22}C_{0.25}$	0.9975	0.135	2500
$Mo_{0.52}Zr_{0.26}C_{0.22}$	0.9950	0.080	2300
$Mo_{0.74}Zr_{0.14}C_{0.12}$	0.9925	0.075	1600
$Mo_{0.70}Zr_{0.17}C_{0.13}$	0.9900	0.045	2100
$Mo_{0.45}Zr_{0.31}C_{0.24}$	0.9825	0.035	1600
		$\bar{K}$ =	2000

A series of melting temperatures (Table II) was determined in the γ + C region. The melting temperature shows a regular decrease from the ZrC + C eutectic 2870 ± 30° (compared to Farr's[3] 2850°) to the Mo_3C_2 + C melting temperature.

Summary.—The Mo–Zr–C system contains the following important features. (1) There is an extensive horn-shaped γ-phase extending from the Zr–C boundary to $Mo_{0.58}Zr_{0.02}C_{0.40}$ with a notable increase in carbon deficiency with increase of Mo. (2) The composition of $Mo_3C_2(\gamma')$ is quite narrow and lies at 38 at. % C at 2100°; however, the carbon-rich boundary lies at 41 at. % C in arc-melted samples. (3) Both the β-and γ'-phases dissolve a small amount of γ-phase. (4) The free energy of formation of Mo_3C_2 expressed as $MoC_{0.61}$ is estimated to be −2.6 ± 1.5 kcal./mole. (5) There are no new ternary phases in the low-carbon portion of the 1500° isothermal section. (6) Along the Mo–C boundary, the melting temperatures are constant (2580 ± 30°) for samples with 38 to 51 at. % C. (7) The melting temperatures in the γ + C region show a regular decrease from ZrC boundary with increase of Mo.

Acknowledgments.—The authors gratefully acknowledge the advice and support of M. G. Bowman during the course of this work; the helpful discussions of J. D. Farr, N. H. Krikorian, and E. K. Storms; and the advice and help given by R. L. Petty on the computer programming of the X-ray data. Thanks are due members of CMB-1 for the analyses and Mrs. M. J. Jorgensen for reading the X-ray diffraction patterns.

(25) M. R. Nadler and C. P. Kempter, *J. Phys. Chem.*, **64**, 1468 (1960).

KINETICS OF THE REACTIONS OF ETHYLENE WITH SULFURIC ACID—REACTION OF ETHYLENE WITH SULFURIC ACID AND ETHYL HYDROGEN SULFATE

BY H. G. HARRIS AND D. M. HIMMELBLAU

Department of Chemical Engineering, University of Texas, Austin 12, Texas

Received September 15, 1962

A kinetic study has been carried out of the reactions of ethylene in diethyl sulfate–sulfuric acid–ethyl hydrogen sulfate solutions. Although by nature a heterogeneous system, the data were obtained from the homogeneous reactions of ethylene in a non-aqueous media. Rate data were obtained, a kinetic model was proposed, and and rate constants determined. The rate constants proved to be functions only of the initial acid concentration. Attempts to obtain a linear correlation between rate constant and some type of acidity function were not successful, indicating that caution is required in the interpretation of rate data in non-aqueous solutions where the variation of activity coefficients is not well understood.

Introduction

The best known reactions in the ethylene–sulfuric acid–ethyl hydrogen sulfate–diethyl sulfate system are

$$C_2H_4 + H_2SO_4 \rightleftarrows C_2H_5SO_4H \quad (1)$$

$$C_2H_4 + C_2H_5SO_4H \rightleftarrows (C_2H_5)_2SO_4 \quad (2)$$

$$2C_2H_5SO_4H \rightleftarrows (C_2H_5)_2SO_4 + H_2SO_4 \quad (3)$$

In dilute sulfuric acid solutions a complex equilibria is established as outlined in Table I. The reactions other than (1), (2), and (3) were curbed by working in essentially non-aqueous solutions of 99.8% H_2SO_4 added to diethyl sulfate (DES).

TABLE I

OVER-ALL REACTIONS IN THE ETHYLENE–DIETHYL SULFATE–ETHYL HYDROGEN SULFATE–SULFURIC ACID–WATER SYSTEM

$$(C_2H_5)_2O + H_2SO_4$$

$$\uparrow\downarrow$$

$$C_2H_5OH$$

$$+$$

$$H_2SO_4 + C_2H_4 \rightleftarrows C_2H_5HSO_4$$

$$+$$

$$H_2O$$

$$\uparrow\downarrow$$

$$C_2H_5OH + H_2SO_4$$

$$C_2H_5HSO_4 + C_2H_5OH$$

$$\uparrow\downarrow$$

$$H_2O$$

$$+$$

$$C_2H_5HSO_4 + C_2H_4 \rightleftarrows (C_2H_5)_2SO_4$$

$$+$$

$$H_2SO_4$$

$$\uparrow\downarrow$$

$$2C_2H_5HSO_4$$

While the character and mechanism of the reactions of ethylene have been investigated to some considerable extent in a qualitative way, quantitative data on the rates of reaction and kinetic constants are scarce.

There have been several qualitative and semi-quantitative studies of reactions 1 and 2. Plant and Sidgwick[1] carried out early rate measurements for these reactions by bubbling C_2H_4 through H_2SO_4 and noting the weight increase of the acid solution. Dalin and Gutyrya[2] measured the rate of ethylene absorption on revolving paddles wetted with H_2SO_4. The rate of decrease in pressure of ethylene in a rotating cylinder partially filled with H_2SO_4 was determined at various conditions by Davis and Schuler[3] and Pigulevskii and Il'ina.[4] Milbauer and others[5] measured the reaction velocity of ethylene bubbling through H_2SO_4. Hellin and Jungers[6] and Kerdivarenko and others[7] noted the decrease in the pressure with time of an ethylene atmosphere over H_2SO_4 in a vibrating vessel.

The major problem in all of the foregoing studies was that reactions 1 and 2 are heterogeneous reactions. In each instance the authors noted that with increased turbulence (mixing) in the liquid phase or increased area available for ethylene dissolution the reaction proceeded more rapidly, indicating that the hydrodynamics of the system was obscuring the true chemical kinetics and that the rate of mass transfer of the gas to the liquid was the controlling factor in the absorption, rather than the chemical reaction rate. Other authors[8,9] have attempted to determine the chemical kinetics of the reactions by examining simultaneous diffusion and reaction of ethylene in the stagnant liquid. These attempts yielded little useful information about the chemical kinetics because of the assumptions and approximations that had to be made to solve the problem, *e.g.*, the solubility of ethylene in sulfuric acid was assumed to be the same as the solubility of ethylene in water, ethylene diffusivity in sulfuric acid was calculated from an equation developed for diffusion of colloidal particles, and a simple kinetic model assuming an irreversible reaction was used to

(1) S. G. P. Plant and N. V. Sidgwick, *J. Soc. Chem. Ind.*, **40**, 14T (1921).
(2) M. A. Dalin and V. S. Gutyrya, *Khim. Referat. Zh.*, **1**, No. 8–9, 84 (1938).
(3) H. S. Davis and R. Schuler, *J. Am. Chem. Soc.*, **52**, 721 (1930).
(4) V. V. Pigulevskii and S. I. Il'ina, *Doklady Akad. Nauk. SSSR*, **45**, 352 (1944).
(5) J. Milbauer, J. Kurka, and J. Mikolasek, *Chem. Obzor*, **14**, 213 (1939).
(6) M. Hellin and J. C. Jungers, *Bull. soc. chim. France*, 386 (1957).
(7) M. A. Kerdivarenko, P. K. Migal, and M. Kh. Kishinevskii, *Zh. Priklad. Khim.*, **28**, 459 (1955).
(8) A. I. Gel'bshtein and M. I. Temkin, *Zh. Fiz. Khim.*, **31**, 2697 (1957).
(9) M. S. Nemtsov, *Khim. Prom.*, No. 8, 15 (1960).

effect several mathematical simplifications. This lack of pure chemical reaction rate data makes the determination of such data of interest and importance.

It became apparent with preliminary trials that the study of a homogeneous reaction would be much preferable to trying to remove the influence of mass transfer from the over-all reaction rate in a heterogeneous reaction. It also became apparent that reactions 1 and 2 are in some respects similar to reaction 3: at high sulfuric acid concentration the reactions are very rapid, but with a decrease in acid concentration the rate of reaction is decreased significantly. The several investigations of (1) and (2) that had been attempted had been carried out at high acid concentration. It proved feasible to collect data on reactions 1 and 2 as homogeneous reactions for mixtures of H_2SO_4 and DES in solutions of relatively high DES concentration.

Experimental

Ethylene (C.P. grade) was physically dissolved by violent agitation in mixtures of purified $(C_2H_5)_2SO_4$, H_2SO_4 (99.8 wt.%), and $C_2H_5SO_4H$ having relatively high initial diethyl sulfate concentrations. The mixtures were then isolated from the source of ethylene, and the component concentrations monitored as reactions 1 and 2 proceeded at 30.00 ± 0.02°.

First, the entire ethylene reaction system was evacuated for more than 30 minutes to remove from the liquid any dissolved inert gases and any light component (such as ether) which might have been formed in trace amounts by some very slow side reaction while reaction 3 was taking place during preparation of the liquid phase. After evacuation, ethylene was added until the pressure in the system was about 200 mm. greater than atmospheric.

Upon agitation of the liquid, the system pressure decreased rapidly by several mm., due to physical dissolution of the ethylene, and then the pressure began to decrease more slowly, corresponding to reaction of ethylene with the solution. The mitxure was allowed to react in this manner for about 15 minutes. Then the stirrer was turned off, and the reaction vessel filled with mercury until the reaction mixture level had risen into a capillryy at the top of the system.

Portions of solution were periodically withdrawn through a rubber serum cap with a calibrated hypodermic syringe. During withdrawal of the samples, mercury was released into the reaction vessel to maintain the reaction mixture level in the capillary. There was thus virtually no area for gas transfer into or out of the solution. The ethylene in each sample was measured volumetrically in a fashion quite similar to that employed in determining gas solubility.[10]

To check the accuracy and reproducibility of this volumetric method of ethylene determination, ethylene was dissolved in diethyl sulfate in the ethylene reaction apparatus and samples analyzed for ethylene content. The average of five different determinations in this manner for ethylene solubility in diethyl sulfate gave a Henry's law constant H = 98.3 atm./mole fr., with a standard deviation of 0.6 atm./mole fr. Although the reproducibility was good, this value for H was 6.4% lower than that reported by Truchard, *et al.*[11] No suitable explanation of this discrepancy was apparent.

Results and Analysis

Preliminary investigations showed that the rate of the ethylene reaction was much more rapid than reaction 3; it was found that the ethylene reaction proceeded to completion with virtually no change in the concentrations of $(C_2H_5)_2SO_4$, H_2SO_4, and $C_2H_5SO_4H$ by reaction 3, even though some of the mixtures were far from equilibrium with respect to reaction 3. In addition, the amount of ethylene dissolved was so small that its reaction to completion did not noticeably affect the concentrations of the other components. Typical results are given in Table II.

TABLE II

ETHYLENE REACTION WITH $(C_2H_5)_2SO_4$–H_2SO_4–$C_2H_5SO_4H$ MIXTURE 6b

Ethylene reaction with mixture 6b

Sample	Time reacted (min.)	$C_{C_2H_4}$ (moles/l.)
1	0.0	4.79×10^{-2}
2	30.3	3.39×10^{-2}
3	68.0	2.30×10^{-2}
4	120.5	1.42×10^{-2}
5	201.0	0.716×10^{-2}
6	300.0	$.429 \times 10^{-2}$
7	435.0	$.254 \times 10^{-2}$
8	1091.5	$.250 \times 10^{-2}$ ($C_{C_2H_4}$ final)

Concentration of mixture 6b

Sample	$C_{(C_2H_5)_2SO_4}$ (moles/l.)	$C_{H_2SO_4}$ (moles/l.)	$C_{C_2H_5SO_4H}$ (moles/l.)
1[a]	5.67	2.39	1.33
2[a]	5.76	2.39	1.23
3[b]	5.53	2.25	1.59
4[b]	5.52	2.24	1.62

Initial concentration of mixture 6b

$C_{(C_2H_5)_2SO_4}$ = 6.34 moles/l.

$C_{H_2SO_4}$ = 3.04 moles/l.

[a] Sampled 145 min. before ethylene reaction began. [b] Sampled 133 min. after ethylene reaction began.

In order to be able to separate the effect of initial acid concentration from component concentration at the time of the ethylene reaction, two mixtures were prepared at each of the different initial acid concentrations. The ethylene reaction was then carried out for different degrees of completion of reaction 3 for each of the two mixtures until the ethylene concentration reached a final, seemingly unchanging value, denoted by $C_{C_2H_4f}$. This was not necessarily the value which would be noted for $C_{C_2H_4}$ at system equilibrium, *i.e.*, equilibrium with respect to each of reactions 1, 2, and 3, so the concentration was not referred to as the equilibrium concentration. The final value of $C_{C_2H_4}$ for a fast reaction mixture was estimated with fairly good accuracy from a $C_{C_2H_4}$ *vs.* time plot. The rate of reaction of ethylene for some mixtures was so slow that it was not possible to follow them to find this terminal value; $C_{C_2H_4f}$ for these mixtures was assumed to be 0.3×10^{-2} mole/l. for purposes of data analysis as discussed later. As will be shown, this assumed value was not critical.

Ethylene could not be reacted with mixtures with a higher initial acid concentration than 37 mole % because the sampling of ethylene would have been necessary at periods of less than 25 minutes, the minimum time for one ethylene determination. Reactions at lower acid concentration than 22 mole % were not run because of the inordinate length of time that would have been required to get useful data.

For most reaction mixtures plots of $C_{C_2H_4}$ *vs.* time resulted in smooth curves. For two mixtures, however, the experimental points on the $C_{C_2H_4}$–time plot had a small amount of scatter, and the data did not seem as accurate. To check the reproducibility of the data, one complete run was repeated; these results were practically identical with the first trial.

(10) A. Weissberger, Ed., "Physical Methods of Organic Chemistry," 2nd Ed., Vol. I, Part I, Interscience, New York, N. Y., 1949, p. 297.

(11) A. M. Truchard, H. G. Harris, and D. M. Himmelblau, *J. Phys. Chem.*, **65**, 575 (1961).

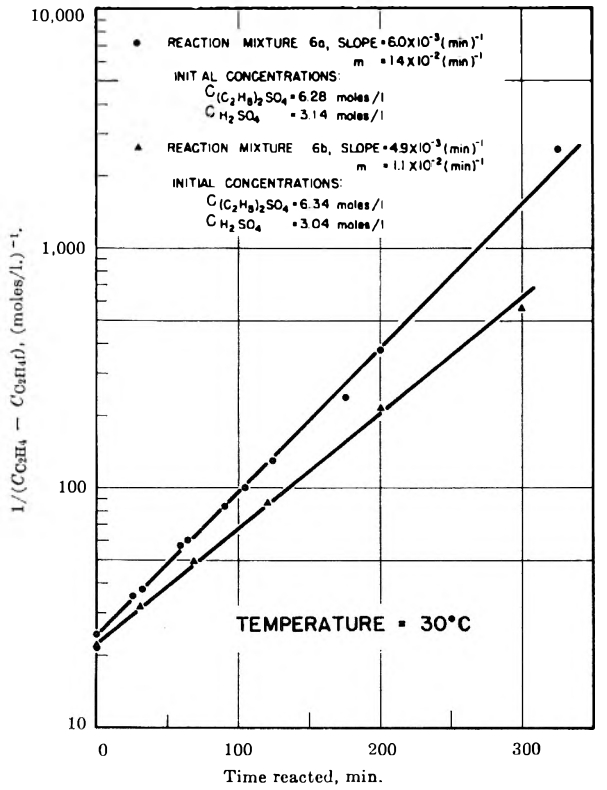

Fig. 1.—Rate constants from slopes of lines—reaction mixtures 6a and 6b.

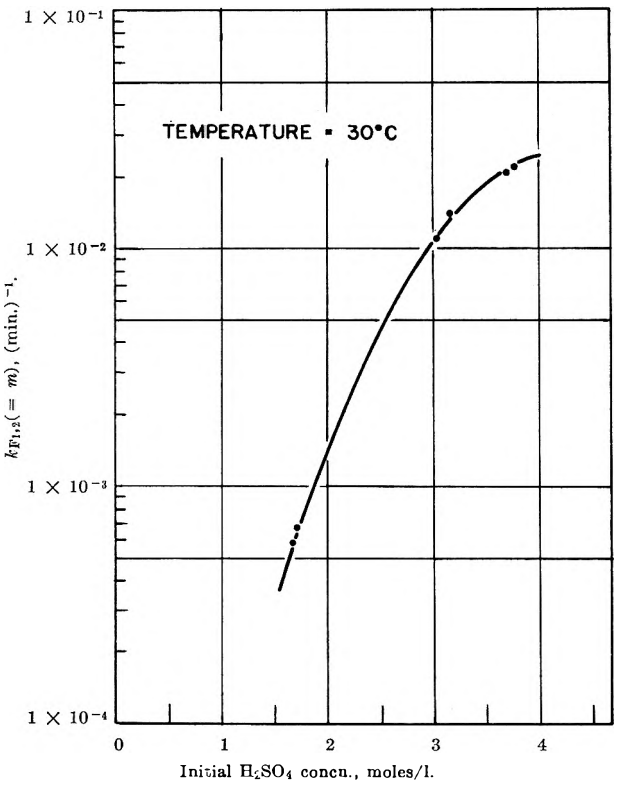

Fig. 2.—Rate constants for C_2H_4 reaction with H_2SO_4 and $C_2H_5SO_4H$ as functions of initial H_2SO_4 concentration.

Kinetic Models

Because of the previously mentioned large difference between the rates of reaction 3 and the ethylene reaction, the concentrations of the components other than ethylene were virtually constant during each of the ethylene reactions. This greatly simplified the data analysis. The rate for any kinetic model could be expressed in terms of only one variable, $C_{C_2H_4}$, could thus be readily integrated, and the rate constants determined.

The following kinetic model based on the over-all stoichiometric equations 1 and 2 was proposed

$$\frac{d(C_{C_2H_4})}{dt} = -k_{F_1}(C_{C_2H_4})(C_{H_2SO_4}) + k_{R_1}(C_{C_2H_5SO_4H}) - k_{F_2}(C_{C_2H_4})(C_{C_2H_5SO_4H}) + k_{R_2}(C_{(C_2H_5)_2SO_4}) = m(C_{C_2H_4}) + b \quad (4)$$

where

$$-m = (k_{F_1}C_{H_2SO_4} + k_{F_2}C_{C_2H_5SO_4H})$$

$$b = (k_{R_1}C_{C_2H_5SO_4H} + k_{R_2}C_{(C_2H_5)_2SO_4})$$

Integrating (4) between the limits

$$t = 0;\ C_{C_2H_4} = C_{C_2H_4 initial}$$

$$t = t;\ C_{C_2H_4} = C_{C_2H_4}$$

gave

$$\log\left[\frac{1}{C_{C_2H_4} - C_{C_2H_4f}}\right] = \frac{m}{2.303}t + b' \quad (5)$$

Thus the data for reactions 1 and 2 plotted according to equation 5 on semilogarithmic graph paper should give straight lines with slopes of $m/2.303$ if the proper kinetic model is that given in equation 4. As can be seen from a typical plot, Fig. 1, the data are well represented by equation 4.

The rate of reaction of ethylene also proved to be dependent only upon the initial acid concentration and not a function of the DES, sulfuric acid, or ethyl hydrogen sulfate concentrations.

This suggests one of two possibilities. The first is that k_{F_1} and k_{F_2} in equation 4 are identical and thus the reaction rate is constant for a fixed sum of $C_{H_2SO_4}$ and $C_{C_2H_5SO_4H}$, and is subsequently constant for all $(C_2H_5)_2SO_4$–$C_2H_5SO_4H$ mixtures having the same initial concentration. Another possibility is that the actual mechanism involves not H_2SO_4 and $C_2H_5SO_4H$ but some property of the system that is constant for a fixed initial concentration. A substantial case has been established[12–16] indicating that the mechanism for the hydration of olefins dissolved in aqueous acid is through reversibly formed π-complex precursors (or perhaps the σ-type) with the later formation of a carbonium ion. The proposed scheme[16] is

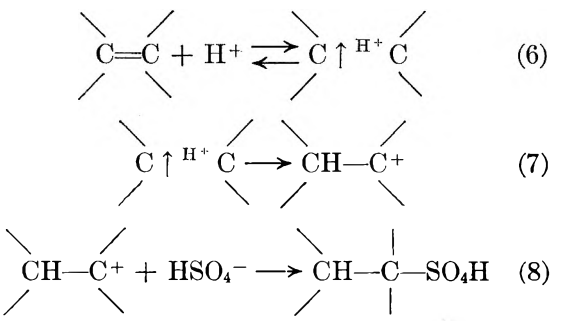

(12) E. R. Alexander, "Principles of Ionic Organic Reactions," John Wiley and Sons, Inc., New York, N. Y., 1950.
(13) B. T. Brooks, "The Chemistry of the Non-benzoid Hydrocarbons," Reinhold Publ. Corp., New York, N. Y., 1950.
(14) E. Kohn, Doctoral Dissertation, The University of Texas, 1956.
(15) R. J. Gillespie and J. A. Leisten, *Quart. Rev.* (London), **8**, 40 (1954).
(16) R. W. Taft, E. L. Purlee, P. Ries, and C. A. Farico, *J. Am. Chem. Soc.*, **77**, 1582 (1955).

with the limiting stage the transition of the π-complex into the carbonium ion, equation 7.

Since reaction 6 is presumed to be in equilibrium, it is easy to show

$$-\frac{d(C_{C_2H_4})}{dt} = k_{f_{1,2}} C_{C_2H_4} C_{H^+} \Gamma \qquad (9)$$

where Γ represents the net product of all the activity coefficients (non-idealities) in the system.

According to the Hammett hypothesis, if the transition state is formed simply by the addition of a proton to the substrate, then the reaction velocity will be proportional to the acidity function h_0, but if the transition state also contains a water molecule, then the reaction velocity will increase less rapidly than h_0 and perhaps may be approximately proportional to the hydrogen ion concentration.

The use of the Hammett acidity function to linearly correlate $k_{f_{1,2}}$ data in the absorption of ethylene in solutions of 80–95% H_2SO_4 (and water) has been demonstrated by Korovina, Entelis and Chirkov[17] and Lumbroso, Hellin, and Coussemant.[18] On the other hand Gel'bshtein and Temkin[8] were unable to find such a linear correlation from their data. In any case, the pertinency of these results to this investigation is not clear, since the diethyl sulfate and ethyl hydrogen sulfate concentrations in their solutions were small, and the water concentrations were substantial—in contrast to the present work which was essentially carried out in non-aqueous solutions. Furthermore, Melander and Myhre[19] point out that the direct proportionality between the acidity function h_0 and the reaction rate is not proof of the mechanism proposed by Taft and co-workers. Taft[20] postulated that the first step in the hydration of olefins has a rapid proton transfer to the π-bond, and that the rate determining step came later in the migration of the proton to one of the carbon atoms forming a carbonium ion. Melander and Myhre's argument indicates that the kinetic evidence alone cannot establish the existence or non-existence of the intermediate π-complex.

How well do the rate constants determined in this work correlate, and what is their significance in connection with the mechanism indicated by equation 9? If log k is plotted against H_0 or $-\log C_{H^+}$, neither plot gives a straight line with slope of unity; neither do they give straight lines with other slopes. Attempts to obtain a linear correlation with other proton indices were also unsuccessful. One of the basic problems is how to evaluate realistically both the proton concentration and the activity coefficients in diethyl sulfate solutions. One might adjust the activity coefficients so the calculated data fit the proposed mechanism, or modify the mechanism assuming the activity coefficient product is essentially constant (or do both at the same time). Figure 2 shows the highly non-linear variation of the rate constant; adjustment of the abscissa scale by one scheme or another to straighten out the curve does not appear to be fruitful. The "true" mechanism must be considerably more complex than that indicated by Taft, perhaps involving orders of reaction greater than unity. One must conclude that considerable caution is needed in interpreting kinetic data in essentially non-aqueous solutions based on models proposed for aqueous solutions.

Acknowledgment.—This research was supported by a grant from The Petroleum Research Fund administered by the American Chemical Society. Grateful acknowledgment is hereby made to the donors of said fund.

(17) G. V. Korovina, S. G. Entelis, and N. M. Chirkov, *J. Appl. Chem.* (English Transl.), **31**, 597 (1958).

(18) D. Lumbroso, M. Hellin, and F. Coussemant, *Compt. rend. Congr. Intern. Chim. 31e Liege, 1958*, **1**, 624 (1959).

(19) L. Melander and P. C. Myhre, *Arkiv för Kemi*, **13**, 507 (1959).

(20) R. W. Taft, Jr., *et al.*, *J. Am. Chem. Soc.*, **74**, 5372 (1952); **77**, 1584 (1955); **78**, 5807, 5811 (1956).

N.M.R. SPECTRA OF SILICON HYDRIDE DERIVATIVES: II. CHEMICAL SHIFTS IN SOME SIMPLE DERIVATIVES[1]

By E. A. V. Ebsworth and J. J. Turner

University Chemical Laboratory, Lensfield Road, Cambridge, England

Received September 15, 1962

The proton and fluorine chemical shifts in a number of simple compounds containing SiH bonds are presented; the SiH chemical shifts are much less sensitive to the nature of the substituents than are the CH chemical shifts in analogous carbon compounds. The SiH resonance shifts to high field from fluorosilane to trifluorosilane. The ^{19}F chemical shifts in fluorosilanes are consistent with a recently developed interpretation of ^{19}F chemical shifts in fluorocarbon derivatives.

We have recently recorded the chemical shifts for protons and fluorine nuclei in a number of simple compounds containing SiH bonds; the results are presented in Tables I–III. The values of the H–H, ^{29}Si–H, H–F, and ^{29}Si–F coupling constants, which were also measured, are discussed elsewhere.[1]

Experimental

The compounds were prepared by standard methods, and were studied in the liquid phase in concentrated (*ca.* 95%) and dilute solutions, using cyclohexane or tetramethylsilane (for proton resonances) or trichlorofluoromethane (for fluorine resonances) as solvent and internal standard. The samples were held in Pyrex tubing of 5 mm. o.d.; the spectra were recorded using a Varian Associates V4300B spectrometer and 12 in. electromagnet, operating at 40 Mc./sec., with flux stabilization and sample spinning; chemical shifts were measured using side-bands generated by a Muirhead-Wigan D695A decade oscillator. Errors quoted for proton resonances are derived from extrapolations, taking at least six measurements at each concentration, unless otherwise stated.

(1) Part I, *J. Chem. Phys.*, **36**, 2628 (1962).

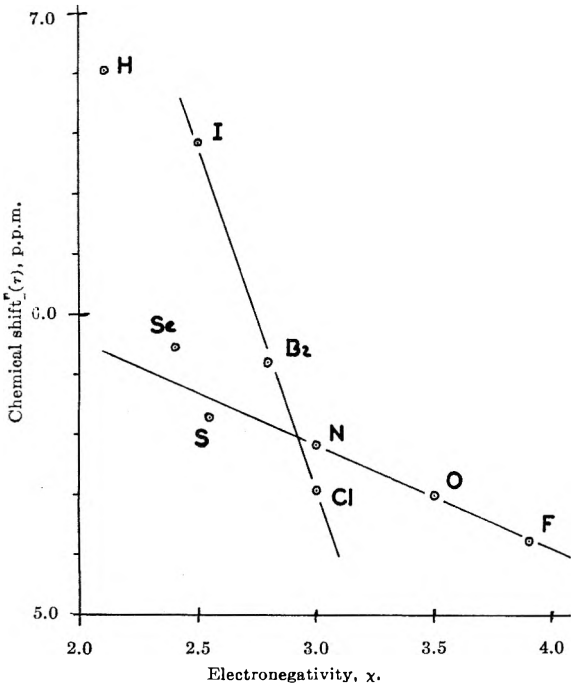

Fig. 1.—Diagram showing variation in proton chemical shift of SiH_3–compounds with the Pauling electronegativity of the substituent. We use the "best valves" of H. O. Pritchard and H. A. Skinner, *Chem. Rev.*, **55**, 745 (1955).

TABLE I

PROTON CHEMICAL SHIFTS IN SIMPLE SILANE DERIVATIVES, IN τ UNITS (C_6H_{12} = 8.56), EXTRAPOLATED TO INFINITE DILUTION

Compound	(±0.01 unless otherwise stated), p.p.m.
SiH_4	6.80
SiH_3I	6.56 ± 0.03
SiH_2I_2	5.97
SiH_3Br	5.83
SiH_2Br_2	4.83
SiH_3Cl	5.41
SiH_2Cl_2	4.60
$SiHCl_3$[a]	3.93
SiH_3F	5.24
SiH_2F_2	5.29 ± 0.02
$SiHF_3$	5.49
SiH_3CN[b]	6.18
$(SiH_3)_2O$	5.39
$(SiH_3)_2S$	5.65
$(SiH_3)SCF_3$[c]	5.58
$(SiH_3)_2Se$	5.88 ± 0.04
SiH_3SeCF_3[d]	5.70
$SiH_3SeC_3F_7$[d]	5.71
$(SiH_3)_3N$[e]	5.56 ± 0.02[h]
$(SiH_3)_2NCH_3$[e]	5.56 ± 0.02[h]
$SiH_3N(CH_3)_2$[e]	5.66 ± 0.04[h]
$(SiH_3)_2CN_2$[f]	5.55
SiH_3NCO[g]	5.58 ± 0.02
SiH_3NCS[f]	5.54 ± 0.02
SiH_3NCSe[g]	5.51 ± 0.02

[a] See also ref. 9. [b] E. A. V. Ebsworth and S. G. Frankiss, *J. Chem. Soc.*, in press. [c] See ref. 7. [d] See ref. 8. [e] See ref. 4. [f] See ref. 5. [g] See ref. 6. [h] From 3 measurements or less.

Discussion

It is interesting to consider the chemical shifts given in Table I with those of the analogous derivatives of methane. The most striking difference is that the SiH chemical shift is much the less sensitive to changes in the nature of the substituent at the central atom; thus although the proton resonance for monosilane appears to low field of that in methane (a point that will be discussed in a later paper),[2] trichlorosilane gives a resonance substantially to high field of chloroform.[3] In the SiH_3– compounds so far studied the chemical shift depends largely on the nature of the substituent atom bound to silicon, and is relatively little affected by changes in the rest of the molecule. Thus out of seven SiH_3N– compounds, six give chemical shifts in the range 5.54 ± 0.03[4–6] and the seventh[4] has τ = 5.66 ± 0.04. In disilyl sulfide[7] and disilyl selenide,[8] replacement of one SiH_3– group by CF_3– changes τ by 0.07 and 0.18 p.p.m., respectively.

The SiH– resonance is also relatively insensitive to dilution. The biggest dilution shift that we have observed is only 0.2 p.p.m. (for SiH_3NCSe),[6] and the mean dilution shift is only 0.05 ± 0.03 p.p.m.; it has previously been noted that the proton chemical shift in trichlorosilane is not very sensitive to changes in solvent.[9] This insensitivity to dilution is of some interest where the fluorosilanes are concerned. It has been suggested that these compounds are associated in the liquid phase[10]; any such association would be expected to lead to unusually large dilution shifts in both proton and fluorine n.m.r. spectra. The observed dilution shifts are given in Table II. In tetramethylsilane the

TABLE II

DILUTION SHIFTS IN FLUOROSILANES (p.p.m.)

Compound	H resonance (solvent $SiMe_4$)	F resonance
SiH_3F	0.03 ± 0.01	3 ± 3
SiH_2F_2	0.04 ± .02	3.8 ± 2.0
$SiHF_3$	0.02 ± .02	0.3 ± 0.5

proton dilution shifts are all small; in the fluorine resonance spectra the dilution shift of difluorosilane is apparently larger, but the uncertainty in the measurement makes the significance of the shift very doubtful. Thus the n.m.r. measurements do not support the idea that the fluorosilanes are associated in the liquid phase.

In the four series of halomethanes of general formula $CH_{4-n}X_n$, where X is fluorine, chlorine, bromine, or iodine, the proton resonance moves to lower fields as n increases from 1 to 3[3,11]; the same is true for the chlorosilanes, while dibromo- and diiodosilane both give resonances well to low field of the analogous monohalosilanes. In the fluorosilanes, on the other hand, increasing fluorine substitution leads to a small *increase* in τ. This may be connected with the anomalous effect of F, O, or N substitution upon the H–H coupling[1]; in this context, the effect of increasing O or N substitution upon the SiH chemical shift would be of interest.

There is a general decrease in τ for SiH_3– compounds as the Pauling electronegativity of the substituent increases. If, however, the chemical shifts in SiH_3– compounds, together with the point for SiH_4,[2] are plotted against the Pauling electronegativity of the

(2) E. A. V. Ebsworth and J. J. Turner, to be published.
(3) See L. M. Jackman, "Nuclear Magnetic Resonance," Pergamon Press, New York, N. Y., 1958.
(4) E. A. V. Ebsworth and N. Sheppard, *J. Inorg. Nucl. Chem.*, **9**, 95 (1959).
(5) E. A. V. Ebsworth and M. J. Mays, *J. Chem. Soc.*, 4879 (1961).
(6) E. A. V. Ebsworth and M. J. Mays, *ibid.*, 4844 (1962).
(7) A. J. Downs and E. A. V. Ebsworth, *ibid.*, 3516 (1960).
(8) E. A. V. Ebsworth, H. J. Emeléus, and N. Welcman, *ibid.*, 2290 (1962).
(9) C. M. Huggins and D. R. Carpenter, *J. Phys. Chem.*, **63**, 238 (1959).
(10) H. J. Emeléus, A. G. Maddock, and C. Reid, *J. Chem. Soc.*, 293 (1944).
(11) S. G. Frankiss, *J. Phys. Chem.*, **67**, 752 (1963).

substituent (see Fig. 1), the pattern obtained is rather different from that given by the analogous CH_3-derivatives.[12] For the CH_3-compounds, the points for F, O, N, and H lie on a straight line; the points for I, Br, Cl, and F lie on a second line, whose gradient $|(d\tau/d\chi)|$ is less, and the failure of the two lines to coincide has been explained in terms of differences in the magnetic anisotropies of the (C–halogen) bonds. For the SiH_3-compounds, the points for F, O, and N lie on a straight line, but the line does not pass through the point for H. Moreover, a line through the points for I, Br, and Cl does not pass through the point for F and is much steeper than the (F, O, N) line. Though these differences between CH_3 and SiH_3 derivatives may be partly due to the different effects of magnetic anisotropy, this sort of explanation is unlikely to account for the high-field shift produced by additional fluorine substitution at silicon. The chemical shifts of protons bound to silicon are likely to be affected by (p→d)π-bonding, and by any contraction in the d-orbitals of silicon that the substituent may cause; the only compound considered here in which there can be no (p→d)π- bonding is SiH_4.

In the fluoromethanes, the fluorine resonance moves to successively lower field values with each additional fluorine substituent.[13] The fluorine resonance in the fluorosilane moves to lower fields as the number of fluorine atoms increases from 1 to 3, but ϕ for tetrafluorosilane is closed to ϕ for difluorosilane (see Table III).

Changes in molecular symmetry may be at least partly responsible for this irregularity; a similar irregularity is also observed in the alkylfluorosilanes.[13] Explanations in terms of changes in electron-density at fluorine are almost certainly inadequate, since it has been shown that fluorine chemical shifts are largely determined by changes in the paramagnetic term. The observed low-field shift as hydrogen is replaced by alkyl groups or fluorine atoms in mono- or difluorosilanes agrees with a recent interpretation of the fluorine chemical shifts in a number of CF-derivatives.[14] This indicates that a substituent at the carbon atom will produce a low-field shift if it has more relatively low-lying excited states than the group it replaces; this is certainly true when methyl groups or fluorine atoms are compared with hydrogen. This type of explanation also accounts for the large low-field shifts in vinyl- and phenyltrifluorosilanes as against trifluorosilane itself.

TABLE III

FLUORINE CHEMICAL SHIFTS IN FLUOROSILANES (p.p.m. RELATIVE TO CCl_3F)

Compound	ϕ
SiH_3F	217 ± 3
SiH_2F_2	151 ± 1.5
$SiHF_3$	109.5 ± 0.5
SiF_4[a]	163.3

[a] Corrected from the measurement in ref. 13 using the value for Et_3SiF given in ref. 13 and by G. Filipovitch and G. V. D. Tiers, *J. Phys. Chem.*, **63**, 761 (1959).

Acknowledgments.—We are grateful to Dr. N. Sheppard for his interest in this work, and to the Wellcome Trustees, who lent the spectrometer to the department.

(12) H. Spiesecke and W. G. Schneider, *J. Chem. Phys.*, **35**, 722 (1961).

(13) E. Schnell and E. G. Rochow, *J. Inorg. Nuclear Chem.*, **6**, 303 (1958).

(14) E. Pitcher, A. D. Buckingham, and F. G. A. Stone, *J. Chem. Phys.*, **36**, 124 (1962).

ULTRAVIOLET ABSORPTION SPECTRA OF o-, m-, AND p-PHENYLENEDIAMINES AND THEIR MONO-AND DIHYDROCHLORIDES IN AQUEOUS SOLUTION[1]

BY P. K. GALLAGHER

Bell Telephone Laboratories, Incorporated, Murray Hill, New Jersey

Received September 18, 1962

Equilibrium quotients were determined at room temperature in aqueous solution for the acidic dissociation reactions of *o*-, *m*-, and *p*-phenylenediamine dihydrochlorides. These values were determined by pH titrations at room temperature and an ionic strength of 1.0 *M*. Acid strengths are of the order $o > m > p$. The ultraviolet absorption spectra were measured for each of the nine species at 25° and an ionic strength of 1.0 *M*. The spectra agreed well with the data available in the literature. The spectra of the ionic species, with the exception of the divalent *ortho* ion, indicate that the addition of a proton to the free electron pair on the nitrogen cancels the original effect of the amine group upon the benzene spectrum.

Introduction

Although there has been considerable effort devoted to the absorption spectra of substituted benzenes, there are only meager data available on the effects of proton association or dissociation reactions on the ultraviolet absorption spectra of the substituted benzene species.[2] It has been observed by numerous investigators that the spectrum of anilinium ion is very similar to that of benzene. Recently Semba[3] has shown that the spectrum of the nitroanilinium ion is similar to that of nitrobenzene. Köhler and Scheibe[4] indicate that the spectrum of the monoprotonated *m*-phenylenediamine ion resembles that of aniline. The contention is that the addition of a proton to the free electron pair on the nitrogen atom cancels the original effect of the amine group upon the absorption spectrum. This investigation extends the work of Köhler and Scheibe to cover all three isomeric phenylenediamines and their divalent ions as well.

The following aqueous equilibria are of interest if the absorption spectra are to be measured for each of the nine species

(1) Presented in part at the 142nd National ACS Meeting, Atlantic City, New Jersey, Sept. 10, 1962.

(2) M. J. Kamlet, "Organic Electronic Spectral Data," Vol. I and II, Interscience Publishers, New York, N. Y., 1960.

(3) K. Semba, *Bull. Chem. Soc. Japan*, **33**, 1640 (1960).

(4) V. H. Köhler and S. Scheibe, *Z. anorg. allgem. Chem.*, **285**, 221 (1956).

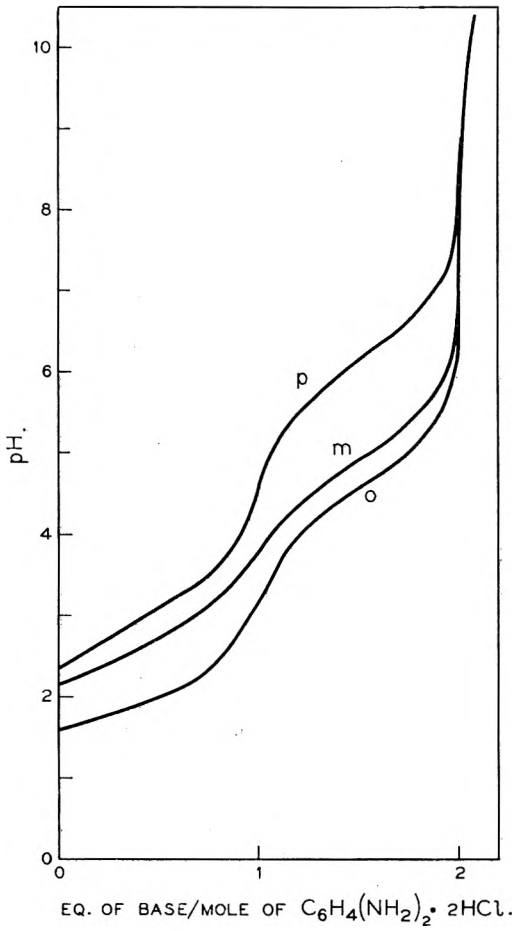

Fig. 1.—Titration of phenylenediamine in 1.0 *M* LiCl.

$$C_6H_4(NH_3)_2^{++} \rightleftharpoons C_6H_4NH_2NH_3^+ + H^+ \quad (1)$$

$$C_6H_4NH_2NH_3^+ \rightleftharpoons C_6H_4(NH_2)_2 + H^+ \quad (2)$$

The values of the equilibrium quotients for these reactions determine the pH necessary to obtain each of the ions in its highest relative concentration. It may be shown that the species $C_6H_4NH_2NH_3^+$ will have its highest concentration at

$$[H^+] = \sqrt{Q_1Q_2} \quad (3)$$

where Q_1 and Q_2 are the equilibrium quotients for reactions 1 and 2 and the brackets denote molar concentration. The maximum fraction of the singly ionized isomer, which occurs at this hydrogen ion concentration is

$$f_{XH^+} = \frac{\sqrt{Q_1/Q_2}}{2 + \sqrt{Q_1/Q_2}} \quad (4)$$

where X = $C_6H_4(NH_2)_2$ and f_i is the fraction of total X present as form i. Since it is necessary to vary the acidity widely in order to obtain the maximum concentration of each species, the ionic strength was maintained constant by the addition of an inert electrolyte. It was hoped that this would minimize medium effects on both the spectra and equilibria.

Experimental

o, *m*-, and *p*-Phenylenediamine dihydrochlorides were obtained from the Eastman Organic Chemical Company. Two samples of each isomer were weighed and dissolved in 200 ml. of 1.0 *M* lithium chloride solution prepared from reagent grade lithium chloride and distilled water. The solutions were titrated with 0.1129 *M* lithium hydroxide solution. A Leeds and Northrup pH meter employing glass and saturated calomel electrodes was used to follow the courses of the titrations.

Absorption spectra were measured using a Cary recording spectrophotometer Model 14, with 1.00 and 0.0504 cm. cells having fused silica windows. The cell compartment was maintained at 25° by the circulation, of water from a thermostat. The spectra were determined for each isomer in 1.00 *M* hydrochloric acid with the solvent as the reference solution. The spectra were again determined in 1.0 *M* lithium chloride to which sufficient lithium hydroxide solution had been added to make the final pH 11.0. Finally the spectra were measured in 1.0 *M* lithium chloride which had been similarly adjusted, by the addition of a small quantity of hydrochloric acid, to the appropriate value of pH given in Table II in order to obtain the maximum concentration of the singly charged ion. The reference solution for these last sets of spectra was 1.0 *M* lithium chloride.

Since these compounds are subject to fairly rapid air oxidation, particularly in weakly acidic or basic solution, it was necessary to make the spectral measurements as rapidly as possible after dissolution. Where it was necessary to adjust the pH of the final solution, the procedure consisted of dissolving the weighed material in a 100-ml. volumetric flask using the 1.0 *M* lithium chloride solution. The pH of this solution was adjusted to the desired value by the dropwise addition of 0.1129 *M* lithium hydroxide solution or dilute hydrochloric acid. The amount of dilution was less than 0.5 ml. and no correction was applied. The spectra were immediately measured and remeasured to see if they had changed during the scanning time of the spectrophotometer. The entire time lapse from weighing to end was less than ten minutes. In no case was the rerun spectra different from the first scan. The entire procedure was performed twice at each pH. One solution was measured in 1.000 cm. cells and the second solution in 0.0504 cm. cells. The shorter cells were necessary in order to obtain good spectra in the region of 196–220 mμ. Absorbancy indices calculated at longer wave lengths for two solutions agreed within experimental error.

Results

Figure 1 presents the averaged titration curves for each of the isomers. The agreement between duplicate titrations and the smoothed curve was ±0.02 pH unit. The values of pQ_1 and pQ_2 were read directly from the curves and are presented in Table I.

TABLE I

VALUES OF THE ACID DISSOCIATION CONSTANTS OF PHENYLENEDIAMINE DIHYDROCHLORIDE. T = 25°, I = 1.0 *M*

Isomer	pQ_1[a]	pQ_2[a]
ortho	2.01	4.58
meta	2.75	4.90
para	3.10	6.16

[a] $pQ_i = -\log Q_i$.

Table II indicates the maximum values of f_{XH^+} which can be obtained in this medium and the values of pH at which they occur. These values are calculated from eq. 3 and 4

TABLE II

MAXIMUM FRACTION OF $C_6H_4NH_2NH_3^+$ AND THE APPROPRIATE pH; T = 25°, I = 1.0 *M*

Isomer	f_{XH^+}	pH
ortho	0.905	3.30
meta	.857	3.82
para	.950	4.63

Absorbancy indices of the uncharged species were calculated directly from the data at pH 11.0 since the conversion is complete at this pH. To a first approximation, the spectral measurements in 1.0 *M* hydrochloric acid were considered as the spectra of the pure divalent isomers. However, contamination with the monovalent ion may be as great as one per cent. Contributions of the other ionic forms are significant in

the region of the maximum concentration of the monovalent species. The spectra observed at these values of pH were corrected to give the absorbancy indices of the pure monovalent isomer by use of the equation

$$a_{HX^+} = \frac{a_{HX^+}^*(2 + \sqrt{Q_1/Q_2}) - a_X - a_{H_2X}}{\sqrt{Q_1/Q_2}} \quad (5)$$

where a_i^* is the absorbancy index calculated on the hypothetical basis that all the isomer is in the form i at this pH.

The spectra of the divalent species were then corrected for the amount of monovalent ion present in 1.0 *M* HCl by use of the analogous equation

$$a_{H_2X^{++}} = \frac{1}{Q_1}[a_{H_2X^{++}}^*(1 + Q_1) - a_{HX^+}] \quad (6)$$

The use of the corrected values of $a_{H_2X^{++}}$ from eq. 6 in eq. 5 does not affect the values of a_{HX^+} calculated and consequently further refinement is not necessary. The corrected spectra for all nine species are plotted in Fig. 2, 3, and 4. A summary of this data is presented in Table III.

TABLE III

CORRECTED VALUES OF WAVE LENGTH AND ABSORBANCY INDEX AT MAXIMA IN THE ABSORPTION SPECTRA OF PHENYLENEDIAMINE AND ITS IONS

		Band A		Band B		Band C	
Isomer	Charge	λ_{max}[a]	log a[b]	λ_{max}[a]	log a[b]	λ_{max}[a]	log a[b]
	0	207	4.60	230	3.83	289	3.47
ortho	+1	198	4.40	230	4.00	280	3.21
	+2	199	4.04	230	3.04	280	2.33
	0	211	4.58	~240[c]	3.95[c]	287	3.45
meta	+1	198	4.41	235	3.97	285	3.24
	+2	..	..	200	3.94	255	2.21
	0	198	4.51	241	3.98	304	3.30
para	+1	198	4.34	235	3.98	285	3.10
	+2	..	..	203	4.05	255	2.23

[a] Units are mμ. [b] a in units of cm.$^{-1}$ M^{-1}. [c] Shoulder.

Discussion

The relationships among the equilibrium quotients are predictable from purely electrostatic considerations similar to those used to explain the relative strengths of the dibasic aliphatic acids.[5] The proximity of the electropositive NH_3^+ groups, particularly for the *ortho* ion, would be expected to facilitate the acid dissociation and similarly the closer the electronegative amine groups the more readily the proton would be added. Hence, the base strengths of the isomeric phenylenediamines follow the order $p > m > o$ for both protonations. The values of Q_1/Q_2 are of the order $o > m > p$ which is also in accordance with the electrostatic interaction of the substituents. As the NH_2 and NH_3^+ groups are further separated they become less interdependent. Consequently the resistance to the formation of two electronegative groups in close proximity to each other by the loss of the second proton is minimized. This is more significant in the comparison of the value of Q_1/Q_2 for the *ortho* ion with the *meta* or *para* isomer than in comparison of the *meta* and *para* ions.

Upon completion of the titrations, the solutions had a noticeable color, suggesting that some oxidation oc-

(5) L. P. Hammett, "Physical Organic Chemistry," McGraw-Hill Book Co., New York, N. Y., 1940, p. 199.

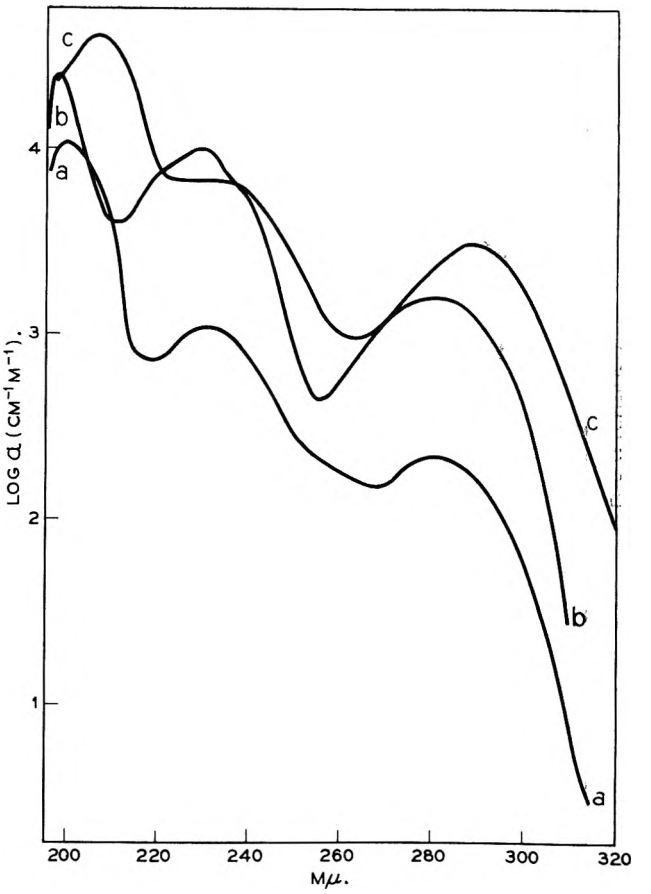

Fig. 2.—Absorption spectra of *o*-phenylenediamine and its ions; I = 1.0 M, T = 25°: (a) $C_6H_4(NH_3)_2^{++}$; (b) $C_6H_4NH_2$-NH_3^+; (c) $C_6H_4(NH_2)_2$.

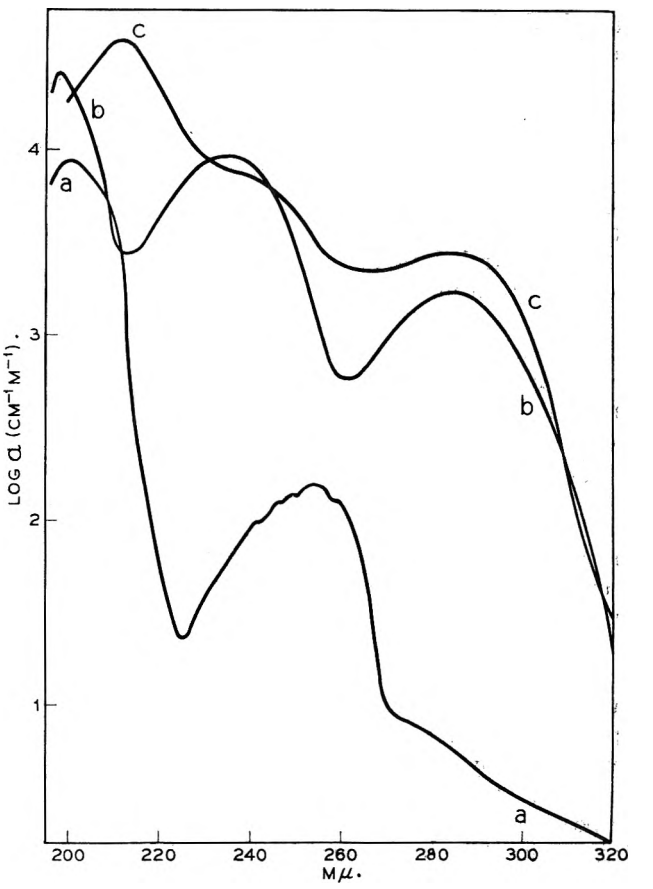

Fig. 3.—Absorption spectra of *m*-phenylenediamine and its ions; I = 1.0 M, T = 25°: (a) $C_6H_4(NH_3)_2^{++}$; (b) $C_6H_4NH_2$-NH_3^+; (c) $C_6H_4(NH_2)_2$.

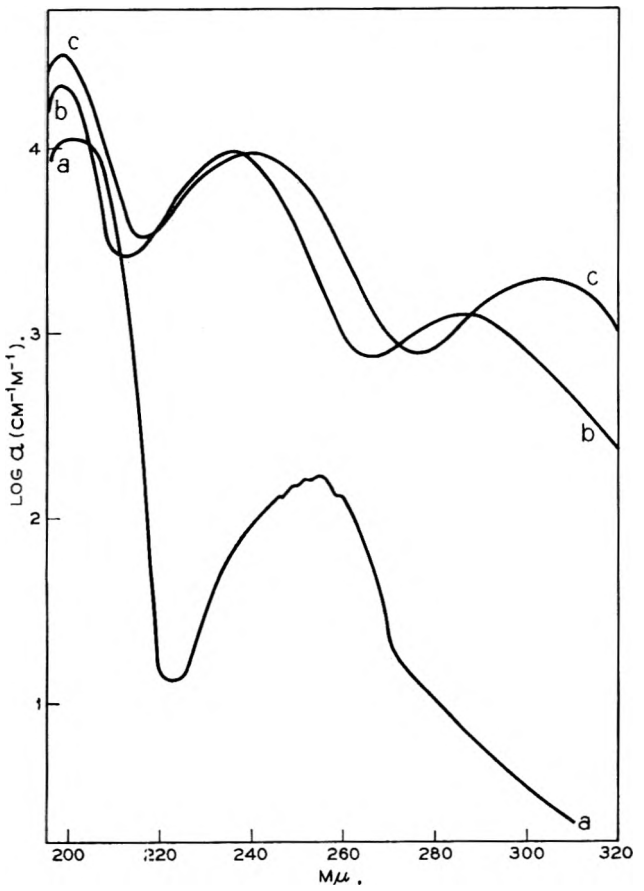

Fig. 4.—Absorption spectra of *p*-phenylenediamine and its ions; $I = 1.0\ M$, $T = 25°$: (a) $C_6H_4(NH_3)_2^{++}$; (b) $C_6H_4NH_2NH_3^+$; (c) $C_6H_4(NH_2)_2$.

curred during the experiment. The time elapsed during the titration was long, however, compared to that necessary to measure the spectra and it is felt that oxidation did not directly introduce errors in the spectral measurements. Any error in the values of Q_2, as a result of oxidation would indirectly introduce a slight error into the corrected spectra of the monovalent ions.

The spectral data for the neutral *ortho* and *meta* isomers, given in Table III are compared in Table IV with values of previous workers.[4,6,7] Some previous effort[4,7] has been devoted to the spectrum of the *meta* isomer as a function of pH and this data is presented in Table V along with selected data from the present work. The agreement in both tables is considered excellent, particularly in view of the unspecified ionic strength and temperature of some of the data. In Table V the first three lines are for the region of pH in which the monovalent ion is the predominant species and the last two lines are for the region of almost pure divalent species.

Doub and Vandenbelt[6,8,9] have explained the spectra of mono- and disubstituted benzene derivatives in terms of a displacement of the benzene bands at approximately 184, 203, and 254 mμ. These bands are referred to by Doub and Vandenbelt as the "Second Primary," "First Primary," and "Secondary" bands, respectively, and correspond to bands A, B, and C in this work. The shift from the parent benzene spectra

(6) L. Doub and J. M. Vandenbelt, *J. Am. Chem. Soc.*, **71**, 2414 (1949).
(7) A. Maschka, M. Seim, and W. Trauer, *Monatsh Chem.*, **85**, 168 (1954).
(8) L. Doub and J. M. Vandenbelt, *J. Am. Chem. Soc.*, **69**, 2714 (1947).
(9) L. Doub and J. M. Vandenbelt, *ibid.*, **77**, 4535 (1955).

TABLE IV

COMPARISON OF SOME SPECTRAL DATA FOR *ortho-* AND *meta-* PHENYLENEDIAMINES

	Band A		Band B		Band C	
Isomer	λ_{max}[a]	log a[b]	λ_{max}[a]	log a[b]	λ_{max}[a]	log a[b]
ortho[c]	207	4.60	230	3.83	289	3.47
ortho[d]	206	4.60	233	3.84	289	3.46
meta[c]	211	4.58	240[e]	3.95[e]	287	3.45
meta[d]	210	4.57	240[e]	3.86[e]	289	3.32
meta[f]	..	..	..	..	288	3.34
meta[g]	210	4.5	240[e]	3.8[e]	290	3.3

[a] Units are mμ. [b] Units of a are cm.$^{-1}$ M^{-1}. [c] This paper. [d] Reference 6. [e] Shoulder. [f] Reference 7. [g] Reference 4.

TABLE V

COMPARISON OF SOME SPECTRAL DATA FOR *m*-PHENYLENEDIAMINE IN ACIDIC SOLUTION

	Band A		Band B		Band C	
Media	λ_{max}[a]	log a[b]	λ_{max}[a]	log a[b]	λ_{max}[a]	log a[b]
pH 1.8[c]	..	..	..	..	283	2.42
Not given[d]	~200	~4.3	235	3.8	285	3.2
pH 3.82[e]	200	4.37	234	3.93	283	3.23
2 *N* HCl[c]	..	..	252	2.09	..	..
1 *N* HCl[e]	200	3.93	254	2.22	..	..

[a] Units are mμ. [b] Units of a are cm.$^{-1}$ M^{-1}. [c] Reference 7. [d] Reference 4, alleged spectra of monovalent ion. [e] Uncorrected data from this paper.

which results upon substitution is correlated with the *ortho-para* directing or *meta* directing nature for a large number or substituents. They observe for disubstituted compounds that if the substituents are of opposite type, the displacement toward longer wave lengths is greater than if both groups are the same. Since NH_2 is electron contributing (*ortho-para* directing) and NH_3^+ is electron attracting (*meta* directing), one would expect the monovalent ion to exhibit the largest shift. This was not the case for any of the three bands or isomers. In each case the shift observed for the monovalent ion was less than or equal to that of the neutral compound. This unusual behavior may be the result of the destruction of the resonance equilibria established by the strongly conjugative substituent, NH_2, when the free electron pair on the nitrogen accepts a proton.

Scheibe[4] has pointed out that the effect of adding a proton to the electron pair on the nitrogen, in general, is to cancel the original effect of the amine group upon the spectrum. He shows that the spectrum of the monovalent *meta* ion is very similar to that of aniline and that the anilinium ion has a spectrum similar to benzene. The data presented here substantiate this. The spectra of the monovalent isomers are similar and resemble that of aniline. The spectra of the *meta* and *para* divalent ions are also similar to that of benzene and the anilinium ion. These comparisons are summarized in Table VI. The agreement is considered excellent.

The fact that the divalent *ortho* ion does not conform to the comparison in Table VI suggests that the second proton does not assume the anticipated position but rather is somehow assimilated into the general structure of the monovalent ion. The result is the general lowering of intensity without a shift in the spectrum. Several factors might contribute to this tendency. The closer proximity of the amine groups in the *ortho* isomer would lead to a greater charge repulsion and possible steric hinderance to the free rotation of the

TABLE VI

COMPARISON OF THE SPECTRA OF BENZENE AND SOME AMINE DERIVATIVES

Species	λ_{max}[a]	log a[b]	λ_{max}[a]	log a[b]	λ_{max}[a]	log a[b]
C_6H_6[c]	203.5	3.87	254	2.31	..	..
$C_6H_5NH_3^+$[c]	203	3.88	245	2.20	..	..
m-$C_6H_4(NH_3)_2^{++}$	200	3.94	255	2.21	..	..
p-$C_6H_4(NH_3)_2^{++}$	203	4.05	255	2.23	..	..
$C_6H_5NH_2$	~198[d]	~4.3[d]	230[c]	3.93[c]	280[c]	3.16[c]
o-$C_6H_5NH_2NH_3^+$	198	4.40	230	4.00	280	3.21
m-$C_6H_5NH_2NH_3^+$	198	4.41	235	3.97	285	3.24
p-$C_6H_5NH_2NH_3^+$	198	4.34	235	3.98	285	3.10

[a] Units are mμ. [b] Units of a are cm.$^{-1}$ M^{-1}. [c] Reference 8. [d] Reference 4 (slight extrapolation of curve from 200 mμ).

nitrogen atoms, if both amine groups add a proton. The hindered rotation has been used to explain the "*ortho* effect" on the dielectric constant of the unprotonated molecule.[10] The largest "*ortho* effect" among the disubstituted benzenes is exhibited by *o*-phenylenediamine.[11] Since this effect is observed for the neutral molecule, the departure from the expected behavior should be even greater for the protonated species. There could also be the added stabilization of the monovalent ion by intrahydrogen bonding as indicated below

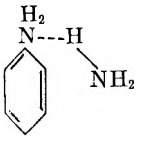

(10) L. Tiganik, *Z. physik. Chem.*, **14B**, 135 (1931).

(11) C. P. Smyth, "Dielectric Behavior and Structure," McGraw-Hill Book Co., New York, N. Y., 1955, p. 332.

Semba[3] has found evidence for such bonds in the *o*-nitroanilinium ion.

Intuitively one would expect that if these factors are operative, the addition of the second proton would be unusually difficult for the *ortho* isomer. This is not reflected in the equilibrium quotients. The lack of an anomalous equilibrium quotient, however, does not preclude the proposed nature of the divalent ion.

Conclusion

The equilibrium quotients were determined for the acidic dissociations of the *o*-, *m*-, and *p*-phenylenediamine dihydrochlorides at room temperature in media having an ionic strength of 1.0 *M*. These values were used to determine the appropriate acidities at which to best evaluate the absorption spectra of each of the nine species. These spectra were measured, at 25° in aqueous solutions having an ionic strength of 1.0 *M*, and corrected, where necessary, for incomplete conversion to the specified species. The spectra agree well with the limited available data. The correlation proposed by Scheibe[4] is substantiated, *i.e.*, the effect of protonating an aromatic amine group is to cancel its effect on the ultraviolet absorption spectrum. This observation is contrary to the empirical correlation of Doub and Vandenbelt[6,8,9] for the case of the monovalent ions. The divalent *ortho* ion does not fit the general picture and it is proposed that the second proton does not add directly to the nitrogen atom.

KINETIC STUDIES WITH ELECTROGENERATED HALOGENS. I. THE MONOBROMINATION OF PHENETOLE

BY GARY S. KOZAK AND QUINTUS FERNANDO

Department of Chemistry, University of Arizona, Tucson, Arizona

Received September 19, 1962

The monobromination of phenetole in aqueous solutions has been investigated by an instrumental technique. Bromine was electrogenerated at a predetermined rate by means of constant current pulses in an acid solution containing potassium bromide and phenetole. The rate of the reaction was followed by recording the diffusion current of bromine at a rotating platinum microelectrode as a function of time. Kinetic measurements at varying hydrogen ion and bromide ion concentrations have shown that molecular bromine is the only brominating species of importance, and that the rate of bromination of phenetole is first order with respect to bromine and first order with respect to phenetole. The second-order rate constant is 4.8 ± 0.2 × 10^4 M^{-1} sec.$^{-1}$ at 25° and 1.1 ± 0.2 × 10^4 M^{-1} sec.$^{-1}$ at 0°. This study has demonstrated that the method we have used is convenient and reliable and can be readily adapted for the study of most halogenation reactions.

A method recently has been described for determining the kinetics of bromination of phenol.[1] In this method bromine was electrogenerated in an acidified solution of potassium bromide in the presence of phenol; the rate at which the diffusion current of the electroreducible species Br_2 and Br_3^- varied with time was followed by means of an amperometric circuit and a recorder, and the rate constants for the bromination reaction were obtained from the resulting curves. Bromine can be electrogenerated by means of constant current pulses or by using a constant direct current. In this work, current pulses of constant magnitude were generated with the aid of a multivibrator and electromechanically counted. A detailed description of the construction, calibration and use of this instrument has been published.[1,2]

The present work was undertaken primarily to demonstrate the utility and general applicability of this instrumental technique. The previous kinetic studies were carried out with phenol using this method[1]; however, the occurrence of several side reactions made the interpretation of the kinetic data difficult. Not only the phenol molecule, but also the phenoxide ion underwent bromination, and furthermore, dibromination as well as tribromination occurred. In this work the kinetics of bromination of phenetole were studied, since this compound was expected to behave in manner

(1) G. S. Kozak and Q. Fernando, *Anal. Chim. Acta*, **26**, 541 (1962).

(2) Q. Fernando, M. A. V. Devanathan, J. C. Rasaiah, J. A. Calpin, and K. Nakulesparan, *J. Electroanal. Chem.*, **3**, 46 (1962).

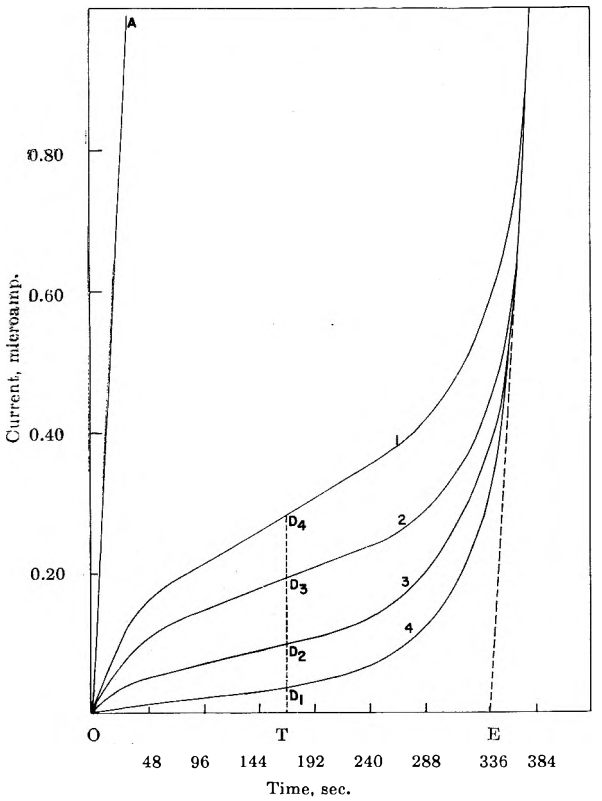

Fig. 1.—The effect of $[Br^-]$ on the monobromination of phenetole: curve 1, $[Br^-] = 0.75\ M$; curve 2, $[Br^-] = 0.50\ M$; curve 3, $[Br^-] = 0.25\ M$; curve 4, $[Br^-] = 0.125\ M$.

exactly analogous to that of anisole, which undergoes only monobromination to form primarily the *para*-bromo compound, *via* the reaction of the neutral molecule with bromine or tribromide ions.[3]

Experimental

Apparatus.—The electrolysis cell consisted of a central compartment having a capacity of about 100 ml. and was connected to two saturated calomel reference electrodes by means of side-arms. Sintered glass disks and agar plugs separated the central compartment from the reference electrodes.[4] The generator electrode consisted of a platinum foil which was connected to the cathode of the tube in the multivibrator circuit,[2] and one of the reference electrodes was connected to ground. A Hewlett-Packard Model 711A power supply served as the source of anode voltage (200 v.) for the multivibrator. The solution in the central compartment was stirred continuously by a magnetic stirrer operating at a constant speed.

The indicator electrode was a platinum microelectrode rotated at a constant speed of 600 rev./min. with a Sargent synchronous motor. This microelectrode and the second reference electrode were connected to a recorder. In this work the recorder of a Sargent Model XV polarograph was found to be quite satisfactory.

Reagents.—HCl, $HClO_4$, KBr, and KNO_3 were of reagent grade purity and were used without further purification.

Phenetole was obtained from Eastman Kodak Co. and was purified by fractional distillation under a pressure of 9 mm. The fraction that had a boiling point between 55.5 and 55.9° was collected and used in this work.

8-Quinolinol was obtained from Lemke and Co., Inc., purified by sublimation, recrystallization from an ethanol–water mixture, and the product was finally dried *in vacuo* in a desiccator. The melting point of the compound was 72.5–74.5°.

All solutions were prepared from distilled water that was passed through a mixed cation–anion exchange resin bed. The effluent had a residual impurity of less than 1 p.p.m. as NaCl.

Determination of Pulse Size.—It has been shown that the oxidation of As(III) to As(V) or the dibromination of 8-quinolinol with electrogenerated bromine can be used to calibrate the size of the constant current pulses.[1,2] In this work a series of standard 8-quinolinol solutions were used to determine the quantity of bromine electrogenerated per pulse and hence the magnitude of each pulse was found to be 3.823×10^{-4} coulomb/pulse.

Bromination of Phenetole.—The central compartment of the titration cell contained 50 ml. of solution which was 0.05 M in hydrogen ion for most experiments, but contained varying amounts of phenetole and bromide ion. The concentration of phenetole brominated in each experiment was determined indirectly since the preparation of standard solutions of phenetole by weighing was subject to errors due to volatilization. It was found more convenient to determine the initial concentration of phenetole in each bromination experiment by a method which is in effect a coulometric determination with electrogenerated bromine utilizing an amperometric end point.

In Fig. 1, point E shows the end point in the titration of a constant quantity of phenetole with varying amounts of bromide ion. The total amount of bromine electrogenerated, in the time interval OE, can be calculated since the pulse rate and the pulse size are known.

A blank titration, OA, in the absence of phenetole, establishes the relationship between the magnitude of the diffusion current and the total number of moles of bromine electrogenerated. It is of interest to note that the total amount of unreacted bromine, *i.e.*, $([Br_2] + [Br_3^-] + [Br_2Cl^-])$, is proportional to the diffusion current at the platinum electrode since an identical blank was obtained in solutions containing varying quantities of Br^- and Cl^-. At time T, the amount of unreacted bromine present as Br_2 and Br_3^- (together with Br_2Cl^- in the presence of Cl^-) is proportional to the diffusion current TD_1, TD_2, TD_3, and TD_4 for the various curves. The difference between the total amount of bromine electrogenerated in the time interval OT and the unreacted bromine is equal to that reacted; if it is assumed that only the monobromination of phenetole takes place, and since the initial concentration of phenetole is known, the concentration of phenetole reacted at time T can be calculated. The above calculation can be repeated for any number of points along the titration curve,[1] and the concentrations of unreacted phenetole and the corresponding concentrations of free bromine and tribromide ions calculated. Table I shows a typical set of data obtained in this manner. It has been assumed in all calculations that the total quantity of bromine electrogenerated is so small ($\sim 10^{-4}\ M$) that the initial concentration of KBr remains constant during each experiment.

Results

When bromine is generated in solutions containing KBr and either 0.05 M $HClO_4$ or HCl, only the following brominating species are assumed to be present[3]: Br_2, Br_3^-, and Br_2Cl^- (in the presence of Cl^-). If k_1, k_2, and k_3 are the second-order rate constants for the bromination of phenetole with Br_2, Br_3^-, and Br_2Cl^-, respectively, the observed rate constant for the bromination of phenetole is given by

$$k = \frac{(k_1 + k_2K[Br^-] + k_3K'[Cl^-])}{(1 + K[Br^-] + K'[Cl^-])} \qquad (1)$$

where

$$K = [Br_3^-]/[Br_2][Br^-]$$

and

$$K' = [Br_2Cl^-]/[Br_2][Cl^-]$$

$K = 16$ at 25° and 20 at 0°[5]; $K' = 1.21$ at 25°.[6]

In the majority of the experiments $HClO_4$ was used instead of HCl. In these cases eq. 1 can be simplified to

$$k = \frac{(k_1 + k_2K[Br^-])}{(1 + K[Br^-])} \qquad (2)$$

(3) R. P. Bell and D. J. Rawlinson, *J. Chem. Soc.*, 63 (1961).

(4) M. A. V. Devanathan and Q. Fernando, *Trans. Faraday Soc.*, **52**, 1332 (1956).

(5) R. O. Griffith, M. McKeown, and A. G. Winn, *ibid.*, **28**, 101 (1932).

(6) I. M. Korenman, *J. Gen. Chem. USSR*, **17**, 1608 (1947).

TABLE I

KINETIC DATA FOR THE BROMINATION OF PHENETOLE AT 25°

Initial concentration of phenetole = 9.350×10^{-5} M
Initial concentration of KBr = 0.500 M
Initial concentration of $HClO_4$ = 0.050 M

Time, sec.	$[Br_2] \times 10^5$, M electrogenerated	$([Br_2] + [Br_3^-]) \times 10^6$, M unreacted	$[Br_2] \times 10^7$, M unreacted	$[Br_2] \times 10^5$, M reacted	$[C_6H_5OC_2H_5] \times 10^5$, M unreacted	$k(1 + K[Br^-]) = k_1 \times 10^{-4}$, M^{-1} sec.$^{-1}$
42.0	1.940	1.149	1.277	1.825	7.525	4.75
48.0	2.215	1.205	1.340	2.094	7.256	4.70
54.0	2.493	1.250	1.390	2.368	6.982	4.71
60.0	2.766	1.298	1.441	2.636	6.714	4.72
66.0	3.045	1.349	1.499	2.910	6.440	4.73
72.0	3.320	1.390	1.545	3.181	6.169	4.79
78.0	3.600	1.448	1.609	3.455	5.895	4.82
84.0	3.880	1.482	1.648	3.732	5.618	4.93

The observed rate constant, k, in $HClO_4$ solutions is given by

$$\frac{d}{dt}[BrC_6H_4OC_2H_5] = k[C_6H_5OC_2H_5]([Br_2] + [Br_3^-]) \quad (3)$$

The rate of formation of monobromophenetole is obtained from the tangent to the plot of the concentration of bromine reacted (see column 5, Table I) as a function of time. The concentration of phenetole at any time during the reaction as well as the sum of the concentrations of unreacted Br_2 and Br_3^- can be obtained from the curves as shown above, since the initial concentrations of phenetole and Br^- are known. A typical set of data is shown in Table I.

Table II summarizes the results obtained by brominating phenetole at bromide ion concentrations varying from 0.25 to 1.00 M. Values of the rate constant, k, are expressed in M^{-1} sec.$^{-1}$ and each k is the average of 4 to 9 values.

TABLE II

EFFECT OF $[Br^-]$ ON THE BROMINATION OF PHENETOLE IN 0.05 M $HClO_4$ AT 25°

$[Br^-]$, M	$k \times 10^{-3}$, M^{-1} sec.$^{-1}$	$k(1 + K[Br^-]) \times 10^{-4}$, M^{-1} sec^{-1}
0.25	9.94	4.97
.50	5.33	4.79
.75	3.73	4.85
1.00	2.86	4.86

Bromination reactions carried out at constant bromide ion concentration but varying perchloric acid concentration (0.03 to 0.075 M) showed no appreciable effect on the observed rate constant.

The results of the bromination of phenetole in 0.05 M HCl and varying bromide ion concentration are shown in Table III. The observed rate constants are not significantly different from the rate constants for corresponding bromide ion concentrations shown in Table II.

A series of bromination experiments was carried out at 0° in a 0.05 M $HClO_4$ solution containing varying amounts of bromide ion, and the kinetic data are given in Table IV.

Discussion

Phenetole can be brominated in aqueous solutions containing bromine by any one or all of the following species: Br_2, Br_3^-, Br^+, HOBr, and H_2OBr^+. In this study, bromination has been carried out in the presence of relatively large concentrations of acid and bromide

TABLE III

EFFECT OF $[Br^-]$ ON THE BROMINATION OF PHENETOLE IN 0.05 M HCl

$[Br^-]$, M	$k \times 10^{-3}$, M^{-1} sec.$^{-1}$	$k(1 + K[Br^-] + k'[Cl^-]) \times 10^{-4} = k_1 \times 10^{-4}$, M^{-1} sec.$^{-1}$
0.25	9.63	4.81
.50	5.30	4.77
.60	4.56	4.84
.75	3.58	4.65
.92	3.01	4.72
1.00	2.73	4.64

TABLE IV

EFFECT OF Br^- ON THE BROMINATION OF PHENETOLE IN 0.05 M $HClO_4$

$[Br^-]$, M	$k \times 10^{-3}$, M^{-1} sec.$^{-1}$	$k(1 + K[Br^-]) \times 10^{-4}$, M^{-1} sec.$^{-1}$
0.125	3.14	1.10
.25	2.00	1.20
.50	0.964	1.06
.64	.797	1.10
.75	.594	0.95
1.00	.424	0.90

ion which preclude the formation of HOBr or Br^+ to any appreciable extent by the reactions

$$Br_2 + H_2O \rightleftharpoons HOBr + H^+ + Br^-$$

and

$$Br_2 \rightleftharpoons Br^+ + Br^-$$

It is therefore reasonable to assume that the only brominating species present in solution are Br_2 and Br_3^-. This also is supported by the fact that the observed rate constant is unaffected by varying the hydrogen ion concentration. Similar findings have been made by other investigators who have studied the bromination of anisole and substituted anisoles in aqueous media.[3,7]

Bromine forms Br_2Cl^- in the presence of chloride ions. In the solutions studied, the relative concentrations of bromide and chloride ions used were such that the concentration of Br_2Cl^- formed was smaller than the concentration of Br_3^- by a factor of about 100. The observed rate constants in Tables II and III are the same (within experimental error) for corresponding bromide ion concentrations. Furthermore a variation in the concentration of Cl^- did not have an appreciable effect on the values of k. These experimental observations indicate that Br_2Cl^- does not participate in the bromination of phenetole.

It is apparent from Fig. 1 that the bromination of phenetole is slowed down by an increase in the concen-

(7) W. J. Wilson and F. G. Soper, *J. Chem. Soc.*, 3376 (1949).

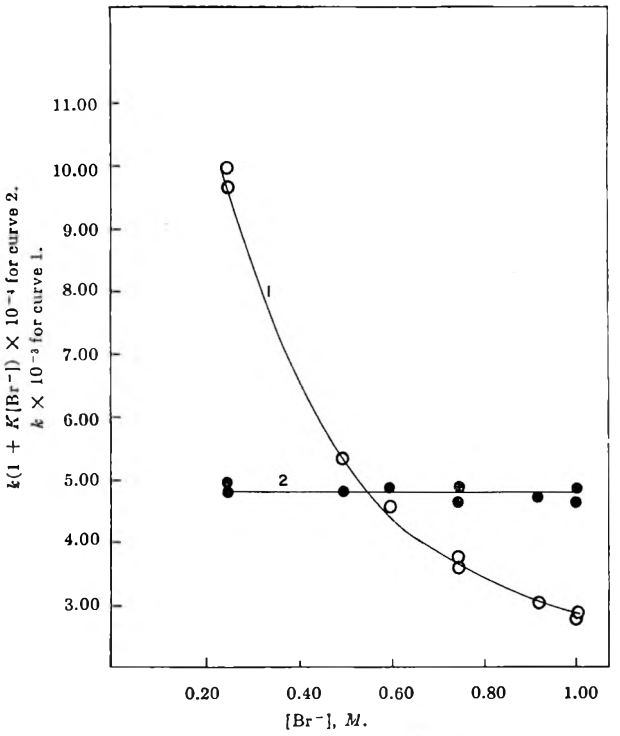

Fig. 2.—Effect of $[Br^-]$ on k and $k(1 + K[Br^-])$: curve 1, k *vs.* $[Br^-]$; curve 2, $k(1 + K[Br^-])$ *vs.* $[Br^-]$.

tration of bromide ions. Therefore the observed rate constant, k, decreases with increasing bromide ion concentration (Fig. 2). The second-order rate constant k_2, for the reaction of tribromide ion with phenetole, can be obtained from a plot of $k(1 + K[Br^-])$ *vs.* Br^- (eq. 2). However, the slope of such a plot (Fig. 2) is zero, *i.e.*, $k(1 + K[Br^-])$ is a constant within experimental error for various bromide ion concentrations. This shows that the tribromide ion is unimportant as a brominating species in the bromination of phenetole in aqueous solutions. The small variation in the value of $k(1 + K[Br^-])$ in Tables II, III, and IV is probably due to a kinetic salt effect. It is possible that the value of the equilibrium constant K is affected at high ionic strengths. Similar salt effects have been observed in the bromination of *o*-bromoanisole.[6]

The rate constant, k_1, was found to be constant over the entire range of phenetole concentration studied, on the assumption that the reaction is first order with respect to phenetole and first order with respect to bromine. Moreover plots of $\log(-d[Br]_2/dt)$ *vs.* $(\log [Br_2] + y/x \log [C_6H_5OC_2H_5])$ where x and y are the orders for the reactants, bromine and phenetole, respectively, gave straight lines only when $x = y = 1$. The analysis of nearly 100 sets of kinetic data by the above method showed that the bromination of phenetole is first order with respect to bromine and first order with respect to phenetole concentration and may be represented by the equation

$$-d[Br_2]/dt = k_1[C_6H_5OC_2H_5][Br_2]$$

The value of k_1 at 25° is $4.8 \pm 0.2 \times 10^4\ M^{-1}$ sec.$^{-1}$ and $1.1 \pm 0.2 \times 10^4\ M^{-1}$ sec.$^{-1}$ at 0°. An average energy of activation of 9.5 kcal. mole^{-1} was obtained from these values for the bromination of phenetole. A value of $4 \times 10^4\ M^{-1}$ sec.$^{-1}$ has been reported as the rate constant for the bromination of anisole at 25° and $6.1 \times 10^3\ M^{-1}$ sec.$^{-1}$ at 0° in an aqueous medium.[3] From these results the rate of bromination of anisole seems to be slightly slower than the rate of bromination of phenetole.

Since this study has established the reliability of the experimental technique, we are presently investigating a number of halogenation reactions which have proved to be far too rapid to follow by conventional methods.

Acknowledgment.—The authors are grateful to the U. S. Atomic Energy Commission for financial assistance.

FLUORINE BOMB CALORIMETRY. V. THE HEATS OF FORMATION OF SILICON TETRAFLUORIDE AND SILICA[1,2]

BY STEPHEN S. WISE, JOHN L. MARGRAVE,

University of Wisconsin, Madison, Wisconsin, and

HAROLD M. FEDER AND WARD N. HUBBARD

Argonne National Laboratory, Argonne, Illinois

Received September 20, 1962

The heat of formation of gaseous silicon tetrafluoride was measured by direct combination of the elements in a bomb calorimeter. ΔHf_{298}^0 was found to be -385.98 ± 0.19 kcal. mole^{-1}. The heats of reaction of vitreous silica and of α-quartz with fluorine were also measured. Combination of these with the heat of formation of $SiF_4(g)$ give ΔHf_{298}^0 (vitreous silica) $= -215.94 \pm 0.31$ kcal. mole^{-1} and ΔHf_{298}^0 (α-quartz) $= -217.72 \pm 0.34$ kcal. mole^{-1}. The excellent agreement between the latter value and Good's determination of the same quantity by an independent method indicates that the generally accepted value, -209.9, should be superceded. The apparent discrepancies between thermochemical and equilibrium values for the free energy of formation of silica, previously noted by Chipman, are now substantially resolved. A value of ΔHf_{298}^0 of -24.04 ± 0.45 kcal. mole^{-1} for the formation of gaseous silicon monoxide is concordant with the reported results. Unresolved discrepancies in the heat of formation of silicon carbide still exist.

Introduction

This research is part of a continuing program to obtain precise thermochemical data by fluorine bomb calorimetry.[3] As an essential preliminary to the study of various silicon-containing compounds by fluorine bomb calorimetry the heat of formation of silicon tetrafluoride was sought. Silicon tetrafluoride is formed whenever silicon-containing compounds react with excess fluorine; hence, it was necessary that its heat of formation be known with high precision. Wartenberg and Schutte[4] made the sole previous determination of the heat of formation of SiF_4 by direct combination of the elements and reported a value of -360 kcal. mole^{-1}. The accuracy of this result was limited by the purities of the silicon and fluorine available at that time; furthermore, Ryss[5] has suggested that the experimental conditions were such that Si_2F_6 may have formed, thus giving a heat of formation of SiF_4 which was insufficiently negative. All other determinations of ΔHf (SiF_4) were made indirectly; *e.g.*, by comparison of the heat of solution of SiF_4 in hydrofluoric acid to form fluorosilicic acid with the heat of solution of silica in hydrofluoric acid to form the same product. Vorob'ev, Kolesov, and Skuratov,[6] reporting the most recent measurements involving the above processes, derived -372.9 kcal. mole^{-1} as the heat of formation of SiF_4. Unfortunately, the indirect determinations of the heat of formation of SiF_4 are uncertain to the same extent as the heats of formation of SiO_2 and HF are uncertain, and the latter uncertainties are far from negligible (see below). It was therefore concluded that a new, direct determination of the heat of formation of SiF_4 by fluorine bomb calorimetry was a necessary adjunct to the determination of the heats of formation of silicon-containing compounds.

The heat of formation of quartz is a quantity of considerable interest to metallurgists and geochemists. The generally accepted value[7] for the heat of formation of α-quartz, -209.9 kcal. mole^{-1}, is based on measurements of the heat of combustion of silicon in oxygen by Humphrey and King.[8] However, Chipman[9] has presented evidence, based on a number of observed equilibria, that the standard free energy of formation of quartz is 3 to 8 kcal. mole^{-1} more negative than the value calculated from this heat of formation. Unless all the observed equilibria are coincidently in error by the same amount, Chipman's observation implies that either the heat of formation of quartz should be 3 to 8 kcal. mole^{-1} more negative or that the generally accepted entropies of crystalline silicon or quartz are in error by absurdly large amounts. On searching the literature we found other evidence that the value -209.9 kcal. mole^{-1} for the heat of formation of quartz may be in error. Potter,[10] in a 1907 paper which has been regarded as of only historical interest, gave results of combustions of silicon in oxygen which yield values for the heat of formation of silica ranging from -212 to -215. Potter, noticing the difficulty of recovering all of the unburned silicon after combustion, used a removable lining in his bomb so that the amount of silicon burned could be determined after the combustion from the gain in weight of the lining and its contents. In more recent times, Golutvin[11] has claimed that Humphrey and King[8] erred in their analytical determination of the quantity of unburned silicon remaining after oxygen bomb combustions. He has reported values for the heat of formation of silica between -215 and -219. Most recently, Good reported[12] the heat of formation of quartz to be -217.5 ± 0.5 kcal. mole^{-1}. This determination was based upon a rather circuitous route and he therefore suggested that

(1) This work was performed under the auspices of the U. S. Atomic Energy Commission.

(2) This paper is based on a thesis submitted by S. S. Wise to the faculty of the University of Wisconsin in partial fulfillment of the requirements for the Ph.D. degree. It is available as Argonne National Laboratory Report No. 6472.

(3) Earlier papers in this series are: I. E. Greenberg, J. L. Settle, H. M. Feder, and W. N. Hubbard, *J. Phys. Chem.*, **65**, 1168 (1961); II. J. L. Settle, H. M. Feder, and W. N. Hubbard, *ibid.*, **65**, 1337 (1961); III. S. S. Wise, J. L. Margrave, H. M. Feder, and W. N. Hubbard, *ibid.*, **65**, 2157 (1961); IV. E. Greenberg, J. L. Settle and W. N. Hubbard, *ibid.*, **66**, 1345 (1962).

(4) H. v. Wartenberg and R. Schutte, *Z. anorg. allgem. Chem.*, **211**, 222 (1933).

(5) I. G. Ryss, "The Chemistry of Fluorine and Its Inorganic Compounds," Moscow, 1956; available in English as AEC-tr-3927 (Pt. 1).

(6) A. F. Vorob'ev, V. P. Kolesov, and S. M. Skuratov, *Russ. J. Inorg. Chem.* (English translation), **5**, 679 (1960).

(7) J. P. Coughlin, U. S. Bur. Mines Bull. 542 (1954).

(8) G. L. Humphrey and E. G. King, *J. Am. Chem. Soc.*, **74**, 2041 (1952).

(9) J. Chipman, *ibid.*, **83**, 1762 (1961).

(10) H. N. Potter, *Trans. Electrochem. Soc.*, **11**, 259 (1907).

(11) Yu. M. Golutvin, *Zhurnal Fiz. Khim.*, **30**, 2251 (1956).

(12) W. D. Good, J. L. Lacina, D. W. Scott, and J. P. McCullough, Preliminary communication to the Calorimetry Conference, Ottawa 1961.

the problem might be better resolved by fluorine bomb calorimetry.

In the present work, very pure silicon, vitreous silica and α-quartz were burned in excess pure fluorine. The heats of formation of silicon tetrafluoride and of α-quartz so determined have been reported in a preliminary communication[13] published concurrently with the results of Good.[14]

Experimental

A. Materials. (i). **Silicon.**—Two samples of elemental silicon were obtained through the courtesy of the Pigments Division, E. I. du Pont de Nemours and Company. One sample was in the form of granules weighing from 0.01 to 0.1 g. each. The other was in the form of 100 mesh powder. X-Ray patterns of both samples corresponded to those of crystalline cubic silicon.[15] The results of chemical analyses follow. Granular silicon: O, 0.0105%; C, 0.0034%; N, 0.0104%; and H, <0.001%. Powdered silicon: O, 0.063%; C, 0.018%; N, 0.0088%; and H, 0.0023%. Spectrochemically, only a trace (<10 p.p.m.) of magnesium was observed in the granular sample and a trace of sodium in the powdered sample. The samples thus contained 99.976 and 99.908% silicon, respectively. If the principal impurities are assumed to be present as SiO_2, Si_3N_4, SiC, and water the purities of the two silicon samples were 99.904 and 99.882 mole % elemental silicon, respectively.

(ii). **Silica.**—Silica glass was obtained from the Englehard Industries in the form of 3 in diameter disks, 3 mm. thick. A second sample of silica glass was obtained through the courtesy of Dr. F. Bickford of the Corning Glass Works. Coupons, $2^1/_2$ in. $\times$ $^1/_2$ in. $\times$ 3 mm., were cut from stock with a silicon carbide saw. Spectrographic analyses of these silica samples showed them to be free from detectable amounts of metallic impurities. The absence of X-ray diffraction lines showed them to be completely amorphous.

A 1-lb. single crystal of synthetic α-quartz was generously supplied by Dr. J. E. Kuntzler, Bell Telephone Laboratories. The spectrographic analysis accompanying the sample showed only the following impurities (in p.p.m.): Na, 30; Al, 50; Li, 10; and Fe, 20. With the assumption that these impurities were present as Na_2SiO_3, Al_2SiO_5, Li_2SiO_3 and Fe_2SiO_4 the sample was calculated to be 99.985 mole % uncombined silica. A sample of naturally-occurring α-quartz was purchased from the P. R. Hoffman Co., Carlisle, Pa. Spectrographic analysis of the impurities in this sample showed only Fe and Al present in the amounts 50 and 10 p.p.m., respectively. The sample was calculated to be 99.996 mole % uncombined silica. The presence of only α-quartz was indicated by X-ray examination of both crystalline materials. The α-quartz samples were crushed to 60–100 mesh size in a "Diamonite" mortar of hardened steel. Chips of steel which contaminated the sample during the pulverization were removed with a large magnet. Representative samples of the pulverized quartz were heated with concentrated hydrofluoric acid in a platinum crucible; the absence of any weighable residue indicated that all of the steel chips had been removed.

(iii). **Fluorine.**—Fluorine was purified by distillation in a low temperature still.[16] Mercury titration analysis[17] showed the distilled fluorine to be more than 99.9% pure; the impurities (by mass spectrometric analysis) were 0.04% oxygen, 0.01% nitrogen, and traces of helium and argon.

B. Calorimeter and Combustion Vessel.—The calorimetric system and operational procedure of this investigation were similar to those described in paper I.[3] The reaction vessel (described in detail elsewhere[18]) was the two-chambered device designed for use with materials that burn spontaneously in fluorine.

C. Calibration.—The energy equivalent of the calorimeter was determined in the standard manner[19] by combustion in oxygen of benzoic acid, NBS standard sample 39g, under prescribed conditions. No nitric acid or carbon monoxide was observed in the combustion products. For the calibration, the fluorine tank was evacuated, the valve was kept closed, and the oxygen, at 30 atm. pressure, was contained within the bomb proper. The energy equivalent of the calorimetric system used in the silicon experiments, as determined by six combustions, was 3348.42 $\pm$ 0.53 cal. deg.$^{-1}$. The energy equivalent of the (slightly different) system used in the silica experiments, as determined by five combustions, was 3351.16 $\pm$ 0.53 cal. deg.$^{-1}$. The uncertainties are standard deviations of the means.

D. Combustion Techniques.—The fluorine tank was filled to the desired pressure and closed by means of a remotely operable toggle valve. The bomb containing the sample was then joined to the tank by a connecting tube. The bomb and tube were pumped down to a pressure of 10^{-3} mm. for approximately one hour and placed in the calorimeter. When the toggle valve was opened fluorine expanded into the bomb proper.

Powdered silicon ignited spontaneously on exposure to more than 300 mm. pressure of fluorine. Because the granular sample did not ignite spontaneously, 30–40 mg. of powdered silicon was added as an igniter. In both cases a mound of sample was supported on a small nickel dish. With the fluorine tank charged initially to 5000 mm. pressure, both samples of silicon, once ignited, burned completely, leaving no trace of residue. The granular silicon immediately fused to form a single molten drop which moved rapidly about the nickel dish until it was completely consumed, much like a drop of water on a hot plate. The nickel dish underwent no significant change in weight or appearance from run to run. It was concluded that no significant attack on the nickel dish by either fluorine or molten silicon (presumably encased in SiF_4 vapor) had taken place.

Neither form of silica reacted spontaneously with fluorine. The vitreous silica, because of its resistance to thermal shock, could be burned as a coupon without being shattered. The internal nickel fittings of the bomb were so arranged that a weighed coupon could be clamped at one end between two nickel nuts while the other end just touched a weighed mound of silicon powder in a nickel dish. The fluorine tank was charged to 6700 mm. pressure for these experiments. The silicon ignited spontaneously on exposure to fluorine and, in turn, ignited the end of the silica coupon. The latter burned until just a sliver, protruding from between the two nickel nuts, remained. After each run this sliver of silica was weighed to determine the extent of combustion. No attack by fluorine on the nuts was observed.

A similar combustion arrangement was not satisfactory for α-quartz because massive samples shattered on ignition and unburned fragments were scattered about. Consequently, the sample was crushed as described, and was burned in the same manner as the granular silicon. A weighed amount of the crushed quartz was placed in a mound on a nickel dish and a small amount of silicon powder was then spread over its surface as an igniter. The fluorine tank was charged to 7600 mm. pressure for these experiments. Approximately 70% of the quartz, and all of the silicon, were burned in each calorimetric combustion. The unburned material was washed from the nickel dish onto a filter funnel, dried and weighed. The unburned material was verified as α-quartz by X-ray examination. Evidence that the nickel support dishes were not significantly fluorinated during the quartz combustion experiments was obtained. In several of these experiments (see Table IV) a vitreous silica support plate was substituted for the nickel dish. The vitreous silica plate reacted slightly during these combustions; however, when a correction for this side reaction was made on the basis of the measured heat of combustion of vitreous silica, there was no detectable difference in the results.

E. Product Analysis.—Infrared spectrometric examination of the bomb gases after the combustions showed bands due only to SiF_4 and none due to Si_2F_6 or to various oxyfluorides. Mass spectrometric analyses showed only SiF_4, O_2 (after silica combustions), and small amounts of N_2 from the impurity in the fluorine and of CF_4 from the carbon impurity in the silicon samples.

F. Blank Experiments.—In the usual[3] calorimetric apparatus for combustions in fluorine, the gas is in contact with the bomb walls for 30 to 45 minutes before the combustion is begun.

(13) S. S. Wise, J. L. Margrave, H. M. Feder, and W. N. Hubbard, *J. Phys. Chem.*, **66**, 381 (1962). The preliminary results have now been revised to accord with the new scale of atomic weights.

(14) W. D. Good, *ibid.*, **66**, 380 (1962).

(15) National Bureau of Standards Circular 539, Vol. II (1953).

(16) A preliminary description is contained in paper I.[3] For further details see L. Stein, J. Settle, and E. Rudzitis, Argonne National Laboratory Report No. 6364.

(17) G. T. Armstrong and R. S. Jessup, *J. Res. Natl. Bur. Std.*, **64A**, 49 (1960).

(18) R. L. Nuttall, S. Wise, and W. N. Hubbard, *Rev. Sci. Instr.*, **32**, 1402 (1961).

(19) J. Coops, R. S. Jessup, and K. van Nees, Chapter 3, "Experimental Thermochemistry," F. D. Rossini, Editor, Interscience Publishers, Inc., New York, N. Y., 1956.

TABLE I

ENERGY OF COMBUSTION OF POWDERED SILICON[a]

(1)	m, g.	0.45240	0.46006	0.45709	0.45807	0.45829	0.45862	0.45714
(2)	Δt_c, deg.	1.85006	1.88140	1.86938	1.87371	1.87377	1.87525	1.86921
(3)	ε(Calor.), cal. deg.$^{-1}$	3348.42	3348.42	3348.42	3348.42	3348.42	3348.33[d]	3348.41[d]
(4)	ε(Calor.)$(-\Delta t_c)$, cal.	−6194.78	−6299.72	−6259.47	−6273.97	−6274.17	−6278.96	−6258.88
(5)	$\Delta E_{contents}$, cal.[b]	−4.58	−4.66	−4.63	−4.64	−4.64	−4.64	−4.63
(6)	ΔE_{gas}, cal.[c]	−0.48	−0.48	−0.48	−0.48	−0.48	−0.48	−0.48
(7)	ΔE_{blank}, cal.	4.0	4.0	4.0	4.0	4.0	4.0	4.0
(8)	$\Delta E_c^0/M$, cal. g.$^{-1}$	−13695.5	−13695.7	−13696.6	−13699.0	−13692.8	−13693.4	−13693.8

(9) Mean $\Delta E_c^0/M$ for sample, cal. g.$^{-1}$ −13695.4 ± 0.8

(10) $\Delta E_c^0/M$ for powdered silicon, cal. g.$^{-1}$ −13707.5 ± 2.1

[a] The symbols employed in these tables are explained in ref. 21. [b] ΔE contents = ε^i(cont.)$(t^i - 25) + \varepsilon^f$(cont.)$(25 - t_f + \Delta t_{corr})$ [c] The sum of items 32 and 34 of ref. 2. [d] Corrected to allow for slight machining changes.

TABLE II

ENERGY OF COMBUSTION OF GRANULAR SILICON

(1)	m, g.	0.42893	0.44825	0.45305	0.45543	0.45539
(2)	Δt_c, deg.	1.89528	1.87845	1.90488	1.89244	1.90667
(3)	ε(Calor.), cal. deg.$^{-1}$	3348.41	3348.41	3348.41	3348.41	3348.41
(4)	ε(Calor.)$(-\Delta t_c)$, cal.	−6346.17	−6289.82	−6378.32	−6336.67	−6284.31
(5)	$\Delta E_{contents}$, cal.	−4.69	−4.65	−4.72	−4.68	−4.70
(6)	ΔE_{gas}, cal.	−0.48	−0.48	−0.48	−0.48	−0.48
(7)	ΔE_{blank}, cal.	4.0	4.0	4.0	4.0	4.0
(7a)	$\Delta E_{kindling}$, cal.	464.00	142.57	164.21	89.70	138.05
(8)	$\Delta E_c^0/M$, cal. g.$^{-1}$	−13716.3	−13716.4	−13718.8	−13719.2	−13718.9

(9) Mean $\Delta E_c^0/M$ for sample, cal. g.$^{-1}$ −13717.9 ± 0.6

(10) $\Delta E_c^0/M$ for granular silicon, cal. g.$^{-1}$ −13721.7 ± 0.8

TABLE III

ENERGY OF COMBUSTION OF VITREOUS SILICA

(1)	m, g.	1.22084	1.22880	1.19919	1.21148	1.21692	1.22401	1.19904[a]
(2)	Δt_c, deg.	1.13231	1.12151	1.11676	1.14375	1.12441	1.12195	1.11406
(3)	ε(calor), cal. deg.$^{-1}$	3351.16	3351.16	3351.16	3351.16	3351.16	3351.16	3351.16
(4)	ε(Calor.)$(-\Delta t_c)$, cal.	−3794.55	−3758.43	−3742.44	−3832.89	−3768.08	−3759.83	−3733.39
(5)	$\Delta E_{contents}$, cal.	−4.80	−4.71	−4.72	−4.86	−4.78	−4.78	−3.75
(6)	ΔE_{gas}, cal.	−0.61	−0.60	−0.61	−0.61	−0.61	−0.61	−0.61
(7)	ΔE_{blank}, cal.	4.0	4.0	4.0	4.0	4.0	4.0	4.0
(7a)	$\Delta E_{kindling}$, cal.	341.70	280.21	351.29	405.79	325.95	298.42	339.37
(8)	$\Delta E_c^0/M$, cal. g.$^{-1}$	−2829.4	−2831.7	−2829.0	−2830.1	−2829.7	−2829.1	−2830.9

(9) Mean $\Delta E_c^0/M$ for sample, cal. g.$^{-1}$ −2830.0 ± 0.4

(10) $\Delta E_c^0/M$ for SiO_2(gl), cal. g.$^{-1}$ −2830.0 ± 0.4

[a] Corning Glass sample; the remainder are Englehard samples.

During this period ample time is available for fluorine to react with impurities, such as water, which may be adsorbed on the bomb surfaces. This is not the case when the two-vessel system is used. The first contact of fluorine with the bomb surfaces occurs when fluorine is expanded into the bomb at the beginning of the reaction period. The thermal effect of the reaction between fluorine and the adsorbed impurities was determined by blank experiments. In these experiments the gas tank was charged with 6–10 atm. of fluorine and a calorimetric run, normal except for the absence of the sample, was made. The measured energy was due to the energy of reaction of fluorine with any adsorbed impurities less the energy absorbed by the expansion of fluorine. The latter quantity was calculated from the equation of state of fluorine and was verified by performing experiments with a bomb freed of adsorbed impurities by prefluorination at 110° for several hours. A net energy of reaction with adsorbed impurities of 4 ± 1 cal. was determined from a series of blank experiments.

Results

The experimental results of this study are presented in Tables I–IV. All energies are expressed in terms of the defined calorie equal to (exactly) 4.1840 absolute joules and all weights were corrected to true mass. The corrections to standard states were applied in the usual manner[20] with suitable modifications for fluorine bomb calorimetry.[21] The entries in Tables I–IV are: (1) the mass of the sample; (2) the observed increase in the calorimeter temperature, corrected for heat exchange between the calorimeter and its surroundings; (3) the energy equivalent of the calorimeter; (4) the energy equivalent of the calorimeter multiplied by the corrected temperature increase; (5) the energy absorbed by the contents of the bomb; (6) the net correction due to the compression and decompression of the bomb gases to the standard states[21]; (7) the blank correction for the reaction of fluorine with adsorbed impurities; (7a) the energy of combustion of any silicon powder kindling used for the ignition; (7b) the energy of combustion of a portion of the vitreous silica support plate used in two of the α-quartz combustions; (8) the energy change per gram of sample burned, with the reactants and products in their respective standard states at 25°; (9) the mean and its standard deviation for the series of experiments; and (10) the standard energy change at 25° per gram of Si, SiO_2(gl), or SiO_2 (α-quartz), after cor-

(20) W. N. Hubbard, D. W. Scott, and G. Waddington, Chapter 5 in ref. 19.

(21) W. N. Hubbard, Chapter 6 in "Experimental Thermochemistry," Vol. II, H. A. Skinner, Editor, Interscience Publishers, Inc., New York, N. Y., 1962.

TABLE IV

ENERGY OF COMBUSTION OF α-QUARTZ

(1)	m, g.	1.10691	0.98937	1.13595[a]	1.08766[a]	1.05216[b]	1.10292[b]	0.79351
(2)	Δt, deg.	1.01577	1.00282	1.05141	1.00889	0.93791	0.96132	0.71981
(3)	ε(Calor.), cal. deg.$^{-1}$	3351.16	3351.16	3351.16	3351.16	3351.16	3351.16	3351.16
(4)	ε(Calor.)$(-\Delta t_c)$, cal.	−3404.01	−3360.61	−3523.44	−3380.95	−3143.09	−3221.54	−2412.20
(5)	$\Delta E_{\text{contents}}$, cal.	−9.43	−9.00	−9.85	−9.08	−9.63	−9.58	−2.31
(6)	ΔE_{gas}, cal.	−0.87	−0.90	−0.87	−0.87	−0.87	−0.87	−0.84
(7)	ΔE_{blank}, cal.	4.0	4.0	4.0	4.0	4.0	4.0	4.0
(7a)	$\Delta E_{\text{kindling}}$, cal.	310.61	592.74	348.41	344.17	200.50	129.97	191.32
(7b)	$\Delta E_{\text{sil. sup.}}$, cal.					4.41	4.92	
(8)	$\Delta E_c^0/M$, cal. g.$^{-1}$	−2800.3	−2803.6	−2801.0	−2797.5	−2798.7	−2804.5	−2797.7

(9) Mean $\Delta E_c^0/M$ for sample, cal. g.$^{-1}$ -2800.3 ± 1.0

(10) $\Delta E_c^0/M$ for SiO_2 (α-quartz), cal. g.$^{-1}$ -2800.3 ± 1.1

[a] Natural quartz samples; the remainder are synthetic quartz samples. [b] Silica support plate used in these runs; nickel dish used in the others.

rection for impurities, for the reactions with fluorine according to equations 1, 2, or 3, respectively.

$$\text{Si(c)} + 2\text{F}_2\text{(g)} \longrightarrow \text{SiF}_4\text{(g)} \quad (1)$$

$$\text{SiO}_2\text{(gl)} + 2\text{F}_2\text{(g)} \longrightarrow \text{SiF}_4\text{(g)} + \text{O}_2\text{(g)} \quad (2)$$

$$\text{SiO}_2(\alpha\text{-quartz}) + 2\text{F}_2\text{(g)} \longrightarrow \text{SiF}_4\text{(g)} + \text{O}_2\text{(g)} \quad (3)$$

Silicon.—The data for seven calorimetric combustions of powdered silicon are presented in Table I and for five calorimetric combustions of granular silicon in Table II.

For the calculation of item (5) the following heat capacities were used: C_p = 0.106 and 0.170 cal. g.$^{-1}$ deg.$^{-1}$ for Ni[22] and Si,[23] respectively; C_v = 5.50 and 15.44 for F_2[24] and SiF_4[24] cal. mole^{-1} deg.$^{-1}$, respectively. For the calculation of item (6) the second virial coefficient and its temperature derivative are required. For F_2 these were estimated[25] from intermolecular force constants.[26] No virial coefficient data were found for SiF_4. However, because the Lennard-Jones 6–12 potential parameters for SiF_4, as derived from gas viscosity drta,[27] are similar to those for CF_4, the virial coefficient data for CF_4[25] were used. All other corrections to standard states were negligible. For the calculation of item (10) the thermal corrections for impurities in the samples were based on the assumption that the impurities were present as SiO_2, SiC,[28] Si_3N_4,[22] and water, and that their combustion products were SiF_4, O_2, CF_4,[29] N_2, and HF[17]; the sources of the required heats of formation are indicated by the superscripts. No corrections were applied for the trace metals found in either sample. In cal. g.$^{-1}$ sample the energies liberated by combustion of the impurities in the powdered silicon were: SiO_2, −2.25; SiC, −8.49; Si_3N_4, −1.53; and H_2O, −0.69. The corresponding values for the granular silicon were SiO_2, −0.55; SiC, −1.63; and Si_3N_4, −1.81. Owing to uncertainties in the chemical analyses and the assumptions as to the chemical state of the impurities generous estimates of the uncertainties in the impurity corrections were allowed.

The powdered silicon sample had a total known impurity content four times as large as the granular silicon sample; hence, the energy of combustion based on the latter is considered to be the more reliable. The results on the powdered sample have been used only for corrections of experiments in which it was used as kindler. It is noteworthy that even after correction for impurities the energies of combustion derived from the two samples differed by 14 cal. g.$^{-1}$ (0.1%), or more than five times the combined standard deviations. Obviously, the two series do not overlap. The source of the difference is unknown.

Silica.—The results of seven combustions of vitreous silica in fluorine are listed in Table III and of seven combustions of α-quartz in Table IV. For the calculation of item (5) the following heat capacities were used: C_p = 0.106, 0.177, 0.176, and 0.170 cal. g.$^{-1}$ deg.$^{-1}$ for Ni,[22] SiO_2(α-quartz),[24] SiO_2(gl),[24] and Si,[23] respectively; C_v = 5.50, 15.44, and 5.04, cal. mole^{-1} deg.$^{-1}$ for F_2,[24] SiF,[24] and O_2.[30] Item (6) was estimated by the method previously discussed. The intermolecular force constants of O_2 were taken from ref. 25. For the calculation of item (10) it was assumed that the impurities were present as Al_2SiO_5, Fe_2SiO_4, Li_2SiO_3, and Na_2SiO_3, and that the products of combustion were O_2, SiF_4, AlF_3, FeF_3, LiF, and NaF. The requisite heats of formation were taken from ref. 31, except for Fe_2SiO_4.[32] The total correction for the reactions of the impurities in the silica samples amounted to about 2700 cal. per gram of impurities. This was so nearly the same as the energy of combustion of the sample that the net impurity corrections were negligible. No significant difference between the energies of combustion of natural and synthetic α-quartz can be discerned from the rather limited data shown in Table IV.

Derived Data.—The standard thermal data derived from the experimental results presented above are presented in Table V. Atomic weights used in the calculations are: Si, 28.086 and O, 15.9994.[33] The

(22) "Selected Values of Chemical Thermodynamic Properties," National Bureau of Standards Circular 500 (1951).

(23) P. Flubacher, A. J. Leadbetter, and J. A. Morrison, *Phil. Mag.*, **4**, 273 (1959).

(24) K. K. Kelley and E. G. King, U. S. Bur. Mines Bull. 592 (1961).

(25) J. O. Hirschfelder, C. F. Curtiss, and R. B. Bird, "Molecular Theory of Gases and Liquids," John Wiley and Sons, Inc., New York, N. Y., 1954.

(26) D. White, J. H. Hu, and H. L. Johnston, *J. Chem. Phys.*, **21**, 1149 (1953).

(27) C. P. Ellis and C. J. G. Raw, *ibid.*, **30**, 574 (1959).

(28) G. L. Humphrey, S. S. Todd, J. P. Coughlin, and E. G. King, U. S. Bureau of Mines Rept. Invest. 4888 (1952).

(29) D. W. Scott, W. D. Good, and G. Waddington, *J. Am. Chem. Soc.*, **77**, 245 (1955).

(30) J. Hilsenrath, C. W. Beckett, W. S. Benedict, L. Fano, H. J. Hope, J. F. Masi, R. L. Nuttall, Y. S. Touloukian, and H. W. Woolley, "Tables of Thermodynamic and Transport Properties of Air, Argon, Carbon Dioxide, Carbon Monoxide, Hydrogen, Nitrogen, Oxygen and Steam," Pergamon Press, New York, N. Y., 1960.

(31) "Preliminary Report on the Thermodynamic Properties of Selected Light-Element Compounds," NBS Report No. 7192, July 1, 1961.

(32) E. G. King, *J. Am. Chem. Soc.*, **74**, 4446 (1952).

(33) International Union of Pure and Applied Chemistry, Information Bulletin Number 14B, Butterworth Scientific Publications, London, 1961; *cf. Chem. Eng. News*, **39**, No. 47, 43 (1961).

TABLE V

DERIVED DATA[a] AT 25°

Silicon

(1) $Si(c) + 2F_2(g) \longrightarrow SiF_4(g)$	$\Delta E_c^0 = \Delta E_f^0 = -385.39 \pm 0.19$	
	$\Delta H_f^0 = -385.98 \pm 0.19$	
	$\Delta S_f^0 = -34.1 \pm 0.5$	
	$\Delta G_f^0 = -375.81 \pm 0.24$	
(2) $SiO_2(gl) + 2F_2(g) \longrightarrow SiF_4(g) + O_2(g)$	$\Delta E_c^0 = \Delta H_c^0 = -170.04 \pm 0.25$	
$Si(c) + 2F_2(g) \longrightarrow SiF_4(g)$	$\Delta H_f^0 = -385.98 \pm 0.19$	
$Si(c) + O_2(g) \longrightarrow SiO_2(gl)$	$\Delta H_f^0 = -215.94 \pm 0.31$	
	$\Delta S_f^0 = -42.2 \pm 0.4$	
	$\Delta G_f^0 = -203.33 \pm 0.34$	
(3) SiO_2 (α-quartz) $+ 2F_2(g) \longrightarrow SiF_4(g) + O_2(g)$	$\Delta E_c^0 = \Delta H_c^0 = -168.26 \pm 0.28$	
$Si(c) + 2F_2(g) \longrightarrow SiF_4(g)$	$\Delta H_f^0 = -385.98 \pm 0.19$	
$Si(c) + O_2(g) \longrightarrow SiO_2$ (α-quartz)	$\Delta H_f^0 = -217.72 \pm 0.34$	
	$\Delta S_f^0 = -43.44 \pm 0.1$	
	$\Delta G_f^0 = -204.77 \pm 0.34$	

[a] Values given in kcal. mole^{-1} except ΔS_f^0 values given in cal. deg.$^{-1}$ mole^{-1}.

symbols ΔE_c^0, ΔH_c^0, ΔE_f^0, ΔH_f^0, ΔS_f^0, and ΔG_f^0 are used for the energy and heat of combustion, and the energy, heat, entropy and Gibbs energy of formation at 25°, respectively. Because there is no net change in the number of moles of gas in equations 2 and 3, the standard energy of combustion is equal to the standard enthalpy of combustion. The standard entropies at 25° of Si,[23] SiO_2(α-quartz),[24] SiO_2(gl),[24] SiF_4,[24] O_2,[24] and F_2[24] were taken as 4.43, 10.00, 11.2, 67.3, 49.01, and 48.49 cal. deg.$^{-1}$ mole^{-1}, respectively. The uncertainties[34] attached to the derived data are equal to twice the combined standard deviations arising from calibration, reproducibility, and the corrections due to impurities and the blank.

Discussion

The result of this research on the heat of formation of α-quartz is a value (-217.72 ± 0.34 kcal. mole^{-1}) which is 7.8 kcal. mole^{-1} more negative than the generally accepted value. Good[14] has burned mixtures of silicon and vinylidene fluoride polymer in oxygen in the presence of aqueous HF in a rotating bomb calorimeter. From these experiments and King's[35] data for the heat of solution of α-quartz in aqueous HF, Good derives a value for the heat of formation of α-quartz (-217.5 ± 0.5 kcal. mole^{-1}) which is in excellent agreement with our result, although obtained by an entirely independent method. The more negative value for the heat of formation of α-quartz suggested by these two researches is consistent with other thermochemical evidence[10,11] and, in addition, substantially resolves the discrepancies which were noted by Chipman.[9] A comparison of the thermochemical and equilibrium measurements is included in Appendix A.

From the values obtained in the present investigation one may calculate the heat of transition of vitreous silica to α-quartz, $\Delta H_{tr.}{}^0{}_{298} = -1.78 \pm 0.46$ kcal. mole^{-1}. Although the combustion method for determining small transition heats is not to be preferred to comparative heat of solution measurements, it is nevertheless satisfying that reasonable agreement with the data of Mullert[36] and Wietzel,[37] -2.21 and -2.33 kcal. mole^{-1}, respectively, is obtained.

(34) F. D. Rossini, Chapter 14 in ref. 19.
(35) E. G. King, *J. Am. Chem. Soc.*, **73**, 656 (1951).
(36) O. Mullert, *Z. anorg. Chem.*, **75**, 198 (1912).
(37) V. R. Wietzel, *ibid.*, **116**, 71 (1921).

We find the heat of formation of gaseous silicon tetrafluoride to be more negative by about 12 kcal. mole^{-1} than the most recent estimate[6] based on the heats of formation of SiO_2 and HF(g), and the heats of solution of HF(g) and SiF_4(g). Most (about 7.8 kcal. mole^{-1}) of this difference is due to the use of Humphrey's value for the heat of formation of SiO_2. The remainder may be due to other incorrect thermochemical data. For example, the true heat of formation of ideal hydrogen fluoride gas may lie closer to the value derived from spectroscopy,[38] -65.1, then to the generally used calorimetric value,[22] -64.2 kcal. mole^{-1}. This question will be discussed elsewhere.

Appendix A

The various lines of reasoning used by Chipman[9] to deduce the existence of a discrepancy in the Gibbs free energy of formation of silica may be re-examined in the light of the present work. For the sake of completeness we have also examined a number of equilibria not considered by Chipman.

I. Two equilibria involving silicon dissolved in liquid iron have been studied.

(a) Matoba, Gunji, and Kuwana[39] have measured the equilibrium expressed by eq. 1A

$$SiO_2(c) + 2H_2(g) = Si(\text{in Fe, l}) + 2H_2O(g) \quad (1A)$$

at low concentrations of dissolved silicon. Combination of their results with the data of Chipman, *et al.*[9,40] on the activity of silicon dissolved in liquid iron gives ΔG_f^0 (SiO_2, c) $= -138.5 \pm 2$ kcal. mole^{-1} at 1600°. Our value for the Gibbs energy of formation of silica at 25°, -204.77 kcal. mole^{-1}, when combined with the tabulated free energy function,[41] gives ΔG_f^0 (SiO_2, c) $= -137.7 \pm 0.7$ kcal. mole^{-1} at 1600°, in good agreement.

(b) Fulton and Chipman[42] have measured the concentration of silicon in liquid iron in the equilibrium expressed by eq. 2A.

(38) J. W. C. Johns and R. F. Barrow, *Proc. Roy. Soc.* (London), **A251**, 504 (1959).
(39) S. Matoba, K. Gunji, and T. Kuwana, *Tetsu to Hagane*, **45**, 229 (1959); *Stahl Eisen*, **80**, 299 (1960).
(40) J. Chipman, J. C. Fulton, N. Gokcen, and C. R. Caskey, *Acta Met.*, **2**, 439 (1954).
(41) JANAF Thermochemical Tables, D. R. Stull, Director, The Thermal Laboratory, Dow Chemical Co., Midland, Mich., 1962.
(42) J. C. Fulton and J. Chipman, *Trans. A.I.M.E.*, **200**, 1136 (1954).

$SiO_2(SiO_2$–CaO slag) + 2C(graphite) =
Si(in Fe, l) + 2CO(g, 1 atm.) (2A)

The combination of this datum, the activity coefficient of silicon in liquid iron,[40] our value of the Gibbs energy of formation of silica, and its free energy function[41] yields $a_{SiO_2} = 0.32$ at 1600° in the slag at a mole fraction $N_{SiO_2} = 0.45$. Yang, McCabe, and Miller[43] have determined the activity of silica in slags by the effusion method. Interpolation of their results to $N_{SiO_2} = 0.45$ and 1600° gives $a_{SiO_2} = 0.28$. The difference in activities is equivalent to 0.5 kcal. mole^{-1} and is well within experimental errors.

II. A number of pertinent studied involve silicon monoxide.

(a) Consider the reactions 3A–5A

$$SiO_2 + H_2(g) = SiO(g) + H_2O(g);\ \Delta H_3 \quad (3A)$$

$$SiO_2 + Si = 2SiO(g);\ \Delta H_4 \quad (4A)$$

$$H_2(g) + {}^1/_2O_2(g) = H_2O(g);\ \Delta H_5 \quad (5A)$$

whence $\Delta H_f(SiO_2) = -2\Delta H_3 + \Delta H_4 + 2\Delta H_5$. Equilibrium pressures for reaction 3A have been reported by Grube and Speidel,[44] Ramstad and Richardson,[45] and Tombs and Welch.[46] If one rejects the results of Tombs and Welch (for reasons discussed in ref. 45), and for the remaining individual results calculates ΔH_{298} (from the third law) one obtains over the range 1200–1600° an average value of $\Delta H_{298°K.}$ (3A) = +135.2 ± 2.4. The equilibrium pressures of reaction 4A have been reported six times. We have accepted the results of Ramstad and Richardson,[45] Tombs and Welch,[46] and Schafer and Hornle[47] because of their reasonable concordance with each other and with the second-law slopes, and have rejected the results of Gel'd and Kochnev,[48] Porter, *et al.*,[49] and Gunther.[50] Over the range 1050–1650° the averaged third law result is $\Delta H_{298°K.}$ (4A) = +168.8 ± 1.0. For reaction 5A the well-established value[22] is $\Delta H_{290°K.}$ (5A) = −57.798. These data lead to the value $\Delta H_f^0{}_{298°K.}(SiO_2, c)$ = −217.2 ± 2.6 kcal. mole^{-1}, in good agreement with our value.

(b) Cochran and Foster[51] have measured the equilibrium pressures over mixtures of gallium with either vitreous silica or magnesia by the Knudsen effusion method. Their results may be summarized by eq. 6A and 7A.

$$2Ga(l) + SiO_2(gl) = SiO(g) + Ga_2O(g);$$
$$\Delta H_{298}^0 = +170.8 \pm 0.7 \quad (6A)$$

$$2Ga(l) + MgO(c) = Mg(g) + Ga_2O(g);$$
$$\Delta H_{298}^0 = +159.3 \pm 0.7 \quad (7A)$$

Foster and Cochran have shown that $\Delta H_f(SiO_2, \alpha$-quartz) may be calculated by combination of their results with data for the transition of silica glass to quartz, reaction 4A, the formation of MgO(c) and the sublimation of magnesium to monatomic vapor. Our evaluation of two of these quantities differs somewhat from theirs. With the use of the experimental value,[36,37] −2.27 ± 0.1 kcal. mole^{-1}, for the heat of transition of silica glass to α-quartz, and the use of +168.8 ± 1.0 kcal. for the mean heat of reaction 4A, we obtain $\Delta H_f^0{}_{298}$ (SiO_2, α-quartz) = −217.0 ± 2.2, in good agreement with our value.

(c) Yang, McCabe, and Miller[43] have studied the dissociation of silica according to

$$2SiO_2 = 2SiO(g) + O_2(g) \quad (8A)$$

Their result at 1600° $\Delta G(8A)$ = +159.3 ± 2, when combined with $\Delta G(4A)$ = +21.0 ± 2[46] leads to $\Delta G_f^0(SiO_2, c)$ = −138.3 ± 2.8 kcal. mole^{-1} at 1600°, again in good agreement with the result (see Ia) based on our value.

(d) Acceptance of the value of $\Delta H_f^0(SiO_2)$ suggested by the present work yields for $\Delta H_f^0{}_{298°K.}$ (SiO, g) the values −25.7 ± 2.5, −24.45 ± 0.5, and −22.0 ± 1.0 kcal. mole^{-1} from reactions 3A, 4A, and 8A, respectively. The weighted average is −24.04 ± 0.45 kcal. mole^{-1}; a widely quoted value (based on the older value for silica) is −21.4.

III. The additional evidence discussed by Chipman[9] depends upon the thermodynamic properties of silicon carbide. A review of the situation, however, reveals that various measurements of the heat or free energy of formation of this substance are in serious disagreement.

Consider, for example, the standard heat of formation of silicon carbide at 25°, as calculated from the following equilibria by the third law. Measurements have been made of the partial pressure of monatomic silicon over a mixture of graphite and silicon carbide (which is known to be stoichiometric[52]), and of the pressure of silicon over silicon saturated with carbon (the solubility of carbon being negligible[53]). Separate sets of measurements have been made by mass spectrometry,[54] effusion,[55,56] transportation,[56] and resonance absorption.[57] The results reported are $\Delta H_f^0{}_{298}$ (SiC, hex.) = −18 ± 2,[54] −17.6 ± 2,[55] −12.4 ± 1.0,[56] and −12.8 ± 0.5[57] kcal. mole^{-1}. Of these four results the first two were corrected for the presence of species other than monatomic silicon in the vapor, whereas the latter two were uncorrected. From measurements of the activities of silicon in liquid lead[58] in equilibrium with either silicon carbide or silicon we calculate $\Delta H_f^0{}_{298}$ (SiC, hex.) = −13.6 ± 1. From similar studies in liquid iron and liquid silver $\Delta H_f^0{}_{298}$ (SiC, cub.) = −13.5 ± 1.5[41] and −15.8 ± 0.9,[59] respectively. Consideration of the Si–C phase diagram,[53] and in particular, of the equilibrium between SiC, C, and liquid Si saturated with C at about 2800°, appears to require $\Delta H_f^0{}_{298}$ (SiC, hex.)

(43) L. Yang, C. L. McCabe, and R. Miller, "Physical Chemistry of Steelmaking," John Wiley and Sons, Inc., New York, N. Y., 1958, p. 63.
(44) G. Grube and H. Speidel, *Z. Elektrochem.*, **53**, 339 (1949).
(45) H. F. Ramstad and F. D. Richardson, *Trans. A.I.M.E.*, **221**, 1021 (1961).
(46) N. C. Tombs and A. J. E. Welch, *J. Iron Steel Inst.*, **172**, 69 (1952).
(47) H. Schafer and R. Hornle, *Z. anorg. allgem. Chem.*, **245**, 1 (1940).
(48) P. V. Gel'd and M. K. Kochnev, *Zhur. Priklad. Khim.*, **21**, 1249 (1948).
(49) R. F. Porter, W. A. Chupka, and M. G. Inghram, *J. Chem. Phys.*, **23**, 216 (1955).
(50) K. G. Gunther, *Glastech. Ber.*, **31**, 9 (1958).
(51) C. N. Cochran and L. M. Foster, *J. Phys. Chem.*, **66**, 380 (1962).
(52) J. A. Lely, *Ber. deut. keram. Ges.*, **32**, 299 (1955).
(53) R. I. Scace and G. A. Slack, *J. Chem. Phys.*, **30**, 1551 (1959).
(54) J. Drowart, G. De Maria, and M. G. Inghram, *J. Chem. Phys.*, **29**, 2015 (1958); J. Drowart and G. De Maria, "Silicon Carbide," Ed., O'Connor and Smiltens, Pergamon Press, New York, N. Y., 1959, p. 16. *Cf.* ref. 50.
(55) S. G. Davis, D. F. Anthrop, and A. W. Searcy, *J. Chem. Phys.*, **34**, 659 (1961).
(56) P. Grieveson and C. B. Alcock, "Special Ceramics," Ed., P. Popper, Heywood and Co., Ltd., London, 1960, p. 183.
(57) G. L. Vidale, General Electric Space Sciences Laboratory TIS Report No. R60-SD-333, Philadelphia, Pennsylvania, 1960.
(58) D. H. Kirkwood and J. Chipman, *J. Phys. Chem.*, **65**, 1082 (1961).
(59) J. d'Entremont and J. Chipman, *ibid.*, **67**, 499 (1963).

more negative than -15.5.[54,60] Note that the lack of agreement among these studies is independent of the heat of formation of SiO_2.

Consider also the two studies which appear to involve silica in the determination of the heat of formation of silicon carbide. From the combustion measurements of Humphrey[28] for the reaction

$$SiC(cub.) + 2O_2 = SiO_2 + CO_2 \quad (9A)$$

we obtain $\Delta H_f^0{}_{298}$ (SiC, cub.) $- \Delta H_f^0{}_{298}$ (SiO_2, α-quartz) $= +196.86 \pm 0.88$ kcal. From the equilibrium pressure measurements of Taylor[61] for the reaction

$$SiO_2 + 3C(graphite) = SiC(cub.) + 2CO(g) \quad (10A)$$

we obtain by the third law (after a minor correction for the presence of SiO in the gas) $\Delta H_f^0{}_{298}$ (SiC, cub.) $- \Delta H_f^0{}_{298}$ (SiO_2, α-quartz) $= +201.9 \pm 1.1$ kcal. It is obvious that these values of the quantity, $\Delta H_f(SiC) - \Delta H_f(SiO_2)$, which is independent of the data for silica, do not agree with each other within their estimated precisions. (For comparison with the results given in the previous paragraph the studies of Humphrey[28] and of Taylor[61] give, with our value of $\Delta H_f^0{}_{298}$ (SiO_2, α-quartz) $\Delta H_f^0{}_{298}$ (SiC, cub.) $= -20.9 \pm 0.9$ and -15.85 ± 1.1 kcal. mole^{-1}, respectively).

From the foregoing discussion it is clear that there exist unknown sources of error in some of the measurements leading to the above values of the heat of formation of silicon carbide. A critical redetermination of the heat of formation of silicon carbide by calorimetry should shed light on these discrepancies.

IV. In conclusion, we find that the value for the heat of formation of α-quartz presented in this work is in good agreement with all the high temperature equilibrium measurements on substances which appear to be reasonably well characterized. Thus, the discrepancies discussed by Chipman (except those involving SiC) appear to be substantially resolved.

(60) J. Smiltens, *J. Phys. Chem.*, **64**, 368 (1960).

(61) J. D. Baird and J. Taylor, *Trans. Faraday Soc.*, **54**, 526 (1958); D. A. R. Kay and J. Taylor, *ibid.*, **56**, 1372 (1960).

HYDROLYSIS OF URANIUM(VI): ABSORPTION SPECTRA OF CHLORIDE AND PERCHLORATE SOLUTIONS[1]

BY RICHARD M. RUSH AND JAMES S. JOHNSON

Chemistry Division, Oak Ridge National Laboratory, Oak Ridge, Tennessee

Received September 21, 1962

Optical absorptions of hydrolyzed U(VI) solutions in 1 *M* chloride have been measured for U(VI) concentrations in the range 0.001–0.1 *M* and for values of **n** (average moles of hydroxide bound per mole of U(VI)) up to 1.3. A few measurements have been carried out for 1 *M* perchlorate solutions with **n** up to 1.0. The molar absorptivity *E* increases sharply with **n**; chloride complexing of the unhydrolyzed species and at least one hydrolyzed species is indicated by higher values of *E* in chloride solutions than in perchlorate solutions with the same **n**. The chloride measurements are correlated with a hydrolysis scheme previously derived from ultracentrifugation and acidity measurements. These results are combined with acidity measurements and spectra in perchlorate media to give values of the formation quotients for hydrolytic species in perchlorate media. The results are consistent with the earlier indication that the species $(UO_2)_3(OH)_4^{+2}$, which appears to be present in substantial amounts in 1 *M* chloride, is of little, if any, importance in 1 *M* perchlorate.

In a recent publication,[2] we presented a hydrolysis scheme for U(VI) in one molar chloride, which was consistent with acidity measurements and with ultracentrifugation estimates of molecular weights (25°). The major species proposed were $(UO_2)_2(OH)_2^{+2}$, $(UO_2)_3(OH)_4^{+2}$, and $(UO_2)_3(OH)_5^{+}$. Formation quotients were given for these species. A scheme, similar except that it did not include $(UO_2)_3(OH)_4^{+2}$, based on literature acidity measurements[3] carried out at 20°, was also presented for one molar perchlorate solutions. Although the species as written do not indicate complexing of other ligands present in the solution, from the fact that $(UO_2)_3(OH)_4^{+2}$ appeared to be of importance only in chloride solution, presumably this species includes complexed chlorides and it seemed possible that other species also complexed anions.

We have recently carried out optical absorption measurements of hydrolyzed uranyl solutions in chloride and perchlorate media. In this paper we attempt to correlate the spectra of the chloride solutions with the hydrolysis scheme earlier reported. From the species absorptivities thus obtained, plus the spectra and acidity measurements in the perchlorate media, we have estimated formation quotients for the hydrolyzed species in 1 *M* $NaClO_4$.

Experimental and Computational Procedure

Spectra of solutions having the following hydroxyl numbers **n** (average number of hydroxyls bound per uranyl) were measured: 1 *M* in total chloride (with Na^+): 0.1 *M* U(VI)—**n** = 0.38, 0.67, 0.90; 0.01 *M* U(VI)—**n** = 0, 0.12, 0.21, 0.30, 0.42, 0.51, 0.61, 0.71, 0.79, 0.89, 0.98, 1.07, 1.21, 1.30; 0.001 *M* U(VI)—**n** = 0.45, 0.73, 0.99, 1.21. In 1 *M* total perchlorate (with Na^+): 0.1 *M* U(VI)—**n** = 0.42; 0.01 *M* U(VI)—**n** = 0, 0.43, 0.62, 0.81; 0.001 *M* U(VI)—**n** = 0.45, 0.64, 0.82, 1.00.

Interpretations are based on measurements in the range 3650–5000 Å., carried out on a Cary Model 14 PM spectrophotometer; cells were of 0.5, 1, 2, 5, or 10 cm. path length. This instrument gives a recording of the absorbance of the solution, $A = \log (I_0/I)$, I being intensity of light transmitted by the solution and I_0, of that transmitted by a reference solution (1 *M* NaCl or 1 *M* $NaClO_4$). From these values, the molar absorptivities $E = A/cb$ are obtained, where c is the total stoichiometric U(VI) concentration (moles/l.), and b is the path length in cm. The molar absorptivity is related to the species absorptivities, $\epsilon_{i,j}$, by the equation

(1) This document is based upon work performed for the United States Atomic Energy Commission at the Oak Ridge National Laboratory, operated by Union Carbide Corporation.

(2) R. M. Rush, J. S. Johnson, and K. A. Kraus, *Inorg. Chem.*, **1**, 378 (1962).

(3) S. Ahrland, *Acta Chem. Scand.*, **3**, 374 (1949).

$$E = \frac{1}{c}\sum_{i,j} c_{i,j}\epsilon_{i,j} = \Sigma F_{i,j}\epsilon'_{i,j} \qquad (1)$$

where $c_{i,j}$ is the concentration of the species $(UO_2)_i(OH)_j^{+(2i-j)}$ (complexing with other ligands being ignored), $F_{i,j} = ic_{i,j}/c$ is the fraction of total uranium found in the (i,j) species, and $\epsilon'_{i,j} = \epsilon_{i,j}/i$.

In the computational procedure, the species fractions $F_{i,j}$ are computed from the formation quotients of the scheme being tested, for the hydroxyl number and total U(VI) concentration of the solution being considered. The formation quotient $k_{i,j}$ is defined as

$$k_{i,j} = \frac{k^0_{i,j}}{G_{i,j}} = \frac{[(UO_2)_i(OH)_j^{+(2i-j)}][H^+]^j}{[UO_2^{+2}]^i} \qquad (2)$$

($k^0_{i,j}$ being the formation constant, $G_{i,j}$ the appropriate activity coefficient ratio, and brackets indicating concentration in moles/l.). For a given solution the hydrogen ion concentration c_H and free uranyl concentration $c_{1,0}$, are obtained from the hydroxyl number n and the formation quotients $k_{i,j}$ by solving the following equations by the Newton–Raphson method

$$F(c_H, c_{1,0}) = \Sigma j c_{i,j} - nc = \Sigma j \frac{k_{i,j}c^i_{1,0}}{c_H{}^j} - nc = 0 \qquad (3)$$

$$G(c_H, c_{1,0}) = \Sigma i c_{i,j} - c = \Sigma i \frac{k_{i,j}c^i_{1,0}}{c_H{}^j} - c = 0 \qquad (4)$$

The species concentrations $c_{i,j}$ and fractions $F_{i,j}$ are then calculated from $c_{1,0}$, c_H, and the formation quotients. With these fractions for each solution in a given medium (chloride or perchlorate), values of $\epsilon'_{i,j}$ at a given wave length for each hydrolyzed species are calculated to give the minimum sum of squares deviation[4] of the values of E for all of the solutions. The values of $\epsilon_{1,0}$ are obtained from the spectra of an unhydrolyzed solution. The program also computes the standard error in each $\epsilon'_{i,j}$ and the deviations between observed E and values computed by equation 1. Computations were carried out on an IBM 7090 computer.

The criterion for correlation is the degree of success with which the observed spectra of individual solutions can be reproduced from the values of $\epsilon'_{i,j}$ obtained in the manner described.

Equilibrium quotients for the same conditions as the measurements on perchlorate solutions (25°, 1 *M* $NaClO_4$) were not available. Estimates of these values were made in a manner to be described in detail below with the help of separate measurements of the solution acidities. The correlation of the absorption spectra was then tested as with the chloride solutions. Acidity measurements were carried out by the technique described previously[2] with the cell

glass electrode$\|(UO_2(OH)_n^{+(2-n)}$, H^+, $Na^+)ClO_4^-$ (1 *M*)$|$HCl (0.01 *M*), $HClO_4$ (0.01 *M*), $NaClO_4$ (0.98*M*), AgCl(s); Ag(s)

Results and Discussion

1. Results—The general features of the absorption spectra can be seen in representative curves given in Fig. 1[5] (measurements were made to 5500 Å. at which point the absorption was negligible indicating the absence of serious turbidity). The values of E increase sharply with hydroxyl number, and the position of maximum absorption shifts to longer wave length in both chloride and perchlorate media. Similar results have been reported in perchlorate by Sutton.[6] Chloride complexing of the unhydrolyzed species is indicated by the difference in spectra at n = 0, and of at least one hydrolyzed species by the greater absorption in 1 *M* NaCl than 1 *M* $NaClO_4$ at a given n. Since free chloride is nearly constant in all experiments, the ratios of species of a given (i,j) which are complexed to different extents by chloride will be essentially constant and the values of $\epsilon'_{i,j}$ will be a composite for species $(UO_2)_i(OH)_jCl_l^{+(2i-j-l)}$.

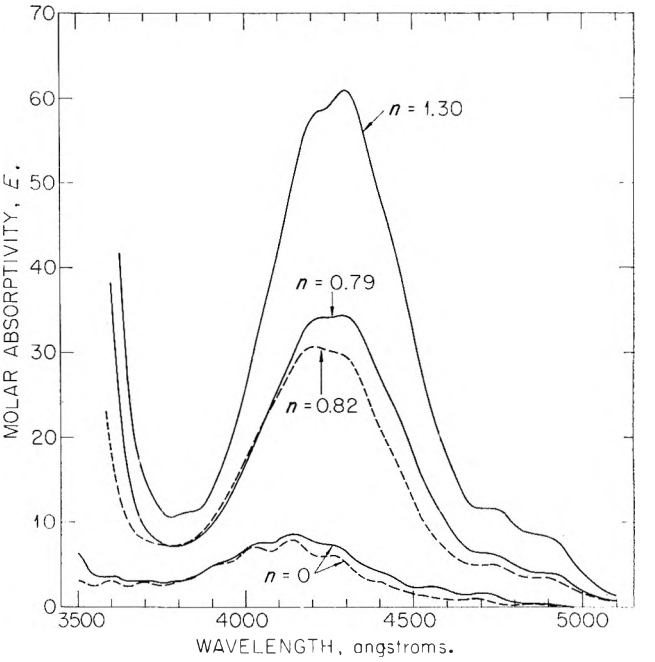

Fig. 1.—Absorption spectra of 0.010 *M* U(VI) solutions in 1 *M* total chloride (———) and 1 *M* total perchlorate (– – – –) at 25°.

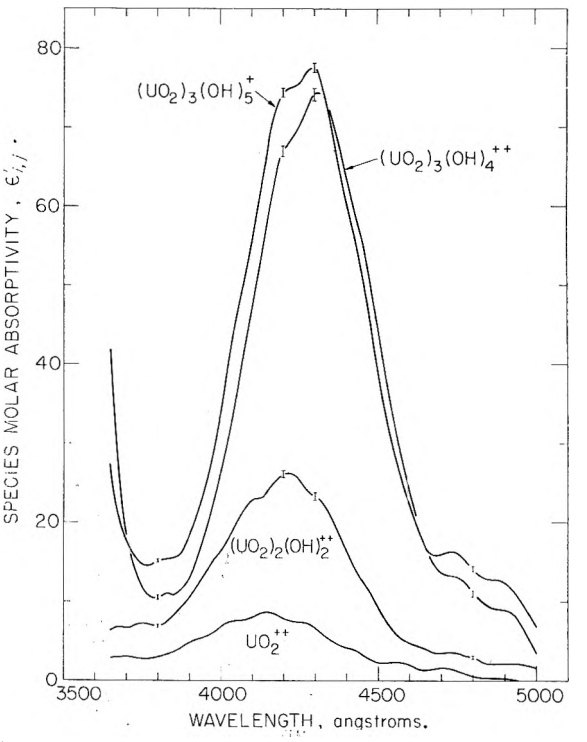

Fig. 2.—Species molar absorptivities for U(VI) species in 1 *M* total chloride: equilibrium quotients used are $k_{2,2} = 6.7 \times 10^{-7}$, $k_{3,4} = 4.7 \times 10^{-13}$, and $k_{3,5} = 1.0 \times 10^{-17}$; vertical lines indicate one standard error on each side of the value.

2. Uranyl Spectra in 1 *M* Chloride Solutions.—In the interpretation[2] of our acidity measurements of U(VI) hydrolysis, the simplest scheme giving an adequate fit involved the hydrolyzed species $(UO_2)_2(OH)_2^{+2}$,

(4) We are indebted to M. H. Lietzke for use of his Fortran generalized least squares subroutine; see U. S. Atomic Energy Commission, ORNL-3259 (1962).

(5) Those interested in a more detailed presentation of the primary data are referred to R. M. Rush, J. S. Johnson, and K. A. Kraus, U. S. Atomic Energy Commission, ORNL-3278 (1963).

(6) J. Sutton, *J. Chem. Soc.*, S275 (1949); see also National Research Council of Canada, Atomic Energy Project, Division of Research, CRC 325 (N. R. C. No. 1612) (1947).

$(UO_2)_3(OH)_4^{+2}$, and $(UO_2)_3(OH)_5^{+}$; these species (as well as the unhydrolyzed uranyl) may further complex chloride ions. An equally satisfactory fit was obtained if the species UO_2OH^+ was included. Although there is some evidence from other studies[7] for this species, especially at higher temperatures,[8] it does not seem to us conclusive at the temperature and concentration range of our studies. In any case, the formation quotients we obtained indicated that, if present, it did not constitute a major fraction of total U(VI) under the conditions of the present study, and we have therefore neglected it for the most part in this discussion.

The formation concentration quotients which we obtained[2] for the scheme without the (1,1) species are as follows: $k_{2,2} = 6.7 \times 10^{-7}$, $k_{3,4} = 4.7 \times 10^{-13}$, and $k_{3,5} = 1.0 \times 10^{-17}$. If the (1,1) species is included, the other quotients are modified slightly.

The values of the species absorptivities, obtained by computing the concentration of the individual species with the above scheme, and finding the values of $\epsilon'_{i,j}$ which give the best fit to the observed spectra for all solutions (see Experimental section) are given in Fig. 2. Vertical lines given at representative wave lengths indicate one standard error in $\epsilon'_{i,j}$ on each side of the "best" value.

Correlation is illustrated in Fig. 3 as deviations of observed values of E from those computed for individual solutions. Most of the deviations represent less than one chart division (0.01 at A) on the recorded spectrum. In the most notable exception, 0.1 M U(VI), n = 0.899, A was very high (up to 2), and the computed values are within 2% in A where the deviation is greatest.

Inclusion of the (1,1) species modified the values of $\epsilon'_{i,j}$ for the other hydrolyzed species shown in Fig. 2 slightly; the over-all fit corresponding to Fig. 3 was about the same.

3. Uranyl Spectra in 1 *M* Perchlorate Solutions.—The equilibrium quotients[2] derived on the basis of Ahrland's acidity measurements in perchlorate media[3] are not strictly applicable to the interpretation of the spectra reported here, since Ahrland's measurements were at 20°. Our interpretation of his results had indicated that the (3,4) species is not present in important amounts in perchlorate solutions. From this, it is reasonable to suppose that this species includes complexed chloride ions. If it is further assumed that the (2,2) and (3,5) species do not complex chloride, and that the values of $\epsilon'_{2,2}$ and $\epsilon'_{3,5}$ are the same in chloride and perchlorate media, the following expressions are obtained which may be solved for the fractions $F_{i,j}$ of the various species ($\epsilon_{1,0}$ is known from measurements on an unhydrolyzed solution)

$$\begin{aligned} \mathrm{n} &= F_{2,2} + (5/3)F_{3,5} \\ E &= F_{1,0}\epsilon_{1,0} + F_{2,2}\epsilon'_{2,2} + F_{3,5}\epsilon'_{3,5} \\ 1 &= F_{1,0} + F_{2,2} + F_{3,5} \end{aligned} \qquad (5)$$

Further, since

$$k_{2,2} = \frac{F_{2,2}[\mathrm{H}^+]^2}{2F^2_{1,0}c}$$

(7) See, *e.g.*, J. Rydberg, *Arkiv Kemi*, **8**, 113 (1956).

(8) (a) C. F. Baes, Jr., and N. J. Meyers, *Inorg. Chem.*, **1**, 780 (1962); see also (b) K. A. Kraus, "Hydrolytic Behavior of the Heavy Elements," Proceedings of the International Conference on the Peaceful Uses of Atomic Energy, Vol. 7, p. 245, Session 10B.1, P/731, United Nations (1956).

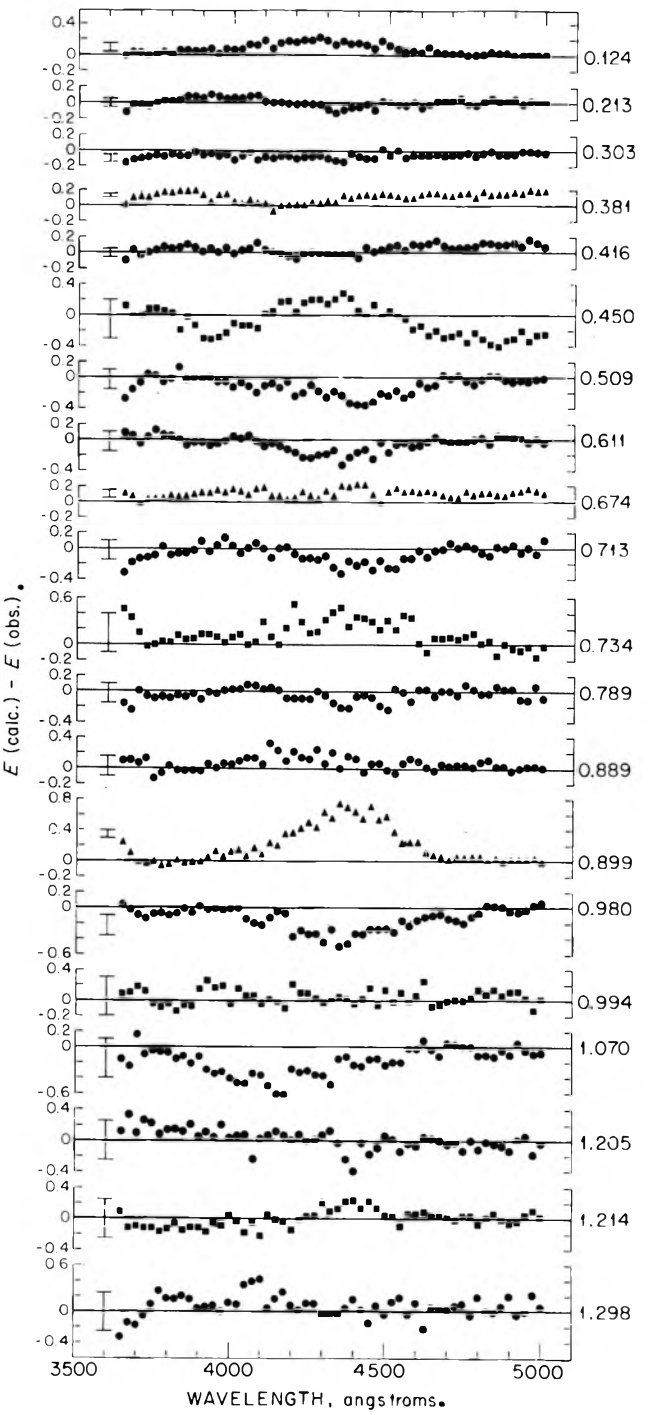

Fig. 3.—Deviations of observed molar absorptivities for U(VI) solutions in 1 M total chloride from values based on $k_{2,2} = 6.7 \times 10^{-7}$, $k_{3,4} = 4.7 \times 10^{-13}$, and $k_{3,5} = 1.0 \times 10^{-17}$. Numbers to the right of each plot are the hydroxyl numbers; vertical lines at the left of each plot represent 0.005 in A, symbols represent M U(VI) as: ▲, 0.1; ●, 0.01; ■, 0.001.

$$k_{3,5} = \frac{F_{3,5}[\mathrm{H}^+]^5}{3F^3_{1,0}c^2} \qquad (6)$$

from the optical absorption of a single solution at one wave length, values of $k_{i,j}$ may in principle be obtained, if the acidity of the solution is also measured. In practice, of course, the solutions must be selected to have an appreciable amount of all species present.

We have carried out such measurements with eight solutions, and the quotients evaluated at 4300 Å. are listed in Table I. Agreement between the values obtained from the individual solutions is about as good as could be expected. The acidity measurements on the

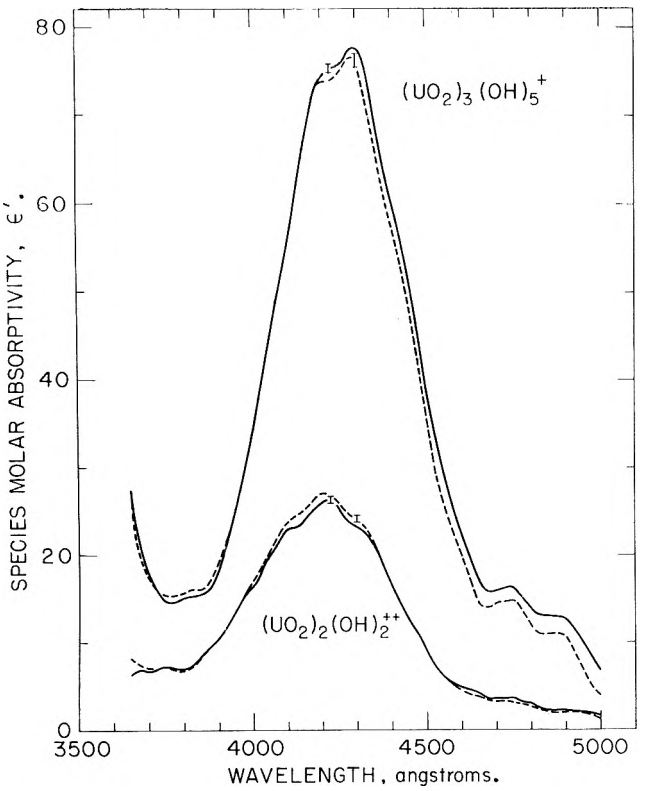

Fig. 4.—Comparison of species molar absorptivities for U(VI) in 1 M total chloride (———) and 1 M total perchlorate (– – – –). Equilibrium quotients used: $k_{2,2} = 6.7 \times 10^{-7}$, $k_{3,4} = 4.7 \times 10^{-13}$, and $k_{3,5} = 1.0 \times 10^{-17}$ for chloride; $k_{2,2} = 1.15 \times 10^{-6}$ and $k_{3,5} = 3.9 \times 10^{-17}$ for perchlorate. Vertical lines on the curves indicate one standard error on each side of the value.

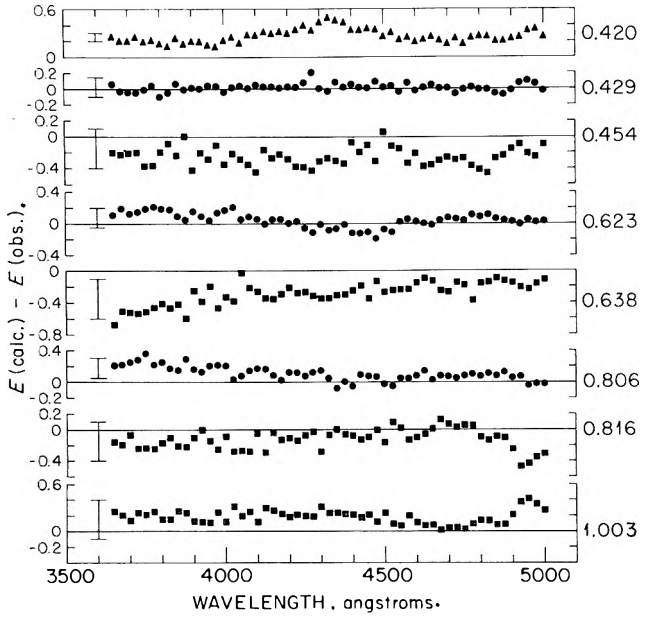

Fig. 5.—Deviations of observed molar absorptivities for U(VI) solutions in 1 M total perchlorate from values based on $k_{2,2} = 1.15 \times 10^{-6}$ and $k_{3,5} = 3.9 \times 10^{-17}$. Numbers to the right of each plot are hydroxyl numbers. Vertical lines to the left of each plot represent 0.005 in A. Symbols represent M U(VI) as: ▲, 0.1; ●, 0.01; ■, 0.001.

eight solutions were also analyzed by the least square procedure described earlier[2] and the results are included in Table I. This agreement is satisfactory in view of the small number of points available for interpretation by acidity data alone and the scatter of individual values of $k_{i,j}$ obtained from analysis of absorption and acidity data.

TABLE I

EQUILIBRIUM QUOTIENTS OBTAINED FROM SPECTRA AND ACIDITY MEASUREMENTS IN 1 M TOTAL PERCHLORATE

c	n	−log [H⁺]	E (4300 Å.)	$k_{2,2}$ × 10⁶	$k_{3,5}$ × 10¹⁷
0.1000	0.420	3.322	13.26	1.33	4.07
.00998	.429	3.833	14.58	1.12	4.06
.01007	.623	3.996	20.95	1.13	4.05
.01005	.806	4.137	28.46	1.13	3.87
.000996	.454	4.299	17.17	1.06	4.28
.001004	.638	4.434	24.00	1.05	3.54
.001002	.816	4.548	31.64	1.05	3.35
.001011	1.003	4.652	39.76	1.34	4.16
			Av.	1.15	3.92
Values obtained from least squares fit of acidity measurements alone (σ = 0.0107 in n)				1.22	3.69

NOTE: At 4300 Å. $\epsilon_{1,0} = 5.233$ from unhydrolyzed perchlorate solution and $\epsilon'_{2,2} = 23.34$, $\epsilon'_{3,5} = 77.59$ from measurements in chloride solution (Fig. 2).

The assumptions made in interpreting the absorption data were tested by correlating the spectra for all wave lengths in the same manner as with the chloride solutions, with the constants $k_{2,2} = 1.15 \times 10^{-6}$ and $k_{3,5} = 3.9 \times 10^{-17}$. Comparison of the values of $\epsilon'_{2,2}$ and $\epsilon'_{3,5}$ obtained from chloride and perchlorate for all wave lengths is shown in Fig. 4, and the deviations between experimental and computed values of E for perchlorate solutions are shown in Fig. 5. The agreement is consistent with the assumption that the (2,2) and (3,5) species do not complex chloride.

The values of $k_{2,2}$ and of $k_{3,5}$ are somewhat smaller in chloride than in perchlorate. This direction is expected if UO_2^{+2} is complexed by chloride, in agreement with the conclusions of many people.[9] More quantitatively, if the only important complex of the unhydrolyzed species is UO_2Cl^+, if the values of $G_{i,j}$ are assumed to be the same in the two media, and if no chloride complexing of the (2,2) or the (3,5) occurs, the ratio of the apparent quotients for the two media should be

$$\frac{(k_{i,j})\text{chloride}}{(k_{i,j})\text{perchlorate}} = \frac{1}{(1 + k_{1,0,1}[Cl^-])^i} \qquad (7)$$

where $k_{1,0,1} = [UO_2Cl^+]/[UO_2^{+2}][Cl^-]$.

An estimate of $k_{1,0,1}$ can therefore be made from comparison of the apparent values of $k_{i,j}$ in chloride and perchlorate media. From such a comparison of the quotients for the (2,2) species, $k_{1,0,1} = 0.35$ is obtained; from the (3,5) species, $k_{1,0,1} = 0.52$. These may be compared with the value of Nelson and Kraus,[10] corrected to $\mu = 1$, $k_{1,0,1} = 0.50$. With the assumptions made, the agreement between these values is good.

4. Discussion.—The optical absorption of hydrolyzed U(VI) chloride solutions seems to be consistent with the species postulated, and the formation quotients evaluated, to explain acidity and ultracentrifugation results.[2] Analysis of the chloride and perchlorate spectra support the conclusion based on acidity data that the (3,4) species, which is important in chloride, is not very important, if present at all, in perchlorate. The values of the equilibrium quotients derived for perchlorate solutions are reasonable. They

(9) J. Bjerrum, G. Schwarzenbach, and L. G. Sillén, "Stability Constants," Part II, The Chemical Society, London, 1958.

(10) F. Nelson and K. A. Kraus, *J. Am. Chem. Soc.*, **73**, 2157 (1951).

are somewhat greater than those estimated from 20° acidity data; however, this is the direction expected, and of the approximate magnitude predicted, from studies of the temperature coefficient of U(VI) hydrolysis in nitrate medium.[8a]

The question of the importance of other species which may be present in minor amounts is no more resolved by the present results than by the earlier study. For example, it was apparent that about as satisfactory an interpretation could be obtained with a scheme including UO_2OH^+, although there would be considerable uncertainty in the values of $\epsilon_{1,1}$. Similarly, our conclusions for the perchlorate solutions agree in general with those of Sutton,[6] though he includes a small contribution of the (3,4) species.

The most important point of disagreement with the interpretation of acidity measurements on a core-link model[11] seems to be resolved, since the Stockholm group now postulate an important contribution by the (3,5) species, which is not of the core-link type.[12] They still postulate the presence of several higher core-link species, for which we do not find any evidence in our results, but since the constants quoted for these species are rather low, the remaining disagreement is perhaps more in a conceptual model of hydrolysis rather than in a practical description of U(VI) solution chemistry. From a recent publication,[13] it appears that even this disagreement may no longer exist.

Acknowledgment.—We wish to express indebtedness to Kurt A. Kraus for many helpful and stimulating discussions and to Neva Harrison for technical assistance.

(11) S. Ahrland, S. Hietenan, and L. G. Sillén, *Acta Chem. Scand.*, **8**, 1907 (1954).
(12) L. G. Sillén, private communication.
(13) L. G. Sillén, *Acta Chem. Scand.*, **16**, 1051 (1962).

IONIZATION BY ALPHA PARTICLES IN BINARY GAS MIXTURES

By T. D. Strickler[1]

Health Physics Division, Oak Ridge National Laboratory,[2] Oak Ridge, Tennessee, and Department of Physics, Berea College, Berea, Kentucky

Received September 21, 1962

The W value (average energy loss per ion pair) for α-particles has been measured in a number of binary gas mixtures of molecular gases as a function of the fractional pressures. The W of the mixture (W_{ij}) can be represented in terms of the W's of the pure constituent gases (W_i, W_j) and the fractional pressures (P_i, P_j) by the relation: $W_{ij} = (W_i - W_j)Z_{ij}'' + W_j$, where $Z_{ij}'' = P_i/(P_i + f_{ij}P_j)$, in which f_{ij} is a constant determined empirically for each pair of gases. These constants very nearly satisfy the relationship $f_{ij} = f_j/f_i = (f_j/f_k)/(f_i/f_k) = f_{kj}/f_{ki}$, where i, j, and k refer to any three gases. Thus, if the following f-values are assigned to the gases in this study (N_2, 1; CO_2, 1.8; H_2, 0.5; O_2, 1.3; CH_4, 1.8; C_2H_4, 3.4; C_2H_6, 3.5; C_3H_6, 4.5; C_3H_8, 4.5; C_4H_8, 6.3) then the constant f_{ij} determined from the ratio of any two of these will serve to predict the W of any mixture of these two gases with an accuracy better than 1%. Slight departures from the W predicted by the above equation have been noted in the case of nitrogen mixtures, indicative of an effect similar to that observed in the noble gases when small amounts of impurities are added.

Introduction

If an α-particle of kinetic energy E_0 is completely stopped in a gas, and in becoming stopped produces N_i ion pairs, then the mean energy lost per ion pair E_0/N_i is commonly called the W of the gas for α-particles. The W of most gases lies in the range 20 to 46 e.v. per ion pair and in many cases is found to be practically independent of the energy of the initial ionizing particle.

The practical importance of W (in the measurement of radiation dose, in the calculation of energies of particles in nuclear reactions, and in the interpretation of radiation-induced chemical reactions) and its theoretical significance have been pointed out in many recent publications on the subject.[3]

In the case of binary mixtures of gases, two distinct phenomena have been observed. One is the marked increase in ionization, and consequent decrease in W, when small amounts of some gases are mixed with the noble gases. This has been studied by Jesse and Sadauskis[4-6] using helium and neon, and by Melton, Hurst, and Bortner[7] using argon. The effect is attributed, in part, to the excitation of the metastable level in the noble gases and the subsequent ionization of the impurity (by interaction with the excited atom), provided the ionization potential of the impurity is lower than that of the metastable state. This has been referred to as the "Jesse effect."[8] The fact that increased ionization occurs in argon, even when the impurity has an ionization potential greater than that of the metastable level, has been demonstrated by Melton, Hurst, and Bortner,[7] but the explanation of the effect is not entirely clear.

On the other hand, in the molecular gases, the W of the mixture is found to lie between the extreme values for the pure gases and to change smoothly from one limit to the other as the composition of the mixture is changed. This has been studied by Huber, *et al.*,[9,10] and by Hurst, *et al.*[11-13] It has been shown that the W of any mixture of two of these gases can be expressed

(1) Dept. of Physics, Berea College, Berea, Kentucky.
(2) Operated by Union Carbide Corporation for the U. S. Atomic Energy Commission.
(3) (a) S. C. Curran and J. M. Valentine, *Rept. Progr. Phys.*, **21**, 1 (1958); (b) W. Binks, *Acta Radiol., Suppl.*, **117**, 85 (1954); (c) R. L. Platzman, NAS-National Research Council Publication 752, 109 (1960).
(4) W. P. Jesse and J. Sadauskis, *Phys. Rev.*, **88**, 417 (1952).
(5) W. P. Jesse and J. Sadauskis, *ibid.*, **90**, 1120 (1953).
(6) W. P. Jesse and J. Saudauskis, *ibid.*, **100**, 1755 (1955).
(7) C. E. Melton, G. S. Hurst, and T. E. Bortner, *ibid.*, **96**, 643 (1954).
(8) R. L. Platzman, "The Physical and Chemical Basis of Mechanisms in Radiation Biology," "Radiation Biology and Medicine," W. D. Claus, Ed., Addison-Wesley Publishing Co., Inc., Reading, Mass., 1958, pp. 15–72.
(9) P. Huber, E. Baldinger, and W. Haeberli, *Helv. Phys. Acta*, **23**, Suppl. 111 (1949).
(10) W. Haeberli, P. Huber, and E. Baldinger, *ibid.*, **26**, 145 (1963).
(11) T. E. Bortner and G. S. Hurst, *Phys. Rev.*, **93**, 1236 (1954).
(12) H. J. Moe, T. E. Bortner, and G. S. Hurst, *J. Phys. Chem.*, **61**, 422 (1957).
(13) G. S. Hurst and T. D. Strickler, NAS-National Research Council Publication 752, 134 (1960).

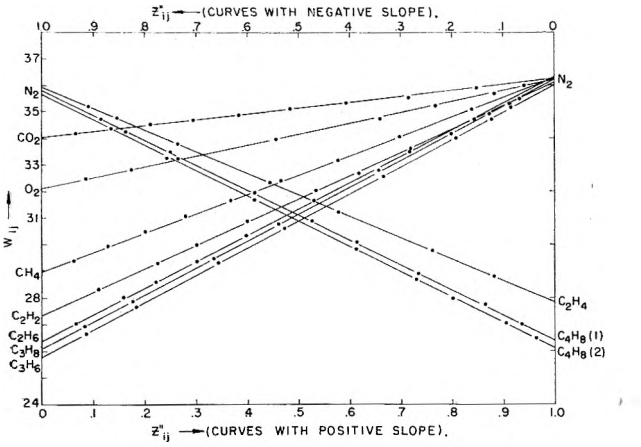

Fig. 1.—Plot of W_{ij} *vs.* Z_{ij}'' for mixtures of N_2 with CO_2, O_2, CH_4, C_2H_2, C_2H_4, C_2H_6, C_3H_6 (cyclopropane), C_3H_8, C_4H_8 (1-butene), and C_4H_8 (2-butene) using Z_{ij}'' calculated from measured constants shown in column 3 of Table II.

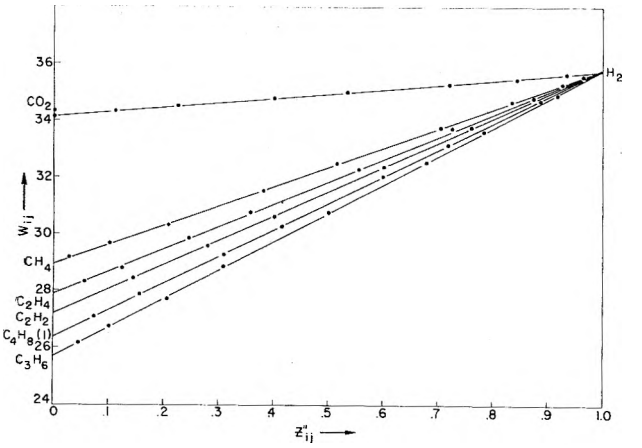

Fig. 2.—Plot of W_{ij} *vs.* Z_{ij}'' for mixtures of H_2 with CO_2, CH_4, C_2H_2, C_2H_4, C_3H_6 (cyclopropane), and C_4H_8 (1-butene) using Z_{ij}'' calculated from measured constants shown in column 3 of Table II.

in terms of the W's of the pure gases, the partial pressures, and an empirical constant characteristic of the two gases.

This report consists mainly of an extension of the work on binary gas mixtures in an attempt to determine more of these empirical constants and to study possible relationships among them.

Experimental Technique and Results with Single Gases

The measurements reported here were made with the same ionization chamber and associated equipment described and used by Bortner and Hurst.[11] This consisted of a large parallel-plate ionization chamber enclosed in a vacuum tank capable of holding gas at pressures up to 2 atm. Alpha particles from the uncollimated source of Pu^{239}, located at the center of the bottom plate, were completely stopped in the chamber and the total ionization was measured by the time required to charge a capacitor to a fixed potential. Electric fields up to 10^3 volts/cm. could be applied to the chamber.

Since W is practically independent of the α-particle energy, a rather strong Pu^{239} source (approximately 3×10^6 c.p.m.) was used in the chamber even though the self-absorption in this source was quite high. A spectral analysis of this source showed that over 90% of the ionization was from α-particles of energy above 3.0 Mev.

No purification techniques were employed and commercially available gases were used throughout. These were reported by the manufacturers to have purities of 99% or more in all cases except acetylene.[14] Since small impurities have no great effect on the particular measurements shown here, it was assumed that these remaining impurities would not greatly affect the results described.

Only relative measurements of W were made by comparing the rate of charge collection in the mixture with that in pure nitrogen.[15] Nitrogen was assumed to have a W of 36.3 e.v./ion pair and all measurements reported are relative to this number.[16]

The gases used in this study are listed in Table I along with the measured W values. These results are comparable to those measured at other laboratories, with the possible exception of hydrogen, for which the value quoted in Table I appears to be somewhat low.[17] The ionization potential also has been included in the table[18] as well as the ratio of W to the ionization potential, since the constancy of this ratio is of some theoretical interest. The constant f shown in column 6 is an empirical constant used in predicting the W of mixtures of the gases listed and is described in the section below.

TABLE I

VALUES OF W AND f FOR VARIOUS MOLECULAR GASES

Formula	Gas	W, e.v./ion pair	Ionization pot., v.	W/Ionization pot.	f
N_2	Nitrogen	36.3[a]	15.6	2.32	1.0[b]
CO_2	Carbon dioxide	34.1	13.85	2.46	1.8
H_2	Hydrogen	35.8	15.43	2.32	0.5
O_2	Oxygen	32.1	12.1	2.65	1.3
CH_4	Methane	28.9	13.12	2.20	1.8
C_2H_2	Acetylene	27.4	11.42	2.40	3.3
C_2H_4	Ethylene	27.85	10.56	2.64	3.4
C_2H_6	Ethane	26.4	11.65	2.27	3.5
C_3H_6	Cyclopropane	25.8	10.23	2.52	4.5
C_3H_6	Propylene	27.0	9.80	2.76	...
C_3H_8	Propane	26.1	11.21	2.33	4.5
C_4H_8	Isobutylene	26.6	9.35	2.85	...
C_4H_8	1-Butene	26.5	9.72	2.73	6.3
C_4H_8	2-Butene	26.1	9.3	2.81	6.3
C_7H_8	Toluene	28[c]	8.7	3.22	15

[a] Assumed value. [b] By definition. [c] Value extrapolated from N_2–C_7H_8 mixture.

Summary of Results Using Mixtures of "Regular Gases"—The f-Ratio

This report is concerned mainly with the determination of the W of mixtures of two gases. It has been shown[11] that the W for a mixture of two "regular gases" (in which the Jesse effect is not pronounced) can be given by

$$\frac{1}{W_{ij}}\left(\frac{1}{W_i} - \frac{1}{W_j}\right) Z_{ij} + \frac{1}{W_j} \qquad (1)$$

where

$$Z_{ij} = \frac{P_i}{P_i + a_{ij}P_j}$$

Here W_{ij} refers to the W of the mixture, W_i and W_j to that of the pure gases, each of which is present with fractional pressures P_i and P_j, and a_{ij} is a constant determined empirically for any particular pair of gases.

(14) Mass spectrographic analysis of a similar tank of acetylene showed: C_2H_2 (97.8%), N_2 + CO (1.4%), acetone (0.5%), H_2O (0.3%).

(15) Mass spectrographic analysis of actual tank of nitrogen showed: N_2 (99.997%), H_2O (0.0008%), and Ar (0.002%).

(16) Measurements by Jesse, substantiated recently by the group at Oak Ridge National Laboratory, indicate that a more accurate value for this W of pure nitrogen for α-particles in this energy range would be 36.6 e.v./ion pair, in which case all measurements reported here would be increased by about 1%.

(17) Mass spectrographic analysis of the tank of hydrogen showed: H_2 (99.3%), H_2O (0.3%), N_2 + CO (0.26%), with traces of CH_4, O_2, HC, Ar, and CO_2.

(18) F. J. Field and L. J. Franklin, "Electron Impact Phenomena," Academic Press, New York, N. Y., 1957, pp. 105–127.

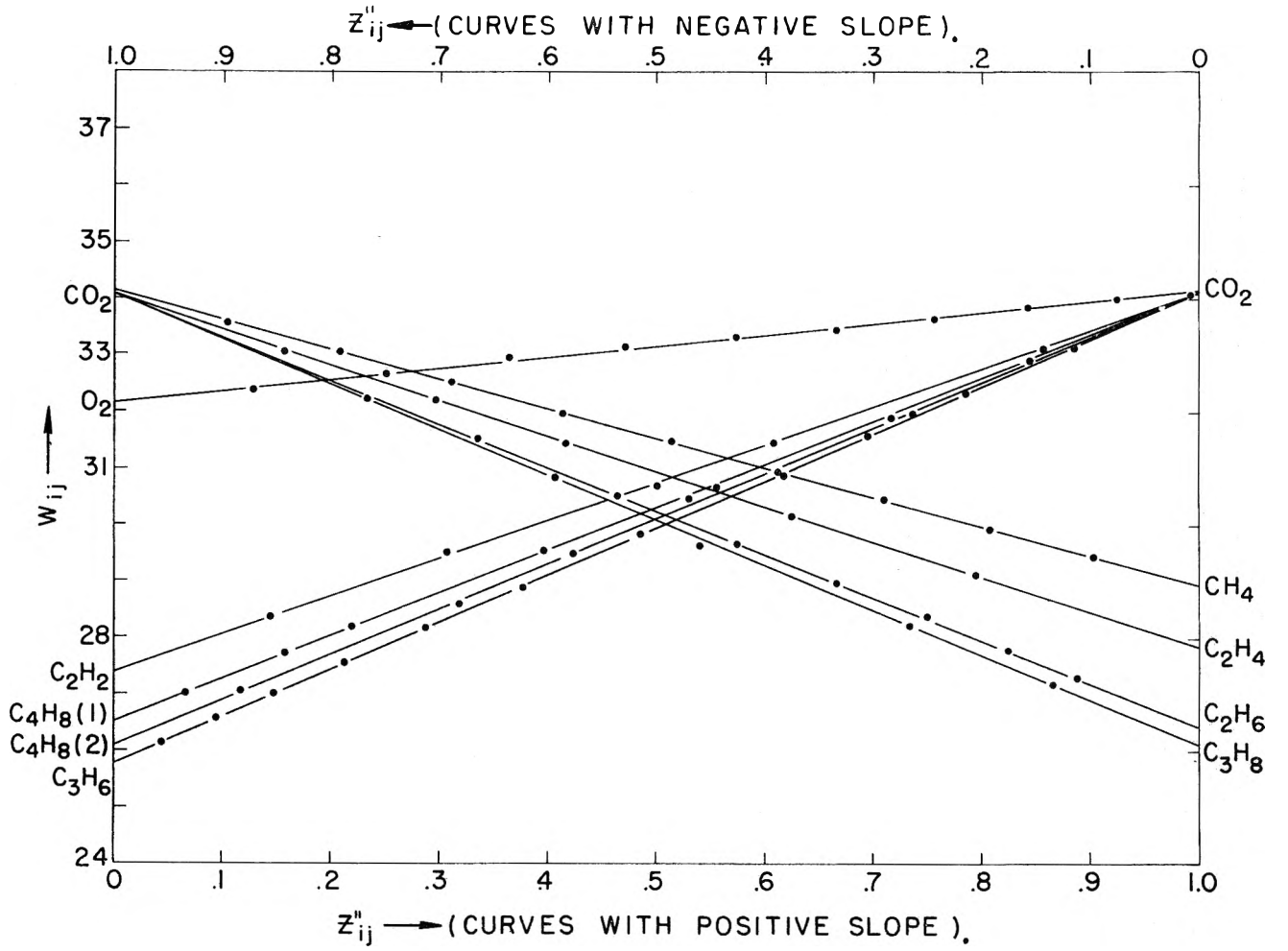

Fig. 3.—Plot of W_{ij} *vs.* Z_{ij}'' for mixtures of CO_2 with O_2, CH_4, C_2H_2, C_2H_4, C_2H_6, C_3H_8 (cyclopropane), C_3H_8, C_4H_8 (1-butene), and C_4H_8 (2-butene), using Z_{ij}'' calculated from measured constants shown in column 3 of Table II.

In many respects it is convenient to replace a_{ij} in eq. 1 by $f_{ij}W_j/W_i$, in which case eq. 1 can be written in simpler form

$$W_{ij} = (W_i - W_j)Z_{ij}'' + W_j \qquad (2)$$

where

$$Z_{ij}'' = \frac{P_i}{P_i + f_{ij}P_j}$$

If the measured value of W_{ij} is plotted against Z_{ij}'', a linear result is obtained (as predicted by eq. 2), provided the proper value of the empirical constant f_{ij} is used for any pair of gases. This has been done for many pairs of gases listed in Table I. The results are shown in Fig. 1 through 5 and the empirical constant f_{ij} associated with each pair of gases can be found in column 3 of Table II. These constants have each been assigned a "probable error" which was obtained by consideration of the accuracy of the W measurements. The probable error in any particular ionization measurement was of the order of 0.2%. The errors listed then

TABLE II

MEASURED AND CALCULATED RATIOS f_j/f_i FOR VARIOUS COMBINATIONS OF MOLECULAR GASES

Gas$_i$	Gas$_j$	f_j/f_i (measured)	f_j/f_i (calcd.)
N_2	CO_2	1.6 ± 0.2	1.8
N_2	O_2	1.2 ± .1	1.3
N_2	CH_4	1.7 ± .05	1.8
N_2	C_2H_2	3.5 ± .1	3.3
N_2	C_2H_4	3.2 ± .1	3.4
N_2	C_2H_6	3.5 ± .1	3.5
N_2	Cyclopropane	4.5 ± .1	4.5
N_2	C_3H_8	4.7 ± .1	4.5
N_2	1-Butene	6.3 ± .2	6.3
N_2	2-Butene	6.3 ± .2	6.3
H_2	CO_2	3.5 ± .6	3.6
H_2	CH_4	3.8 ± .15	3.6
H_2	C_2H_2	6.0 ± .2	6.6
H_2	C_2H_4	7.2 ± .2	6 8
H_2	Cyclopropane	9.0 ± .25	9.0
H_2	1-Butene	12.7 ± .3	12.6
CO_2	O_2	0.75 ± .1	0.72
CO_2	CH_4	1.05 ± .05	1.0
CO_2	C_2H_2	1.5 ± .05	1.83
CO_2	C_2H_4	1.7 ± .06	1.89
CO_2	C_2H_6	2.0 ± .06	1.95
CO_2	Cyclopropane	2.5 ± .1	2.5
CO_2	C_3H_8	2.7 ± .1	2.5
CO_2	1-Butene	3.55 ± .1	3.5
CO_2	2-Butene	3.2 ± .1	3.5
CH_4	C_2H_2	1.25 ± .2	1.83
CH_4	C_2H_4	2.0 ± .4	1.89
CH_4	C_2H_6	1.7 ± .15	1.95
CH_4	Cyclopropane	2.3 ± .2	2.5
CH_4	C_3H_8	2.25 ± .2	2.5
CH_4	1-Butene	4.0 ± .4	3.5
C_2H_2	Cyclopropane	1.5 ± .2	1.36
C_2H_2	1-Butene	2.0 ± .4	1.91
C_2H_4	Cyclopropane	1.3 ± .1	1.32
C_2H_4	2-Butene	2.0 ± .2	1.85
Propylene	Cyclopropane	0.95 ± .15	

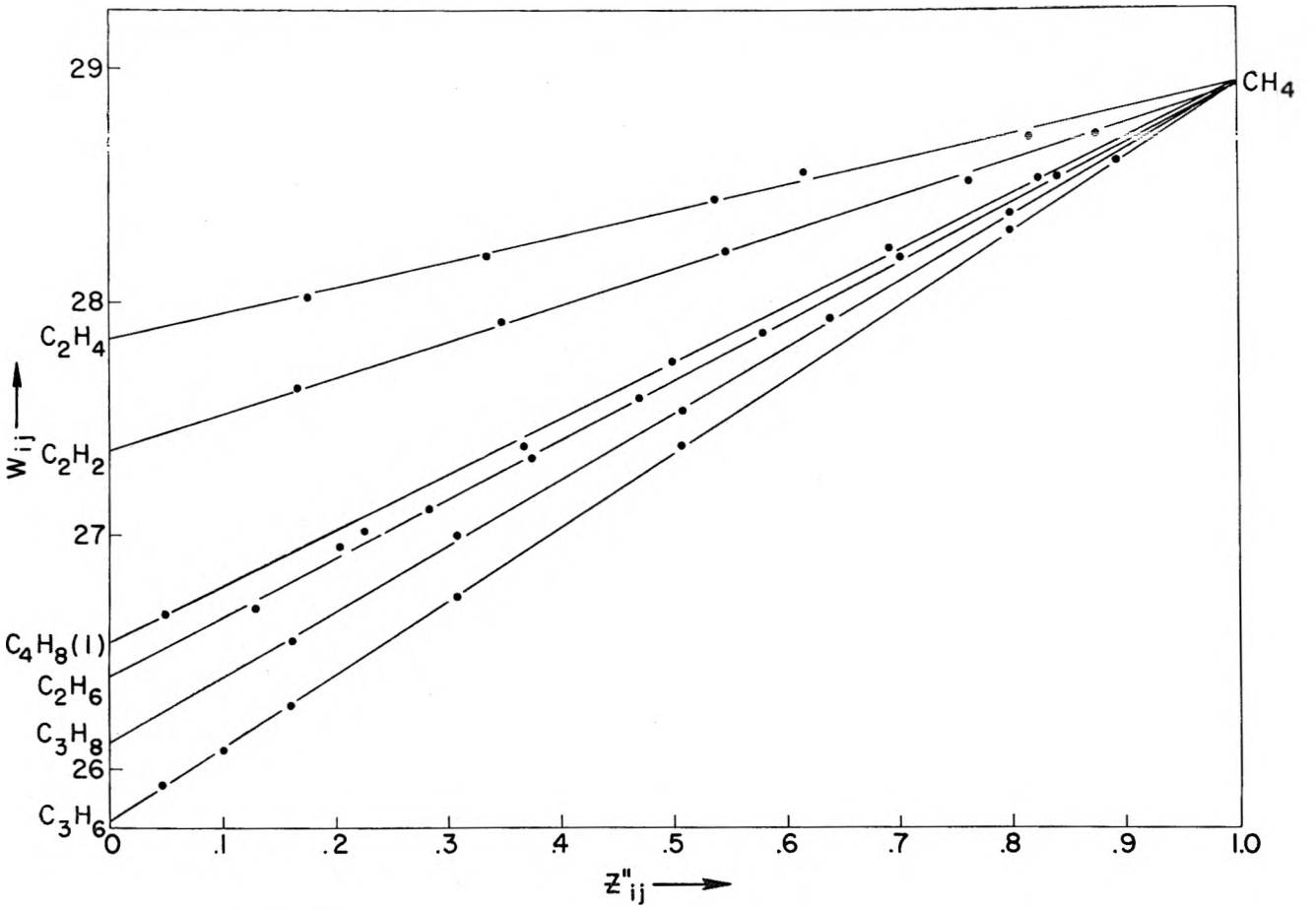

Fig. 4.—Plot of W_{ij} *vs.* Z_{ij}'' for mixtures of CH_4 with C_2H_2, C_2H_4, C_2H_6, C_3H_6 (cyclopropane), C_3H_8, and C_4H_8 (1-butene), using Z_{ij}'' calculated from measured constants shown in column 3 of Table II.

were determined by finding the variation in f_{ij} which would change the W value at the mid-point of the curve ($Z_{ij}'' = 0.5$) by as much as 0.2%. This variation is therefore large in the case of mixtures whose two component gases have W's which are close together. In these cases, large changes in f_{ij} have little effect in shifting the curve from a straight line.

Closer observation of the constants listed in this column shows that, with a few exceptions, they very nearly satisfy the relationship

$$f_{ij} = f_{kj}/f_{ki} \qquad (3)$$

where i, j, and k refer to any three gases in the table. In fact, if the constants are replaced by the values shown in column 4 of this table, the relationship given by eq. 3 is made to hold exactly. Many of these constants are within the probable error of those listed in column 3 and most of the others are close approximations. Moreover, if these constants are used in computing Z_{ij}'', instead of those in column 3, the curves obtained are very nearly straight lines identical with those in Fig. 1–5, with no points deviating from the straight lines by as much as 1% except in the case of acetylene mixtures, where the variation from a straight line is as high as 1.5% at $Z_{ij}'' = 0.5$. Thus, if each gas is assigned an f value such as that shown in column 6 of Table I (where nitrogen was arbitrarily assigned the value 1), then the constant $f_{ij} = f_j/f_i$ determined from any two of these can be used in eq. 2 to give the W of any mixture of the gases within the accuracy described above.

Distinction between "Regular Effects" and Other Effects

Neglecting the effects (such as the Jesse effect) of the addition of small amounts of impurities in the gases helium, neon, and argon, it has been shown[11,12] that further addition of the second gas leads to more regular changes in W similar to that observed in the molecular gases. These latter changes can be represented by eq. 1, and, therefore, also by eq. 2 by proper choice of constants. In these cases, the straight lines obtained do not necessarily intersect the axis at the W of the pure noble gas but at some point characteristic of the "contaminated" gas.

Closer examination of Fig. 1 shows an effect in nitrogen similar to the Jesse effect. This first became apparent in the case of mixtures of nitrogen and acetylene where the best straight line was obtained with $f_{ij} = 3.5$. This line, however, intersected the axis at 36.1 e.v./ion pair instead of 36.3 e.v./ion pair (the W of pure nitrogen).

Subsequent mixtures of nitrogen with ethylene, cyclopropane, and 1-butene showed the same rapid decrease in W as the first 1 to 3% of the second gas was added to the nitrogen and the more "regular" decrease from there on. Figure 6 shows an expanded view of the upper portion of these curves from $Z_{ij}'' = 0.5$ to $Z_{ij}'' = 1.0$ in the region near that of pure nitrogen. In the case of CO_2, the line approaches 36.3 e.v./ion pair but in the case of C_2H_2, C_3H_6, and C_4H_8, the straight lines approach points considerably below the W of nitrogen. Furthermore, in the cases shown, the lower

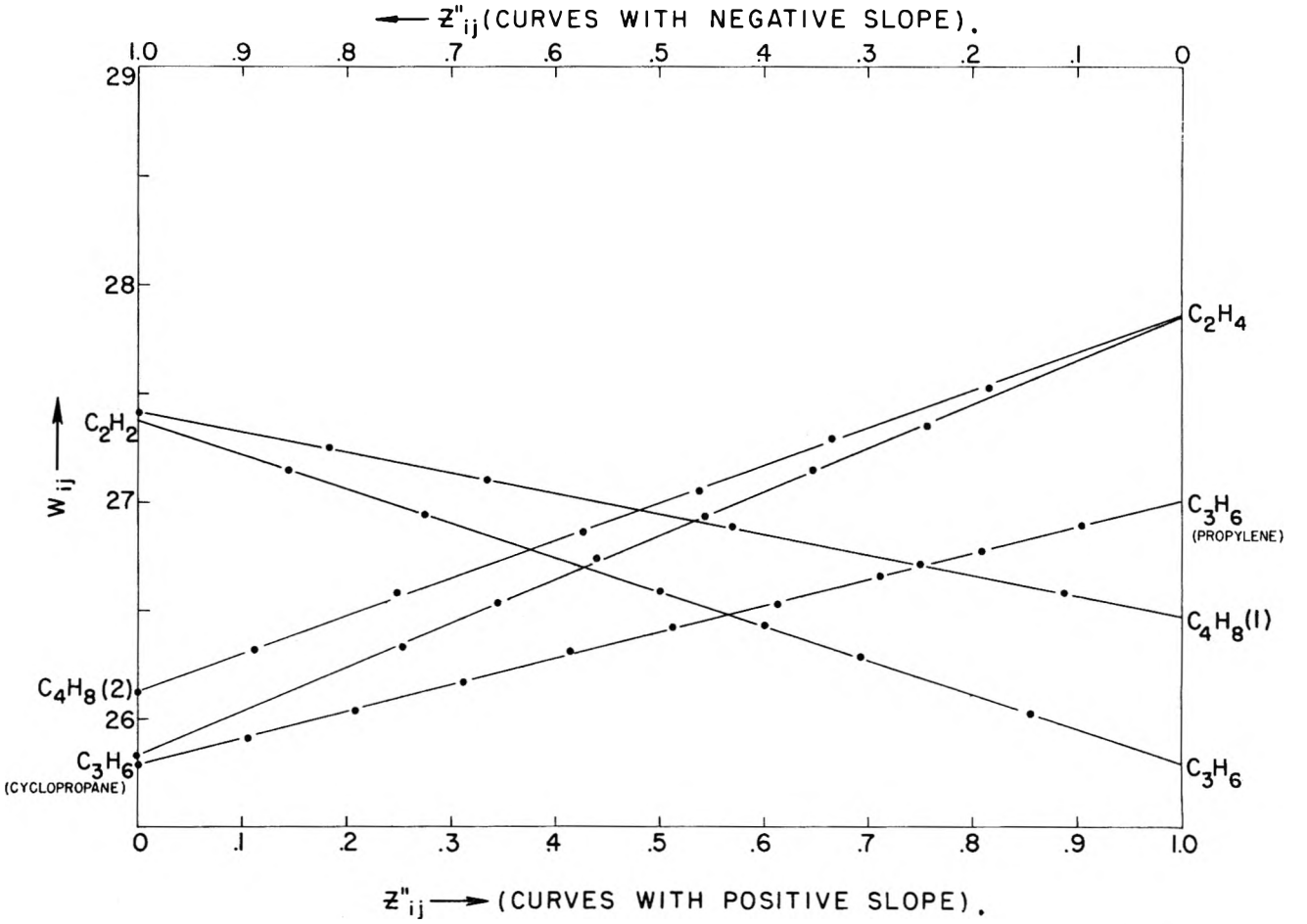

Fig. 5.—Plot of W_{ij} *vs.* Z_{ij}'' for mixtures of C_2H_2 with C_3H_6 (cyclopropane) and C_4H_8 (1-butene); for mixtures of C_2H_4 with C_3H_6 (cyclopropane) and C_4H_8 (2-butene); and for the C_3H_6 (propylene)–C_3H_6 (cyclopropane) mixture; all using Z_{ij}'' calculated from measured constants shown in column 3 of Table II.

the ionization potential of the second gas, the greater is the depression of the line. In fact, in the case of cyclopropane and 1-butene, the butene has a lower ionization potential than the cyclopropane but a higher W. The initial drop in W from 36.3 e.v./ion pair therefore is greater for butene and the two lines subsequently cross at about $Z_{ij}'' = 0.8$.

A further check on this effect was made by mixing small amounts of toluene vapor with nitrogen, since toluene has a rather low ionization potential. At room temperature, as much as 3 cm. pressure of this vapor could be admitted to the chamber with nitrogen, resulting in a mixture up to 12% toluene–88% nitrogen. Above 1% toluene, the W's of the mixtures fall on a fairly straight line, when plotted against Z_{ij}'', provided f_{ij} is set equal to about 15. Figure 7 shows this line as well as the curvature which results when the constant f_{ij} is made as low as 10 or as high as 20. The line approaches the point 35.3 e.v./ion pair on the nitrogen side, indicating a large initial drop from the value of pure nitrogen (the upper portion of this curve also is reproduced in Fig. 6), and approaches the point 28 e.v./ion pair on the toluene side. This extrapolated estimate for the W of pure toluene, which has been included in Table I, may be in error by as much as 5%. It points out the possibility of using this method of mixtures to obtain the W of other vapors, particularly heavy vapors, when the vapor pressure of the pure substance, at room temperature, is not sufficient to completely stop the α-particles in the chamber. To substantiate further this W value for toluene, mixtures also were run of toluene and cyclopropane. Assuming the validity of eq. 3 in this case, the constant $f_{ij} = 15/4.5 = 3.3$ (using Table I) and the resulting line for this mixture is shown at the bottom of Fig. 7. The W of this mixture increases with increasing amounts of toluene and extrapolates roughly to 27 e.v./ion pair.

Conclusions

The results described in this report are an attempt to show the wide applicability of eq. 2 (or equally well, eq. 1) in presenting data on W's of binary gas mixtures. By plotting W's in this way, it is possible to pick out those regions where other effects, such as the Jesse effect, are predominant, whereas these other effects might not be otherwise distinguished. Such is the case in nitrogen, where the effects of small impurities of gases with low ionization potential become noticeable only when the data are plotted in this way. It also is possible to extrapolate the straight line obtained with these equations to predict the W of pure vapors even when the vapor is part of a mixture and can only be obtained in concentrations up to 10% (by volume).

The relationship between the f constants given by eq. 3 is somewhat surprising, and is of considerable practical interest in that it allows one to predict unknown W's of mixtures of gases such as might be found in nuclear counters. The extensive application of this relationship to other gases has not been tested,

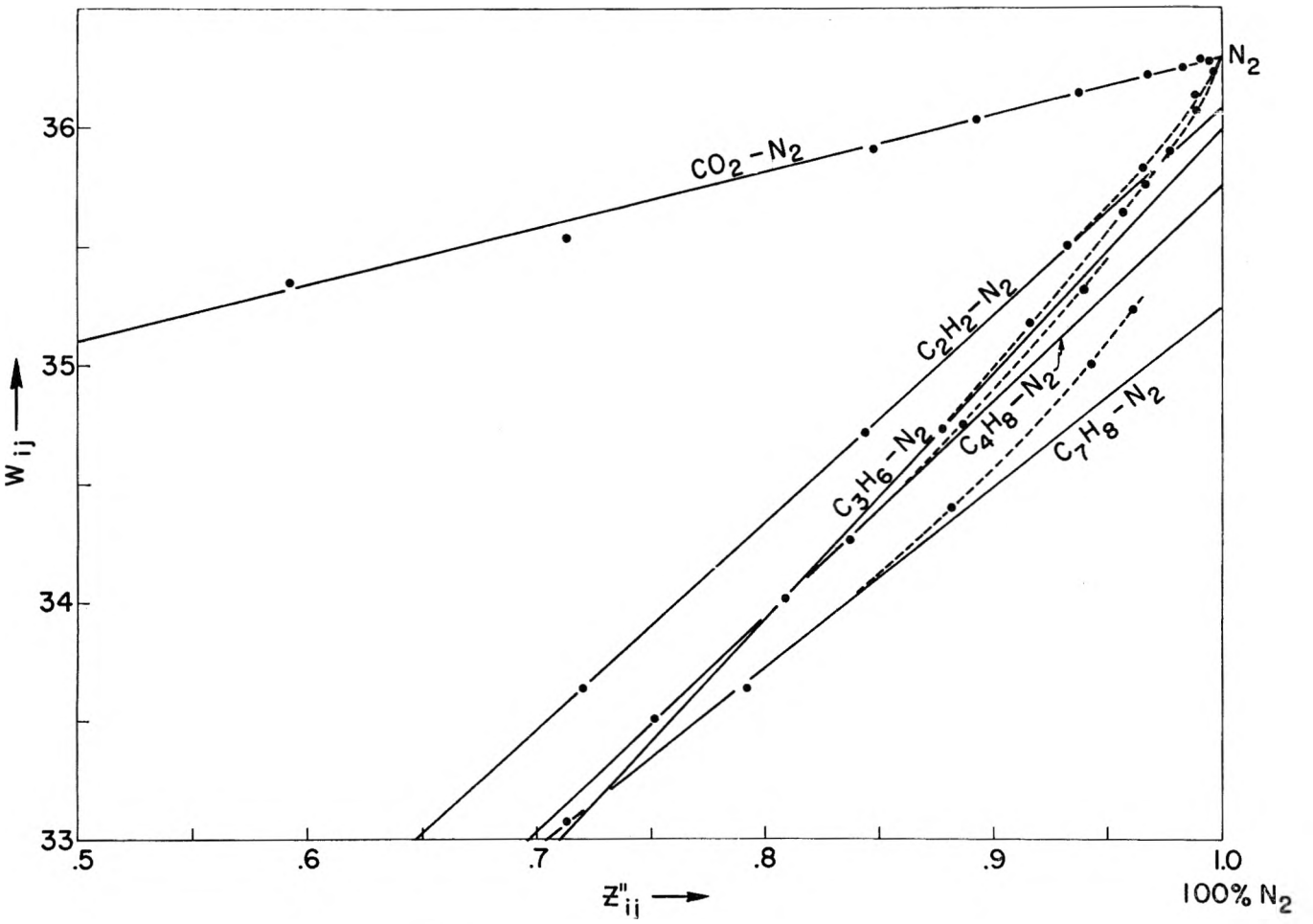

Fig. 6.—Expanded scale plot of W_{ij} *vs.* Z_{ij}'' for mixtures of N_2 with CO_2, C_2H_2, C_3H_6 (cyclopropane), C_4H_8, and C_7H_8 (toluene).

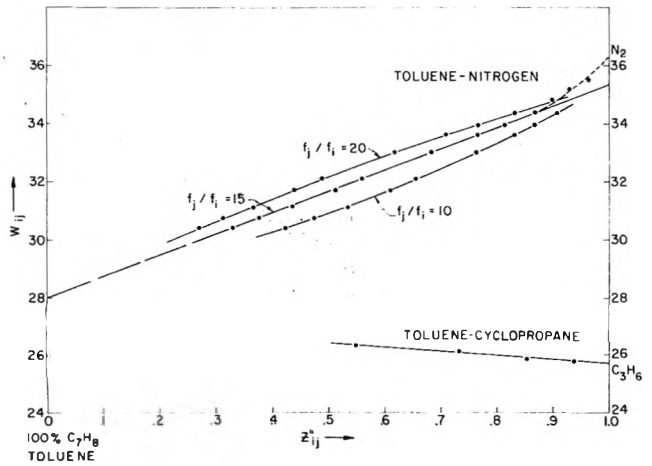

Fig. 7.—Plot of W_{ij} *vs.* Z_{ij}'' for mixtures of N_2–C_7H_8 using three different values of f_{ij}.

but it might be found to apply to many other molecular gas mixtures.

The accuracy of any particular combination may be limited by gas purity since no attempt was made to purify the gases used. It is worth repeating that the W's were measured *relative to nitrogen*, which was assumed to have a W of 36.3 e.v./ion pair. The results do not necessarily apply to monoenergetic α-particles of 5 Mev., but since the W is practically independent of energy over the spectral range of the source, they probably are representative.

Acknowledgments.—This work was performed at Berea College under the encouragement and guidance of G. S. Hurst of the Health Physics Division of the Oak Ridge National Laboratory. Thanks also are due to T. E. Bortner, H. B. Eldridge, R. H. Ritchie, and others of the Health Physics Division for their help and suggestions. In addition, M. G. Payne, E. M. Purcell, and N. C. Cornett, physics majors at Berea College, were actively engaged in the work of the project at one time or another.

THE RADIATION CHEMISTRY OF SOME OF THE HIGHER ALIPHATIC ALCOHOLS—FURTHER STUDIES ON RADICALS TRAPPED AT LOW TEMPERATURES[1]

BY RUSSELL H. JOHNSEN AND D. A. BECKER[2]

Department of Chemistry, Florida State University, Tallahassee, Florida

Received September 21, 1962

The radiation chemistry of iso-propyl alcohol, 1-butanol, *sec*-butyl alcohol and *t*-butyl alcohol has been investigated in both liquid and solid states. The effect of bleaching with visible and ultraviolet light on free radicals trapped in the low-temperature alcohol samples has been studied. The results of these experiments have been interpreted in terms of ionic and free radical reactions and applied to the problem of alcohol radiation chemistry in general.

Introduction

In an earlier study[3] the radiation chemistry of methanol, ethanol, and 1-propanol at 25° and at liquid nitrogen temperatures was investigated. This study was especially concerned with the nature of the paramagnetic species trapped in the low-temperature solids and the decomposition of these by the action of ultraviolet and visible light. It was concluded on the basis of these experiments that the principal products of irradiation are the alcohol radicals formed by the removal of an α-hydrogen and hydrogen.

The alcohol radicals subsequently react to produce glycol and aldehyde in the absence of bleaching. Illumination of the glassy solid with light below 3000 Å. results in the photolysis of these radicals with the production of smaller stable molecules such as methane, carbon monoxide, and additional hydrogen.

In the present work we have extended this type of investigation to some of the higher members of the homologous series and their structural isomers, with the view of studying particularly the effect of structure on photolytic behavior.

Experimental

Irradiation, analytical procedures, and dosimetry were identical with those described in the preceding paper, with the exception that glycols were determined using vapor fractometry, as well as by the periodic acid method. A 38-centimeter Carbo-Wax-400 column operated at 210°, and a helium flow rate of 54 ml./min. was employed in these determinations. Total dosages are indicated in connection with the experimental data.

The alcohols employed in these studies were purified by first drying over appropriate drying agents followed by fractional distillation. Samples were then transferred to the vacuum line where they were subjected to three bulb-to-bulb distillations prior to distillation into the irradiation vessels. In every case sample boiling over a one degree (or less) range was employed.

Experimental Results

The results of these experiments are displayed in Tables I–VIII. The experiments labeled "liquid (25°)"[4] refer to experiments carried out at room temperature but under the same conditions of geometry and radiation flux as those carried out at lower temperatures. Those samples labeled "solid (−196°)" were allowed to melt in the dark and reach room temperature prior to analysis. Samples labeled "solid (−196°) visible bleach" were held at −196° in a quartz dewar and exposed to a 100-watt fluorescent lamp for one hour prior to melting. The "solid (−196°) ultraviolet bleach" samples were treated in the same manner except that the unfiltered output of an AH-6 mercury arc lamp was

TABLE I

GASEOUS RADIOLYTIC PRODUCTS FROM ISOPROPYL ALCOHOL

Conditions of irradiation	100 e.v. Yields $G(H_2)$	$G(CH_4)$	$G(CO)$	$G(C_2-C_3)$	Total dose, e.v./g.
Liquid (25°)	3.74	1.53	0.19	0.51	1×10^{19}
Solid (−196°)	3.63	.78	.06	.62	1×10^{19}
Solid (−196°)	4.34	.99	.12	.72	1×10^{19}
Visible bleach					
Solid (−196°)	15.61	1.53	.77	4.50	1×10^{19}
Ultraviolet bleach[a]					

[a] Yield based on γ-ray energy absorbed.

TABLE II

GASEOUS RADIOLYTIC PRODUCTS FROM 1-BUTANOL

Conditions of irradiation	100 e.v. Yields $G(H_2)$	$G(CH_4)$	$G(CO)$	$G(C_2)$	Total dose, e.v./g.
Liquid (25°)	4.18	0.10	0.08	0.65	1×10^{19}
Solid (−196°)	3.54	.20	.36	.18	1×10^{19}
Solid (−196°)	3.37	.14	.70	.34	1×10^{19}
Visible bleach					
Solid (−196°)	18.40	.75	4.05	5.01	1×10^{19}
Ultraviolet bleach[a]					

[a] Yield based on γ-ray energy absorbed.

TABLE III

GASEOUS RADIOLYTIC PRODUCTS FROM *sec*-BUTYL ALCOHOL

Conditions of irradiation	100 e.v. Yields $G(H_2)$	$G(CH_4)$	$G(CO)$	$G(C_2)$	Total dose, e.v./g.
Liquid (25°)	2.56	0.51	0.64	2.40	1×10^{19}
Solid (−196°)	2.62	.32	.20	1.44	1×10^{19}
Solid (−196°)	2.82	.40	.28	1.52	1×10^{19}
Visible bleach					
Solid (−196°)	7.67	.89	2.15	3.97	1×10^{19}
Ultraviolet bleach[a]					

[a] Yield based on γ-ray energy absorbed.

TABLE IV

GASEOUS RADIOLYTIC PRODUCTS FROM *t*-BUTYL ALCOHOL

Conditions of irradiation	100 e.v. Yields $G(H_2)$	$G(CH_4)$	$G(CO)$	$G(C_2)$	Total dose, e.v./g.
Liquid (30°)	0.97	2.98	0.55	2.91	1×10^{19}
Solid (−196°)	1.33	1.00	.18	2.06	1×10^{19}
Solid (−196°)	1.45	1.21	.20	1.24	1×10^{19}
Visible bleach					
Solid (−196°)	1.52	0.29	.81	6.84	1×10^{19}
Ultraviolet bleach[a]					

[a] Yield based on γ-ray energy absorbed.

(1) This work was supported in part by the U. S. Atomic Energy Commission under Contract AT-(40-1)-2001.

(2) Abstracted in part from the M. S. thesis of D. A. Becker, Florida State University, June, 1961. Presented before the Second International Congress of Radiation Research, Harrogate, England, August, 1962.

(3) R. H. Johnsen, *J. Phys. Chem.*, **65**, 2144 (1961).

(4) *t*-Butyl alcohol was irradiated at 30° to maintain the liquid condition.

TABLE V

CONDENSED PRODUCTS FROM ISOPROPYL ALCOHOL RADIOLYSIS

100 e.v. Yields

Product	Condition: Liquid (25°)	Solid (−196°)	Solid (−196°) ultraviolet bleach
Isopropyl ether	0.10	0.02	0
Other ether	.15	.06	0
Acetaldehyde	.30	.13	0
Acetone	1.47	1.57	2.04
Water	trace	trace	1.41
Glycol	.20	trace	trace
Total dose, e.v./g.	13×10^{20}	9×10^{20}	8×10^{20}

TABLE VI

CONDENSED PRODUCTS FROM 1-BUTANOL RADIOLYSIS

100 e.v. Yields

Product	Condition: Liquid (25°)	Solid (−196°)	Solid (−196°) ultraviolet bleach
Butyraldehyde	0.62	1.24	1.89
Formaldehyde	1.44	0	0
Ethanol	1.47	.35	.35
1-Propanol	0.25	.11	.81
Water	.37	.23	.54
Glycol	.10	trace	trace
Total dose, e.v./g.	4×10^{20}	8×10^{20}	12×10^{20}

TABLE VII

CONDENSED PRODUCTS FROM *sec*-BUTYL ALCOHOL RADIOLYSIS

100 e.v. Yields

Product	Condition: Liquid (25°)	Solid (−196°)	Solid (−196°) ultraviolet bleach
Acetaldehyde	0.46	0.24	0.21
Propionaldehyde	.09	.07	.06
Acetone	.15	.26	.28
Methyl ethyl ketone	.42	.94	3.66
Ethanol	0	0.03	0
Water	trace	trace	trace
Glycol	.1 (2)	0	0
Total dose, e.v./g.	5×10^{20}	8×10^{20}	8×10^{20}

TABLE VIII

CONDENSED PRODUCTS FROM *t*-BUTYL ALCOHOL RADIOLYSIS

100 e.v. Yields

Product	Condition: Liquid (25°)	Solid (−196°)	Solid (−196°) ultraviolet bleach
Ether	0.17	0.03	0.03
Unidentified	.11	.22	.19
Acetone	1.08	.91	2.17
sec-Butyl alcohol	0.16	.12	0.16
Water	.26	1.15	.81
Glycol	trace	0	0
Total dose, e.v./g.	9×10^{20}	7×10^{20}	8×10^{20}

employed as the bleaching agent. In the case where analysis was to be made of the liquid products, that is, those not appreciably volatile or quite soluble in the alcohol, irradiations were carried out with a 3 Mev. Van de Graaff Accelerator employing much larger total doses, while for those samples on which gaseous products were determined a cobalt-60 source was used.

Clear, glassy samples were readily obtainable for all alcohols except *t*-butyl alcohol. Thus the results obtained from *t*-butyl alcohol in the solid state are not strictly comparable with the others since, as has been pointed out previously, considerable scatter in the data is observed when crystalline samples are used. Bleaching is especially difficult due to scattering of light from the opaque crystalline mass of the sample, and there is considerable doubt as to the effectiveness of the bleaching agents in this case.

Analyses of the gaseous products from liquid irradiation are generally reproducible to 1%. For the solid irradiation this is reduced to around 5%. Analyses for major liquid products were reproducible to a like degree, but for minor products this reproducibility was considerably reduced.

Discussion of Results

Two major differences are to be noted when the results for the substances studied in the present work are compared with those reported earlier. First of all, the yields of glycol are considerably reduced in relative importance, and, secondly, the simple relationships that were to be found among the radiolysis and photolytic products from the lower alcohols are apparent only for the normal and secondary butanol cases. The more complicated relationships can largely be understood in terms of the increased molecular complexity which results in a wider variety of possible decomposition products, higher steric requirements for radical–radical interactions, and the absence (except for 1-butanol) of the primary-CHOH grouping which seems particularly susceptible to photolytic decomposition.

A. Radiation Decomposition of Liquid Alcohols. (i) **Gaseous Products.**—All of these alcohols have been previously studied by McDonnell and Newton[5] using 28 Mev. helium ions. Irradiation by X-rays results in a comparative increase in the hydrogen yield ranging from 63.5 to 16.5% in the normal series from methanol to 1-butanol. In the case of secondary and *t*-butyl alcohol the hydrogen yields are lower (but only slightly) than those reported by McDonnell and Newton using helium ions. These results would seem to suggest that the recombination of hydrogen atoms in the track of the ionizing particle is a relatively unimportant mode of hydrogen formation in the liquid state. It should also be noted that there is no regular change in the hydrogen yield as one goes to alcohols of higher molecular weight. This is true of both the X-rays and helium ion studies, a secondary maximum being present for 1-butanol in both studies.

Methane yields are uniformly higher for the X-ray case, as are the yields of the C_2–C_4 hydrocarbons. This suggests that reactions leading to products of higher molecular weight than these occur with greater frequency in the higher L.E.T. case than here.

(ii) **Liquid Products.**—In Table IX the yields of carbonyl compounds and glycols for six alcohols studied in this Laboratory are juxtaposed with the results of McDonnell and Newton[5] in order more clearly to illustrate a rather unexpected linear energy transfer effect. Heretofore it has generally been assumed that glycols arise from the combination of two alcohol free radicals, while carbonyl compounds are the result of the molecular elimination of hydrogen. If these mechanisms are essentially correct, implying that the sole fate of the radicals is glycol formation, one would expect that high L.E.T. radiation would favor glycol formation,

(5) W. R. McDonnell and A. S. Newton, *J. Am. Chem. Soc.*, **76**, 4651 (1954).

while in the case of the relatively lower concentrations of free radicals provided by γ-rays the yield of glycol would be relatively lower.

Examination of Table IX reveals that in the case of

TABLE IX

	100 e.v. Yields			
	Carbonyl		Glycol	
	γ-rays	α-rays	γ-rays	α-rays
Ethanol	1.40	1.71	1.95	1.00
1-Propanol	1.22	2.14	1.43	1.46
Isopropyl alcohol	1.47	2.02	0.20	0.40
1-Butanol	0.62	1.50	.10	.92
sec-Butyl alcohol	.42	1.12	.10	.56
t-Butyl alcohol	1.08[a]	2.78	trace	.10

[a] Acetone.

the six alcohols considered the yield of carbonyl compound is *higher* for the high L.E.T. radiation in every case, in direct contradiction to our expectations. This same effect has also been observed by Choi and coworkers[6] for the case of methanol when Co-60 γ-rays were compared with the recoils from the $B^{10}(n,\alpha)Li^7$ reaction. These results would suggest that the rate of formation of the carbonyl compound is also a function of the local concentration of free radicals and would be most easily explained if the reaction involves a hydrogen atom transfer reaction between two radicals. This type of disproportionation reaction would be favored if the radicals involved had energies somewhat above average.

For methanol, ethanol, and 1-propanol the yields of glycol produced by γ-rays are greater than or equal to those resulting from high L.E.T. irradiation, which again is inconsistent with the view that glycol formation would be favored by a high local concentration of free radicals, other factors being equal. Only for the larger, more complex molecules does the ratio fall below one, which is consistent with the observation that for smaller radicals recombination is favored over disproportionation.

It is obvious from these observations that the mechanism of formation of these two types of molecules is not to be understood in terms of simple competition between bimolecular radical reactions and monomolecular decomposition but rather involves a complex of factors among which the residual energy of the radical following hydrogen atom loss plays an important role in determining whether hydrogen transfer or coupling takes place. Also to be considered are reactions in which the appropriate types of radicals are formed in close proximity, independent of the L.E.T. of the radiation. For example

$$RCH_2OH^+ + RCH_2OH \longrightarrow RCH_2OH_2^+ + \dot{R}CHOH$$

$$RCH_2OH_2^+ \xrightarrow{\epsilon^-} \dot{R}CHOH + H_2$$

B. Comparison of Solid State Irradiation with Liquid State. (i) **Gaseous Products.**—Hydrogen yields are somewhat affected by change of state and by the accompanying lower temperature for this group of compounds, but to a lesser extent than for methanol or ethanol. This either points to a molecular process for hydrogen formation or indicates that the reactions of the hydrogen atom are not so seriously impeded at $-196°$ in these compounds as they are for the smaller molecules. *t*-Butyl alcohol however, provides an exception in that it shows about a 38% increase in hydrogen production on going to the solid state.

In *t*-butyl alcohol the formation of hydrogen is of less importance than the formation of methane, and it seems reasonable to assume that H-atom and methyl radical loss compete as modes of energy dissipation on about equal footing in contrast to the situation involving the other alcohols where hydrogen atom loss is by far the more important process. In the solid state the escape of the methyl radical from the spur would be less probable and thus the formation of hydrogen increased in relative importance as the methyl radicals recombine with the parent radical. That this is a reasonable assumption can be seen from the fact that the methane yield from solid *t*-butyl alcohol is lowered by a factor of three from that observed for the liquid alcohol. Lower methane yields from solid state irradiations seem to be generally observed, with the exception of 1-butanol, where one sees the expected accompanying decrease in hydrogen production; and methanol where C–C bond cleavage is not involved in methyl radical formation.

The question of the abstraction of hydrogen from carbon by hydrogen atom at $-196°$ is not completely resolved. The stoichiometry of our results strongly suggests, however, that in the case of methanol no abstraction occurs at this temperature but that, as the alcohols become more complex structurally, abstraction plays an increasingly important role. This is consistent with the widely held view that secondary and especially tertiary hydrogen atoms are much more labile than primary ones.

The hydrocarbon products higher than methane also show this same general behavior on going from liquid to solid state irradiations, the only exception being isopropyl alcohol, for which there is a slight increase in the C_2–C_3 fraction on going from the liquid to the glassy state.

(ii) **Liquid Products.**—In general the effect of going to the solid state on the production of carbonyl compounds and glycols is similar to that observed for the lower alcohols. Yields of carbonyls are slightly increased, but the already low glycol yields essentially vanish. The one exception to this is the case of *t*-butyl alcohol where the yield of acetone is slightly lower in the solid state. However, this is consistent with the previous observation that products requiring the breakage of C–C bonds are consistently lower in the solid state. For example, formaldehyde and ethanol are important products from the radiolysis of liquid 1-butanol, while at $-196°$ no formaldehyde is produced and the yield of ethanol is approximately 20% of that observed for the liquid state.

All of these results suggest that the distribution of stable products observed is ultimately a function of the ability of the various intermediates to escape the solvent cage. On going to the solid state the rate of diffusion of the larger fragments is considerably inhibited, while the diffusion of hydrogen atoms seems little affected. The *total* amount of decomposition is, however, not much influenced.

(6) S. U. Choi, N. N. Lichtin, and J. J. Rush, *J. Am. Chem. Soc.*, **82**, 3225 (1960).

C. The Effect of Bleaching with Ultraviolet Light. (i) Gaseous Products.—Of the four alcohols studied in this investigation only 1-butanol and *sec*-butyl alcohol show the kind of photolytic behavior that was observed for the lower alcohols previously reported on. Thus for these two compounds the yields of carbon monoxide produced upon ultraviolet photolysis of the X-irradiated materials shows a reasonable correlation with the expected initial free radical yield and with the yield of hydrogen produced in the "dark" samples. Thus examination of Tables II and III reveals that for 1-butanol the "dark" hydrogen yield is 3.5 and the photolytic carbon monoxide yield is equal to 4.0, while these values for *sec*-butyl alcohol are 2.62 and 2.15, respectively. This is identical with the behavior observed for the case of 1-propanol but differs from the two lower alcohols, for which $G(CO)$ bleach $= 2G(H_2)$ dark.

Neither isopropyl alcohol nor *t*-butyl alcohol shows these simple relationships. In the case of *t*-butyl alcohol the opaque character of the samples employed, which in turn prohibited efficient bleaching, cannot be excluded as a cause for this discrepancy. However, isopropyl alcohol at $-196°$ produces clear glasses which should behave in a normal fashion. Nevertheless, the yield of carbon monoxide produced upon bleaching remains low. At this time it can only be conjectured that the radical resulting from the removal of the carbinol hydrogen is not capable of being photolyzed to carbon monoxide. Since the same radical would result from loss of a methyl group from the *t*-butyl alcohol molecule, it is also reasonable to suppose that similar considerations may apply here.

We thus see that the seven alcohols that have so far been studied fall into three classes. For one class, consisting of methanol and ethanol, $G(CO)$ bleach $= 2G(H_2)$ dark. For the second class composed of 1-propanol, 1-butanol, and *sec*-butyl alcohol, $G(CO)$ bleach $= G(H_2)$ dark. For the third group no simple relationship seems apparent. It is postulated that the following sequence of events transpires for the first group

A. At $-196°$ in the dark

$$CH_3OH \longrightarrow CH_3OH^+ + \epsilon^- \quad (1)$$

$$CH_3OH^+ + CH_3OH \longrightarrow CH_3OH_2^+ + \dot{C}H_2OH \quad (1a)$$

$$CH_3OH_2^+ + \epsilon^- \longrightarrow CH_3OH + H\cdot \quad (1b)$$

$$CH_3OH \longrightarrow \dot{C}H_2OH + H\cdot \quad (2)$$

$$H\cdot + H\cdot \xrightarrow{M} H_2 \quad (2a)$$

$$2CH_3OH \longrightarrow [CH_3OH^+ \ldots CH_3OH^-] \longrightarrow 2\dot{C}H_2OH + H_2 \quad (3)$$

B. Upon bleaching

$$\dot{C}H_2OH \longrightarrow H_2 + H\dot{C}O \quad (4)$$

$$H\dot{C}O \longrightarrow H\cdot + CO \quad (5)$$

The work of Baxendale and Mellows[7] using low concentrations of scavengers has shown that a process of the type suggested by equations 1 contributes a yield of hydrogen equal to 0.7 molecule per 100 electron volts in the solid state at $-196°$ and 1.4 molecules at room temperature where abstraction rather than dimerization takes place. The fact that abstraction rather than dimerization takes place in methanol is attested to by the sharp drop in hydrogen yields in going from the liquid to the solid state; this same laboratory[8] has also shown that $G(H_2)$ molecular (process 3) is 1.6 molecules per 100 e.v. Since $G(H_2)$ total $= 3.6$, $G(H\cdot)$ and $G(\dot{C}H_2OH)$ from process 2 must be equal to 2.5, again assuming no abstraction. On this basis we can calculate that the total yield of $G(\dot{C}H_2OH)$ trapped is 7.2 which is in excellent agreement with the value of ~ 7 reported by Alger, *et al.*[9] A similar reaction scheme can be developed for ethanol, which also leads to the relationship: $G(CH_3\dot{C}HOH) = 2G(H_2)$, although in this case some hydrogen abstraction by hydrogen must occur even in the solid phase. Thus we would expect only one kind of radical to be observed by e.p.r. studies on this type of alcohol irradiated in the dark (excluding a small amount of $H\dot{C}O$ produced initially) and equivalent amounts of $H\dot{C}O$ (or HCHO) and subsequently CO produced upon bleaching. These postulates have been confirmed experimentally. The $H\dot{C}O$ radical is produced from $\dot{C}H_2OH$ upon bleaching with light in the region of 2537 Å. and is decomposed to CO by visible light.[10] The behavior of the e.p.r. spectrum upon both photolytic and thermal bleaching is consistent with the presence of a single species.

The mode of formation of the additional hydrogen produced upon bleaching is complex. For example, in the case of methanol $\Delta G(H_2)$ bleach is 16. If hydrogen is produced molecularly from the $\dot{C}H_2OH$ radical this results in a yield of ~ 7 molecules. The fate of the simultaneously produced $H\dot{C}O$ radical is ultimately to produce carbon monoxide and a hydrogen atom. If these recombine a further increment of 3.5 molecules of H_2 results, far short of the observed 16 molecules. On the other hand, if these H-atoms react by abstraction they would lead to the further production of $\dot{C}H_2OH$ and a chain reaction. That a chain of this type does not occur is attested to by the fact that bleaching results in a complete disapperance of paramagnetic species rather than a steady state. This disappearance is probably not due to the recombination of large radicals since these are stable over long periods of time at $-196°$. One possible source of additional hydrogen should be mentioned. If the mechanism of photolysis of matrix alcohol molecules outlined below is valid molecular hydrogen in an amount nearly sufficient to make up the deficit would be formed.

In the case of the second class of compounds (where $G(CO)$ bleach $= G(H_2)$ dark) the basic reactions are much the same, but now the abstraction of hydrogen by the RCH_2OH^+ ion, or H-atom (which is more likely in these complex molecules), can take place at at least two positions in the molecule, thus leading to two types of trapped free radicals. It is presumed that only one of these ($R\dot{C}HOH$) is capable of being decomposed photolytically to carbon monoxide. Thus each molecule of H_2 produced in the dark is accompanied by the formation of only one carbon monoxide molecule. Such a series of postulates requires that *two* types of free radicals be trapped in the initially irradiated

(7) J. H. Baxendale and F. W. Mellows, *J. Am. Chem. Soc.*, **83**, 4720 (1961).

(8) G. E. Adams and J. H. Baxendale, *J. Phys. Chem.*, **63**, 854 (1959).

(9) R. S. Alger, T. H. Anderson, and L. A. Webb, *J. Chem. Phys.*, **30**, 695 (1959).

(10) R. H. Johnsen, unpublished results.

material. There is some evidence for this in the e.p.r. spectra of both 1-propanol and 1-butanol.

(i) **Liquid Products.**—As in the case of the alcohols previously studied, while bleaching with ultraviolet light presumably destroys the free radical precursors here postulated to lead to the formation of aldehydes, these products are nevertheless seen in bleached samples. (In the case of the compounds studied herein glycols are not important products in the solid state irradiations.) The yield of carbonyl compound is in every case higher than that observed for the "dark" and liquid state experiments. While other possibilities cannot be excluded it again seems reasonable to consider the effect that the presence of the paramagnetic free radicals trapped in the matrix has on the photochemistry of the matrix. Studies have now been conducted on the effect of a variety of paramagnetic solutes upon the photochemistry of ethanol[11]; and such diverse substances as oxygen, nitric oxide, and a variety of paramagnetic metal ions all have a similar effect—namely, the formation of acetaldehyde at wave lengths completely ineffective in the pure alcohol. Furthermore, this same study has shown that all of these alcohols form complexes with oxygen which have absorptions at wave lengths considerably shifted to longer wave lengths.

Acknowledgments.—The authors wish to thank Mr. M. Riggenbach for assistance with the analyses and Mr. K. Chellis for performing the Van de Graaff irradiations.

(11) R. H. Johnsen and D. A. Becker, to be published.

THE SOLUBILITY OF CORUNDUM IN BASIC HYDROTHERMAL SOLVENTS

BY R. L. BARNS, R. A. LAUDISE AND R. M. SHIELDS

Bell Telephone Laboratories, Incorporated, Murray Hill, New Jersey

Received September 24, 1962

The solubility of corundum has been measured in sodium hydroxide and in sodium carbonate solutions from about 400 to 600° at pressures up to about 2800 bars. In sodium hydroxide, the solubility was independent of pressure but dependent almost linearly on base concentration up to 10 *m* NaOH. In sodium carbonate, the solubility depended almost linearly on pressure up to about 1370 bars beyond which it was almost independent of pressure. The solubility in Na_2CO_3 depended almost linearly on base concentration up to 4.3 *m* beyond which it was independent of base. The temperature coefficient of solubility was large in Na_2CO_3 and nearly zero in NaOH. The solubility in LiOH, KOH, CsOH, K_2CO_3, Cs_2CO_3, and several other mineralizers is reported. The solubility data suggest that in $(OH)^-$ the predominant species is $(AlO_2)^-$ or $(AlO_3)^=$ while several species are present in $(CO_3)^{=2}$.

Introduction

Alpha-Al_2O_3 has been grown on a seed crystal from dilute NaOH and Na_2CO_3 solutions at temperatures above 400° and pressures from about 500 bars upward. The method of preparation has been reported by Laudise and Ballman[1] and more recently by Bashuk, *et al.*[2] It is of interest to determine the solubility of corundum in the hydrothermal solvents from which it has been or might be grown. Such solubility data will aid in elucidating the mechanisms of hydrothermal crystal growth in general and hopefully will suggest conditions for the more rapid growth of corundum.

The hydrothermal solubility of refractory oxides is of general interest and a considerable body of theoretical work has been done on the thermodynamics of hydrothermal systems.[3-5] However, the only experimental solubility data under hydrothermal conditions in existence was for α-quartz.[5-7] In general, theoretical treatments of solubility have restricted themselves to systems containing only water and solute. For the growth of crystals under hydrothermal conditions, the solubility usually must be increased by the addition of a mineralizer. Previous work in the system SiO_2–NaOH–H_2O has shown that the function of the $(OH)^-$ mineralizer is to promote the formation of new silica containing species other than those found in pure water.[5,7] It would be of interest to test hydrothermal solubility theories and postulates concerning the role of a mineralizer in a system containing some other refractory oxide besides SiO_2. Consequently, it was decided to study the hydrothermal solubility of Al_2O_3 in the presence of mineralizers. Further work has extended these solubility studies to ZnO.[8]

Experimental

Hydrothermal equipment has been discussed elsewhere,[9] so only a brief description will be given here. Previous hydrothermal solubilities have been determined by (1) sampling the fluid phase at the chosen *p–t* conditions or (2) determining the loss in weight of the solid phase following rapid quenching to room temperature. Method (2) is satisfactory provided the solid phase does not recrystallize on the solid piece during the quench and provided but one fluid phase co-exists in equilibrium with the crystalline phase. Method (2) was used in our previous determinations of solubility in the SiO_2–Na_2O–H_2O system.[5] The hydrothermal vessel had a volume of about 100 cm.[3] and was arranged in a rocking furnace to accelerate equilibrium. Recently we have found that with a small sacrifice in precision and much less effort, it is possible to carry out solubility determinations, at least where the solubility is above about one per cent, in welded platinum capsules whose volume is one cm.[3] or less.

The procedure used was as follows. One end of a thin walled

(1) R. A. Laudise and A. A. Ballman, *J. Am. Chem. Soc.*, **80**, 2655 (1958).

(2) R. P. Bashuk, V. P. Basaev, R. B. Tsadkina, and S. A. Faivusovich, *Kristallografiya*, **5**, 666 (1960). (Eng. Translation—*Soviet Physics Crystallography*, **5**, 638 (1961).

(3) E. U. Franck, *Z. physik. Chem.* (Frankfurt), **6**, 345 (1956).

(4) G. J. Wasserburg, *J. Geol.*, **66**, [5], 559 (1958).

(5) R. A. Laudise and A. A. Ballman, *J. Phys. Chem.*, **65**, 1396 (1961).

(6) G. W. Morey and J. M. Hesselgesser, *Am. J. Sci.*, Bowen Volume, 343 (1952).

(7) A more complete compilation of references of theoretical and experimental publications on quartz solubility is given in "Hydrothermal Synthesis of Single Crystals," R. A. Laudise in "Progress in Inorganic Chemistry" Vol. III, edited by F. A. Cotton, Interscience, New York, N. Y., 1962, p. 1ff.

(8) R. A. Laudise and E. D. Kolb, *Am. Mineralogist*, in press.

(9) R. A. Laudise and J. W. Nielsen, "Solid State Physics," Vol. 12, ed. by F. Seitz and D. Turnbull, Academic Press, New York, N. Y., 1961, p. 149ff.

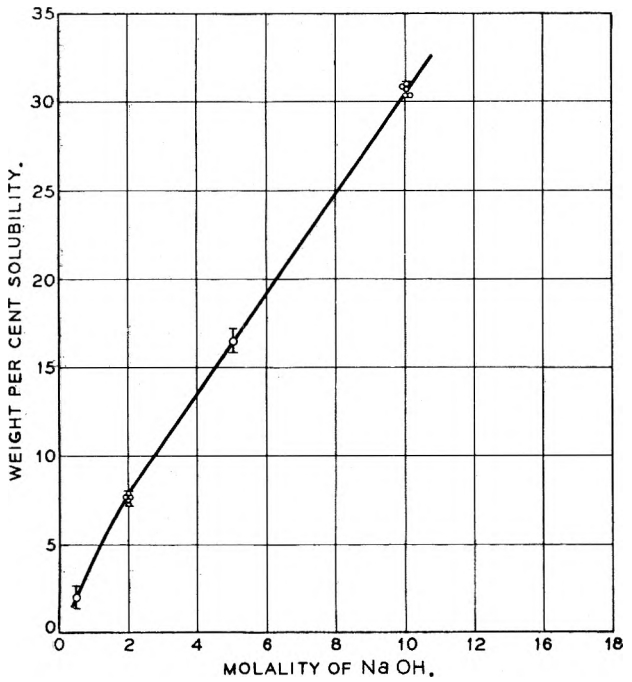

Fig. 1.—Solubility of corundum as a function of NaOH concentration at 430° and 1450 bars.

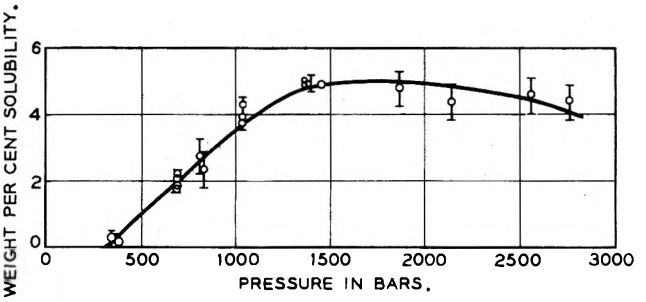

Fig. 2.—Solubility of corundum as a function of pressure in 3.4 *m* Na_2CO_3 at 430°.

C.P. platinum tube (typically 0.19 in. o.d. × 1.5 in. long × 0.007 in. wall) was crimped and welded with a d.c. arc welder. The tube was then weighed. A length of single crystal corundum (Linde Co. white sapphire rod) was weighed. The rod and the desired solvent were loaded into the tube and the open end was crimped and welded. The whole capsule was then weighed. The capsule was tested for leaks by placing it in an oven at 225° for at least 10 min., after which it was reweighed. The capsule was placed in a 0.25 in. i.d. Tuttle cold seal test-tube type autoclave.[10] The autoclave was attached to an air driven intensifier (which pumped water at any desired pressure up to 4,000 bars) and a pressure gage (calibrated to ±10 bars with a dead weight tester).

Water was pumped into the autoclave up to the desired pressure (controlled within ±30 bars) and a furnace (controlled to ±3°) by a conventional contactor controller with a chromel–alumel thermocouple was placed around the autoclave. Another thermocouple was inserted in a cavity in the autoclave wall and its output was recorded.

At the end of the run, the autoclave was quenched with cold water and the capsule was reweighed to determine if any leaks had occurred. The capsule was then opened and the contents carefully examined for evidence of foreign phases. The sapphire rod was then rinsed in 6 *N* HCl, carefully dried and weighed.

In all cases where a solubility is reported, the rod surface was smooth with no evidence of redeposition. In those cases where corundum was found not to be the stable phase, the rod usually had a rough, chalky surface.

Reagent purity chemicals were used in all experiments and solutions were standardized against potassium acid phthalate. All mineralizer concentrations are expressed in terms of molality, *m*.

(10) The autoclaves and associated pressure and furnace system were purchased from Tempress, Inc., State College, Pa.

Using five replicate determinations of solubility in 3.4 *m* Na_2CO_3 at 430° and 1,450 bars, the standard deviation of a single observation was found to be 0.19% at an average value of 4.94 wt. % solubility. The bars on the graph indicate the ±3 σ limits for either single or multiple determinations. For multiple determinations the bar height shows the ±3 σ limits for the mean of the several determinations.

Results

The apparent solubility of corundum was determined as a function of time under representative conditions from 5 to 100 hours and it was found that equilibrium was achieved in five hours. All experiments were for at least 18 hr. Phase equilibrium experiments were performed by using as starting material γAl_2O_3, $Al(OH)_3 \cdot nH_2O$, or both. Solubilities are reported only for those conditions where the stable solid phase was observed to be α-Al_2O_3. Per cent solubility was calculated as wt. of corundum lost × 100/wt. of water + wt. of mineralizer. Solid phases were always identified by X-ray powder patterns and verified in some cases by petrographic microscopy.

Solubility in NaOH.—Certain pertinent solubility data are shown in Table I. As can be seen, and as other data not shown here substantiate, the solubility from 0.5–10.0 *m* NaOH in the temperature range from 400–600° is apparently independent of pressure for pressures from 140 to 2,760 bars. The solubility has a slight positive temperature coefficient and other data not shown here indicate that the Van't Hoff equation is obeyed in 10 *m* NaOH with a pressure independent ΔH of about 0.2 kcal./mole between 430 and 600°. The slope in 2.0 *m* NaOH is probably similar, but the data scatter rather badly.

TABLE I

SOLUBILITY OF CORUNDUM IN NaOH–WATER SOLUTIONS

Base concn., *m*	Temp., °C.	Pressure, bars	Solubility, wt. %	No. of determinations	
0.5	400	310–2,680	2.0	5	Indep. of *p*
2.0	430–600	1,450	7.5 at 430° 8.0 at 600°	10	Slight pos. slope
2.0	430	1,380–2,760	7.5	7	Indep. of *p*
2.0	600	1,380–2,760	8.0	2	Indep. of *p*
10.0	430–600	1,450	30.5 at 430° 31.5 at 600°	12	Slight pos. slope
10.0	430	140–2,760	30.5	9	Indep. of *p*

Figure 1 shows the dependence of solubility on base concentration to be nearly linear up to 10 *m* NaOH.

Solubility in Na_2CO_3.—The dependence of solubility on pressure in 3.4 *m* Na_2CO_3 at 430° is shown in Fig. 2, while Fig. 3 shows the dependence on temperature at 1450 bars. Figure 4 shows the solubility dependence on Na_2CO_3 concentration at 1450 bars and 430°. As can be seen, the solubility depends almost linearly on pressure up to 1380 bars above which the pressure coefficient is either zero or slightly negative. The temperature coefficient of solubility is large, while the Van't Hoff equation is only imperfectly obeyed with $\Delta H_{574°} \simeq 1$ kcal./mole while $\Delta H_{450°} \simeq 5$ kcal./mole. The solubility increases with increasing base concentration up to about 3.4 *m* beyond which it is independent of base concentration until sodium aluminate becomes the stable phase.

Solubility in Other Mineralizers.—A number of other mineralizers for Al_2O_3 were investigated, and the results are summarized in Table II.

TABLE II

PHASE EQUILIBRIA AND SOLUBILITY IN VARIOUS MINERALIZERS

Mineralizer	Temp., °C.	Pressure, bars	Stable phase	Solubility, wt. %	Remarks
4 *m* LiOH	430	1,450	$LiAlO_2$		Well crystallized
2 *m* NaOH	430	1,450	α-Al_2O_3	7.5	
2 *m* KOH	430	1,450	α-Al_2O_3	6.6	
	600	1,450	α-Al_2O_3	6.9	
2 *m* CsOH	430	1,450	α-Al_2O_3	5.2	
	600	1,450	α-Al_2O_3	5.7	
2 *m* $Ba(OH)_2$	430	1,450	Not α-Al_2O_3		Unidentified hexagonal plates
	600	1,450	$BaAl_2O_4$		
2 *m* Na_2CO_3	430	1,450	α-Al_2O_3	4.9	
	600	1,450	α-Al_2O_3	7.0	
2 *m* K_2CO_3	430	1,450	α-Al_2O_3	4.3	
	600	1,450	α-Al_2O_3	5.8	
2 *m* Cs_2CO_3	430	1,450	α-Al_2O_3	3.4	
	600	1,450	α-Al_2O_3	4.8	
20 *m* NaCl	430	1,450	?	<0.2%	
2–20 *m* KCl	430	1,450	?	<0.2%	
3.3 *m* HCl	430	1,450	?	<0.2%	
7.8 *m* HF	430	1,450	$Al(OH, F)_3$		
2 *m* KF	430	1,450	Not α-Al_2O_3		
10 *m* KF	600	1,380	K_3AlF_6		
Concd. NH_4OH	430–600	1,450–2,760	?	<0.2%	

Discussion

Solubility in NaOH.—The equation describing the dissolving of Al_2O_3 in pure water is by analogy with previous work on SiO_2[5]

$$Al_2O_3 \text{ (solid corundum)} + nH_2O \text{ (liquid or gas)} \rightleftharpoons Al_2O_3 \cdot nH_2O \text{ (liquid or gas soln.)} \quad (1)$$

Equation 1 assumes no ionization of the aluminum hydroxide formed.

Since no quantitative data are available for the solubility in pure water, and since the present method lacked sufficient sensitivity to determine such data, we were not able to determine the value of n. However, since the simplest hydroxy compound is $Al(OH)_3$, a plausible assumption is that $n = 3$. In this connection it is interesting to point out that Wasserburg[4] has suggested that, although the assumptions and methods used by others to calculate n in the SiO_2 reaction analogous to equation 1 were incorrect, the result that $n \simeq 2$ leading to $Si(OH)_4$ as the predominant species is correct. In any case, qualitative determinations of Al_2O_3 solubility in pure water at 430° and 1450 bars indicate that the solubility is less than 0.5 wt. %.

It is suggested that the equation describing the dissolving of Al_2O_3 in basic media is similar to that suggested for SiO_2.[5]

$$1/2\ Al_2O_3 + (2a - 3)(OH)^- \rightleftharpoons AlO_a^{(2a-3)-} + (a - 3/2)H_2O \quad (2)$$

Equation 2 assumes complete ionization of the aluminates formed.

Figure 1 shows that up to 10 *m* NaOH the solubility of Al_2O_3 is linearly dependent on the $(OH)^-$ concentration. The solubilities of Fig. 1 lead to the ratios: moles Al_2O_3/ moles NaOH $\simeq$ 0.38–0.42. This suggests a ratio of $^1/_2$ or $^1/_3$ which, for $^1/_2$, would make equation 2

$$1/2\ Al_2O_3 + (OH)^- \rightleftharpoons (AlO_2)^- + 1/2\ H_2O \quad (3)$$

Thus, $a \simeq 2$ and the predominant species in $(OH)^-$ up to 10 *m* would be $(AlO_2)^-$. For $^1/_3$ the predominant species would be $(AlO_3)^{-2}$. Surely, however, this species is, in any case, in equilibrium with other aluminates. However, in view of the marked increase in solubility in the basic solution, aluminates must predominate over species of the $Al_2O_3 \cdot nH_2O$ type. The results here

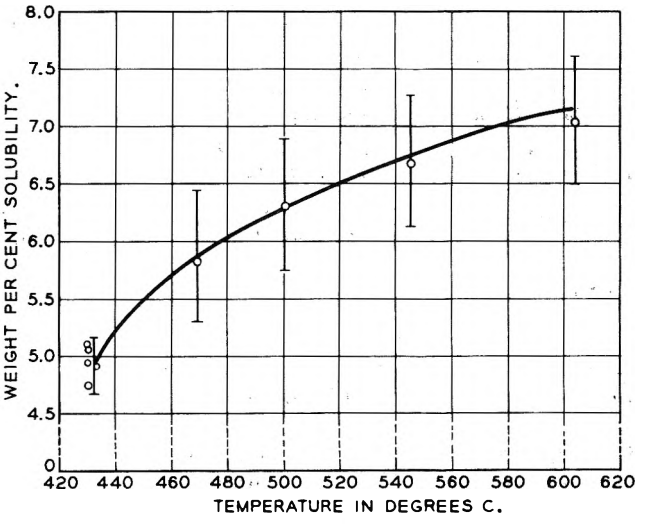

Fig. 3.—Solubility of corundum as a function of temperature in 3.4 *m* Na_2CO_3 at 1450 bars.

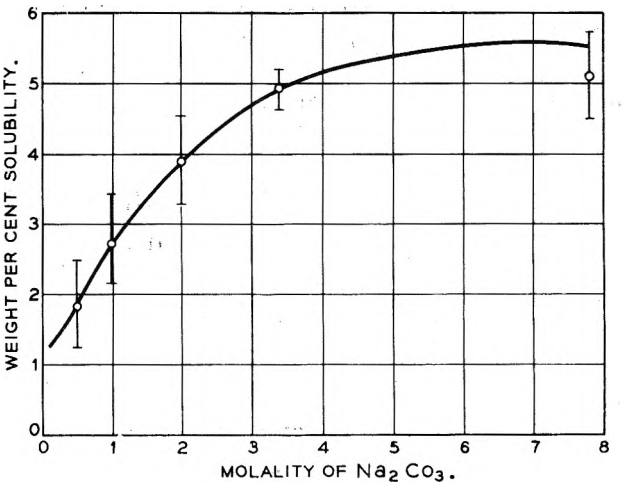

Fig. 4.—Solubility of corundum as a function of Na_2CO_3 concentration at 430° and 1450 bars.

are generally commensurate with those obtained in our study of the SiO_2–H_2O–NaOH system.[5]

The dependence of the solubility of Al_2O_3 in $(OH)^-$ upon pressure and temperature are, however, in marked contrast to the results found for quartz. The solubility of Al_2O_3 is almost independent of pressure, and the temperature coefficient of solubility is small. Unfortunately, the dependence of solubility on density (specific volume) of the solvent cannot be estimated without data on the equation of state of the solution.

It is indeed surprising that solubility is independent of pressure. Once we grant that solubility is independent of pressure, then, of course, it follows that the temperature coefficient of solubility and ΔH will be independent of pressure. It is true, of course, that if the solubility is expressed in g./cc. of free volume[11] then the solubility values of this work will to a first approximation be a linear function of the density.

However, the solubility is a logarithmic function of the density in the SiO_2–NaOH–H_2O system and ΔE is a function of solvent density (or pressure) in basic solutions but not in pure water.[5]

Several reasons may be advanced for the lack of solubility dependence on pressure. Perhaps over the pressure range investigated, the density changes very little in comparison with a similar pressure range for quartz. However, this seems unlikely.

It would also be useful to consider the over-all reaction for the dissolving of Al_2O_3 in aqueous sodium hydroxide. This would be the sum of D times reaction 1 plus E times reaction 2 where D and E are coefficients which produce the observed ratio of $Al_2O_3 \cdot nH_2O/AlO_a^{(2a-3)-}$.[12]

In view of the marked increase in solubility in base, it is probably fair to assume that in pure water, equation 1 describes the situation, while in basic solutions, equation 2 is applicable. Therefore, one would expect that Δv, the change in volume in reaction 2 in NaOH, is zero. Since the change in the number of compressible species is not zero, there must be appreciable differences in the compressibilities of the species.

We should now consider the low value for ΔH of Al_2O_3 in NaOH in contrast with the values of ΔH obtained for quartz in basic solutions.[13] If we consider the dissolving of Al_2O_3 in basic media to be principally described by the over-all reaction of equation 2 and break this reaction into several steps as

$$1/2\ Al_2O_3(\text{solid}) \rightleftarrows 1/2\ Al_2O_3(\text{gas}) \quad \Delta H_4 \text{ sublimation (endothermic)} \quad (4)$$

$$1/2\ Al_2O_3(\text{gas}) + (OH)^-(\text{soln.}) \rightleftarrows (AlO_2)^-(\text{soln.}) + 1/2\ H_2O \quad \Delta H_5 \text{ (exothermic)} \quad (5)$$

Since

$$\Delta H_2 = \Delta H_4 + \Delta H_5 = 0$$

$$\Delta H_4 \simeq \Delta H_5$$

that is, the exothermic heat of reaction 5 just about equals the heat of sublimation of sapphire.

Solubility in $(CO_3)^{-2}$.—Equation 2 describes the dissolving of Al_2O_3 in $(CO_3)^=$ with the $(OH)^-$ being formed due to the hydrolysis of $(CO_3)^=$. Consequently, one would expect that the solubility in $(CO_3)^=$ under similar conditions would be lower than in $(OH)^-$ since the hydrolysis of $(CO_3)^=$ is by no means complete. The dependence of solubility on pressure could be best rationalized if we knew the equation of state so as to examine the dependence on specific volume. Even as a crude approximation it is not justified to assume applicability of the p–v–t data for water since the formation of CO_2 will markedly influence the equatino of state for $(CO_3)^=$ solutions. The hydrolysis of carbonate results in the formation of CO_2 which has a large compressibility and, therefore, it might be expected that Δv, the change in volume for reaction 2 in $(CO_3)^=$ would be larger than in $(OH)^-$ and that the pressure coefficient of solubility would be larger than for $(OH)^-$ solutions. Up to 1380 bars, this is the case. The cause of the leveling in the pressure–solubility curve beyond 1380 bars is not understood.

The large values of ΔH in $(CO_3)^=$ and the large positive temperature coefficient of solubility can be explained if we realize that

$$\Delta H_{(CO_3)^=} \simeq \Delta H_4 + \Delta H_5 + \Delta H_6$$

where ΔH_6 is for the hydrolysis reaction

$$H_2O + (CO_3)^= \rightleftarrows (HCO_3)^- + (OH)^- \quad (6)$$

Since equation 6 is endothermic, ΔH_6 is positive and, since

$$\Delta H_4{}^= = \Delta H_5$$

$$\Delta H_{(CO_3)^=} \simeq \Delta H_6$$

The dependence of solubility on base concentration suggests that several aluminum containing species may be responsible for the observed solubilities in $(CO_3)^=$.

Solubility in Other Mineralizers.—In agreement with the work of Yalman, Shaw, and Corwin[14] it was found that in the presence of $(H)^+$ and of $(F)^-$, hydrates and fluorides of Al_2O_3 are often stable.

Implications for the Growth of Sapphire.—The small temperature coefficient in $(OH)^-$ explains the slow growth rates obtained with this mineralizer.[1] In several cases, growth was probably mainly due to the supersaturation caused by the presence of metastable $Al(OH)_3 \cdot nH_2O$ nutrient. Such growth, of course, ceases when the $Al(OH)_3 \cdot nH_2O$ has converted *in situ* to Al_2O_3.

In sodium carbonate solutions pressures much above

(11) This is calculated by dividing the solubility data as presently expressed in this work by the density of the solution at the condition of the experiment. To a first approximation, the p–v–t data for water were used to estimate the density.

(12) In a previous publication[5] on the solubility of quartz D and E were incorrectly assumed to be equal, and equations 2 and 3 of ref. 5 should not have been added as they were to yield equation 10. Instead, reasoning analogous to that applied in this work leads to the conclusion that the over-all reaction is essentially that of equation 8. Then, the order for the values of a found in ref. 5 reflects the values of Δv, the volume change in the appropriate reaction, in the three cases—dissolving of SiO_2 in pure water, dissolving of SiO_2 in NaOH, and dissolving of SiO_2 in Na_2CO_3. That is, since $a_{H_2O\text{-}SiO_2} > a_{NaOH\text{-}SiO_2} > a_{Na_2CO_3\text{-}SiO_2}$, $\Delta v_{H_2O\text{-}SiO_2} > \Delta v_{NaOH\text{-}SiO_2} > \Delta v_{Na_2CO_3\text{-}SiO_2}$. The value of Δv for each of the cases is established by the change in the number of compressible species in the reaction and by the relative compressibilities of the various species.

(13) The ΔH values for quartz were calculated from the ΔE values of ref. 5, assuming a reasonable value for Δv in $\Delta H = \Delta E + p\Delta v$.

(14) R. G. Yalman, E. R. Shaw, and J. F. Corwin, *J. Phys. Chem.*, **64**, 300 (1960).

1380 bars will not increase the solubility, nor will base concentrations above 2 *m*. Sodium, potassium, rubidium, or cesium carbonate in this range appear to be promising solvents.

Acknowledgments.—We wish to thank E. D. Kolb for several useful discussions and Miss A. D. Mills for identifying phases by X-ray powder diffraction.

THE FREE ENERGY OF SiC FROM ITS SOLUBILITY IN Fe AND FROM GAS-SOLID EQUILIBRIA WITH SiO_2, GRAPHITE, AND CO

BY RICHARD H. REIN AND JOHN CHIPMAN

Department of Metallurgy, Massachusetts Institute of Technology, Cambridge, Mass.

Received September 24, 1962

Concordant values for the free energy of formation of β-SiC at temperatures of 1533–1600° are found by three methods: I, its solubility in graphite-saturated Fe–Si–C alloys; II, the concentration and activity of Si in similar alloys in equilibrium with SiO_2, SiC, and Co; III, the temperature (1533°) at which p_{CO} = 1 atm. in the formation of SiC from SiO_2 and graphite. Results confirm recent values of ΔH_f for SiO_2 and give for β-SiC the average value $\Delta H_{f298} = -15.6$ kcal.

Several experimental methods have been used to obtain values of the free energy of formation of SiC at elevated temperatures. In connection with their recent study of its solubility in molten Ag, d'Entremont and Chipman[1] summarized the results of recent investigations and suggested a value of $\Delta H_{f298} = -15.8$ kcal. for β-SiC in preference to the older calorimetric value, −13.4 kcal. This paper presents the results of further experiments at high temperatures in which two entirely different methods are combined to yield concordant results and thereby to confirm the recently revised value for the heat of formation[2,3] of SiO_2 (α-quartz), $\Delta H_{f298} = -217.6$ kcal.

Experimental Procedure

The experiments formed a part of a broad study of the activity of SiO_2 in metallurgical slags (to be reported elsewhere) based on establishment of equilibrium in the reaction

$$SiO_2(\text{in slag}) + 2C(\text{graph.}) = Si(\text{in C-sat. Fe}) + 2CO(1\text{ atm.}) \quad (1)$$

The experiments were carried out in a horizontal graphite-tube resistance furnace 50 mm. i.d. having a uniformly heated central zone 10 cm. long, and controlled within ±2°. Carbon monoxide of C.P. grade flowed through the tube at 100 cm.³/min. at atmospheric pressure. Samples were heated in groups of 3 or 4 in small graphite crucibles mounted on a carbon boat. At the termination of the run, usually 24 hr., the boat was withdrawn to the cold end of the tube. The Fe–Si alloys were separated from the crucibles and the adhering graphite removed with a wire wheel. The alloys were then analyzed for Si and C. Temperature was measured with an optical pyrometer sighted directly on the carbon boat. The pyrometer was calibrated frequently against a Pt, Pt 10% Rh thermocouple inserted from the opposite end of the furnace.

Solubility of β-SiC in Graphite-Saturated Iron (Method I).—The alloys used in this study were prepared from electrolytic Fe and high-purity Si and initially contained approximately the silicon required to form SiC. The alloys were melted under silica slags, not saturated but of sufficiently high silica content so that silicon was transferred slowly to the metal according to reaction 1. After 24 hours of equilibration, the metal sample was separated from the graphite crucible and the interface was examined to determine whether SiC had formed. The results are presented in Table I. Samples marked with a superscript *a* were used to determine the average minimum value at which SiC is formed; this was found to be 22.0 % Si at 1550° and 22.4 % Si at 1600°.

TABLE I

THE SILICON CONTENT OF IRON IN EQUILIBRIUM WITH β-SiC AND GRAPHITE

Run no.	Temp., °C.	Initial wt. % Si	Final wt. % Si	SiC at metal–graphite interface
52–1	1550	21.95	22.4	Yes
52–2	1550	21.4	22.1	Yes[a]
53–1	1550	21.95	22.6	Yes
53–2	1550	21.4	22.3	Yes
53–3	1550	20.5	21.5	No
54–1	1550	22.0	22.2	Yes
54–2	1550	21.5	21.8	Yes[a]
55–1	1550	21.95	21.9	Yes[a]
55–2	1550	21.0	22.0	Yes[a]
56–1	1550	22.0	21.8	No[a]
56–2	1550	21.4	21.7	No
78–12	1600	22.5	22.4	Yes[a]
80–2	1600	23.0	22.4	Yes[a]

[a] Samples used to establish the average Si content of iron in equilibrium with β-SiC and graphite.

These values are somewhat lower than those reported by Chipman, Fulton, Gokcen, and Caskey[4] who found 22.7% Si at 1550° and 23.0 % Si at 1600°. The carbon solubilities determined by both investigators were in agreement.

Chipman and Baschwitz[5] have determined the activity of Si in Fe–Si–C solutions by means of its distribution between this solution and liquid Ag and related experimental data. Their results are reproduced in Fig. 1. For concentrations approximating the solubility of SiC they showed that log γ_{Si} bears the same relation to $N_{Si} + N_C$ as to N_{Si} in the binary solution. Calculations from the solubility data are summarized in Table II.

TABLE II

FREE ENERGY OF SiC FROM SOLUBILITY MEASUREMENTS

Temp., °C.	Solubility: %Si	N_{Si}	N_C	log γ_{Si}	a_{Si}	$\Delta F°_{SiC}$, cal./mole
1550	22.0	0.357	0.011	−0.94	0.041	−11,600
1600	22.4	0.364	0.016	−0.82	0.052	−11,000

The Equilibrium $SiO_2(c) + 2SiC(\beta) = 3Si(\text{in Fe}) + 2CO(1\text{ atm.})$ (Method II).—The equilibrium in this reaction was determined by equilibrating silica-saturated slags with liquid Fe–Si–C alloys contained in an SiC crucible. The SiC crucibles were prepared by forming a layer of SiC on the inside of a graphite crucible by reaction with silicon vapor for 1 hr. at 1650°. The crucibles were 20 mm. in diameter and 25 mm. in height and were fitted

(1) J. C. d'Entremont and J. Chipman, *J. Phys. Chem.*, **67**, 499 (1963).
(2) W. D. Good, *ibid.*, **66**, 380 (1962).
(3) S. S. Wise, J. L. Margrave, H. M. Feder, and W. N. Hubbard, *ibid.*, **66**, 381 (1962).
(4) J. Chipman, J. C. Fulton, N. A. Gokcen, and G. R. Caskey, *Acta Met.*, **2**, 439 (1954).
(5) J. Chipman and R. Baschwitz, paper submitted to *Trans. Met. Soc. AIME*.

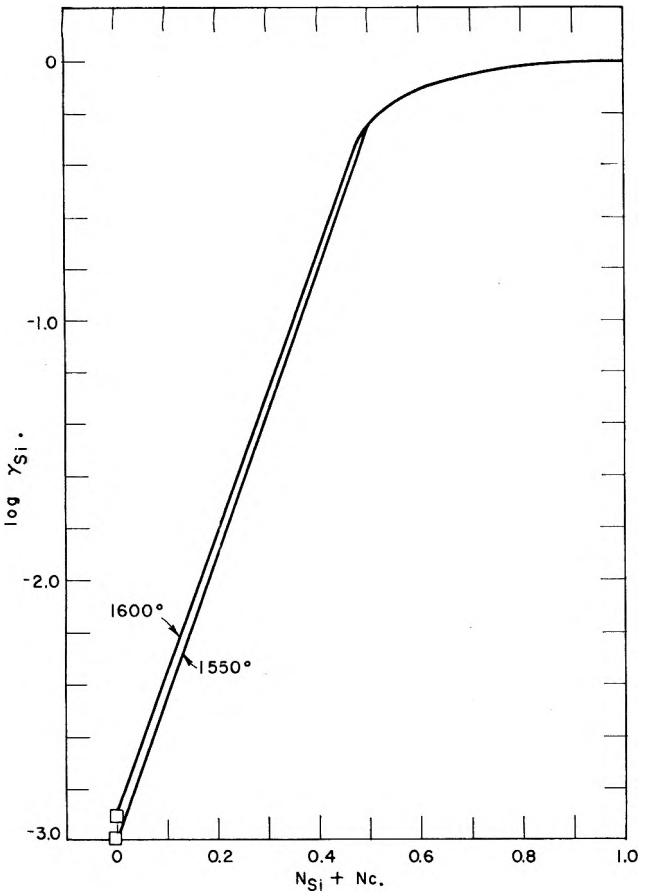

Fig. 1.—Activity coefficient of Si in iron and iron-carbon alloys at 1550 and 1600°.

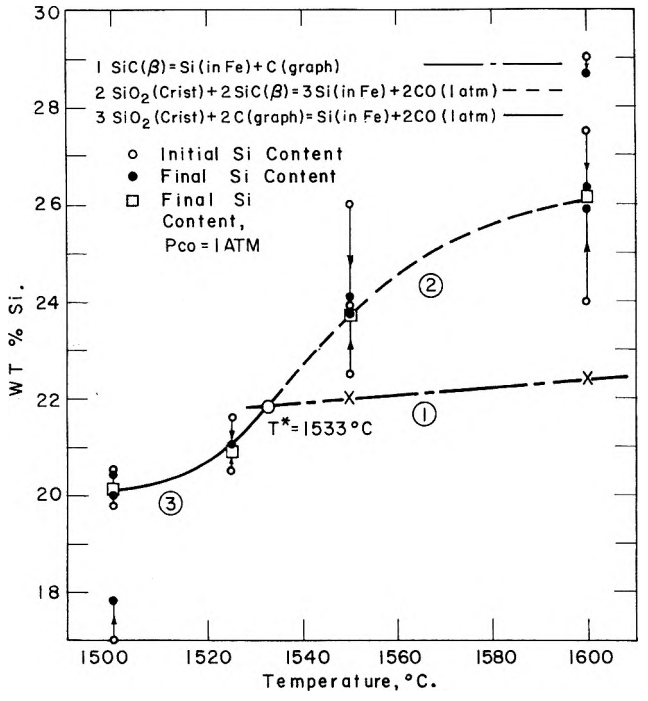

Fig. 2.—Interpolation to establish T^* for the equilibrium SiO_2(crist.) + 3C(graph.) = SiC(β) + 2CO (1 atm.).

with graphite covers to reduce the SiO loss. The charge in the crucible consisted of 3 g. of an Fe–Si alloy and 3 g. of slag. The slags consisted of prefused SiO_2–CaO–Al_2O_3 saturated with SiO_2. The slag and metal were permitted to equilibrate for 24 hr. which was found to be sufficient for equilibrium to be reached in most cases. The carbon monoxide pressures were determined from gas analysis and barometric pressures and corrected for the presence of silicon monoxide, using the data of Ramstad and Richardson.[6] The equilibrium data are presented in Table III. The final average Si content of the iron was calculated to correspond to a CO pressure of 1 atm.

TABLE III

COMPOSITION OF Fe–Si–C ALLOYS IN EQUILIBRIUM WITH SiO_2-SATURATED SLAG, β-SiC, AND CO

Run no.	Temp., °C.	Initial wt. % Si	Final wt. % Si	P_{CO}, atm.	N_{Si}	N_C	$K = a^s_{Si} \times P^2_{CO}$
58–2	1550	22.5	23.7	0.964	0.380	0.006	1.34×10^{-4}
60–2	1550	26.0	24.0	.984	.384	.005	1.62×10^{-4}
60–3	1550	24.0	23.8	.984	.381	.006	1.50×10^{-4}
60–4	1550	26.0	24.1	.984	.386	.005	1.72×10^{-4}
Av. adjusted	1550	..	23.7	1.0	.380	.006	1.55×10^{-4}
61–3	1600	29.0	28.7	0.967	.446	.002	Not equilibrium
61–4	1600	24.0	25.9	0.967	.410	.007	8.7×10^{-4}
80–1	1600	27.5	26.2	0.980	.413	.007	9.8×10^{-4}
Av. adjusted	1600	..	26.1	1.0	.411	.007	9.25×10^{-4}

The free energy of formation of silica can be calculated from the heat of formation determined recently by Good,[2] and by Wise, Margrave, Feder, and Hubbard[3] using the thermal data of Mosesman and Pitzer[7] and of Kelley[8] and entropies given by Kelley and King.[9] The resulting equation useful at 1700–2000°K. is

$$Si(l) + O_2(g) = SiO_2(crist.)$$

$$\Delta F^0 = -226{,}500 + 47.5T \quad (2)$$

The free energy of formation of carbon monoxide was derived from the National Bureau of Standards' selected values in the same temperature range

$$2C(gr.) + O_2(g) = 2CO(g)$$

$$\Delta F^0 = -56{,}200 - 40.4T \quad (3)$$

The average results of Table III and the other data cited lead to values for ΔF^0_f for SiC as follows: $\Delta F^0_{1823} = -10.8$ kcal.; $\Delta F^0_{1873} = -10.1$ kcal.

The Equilibrium SiO_2(c) + 2C(graph.) = Si(in Fe) + 2CO(1 atm.).—Silica-saturated slags were also equilibrated at 1500 and 1525° with Fe–Si alloys in graphite crucibles in a manner similar to the experiments just described. Under these conditions SiC does not form and the equilibrium represented by equation 1 is attained. The results are presented in Table IV.

TABLE IV

COMPOSITION OF Fe–Si–C ALLOYS IN EQUILIBRIUM WITH SiO_2-SATURATED SLAG, GRAPHITE, AND CO

Run no.	°C.	Initial wt. % Si	Final wt. % Si	P_{CO}, atm.
63–1	1500	19.8	20.0	0.993
63–2	1500	17.0	17.8	.993
73–1	1500	20.5	20.4	.990
62–1	1525	21.6	21.0	.999
72–1	1525	20.5	20.9	.995

The Equilibrium SiO_2(c) + 3C(graph.) = SiC(β) + 2CO(1 atm.) (Method III).—At unit pressure the three solid phases can coexist in equilibrium at only one temperature. This temperature, called T^*, is obtained by interpolation using the data of Tables I, III, and IV. This is shown in Fig. 2. The solubility data are plotted in curve 1 and extrapolated downward to intersect the interpolation curve connecting the data of Tables III and IV. The intersection at 1533° is taken as T^*. At this temperature, ΔF^0 for the reaction SiO_2(crist.) + 3C(graph.) = SiC(β) + 2CO(1 atm.) is zero. Combining this with equations 2 and 3 yields a value for the free energy of formation of SiC at T^*, $\Delta F^0_{1806} = -11.6$ kcal.

The data on the free energy of SiC are summarized in Fig. 3, each set of results being represented in its experimental tempera-

(6) J. F. Ramstad and F. D. Richardson, *Trans. Met. Soc. AIME*, **221**, 1021 (1961).
(7) M. H. Mosesman and K. S. Pitzer, *J. Am. Chem. Soc.*, **63**, 2348 (1941).
(8) K. K. Kelley, U. S. Bureau of Mines Bulletin 584, 1960.
(9) K. K. Kelley and E. G. King, Bureau of Mines Bulletin 592, 1691.

ture range. The calorimetric lines include ΔH by Humphrey, Todd, Coughlin, and King[10] and entropy and enthalpy data of Kelley.[8,9] For temperatures of 1700–2000°K, their data for either α or β may be represented by the equation

$$\Delta F^0_f = \Delta H_{298} - 11{,}850 + 8.88T$$

Of the dissociation pressure determinations, those of Davis, Anthrop, and Searcy[11] and of Grieveson and Alcock[12] agree well with the present results while those of Drowart, de Maria, and Inghram[13] and of Vidale[14] differ by about 2.5 kcal. in opposite directions.

Our results are shown as individual points and by an average line whose equation is

$$SiC(\beta);\ \Delta F^0 = -27{,}400 + 8.88T$$

The limits of error are not readily assessed. The accuracy of Method I depends upon the activity coefficient of Si in Fe in which the uncertainty is about ±0.8 kcal. The solubilities reported here are more dependable than those of Chipman, *et al.*,[4] from which they differ by 3%. Recent solubility data of Kirkwood and Chipman[15] in Pb and of d'Entremont and Chipman[1] in Ag are in better agreement, particularly the latter.

Method III depends upon the heat of formation of SiO_2, probably good to ±0.3 kcal. at 298° but less precise at high temperatures, and upon interpolation to obtain T^*. The latter is confirmed within 8° by the work of Kay and Taylor[16] and the over-all result of this method is about as good as that of Method I. The accuracy of Method II is inferior to either of the others in that it involves both of the subsidiary data and γ_{Si} appears in the $^3/_2$ power.

In view of the agreement among independent methods, it seems unlikely that the proposed equation for ΔF^0 can be in error by as much as 1 kcal. The derived heat of formation ΔH_{298} = −15.6 kcal., which is of less importance to high-temperature chemistry, is subject to somewhat greater uncertainty.

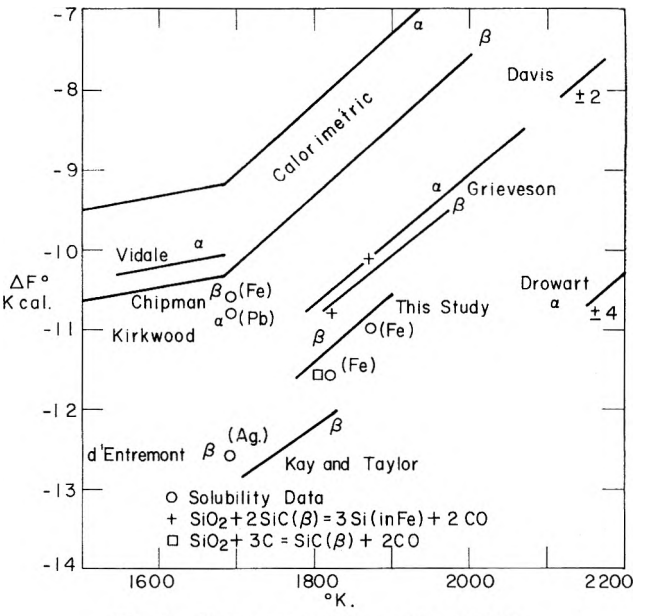

Fig. 3.—Free energy of formation of SiC.

It is of especial interest that equilibria involving SiO_2, both as determined in this study and as reported earlier by Baird and Taylor[17] and by Kay and Taylor,[16] now lead to values for the free energy of SiC which are in agreement with solubility and dissociation pressure results. It was the earlier disagreement in such studies that first called attention[18] to an error in the free energy of SiO_2 and the present agreement may be taken as confirmatory evidence for the validity of the new heat of formation.

Acknowledgments.—The authors wish to thank Mr. D. L. Guernsey for the careful analytical work. This study was sponsored in part by the American Iron and Steel Institute and in part by the National Science Foundation.

(10) G. L. Humphrey, S. S. Todd, J. P. Coughlin, and E. G. King, U. S. Bureau of Mines, Report of Investigations 4888, 1952.

(11) S. G. Davis, D. F. Anthrop, and A. W. Searcy, *J. Chem. Phys.*, **34**, 659 (1961).

(12) P. Grieveson and C. B. Alcock, "Special Ceramics," Haywood & Co., Ltd., London, 1961, p. 183–208.

(13) J. Drowart, G. de Maria, and M. G. Inghram, *J. Chem. Phys.*, **29**, 1015 (1958).

(14) G. L. Vidale, General Electric Co., Missile & Space Vehicle Dept., TIS Report R60 SO333 (1960).

(15) D. H. Kirkwood and J. Chipman, *J. Phys. Chem.*, **65**, 1082 (1961).

(16) D. A. R. Kay and J. Taylor, *Trans. Faraday Soc.*, **56**, 1372 (1960).

(17) J. D. Baird and J. Taylor, *ibid.*, **54**, 526 (1958).

(18) J. Chipman, *J. Am. Chem. Soc.*, **83**, 1762 (1961).

CATALYTIC ACTIVITY AND SINTERING OF PLATINUM BLACK. I. KINETICS OF PROPANE CRACKING[1]

By D. W. McKee

General Electric Research Laboratory, Schenectady, New York

Received September 26, 1962

The activity of unsupported platinum black for the catalytic cracking of propane has been studied between 100 and 200° by a static volumetric technique. The results indicated that the specific activity of platinum (activity per unit area of catalyst surface) was considerably less than that of nickel for this reaction. However, the activity of platinum black was very dependent on the degree of sintering, a process which occurred readily with the reduced metal at temperatures above 100°. The specific activity of the metal decreased rapidly as sintering proceeded, indicating that the sintering process involved reduction in both surface area and density of surface sites (vacancies or point defects) which were responsible for the catalytic activity. The ratio of ethane:methane in the products of cracking of propane was generally greater for platinum than for nickel. The activation energy for the cracking reaction was found to be 24 kcal./mole but this value decreased with increasing density of active sites.

Introduction

Platinum catalysts for use in gas phase hydrocarbon reactions are generally employed in the supported state, the essentially inert support providing mechanical strength and inhibiting the sintering of the finely divided metal. For certain purposes, however, it is necessary to use the metal in the unsupported powdered form. For example, in the preparation of electrodes for fuel cells, the metal particles must be in good electrical contact and possess a high surface area; hence platinum black is widely used as an electrode material[2]

(1) This work was made possible by the support of the Advanced Research Projects Agency (Order Number 247-61) through the United States Army Engineer Research and Development Laboratories, Ft. Belvoir, Virginia, under Contract Number DA-44-009-ENG-4853.

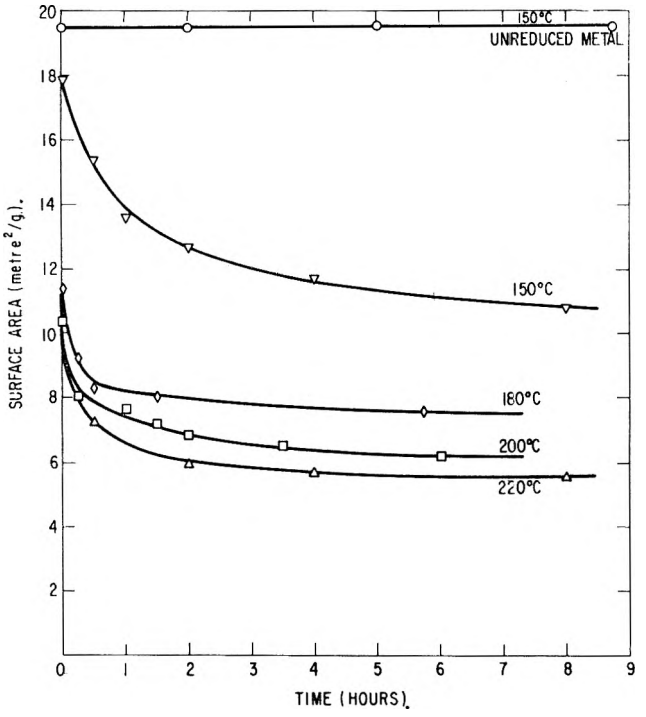

Fig. 1.—Sintering of platinum black: surface area (m.²/g.) *vs.* time (hr.).

in these devices. For this reason and because of the lack of available information on the change of catalytic activity of platinum black as a function of sintering, it was decided to study this effect for the cracking of propane at elevated temperatures. It was hoped to compare the results of this work with those of previous investigations of the kinetics of propane cracking on unsupported nickel[3a] and on evaporated rhodium films prepared under ultra-high vacuum.[3b]

Although it has been known for many years[4] that hydrocarbons crack on metals at elevated temperatures, there have been few detailed studies of these reactions. Most of the literature on catalytic cracking has been devoted to the behavior of acidic materials such as aluminosilicates, which are commercially more important than metals for this purpose. However, the cracking of hydrocarbons on metallic catalysts is important in fuel cell technology as methane is inert electrochemically except at high temperatures and extensive cracking of hydrocarbon fuels on the electrodes could limit the performance of hydrocarbon fuel cells above 100°.

Experimental

Apparatus.—The static volumetric technique used in this work has been described previously.[3a] Samples of platinum black were sealed into the apparatus and protected from mercury vapor by means of gold foil traps. Small plugs of glass wool prevented blowing of the catalyst during evacuation. The platinum black was found to be initially covered with a layer of chemisorbed oxygen and this was removed by reduction with hydrogen, obtained by diffusion through a palladium thimble. Considerable difficulty was experienced, however, in maintaining the high surface area of the catalyst during the reduction, as the heat liberated during the removal of the chemisorbed oxygen was often sufficient to cause appreciable sintering and consequent loss in area of the metal, as is discussed below. The most favorable procedure was found to consist in initially cooling the metal to 0° in a bath of melting ice and carrying out the reduction slowly with about 10% hydrogen in a stream of nitrogen at 15–20 cm. pressure. After reduction at 0° for 30 min., the metal was then allowed to warm up to room temperature and the reduction continued for a further 30 min. Finally the reduced metal was evacuated at 100° to a residual pressure less than 1×10^{-6} mm. before the catalytic measurements were carried out. Even with this technique it was found that at least 10% of the initial surface area was lost during the reduction.

The adsorption and cracking of propane was studied by allowing a measured quantity of propane to stand over the metal for varying periods of time, changes in gas pressure being followed by means of a wide bore mercury manometer to within ±0.01 mm. The temperature of the catalyst was kept constant during runs by means of a Honeywell controller and furnace to within ±0.5°. Analysis of the products of reaction were carried out on condensed portions of the gas phase by means of an F & M temperature programmed gas chromatograph, using an 8 ft. silica gel column and helium as carrier gas. In most of the cracking experiments, the initial pressure of the propane in the storage part of the apparatus was adjusted to about 17.5 mm. After expansion into the catalyst bulb, the initial pressure over the metal was about 14.6 mm. in a total gas volume of 117.7 ml. These values, however, depended somewhat on conditions. Although liberation of methane by catalytic cracking generally resulted in a rise in gas pressure over the metal, an initial rapid chemisorption of propane occurred in every case, so that the pressure fell to a minimum value during the first few minutes of contact. After generally one hour contact the final gas pressure was read, a known fraction of the gas phase condensed into sample bulbs cooled in liquid nitrogen, and the composition of the gas phase was calculated from the gas chromatographic analysis. The residual non-condensable pressure after cooling in the traps was found to be due only to methane, no hydrogen being detected in any of the measurements.

The change in surface area of the platinum black was followed by nitrogen adsorption at −195° and application of the B.E.T. method, the generally accepted value of 16.2 Å.² being used for the cross-sectional area of the nitrogen molecule in the surface area calculations. Surface area determinations and cracking activity measurements were often carried out alternately, but owing to the fact that the cracking reaction generally resulted in the formation of a non-volatile carbonaceous deposit on the metal surface, which was only removed by prolonged reduction at elevated temperatures, fresh samples were generally used for each catalytic run. Nitrogen and physically adsorbed propane could, however, be removed reversibly by evacuation at room temperature and hence the sintering process could be followed by alternate heating periods and nitrogen adsorption measurements. The carbonaceous residue mentioned above could be removed by reduction for 2 hours at temperatures above 150°, but this treatment generally resulted in a large decrease in surface area of the black.

Materials.—The platinum black used in this work was obtained from Fisher Co. and was of high purity (>99.8%). The unreduced metal had a B.E.T. nitrogen surface area of 19.5 m.²/g. Examination by electron microscopy revealed that the black consisted of roughly spherical particles, probably microcrystallites, of approximately 100 Å. diameter.

Phillips "Research Grade" 99.98% pure propane was used throughout, the gas being condensed and fractionally distilled from a trap cooled in liquid nitrogen before being admitted into the apparatus.

Results

Sintering of Platinum Black.—The loss of surface area of the platinum black as a function of time at different temperatures is shown in Fig. 1, the surface area being measured by nitrogen adsorption as described above. Owing to the rapid and unavoidable decrease in surface area during the reduction process, it was difficult to obtain reproducible results or to examine quantitatively the kinetics of the sintering process. However the metal lost up to 50% of its surface area during the first 30 min. of heating at the sintering temperature, this rapid decrease being followed by a more gradual loss in area which continued for a con-

(2) E. J. Cairns, D. L. Douglas, and L. W. Niedrach, *A.I.Ch.E. J.*, **7**, 551 (1961).

(3) (a) D. W. McKee, *J. Am. Chem. Soc.*, **84**, 4427 (1962); (b) R. W. Roberts, *J. Phys. Chem.*, **66**, 1742 (1962).

(4) *E.g.*, F. E. Frey and D. F. Smith, *Ind. Eng. Chem.*, **20**, 948 (1928).

siderable period. Even after sintering at 200° for over 8 hours, the metal showed a residual porosity and surface area of over 5 m.²/g. Similar characteristics are shown during the sintering of other materials, such as magnesium oxide.[5] Figure 1 also illustrates the effect of an adsorbed film of oxygen on the sintering process, the unreduced metal remaining unchanged in surface area after heating for over 8 hours at 150°, whereas the reduced metal showed a decrease of over 40% during the same period. It is probable that chemisorbed layers of other substances, for example hydrocarbons, would also tend to inhibit the sintering process. Measurements of sintering below 150° were difficult owing to the fact that temperatures of at least 100° were necessary to remove chemisorbed hydrogen after the reduction process. For this reason maxima were sometimes found in the curves of surface area *vs.* time for temperatures below 100°. These results are not shown in Fig. 1.

Electron micrographs were also used to follow the changes which took place during sintering. The particles in the original unsintered black were quite uniform, roughly spherical in shape and of approximately 100 Å. in diameter. The particles readily aggregated into loose clusters in which, however, the individual particles remained discernable. After sintering at 200° for four hours, the particles had fused together into irregular amorphous conglomerates which still retained some porosity. This coalescence of the metallic particles was attended by a contraction and increase in density of the catalyst mass.

Cracking of Propane on Platinum Black.—The products of the cracking of propane on platinum black between 100 and 200° were found to be methane, small amounts of ethane and a carbonaceous residue of variable composition $(CH_n)_x$ which remained on the solid surface. No hydrogen, olefins or higher paraffins were detected in the gaseous products. Identical products were obtained from the cracking of propane on evaporated rhodium films at 100°.[3b] As with nickel,[3a] the surface residues remaining after reaction tended to poison the metal. These residues were not desorbed by evacuation at the reaction temperature but reduction with hydrogen at 150° and above for several hours was necessary to regenerate the activity of the metal. However, such drastic treatment usually resulted in substantial sintering of the metal and, for this reason, a fresh sample was generally used for each catalytic run.

At the beginning of this investigation it became apparent that the catalytic activity of the metal depended to a large extent on the degree of sintering which had taken place. If this involved merely the reduction in surface area without decrease in the density of catalytically active sites, then the specific activity of the metal (activity/surface area) should be a constant throughout the sintering process. Figure 2 illustrates the results of a number of measurements of platinum black samples with various degrees of sintering, the BET nitrogen surface area being determined before each catalytic run. The catalytic activity of the metal was determined by measuring the amount of methane formed after one hour contact with propane at the same initial pressure. As the rate of methane evolution was found to be approximately linear with respect to

(5) S. J. Gregg, R. K. Packer, and K. H. Wheatley, *J. Chem. Soc.*, 46 (1955).

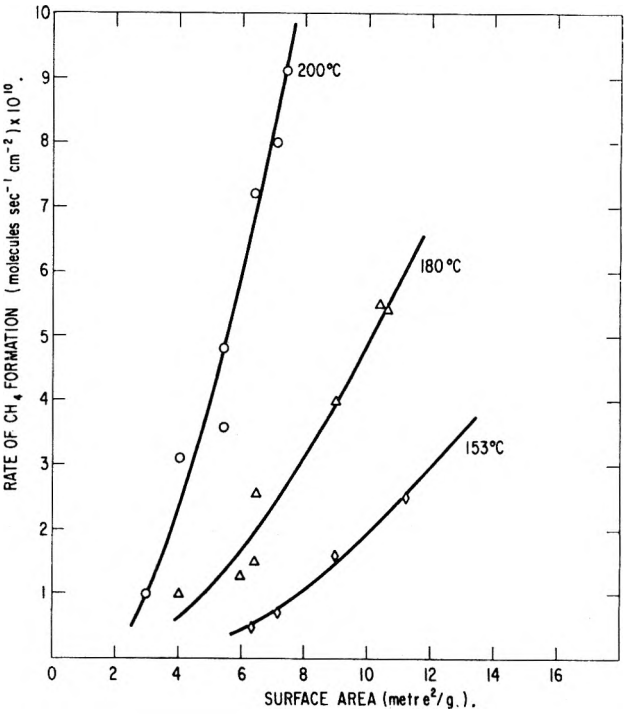

Fig. 2.—Change of catalytic activity of Pt black during sintering: initial C_3H_8 pressure = 14.6 mm.; 1 hr. contact time.

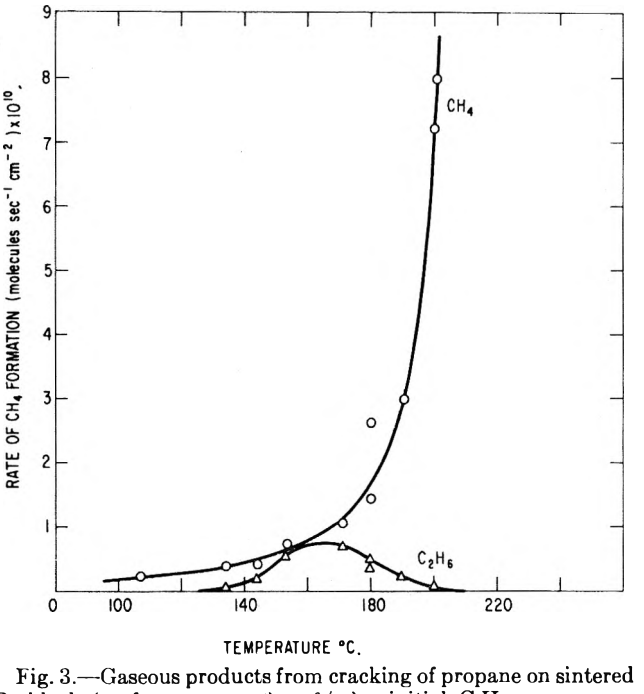

Fig. 3.—Gaseous products from cracking of propane on sintered Pt black (surface area ~6 m.²/g.): initial C_3H_8 pressure = 14.6 m.; 1 hr. contact time.

time for at least one hour at the beginning of the reaction, the specific activity was then calculated in molecules CH_4 sec.$^{-1}$ cm.$^{-2}$. The total amount of methane produced was always less than 30% of the propane present, so that an excess of the latter remained in contact with the metal at all times. The results of Fig. 2 indicate that, far from being constant, the specific activity decreases rapidly with loss of surface area, the rate of decrease increasing with increasing temperature. Although some additional sintering may have taken place during the catalytic run, this effect is likely to have been reduced by the presence of the film of adsorbed propane. However, if the measured nitrogen

surface area values are slightly high, the true values would tend to accentuate the effect shown in Fig. 2.

Small amounts of ethane were also produced during the cracking reaction, as shown in Fig. 3, which gives the average yields of the two gaseous products as a function of temperature for sintered samples of approximate area 6 m.²/g. The volume of ethane produced, although small, reached a maximum at about 170°. The yield of methane increased rapidly above 150° and from the rate of formation of methane with temperature the apparent activation energy was calculated to be 24 ± 1 kcal./mole and the frequency factor A (in molecules sec.$^{-1}$ cm.$^{-2}$) was given by log A = 20.5 ± 0.3.

The liberation of methane was always observed to be preceded by adsorption of propane on the metal surface and it was possible to measure the extent of this adsorption at temperatures too low for cracking to be appreciable. At 0° a platinum black sample, having a B.E.T. nitrogen surface area of 16.7 m.²/g., required 1.47 ml. STP/g. of propane to cover the surface with a monolayer (calculated from the BET plot for the propane adsorption isotherm), whereas a sintered sample with 6.8 m.²/g. surface area adsorbed 0.6 ml. STP/g. propane in the monolayer. The ratios of nitrogen surface area to propane monolayer values are identical in the two cases, indicating that no "molecular sieve" effect was responsible for excluding propane from the pores of the sintered sample, the loss in catalytic activity being entirely due to the elimination of active sites. The adsorption of propane at 0° was physical in nature and entirely reversible, the effective cross-sectional area of the propane molecules in the monolayer being 41 Å.² compared with 16.2 Å.² for nitrogen. This value is reasonable in comparison with the value of 27.4 Å.² which is frequently shown by propane physically adsorbed at its boiling point of −42°.[6]

Discussion

Mechanism of Sintering of Platinum Black.—The sintering of a finely divided metal results in a decrease in the surface free energy and a consequent loss in the area of the solid-gas interface. This process is of great importance in ceramics and powder metallurgy and the subject has an extensive literature.[7] The material transport involved during sintering can take place by several different mechanisms, for example, (i) evaporation and condensation as a result of differences in vapor pressures over the curved solid surfaces, (ii) viscous flow and plastic deformation at points of contact, and (iii) surface diffusion and migration of vacancies. In the present case, mechanisms (i) and (ii) seem unlikely owing to the low vapor pressure and high melting point of platinum, however the physical properties of platinum in fine dispersion may be quite different from those of the bulk metal. Plastic flow is not generally considered appreciable at least until the Tammann temperature ($0.5T_m$, where T_m is the melting point of the solid) is reached but migration of defects can take place at much lower temperatures. Thus lattice vacancies could migrate away from the contact area between two spherical particles and be discharged at the surface or at grain boundaries (if these exist in the microcrystallites of the Pt black). As a result a net transfer of material to the contact zone would occur and growth of necks between particles take place. Calculations based on this model[8] yield the relation

$$\frac{x}{r} = kr^{-3/5}\,t^{1/5}$$

where x is the neck radius, and r is the radius of the spherical particle. No exact formulation of this process is possible as the relation between the increase in neck radius and decrease in surface area is not known and, in any case, the variation of sintering rate with particle size and temperature for real systems of irregular particles would be too complex to be represented by this equation. However, the data of Fig. 1 were found to give straight lines of constant slope when log s was plotted against log t, for times greater than 15 min. This result suggests that the sintering process follows the relation, $s = Kt^{-0.11}$, where K is a function of temperature.

The initial rapid decrease in surface area can be attributed to the large amount of heat liberated during the reduction process. The heat evolved during the reaction

$$PtO + H_2(g) \longrightarrow Pt + H_2O(ads.)$$

has recently been determined to be 42 kcal./mole of H_2.[9] This heat, unless dissipated rapidly, would be capable of producing high local temperatures at asperities and points of contact of the metal particles, even when the catalyst mass is cooled to temperatures as low as 0°. It may be possible to reduce this initial sintering further by using lower concentrations of hydrogen in the carrier gas stream.

Sintering and Catalytic Activity.—The marked dependence of catalytic activity on extent of sintering, shown in Fig. 2, is consistent with the idea that the sintering process involves the migration and elimination of surface defects which may be responsible for the activity of the metal in the cracking reaction. Such an effect has rarely been reported before. In a recent authoritative work on catalysis,[10] the author states, "No successful attempt has been made to demonstrate an inherent change in catalytic activity per atom or per unit weight with particle size, as might be expected if very small particles had properties significantly different from those of the massive metal. Such effects as have been observed are adequately interpreted in terms of the varying surface area." Previous failure to observe this effect may have been due to the fact that catalysts are usually chosen which have been annealed to a stable state before use. However, it has been found possible to induce catalytic "superactivity" in copper and nickel wires by flashing at high temperature.[11] It is suggested that the enhanced activity is due to the production of a high concentration of vacancies by the flashing procedure. Assuming that a similar process operates in the case of platinum black,

(6) D. W. McKee, *J. Phys. Chem.*, **63**, 1256 (1959).

(7) *E.g.*, W. D. Kingery, "Introduction to Ceramics," John Wiley and Sons, New York, N. Y., 1960, p. 369.

(8) R. L. Coble, *J. Am. Ceram. Soc.*, **41**, 55 (1958).

(9) H. Chon, R. A. Fisher, E. Momezsko, and J. G. Aston, "Proc. 2nd. International Congress on Catalysis," Paris, 1960, paper 3.

(10) G. C. Bond, "Catalysis by Metals," Academic Press, New York, N. Y., 1962, p. 31.

(11) M. J. Duell and A. J. B. Robertson, *Trans. Faraday Soc.*, **57**, 1416 (1961).

the rate of the cracking reaction will be related to the activation energy for the disappearance of active sites and to the true activation energy for the cracking reaction. Hence, for a first-order reaction, the rate of methane formation in molecules cm.$^{-2}$ sec.$^{-1}$ is given by

$$v = c_g c_s \frac{kT}{h} \frac{f_{\pm}}{F_g f_s} \exp\left[-\frac{\epsilon_0}{kT}\right]$$

where c_s is the density of active sites at T°K., ϵ_0 is the activation energy of the cracking reaction at the absolute zero, and the other terms have their usual significance.[12] If the number of active sites per cm.^{2} decreases with increasing temperature as a result of sintering according to the relation

$$c_s = c_0 \exp\left[\frac{E_D}{kT}\right]$$

where E_D is the activation energy for the elimination of active sites, than the apparent rate of the cracking reaction is

$$v' = c_g c_s \frac{kT}{h} \frac{f_{\pm}}{F_g f_s} \exp\left[\frac{-(\epsilon_0 - E_D)}{kT}\right]$$

Although the rate law for the disappearance of active sites is not known the over-simplified equation above suggests that the removal of active sites should give rise to an increase in the apparent activation energy for the cracking reaction. This effect was in fact observed, as shown in Fig. 4, the value of E varying by a factor of almost two between the fresh and completely sintered catalyst.

Comparison of Propane Cracking on Nickel and Platinum Catalysts.—A comparison can be made between the rates of propane cracking on platinum black and on nickel previously reported.[3a] Although the measurements with nickel were carried out with a lower initial pressure of propane (5.6 mm., compared with 14.6 mm. in the present work), the rate of cracking on nickel was considerably greater than that on platinum, even for unsintered samples. Thus the rate constant for methane formation on Ni at 156° was 1.27 × 10^{11} molecules sec.$^{-1}$ cm.$^{-2}$, compared with 2.5 × 10^{10} molecules sec.$^{-1}$ cm.$^{-2}$ for the maximum rate obtainable on Pt black. This generalization may not, however, apply over different temperature ranges. Comparing the nickel results with those of sintered Pt black in Fig. 3, it is apparent that cracking of propane became appreciable at lower temperatures on Ni than on Pt, methane being present in about 2% concentration in the gas phase at 60° with Ni, but only at above 100° with Pt. The kinetic parameters for the two metals are compared in Table I.

TABLE I

Meta	Temp. range, °C.	E (kcal./mole)	log A (molecules sec.$^{-1}$ cm.$^{-2}$)
Ni	130–183	15 ± 1	18.8 ± 0.3
Pt	150–200	24 ± 1	20.5 ± 0.3

The amount of ethane produced during cracking is also different with the two metals, the yield being somewhat greater for platinum than for nickel. The maximum concentration of ethane in the gas phase occurred with Ni at about 130°, the rate of formation of this product then being 0.37 × 10^{10} molecules sec.$^{-1}$ cm.$^{-2}$. By comparison, the maximum yield of ethane occurred with Pt at 170°, the rate then being 0.66 × 10^{10} molecules sec.$^{-1}$ cm.$^{-2}$.

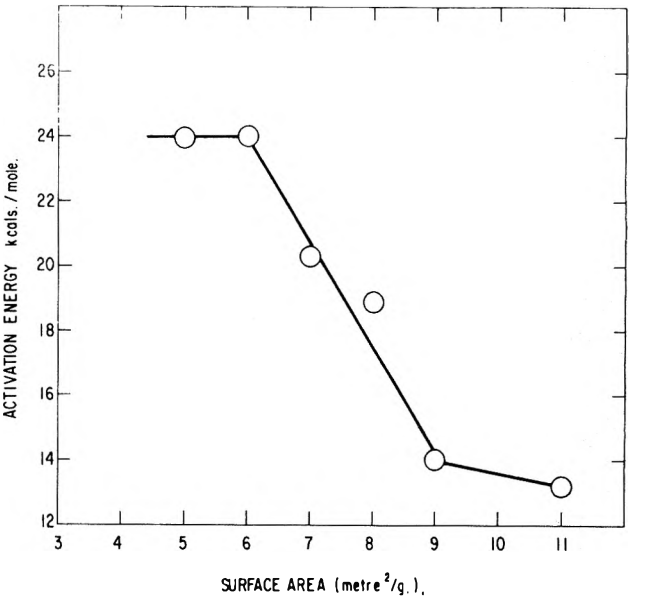

Fig. 4.—Change of activation energy for propane cracking during sintering.

Little information can be obtained concerning the detailed steps involved in the breakup of the propane molecule, although it is probable that the reaction proceeds in a similar way for both nickel and platinum. It seems plausible that the hydrocarbon is initially chemisorbed on the metal surface, almost a monolayer being formed at the lower temperatures before cracking becomes appreciable. Dissociation of the adsorbed hydrocarbon gives rise to mono- and di-carbon fragments and chemisorbed hydrogen atoms which migrate along the surface to hydrogenate the surface radicals to methane and ethane which are desorbed. The concentration of ethane in the gas phase may be limited by cracking at elevated temperatures.

According to the early work of Frey and Smith,[4] the cracking of propane on platinum gives a higher proportion of hydrogen in the products above 400° than does nickel. Although no hydrogen was observed in the gaseous products in the present work, the amount of chemisorbed hydrogen on the metal surface may be greater for Pt than for Ni, which might tend to increase the ethane concentration in the former case. The activation energies shown in Table I above may be compared with the value of 34 kcal./mole found for the hydrocracking of propane on a supported nickel catalyst by Morikawa, Trenner, and Taylor.[13] It is possible that the effect of increasing concentrations of hydrogen in the adsorbed layer is to increase the activation energy for the dissociation of propane. However, in view of the different conditions under which these values were obtained it would be unwise to attach too much significance to this result.

It has been suggested in this work that the activity of platinum black is influenced by the concentration of defects or active sites on the metal surface. However,

(12) S. Glasstone, K. Laidler, and H. Eyring, "The Theory of Rate Processes," McGraw-Hill Book Co., New York, N. Y., 1941, Chap. VII.

(13) K. Morikawa, N. R. Trenner, and H. S. Taylor, *J. Am. Chem. Soc.*, **59**, 1103 (1937).

electronic considerations must also be responsible to some extent for the observed differences between nickel and platinum for this reaction. Both of these metals belong to group $VIII_3$ and therefore possess partially filled d-bands, but it is not possible at this stage to assess the relative importance of morphological and electronic factors in determining the catalytic activity.

Acknowledgments.—The author wishes to thank Dr. E. J. Cairns and W. T. Grubb for many helpful discussions during the course of this investigation.

N.M.R. STUDIES OF HYDROGEN BONDING. I. BINARY MIXTURES OF CHLOROFORM AND NITROGEN BASES[1]

BY PETER J. BERKELEY, JR., AND MELVIN W. HANNA

Department of Chemistry, University of Colorado, Boulder, Colorado

Received October 6, 1962

A discussion is given of the theory of the dilution-shift technique for examining 1:1 hydrogen-bonded complexes by n.m.r. It is shown that at infinite dilution of the proton donor in an acceptor solvent, the limiting slope and the intercept (the limiting shift) of a plot of donor concentration *vs.* shift of the donated proton is sufficient to determine uniquely the equilibrium constant for hydrogen-bond formation and the shift of the pure hydrogen-bonded species. A method for taking solvent effects into account is included. Data for chloroform plus pyridine, ethylideneisopropylimine, acetonitrile, and N-methylpyrrolidine are reported. These data are analyzed by the above theory and the importance of solvent effects is evaluated. A qualitative discussion is given of the calculated equilibrium constants and shifts upon complex formation.

Introduction

It is now well known that the position of a hydrogen-bonded proton in an n.m.r. spectrum is shifted downfield with respect to the position of a non-hydrogen-bonded proton.[2] This shift has become known as the hydrogen-bond shift. In recent years an abundance of experimental information has appeared on many different systems in an attempt to correlate the hydrogen-bond shift with hydrogen-bond strength, infrared stretching frequencies, and other physical properties of the hydrogen-bond.[3] There has been considerable variation in the means of interpreting this data, however, with the result that it is difficult to get a clear picture of the relation between n.m.r. hydrogen-bond shifts and properties of the hydrogen-bond itself.

This recent growth of the literature has also introduced certain nomenclature ambiguities. The situation is aggravated by the fact that two distinct types of dilution-shift experiments may be carried out. In the case of hydroxylic materials, one compound can act as both proton donor and acceptor, and here it is usual to observe the shift of the hydroxyl proton as such a compound is diluted with *inert* solvent. This paper concerns itself, however, with the situation where a proton donor is diluted with *acceptor* and the shift of the donated proton observed. It is common to utilize, in both cases, the shift at infinite dilution of the acid–base in the first case, or of the acid in the second case. These two kinds of infinite dilution shifts, however, have quite a different significance. Unless otherwise stated, all that follows will be concerned with the second case.

A further nomenclature difficulty involves the meaning of the phrase "hydrogen-bond shift." In both kinds of experiment mentioned above, a distinction should be made between the observed dilution shift and a quantity which can be calculated from this observed shift, the hydrogen-bond shift of pure dimer. In this paper the former quantity will be distinguished from the latter by being called the *observed* H-bond shift.

It is the purpose of this paper to present a simplified approach that is applicable to the study of 1:1 hydrogen-bonded complexes by n.m.r. and to point out the significance of "observed H-bond shifts" as a criterion of hydrogen-bond strength. Specifically, it will be shown that for the case of a 1:1 complex the data relating the chemical shift of the donated proton to apparent concentration of this proton are sufficient to determine uniquely the association constant of the complex without resorting to iterative procedures, to curve fitting, or to information from other sources (such as infrared). This theory is then applied to data for the association of chloroform with pyridine, acetonitrile, ethylideneisopropylimine, and N-methylpyrrolidine.

Theory

Consider the equilibrium

$$A + D \rightleftharpoons AD$$

where A is the proton acceptor and D, the donor. If the usual[4] assumption is made that the system is an ideal mixture of species (after the above equilibrium has been taken into account), concentrations can be substituted for activities and the equilibrium expression takes the form

$$K = \frac{X_{AD}}{X_A X_D} = \frac{\lambda}{(N_A^0 - \lambda)(N_D^0 - \lambda)}(N_A^0 + N_D^0 - \lambda) \quad (1)$$

where the X's are the mole fractions, the N^0's are the initial number of moles, and λ is the moles of complex at equilibrium. Applying equation 1 to cases where only an average spectral line is observed for the hydrogen-

(1) Supported in part by Grant GM 09187-01S1 from the National Institutes of Health, Public Health Service.

(2) See for instance: J. A. Pople, W. G. Schneider, and H. J. Bernstein, "High Resolution Nuclear Magnetic Resonance," Chapter 15, McGraw-Hill Book Co., New York, N. Y., 1959.

(3) G. C. Pimentel and A. L. McClellan, "The Hydrogen Bond," W. H. Freeman and Co., San Francisco, Calif., 1960. Chapter 4.

(4) J. E. Hildebrand and R. L. Scott, "The Solubility of Non-electrolytes," 3rd Edition, Chapter XI, Reinhold Publ. Corp., New York, N. Y., 1950.

bonded and non-hydrogen-bonded protons, Huggins, *et al.*,[5] have shown that

$$\delta_0 = \frac{K}{1 + K}(\delta_{AD} - \delta_D) + \delta_D \qquad (2)$$

where δ_0, δ_{AD} and δ_D are the chemical shifts of the donated proton in infinitely dilute donor, of the pure complex, and of the pure donor, respectively. For compactness in what follows, the symbol Δ_{AD} will be introduced to represent the hydrogen bond shift of pure donor, *i.e.*, $\Delta_{AD} = \delta_{AD} - \delta_D$. It is necessary to realize here that the above applies only to binary systems with the acceptor being the second component. When one component is both acceptor and donor and the other is inert solvent, the shift at infinite dilution equals that of the monomer.[3]

An important point to be re-emphasized[6] in these equations is that the *observed hydrogen-bond shift* ($\delta_0 - \delta_D$) *depends on both the equilibrium constant, K, and the H-bond shift of the pure dimer*, Δ_{AD}. Thus, when a correlation between n.m.r. data and hydrogen-bond properties is attempted, it is extremely important to state precisely what is being correlated. As shall be seen below, the values of K and Δ_{AD} sometimes go in opposite directions for a series of acceptors with the same donor, and a decision must be made as to which quantity is to be used as a criterion of hydrogen-bond strength. In some cases, however, the observed hydrogen-bond shift is a good criterion of the H-bond shift of the pure dimer. Thus if K is very large $\Delta_{AD} = (\delta_0 - \delta_D)$, but this condition does not hold in many instances.

Additional information can still be obtained from the data, however. The use of limiting slope in n.m.r. studies of hydrogen-bonding was introduced in connection with self-association of phenols.[7] Applying standard mathematical procedures to a plot of observed chemical shift *vs.* apparent mole fraction of acceptor, the slope at high X_A^0 is given by

$$\frac{d\delta}{dX_D^0} = -\Delta_A \frac{K}{(1 + KX_A^0)^2} \qquad (3)$$

Therefore the limiting slope, S_0, is

$$S_0 \equiv \left(\frac{d\delta}{dX_D^0}\right)_{X_D^0 \longrightarrow 0} = -\Delta_{AD}\frac{K}{(1+K)^2} \qquad (4)$$

Now if Δ_{AD} is eliminated between (2) and (4)

$$\Delta_{AD} = \frac{1 + K}{K}(\delta_0 - \delta_D) = -S_0\frac{(1 + K)^2}{K} \qquad (5)$$

and

$$K = \left(\frac{\delta_0 - \delta_D)}{-S_0}\right) - 1 \qquad (6)$$

Thus S_0 (the limiting slope) and δ_0 (the shift at infinite dilution) of a plot of observed shift *vs.* proton donor concentration are sufficient information to yield Δ_{AD} and K uniquely.

Equation 6 is not satisfactory, however, in the cases where $\delta_0 - \delta_D$ is small (say less than 1.0 p.p.m.) because it is known that the chemical shift is solvent dependent.[8] That is to say, part of the observed H-bond shift, ($\delta_0 - \delta_D$), will be dependent upon the solvent used, unless the shifts are referred to the gas phase. Bothner-By[9] has recently provided an empirical means of taking this into account. He has found that the unexpected downfield shift of a proton in a material "i" dissolved in a solvent "j" can be expressed as a product of two numbers: x_i, characteristic of the compound containing the proton and y_j, characteristic of the solvent. Thus he writes for a cylindrical sample tube

$$\delta_i^j = \delta_i^0 - x_i y_j + \frac{2\pi}{3}\chi_j \qquad (7)$$

where δ_i^0 is the shift of the proton in the gas phase and χ_j is the volume diamagnetic susceptibility of the solvent.

Experimentally, δ has to be observed with respect to some reference compound, either external or internal. If the absolute shift of an internal reference is δ_r, the measured shift (δ_M) can then be expressed as

$$\delta_M = \delta - \delta_r$$

If equations 5 and 6 are now rederived with the inclusion of solvent effects, there results

$$\Delta_{AD} = \frac{1 + K}{K}[(\delta_M)_0 - \Delta^0 + y_A\Delta_x] \qquad (8)$$

and

$$K = \left[\frac{(\delta_M)_0 - \Delta^0 + y_A\Delta_x}{-S_0 + \Delta_x\left(\frac{dy_A}{dX_D^0}\right)_0}\right] - 1 \qquad (9)$$

where $(\delta_M)_0$ is the measured shift at infinite dilution, y_A is the "y_j" of the acceptor (base), and Δ_x is the difference in x value between donor and reference. The term Δ^0, which is the gas phase difference in shifts between pure donor and reference, can be obtained by an independent measurement in the gas phase or it can be obtained from liquid phase measurements using equation 7 if the appropriate x and y values and susceptibilities are known. The use of equation 8 eliminates the influence of differential solvent effects on donor and reference. It automatically takes into account the small self-association of chloroform,[10] for example.

Experimental

The reagent grade chloroform used was extracted with water to remove alcohol, dried over anhydrous potassium carbonate and distilled immediately before use. Reagent grade cyclohexane was used without further purification. Reagent grade pyridine was dried over anhydrous K_2CO_3 and distilled. N-Methylpyrrolidine, obtained from the Aldrich Chemical Company, was placed in contact with metallic sodium overnight and then distilled from over metallic sodium. Reagent grade acetonitrile was extracted with a saturated solution of potassium hydroxide, dried over anhydrous K_2CO_3, and then distilled over K_2CO_3. The ethylideneisopropylimine was prepared in the manner outlined by Campbell, *et al.*[11]

(5) C. M. Huggins, G. C. Pimentel, and J. N. Shoolery, *J. Chem. Phys.*, **23**, 1244 (1955).

(6) This point was made sometime ago by Huggins, *et al.*, ref. 5.

(7) C. M. Huggins, G. C. Pimentel, and J. N. Shoolery, *J. Phys. Chem.*, **60**, 1311 (1956); see also E. D. Becker, U. Liddel, and J. N. Shoolery, *J. Mol. Spectry.*, **2**, 1 (1958).

(8) Reference 1, Chapter 16.

(9) A. A. Bothner-By, *J. Mol. Spectry*, **5**, 52 (1960).

(10) C. F. Jumper, M. T. Emerson, and B. B. Howard, *J. Chem. Phys.*, **35**, 1911 (1961).

(11) K. N. Campbell, A. H. Sommers, and B. K. Campbell, *J. Am. Chem. Soc.*, **66**, 82 (1944).

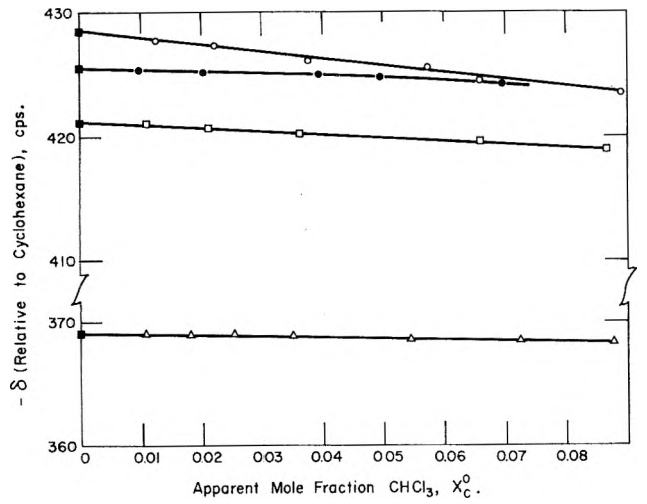

Fig. 1.—Plots of the shift of the chloroform proton (with respect to an internal cyclohexane standard) at low chloroform concentrations in various bases: O, pyridine; ●, ethylidene-isopropylimine; □, N-methylpyrrolidine; △, acetonitrile.

The samples were prepared by weight and were approximately 5 ml. in volume to which about 0.2 ml. of cyclohexane was added. A Varian A-60 analytical spectrometer was used. The audio side band technique was employed to measure the separation of the $CHCl_3$ and internal C_6H_{12} reference. All measurements were made at 37.5 ± 1.0°. Duplicate runs on the same samples indicated a measurement error of about ±0.1 c.p.s. Most error, therefore, arose from uncertainties in the concentrations due to evaporation.

Results and Discussion

The observed shift of the chloroform proton was measured at low concentrations (less than 0.1 mole fraction $CHCl_3$) in binary mixtures of $CHCl_3$ + pyridine, $CHCl_3$ + CH_3CN, $CHCl_3$ + $CH_3CH{=}NCH(CH_3)_2$, and $CHCl_3$ + N-methylpyrrolidine. The experimental points are plotted in Fig. 1 along with the least-square lines (found assuming all error in $CHCl_3$ concentration). The slopes and intercepts found are listed in Table I.

TABLE I

EXPERIMENTALLY OBSERVED PROPERTIES OF CHLOROFORM–PROTON ACCEPTOR SOLUTIONS[a]

Proton acceptor	$(\delta_M)_0$, c.p.s.	S_0, c.p.s./m.f.
Pyridine	−428.5	56.5
N-Methylpyrrolidine	−421.2	26.6
$CH_3CH{=}NCH(CH_3)_2$	−425.4	14.0
Acetonitrile	−369.1	6.84

[a] Shifts were measured at 60 Mc. and negative numbers refer to lines downfield from the internal cyclohexane reference.

Data were also obtained over the whole concentration range of $CHCl_3$ + pyridine; and the curve had the S-shape characteristic of complex-forming systems.

Of course, the above theory cannot be used unless one is dealing with 1:1 complexes. That such is the case with chloroform and nitrogen bases is very plausible for three reasons: A 1:1 complex is the most reasonable on structural grounds; higher complexes would not give straight lines at low X_D^0; and, finally, freezing point–concentration data of Korinek and Schneider[12] indicate the formation of 1:1 complexes at low chloroform concentrations.

Before this data could be used for calculations, the contributions from the solvent effect terms in equations 8 and 9 had to be evaluated. The various x's and y's were obtained[13] by experiments using concentric sample tubes in conjunction with equation 7. For instance, in order to calculate the y_A's, a drop of A in cyclohexane was placed in the center tube and pure cyclohexane in the other tube, $\delta_r^r - \delta_r^A$ measured, and the following equation applied

$$y_A = \frac{(\delta_r^r - \delta_r^A) + x_r y_r + \frac{2\pi}{3}(\chi_A - \chi_r)}{x}$$

The susceptibilities needed were obtained from reference (2) (except as listed in Table II) and corrected for temperature. The quantity $(dy_s/dX_D^0)_0$ was found to be negligible.

The observed hydrogen-bond shifts corrected for solvent effects are given in Table II, along with the solvent effect parameters needed for these corrections. (Note that Δ^0 was obtained from a gas phase measurement of W. G. Schneider.[14]) Significant contributions from solvent corrections (>10%) are not obtained until $(\delta_M)_0$ falls below 1.0 p.p.m., which is the case only with acetonitrile. It is of interest that the values of the solvent effect-corrected shifts of pyridine and acetonitrile are in good agreement with those found by Martin[15] for what she calls Δ_∞ (shift of pure liquid chloroform minus shift of infinitely dilute chloroform).

TABLE II

INFLUENCE OF SOLVENT EFFECT CORRECTIONS UPON OBSERVED HYDROGEN BOND SHIFTS

Proton acceptor	$-\chi_A \times 10^6$	y	$y\Delta_x$, c.p.s.	$(\delta_M)_0 - \Delta^0 + y_s\Delta_x$, c.p.s.
Pyridine	0.600[a]	− .078	−4.3	−95.6
N-Methylpyrrolidine	.710[b]	~0	0	−84.0
$CH_3CH{=}NCH(CH_3)_2$	.509[c]	0.037	2.0	−86.2
Acetonitrile	.514[d]	0.059	3.2	−28.7

[a] Reference 2 after correction to 37.5°. [b] Estimated from that of pyrrolidine found in A. Pacault, *Ann. Chim.* [12], **1**, 527 (1946). [c] Measured using the A-60 spectrometer, see equation (4-2), page 79, in reference 2. [d] H. Francois and J. Hooran, *Compt. rend.*, **240**, 1220 (1955).

In Table III are listed the values of K and Δ_{AD} calculated using equations 8 and 9, neglecting the derivative in the denominator of equation 9. It would be tempting to spend some discussion on the relative order of magnitudes of the derived K's. However, it is felt at this time that such discussion would of necessity be highly speculative. Experiments are currently under way to determine the full significance of these K's. ΔH^0 values for such weak interactions will be sufficiently small that the ΔS^0 values will be of major

TABLE III

CALCULATED PROPERTIES OF CHLOROFORM–PROTON ACCEPTOR SOLUTIONS

Proton acceptor	K	Δ_{AD} c.p.s.	Δ_{AD} p.p.m.
Pyridine	0.69	−234	−3.90
N-Methylpyrrolidine	2.2	−123	−2.05
$CH_3CH{=}NCH(CH_3)_2$	5.2	−119	−1.98
Acetonitrile	3.2	− 37.6	−0.63

(12) G. Korinek and W. G. Schneider, *Can. J. Chem.*, **35**, 1157 (1951).

(13) The x's for cyclohexane and chloroform were found to be 5.1 and 7.0, respectively. y of cyclohexane is given by Bothner-By[9] as 0.033. All other y's used are given in Table II.

(14) Private communication: −337.2 c.p.s. (at 60 Mc.) after correction from a gaseous neopentane reference to a gaseous cyclohexane reference.

(15) M. Martin, *Ann. Phys.*, **7**, 35 (1962).

significance in determining K. However, these values are of the correct magnitude as can be seen by comparison with data of Huggins[5] for triethylamine–chloroform and with that of Jumper[16] for acetonitrile– and pyridine–chloroform. Classical physical chemistry techniques also give similar results. For example, for the chloroform–dioxane system,[17] $K_1 = 1.1$. It should not be expected, however, that these K's will follow the same order as found for the K_B's of the same bases because of the lesser importance of entropy effects.

The calculated Δ_{AD}'s are of interest, however, because they *do appear* to be related to the basicity of the acceptor. At the same time, they demonstrate the care which must be exercised when n.m.r. data are compared with other properties of hydrogen-bonded systems. On the basis that the base strength (K_B) is what determines the strength of the hydrogen-bond shift and hopefully the value of Δ_{AD}, one would expect the Δ_{AD}'s to decrease in the order $sp^3 > sp^2 > sp$.[18] In fact, with the exception of pyridine this is the order that is observed even though the sp^2 and sp^3 unshared pairs give Δ_{AD}'s which are very close to each other. This correlation, however, must take magnetic anisotropy effects into account. Thus, there is an *additional* downfield shift in the pyridine–chloroform complex because of the aromatic ring currents[19] in the base. The Δ_{AD} in pyridine is, therefore, *not a measure of a property of the hydrogen-bond until the effect of the aromatic ring currents has been subtracted out.* A similar argument can be applied to acetonitrile except that in this case paramagnetic contributions to the nuclear screening of the hydrogen-bonded proton produce an *upfield* shift. The "true" hydrogen-bond Δ_{AD} is therefore larger than the Δ_{AD} in Table III. A schematic representation of these effects is shown in Fig. 2. It is also highly possible that a larger difference between sp^3 and sp^2 unshared pair shifts would be found if the paramagnetic contribution to the shift due to the carbon–nitrogen double bond were subtracted. Since theoretical estimations of these effects are about as uncertain as the magnitudes of Δ_{AD}'s themselves, it is difficult to take these contributions into account in any satisfying quantitative way. The basic point is that it would be unsound to try to correlate these n.m.r. shifts in any more than a general way with the properties of the hydrogen bond formed in these systems, but it does seem that the general order of expected H-bond strength $sp^3 > sp^2 > sp$ is confirmed for the non-aromatic compounds since it is likely that the correction to the acetonitrile would be of the order of 0.5 p.p.m.[20]

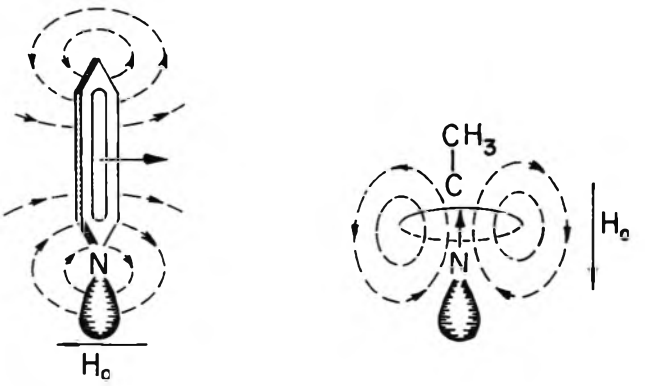

Fig. 2.—Schematic representation of ring currents in pyridine and acetonitrile. The small arrows in the center of the ring represent the direction of the field induced by H_0, the applied field. The dashed lines represent the lines of force of the induced field; and their direction at the nitrogen lone-pair orbitals indicate whether the induced field adds to or subtracts from H_0 from the point of view of the chloroform proton.

It appears on the basis of the above work, therefore, that in cases where the magnetic anisotropy does not vary greatly, Δ_{AD} might be a useful criterion of H-bond and could be correlated with other properties such as infrared hydrogen-bond shifts.

Acknowledgments.—The authors wish to thank Professor E. King for many helpful discussions, and Dr. W. G. Schneider for communicating his gas phase chloroform shift.

(16) C. F. Jumper, "A Study of Hydrogen Bonding by Dielectric Methods and by Nuclear Magnetic Resonance," Thesis, Florida State University, L. C. Card No. Mic 61-1285 (1961).

(17) M. L. McGlashan and R. P. Rastogi, *Trans. Faraday Soc.*, **54**, 498 (1950).

(18) C. R. Noller, "Chemistry of Organic Compounds," W. B. Saunders Co., Philadelphia, Pa., 1951

(19) J. A. Pople, *Proc. Roy. Soc.* (London), **A239**, 541, 550 (1957).

(20) In reference 2, page 179, a calculated value of 10 p.p.m. is given for the upfield shift of the acetylene proton. Because this shift varies as the reciprocal of the bond length to the third power, the 10 p.p.m. must be multiplied by about $1^3/(\sim 2.7)^3 \approx 0.05$.

THE REACTION OF HYDROGEN ATOMS WITH LIQUID OZONE[1]

By J. A. Wojtowicz, F. Martinez, and J. A. Zaslowsky[2]

Olin Mathieson Chemical Corporation, Organics Division, New Haven, Connecticut

Received October 5, 1962

The reaction of atomic hydrogen with liquid ozone at −196° gives a product which upon warming evolves molecular oxygen and leaves a residue of aqueous hydrogen peroxide. It is shown that under certain reproducible conditions the ratio of evolved oxygen to residual hydrogen peroxide is unity. The absence of hydrogen peroxide as a primary reaction product (under these conditions) was confirmed by infrared examination.

Introduction

Many investigators have reported the formation of hydrogen peroxide in frozen condensates obtained by the reaction of hydrogen and oxygen containing radicals.[3] Despite the general accord regarding the formation of hydrogen peroxide, there is disagreement as to the explanation of the evolution of oxygen which occurs when the condensates are warmed from −196° to

(1) Presented in part at the Fifth International Symposium on Free Radicals, Uppsala, Sweden, July, 1961.

(2) Address inquiries to J. A. Zaslowsky.

(3) (a) A. M. Bass and N. P. Broida, "Formation and Trapping of Free Radicals," Academic Press, New York, N. Y., 1960; (b) G. J. Minkoff, "Frozen Free Radicals," Interscience, New York, N. Y., 1960.

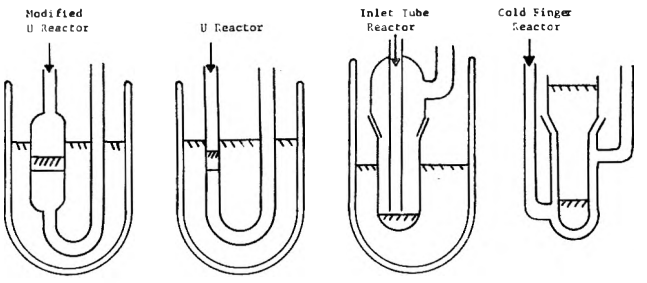

Fig. 1.—Reactors used in the hydrogen atom–liquid ozone studies: →, flow of hydrogen atoms; \\\\, liquid nitrogen; ////, liquid ozone film.

temperatures above −120°. The reported ratios of evolved oxygen to residual hydrogen peroxide vary from about 0.15, in the case of dissociated water vapor, to a value of 1 when hydrogen atoms react with liquid ozone.[4] The suggestion that the oxygen is formed by the decomposition of a hydrogen superoxide was seriously advanced by Ohara,[5] who studied the condensates of dissociated water and the product of hydrogen atom–oxygen reaction. Other theories which have been advanced include the decomposition of an unstable hydrogen peroxide isomer, the decomposition of the solvates $H_2O \cdot O_2$ and $H_2O_2 \cdot O_2$, and the liberation of occluded oxygen at the phase change exhibited by ice–peroxide mixtures at about −115°.

The species responsible for the oxygen evolution cannot be the HO_2 radical on the basis of studies which have indicated that its concentration at the decomposition temperature is negligible.[6]

Kobozev and co-workers[4] have reported that the product obtained by the reaction of a thin film of liquid ozone with hydrogen atoms evolves, upon warming, one mole of oxygen per mole of residual hydrogen peroxide. This unexpected result suggests that the species responsible for the evolved oxygen is hydrogen superoxide

$$H_2O_4 \longrightarrow H_2O_2 + O_2$$

Giguère and Chin[7] claimed to have examined this reaction product by low temperature infrared spectrophotometry and concluded that the only products formed were hydrogen peroxide and water. It was concluded that the reported existence of H_2O_4 was in error.

It was of interest to study the reaction of hydrogen atoms with ozone in order to confirm the stoichiometry of decomposition and to ascertain the experimental conditions which determine the ratio of evolved oxygen to residual hydrogen peroxide.

Infrared examination of the product was undertaken to ascertain whether hydrogen peroxide was present in a frozen matrix which evolved oxygen corresponding to the stoichiometry $H_2O_4 \rightarrow H_2O_2 + O_2$ (at −115°).

Experimental

The Wood discharge tube for producing atomic hydrogen was of conventional design employing aluminum electrodes. A neon sign transformer rated at 9 kv. and 150 ma. was used as a power source. Flow conditions were maintained using a Welch Duoseal vacuum pump (1 mm. pressure).

Ozone was prepared by subjecting oxygen to either glow or silent discharge and condensing the gas at −196° on the reactor wall as a film (5–10 cm.²). The ozone (at −196°) was exposed to a stream of dissociated hydrogen (0.1 to 0.6 mmole H or D/min.) at a linear velocity of 3 to 6 m./sec. The reaction time (10 min. to 2 hr.) usually depended upon the rate of ozone consumption as noted by the disappearance of the blue color. This was shown to be dependent on the reactor design, the amount of ozone, the area of ozone film, the hydrogen atom flow rate and the level of liquid nitrogen refrigerant. The glassy product sometimes had a slightly blue haze due to traces of unreacted ozone. This was removed prior to the evolution of oxygen by evacuating at about −130°. The four reactors used in this study are depicted in Fig. 1.

The quantity of unreacted ozone was determined manometrically by warming the product to about −130° in a calibrated vacuum system. The oxygen evolved from the product (above −120°) was determined after warming the product to about −15°. The residual non-volatile (at −15°) product was analyzed for hydrogen peroxide by a standard permanganate titration. The water content was found by difference from the amount of peroxide and the total product weight.

In some experiments oxygen which was produced during the reaction and which escaped from the reaction zone was catalytically converted to water by reaction with hydrogen over palladium black. The amount of this oxygen was determined by measuring the heat evolved on conversion to water or by determining the amount of water formed by weighing or by use of Karl Fischer reagent.

The hydrogen atom flow rate was determined using an isothermal calorimeter based on the evaporation of liquid nitrogen. It was confirmed[8] that hydrogen atoms recombined quantitatively on passing through a tube cooled to −196°.

The data are summarized in Table I.

TABLE I

THE STOICHIOMETRY OF DECOMPOSITION OF THE REACTION PRODUCT

Expt. no.	mmoles ozone[a]	mmoles residual H_2O_2	mmoles evolved O_2	Reactor	Ratio O_2/H_2O_2
1	2 (initial)	0.18	0.18	U	1.00
2	2 (initial)	.34	.33	U	0.97
3	2 (initial)	.43	.42	U	0.98
4	2 (initial)	.59	.60	U	1.02
5	2 (initial)	.88	.82	U	0.94
7	2.84	1.05	.46	Modified U	.44
8	1.72	0.48	.28	Modified U	.58
9	1.99	.89	.18	Modified U	.20
10	1.03	.54	.31	Modified U	.57
11	0.67	.14	.09	Modified U	.64
13	1.48	.42	.22	Inlet-tube	.52
14	1.37	.22	.18	Inlet-tube	.82
15	1.95	.83	.27	Inlet-tube	.33
17	1.87[c]	1.35		Inlet-tube	
18	1.77[c]	1.41	.32	Inlet-tube	.23
19	2.40[b] (initial)	0.69	.73	Inlet-tube	1.06
20	2.40[b] (initial)	0.43	.40	Inlet-tube	0.93
22	2 (initial)	Trace		Cold finger	
23	2 (initial)	0.65(D_2O_2)	.70	U	1.08
24	2 (initial)	0.41(D_2O_2)	.43	U	1.05

[a] Reacted unless indicated otherwise. [b] The power to the discharge was lowered. The hydrogen atom concentration thus was lowered. [c] Decreased ozone area by forming a pool at the bottom of the reactor.

The low temperature infrared cell used in these studies is of conventional design. The optical system consisted of two sodium chloride windows, sealed to the cell body by means of wax (Cenco Softseal Tackiwax, Central Scientific Co., Chicago, Illinois), and two Irtran-2 windows (Eastman Kodak Company, Rochester, New York) which were used to contain the sample. The Irtran windows (1-in. diam.) were placed in a heavy copper

(4) M. I. Kobozev, I. I. Skorokhodov, L. I. Nekrasov, and E. I. Makarova, *Zh. Fiz. Khim.*, **31**, 1843 (1957).

(5) E. Ohara, *J. Chem. Soc., Japan*, **61**, 569 (1940).

(6) (a) R. Livingston, J. A. Ghormley, and H. Zeldes, *J. Chem. Phys.*, **24**, 483 (1956); (b) A. Gorbanev, S. Kaitmazov, A. Prokhorov, and A. Tsentsiper, *Zh. Fiz. Khim.*, **31**, 515 (1957); (c) unpublished data, these Laboratories.

(7) P. Giguère and D. Chin, *J. Chem. Phys.*, **31**, 1685 (1959).

(8) K. F. Bonhoeffer, *Ergeb. exakt. Naturw.*, 231 (1927).

ring soldered to a 1-in. diam. Kovar–Pyrex seal. This assembly was connected to a vacuum jacket by means of a 45/50 standard taper joint to permit rotation of the Irtran window from the reaction path to the optical path. The temperature of the Irtran window under operating conditions was maintained at −194° to −191°, as determined with an iron–constantan thermocouple. Oxygen and hydrogen at 1–2 mm. pressure, admitted into the system as required through a needle valve, were electrically dissociated using a 125 watt microwave apparatus (Model No. CMD-10, 2450 Mc, Raytheon Manufacturing Company, Waltham, Mass.). The infrared cell was connected to a high speed vacuum pump (Welch Duo-Seal, Model No. 1402, W. M. Welch Manufacturing Company, Chicago, Illinois). The infrared spectra were recorded in the 700 to 4000 cm.$^{-1}$ region with an Infracord spectrophotometer (Model No. 137, Perkin–Elmer Corporation, Norwalk, Connecticut).

The product was prepared by the following techniques:

1. *In situ* on the Irtran window. (a) Using the infrared cell, ozone was deposited on the Irtran window, positioned in the reaction path. The ozone was then exposed to a hydrogen atom stream until the bulk of the ozone had reacted as noted by the disappearance of the blue color. (b) Using an apparatus wherein the Irtran window, maintained at −196°, formed the base of a U-reactor. The lens was transferred to the infrared cell following conversion of the ozone as described in (a).

2. Ozone was condensed on the walls of a U-tube which was cooled to −196°. The cold film was exposed to a stream of dissociated hydrogen until the blue color had essentially disappeared. The U-tube was disconnected from the vacuum line after pressuring with nitrogen. The tube was filled with liquid nitrogen and the product removed from the wall with a spatula. The slurry was placed on the Irtran window (maintained close to −190° by means of liquid nitrogen in the reservoir). The material then was examined as described.

A mixture of gaseous water and hydrogen peroxide was condensed at −196° using procedures 1(a) and 2. The product was examined as described.

Discussion

The data presented in Table I indicate that in the U-tube reactor the ratio of oxygen evolved to residual peroxide was approximately one in agreement with Kobozev and co-workers.[4] On the other hand, it is seen that when the reactor geometry was modified the ratio was no longer 1:1. It was evident that the mechanism of formation of the product which gave a 1:1 ratio was closely related to geometrical and flow parameters.

It was observed that oxygen was lost from the reaction mixture during the reaction. A closer check revealed that most of the oxygen was lost in the early stages of the reaction. It was also shown that the hydrogen atoms degraded very rapidly in the liquid nitrogen cooled zone. When the liquid nitrogen level in the U-tube was raised several inches above the film of ozone, no reaction occurred. Other pertinent observations included the effect of decreasing the hydrogen atom concentration (by lowering the discharge power), and decreasing the area of the exposed ozone (forming a pool at the bottom of the reactor). The effect of decreasing the hydrogen atom concentration was to increase the ratio of evolved oxygen to hydrogen peroxide to the value of 1 even in the inlet tube reactor. Decreasing the area of exposed ozone markedly increased the production of hydrogen peroxide and decreased the amount of evolved oxygen.

It should be noted that only trace quantities of peroxide were formed in the cold finger reactor.

The above observations are in accord with the following mechanism of formation of the postulated superoxide. For the present purposes, the concentration of superoxide relative to hydrogen peroxide is measured by the ratio of evolved oxygen to residual peroxide. The value of 1 for this ratio signifies the absence of hydrogen peroxide. A value of zero indicates the absence of a higher peroxide.

$$\mathrm{H}\cdot + \mathrm{O_3} \xrightarrow{-196^\circ} \mathrm{HO}\cdot + \mathrm{O_2} \qquad (1)$$

$$\mathrm{H_2} + \mathrm{OH}\cdot \longrightarrow \mathrm{H_2O} + \mathrm{H}\cdot$$

or

$$\mathrm{H}\cdot + \mathrm{OH}\cdot \xrightarrow{\text{Wall}} \mathrm{H_2O} \qquad (2)$$

$$\mathrm{H}\cdot + \mathrm{O_2} \longrightarrow \mathrm{HO_2}\cdot \longrightarrow {}^1/_2\mathrm{H_2O_4} \qquad (3)$$

$$\mathrm{HO_2}\cdot + \mathrm{H}\cdot \longrightarrow \mathrm{H_2O_2} \qquad (4)$$

The oxygen formed in reaction 1 can either escape from the system or react with an atom of hydrogen.

The concentration of hydrogen atoms and the residence time of the liberated molecular oxygen in its environment determines the fate of the oxygen. A decrease in these factors results in an increase in the amount of oxygen lost. Thus, in the cold-finger reactor almost complete loss of oxygen occurs as evidenced by the fact that only a trace of peroxide is formed.

Step 4 determines:

1. The quantity of superoxide which remains as a product. In this connection, the product obtained in the U-tube was exposed to further reaction with hydrogen atoms following complete conversion of the ozone. The ratio of oxygen evolved to hydrogen peroxide after several hours of reaction was 1. This result indicates that the product was inert to hydrogen atoms once dimerization of the superoxide radical had occurred.

2. The quantity of hydrogen peroxide obtained. Each HO_2 radical can produce either 1 or $^1/_2$ molecules of hydrogen peroxide depending upon whether dimerization or reaction with hydrogen atoms predominates. This difference is noted by comparing the data of 17 and 18 with those of experiments 19 and 20. The larger quantities of hydrogen peroxide formed in experiments 17 and 18 led to low ratios of evolved oxygen to peroxide. In contrast, smaller quantities of peroxide in 19 and 20 gave a value of 1 for the ratio of evolved oxygen to residual hydrogen peroxide. The quantities of ozone used in the above experiments were approximately equal. These results are readily explained on the basis of the postulated mechanism. When the ozone area is decreased, the consumption of hydrogen atoms by reaction with the ozone is reduced. The net result is a greater availability of hydrogen atoms for reaction with the oxygen liberated in step 1. The oxygen does not leave the reaction zone but reacts with the excess hydrogen atoms to form $HO_2\cdot$ and H_2O_2. Conversely, when the hydrogen atom concentration was deliberately lowered, the ratio of evolved oxygen to residual peroxide was increased to 1 and the total quantity of peroxide formed was lowered. The $HO_2\cdot$ radicals dimerize to give a product which is unreactive to atoms. The hydrogen atom concentration determines the quantity of hydrogen peroxide formed as well as the ratio of evolved oxygen to peroxide.

The fate of the OH · radical can be shown from the extensive data of Kobozev and co-workers[4] and also

from data obtained in the present research. An analysis of Kobozev's data indicated that one mole of water was formed for each mole of consumed ozone as required by the suggested mechanism.

The following indicates the quantities of water formed in some experiments in the present studies

	mmoles				
Expt. no.	O_2 Initial	O_3 Final	O_2 Reacted	H_2O	H_2O_2
9	2.01	0.02	1.99	2.11	0.89
18	1.83	0.06	1.77	1.73	1.41

The quantity of water formed is in close agreement with the ozone consumed whereas the peroxide concentrations vary considerably. The presence of ice (with a trace of hydrogen peroxide) on the inlet tube was observed in some experiments. The water analyses in these experiments were vitiated since no provision was initially made to account for the water condensed in this zone of the system. The transfer of ice (and/or hydrogen peroxide) to the inlet suggests that a vapor phase reaction could occur by vaporization of some ozone due to the heat of reaction. This would lead to the vapor phase reaction

$$H\cdot + O_3 \longrightarrow O_2 + OH$$

postulated by McKinley and Garvin.[9]

A reasonable confirmation of the validity of the analytical methods employed in this research is obtained from expt. 9.

		(O) mmoles
mmoles of ozone reacted	1.99	5.97 (in)
mmoles of water formed	2.11	2.11
mmoles of peroxide formed	0.89	1.78
mmoles of oxygen lost	.70	1.40
mmoles of oxygen evolved	.18	0.36
		5.65 (out)

The 1:1 ratio of oxygen evolved to residual peroxide noted when deuterium atoms were employed suggests that an analogous higher deuterated peroxide was formed using the same operating conditions.

The "hydrogen superoxide" product prepared by procedures 1(a) and (b) sometimes contained traces of occluded ozone as evidenced by absorption in the regions 2130 to 2040 and 1030 to 1020 cm.$^{-1}$. The absorption peaks exhibited by the hydrogen atom–ozone product in the 3330 to 2780 and 1610 cm.$^{-1}$ regions were attributed to ice. The product obtained by procedures 1(b) and 2 was examined at −130° by replacing the liquid nitrogen refrigerant with a pentane "slush" bath. No significant change in the spectrum was noted. The appearance of the strong hydrogen peroxide absorption at about 1370 cm.$^{-1}$ was observed when the product was allowed to warm to −78° (Dry Ice–acetone).

In contrast to these results, examination of the hydrogen peroxide–water mixture at −196° and the product obtained by procedure 1(a) exhibited absorption bands at about 1370 cm.$^{-1}$.

The infrared spectra of the hydrogen atom–liquid ozone product, prepared using techniques 1(b) and 2 comfirmed the absence of hydrogen peroxide in the temperature region −196° to −130°. At higher temperatures hydrogen peroxide was readily detected. In agreement with Giguère and Chin,[7] no absorption which could be attributed to a higher peroxide was noted. The appearance of hydrogen peroxide when the samples were warmed is in agreement with the view that a higher peroxide (H_2O_4) which decomposes to H_2O_2 ($+O_2$) is formed by the reaction of hydrogen atoms with ozone at −196°.

Further physical and chemical studies are required to establish whether the source of hydrogen peroxide is the postulated superoxide, H_2O_4.

If the mechanism presented in the present paper is valid, the reaction of hydrogen atoms with ozone involves the reaction of H · with O_2 in the peroxide forming step. Thus, the results and the nature of the product obtained are not unique to this reaction but are related to the numerous experiments in the literature involving radicals containing oxygen and hydrogen as typified by the reaction of hydrogen atoms with molecular oxygen. The source of evolved oxygen would then be the same hydrogen superoxide.

Conclusions

The data suggest that under certain conditions hydrogen or deuterium atoms react with liquid ozone to give a product which, based upon the stoichiometry of decomposition, can be described as a hydrogen superoxide.

Infrared studies have confirmed the absence of hydrogen peroxide as a primary product of the reaction when the ratio of evolved oxygen to residual hydrogen peroxide is unity.

Acknowledgment.—The authors are grateful to the Directorate of Research Analysis, Air Force Office of Scientific Research, for support of this work under contract AF 29(600)-1667.

(9) J. D. McKinley and D. Garvin, *J. Am. Chem. Soc.*, **77**, 5802 (1955).

ON THE THEORY OF OXIDATION–REDUCTION REACTIONS INVOLVING ELECTRON TRANSFER. V. COMPARISON AND PROPERTIES OF ELECTROCHEMICAL AND CHEMICAL RATE CONSTANTS[1]

BY R. A. MARCUS[2]

Departments of Chemistry, Brookhaven National Laboratory, Upton, New York, and Polytechnic Institute of Brooklyn, Brooklyn 1, New York

Received October 11, 1962

Using a theory of electron transfers which takes cognizance of reorganization of the medium outside the inner coördination shell and of changes of bond lengths inside it, relations between electrochemical and related chemical rate constants are deduced and compared with the experimental data. A correlation is found, without the use of arbitrary parameters. Effects of weak complexes with added electrolytes are included under specified conditions. The deductions offer a way of coördinating a variety of data in the two fields, internally as well as with each other, and a way of predicting results in one field from those in another. For example, the rate of oxidation or reduction of a series of related reactants by one reagent is correlated with that of another and with that of the corresponding electrochemical oxidation–reduction reaction, under certain specified conditions. These correlations may also provide a test for distinguishing an electron from an atom transfer mechanism.

In recent years many rate constants of electron transfer reactions in solution and at electrodes have been measured,[3,4] and some quantitative comparison of the data in the two fields now seems appropriate. As a guide we shall employ a theory formulated in earlier papers.[5] This theory yielded an expression for the rates of each of these processes, taking into consideration the solvent reorganization occurring outside the inner coördination shell of each reactant prior to (and necessary for) electron transfer.[5a–d]

The theoretical rate constant for either process was given by eq. 1–3[5c,g]

$$k = Ze^{-\Delta F^*/RT} \tag{1}$$

where

$$\Delta F^* = w + m^2\lambda \tag{2}$$

and

$$m = -\left(\tfrac{1}{2} + \frac{\Delta F^0 + w^p - w}{2\lambda}\right) \tag{3}$$

In eq. 1 Z is the collision frequency of (hypothetical) uncharged species in solution. It will be taken to be $\sim 10^{11}$ l. mole^{-1} sec.$^{-1}$ and $\sim 10^4$ cm. sec.$^{-1}$ for homogeneous and electrochemical reactions, respectively. w is the work needed to bring the two reactants (or reactant plus electrode) together and w^p is the corresponding term for the products. ΔF^0 is the "standard" free energy of the elementary electron transfer step *in the prevailing electrolyte medium*. It is $-nF\eta_a$ for the electrode case. (n = number of electrons transferred; η_a = activation overpotential.) λ was given by eq. 10 in ref. 5c, which is reproduced in eq. 5 below.

More recently this theory was extended to include the effect of changes (Δq_j^0, below) in bond distances and bond angles in the inner coördination shell of each reactant.[5e,f] Equations 1 to 3 were again obtained with λ now equal to

$$\lambda = \lambda_o + \lambda_i \tag{4}$$

λ_o (λ_{outer}) depends on the size and shape of the reactants. For spherical particles undergoing a homogeneous reaction, λ_o is given by eq. 5 below, and for a spherical reactant undergoing an electrochemical reaction it is one-half that expression. λ_i (λ_{inner}) is given by eq. 6 where k_j and k_j^p denote the force constant of the jth vibrational coördinate in a species involved in the reaction when that species is a reactant and when it is a product, respectively. The summation is over both reactants in the homogeneous case and over the one reactant in the electrode one. A rather general expression for the inner shell reorganization barrier is given in ref. 5e, but this one suffices for the purpose of this paper. A more general but formal expression for λ_0, based on statistical mechanics rather than on a dielectric continuum treatment, is given in part VI.[5h]

$$\lambda_o = \left(\frac{1}{2a_1} + \frac{1}{2a_2} - \frac{1}{r}\right)\left(\frac{1}{D_{op}} - \frac{1}{D_s}\right)(ne)^2 \tag{5}$$

$$\lambda_i = \Sigma_j \frac{k_j k_j^p}{k_j + k_j^p}(\Delta q_i^0)^2 \tag{6}$$

a_1 and a_2 are the radii of the spherical particles undergoing reaction, the inner coördination shell of each particle being included in the estimation of a_1 and a_2. r is the mean distance between the centers of the reactants in the activated complex. (We take $r = a_1$

(1) Research performed in part under the auspices of the U. S. Atomic Energy Commission. Presented at the "Symposium on Mechanisms of Electrode Reactions," 142nd American Chemical Society National Meeting, Atlantic City, 1962. For Part IV see ref. 5e. Related papers are listed under ref. 5. A still more general proof of eq. 1 to 4 is given in part VI.[5h]

(2) Alfred P. Sloan Fellow. Visiting Senior Scientist at B.N.L. Present address: Department of Chemistry, Polytechnic Institute of Brooklyn.

(3) For detailed reviews of homogeneous reactions, see (a) N. Sutin, *Ann. Rev. Nuclear Sci.*, **12**, 285 (1962), and (b) J. Halpern, *Quart. Rev.* (London), **15**, 207 (1961).

(4) For detailed summary of electrode kinetic data, see (a) N. Tanaka and R. Tamamushi, "Kinetic Parameters of Electrode Reaction," a report presented to the Commission on Electrochemical Data of the Section of Analytical Chemistry of I.U.P.A.C., at the International Congress of Pure and Applied Chemistry, Montreal, 1961. Copies are obtainable from H. Fischer, Department of Electrochemistry, Institute of Technology, Karlsruhe, Germany. (b) J. Jordan and N. A. Stalica, in "Handbook of Analytical Chemistry," L. Meites, Ed., McGraw-Hill Book Co., New York, N. Y., 1963.

(5) R. A. Marcus (a) *J. Chem. Phys.*, **24**, 966 (1956); (b) O.N.R. Technical Report No. 12. Project NR 051-331 (1957); (c) *Can. J. Chem.*, **37**, 155 (1959); (d) "Trans. Symposium Electrode Processes," E. Yeager, Ed., John Wiley and Sons, New York, N. Y., 1961, p. 239; (e) *Discussions Faraday Soc.*, **29**, 21 (1960); eq. 6 below is actually obtained in ref. 5h, by simplifying those in part IV; (f) unpublished results for the electrochemical case, analogous to those in (e). Equation 9 of the present paper, which is a convenient approximation to the results obtained in sections (ii) and (iii) of ref. 5e, will be discussed in detail in part VI.[5h] As will be pointed out in ref. 5h, there is also a relatively minor reorganization term for the surrounding electrolyte but one which does not alter the correlations in this paper. For brevity, we have omitted it in the present paper. (g) Note on eq. 1 to 3: in a notational change to conform with ref. 5e, w^* and w in ref. 5c are now written as w and w^p, respectively. The factor of $\frac{1}{2}$ in eq. 8 of ref. 5c is now incorporated in the present definition of λ_0 for the electrode system, and "e" has been replaced by its molar equivalent, the Faraday F. The values of Z in the present paper are the gas kinetic values. (*h*) *J. Chem. Phys.*, to be submitted.

$+ a_2$.) In the electrochemical case a_1 and a_2 are equal and r is twice the distance from the center of the reacting particle to the electrode surface. D_{op} and D_s are the square of the refractive index and static dielectric constant, respectively.

For making the correlation described in this paper, an essential feature of eq. 4 to 6 is that

$$\lambda_{soln} = \lambda_1 + \lambda_2 - \lambda_r \qquad (7)$$

where λ_1 depends on the properties of particle 1 (size, force constants, difference of corresponding equilibrium bond distances in reactant and product state) and not on those of particle 2. Similarly, λ_2 depends only on properties of 2. λ_r is the r term in eq. 5. In the electrochemical case we find

$$\lambda_{el} = \lambda_1 - \frac{\lambda_r}{2} \qquad (8)$$

where the value of λ_r in eq. 8 will be equal to or less than that in eq. 7, according as the reacting species can or cannot penetrate any bound layer of solvent molecules adjacent to the electrode surface.[5c]

Particularly pertinent to the following arguments is eq. 9, obtained from eq. 2 and 3 when $|(\Delta F^0 + w^p - w)/\lambda|$ is small (say, 1/4).

$$\Delta F^* \cong \frac{w + w^p}{2} + \frac{\lambda}{4} + \frac{\Delta F^0}{2} \qquad (9)$$

ΔF^* is then linear in ΔF^0 with a slope of 0.5. When w and w^p are small, λ is seen to be four times the value of ΔF^* when $\Delta F^0 = 0$, *i.e.*, $4(\Delta F^*)_0$ say. Thus, the above condition for linearity in ΔF^0 can be written as

$$\left|\Delta F^0/(\Delta F^*)_0\right| \leqslant 1 \qquad (10)$$

a condition often fulfilled in practice.[6] More generally, the *instantaneous* slope of a plot of ΔF^* *vs.* ΔF^0 is, according to eq. 2 and 3, $^1/_2[1 + \Delta F^0/4(\Delta F^*)_0]$ when the work terms are small.

Effect of Standard Free Energy of Reaction or of Overpotential on Reaction Rate.—Two immediate deductions may be drawn from eq. 9 when the work terms can either be made small, say by using high electrolyte concentration, or when they are essentially constant in the following variations: In the oxidation–reduction reaction of a series of related compounds with a given reagent such that ΔF^0 is essentially the only parameter varied, a plot of ΔF^* *vs.* ΔF^0 and hence of log k *vs.* log K should be linear with a slope of 0.5 for ΔF^0's satisfying eq. 10. In the electrochemical case, the corresponding plot of ΔF^* *vs.* $-nF\eta_a$ (or of $-RT/nF$ ln k *vs.* electrode potential) should also be linear with a slope of 0.5. The first deduction, predicted first in ref. 5e, was recently confirmed experimentally for the homogeneous oxidation of Fe(II) by a series of substituted $Fe(phen)_3^{+3}$ ions.[7] Again, the slope of the electrochemical plot of RT/nF ln k *vs.* electrode potential is the so-called electrochemical "transfer coefficient." At appreciable salt concentrations transfer coefficients have been found to be near 0.5 (0.4 to 0.6),[8] in agreement with the second deduction.

By analogy, we shall call the slope of the ΔF^* *vs.* ΔF^0 plot the "chemical transfer coefficient" of the reaction.

Two deductions may also be made on the direct relation between electrochemical and related chemical rate constants:

Comparison of Isotopic Exchange Rate and Corresponding Electrochemical Exchange Current.—For an isotopic exchange reaction between ions differing only in valence state, $\Delta F^0 = 0$, $w = w^p$, and hence $m = -0.5$ in eq. 3. In the "exchange current" of the corresponding electrochemical system $\eta_a = 0$ by definition, and $m = -0.5$, if the work term $w - w^p$ is small. The λ_1's and λ_2's in eq. 7 and 8 are all equal. According to the remarks following eq. 8, it then follows that $\lambda_{ex} \leqslant 2\lambda_{el}$ (= or < according as the reactant can or cannot penetrate the solvent layer adjacent to the electrode). From a physical viewpoint, the factor of two enters in the exchange system because two ions and their solvation shells are undergoing rearrangement in forming the activated complex while in the electrochemical system there is but one such particle. It thus follows that $\Delta F_{ex}^* \leqslant 2\Delta F_{el}^*$ when w and w^p are small in both the ex and el experiments. From eq. 1 we then expect that $\sqrt{k_{ex}/10^{11}} \geqslant k_{el}/10^4$, where k_{ex} and k_{el} are in units of l. mole sec.$^{-1}$ and cm. sec.$^{-1}$, respectively. Another factor tending to favor the "$>$" sign is the existence, if any, of inactive sites on the electrode due, say, to any strongly absorbed foreign particles.

More recently it has been concluded theoretically that under certain conditions neither the above deduction of this $\sqrt{k_{ex}}/k_{el}$ relation nor that of the 0.5 slopes of the ΔF^* plots should be affected if one or both of the reactants form relatively weak complexes with other ions.[9] (The ΔF^*'s are then those corresponding to the

(6) *E.g.*, in ref. 7, the intercept of Fig. 2 yields $(\Delta F^*)_0 \sim 12$ kcal. mole^{-1}. (Ref. 7 gives $\Delta F^{\ddagger}$'s but $\Delta F^* = \Delta F^{\ddagger} - RT \ln hZ/kT = \Delta F^{\ddagger} - 2.8$ kcal. mole^{-1} when the standard state in $\Delta F^{\ddagger}$ is 1 mole liter^{-1}.)[5a] Since the largest $|\Delta F^0|$ there was 12 kcal. mole^{-1}, (10) is fulfilled. Again, in electrochemical systems in which the transfer coefficient is measured over an electrode potential range of perhaps 0.2 volt from the equilibrium potential, and in which the typical $(\Delta F^*)_0$ (value of ΔF^* at $\eta_a = 0$) in Table I is of the order of 7 kcal. mole^{-1}, condition (10) is again fulfilled since $|\Delta F^0/(\Delta F^*)_0| \sim 0.2 \times 23/7$.

(7) M. H. Ford-Smith and N. Sutin, *J. Am. Chem. Soc.*, **83**, 1830 (1961). The data satisfy condition (10).[6] It is assumed that in the first approximation the substituents leave the k_j's and Δq_j^0's unaltered. Still more extensive data supporting this predicted value of the slope have been obtained by N. Sutin and collaborators (private communication).

(8) Data are largely but not entirely taken from ref. 4a. The transfer coefficients are either those of the reduction process or are (1-transfer coefficient of the oxidation step): Fe(II)–Fe(III) in 1 *M* H_2SO_4 0.42,[a,b] 0.62,[c] 0.61[c]; $Fe(CN)_6^{-4,-3}$ in 1 *M* KCl 0.45,[c] 0.50,[c] and (graphite) 0.5[d]; V(II)–V(III) in 1 *M* $HClO_4$ 0.52,[e] 0.50 to 0.57,[f] and in 1 *M* H_2SO_4 0.46[f]; Tl(I)–Tl(II) in 1 *M* $HClO_4$ 0.5[g]; Tl(III)–Tl(II) in 1 *M* $HClO_4$ 0.5.[g]

At lower supporting electrolyte concentration: Fe(II)–Fe(III) in 0.1 *M* $HClO_4$, 0.78[b]; $Cr(CN)_6^{-3,-4}$ in 0.2 *M* NaCN 0.67.[i] (The exchange current in the latter system was very sensitive to salt concentration.)

Low values are: Ce(III)–Ce(IV) in 1 *N* H_2SO_4, 0.25,[b] and Mn(II)–Mn(III) in 15 *N* H_2SO_4, 0.28.[a,b] (a) R. Parsons, "Handbook of Electrochemical Constants," Butterworths, London (1959); (b) K. J. Vetter, "Electrochemische Kinetik," Springer-Verlag, 1961; (c) M. D. Wijnen and W. M. Smit, *Rec. trav. chim.*, **79**, 289 (1960); (d) A. Regner and J. Balej, *Collection Czechoslov. Chem. Commun.*, **26**, 237 (1961); (e) K. M. Joshi, W. Mehl, and R. Parsons, "Trans. Symposium Electrode Processes," E. Yeager, Ed., John Wiley and Sons, New York, N. Y., 1961, p. 249; (f) J. E. B. Randles, *Can. J. Chem.*, **37**, 238 (1959); (g) H. Catherino and J. Jordan, private communication; (h) J. Jordan and R. A. Javick, *Electrochim. Acta*, **6**, 23 (1962); (i) P. Delahay and M. Kleinerman, *J. Am. Chem. Soc.*, **82**, 4509 (1960).

(9) R. A. Marcus (unpublished). The conditions imposed in the derivation were that (i) for every pair of reacting complexes the corresponding ΔF^* for electron transfer between the pair is in the linear ΔF^0 region described earlier; (ii) the added ions do not act as bridging groups to any appreciable extent; and (iii) dissociation of any complex does not constitute an important reaction coördinate at the intersection surface of ref. 5e, though it can occur before or later; see, in part, ref. 5h.

If A and B denote different reactants, A^p and B^p the corresponding products, and X and Y any ions forming complexes with these species, condition (i) is fulfilled only if the standard free energy of reaction of $AX_m + BY_n \rightleftarrows A^pX_m + B^pY_n$, ΔF_{mn}^{0xy}, satisfies condition (10) for every important

TABLE I

COMPARISON OF ISOTOPIC EXCHANGE AND ELECTROCHEMICAL RATE CONSTANTS FOR ONE-ELECTRON TRANSFERS AT 25°

System	Medium	$\sqrt{k_{ex}/10^{11}}$	$k_{el}/10^4$	Electrode	Reference
$Fe(CN)_6^{-3,-4}$	1 M K^+	(1×10^{-3})	1×10^{-5}	Pt	a
$MnO_4^{-1,-2}$	0.9 M Na^+	2×10^{-4}	$\sim 2 \times 10^{-5}$	Pt, see ref. 11	b
$Fe^{+2,+3}$	1 M $HClO_4$	9×10^{-6}	7×10^{-7}	Pt	c
$V^{+2,+3}$	1 M $HClO_4$	4×10^{-7}	4×10^{-7}	Hg	d
$Eu^{+2,+3}$	1 M Cl^-	6×10^{-8}	3×10^{-8}	Hg	e
$Tl^{+1,+3}$	1 M $HClO_4$	3×10^{-8}[h]	2×10^{-8}	Pt	f
$Co(NH_3)_6^{+2,+3}$	0.14 M H^+	$<5 \times 10^{-11}$	$\sim 5 \times 10^{-12}$	Hg	g

Exchange data: [a] Reference 10; [b] J. C. Sheppard and A. C. Wahl, *J. Am. Chem. Soc.*, **79**, 1020 (1957); [c] J. Silverman and R. W. Dodson, *J. Phys. Chem.*, **56**, 846 (1952); [d] K. V. Krishnamurty and A. C. Wahl, *J. Am. Chem. Soc.*, **80**, 5921 (1958); [e] D. J. Meier and C. S. Garner, *J. Phys. Chem.*, **56**, 853 (1952); [f] E. Roig and R. W. Dodson, *ibid.*, **65**, 2175 (1961). [g] See Appendix II. Electrochemical data: [a] Reference 8c; [b] Reference 11; [c] J. E. B. Randles and K. W. Somerton, *Trans. Faraday Soc.*, **48**, 937 (1952); [d] Ref. *c*, J. E. B. Randles, *Can. J. Chem.*, **37**, 238 (1959), ref. 8i; [e] Ref. *c:* note that the corresponding isotopic exchange data were insensitive to (H^+), so this comparison could be made; [f] Ref. 8g. See Appendix I. All data are corrected to 25° and to the cited salt concentration listed under "Medium." [g] See Appendix II. [h] Assuming exchange proceeds *via* two one-electron transfers. Otherwise, value is an upper limit for the one-electron transfer rate.

TABLE II

RELATIVE REDUCTION RATES OF $Co(NH_3)_5X$ (III)

X	V^{+2}	$Cr(dipy)_3^{+2}$	DME[a]
NH_3	1	1	1
H_2O	135	91	124
Cl^-	1.6×10^3	1.5×10^3	..

[a] At E of 0.1 N calomel electrode.

pseudo-rate constants, "constants" which depend on the concentrations of these other ions.)

A comparison of $\sqrt{k_{ex}/10^{11}}$ and $k_{el}/10^4$ on the basis of the existing experimental data is given in Table I. All rate constants are pseudo-rate constants, their use being justified under the conditions cited.[9] The qualitative trend in both k_{el} and k_{ex} is seen to be the same, and the values in the two columns are relatively close to each other, considering the fact that approximations in the theory enter exponentially (a fairer comparison would be of $\Delta F_{ex}^*/2$ and ΔF_{el}^*), that stationary electrodes (and their adsorption problems) were usually necessary, and that the work terms may not have been negligible. Other reactions for which the data are more fragmentary are described in Appendix II.

Comparison of Chemical and Electrochemical Oxidation–Reduction Rates of a Series of Related Reactants.—In this comparison we shall consider systems in which a constant reagent is used in the chemical system, and a constant electrode potential in the electrochemical one, to oxidize or reduce a series of related compounds. In a series of a given charge type, the work terms are either exactly or roughly constant in each of these two systems. Furthermore, if the ΔF^*'s are in the region where they would depend linearly on ΔF^0, then according to eq. 1 and 7 to 9 the ratio k_{soln}/k_{el} should be the same for each member of the series: In both cases, the terms λ_1, ΔF^0, and, at a constant E, η $(=E - E^0)$ will normally vary from member to member. (λ_2 refers to the constant reagent.) However, since ΔF^0 equals $(-nFE^0 +$ constant) in the series, one sees from eq. 7 to 9 that these variations in λ_1, ΔF^0, and E^0 cancel when one compares values of $(\Delta F_{soln}^* - \Delta F_{el}^*)$, that is of k_{soln}/k_{el}. Vlcek[12] has recently observed that the electroreduction and the $Cr(dipy)_3^{+2}$ reduction[13] of $Co(NH_3)_6^{+3}$ and $Co(NH_3)_5(H_2O)^{+3}$ had essentially the same k_{soln}/k_{el} for both Co compounds (see Table II). This experimental result is in agreement with the above theoretical deduction. Presumably both E^0 and λ_1 differed in the two compounds. Extension of these comparative studies to other Co compounds would of course be desirable.

Similarly, the ratio k^a_{soln}/k^b_{soln} for each member of the series oxidized or reduced by two reagents, a and b, should be constant. This result was found experimentally for the $Co(NH_3)_5X$ (III) compounds reduced by $V(H_2O)_6^{+2}$ and $Cr(dipy)_3^{+3}$, respectively, with X being NH_3, H_2O, and Cl^-[14,15] (Table II). The restriction to a given charge type will not be important if the work terms are relatively minor. The comparison involving V^{+2} should be accepted with some reserve since the V(II) reaction is not necessarily an "outer sphere" one, as Taube has pointed out.

Salt and Solvent Effects.—The above comparisons suggest that some of the interesting phenomena observed in isotopic exchange reactions should be looked for in the corresponding electrochemical ones. For example, traces of Cl^- inhibit Tl(I)–Tl(III) isotopic exchange but greater amounts catalyze it.[16] Again, substitution of water by isopropyl alcohol decreased the rate of Fe(II)–Fe(III) exchange 10^8-fold.[17] This factor could be due to the enhanced coulombic repul-

mn pair, *i.e.*, if $|\Delta F_{mn}^{0xy}/(\Delta F_{mn}^{*xy})_0| \leqslant 1$. If any of these complexes decomposes in less than a vibrational period, ΔF_{mn}^{0xy} is to be computed for a "frozen" value of the unstable coördinate, the same value for both sides of the above equilibrium. There is some possibility that for certain deductions these conditions can be relaxed, a point which we shall investigate further.

(10) P. King, C. F. Deck and A. C. Wahl, 139th American Chemical Society National Meeting, 1961, Abstracts, p. 30R, and private communication. The value in Table I is a long extrapolation which was made using their equation describing data in the 0.0025 to 0.05 M KCl region. At 0.05 M KCl and corrected to 25°, $\sqrt{k_{ex}/10^{11}}$ was 1.6×10^{-4}.

(11) Z. Galus and R. N. Adams, Paper presented at the "Symposium on Mechanisms of Electrode Reactions," 142nd American Chemical Society National Meeting (1962). These authors found that in a variety of electrochemical reactions k_{el} averaged about 20-fold less for a carbon paste electrode than it did for a platinum one. Accordingly, their k_{el} for $MnO_4^{-1,-2}$ (0.01 cm. sec.$^{-1}$), which was obtained with carbon paste, was increased by a factor of twenty to obtain the value cited in Table I, so as to permit its comparison with the other systems.

(12) A. A. Vlcek, in "Sixth International Conference on Coördination Chemistry," S. Kirschner, Ed., The Macmillan Co., New York, N. Y., 1961, p. 590.

(13) A. M. Zwickel and H. Taube, *Discussions Faraday Soc.*, **29**, 42, (1960).

(14) A. M. Zwickel and H. Taube, *J. Am. Chem. Soc.*, **83**, 793 (1961).

(15) Condition (10) is fulfilled for the V^{+2}–$Co(NH_3)_6^{+3}$ reaction, since $\Delta F^0 = -8$ kcal. mole^{-1}, $\Delta F^* = 18$ kcal. mole^{-1} whence $(\Delta F^*)_0 \sim (18 + 8/2)$ and $|\Delta F^0/(\Delta F^*)_0| \sim 1/3$. An E^0 or $E^1/_2$ for $Cr(dipy)_3^{+2,+3}$ could not be found, so that condition (10) was not checked for the $Cr(dipy)_3^{+2}$–$Co(NH_3)_6^{+3}$ reaction. In the electrochemical reduction of $Co(NH_3)_5X$ (III), most of the transfer coefficients were near 0.5, though that for X = NH_3 was apparently 0.67.

(16) G. Harbottle and R. W. Dodson, *J. Am. Chem. Soc.*, **73**, 2442 (1951). For other references to anions which inhibit Tl(I)–Tl(III) exchange, see N. Sutin, ref. 3a.

(17) N. Sutin, *J. Phys. Chem.*, **64**, 1766 (1960).

sion. If not, the electrochemical exchange current may be reduced 10^4-fold.

Sutin has suggested[18] that it would also be interesting to study the electro-reduction of $Co(NH_3)_5X$ (III) when X is a fumarate methyl or phenyl ester, to see whether this reduction resembles more closely a reduction by $Cr(dipy)_3^{+2}$ or by V^{+2}. Hydrolysis of the ester accompanies the reduction in the second case but not in the first.

Cross-Reaction Rate Constants.—It follows from eq. 1, 7, and 9 that when condition (10) is fulfilled the forward rate constant k_{12} of the cross-reaction (11)

$$Ox_1 + Red_2 = Red_1 + Ox_2 \qquad (11)$$

is given by (12).

$$k_{12} \cong \sqrt{k_{11}k_{22}K_{12}}e^{-(w_{12} + w_{12}^{p} - w_{11} - w_{22})/2RT} \qquad (12)$$

where k_{11} and k_{22} are the isotopic exchange rate constants in systems 1 and 2, w_{11} and w_{22} are the corresponding work terms, and K_{12} and w_{12}, w^{p}_{12} denote the equilibrium constant and the work terms of (11).

Equation 12 was derived earlier[5d] under a more eestrictive assumption ($k_j = k_j^{p}$) and for negligible rxponent. Even if any or all of the species in (11) form weak complexes with other ions, (12) should still hold for the pseudo k's, provided (i) the conditions listed earlier[9] prevail, (ii) the coulombic contribution to $w_{12} + w^{p}_{12} - w_{11} - w_{22}$ is negligible for each elementary electron transfer, and (iii) the non-coulombic one (see below) is either essentially the same for each pair or vanishes. When the coulombic term is not negligible, eq. 12 is to be used for each elementary electron transfer; if a participating complex is very unstable, K_{12} for this step is that computed when a coördinate is "frozen."[9]

For a somewhat more accurate comparison, k_{12} may be estimated from k_{11} and k_{22} using the complete equations 1 to 3, noting that $\lambda_{12} = (\lambda_{11} + \lambda_{22})/2$. (However, the generalization to weak complexes has not been established for the case where condition (10) does not hold.) When the work terms are negligible, eq. 1 to 3 yield

$$k_{12} = \sqrt{k_{11}k_{22}K_{12}f} \qquad (13)$$

where

$$\ln f = (\ln K_{12})^2/4 \ln (k_{11}k_{22}/Z^2)$$

When reaction 11 is one in which the reactants are aquo ions which interchange charges, one would expect $w_{12} = w^{p}_{12} = w_{11} = w_{22}$. The work term in (12) then vanishes. On the other hand, when (11) is a reaction between an ion with hydrogen bonding ligands and one with organic ligands (*e.g.*, $Fe(H_2O)_6^{+2}$ + $Fe(phen)_3^{+3}$) one would expect that the non-coulombic contributions to the work terms will not cancel: w_{11} and w_{22} may have attractive non-coulombic contributions and (w_{12} + w_{12}^{p}) repulsive ones. In this event two deductions may be made: (i) k_{12} will be less than $\sqrt{k_{11}k_{22}K_{12}}$ and (ii) when suitable ratios k_{12}/k_{13} are taken, the non-coulombic contribution to the work term can essentially cancel in the ratio (*e.g.*, if k_{12} corresponds to the reaction of $Fe(phen)_3^{+1}$ or $^{+2}$ with $Fe(H_2O)_6^{+2}$ or $^{+3}$ and k_{13} corresponds to the reaction of $Fe(phen)_3^{+3}$ or $^{+2}$ with another aquo-ion).

(18) N. Sutin, private communication.

Deduction (i) may explain the results of a comparison[3a] of k_{12} and $\sqrt{k_{11}k_{22}K_{12}}$ for the Fe^{+2}–$Fe(phen)_3^{+3}$ system. A value of a few kcal. mole^{-1} for (w_{12} + w_{12}^{p} − w_{11} − w_{22})/2 would suffice to explain the results. Deduction (ii) was suggested by a comparison of k_{12}/k_{13} with $\sqrt{k_{22}K_{12}/k_{33}K_{13}}$ made by N. Sutin.[18] A variety of experimental tests involving the cross-relations is now in progress by Sutin and collaborators.[18]

Often in the literature the role of ΔF^0 (and hence of K_{12}) has been ignored in explaining the values of certain rate constants. Equation 12 (or indeed eq. 1 to 3) illustrates how important it can be for the present class of reactions.

Ligand-Field Effects.—The influence of ligand-field effects on the rate constants of oxidation–reduction reactions and on other properties of complex ions has been the subject of much interest. They are incorporated in the present theory; in particular they influence k_j, Δq_j^0, and ΔF^0. Accordingly, the present approach converts discussions of ligand-field effects on kinetic problems into a discussion of the problem of estimating k_j, Δq_j^0, and ΔF^0. Moreover, according to eq. 1, 7, 8, and 9, these effects cancel when certain correlations of the experimental data are made: the correlations embodied in chemical and electrochemical transfer coefficients of 0.5, in the comparison of chemical and electrochemical exchange "currents," and in the comparison of cross and isotopic exchange rate constants.

One *vs.* Two-Electron Transfers.—In some reactions involving 2-electron oxidation–reduction reagents, it has not been possible to decide whether the mechanism proceeds *via* two successive one-electron transfers or *via* one two-electron transfers. However, it is sometimes possible to distinguish between the two alternative mechanisms in a corresponding electrochemical reaction. For example, the Tl(I)–Tl(III) electrochemical process has been found to proceed *via* two one-electron transfers.[8g] From the electrochemical rate constants for the Tl(I)–Tl(II) and Tl(III)–Tl(I) reactions, we have computed in Appendix I a rate constant which may be compared with the homogeneous rate constant. Agreement would be expected only if the homogeneous rate constant proceeds *via* two one-electron transfers. The agreement in Table I for this comparison would appear to favor this mechanism for the homogeneous reaction. Had the value for $\sqrt{k_{ex}/10^{11}}$ been appreciably greater than that for $k_{el}/10^4$ (or really appreciably more than 10-fold greater since the electrode was Pt rather than Hg) one would have obtained evidence for the one two-electron homogeneous reaction instead.

Concluding Remarks.—The above correlations offer a possible way of systematizing and comparing experimental data both on electrochemical and on chemical electron transfer reactions. Some of the isotopic exchanges discussed earlier may not involve electron transfer and could involve atom transfer instead. The extent of correlations such as those in Table I may eventually provide a test of the mechanism, at least in the cases of extreme discrepancy.

There are a variety of other reactions for which the experimental electrochemical and isotopic exchange rate constants could be compared, and of related reactions for which chemical and electrochemical trans-

fer coefficients could be determined. Several recent detailed surveys of the literature[3,4] should be very helpful for this purpose. More frequent collaboration between electrochemists and chemical kineticists would be useful for this purpose.

Acknowledgment.—The author has benefitted considerably from the many stimulating discussions on this subject with Dr. N. Sutin of Brookhaven National Laboratory. He is also particularly indebted to Drs. R. W. Dodson and J. Jordan for their very helpful comments, and to Dr. Dodson and his department for their hospitality during the author's stay at Brookhaven. This work was supported by the U. S. Atomic Energy Commission, the National Science Foundation, and the Alfred P. Sloan Foundation, a support which the author deeply appreciates.

Appendix I

An Analysis of the Tl(I)–Tl(III) System.—In ref. 8g the following k values were estimated at the formal potential of Tl(I) = Tl(III) + 2e in 1 M $HClO_4$ at 25°

$$Tl(III) \longrightarrow Tl(II) - e \qquad k_{32}^{el} = 1 \times 10^{-5} \text{ cm. sec.}^{-1}$$

$$Tl(I) \longrightarrow Tl(II) + e \qquad k_{12}^{el} = 3.5 \times 10^{-3} \text{ cm. sec.}^{-1}$$

We shall designate λ by appropriate subscripts and let E_{ij}^0 be the formal half-cell potential (in 1 M $HClO_4$ at 25°) of Tl(i) = Tl(j) + $(j - i)$e $(j > i)$. Equations 1, 8, and 9 then yield, when the work terms are neglected

$$-RT \ln k_{32}^{el}/Z^{el} = \frac{\lambda_{23}^{el}}{4} + \frac{F\eta_{32}}{2}, \quad \eta_{32} = -(E^0_{13} - E^0_{23})$$

$$-RT \ln k_{12}^{el}/Z^{el} = \frac{\lambda_{12}^{el}}{4} + \frac{F\eta_{12}}{2}, \quad \eta_{12} = E^0_{13} - E^0_{12}$$

since the transfer coefficients are in fact 0.5,[8g] so eq. 9 applies, and since the k's were given at E^0_{13}, rather than at the unknown E^0_{23} or E^0_{12}.

Noting further that $(E^0_{23} - E^0_{12})F$ is ΔF^0, the "standard" free energy of reaction A1 in the prevailing medium

$$Tl(III) + Tl(I) = 2Tl(II) \qquad (A1)$$

one obtains

$$-RT \ln k_{32}^{el} k_{12}^{el}/Z^{el^2} = \frac{\lambda_{23}^{el} + \lambda_{12}^{el}}{4} + \frac{\Delta F^0}{2}$$

However, it can be shown from eq. 1, 7, and 8 that the forward rate constant of the homogeneous reaction (A1), k^{ex}, should be given by

$$-RT \ln k^{ex}/Z^{soln} = \frac{\lambda_{23}^{ex} + \lambda_{12}^{ex}}{8} + \frac{\Delta F^0}{2}$$

Since $\lambda^{ex} \leq 2\lambda^{el}$ it then follows that to test the theory $\sqrt{k^{ex}/Z}$ should be compared with $\sqrt{k_{32}^{el} k_{12}^{el}/Z}$. For this reason the geometric mean of k_{32}^{el} and k_{12}^{el} was used in Table I.

Appendix II

Comparisons in Other Systems.—Fragmentary information exists about electrochemical and chemical exchange rates in a number of other systems.

$Co(NH_3)_6^{+2,+3}$.—Both the electrochemical and chemical rates are extremely small. The electrochemical reduction of $Co(NH_3)_6^{+3}$ in 0.14 M $HClO_4$ and 1.26 M $NaClO_4$ at 25° has a rate constant of $2.1 \times 10^{-4} \sqrt{D}$ cm. sec.$^{-1}$ when the formal applied potential E is 0 *vs.* 0.1 N calomel electrode[10] (D is the diffusion coefficient). Taking the formal E^0 for the $Co(NH_3)_6^{+2,+3}$ system to be[19] ~0.22 volt *vs.* 0.1 N calomel, the transfer coefficient to be 0.67,[12] and $D \sim 10^{-5}$ cm.^{2} sec.$^{-1}$, the value of $k_{el}/10^4$ at $\eta_a = 0$ is found to be 2×10^{-12}. If a transfer coefficient of 0.5 had been used, the value would have been 9×10^{-12}.

From isotopic exchange rate constants and equilibrium constants obtained at 65°,[20] one may estimate that $\sqrt{k^{ex}/10^{11}} < 5 \times 10^{-11}$ in 0.14 M H^+ at 65°. Presumably, therefore, $\sqrt{k^{ex}/10^{11}} << 5 \times 10^{-11}$ at 25°, a result consistent with the above value of $k^{el}/10^4$.

Ce(III)–Ce(IV).—The value of $k_{el}/10^4$ for this system in 1 N H_2SO_4 at 25° is 8b ~ 10^{-8}. Unfortunately, the electrochemical transfer coefficient for oxidation was apparently 0.75, a value so different from 0.5 that a comparison with the exchange data can be questioned. (The magnitude of the chemical transfer coefficient for the Ce(IV)–$Fe(phen)_3^{+2}$ system is of particular interest and is under current investigation.[18]) The value of $\sqrt{k_{ex}/10^{11}}$ is 7×10^{-6} in 0.8 N H_2SO_4 at 25°.[21]

Cr(II)–Cr(III).—The electrochemical exchange current for this system has been measured at 20° in 1 M KCl where hydrolysis is presumably appreciable.[22] The value of $k_{el}/10^4$ is 1.0×10^{-9}. From the isotopic exchange rate data[23] at the lowest acid concentration studied (0.2 M $HClO_4$, 0.8 M $NaClO_4$), one may estimate $\sqrt{k_{ex}/10^{11}} = 5 \times 10^{-7}$ at 20°.

(19) W. M. Latimer, "Oxidation Potentials," Second Ed., Prentice-Hall, New York, N. Y., 1952.
(20) D. R. Stranks, *Discussions Faraday Soc.*, **29**, 73 (1960).
(21) P. B. Sigler and B. J. Masters, *J. Am. Chem. Soc.*, **79**, 6353 (1957).
(22) J. E. B. Randles and K. W. Somerton, *Trans. Faraday Soc.*, **48**, 937 (1952).
(23) A. Anderson and N. A. Bonner, *J. Am. Chem. Soc.*, **76**, 3826 (1954).

A DEUTERIUM ISOTOPE EFFECT ON THE EXCESS ENTHALPY OF METHANOL–WATER SOLUTIONS[1]

BY L. BENJAMIN[2] AND G. C. BENSON

Division of Pure Chemistry, National Research Council, Ottawa, Canada

Received October 11, 1962

Heats of mixing of methanol and water and of methanol-*d* and heavy water were determined at 25° in an adiabatic calorimeter. Deviations between the two systems are most pronounced for solutions dilute in alcohol and a Tian–Calvet microcalorimeter was used for additional measurements in this region. The results are consistent with the concept of the strengthening of hydrogen bonding by deuterium substitution.

Introduction

Differences in the physicochemical properties of a system due to isotopic substitution are of interest since in general they reflect variations in the degree of interaction within the system as distinct from changes in the fundamental nature of the interaction. Thus the substitution of hydrogen by deuterium has been used to study hydrogen bonding in a number of cases.[3]

In one recent investigation by Rabinovich and coworkers[4] the mutual solubility behavior of a number of organic liquids in water was compared with that of their suitably deuterated analogs in heavy water and the changes in miscibility attributed to differences between hydrogen bonds involving normal and heavy hydrogen. The present study of heats of mixing was undertaken to investigate further the isotope effect in hydrogen bonding. The methanol–water system was chosen because of the relative simplicity of the two species and the availability of deuterated analogs, *viz.*, methanol-*d* and heavy water.

Calorimetric studies of the mixing of methanol and water were carried out by Bose[5] over 50 years ago and more recently by Ocón and Taboada.[6,7] However, since only a small isotope effect was expected it seemed advisable to repeat the methanol–water determinations and thus to ensure that the same experimental techniques were used for this system as for the methanol-*d*–heavy water system.

Experimental

In the study of aqueous methanol solutions, Matheson Coleman and Bell "Spectroquality Reagent" methanol and conductivity water were used. The latter was obtained by distillation of alkaline permanganate solutions in a Pyrex still. Heavy water (D_2O content 99.82%) purchased from Atomic Energy of Canada Ltd. and Merck methanol-*d* having an isotopic purity greater than 98% were used for measurements on the corresponding deuterated system.

In both systems heats of mixing for values of x_2, the mole fraction of alcohol in the final solution, in the range 0.03 to 0.95 were measured in the adiabatic calorimeter described by Benson and Benson.[8] The only modification of this equipment was the replacement of the guillotine arrangement inside the stainless steel vessel by the Pyrex mixing cell shown in Fig. 1. The liquids to be mixed in the cell are separated by mercury; filling is accomplished by displacing mercury from the outer chamber with one of the liquids and removing mercury from the central tube to accommodate the second liquid. The amounts of the two liquids are determined from an appropriate series of weighings. In general the total weight of the mixture was 10 to 20 g. and the vapor volume above the liquid in the central tube was about 2 cc. The ratio of the volumes of the two liquids to be mixed in the cell was 5 to 1 or greater. In order to cover the whole concentration range it was necessary to work from both ends and to reach concentrations with mole fractions 0.3 to 0.7 by multiple dilutions; the overlap of results around $x_2 = 0.5$ was quite satisfactory and indicated the self-consistency of the technique.

The mixing cell is supported by a metal frame inside the steel calorimeter vessel and the intervening space filled with water to improve the thermal contact. Mixing is initiated by tipping the calorimeter assembly through 180°. The experimental procedure followed during a calorimetric determination has been described previously.[8] Quantities of heat evolved by the mixing process ranged from 10 to 100 cal.

All calorimetric measurements were carried out at temperatures close to 25° (generally within ±0.1°) and heat capacity values were used to correct the results to 25.00°. Vapor volumes in each determination were noted and a correction applied for heat effects arising from the change in vapor composition which accompanied the mixing. Data for heat capacities and vapor pressures needed for these corrections are available in the literature for aqueous methanol solutions.[5,9,10] Similar information is lacking for the deuterated system and corrections were estimated on the basis of the values for the ordinary methanol solutions. In all cases the total correction amounted to less than 1% of the measured heat and usually was less than 0.5%.

In addition to the work in the adiabatic calorimeter, a number of solutions with mole fractions of alcohol less than 0.1 were investigated in a Tian–Calvet microcalorimeter.[11,12] The present form of this apparatus, which is similar in many respects to the calorimeter used by Attree, *et al.*,[13] has been described briefly by Benjamin and Benson.[14] In it the transfer of thermal energy from a silver reaction tube to a large Dural block surrounding the tube is measured by a calibrated thermopile; a flux of less than 1×10^{-6} cal. sec.$^{-1}$ can be detected. The dilution studies were carried out in a metal cell immersed in silicone oil in the reaction tube. A drawing of the mixing cell is shown in Fig. 2. A thin (0.0005 in.) platinum foil separates the two liquids before mixing. The position of this divider is adjustable in the metal cell. After a steady state has been reached the foil is pierced by a pointed cutter and the e.m.f. of the thermopile measured continuously until the steady state is re-established. The area under the e.m.f.–time curve is proportional to the heat effect taking place in the reaction tube. A manganin heater wound on the outside of the metal cell is used for electrical calibration. The heat associated with rupture of the foil is determined in a blank experiment and a correction applied. In general the heat effects studied in the microcalorimeter were in the range 0.05 to 2.0 cal. The accuracy with which these could

(1) Issued as N.R.C. No. 7314. Paper presented in part at the 17th Annual Calorimetry Conference, University of California, Berkeley, August 23, 1962.

(2) National Research Council of Canada Postdoctorate Fellow, 1958–1960.

(3) G. C. Pimentel and A. L. McClellan, "The Hydrogen Bond," W. H. Freeman and Co., San Francisco, Calif., 1960.

(4) I. B. Rabinovich, V. D. Fedorov, N. P. Pashkin, M. A. Avdesnyak, and N. Ya. Pimenov, *Dokl. Akad. Nauk SSSR*, **105**, 108 (1955) (English translation NRC TT-875).

(5) E. Bose, *Z. physik. Chem.*, **58**, 585 (1907).

(6) J. Ocón and C. Taboada, *Anales fis. y quim.* (Madrid), **55B**, 243 (1959).

(7) J. Ocón and C. Taboada, *ibid.*, **55B**, 263 (1959).

(8) G. C. Benson and G. W. Benson, *Rev. Sci. Instr.*, **26**, 477 (1955).

(9) G. Bredig and R. Bayer, *Z. physik. Chem.*, **130**, 1 (1927).

(10) J. B. Ferguson and W. S. Funnell, *J. Phys. Chem.*, **33**, 1 (1929).

(11) E. Calvet and H. Prat, "Microcalorimetrie," Masson et Cie, Paris, 1956.

(12) F. D. Rossini, "Experimental Thermochemistry," Interscience Publishers, New York, N. Y., 1956, Chapter 12.

(13) R. W. Attree, R. L. Cushing, J. A. Ladd, and J. J. Pieroni, *Rev. Sci. Instr.*, **29**, 491 (1958).

(14) L. Benjamin and G. C. Benson, *Can. J. Chem.*, **40**, 601 (1962).

be measured was optimum (about ±2%) in the middle of this range.

Results and Discussion

The excess enthalpy h^E is equal to the integral heat of mixing per mole of solution at constant temperature and pressure. Excess enthalpies at 25.00° measured in the adiabatic calorimeter are summarized in Table I (the defined thermochemical calorie, equal to 4.184 absolute joules, is used); results for normal methanol solutions are given in the first and second columns, those for methanol-*d*–heavy water in the last two columns. The accuracy of the results as estimated from consideration of the experimental procedure and the internal consistency of the data is about ±0.2%. The data are displayed graphically in Fig. 3. Over the whole concentration range the excess enthalpy is negative and exhibits a simple minimum. This occurs close to $x_2 = 0.3$ for both systems and has a depth of 212.2 and 216.9 cal. mole^{-1} for the normal and deuterated solutions, respectively. Qualitatively the effect of deuterium substitution is somewhat similar to that of reducing the temperature which may indicate that the structure of the deuterated system at 25° is similar to that of the normal system at a lower temperature. However, the analogy is not perfect.

TABLE I

EXPERIMENTAL VALUES OF THE EXCESS ENTHALPY AT 25.00°

CH_3OH–H_2O system		CH_3OD–D_2O system	
x_2	h^E, cal. mole^{-1}	x_2	h^E, cal. mole^{-1}
0.02916	− 47.77	0.06157	−100.1
.08310	−119.4	.1225	−164.3
.1029	−139.5	.1850	−199.6
.1091	−145.2	.2490	−214.4
.1725	−187.3	.2970	−216.8
.2045	−198.4	.3167	−216.9
.2949	−212.3	.3732	−212.4
.3222	−211.7	.4026	−209.0
.3864	−207.6	.4705	−198.4
.4786	−195.7	.5399	−185.3
.5978	−172.5	.6072	−170.5
.6785	−152.3	.7124	−141.9
.7684	−123.3	.8137	−105.1
.8614	− 83.9	.8396	− 94.0
.9528	− 32.65	.9476	− 35.88

TABLE II

VALUES OF THE EXCESS ENTHALPY AT 25.00° AT ROUNDED CONCENTRATIONS

	CH_3OH–H_2O	CH_3OD–D_2O		CH_3OH–H_2O data of Bose[5]		CH_3OH–H_2O data of Ocón and Taboada[6,7]	
x_2	h^E, cal. mole^{-1}	h^E, cal. mole^{-1}	% diff. from col. 2	h^E, cal. mole^{-1}	% diff. from col. 2	h^E, cal. mole^{-1}	% diff. from col. 2
0.00	0	0	0	0	0	0	0
.05	− 78.0	− 84.3	8.1	− 76.5	1.9	− 72.5	7.1
.10	−136.7	−144.5	5.7	−135.5	0.9	−125.0	8.6
.15	−175.2	−182.9	4.4	−174.0	0.7	−163.0	7.0
.20	−197.1	−204.5	3.8	−200.5	−1.7	−187.5	4.9
.25	−208.1	−214.5	3.1	−210.0	−0.9	−202.0	2.9
.30	−212.2	−216.8	2.3	−211.0	0.6	−209.0	1.5
.35	−210.7	−215.1	2.1	−208.0	1.3	−209.0	0.8
.40	−206.1	−210.0	1.9	−204.0	1.0	−205.0	0.5
.45	−199.8	−202.9	1.6	−196.5	1.7	−197.5	1.2
.50	−192.4	−199.4	1.0	−187.5	2.5	−188.5	2.0
.55	−183.1	−184.1	0.6	−177.5	3.1	−178.0	2.8
.60	−172.1	−172.1	0	−164.5	4.4	−168.5	2.1
.65	−160.0	−159.4	−0.4	−152.5	4.7	−154.0	3.8
.70	−146.0	−145.2	− .6	−137.5	5.8	−140.5	3.8
.75	−129.9	−129.3	− .5	−123.0	5.3	−126.5	2.6
.80	−111.3	−110.7	− .5	−104.5	6.1	−110.0	1.2
.85	− 89.4	− 89.2	− .2	− 82.0	8.3	− 91.0	− 1.8
.90	− 63.9	− 63.8	− .2	− 56.0	12.4	− 67.0	− 4.9
.95	− 34.5	− 34.3	− .6	− 28.5	17.4	− 38.0	−10.1
1.00	0	0	0	0	0	0	0

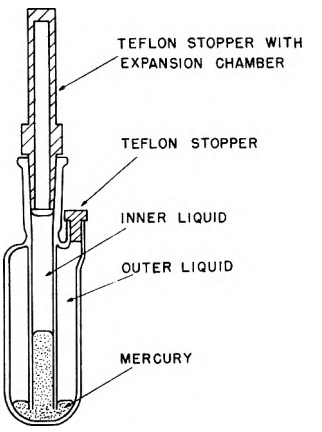

Fig. 1.—Diagram of the mixing cell used in the adiabatic calorimeter.

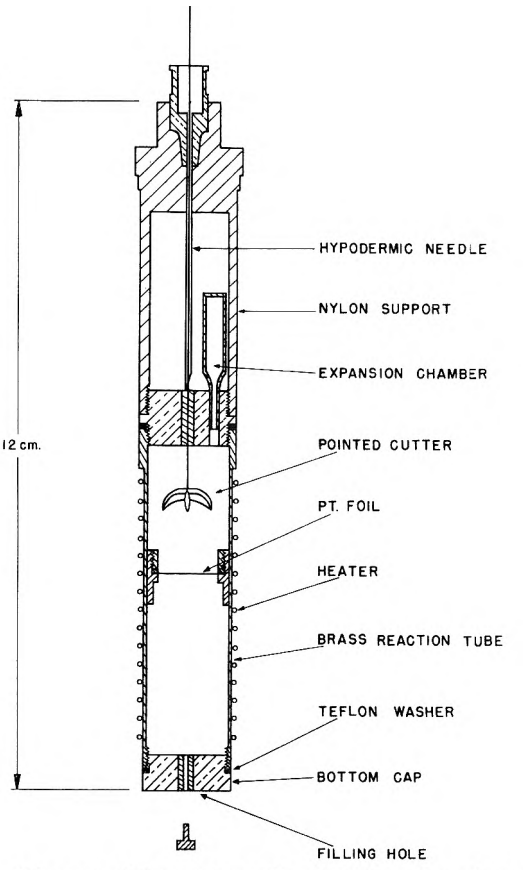

Fig. 2.—Diagram of the mixing cell used in the microcalorimeter.

In Table II values of the excess enthalpy interpolated at rounded concentrations are given. These were obtained through the use of smoothed plots of the deviation of the experimental points from suitable algebraic forms.

As mentioned in the Introduction, heats of mixing of methanol and water have been determined by several previous investigators. The measurements of Bose[5] were made at 0, 19.69, and 42.37°, those of Ocón and Taboada[6,7] at 16.0, 35.4, and 53.5°. Graphical interpolation in these two sets of data leads to the values at 25° listed in columns 5 and 7 of Table II. Percentage differences of these results from those obtained in the present investigation are given in columns 6 and 8. Below $x_2 = 0.5$ the deviation of Bose's data is 2% or

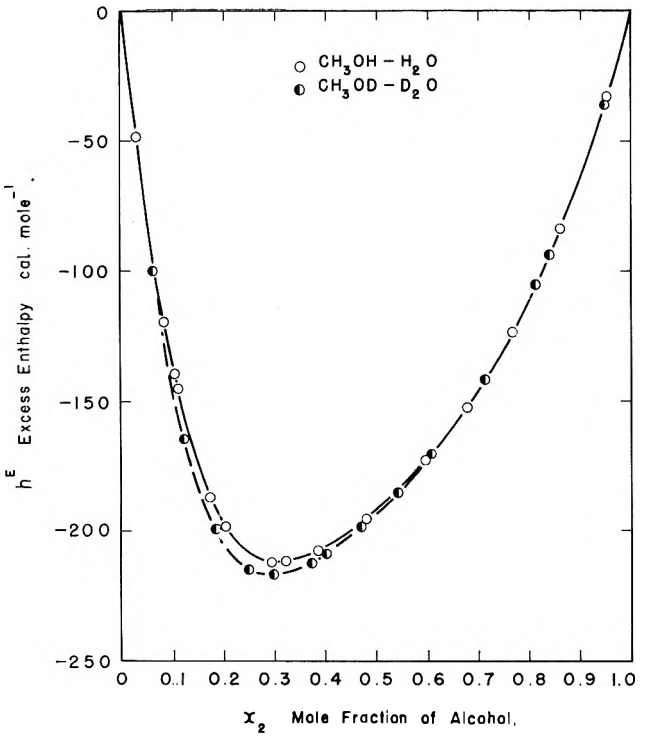

Fig. 3.—Plot of excess enthalpies measured in the adiabatic calorimeter at 25.00°.

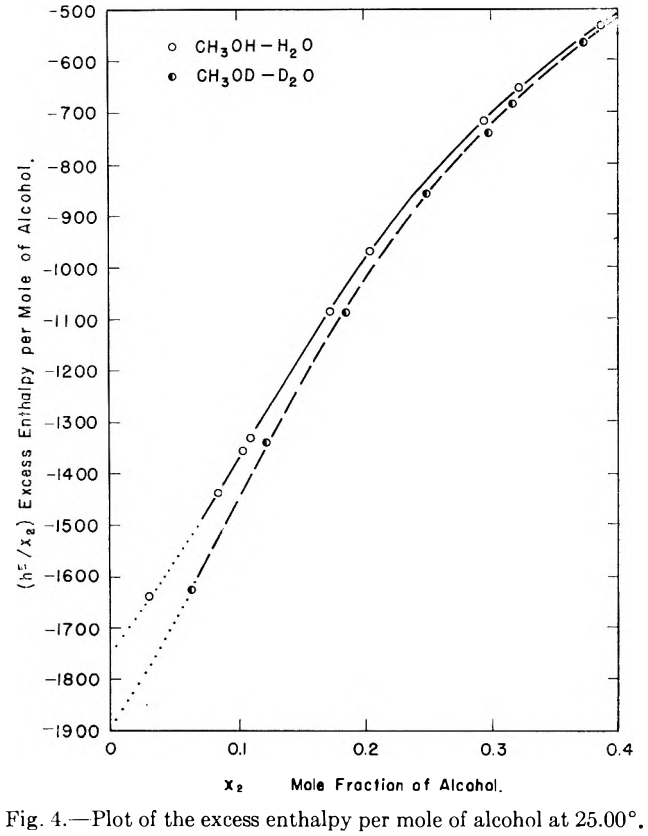

Fig. 4.—Plot of the excess enthalpy per mole of alcohol at 25.00°.

less, in magnitude, but increases at higher mole fractions. For most of the range above $x_2 = 0.5$ the new results are closer to those of Ocón and Taboada and numerically exceed Bose's values by about 7 cal. mole^{-1}. This difference is larger than can be explained by the estimated experimental error in the present measurements.

Percentage differences between the excess enthalpies for the deuterated and normal systems are given in the 4th column of Table II. The deviations above $x_2 = 0.5$ are not much larger than twice the estimated error of an individual determination, but become quite significant as the dilution of the alcohol increases. This conclusion is further substantiated by the divergence, at small x_2 values, of plots of (h^E/x_2) for the two systems (see Fig. 4).

The measurements in the microcalorimeter were designed to study solutions dilute in alcohol at concentrations lower than was feasible in the adiabatic calorimeter. Results for the two systems are given in Table III; the data in the first three columns are, respectively, the initial mole fraction x_2', the final mole fraction x_2, and the intermediate heat of dilution $\Delta H_{(x_2' \rightarrow x_2)}$ (in calories per mole of alcohol). The last column of Table III contains values of ϕ_L, the relative apparent molal enthalpy (referred to the infinitely dilute solution) at concentration x_2, derived from the intermediate heats by graphical superposition and extrapolation.

In Fig. 5 ϕ_L is plotted against x_2 for both systems. The curve for the deuterated solutions has been lowered 100 cal. mole^{-1} to separate it from the normal methanol results. The 5 points on the latter plot at concentrations below $x_2 = 0.006$ are based on the work of Lange and Markgraf.[15] These data appear to be consistent with the present results.

The values of the relative apparent molal enthalpy in dilute solutions were used in drawing the dotted parts of the curves in Fig. 4. It can be shown that the intercept at zero concentration in this figure is equal to

$$h_2^* - h_2^0 = -\bar{L}_2^C \qquad (1)$$

where h_2 is a partial molal enthalpy, and $\bar{L}_2$ is a relative partial molal enthalpy; the superscript asterisk and zero denote a solution infinitely dilute in alcohol and the pure substance, respectively. Values of the relative molar enthalpy of the pure alcohol obtained in this way are 1742 cal. mole^{-1} for methanol and 1885 cal. mole^{-1} for methanol-*d* with an uncertainty of about ±10 cal. mole^{-1} in each case. The difference of the two intercepts in Fig. 4 leads to the expression

$$(h_2^0)_D - (h_2^0)_H - [(h_2^*)_D - (h_2^*)_H] \approx 140 \text{ cal. mole}^{-1} \qquad (2)$$

where subscripts D and H are used to indicate the deuterated and normal systems

The difficulties associated with theoretical calculations of hydrogen bond energies have been summarized by Coulson.[16] In addition, experimentally measured values for the strength of hydrogen bonds lack precision and vary over a considerable range depending on the method of measurement.[3] It appears that in neither of these areas can the effect of deuterium substitution on hydrogen bonding be quantitatively established at the present time. The isotope effect in crystals, particularly with regard to changes in bond lengths, has been extensively studied and interpreted qualitatively in terms of differences in zero point energies.[3,17]

Approximately 15% of the sublimation energy of ice is gained on fusion and the remainder during evaporation of water at room temperature. The heat of fusion

(15) E. Lange and H. G. Markgraf, *Z. Elektrochem.*, **54**, 73 (1950).
(16) C. A. Coulson in "Hydrogen Bonding," ed. by D. Hadzi, Pergamon Press, London, 1959, see p. 339.
(17) A. R. Ubbelohde and K. J. Gallagher, *Acta Cryst.*, **8**, 71 (1955).

TABLE III

HEATS OF DILUTION MEASURED IN THE MICROCALORIMETER AT 25.00°

x'_2 (initial)	x_2 (final)	$\Delta H(x'_2 \rightarrow x_2)$, cal./mole alcohol	ϕ_L, cal./mole alcohol
	CH_3OH–H_2O system		
0.05697	0.05697	(0.0)	−202.5
	.04374	− 48.8	−153.7
	.03865	− 64.7	−137.8
	.03173	− 94.7	−107.8
	.02473	−114.5	− 88.8
	.02462	−112.6	− 89.9
.01834	.01834	(0.0)	− 62.7
	.01563	− 9.7	− 53.0
.01743	.01743	(0.0)	− 59.5
	.01237	− 17.3	− 42.2
	.00769	− 34.0	− 25.5
.01622	.01622	(0.0)	− 55.5
	.01149	− 16.4	− 39.1
	CH_3OD–D_2O system		
0.06486	0.06486	(0.0)	−272.0
	.05444	− 39.3	−232.7
	.04484	− 87.3	−184.7
	.03470	−138.3	−133.7
	.02828	−161.7	−110.3
.01835	.01835	(0.0)	− 67.5
	.01650	− 7.1	− 60.4
	.01403	− 16.7	− 50.8
	.01072	− 27.7	− 39.8
	.00825	− 37.5	− 30.0
.00558	.00558	(0.0)	− 21.5
	.00493	− 5.1	− 16.4
	.00409	− 6.4	− 15.1
	.00317	− 5.6	− 15.9
	.00249	− 15.0	− 6.5

for ice is 1436 cal. mole^{-1} and is increased by 65 cal. mole^{-1} for D_2O; the values of the heat of vaporization for water and heavy water at 25° are 10,520 and 10,851 cal. mole^{-1}, respectively.[18] Recent vapor pressure measurements show that the heat of vaporization is increased by 127 cal. mole^{-1} for methanol and 145 cal. mole^{-1} for isopropyl alcohol by deuterium substitution in the hydroxyl group.[19] Increased strength of the D-bond is also indicated by elevated boiling points of a number of substituted aliphatic alcohols.[20] In liquid water the statistical distribution of H-bonds is complex and any quantitative estimate of the enthalpy must take into account the extent and strength of the bonds (weaker than those in ice[21]), coördination number, and molecular aggregation.[22] However, the 3–4% increase in the heats of fusion and vaporization for D_2O as compared to H_2O, together with the increased heat of vaporization values for methanol and isopropyl alcohol, suggest that for these compounds in the liquid state the D-bond is ~150 cal. mole^{-1} stronger than the corresponding H-bond.

(18) "Selected Values of Chemical Thermodynamic Properties," Circular 500 of the National Bureau of Standards, U. S. Government Printing Office, Washington, D. C., 1952.

(19) A. A. Efremov and Ya. D. Zel'vinskii, *Zh. Vses. Khim. Obshch. im. D. I. Mendeleeva*, **6**, 359 (1961).

(20) I. B. Rabinovich, V. G. Golov, N. A. Efimova, and S. M. Rustamov, *Proc. Acad. Sci. USSR (Phys. Chem.)*, Eng. Transl., **114**, 339 (1957).

(21) C. L. van P. van Eck, H. Mendel, and J. Fahrenfort, *Proc. Roy. Soc.* (London), **A247**, 472 (1958).

(22) G. Némethy and H. A. Scheraga, *J. Chem. Phys.*, **36**, 3382 (1962).

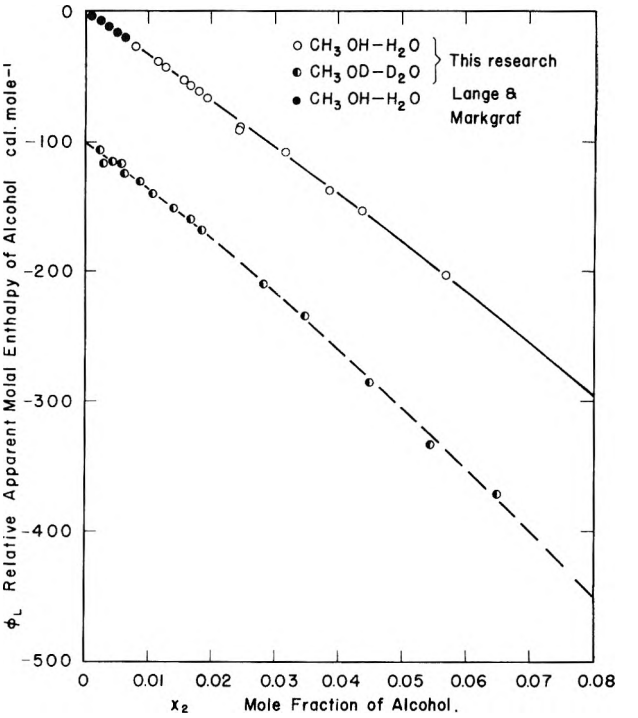

Fig. 5.—Plot of the relative apparent molal enthalpy at 25.00°. The data for the deuterated system have been lowered 100 cal. mole^{-1}.

Interactions in aqueous solutions of non-electrolytes have been classified in terms of the strength and number of solute–water bonds present,[23,24] and alcohols are seen to belong to a group which exhibits asymmetric negative excess enthalpies over the whole concentration range as in Fig. 3, but with positive excess free energies of mixing (see Mitchell and Wynne-Jones[25] for methanol–water data). Thus the bonds formed between methanol and water molecules are stronger or are present to a greater extent than those in the pure liquids. The observed isotope effect is in agreement with this picture and with the interpretation of solubility phenomena by Rabinovich, *et al.*[4] Although the number of formal H-bonds present must necessarily be reduced[24] when water is mixed with molecules containing inert groups such as $-CH_3$, the mean number of bonds may actually increase due to the stabilization of ice-like aggregates around the inert group. This concept, first formalized by Frank and Evans[26] and recently treated more quantitatively[27] was suggested by Butler[28] in discussing the hydration of aliphatic alcohols and hydrocarbons. The isotope effect expressed in eq. 2 is of reasonable magnitude for the increase in hydrogen bonding which might be expected to occur in the water around the methyl group.

Acknowledgment.—The authors wish to thank Mr. P. D'Arcy for invaluable assistance during the calorimetric measurements.

(23) J. S. Rowlinson in "Hydrogen Bonding," edited by D. Hadzi, Pergamon Press, London, 1959, see p. 423.

(24) J. S. Rowlinson, "Liquids and Liquid Mixtures," Butterworths Publ. Ltd., London, 1959, see pp. 183–186.

(25) A. G. Mitchell and W. F. K. Wynne-Jones, *Discussions Faraday Soc.*, **15**, 161 (1953).

(26) H. S. Frank and M. W. Evans, *J. Chem. Phys.*, **13**, 507 (1945).

(27) G. Némethy and H. A. Scheraga, *ibid.*, **36**, 3401 (1962).

(28) J. A. V. Butler, *Trans. Faraday Soc.*, **33**, 229 (1937).

ANODIC OXIDATION OF N-METHYLANILINE AND N,N-DIMETHYL-*p*-TOLUIDINE

BY Z. GALUS AND RALPH N. ADAMS

Department of Chemistry, University of Kansas, Lawrence, Kansas

Received October 11, 1962

The anodic oxidation of N-methylaniline was studied at carbon paste and platinum electrodes using cyclic voltammetry and rotating disk techniques. N-Methylaniline oxidizes to give N,N′-dimethylbenzidine as a primary product which is further oxidized to the corresponding diquinoid. The anodic reaction is very similar to that of N,N-dimethylaniline. However, if the *para* position of an N-methylated aniline is blocked, as in N,N-dimethyl-*p*-toluidine, the reaction is entirely different. Here anodic oxidation of the *para* methyl group occurs leading to the corresponding aldehyde and acid.

The anodic oxidation of N,N-dimethylaniline (DMA) was investigated in this Laboratory and shown to consist of a 2-electron charge transfer step followed by a chemical reaction to yield N,N′-tetramethylbenzidine (TMB). This compound, being more easily oxidized than the parent DMA, undergoes further oxidation to the quinone diimine (TMBOx). Further complicating side reactions of the TMBOx with excess DMA were identified and the entire reaction scheme was studied in detail.[1-3]

It is therefore of considerable interest to investigate the anodic oxidation of monomethylaniline to see if it proceeds in similar fashion. Further, by blocking the *para* position, as in N,N-dimethyl-*p*-toluidine, it is possible to see if an *ortho* type coupling can occur to give a benzidine-like product or if some entirely new electrode reaction occurs. The following studies of the anodic oxidation of N-methylaniline (MA) and N,N-dimethyl-*p*-toluidine (DMPT) were carried out using single and multi sweep cyclic voltammetry as well as rotated disks. In addition some random tritium labeled electrolyses were investigated. Experimental details have been presented previously.[1-3]

Oxidation of MA.—The oxidation of MA was carried out over a wide pH range from 3 *N* H_2SO_4 to pH 9 buffer. The buffer solutions were Britton and Robinson and contained 1 *M* Na_2SO_4 to maintain reasonably constant ionic strength All polarograms were carried out with a controlled potential scanner.

Over the entire pH range MA showed a single anodic wave with $E_{p/2}$ varying with pH as expected. The $E_{p/2}$ values at Pt and carbon paste electrodes were very similar below pH 6–7. Above this pH range results on carbon paste showed considerable scatter. Below pH 5.5, the mean slope of the peak polarograms on Pt is 55 mv. and about 60 mv. for carbon paste electrodes.

The family of curves in Fig. 1A shows the cyclic voltammetry of MA at pH 2.4 at a carbon paste electrode. The first anodic scan (1) shows only the oxidation wave for MA at *ca.* 0.7 v. *vs.* s.c.e. Upon reversal of the scan two cathodic waves are obtained at *ca.* +0.45 and 0.35 v. In the subsequent anodic scans two anodic waves appeared at the corresponding potentials.

Following the reasoning used in the DMA studies, the oxidation–reduction system at *ca.* 0.45 v. was presumed to be that of N,N′-dimethylbenzidine (DMB) and its corresponding diquinoid DMBOx. Therefore DMB was prepared by standard methods and subjected to cyclic voltammetry under identical conditions. The system of almost reversible cyclic polarograms seen in Fig. 1B resulted. There is very little doubt that the DMB–DMBOx system is present after electrolysis of MA. The magnitude of the currents for the DMB–DMBOx system obtained in electrolysis of MA (Fig. 1A) is small since DMBOx reacts rapidly with excess MA as indicated below.

The oxidation–reduction system at *ca.* +0.35 v. was assumed to result from coupling of DMBOx and excess MA Accordingly, DMB was oxidized in the presence of excess MA, *care being taken to keep the potential below that at which MA oxidizes.* The family of polarograms in Fig. 1C resulted. Note especially that on the first anodic scan (1), only a wave for DMB oxidation is obtained. On the reverse (cathodic going) cycle both cathodic waves are observed and on the second and subsequent anodic scans the semi-reversible oxidation–reduction couple at +0.35 v. is clearly evident. It is clear then that the compound formed which gives rise to the oxidation–reduction system at +0.35 v. is formed by interaction between DMBOx and MA.

It is fairly clear then that DMB is formed in MA anodic oxidation and that DMB, being more easily oxidized than the parent MA, is found finally as DMBOx. In this respect the oxidation of MA is almost identical with that of dimethylaniline. However, the secondary reaction between DMBOx and MA is much faster and occurs even in acidic media whereas this reaction was only prevalent in alkaline media with dimethylaniline. It remained to be decided if the DMB arises from a free radical coupling of two MA molecules which had lost one electron each, or by the dipositive species interacting with an unoxidized molecule of MA. This question can be decided by studying the order of the reaction with respect to MA and the number of electrons in the charge transfer step.

The reaction order was determined by studies at a rotated disk of carbon paste. The rotation speed was varied between 0 and 30 r.p.s. Figure 2 shows some typical results. Here the current *vs.* the square root of rotation speed ($N^{1/2}$) is plotted for MA oxidation at various applied potentials. At low E_{app} (0.87 v.) the current is almost independent of rotation speed, *i.e.*, the current is practically limited by the charge transfer process. At the highest potential, 0.95 v., the current increases with rotation speed but is still not linear with $N^{1/2}$. Such behavior is typical of a reaction controlled both

(1) T. Mizoguchi and R. N. Adams, *J. Am. Chem. Soc.*, **84**, 2058 (1962).
(2) Z. Galus and R. N. Adams, *ibid.*, **84**, 2061 (1962).
(3) Z. Galus, R. M. White, F. S. Rowland, and R. N. Adams, *ibid.*, **84**, 2065 (1962).

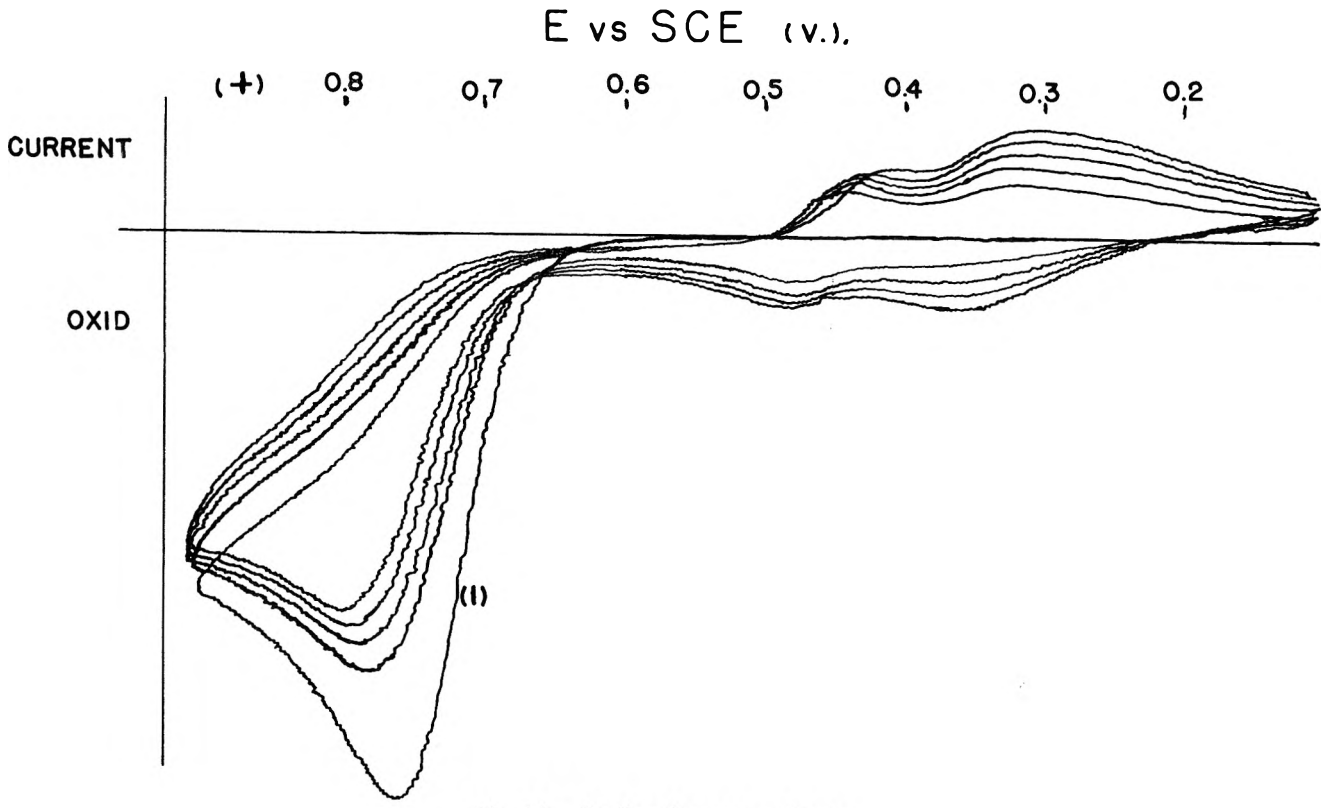

Fig. 1A.—Cyclic polarograms of MA.

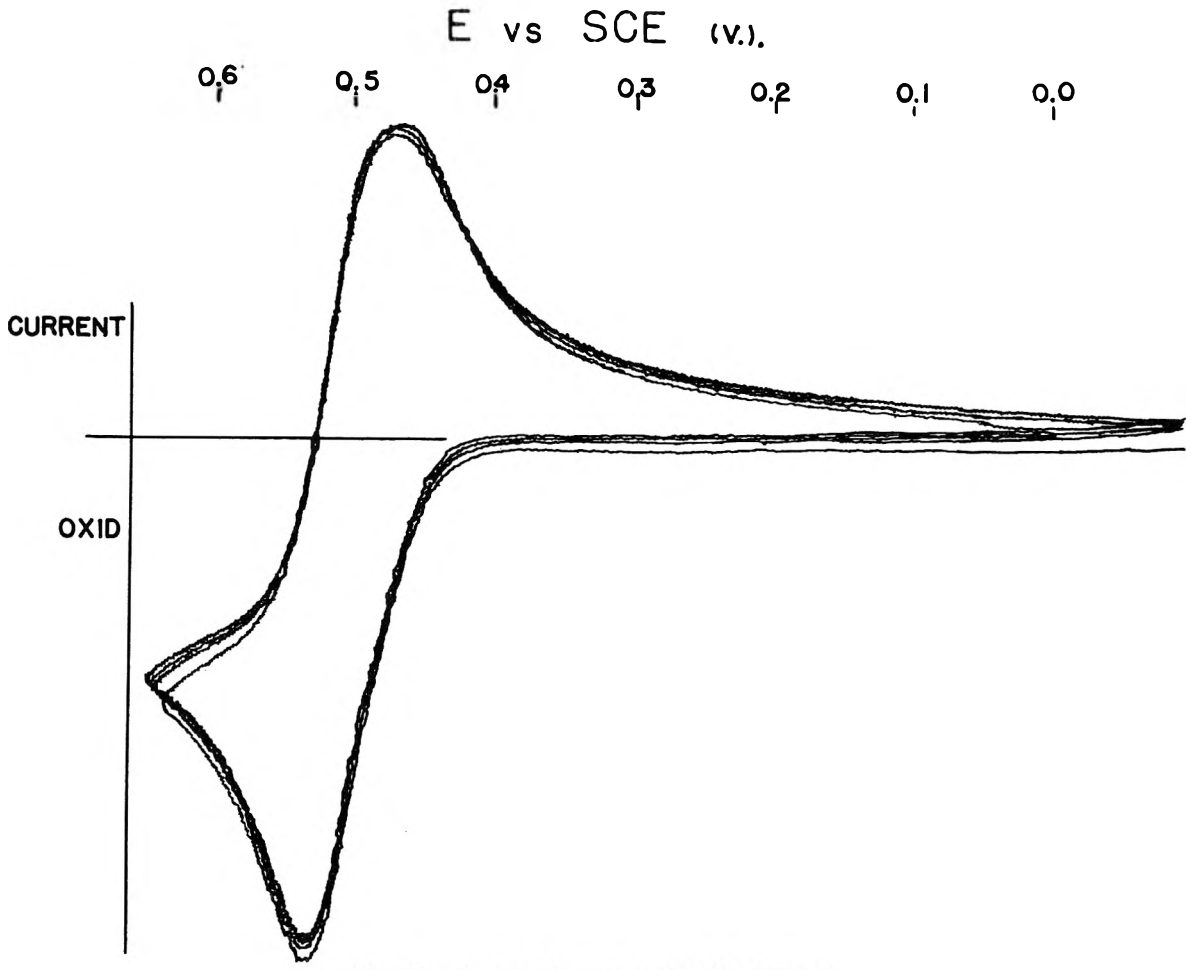

Fig. 1B.—Cyclic polarograms of DMB–DMBOx.

by mass transfer and rate of electrochemical reaction. This case has been treated extensively by Levich.[4] The reaction order, m, was calculated by the method used for DMA previously (see ref. 2, eq. 8). The δ-values were calculated for 3 and 21 r.p.s. and found to

(4) V. G. Levich, "Fiziko-khimicheskaya gidrodinamika (Physico-Chemical Hydrodynamics)," p. 77, Godudarstvennoe, Izdatel'stvo Fiziko-matematicheskoi Literatury, Moscow, 1959.

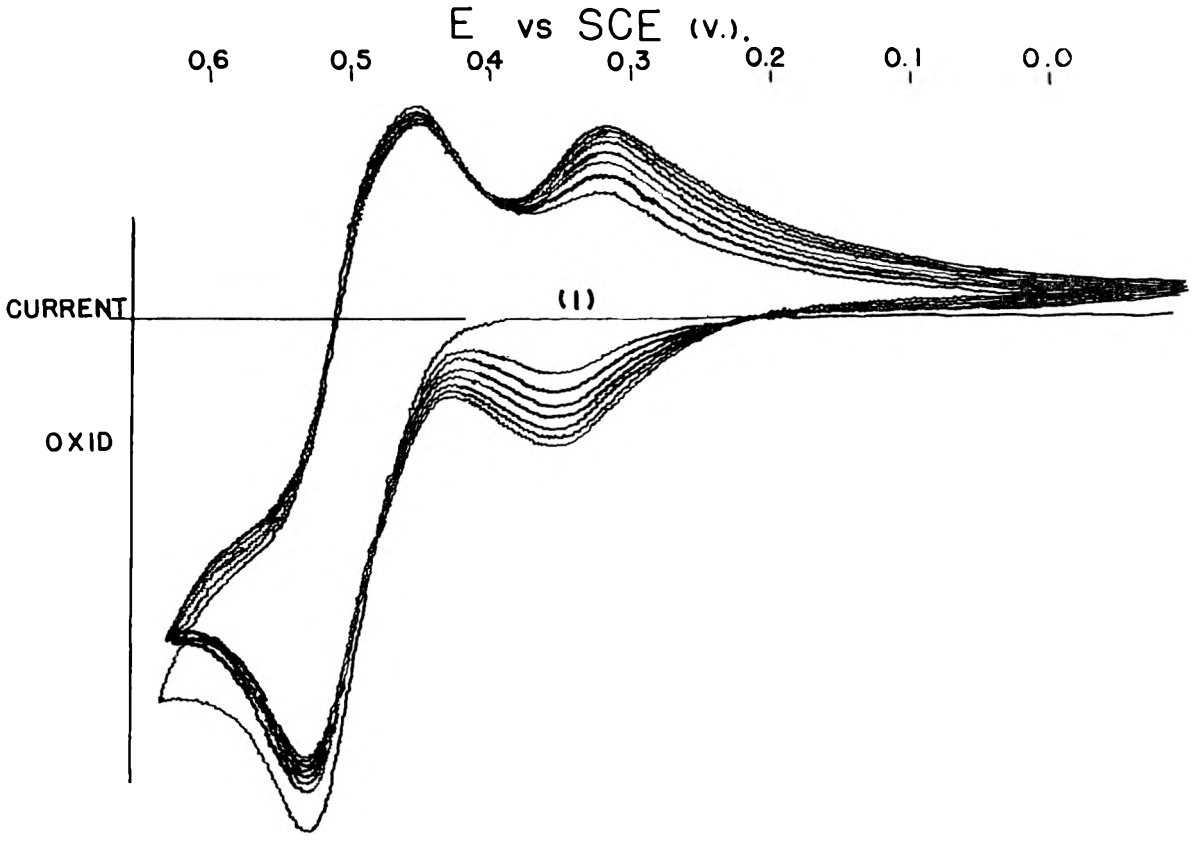

Fig. 1C.—Cyclic polarograms of mixture of DMBOx and excess MA.

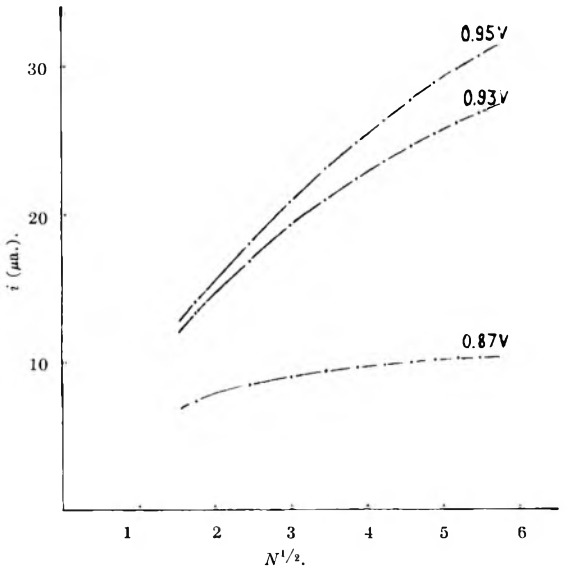

Fig. 2.—Oxidation of MA at rotated disk electrode.

have the values 3.39×10^{-3} and 1.28×10^{-3} cm., respectively. The corresponding fluxes at these speeds were calculated from the currents of Fig. 2. D values were evaluated from peak current polarograms with $n_T = 2$ electrons. The kinematic viscosity was assumed to be 0.01 cm.^{2}/sec. The value of m at 0.93 v. was found to be 0.87; at 0.95 v. m was 0.85. This is fairly conclusive evidence that one molecule of MA is involved in the charge transfer step.

The quantity (βn_a), the product of the anodic transfer coefficient by the number of electrons in the charge transfer step, was next evaluated from the peak polarograms using the well known relations for an irreversible process given by Matsuda and Ayabe[5]

(5) H. Matsuda and Y. Ayabe, *Z. Elektrochem.*, **59**, 494 (1955).

$$\beta n_a = \frac{0.048}{E_p - E_{p/2}} \text{ at } 25°$$

The results are shown in Table I. (βn_a) is difficult to evaluate for Pt at slow scan rates since the peak polarograms are drawn out (*i.e.*, $(E_p - E_{p/2})$ is difficult to evaluate). At the higher scan rates the mean value is about 0.83. The results are excellent at carbon paste with a mean value of 0.91 The values of (βn_a) obtained strongly suggest $n = 2$ assuming a reasonable value for β of *ca.* 0.5. Higher values of n_a are not excluded by this evaluation.

TABLE I

KINETIC PARAMETERS FOR MA OXIDATION[a]

Scan rate (v./min.)	βn_a Pt	βn_a C.P.	log K_b^0 Pt	log K_b^0 C.P.
0.00083	..	0.88	....	−18.5
.0033	0.73	.91	−15.9	−18.8
.0083	.81	.92	−17.1	−18.9
.0167	.82	.92	−17.1	−18.9
.033	.85	.90	−17.6	−18.5

[a] In sulfuric acid–sulfate buffer pH 1.32.

On the basis of the above data we propose the electrochemical oxidation of MA proceeds according to

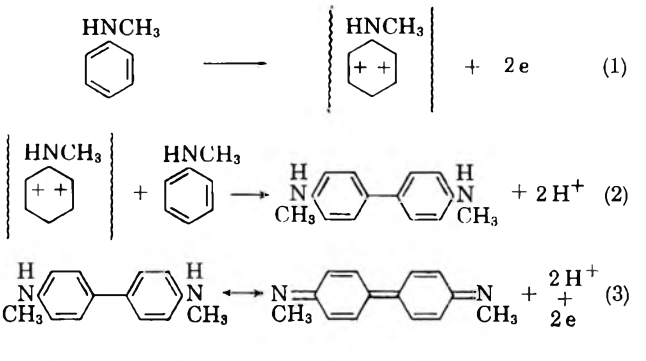

In actual fact DMB was not identified positively. The identification *via* a double rotated disk technique, which was successful with DMA (see ref. 2), was not possible in the present study since the secondary reaction of DMBOx with MA was so rapid. The product of this secondary reaction interferes with the double disk method.

The subsequent reaction of DMBOx and MA was investigated in more detail by classical potentiometry. A solution of DMBOx was prepared by oxidizing a known amount of DMB with bromine *via* a bromate–bromide reaction in acid solution. Care was taken to add an amount of bromine which would oxidize only about one half of the known quantity of DMB (*i.e.*, no excess bromine was present at the end of the reaction). Next, this solution of DMBOx was titrated potentiometrically with MA solution using a carbon paste indicator electrode *vs.* s.c.e. Figure 3 shows a typical potentiometric curve. In solutions from 0.1 to 1.5 *N* H_2SO_4, the ratio of MA to DMBOx was found to be very close to 2. Thus, it can be postulated that the oxidation–reduction system which develops at *ca.* +0.35 v. is that of a compound with the generic formula

$$\text{DMBOx (MA)}_2$$

This material is oxidizable and forms a semi-reversible oxidation–reduction system. The exact structure of the coupling product is somewhat speculative. At higher pH's, the ratio of MA/DMBOx is less than 2 indicating partial reduction of DMBOx prior to reaction.

The latter point is borne out by examination of the tritium content of random labeled MA after usual oxidation procedures. The activity was always lower than expected on the basis of the postulated reactions at high pH's. Either deamination reactions occur at high pH's or rapid exchange of the tritium occurs.

Finally, at low pH's, when the formation of the DMBOx–MA compound is relatively slow, the rate constants for MA oxidation were determined from the peak polarogram behavior using the expression of Matsuda and Ayabe

$$E_{p(Irr)} = \frac{RT}{\beta n_a F}\left[0.78 - \ln\frac{K^0{}_b f_{Red}}{D_{Red}^{1/2}} + \frac{1}{2}\ln\frac{\beta n_a F V}{RT}\right]$$

where K_b^0 is the rate constant evaluated at $E = 0$ (*i.e.*, *vs.* $H_2 = 0$). In Table I, the rate constants (actually log ($K_b^0 \times f_{Red}$)) are seen to be independent of scan rate and have the mean value −18.7 on carbon paste. The reaction appears slightly more rapid at Pt with a mean log $K_b^0 = -17.3$.

The apparent activation energies were calculated by varying the temperature between 25.2 and 56.5°. The product βn_a was practically constant over the temperature interval. A plot of log K_b^0 *vs.* $1/T$ gives an apparent activation energy of 30.8 kcal. This is quite a bit smaller than that found for DMA under similar conditions.

Rate constants evaluated at other than the equilibrium potential cannot be compared for different substances. However, since the hypothetical equilibrium potentials for DMA and MA can be supposed to be quite similar, it is possible to make an approximate correlation of the anodic oxidation rates of DMA[2] and MA. Thus, in the same pH region we have

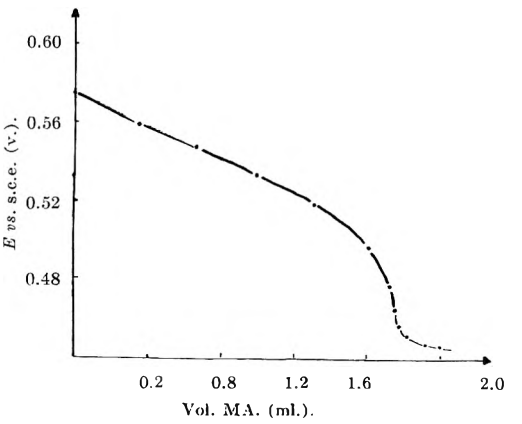

Fig. 3.—Potentiometric titration of DMBOx with MA.

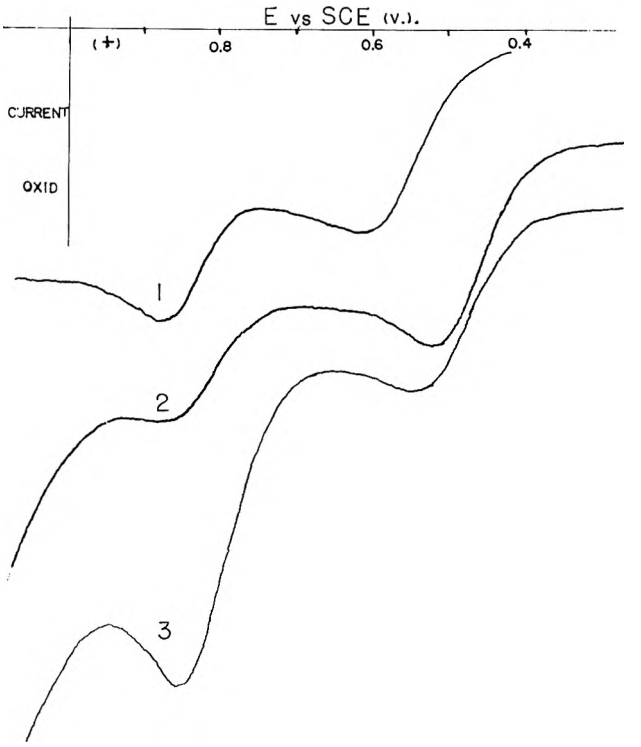

Fig. 4.—Anodic oxidation of DMPT: 1, carbon paste electrode; 2, platinum electrode; 3, DMPT plus *p*-dimethylaminobenzaldehyde.

DMA $\log K_b^0 = -19.8$

MA $\log K_b^0 = -17.2$

Oxidation of N,N-Dimethyl-*p*-toluidine.—Since some 20% *ortho–para* coupling was shown to exist in the oxidation of DMA,[3] a study of N,N-dimethyl-*p*-toluidine (DMPT) was of interest to see if similar coupling would occur or whether the blocking of the *para* position would result in an entirely new electrode reaction. It was found, indeed, that the oxidation of DMPT is quite different.

During cyclic scanning of DMPT in solutions from 3 *N* H_2SO_4 to pH 11 buffer, at both carbon paste and Pt electrodes, *no reversible electroactive systems were formed* in the region 0 to + 1.2 v. This alone is evidence that the *o,o'*-dimethyl-N,N'-tetramethylbenzidine is not formed.

Instead only anodic waves were found in DMPT oxidation. Two waves were always seen with even a small third anodic wave occurring in the pH interval 2–6. The slopes of these waves were not very repro-

ducible and the value of $E_{p/2}$ varied with scan rate. The peculiar behavior was not caused by film formation on the electrode since repeat scans were quite reproducible. However, quantitative measurements of βn_a were not attempted.

The nature of the various waves in DMPT oxidation can be explained qualitatively. Since no reversible oxidation–reduction systems were observed it is reasonable to assume the *para* CH_3 group is oxidized. In alkaline solution, where 2 waves are observed, the ratio of peak currents was about 2:1. This is seen in Fig. 4. Curve 1 was obtained on C paste and curve 2 on Pt. By comparison of the peak currents for oxidation of DMA and DMPT (assuming $D_{DMA} = D_{DMPT}$) and taking into account the ratio of the apparent transfer coefficients a reasonable value for n of the DMPT oxidation is 4 electrons. Thus, it is most likely that the first wave corresponds to oxidation to aldehyde. The second wave (2 electrons) is then an oxidation to the corresponding acid.

Support of this mechanism is afforded by adding *p*-dimethylaminobenzaldehyde to a solution of DMPT and examining the second wave. Curve 3 of Fig. 4 shows the polarogram obtained at pH 6.8 where 5.0×10^{-4} *M* aldehyde was added to 4×10^{-4} *M* DMPT. The 2nd wave quite clearly is due to the presence of the aldehyde formed from the oxidation during the 1st wave.

Summary.—The anodic oxidation pathways of N-methyl and N-dimethylaniline have been shown to be quite similar. Both lead to the formation of N-substituted benzidines. However, with the *para* position blocked, as in N,N-dimethyl-*p*-toluidine, oxidation of the *para* methyl substituent occurs.

Acknowledgments.—It is a pleasure to acknowledge the support of this work by the Atomic Energy Commission through contract AT(11-1)-686. We are indebted to A. Rogers for technical assistance.

THE INVESTIGATION OF THE KINETICS OF MODERATELY RAPID ELECTRODE REACTIONS USING ROTATING DISK ELECTRODES[1]

BY Z. GALUS AND RALPH N. ADAMS

Department of Chemistry, University of Kansas, Lawrence, Kansas

Received October 12, 1962

The capabilities and limitations of rotated disk electrodes for the measurement of heterogeneous rate constants (k_s) have been examined in detail. Values of k_s for the oxidation–reduction systems Fe(III)–Fe(II), $Fe(CN)_6^{-3}$–$Fe(CN)_6^{-4}$, MnO_4^-–$MnO_4^=$, and Ce(IV)-Ce(III) were determined at platinum and carbon paste rotated disks as a function of solution environment. The results for moderately rapid charge transfer rates are in good agreement with existing data. Further correlations of k_s and the homogeneous exchange rate are possible *via* recent theoretical interpretations of Marcus.

The rotating disk electrode (r.d.e.) is uniquely suited to the determination of the heterogeneous rate constants for moderately rapid electron transfer (charge transfer) processes. As was shown by Levich,[2] the mass transport rate to the disk surface is independent of the distance from the axis of revolution. Thus, the concentration of the electroactive species at the electrode surface (C^e) is everywhere equal on the surface and the thickness of the diffusion layer is given by Levich as

$$\delta = 1.61 D^{1/3} \gamma^{1/6} \omega^{-1/2} \qquad (1)$$

where

D = diffusion coefficient, cm.²/sec.

γ = kinetic viscosity, cm.²/sec.

ω = angular velocity of disk given by $\omega = 2\pi N$ where N = revolutions per sec.

It follows that the rate of an electrochemical reaction at the surface of the r.d.e. is equal at all points on the surface (disregarding micro heterogeneity, *i.e.*, active sites on the surface).

To investigate the kinetics of an electrode reaction, mass transport (m.t.) should be fast in comparison to the charge transfer (c.t.) rate. With the r.d.e., the m.t. rate can be regulated *via* the disk rotation velocity. One might think it would be possible to determine very fast c.t. rates by increasing rotation velocity to very high values. With high rotation velocities, the fluid flow at the r.d.e. becomes turbulent and relations based on laminar m.t. are no longer valid.

According to Levich,[3] the m.t. at smooth and well centered r.d.e.'s ceases to be laminar at values of the Reynolds number (Re) between 10^4 and 10^5. The dimensionless parameter Re is given by

$$\mathrm{Re} = \frac{r^2\omega}{\nu} \qquad (2)$$

where

r = radius of r.d.e. in cm.

Non-turbulent conditions are favored by using an electrode of small radius (this includes the working plus non-working shield radius). On the other hand, the size of the disk working surface must be large enough to allow one to neglect edge effects. In the present work good results were obtained with disk diameters of 2 mm. (working surface). Smaller disks have been described by Vielstich and Jahn,[4a] Azzim and Riddiford,[4b] and Frumkin and Teodoradse.[5]

(1) Based on material presented at Symposium on Electrode Processes, Division of Physical Chemistry., 142nd National Meeting of the American Chemical Society, Atlantic City, N. J., Sept., 1962.

(2) V. G. Levich, "Physicochemical Hydrodynamics," Prentice–Hall, Inc., Englewood Cliffs, N. J., 1962.

(3) Ref. 2, p. 86.

(4) (a) W. Vielstich and D. Jahn, *Z. Elektrochem.*, **64**, 63 (1960); (b) S. Azzim and A. C. Riddiford, *Anal. Chem.*, **34**, 1023 (1962).

(5) A. N. Frumkin and G. Teodoradse, *Z. Elektrochem.*, **62**, 251 (1958).

Assuming a radius (working plus shield) of 1.4 mm. as a practical size, then substituting in eq. 2 a rounded value of $\gamma = 10^{-2}$ cm.^{2}/sec. and a limit of Re $= 2 \times 10^4$, one finds the highest non-turbulent rotation velocity is about $\omega = 10^4$ rad./sec. The m.t. rate at this upper limit of rotation velocity is

$$V_{mt} = \frac{D}{\delta} \tag{3}$$

Combining equations 3 and 1, one has

$$V_{mt} = 0.62 D^{2/3} \nu^{-1/6} \omega^{1/2} \tag{4}$$

Using $\omega = 10^4$, $\gamma = 10^{-2}$ cm.^{2}/sec., and $D = 10^{-5}$ cm.^{2}/sec., one has $V_{mt} = 6.2 \times 10^{-2}$ cm./sec. as an upper limit.

Under such experimental conditions one expects that electrochemical systems having c.t. rate constants smaller than about 6×10^{-3} cm./sec. will show i–E curves with definite irreversible character. Conversely, the i–E curves for systems with c.t. rate constants greater than about 0.6 cm./sec. will appear to be controlled predominantly by mass transport (ordinarily called diffusion controlled or reversible).

In summary, the r.d.e. is best suited to the measurement of *moderately* fast electrode processes. Using the *highest*, non-turbulent rotation velocities ($\omega = 10^4$ rad./sec. and the previous assumptions regarding practical size, etc.), the upper limit of rate constants which could be evaluated with a precision of a few per cent is *ca.* 6×10^{-2} cm./sec. Presumably with precisions of ±20–30% values of k_s up to 2.5×10^{-1} cm./sec. could be determined. The r.d.e. could be approximately competitive with potentiostatic and galvanostatic methods.

We feel, however, that mechanical problems limit practical rotation velocities to about $\omega = 10^3$ rad./sec. (For instance, vortex formation is difficult to control much above these speeds. While it apparently is unnecessary to maintain laminar flow if the data are treated by the calculations of Randles discussed later, if turbulent flow is present, it *must be reproducible.* The latter condition is not easily achieved experimentally.)

It also should be pointed out that the m.t. rate increases only with $\omega^{1/2}$. The highest rotation velocity used in this study, 754 rad./sec., which is about 13 times smaller than the highest non-turbulent velocity, gives $V_{mt} = 1.7 \times 10^{-2}$ cm./sec. This is smaller than the estimated upper limit of $V_{mt} = 6.2 \times 10^{-2}$ cm./sec. by only a factor of 3.65. In terms of measured rate constants little is gained by going to higher rotation velocities.

Using the r.d.e.'s described herein, with the upper practical limit of $\omega = 754$ rad./sec., one is able to determine k_s up to *ca* 1.5×10^{-2} cm./sec. with estimated precisions of ±5%. With decreasing precision, one could measure k_s up to 6×10^{-2} cm./sec. Since this work was completed a report by Jahn and Vielstich appeared in which values of k_s up to 0.1 cm./sec. were measured with the r.d.e.[6]

Methods for Evaluation of Rate Constants.—Methods for calculating rate constants from i–E curves have been given by Levich,[7] Randles,[8] Jordan and coworkers,[9] and others.

1. Levich Method.—For the first-order electrode reaction which is controlled both by m.t. and c.t., Levich writes

$$i = \frac{nFADC^b}{1.61 D^{1/2} \nu^{1/6} \omega^{-1/2} + \frac{D}{k}} \tag{5}$$

This relation can be written as

$$i = \frac{nFADC^b}{\delta + \frac{D}{k}} \tag{5a}$$

Here, C^b is the bulk concentration of electroactive species, A is the electrode area, and k is the heterogeneous rate constant at the given potential. The other symbols have their usual significance. Depending on the relative magnitudes of δ and the ratio D/k, equation 5 or 5a has limiting forms corresponding to control of the electrode process by c.t. or m.t.

If $\delta = 10^{-3}$ cm. (a reasonable value under the experimental conditions used herein), then for values of $k > 10^{-1}$ cm./sec. the term D/k can be dropped to give the familiar relation for the limiting current of a diffusion controlled process at the r.d.e.

$$i = 0.62 nFAD^{2/3} \nu^{-1/6} \omega^{1/2} C^b \tag{6}$$

On the other hand, if, under the same experimental conditions, $k < 10^{-4}$ cm./sec., then δ is negligible with respect to D/k and one has

$$i = nFAkC^b \tag{7}$$

It is clear that the observed current in this case is independent of the m.t.—the current is entirely controlled by c.t. As will be apparent in the Experimental section, the rate constant can be evaluated from equations 5 and 7.

Next log k_f and log k_b can be plotted as a function of electrode potential. According to the relations

$$k_f = k_f^0 \exp\left(\frac{-\alpha n_a FE}{RT}\right) \tag{8}$$

and

$$k_b = k_b^0 \exp\left(\frac{(1-\alpha) n_a FE}{RT}\right) \tag{9}$$

where k_f = "forward" rate constant for cathodic direction. Two straight lines should be obtained from the slopes of which the transfer coefficient, α, can be evaluated. The intersection, at the formal potential of the system, E_f^0, gives the rate constant at the formal potential, k_s. In the Levich method only one of the conjugate pair Ox–Red is in the bulk of solution, and measurements are made at high overpotentials so the inverse reaction can be neglected.

2. Randles Method.—The technique given by Randles is preferred and is applied to systems where mixed anodic–cathodic polarograms are obtained.[8]

(6) D. Jahn and W. Vielstich, *J. Electrochem. Soc.*, **109**, 849 (1962). While these workers indicate values of k_s up to 0.1 cm./sec. can be measured, no indications of precision are given.

(7) Ref. 2, p. 83.

(8) J. E. B. Randles, *Can. J. Chem.*, **37**, 238 (1959).

(9) J. Jordan, *Anal. Chem.*, **27**, 1708 (1955); J. Jordan and R. A. Javick *Electrochim. Acta*, **6**, 23 (1962).

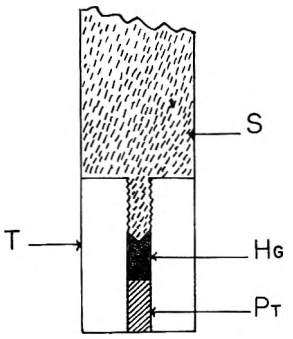

Fig. 1.—Interchangeable rotated disk electrode: S, brass extension of motor shaft, threaded on projection as indicated; T, Teflon shield; Hg, mercury resevoir for electrical connection; Pt, disk electrode, pressure fitted in Teflon shield.

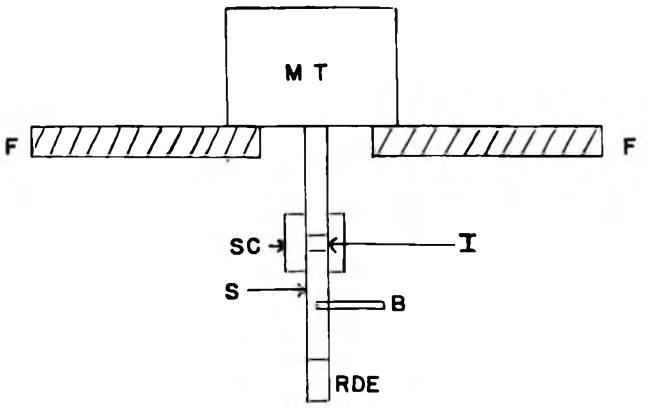

Fig. 2.—Rotated electrode assembly: MT, motor-tachometer generator; F, steel support frame, bolted *via* Unistrut to laboratory wall; SC, shaft coupler, set-screw adjust; S, brass shaft extension, see Fig. 1; I, air space insulation between motor shaft and brass extension; B, brush type external electrical connection; RDE, interchangeable rotated disk electrode, see Fig. 1.

In terms of the limiting cathodic and anodic currents i_c and i_a, and the current, i, at any point on the wave, one has

$$-\log nFk_f C_{Ox}{}^b = \log\left[\left(\frac{1}{i}-\frac{1}{i_c}\right)-\left(\frac{1}{i}+\frac{1}{i_a}\right)\exp\left(\frac{nE\eta}{RT}\right)\right] \quad (10)$$

where the overpotential, η, is given as $\eta = E - E_f{}^0$. A similar expression can be written to evaluate k_b. Experimentally, the k's are evaluated at various values of η. As before, a log plot of k_f and k_b *vs.* η gives two straight lines with an intersection at $\eta = 0$ where k_s is evaluated. Unless otherwise noted Randles' calculations were used. We are indebted to the referee for pointing out that the Levich treatment results from eq. 10 when the term exp $(nF\eta/RT)$ is either << or >> 1 and i_c or i_a is given by eq. 6 for mass transport conditions at the r.d.e.

Obviously, using the Randles method of treating the experimental data, rate constants for c.t. can be evaluated only if the recorded i–E curve shows sufficient deviation from "reversible" behavior. This is most easily checked by a quick evaluation of $(E_{3/4} - E_{1/4})$ on the wave. For a completely m.t. controlled process one has

$$(E_{3/4} - E_{1/4}) = \frac{0.056}{n} \text{ v.} \quad (11)$$

It can be observed that the precision in determining k is greater, the greater is the deviation from reversibility. Using the r.d.e., one essentially "tunes in" irreversible character by increasing the rotation velocity of the disk.

Experimental

Doubly distilled water was used for all work. Solutions of sulfuric acid were prepared after fuming the concentrated acid according to the directions of Anson.[10] Hydrochloric acid was distilled at room temperatures. Approximately 0.6 *M* hydrochloric acid was prepared by placing a beaker of the concentrated acid and a beaker of pure water in a desiccator. After about 20 hours, the *ca.* 0.6 *M* acid was obtained by effusion. Sodium perchlorate was prepared by neutralization of pure perchloric acid with high purity sodium bicarbonate. Other salts used as background electrolytes were recrystalized and carefully dried. The ferric and ferrous solutions were standardized by conventional cerimetric titrations. Permanganate solutions were standardized *vs.* oxalic acid. The solutions of potassium ferro- and ferricyanide were prepared by dissolving the twice recrystallized salts in pure water.

The platinum r.d.e. was prepared from 3 mm. diameter platinum wire. This was pressure fitted in a drilled Teflon rod and both surfaces cut smooth on the working end. Figure 1 illustrates the electrode design. The Teflon rod was threaded on the upper end to attach to the brass extension (S, in Fig. 1) of the motor shaft. In this way a variety of electrodes can be interchanged without disturbing the shaft coupling itself. Electrical connection between the disk and the brass rod was *via* a mercury pool and the external electrical contact was a copper wire acting as a brush on the brass rod. The contact area on the brass rod was amalgamated frequently to eliminate electrical noise. Figure 2 illustrates the entire electrode assembly. The motor with integral tachometer generator (MT) was bolted to a steel plate and supported on the laboratory wall by a Unistrut frame. This reduced vibration problems and allowed free working space under the electrode. The polarographic vessel was supported on an adjustable platform. The output of the tachometer generator was fed to an operational amplifier speed controller. Many other forms of speed control are possible. Calibration of rotation velocities was accomplished with a stroboscope type arrangement. (Exact rotation velocities are not needed in the Randles type treatment.)

The carbon paste electrodes were prepared similar to the platinum except that the hole in the Teflon contained carbon paste. Slightly different forms of carbon paste r.d.e.'s have been described previously.[11] Unless otherwise noted, the carbon paste was a standard Nujol composition as described previously. Platinum electrodes were pretreated in a fashion similar to that used by Anson using electrical oxidation at 1.5 v. *vs.* s.c.e., followed by chemical reduction in 10^{-3} *M* ferrous sulfate solution.

All measurements were made at 25° with an operational amplifier controlled potential polarograph.

Results

The measurement of rate constants, in itself, is not particularly significant. However, recent advances in the interpretation of electrochemical and homogeneous electron transfer reactions allow intriguing correlations to be made between these processes.[12] Thus the measurement of k_s values for oxidation–reduction systems as a function of solution environment and electrode system becomes of considerable significance. In this study with the r.d.e. electrochemical systems were examined for which kinetic data already existed. Further, since carbon paste electrodes are relatively new, comparisons of k_s between platinum and Nujol carbon pastes were made. The results are summarized in terms of the electrochemical systems.

A. Fe(III)–Fe(II)–Sulfuric Acid Media. 1. Platinum R.d.e.—As a first check of the validity of k_s

(10) F. C. Anson, *Anal. Chem.*, **33**, 934, 939 (1961).

(11) Z. Galus, C. Olson, H. Y. Lee, and R. N. Adams, *ibid.*, **34**, 164 (1962).

(12) R. A. Marcus, Abstracts of Papers, Division of Physical Chemistry, 142nd National Meeting of the American Chemical Society, Atlantic City, N. J., Sept., 1962, p. 7T.

measurements at the r.d.e., the ferric–ferrous system in 1 M sulfuric acid was examined at the platinum disk. The value of E_f^0 was determined with a stationary platinum wire electrode. The value of $k_s = 4.3 \times 10^{-3}$ cm./sec. in 1 M sulfuric acid is in good agreement with existing literature data. Wijnen and Smit[13] reported 5.0×10^{-3} using a square wave technique; Gerischer[14] gave 3×10^{-3} and, most recently, Anson[10] obtained 5.3×10^{-3} cm./sec. by galvanostatic methods for this system. There is excellent assurance that the r.d.e. technique yields accurate rate constants in this range.

Table I summarizes the k_s values and transfer coefficients for Fe(III)–Fe(II) in other concentrations of sulfuric acid and sulfate ion. These results partially confirm the results of Anson for varying acidities and sulfate ion concentrations[10] but detailed studies were not made.

TABLE I

KINETIC DATA FOR Fe(III)–Fe(II) SYSTEM IN SULFATE MEDIA PLATINUM R.D.E.[a]

Mixture no.[b]	Background composition	k_s (cm./sec.)	α	β[c]
1	1 M H_2SO_4	4.3×10^{-3}	0.46	0.53
2	0.1 M H_2SO_4	4.3×10^{-3}	.60	.39
3	4 M H_2SO_4	3.1×10^{-3}	.44	.55
4	1 M H_2SO_4, 2.8 M Na_2SO_4	1.4×10^{-3}	.55	.45

[a] Rotation velocity 100 rev./sec., data treated by calculations of Randles. [b] Fe(III) and Fe(II) concentrations 10^{-3} M in all cases. [c] The anodic transfer coefficient evaluated independently from slope of log k_b *vs.* η plot.

2. Carbon Paste r.d.e.—The value of k_s was only measured in 1 M sulfuric acid with carbon paste electrodes. The E_f^0 determined with the platinum wire was used since it was known that the rate was markedly slower at carbon paste electrodes. In fact, single sweep, stationary electrode polarograms at carbon paste exhibited the characteristics of a totally irreversible system with sweep rates of 2 v./min. Thus, as an independent check, it was possible to evaluate k_s from the treatment of Matsuda and Ayabe for peak polarograms.[15] The pertinent equations are

$$\log k_s = 1.13 - \frac{\alpha n}{0.059}(E_f^0 - E_{p,c}) - \log \frac{1}{D_{Ox}^{1/2}} + \frac{1}{2}\log \alpha n V \quad (12)$$

and

$$\log k_s = 1.13 - \frac{\beta n}{0.059}(E_{p,a} - E_f^0) - \log \frac{1}{D_{Red}^{1/2}} + \frac{1}{2}\log \beta n V \quad (13)$$

where

α and β = cathodic and anodic transfer coefficients
n = number of electrons in rate-determining step
$E_{p,c}E_{p,a}$ = peak potential of cathodic and anodic polarograms
V = voltage sweep rate, volts/sec.

The values of αn and βn are first determined from the slopes of the individual peak polarograms as

(13) M. D. Wijnen and W. M. Smit, *Rec. trav. chim.*, **79**, 289 (1960).
(14) H. Gerischer, *Z. Elektrochem.*, **67**, 366 (1950).
(15) H. Matsuda and Y. Ayabe, *ibid.*, **59**, 494 (1955).

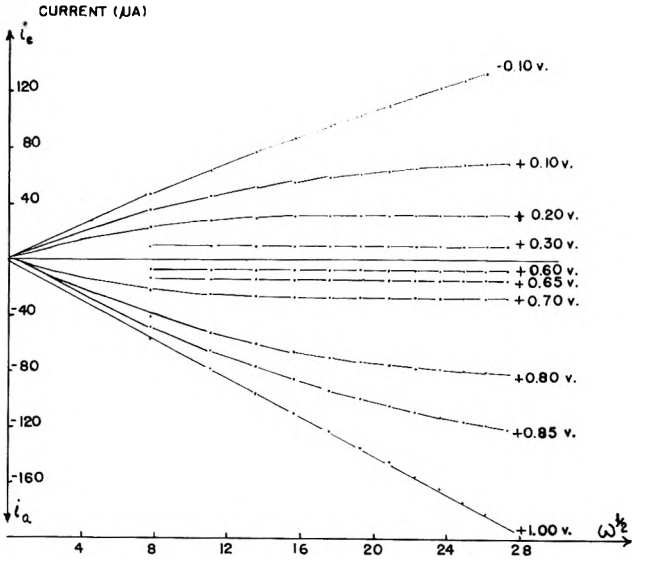

Fig. 3.—Limiting current *vs.* rotation velocity for Fe(III)–Fe(II) system.

$$\alpha n = \frac{0.048}{(E_{p/2,c} - E_{p,c})} \quad (14)$$

$$\beta n = \frac{0.048}{(E_{p,a} - E_{p/2,a})} \quad (15)$$

where $E_{p/2}$ is the corresponding half-peak potential. The results are summarized in Table II. Obviously, the anodic and cathodic waves should yield the same k_s in the Matsuda and Ayabe treatment—however, the difference is not great. Both values are slightly lower than that obtained from the r.d.e.. When one considers the large difference in mass transfer characteristics of the two types of measurement, the agreement is probably good. In any event, the comparison shows that widely differing treatments of irreversible electrode kinetics give relatively concordant results (for this particular range of moderately rapid reactions). The value of k_s measured at the r.d.e. is felt to be the most reliable.

TABLE II

Fe(III)–Fe(II) SYSTEM IN 1 M SULFURIC ACID AT CARBON PASTE R.D.E.[a]

Type measurement	k_s (cm./sec.)
R.d.e.	5.4×10^{-5}
Matsuda and Ayabe	4.5×10^{-5} (cathodic)
	3.2×10^{-5} (anodic)

[a] Rotation velocity, 100 rev./sec.

B. Fe(III)–Fe(II)–Chloride Media.—Measurements were made at varying chloride ion concentration with constant ionic strength. A few experiments at varying ionic strength were also carried out. All studies in chloride media were at the carbon paste r.d.e. The results are given in Table III.

It can be observed first that k_s is greater in chloride media (a fact well known in solid electrode voltammetry). Further, the rate is only slightly dependent on chloride ion concentration. A small dependence of k_s on ionic strength may be present. The effects are small but in general accord with the work of Silverman and Dodson on the homogeneous electron exchange of the Fe(III)–Fe(II) system.[16]

(16) J. Silverman and R. W. Dodson, *J. Phys. Chem.*, **56**, 896 (1952).

TABLE III

Fe(III)-Fe(II) SYSTEM IN CHLORIDE MEDIA AT CARBON PASTE R.D.E.

Background composition	k_s (cm./sec.)
0.1 *M* $NaClO_4$, 0.1 *M* HCl	8.5×10^{-5}
3.9 *M* $NaClO_4$, 0.01 *M* HCl, 0.09 *M* $HClO_4$	1.37×10^{-4}
3.9 *M* $NaClO_4$ + 0.1 *M* HCl	1.41×10^{-4}
3.4 *M* $NaClO_4$, 0.5 *M* NaCl, 0.1 *M* HCl	1.41×10^{-4}
3.8 *M* KCl, 0.1 *M* HCl	2.29×10^{-4}
3.9 *M* LiCl, 0.1 *M* HCl	2.19×10^{-4}
0.1 *M* HCl	7.4×10^{-5} (Randles)
0.1 *M* HCl	1.0×10^{-4} (Levich)

TABLE IV

EFFECT OF BACKGROUND SALT ON k_s CARBON PASTE R.D.E.[a]

Background composition	k (cm./sec.)
A. $Fe(CN)_6^{-3}$–$Fe(CN)_6^{-4}$	
0.1 *M* KCl	1.48×10^{-3}
0.3 *M* KCl	2.65×10^{-3}
1 *M* KCl	7.08×10^{-3}
1 *M* LiCl	1.06×10^{-3}
B. MnO_4^-–$MnO_4^{=}$ [b]	
0.9 *M* LiOH	6.92×10^{-3}
0.9 *M* NaOH	1.45×10^{-2}

[a] Rotation velocity 100 rev./sec. for ferri–ferrocyanide; 120 rev./sec. for permanganate–manganate. [b] To prepare solutions, permanganate in lithium or sodium hydroxide solution was added to the polarographic cell, deaerated, then one-half of permanganate reduced with sodium sulfite.

they are slower. The results are given in Table IV. The strong dependence of the k_s of ferri–ferrocyanide on background composition is clear. These changes are probably due to an alteration of double layer structure with background composition, although the effect may be more subtle. Wahl and co-workers have reported strong cation catalysis of the homogeneous exchange.[17] Further studies of this system are in progress.

The rates of the permanganate–manganate system vary with lithium and sodium hydroxide background. The effect of alkali metals on the homogeneous exchange was investigated by Sheppard and Wahl.[18]

D. Ce(IV)–Ce(III) System in 1 *M* Sulfuric Acid.—Because of the very positive E_f^0 of this system it was not possible to study properly the oxidation of Ce(III) species. Hence the Levich type calculations were used. Even with the reduction of Ce(IV) the background currents were quite high so that 10^{-2} *M* Ce(IV) solutions were studied. The Ce(IV) reduction current was examined as a function of ω at different potentials.

Using the platinum electrode k_s was found to be 3.7×10^{-4} cm./sec. This value is in good agreement with 4.5×10^{-4} found by Vetter.[19] On the carbon paste r.d.e., k_s was found to be almost identical having the value 3.8×10^{-4} cm./sec. The cathodic transfer coefficients at platinum and carbon paste were 0.21 and 0.28, respectively.

E. Comparison of k_s at Platinum and Carbon Paste Electrodes.—Table V summarizes the comparisons between platinum and carbon paste electrodes. The values marked with subscripts are from the literature, all others were measured in this work. For the same electroactive system in identical media, k_s at carbon paste is somewhat smaller than at platinum. In the case of Ce(IV)–Ce(III) the rates are about identical.

TABLE V

COMPARISON OF k_s VALUES AT PLATINUM AND CARBON PASTE ELECTRODES

System	Background	k_s (cm./sec.) Pt	k_s (cm./sec.) CE-NjP	k_s (cm./sec.) Graphite	Ratio k_s (Pt)/k_s (CE)
Fe(III)–Fe(II)	1 *M* H_2SO_4	4.3×10^{-3}	5.4×10^{-5}		80
Ferricy–ferrocy	1 *M* KCl	9×10^{-2}[c]	7.1×10^{-3}		13
		8×10^{-2}[b]			
	0.5 *M* K_2SO_4	1.3×10^{-1}[a]		6×10^{-3}[c]	22
Ce(IV)/Ce(III)	1 *M* H_2SO_4	3.7×10^{-4}	3.8×10^{-4}		0.97
		4.5×10^{-4}[d]			(1.18)

[a] J. E. B. Randles and K. W. Somerton, *Trans. Faraday Soc.*, **48**, 937 (1952), a.c. methods. [b] J. Jordan and R. A. Javick, *Electrochim. Acta*, 6, 23 (1962), using flow apparatus. [c] A. Regner and J. Balej, *Coll. Czech. Chem. Comm.*, **26**, 237 (1971), on plane graphite (*not* wax impregnated). [d] K. Vetter, *Z. physik. Chem.*, **196**, 360 (1950).

The iron–chloride medium was used to test the agreement of evaluating k_s by Levich's calculations *vs.* Randles' method. To determine k_s by Levich's method, the anodic and cathodic currents were determined at different applied potentials and varying disk rotation speeds. These data are shown in Fig. 3. As shown, at anodic potentials of +0.60, +0.65, and +0.70 v. *vs.* s.c.e., the current is independent of $\omega^{1/2}$, *i.e.*, is determined only by c.t. Hence, equation 7 can be used to evaluate k. For higher potentials, both m.t. and c.t. control the current (i_{Lim} is nonlinear with $\omega^{1/2}$) and equation 5 was used to evaluate k. Similar considerations apply to the cathodic current. The values of k are compared at the bottom of Table III.

C. Ferri–Ferrocyanide and Permanganate–Manganate Systems.—Both the homogeneous exchange and the electrochemical rate are rapid for these systems where the coördination shells of oxidized and reduced forms are very similar. Both systems are slightly too rapid at platinum to be measured *with good precision* using our techniques (see, however, ref. 6). Therefore both were measured at the carbon paste r.d.e. where

In reality it is quite surprising to find the rates at platinum and carbon paste so similar. At most, for the Fe(III)–Fe(II) system the ratio k_s(Pt) to k_s(carbon paste) is only 80. To understand the influence of the organic liquid (*i.e.*, Nujol, bromoform, etc) used in carbon paste electrodes it would be valuable to compare k_s values with those determined at pure carbon (graphite). Since such electrodes normally have very high residual currents they are seldom used. Apparently the only k_s value at pure graphite is that given by Regner and Balej for ferri–ferrocyanide in 0.5 *M* potassium sulfate.[20] As seen in Table V, this

(17) A. C. Wahl, R. J. Campion, and P. King, Abstracts of Papers, Division of Inorganic Chemistry, 142nd Natl. ACS Meeting, Atlantic City, N. J., Sept. 1962, p. 32N.

(18) J. C. Sheppard and A. C. Wahl, *J. Am. Chem. Soc.*, **73**, 1020 (1957).

(19) K. Vetter, *Z. physik. Chem.*, **196**, 360 (1951).

(20) A. Regner and J. Balej, *Coll. Czech. Chem. Comm.*, **26**, 237 (1961).

is quite close (*ca.* 1/22 as large) to that found by Randles and Somerton using a.c. techniques for the same system as platinum.[21] While we did not measure k_s in this background at carbon paste, we do check well with the platinum data in 1 *M* potassium chloride. It is probably safe to conclude there is little difference between k_s values at carbon paste and untreated carbon electrodes (where these can be used). It appears then that the effect of the organic liquid in the carbon paste on charge transfer rates is relatively small.

(21) J. E. B. Randles and K. W. Somerton, *Trans. Faraday Soc.*, **48**, 951 (1952).

One useful consequence of the slower rate at carbon paste may be that such electrodes can be used to "slow down" reactions to the region where precision r.d.e. studies are possible. A detailed treatment of rates at the two electrodes will be given elsewhere.

Acknowledgments.—We are indebted to F. O'Brien and R. Gillmore for the design and construction of the disk electrodes and to A. Rogers for technical assistance. This work was supported by the Atomic Energy Commission through contract AT(11-1)-686 and this support is gratefully acknowledged.

THE KINETICS OF THE REACTION BETWEEN SULFUROUS ACID AND FERRIC ION[1]

By D. G. Karraker

Savannah River Laboratory, E. I. du Pont de Nemours & Co., Aiken, South Carolina

Received October 15, 1962

The rate of oxidation of sulfurous acid to sulfate by ferric ion in perchloric acid solution was found to agree with a kinetic route that required a thionate (HSO_3) free radical as a primary reaction product. The proposed mechanism requires (1) the disproportionation of the $Fe(HSO_3)^{+2}$ complex ion to form Fe^{+2} and HSO_3, (2) the reverse of reaction (1), and (3) the oxidation of the HSO_3 radical to sulfate by Fe^{+3}. At 25° and in a perchlorate medium of unit ionic strength, k_1 is estimated to be 7 min.$^{-1}$ and $k_2/k_3 = 22$. From measurements of the reaction rate in the presence of oxygen, it is estimated that the scavenging of HSO_3 radicals by oxygen is about thirty-fold faster than by ferric ion.

Introduction

This study is concerned with the oxidation of sulfurous acid to sulfuric acid. Previous work indicated a probable route for this reaction, but no specific studies of the reaction have been reported. The kinetic route for production of sulfate by oxidation of sulfurous acid was of interest because of the probability that the mechanism and kinetics of this reaction would be pertinent to similar reactions of possible commercial interest, such as the ferric-catalyzed oxidation of SO_2 by O_2[2] and the radiation-catalyzed oxidation of SO_2 by O_2 to produce sulfuric acid.

Sulfurous acid is oxidized by ferric ion to produce either sulfate or dithionate ions, depending on the reaction conditions. The net reactions involved are

$$H_2SO_3 + 2Fe^{+3} + H_2O \longrightarrow 2Fe^{+2} + 4H^+ + SO_4^{-2} \quad (A)$$

$$2H_2SO_3 + 2Fe^{+3} \longrightarrow S_2O_6^{-2} + 4H^+ + 2Fe^{+2} \quad (B)$$

Previous investigators[3,4] have studied the stoichiometry of reactions A and B under different reaction conditions, and the kinetics of the cupric-catalyzed oxidation of sulfurous acid to dithionate has been studied by Higginson and Marshall.[5] The latter investigators explained their results by a mechanism involving the reaction of the thionate (HSO_3) radical. An attempt to measure the kinetics of the uncatalyzed reaction by Pollard, *et al.*,[6] did not lead to a satisfactory agreement with the mechanism proposed by Higginson and Marshall.

Experimental

Reagents.—Ferric perchlorate stock solutions were prepared by dissolving analytical grade iron wire in perchloric acid, oxidizing the ferrous ion with hydrogen peroxide, and destroying the excess peroxide by boiling. In some experiments, the ferric perchlorate was purified by crystallization from 60% perchloric acid. Ferrous perchlorate solution was prepared by dissolving iron wire in perchloric acid. Sodium perchlorate stock solution was prepared by neutralizing standardized sodium hydroxide solution with perchloric acid. Gaseous SO_2 was absorbed in water to prepare a stock solution of sulfurous acid. Perchloric acid was of reagent grade and was used without further purification. Ordinary distilled water was used in most of the experiments; triple-distilled water in the remainder.

Analyses.—Conventional analytical methods were used to measure the concentrations of most of the reagents in this work: ferrous iron was determined by titration with standard ceric sulfate solution with *o*-phenanthroline ("ferroin") as an indicator; ferric ion was determined colorimetrically by reduction to ferrous ion and measurement of the absorbance of the ferrous *o*-phenanthroline complex; sulfurous acid was determined by titration with standard iodine solution; and hydrogen ion was determined by titration with standard sodium hydroxide in the presence of sodium oxalate solution to prevent interference by iron. Dithionate was detected by a modification of the method of Glasstone and Hickling,[7] which involved oxidation of dithionate ion to sulfate by boiling with standard dichromate in 6 *M* $HClO_4$, reduction of the excess dichromate with a standard ferrous sulfate solution, and measurement of the excess ferrous ion by titration with ceric sulfate solution.

Oxygen was measured indirectly by assuming that the difference between the sulfate produced by the reaction between Fe^{+3} and H_2SO_3 and the total sulfate (after blank correction for reagents) was due to the reaction: $2H_2SO_3 + O_2 \rightarrow 2H_2SO_4$. Sulfate was measured turbidimetrically by comparing the turbidity developed by samples in dilute barium chloride solutions with the turbidity developed by weighed sodium sulfate standards.

(1) The information contained in this article was developed during the course of work under contract AT(07-2)-1 with the U. S. Atomic Energy Commission.

(2) (a) D. M. Yost and H. Russelll, Jr., "Systematic Inorganic Chemistry of the Fifth-and-Sixth-Group Nonmetallic Elements," Prentice-Hall, Inc., New York, N. Y., 1944; (b) F. H. Neytzell-deWilde and L. Traverner, *Proc. U. N. Intern. Conf. Peaceful Uses At. Energy, 2nd*, Geneva, **3**, 303 (1958).

(3) H. Bassett and A. J. Henry, *J. Chem. Soc.*, 914 (1935).

(4) H. Bassett and W. G. Parker, *ibid.*, 1540 (1951).

(5) W. C. E. Higginson and J. W. Marshall, *ibid.*, 447 (1957).

(6) F. H. Pollard, P. Hanson, and G. Nickless, *J. Chromatog.*, **5**, 68 (1961).

(7) S. Glasstone and A. Hickling, *J. Chem. Soc.*, 5 (1933).

Analytical determinations of iron, acid, etc., were estimated to be accurate to ±5%, with a precision of about ±2%. The turbidimetric analysis for sulfate was considered to be accurate to ±10%.

Run Procedure.—Solutions of $Fe(ClO_4)_3$, $HClO_4$, and $NaClO_4$ were mixed in the desired proportions to produce the desired acidity and iron concentrations, and an ionic strength of unity; oxygen was removed from the solutions by boiling. Nitrogen-saturated kerosene was poured on the surface of the boiling solution to prevent readsorption of air and, after cooling, the solution was transferred by nitrogen pressure into a volumetric flask. Sufficient deaerated water was added to provide the correct volume. A layer of kerosene covered the surface of the deaerated solution in all subsequent steps. These measures were not always successful in removing oxygen. In many experiments a small amount of H_2SO_3 was added 20–30 minutes before initiating the reaction, to react with and destroy any residual oxygen. In these experiments, the initial concentration of ferrous ion was measured before starting the reaction. Portions of this solution were pipetted into the flask that served as a reaction vessel, and were allowed to reach thermal equilibrium in a constant-temperature (25.6°) bath. In the experiments with air-saturated solutions, the precautions to exclude air were omitted.

The reaction was initiated by adding and mixing a measured amount of sulfurous acid solution. Some SO_2 escaped during the addition, but after this initial loss, experiments with air-tight apparatus showed identical results compared to experiments in which no effort was made to prevent SO_2 loss. It was concluded that after the initial loss of SO_2, there was no further loss during the reaction.

The progress of the reaction was followed by withdrawing samples at timed intervals. These samples were immediately diluted with 20 ml. of 3 *M* $HClO_4$ and the unreacted H_2SO_3 was removed from solution by sparging with a stream of nitrogen for 8–10 minutes. The ferrous ion produced by the reaction was determined by titration with Ce(IV) with pre-neutralized "ferroin" as an indicator. This procedure was evolved after preliminary tests showed that there was essentially no reaction in 3 *M* $HClO_4$, and that a 5-minute sparge with nitrogen was sufficient to remove unreacted H_2SO_3.

Data obtained in this manner showed that the concentration of Fe^{+2} increased with time to a constant value that was taken to be equivalent to the final concentration of sulfate produced by the reaction between Fe^{+3} and H_2SO_3, and thus was equivalent to the initial concentration of H_2SO_3. It was determined that the difference between the final Fe^{+2} concentration and the Fe^{+2} concentration at any time decreased logarithmically with time. The half-life of the reaction was determined graphically for each run with an estimated precision of ±10%. The data from a typical run are shown in Table I, and a graph of log $[(Fe^{+2})_\infty - (Fe^{+2})_t]$ *vs.* time for these data is a straight line.

The reaction conditions were designed to oxidize H_2SO_3 to sulfate rather than dithionate, and therefore all reactions used a large excess of Fe^{+3} and low concentrations of both reactants. The absence of any substantial amount of dithionate in the reaction products was verified in many of the experiments by analysis for dithionate. It was observed experimentally that the production of dithionate was also indicated by a second component in the first-order rate curve. Data for these runs were discarded; pertinent reaction data were restricted by dithionate interference to Fe^{+3} concentrations below 0.09 *M*, and H_2SO_3 concentrations below 0.006 *M*.

TABLE I

TYPICAL RUN DATA FOR Fe^{+3} OXIDATION OF H_2SO_4

Initial concn.: 0.089 *M* Fe^{+3}, 0.255 *M* $HClO_4$, 0.0027 *M* H_2SO_3

Time of reaction, min.	Fe^{+2}, *M*	$(Fe^{+2})_\infty - (Fe^{+2})_t$, *M*
1	1.43×10^{-3}	4.9×10^{-3}
3	2.08×10^{-3}	3.3×10^{-3}
6	2.73×10^{-3}	2.6×10^{-3}
11	4.16×10^{-3}	1.2×10^{-3}
17	4.82×10^{-3}	0.5×10^{-3}
25	5.20×10^{-3}	1×10^{-3}
35	5.33×10^{-3}	...
50	5.33×10^{-3}	...

The results of these experiments are shown in Table II. One run in an air-saturated system is reported.

TABLE II

EXPERIMENTAL RESULTS

Initial run conditions				Reaction half-life, min.
Fe^{+2}, *M*	H_2SO_4, *M*	H^+, *M*	Fe^{+2}, *M*	
6.53×10^{-2}	3.64×10^{-3}	0.255	...	6.4
6.53×10^{-2}	5.53×10^{-3}	.255	...	10
6.53×10^{-2}	2.67×10^{-3}	.255	...	5.5
6.53×10^{-2}	3.51×10^{-3}	.255	4.94×10^{-3}	10.2[a]
6.53×10^{-2}	3.43×10^{-3}	.255	11.4×10^{-3}	13.7
6.53×10^{-2}	1.35×10^{-3}	.255	...	3.3
6.53×10^{-2}	4.81×10^{-3}	.255	...	7.6
8.90×10^{-2}	3.06×10^{-3}	.255	...	4.9
6.53×10^{-2}	1.43×10^{-3}	.255	...	3.9
7.50×10^{-2}	2.80×10^{-3}	.255	...	5.3
4.32×10^{-2}	2.02×10^{-3}	.255	...	8.5
6.53×10^{-2}	2.50×10^{-3}	.255	0.9×10^{-3}	8.2
6.53×10^{-2}	3.84×10^{-3}	.255	0.9×10^{-3}	8.4
6.53×10^{-2}	1.63×10^{-3}	1.0	0.1×10^{-3}	18
6.53×10^{-2}	2.60×10^{-3}	0.63	1.3×10^{-3}	17
6.53×10^{-2}	2.25×10^{-3}	.51	1.0×10^{-3}	10.6
6.55×10^{-2}	3.20×10^{-3}	.255	4.9×10^{-3}	7.5[b]

[a] Compared with the air-saturated experiment to estimate the rate constant for the O_2–HSO_3 reaction. [b] Air-saturated; O_2 concentration = 8×10^{-4} *M*.

Results

Derivation of the Rate Expression.—A mechanism similar to that proposed by Higginson and Marshall for the production of dithionate was found to be in reasonable agreement with the experimental results. This mechanism depends upon the reactions of the thionate radical (HSO_3) and involves the steps

$$H_2SO_3 \overset{K_1}{\rightleftharpoons} H^+ + HSO_3^-$$

$$Fe^{+3} + HSO_3^- \overset{K_2}{\rightleftharpoons} Fe(HSO_3)^{+2}$$

$$Fe(HSO_3)^{+2} \xrightarrow{k_1} Fe^{+2} + HSO_3$$

$$HSO_3 + Fe^{+2} \xrightarrow{k_2} Fe^{+3} + HSO_3^-$$

$$HSO_3 + Fe^{+3} + H_2O \xrightarrow{k_3} SO_4^{-2} + Fe^{+2} + 3H^+$$

The rate expression for the oxidation of H_2SO_3 by this series of reactions is

$$\frac{d(H_2SO_3)}{dt} = \frac{-k_1K_1K_2(Fe^{+3})}{(H^+)}(H_2SO_3) + k_2(Fe^{+2})(HSO_3) \quad (1)$$

From the steady-state approximation

$$(HSO_3) = \frac{k_1K_1K_2(H_2SO_3)(Fe^{+3})}{k_2(Fe^{+2})(H^+) + k_3(Fe^{+3})(H^+)} \quad (2)$$

Replacing (Fe^{+2}) by the identity $(Fe^{+2}) = (Fe^{+2})_0 + 2(H_2SO_3)_0 - 2(H_2SO_3)$ and substituting (2) into (1), the variables in the rate expression can be separated for conditions applying to these experiments; *i.e.*, Fe^{+3} and H^+ are essentially constant for each experiment. Performing the integration and evaluating the integration constant, the following expression is obtained

$$\ln \frac{(H_2SO_3)}{(H_2SO_3)_0} = \frac{-k_1K_1k_3K_2(Fe^{+3})^2t + 2k_2(H^+)[(H_2SO_3) - (H_2SO_3)_0]}{k_2(H^+)[(Fe^{+2})_0 + 2(H_2SO_3)_0] + k_3(Fe^{+3})(H^+)} \quad (3)$$

The term $2k_2(H^+)[(H_2SO_3) - (H_2SO_3)_0]$ in the numerator is neglected; its effect is to introduce an additive term of increasing magnitude to the first-order rate expression. This term is zero at the start of the reaction, so its effect on the initial slope of the first-order rate is negligible. Experimentally, no appreciable deviation from a first-order rate equation was observed. Neglecting this term, the rate expression becomes

$$\ln \frac{(H_2SO_3)}{(H_2SO_3)_0} = \frac{k_1'k_3(Fe^{+3})^2t}{k_2(H^+)[(Fe^{+2})_0 + 2(H_2SO_3)_0] + k_3(Fe^{+3})(H^+)} \quad (4)$$

where

$$k_1' = k_1K_1K_2$$

Comparison with Experiment.—Rate data were compared with eq. 5, obtained by substituting $t_{1/2} = t$, $0.693 = \ln [(H_2SO_3)/(H_2SO_3)_0]$ and rearranging eq. 4

$$(Fe^{+3})^2t_{1/2} = 0.693\frac{k_2(H^+)}{k_1'k_3}[(Fe^{+2})_0 + 2(H_2SO_3)_0] + \frac{0.693}{k_1'}(Fe^{+3})(H^+) \quad (5)$$

The constants, k_1' and k_2/k_3, in (5) were evaluated graphically from data at 0.0655 M Fe^{+3}, 0.255 M H^+, and varying $[(Fe^{+2})_0 + 2(H_2SO_3)_0]$. Equation 5 predicts that a graph of $t_{1/2}$ *vs.* $[(Fe^{+2})_0 + 2(H_2SO_3)_0]$ will be a straight line and this prediction was verified. The constant k_1' was calculated to be 1.35 min.$^{-1}$ from the intercept on the y-axis, $k_2/k_1'k_3 = 16.3$ min. from the slope, and thus $k_2/k_3 = 22$. A further test of the kinetic expression was made by calculating the agreement of the data at 25° with eq. 5; $k_1' = 1.35$ min.$^{-1}$ and $k_2/k_3 = 22$. The results of the comparison of the left and right sides of eq. 5 are shown in Table III.

Table III

Comparison of Results with Equation 5

(1) $0.693\frac{k_2(H^+)}{k_1'k_3} \times [(Fe^{+2})_0 + 2(H_2SO_3)_0]$	(2) $\frac{0.693}{k_1'} \times (Fe^{+3})(H^+)$	Sum of columns 1 and 2	(10) $(Fe^{+3})^2t_{1/2}$	Dev., %
0.209×10^{-2}	0.87×10^{-2}	2.96×10^{-2}	2.73×10^{-2}	− 8
3.10×10^{-2}	$.87 \times 10^{-2}$	3.97×10^{-2}	4.27×10^{-2}	7
1.54×10^{-2}	$.87 \times 10^{-2}$	2.41×10^{-2}	2.34×10^{-2}	− 3
3.41×10^{-2}	$.87 \times 10^{-2}$	4.28×10^{-2}	4.36×10^{-2}	2
4.97×10^{-2}	$.87 \times 10^{-2}$	5.84×10^{-2}	5.85×10^{-2}	..
0.78×10^{-2}	$.87 \times 10^{-2}$	1.65×10^{-2}	1.41×10^{-2}	−16
2.77×10^{-2}	$.87 \times 10^{-2}$	3.64×10^{-2}	3.34×10^{-2}	− 9
1.78×10^{-2}	1.17×10^{-2}	2.95×10^{-2}	3.87×10^{-2}	27
0.82×10^{-2}	0.87×10^{-2}	1.69×10^{-2}	1.67×10^{-2}	− 1
1.61×10^{-2}	$.98 \times 10^{-2}$	2.59×10^{-2}	2.98×10^{-2}	14
1.17×10^{-2}	$.56 \times 10^{-2}$	1.73×10^{-2}	1.58×10^{-2}	− 9
1.68×10^{-2}	$.87 \times 10^{-2}$	2.55×10^{-2}	3.50×10^{-2}	31
2.46×10^{-2}	$.87 \times 10^{-2}$	3.33×10^{-2}	3.58×10^{-2}	7
3.7×10^{-2}	3.4×10^{-2}	7.1×10^{-2}	7.7×10^{-2}	8
3.7×10^{-2}	2.1×10^{-2}	5.8×10^{-2}	7.2×10^{-2}	22
3.1×10^{-2}	1.7×10^{-2}	4.8×10^{-2}	4.3×10^{-2}	−11
			Av. dev.	11

Discussion

The Ferric Ion–Sulfurous Acid Reaction.—The results of this work on the oxidation of sulfurous acid by ferric ion are considered to be in good agreement with the proposed mechanism in every detail. For the acidity range studied, sulfurous acid is largely unionized, but the assumption that the reacting species is H_2SO_3 leads to a consistent deviation from the derived rate expression of −35% at higher acidities, compared to an average deviation of 14% if bisulfite is assumed to be the reacting species. The assumption of a ferric–bisulfite complex does not affect the rate expression, but is included because the obvious color change that occurs on addition of H_2SO_3 to ferric ion is considered to be strong evidence for the formation of a complex. Under the conditions of this work, where ferric ion is in large excess, a 1:1 complex is considered to be the most reasonable.

The constants determined in this work, k_1' and k_2/k_3, may be compared to those obtained from the data of Higginson and Marshall, which are $k_1' = 0.73$ min.$^{-1}$ and $k_2/k_3 = 0.1$ at 25°, $\mu = 2.0$, and $H^+ = 0.08$ M, in a sulfate medium. These values do not agree with the values determined in this work, $k_1' = 1.35$ min.$^{-1}$ and $k_2/k_3 = 22$. Under the conditions of Higginson and Marshall's work, ferric ion is totally complexed by sulfate, and the major difference between their constants and those of this work is ascribed to that cause.

Combining k_1' with values for K_1 and K_2 will lead to the rate constant, k_1, for the disproportionation of the ferric–sulfite complex ion. Values for K_2 are unknown, and the accepted[8] value of 1.72×10^{-2} for K_1 becomes quite uncertain when extrapolated to an ionic strength of unity. However, from Higginson and Marshall's report that no visual indication of a ferric–bisulfite complex was formed in their work, K_2 is much less than 95,[9] the complex constant constant for $Fe(SO_4)^+$. An estimate of 7 min.$^{-1}$ for k_1 is obtained by using $K_1 = 0.02$, and assuming that K_2 is of the order of 10.

Effect of Oxygen.—Reactions carried out in air-saturated solutions were more rapid than those in the absence of oxygen. This effect is due to competition by the well known[5,6] ferric-catalyzed oxidation of sulfurous acid by oxygen. A reasonable mechanism for the reaction of oxygen is

$$HSO_3 + O_2 + H_2O \xrightarrow{k_4} SO_4^{-2} + 2H^+ + HO_2$$

$$HO_2 + Fe^{+2} + H_2O \longrightarrow Fe(OH)^{+2} + H_2O_2$$

$$H_2O_2 + Fe^{+2} \longrightarrow Fe(OH)^{+2} + OH$$

$$HSO_3 + OH \longrightarrow 2H^+ + SO_4^{-2}$$

This mechanism, due in essence to Haber,[10] embodies reactions similar to those demonstrated for the Fricke dosimeter[11] and the decomposition of H_2O_2 by ferrous

(8) H. V. Tartar and H. H. Garretson, *J. Am. Chem. Soc.*, **63**, 808 (1941).
(9) R. A. Whiteker and N. Davidson, *ibid.*, **75**, 3081 (1953).
(10) F. Haber, *Naturwiss.*, **19**, 450 (1931), quoted in ref. 2b.
(11) A. O. Allen, "The Radiation Chemistry of Water and Aqueous Solutions," D. Van Nostrand Co., Princeton, N. J., 1961.

ion.[12] It is chosen in preference to a mechanism proposed by Bäckström[13] involving peroxysulfuric acid (H_2SO_5) because the known properties of H_2SO_5 do not correspond to those of the active intermediate required. However, in derivation of the rate expression, the intermediates are eliminated and the same kinetic expression results for either mechanism. In the absence of any net reaction between Fe^{+++} and HSO_3, the rate expression can be derived to be

$$\frac{-\mathrm{d} \ln H_2SO_3}{\mathrm{d}t} = \frac{k_1'(Fe^{+3})}{(H^+)}\left(1 - \frac{k_2(Fe^{+2})}{2k_4(O_2)}\right) \quad (6)$$

This expression can be integrated when Fe^{+2}, Fe^{+3}, and O_2 are constant to yield

$$\ln \frac{H_2SO_3}{(H_2SO_3)_0} = \frac{k_1'(Fe^{+3})_t}{(H^+)}\left(1 - \frac{k_2(Fe^{+2})}{2k_4(O_2)}\right) \quad (7)$$

The data of Neytzell-deWilde and Taverner,[2b] obtained at 10° in *ca.* 10^{-2} *M* H_2SO_4, show general agreement with this expression. These investigators found the reaction between O_2 and SO_2 to depend directly on ferric ion, inversely on the acidity, and to be essentially independent of O_2, under conditions where there was a twofold excess of O_2. They state that the reaction is second order in H_2SO_3, but careful examination of their data shows that most of their data under conditions where the reaction was rapid ($t_{1/2}$ = 25 minutes or less) fits a first-order rate expression, with $k_1' \approx 0.3$. During reactions that were quite slow ($t_{1/2}$ greater than 30 minutes), their data are no longer first order in H_2SO_3. It may be that some other mechanism is affecting the reaction, or that experimental difficulties, such as the loss of SO_2, affected their measurements.

Considering all the competitive reactions in an air-saturated system, the rate expression can be derived as

$$\frac{-\mathrm{d} \ln H_2SO_3}{\mathrm{d}t} = \frac{k_1'(Fe^{+3})}{(H^+)} \times \frac{k_3(Fe^{+3}) + 2k_4(O_2)}{k_2(Fe^{+2}) + k_3(Fe^{+3}) + 2k_4(O_2)} \quad (8)$$

From data obtained during comparable reactions both in the presence and absence of oxygen, the ratio k_4/k_3 can be estimated. This estimate involves (a) integrating eq. 8 assuming Fe^{+++}, Fe^{++}, H^+, and O_2 are constant, (b) equating the right side of this expression with an equivalent expression for the case where O_2 is absent, and (c) eliminating common terms to obtain

$$\frac{t_{1/2}\,[k_3(Fe^{+3}) + 2k_4(O_2)]}{k_2(Fe^{+2}) + k_3(Fe^{+3}) + 2k_4(O_2)} = \frac{t_{1/2}\,[k_3(Fe^{+3})]}{k_2(Fe^{+2}) + k_3(Fe^{+3})} \quad (9)$$

Substituting the data from an experiment in the presence of oxygen in the left of (9) and data at the approximately equal Fe^{+3} and H_2SO_3 concentrations in the absence of oxygen on the right, the equation can be solved to yield $k_4/k_3 \simeq 30$, and thus $k_2/k_4 \simeq 0.7$.

Despite the approximate nature of these estimates, the results demonstrate that oxygen reacts with the HSO_3 radical much more rapidly than does Fe^{+3}, and about as rapidly as Fe^{+2}. It is unfortunate that this investigation results in the determination of ratios of rate constants, rather than the rate constants themselves. It is suggested that measurement of the free radical concentration by e.s.r. techniques in this system and other systems could lead to the determination of the individual rate constants for the individual reactions.

Acknowledgment.—The author is indebted to R. S. Dorsett for performing many of the analyses.

(12) W. G. Barb, *et al.*, *Trans. Faraday Soc.*, **47**, 462 (1951).
(13) H. L. J. Bäckström, *J. Am. Chem. Soc.*, **49**, 1460 (1927).

QUANTUM YIELDS FOR THE PHOTOCHROMISM OF 2-(2-NITRO-4-CYANOBENZYL)-PYRIDINE

BY GUNNAR WETTERMARK[1] AND JOHN SOUSA

Pioneering Research Division, Quartermaster Research and Engineering Center, U. S. Army, Natick, Massachusetts

Received October 17, 1962

2-(2-Nitro- 4-cyanobenzyl)-pyridine has been shown to display photochromism in EPA glass at liquid nitrogen temperature. The molar absorptivities for the photochemically produced species have been measured; 1.3×10^4 and 1.1×10^4 were obtained for the absorption maxima at 450 and 590 mμ, respectively. The quantum yields for the production of the colored species were found to be low (0.032 for 254 mμ and 0.014 for 365/366 mμ).

Introduction

The long-known photochromism of 2-(2,4-dinitrobenzyl)-pyridine[2] recently has been the subject of many investigations.[3,4] The color change phenomenon can be observed with crystals of the compound or in solution.

During the last two years it has also been found that several compounds which are closely related structurally to 2-(2,4-dinitrobenzyl)-pyridine also exhibit photochromism. Mosher, *et al.*,[5] found that the γ-isomer [4-(2,4-dinitrobenzyl)-pyridine] showed photochro-

(1) National Academy of Sciences–National Research Council Visiting Scientists Research Associate and Guest of the Massachusetts Institute of Technology associated with Prof. L. J. Heidt of the Department of Chemistry.
(2) A. E. Tschitschibabin, B. M. Kuindshi, and S. W. Benewolenskaja, *Ber.* **58**, 1580 (1925).
(3) R. Hardwick, H. S. Mosher, and P. Passailaigue, *Trans. Faraday Soc.*, **56**, 44 (1960).
(4) (a) J. Sousa and J. Weinstein, *J. Org. Chem.*, **27**, 3155 (1962); (b) G. Wettermark, *J. Am. Chem. Soc.*, **84**, 3658 (1962).
(5) H. S. Mosher, C. Souers, and R. Hardwick, *J. Chem. Phys.*, **32**, 1888 (1960).

mism in solution at Dry Ice temperatures. Using a low temperature technique Sousa and Weinstein[4a] showed that 2-(2-nitro-4-cyanobenzyl)-pyridine and 2,4-dinitrobenzyl alcohol undergo a reversible color change on exposure to light.

Flash photolysis studies in solution at room temperature by Wettermark[6,7] revealed that *o*-nitrotoluene and derivatives of *o*-nitrotoluene on exposure to light develop species which absorb strongly in the visible region of the spectrum. These experiments indicate that this is a general behavior of compounds having a nitro- and a methyl-group in *ortho* position to each other and where at least one hydrogen atom on the methyl group is left unsubstituted. For all compounds investigated the colored species fades in a reaction following first order kinetics.

The present study has been undertaken to evaluate the molar absorptivity of the photochemically produced colored species and also the quantum yield for the production of these species, and 2-(2-nitro-4-cyanobenzyl)-pyridine was chosen as a model compound. From earlier work it has been observed that an irreversible decomposition accompanies a cycle of turning colored on exposure to light and then reverting to colorless in the dark. However, for 2-(2-nitro-4-cyanobenzyl)-pyridine the irreversible decomposition is very small.

Crystals of 2-(2-nitro-4-cyanobenzyl)-pyridine are faint yellow when kept in the dark. On exposure to light at room temperature the crystals turn deep green and revert to faint yellow in the dark over a period of a few hours. At low temperatures the color change can also be seen in solution.[4a] The rate constant for the fading reaction is 3.7×10^{-1} sec.$^{-1}$ at room temperature in an alcohol solution.[4a,6] The rate constant in ethanol solution at $-88°$ is 3.24×10^{-3} sec.$^{-1}$ and measurements[4a] of the activation energy showed that the rate of fading markedly decreases with decreasing temperatures.

Experimental

Principal Equipment.—Irradiations were made in a cryostat which will be described elsewhere. All exposures were made with the solution at about liquid nitrogen temperatures, except when otherwise stated. The cryostat was provided with quartz windows and constructed in such a way as to fit the cell compartment of a Cary 14 spectrophotometer, which was used for all spectrophotometric analyses. The optical path length of the cell was 2.50 cm. As light sources for the irradiations a high pressure mercury arc (General Electric AH-6) and a low pressure mercury arc were used. Various wave length regions were isolated by applying appropriate filters and will be specified in the text together with the actual experiments.

Solutions.—2-(2-Nitro-4-cyanobenzyl)-pyridine was prepared by Sousa and Weinstein and purified by repeated crystallization from ethanol, followed by chromatographic purification using a column with neutral aluminum oxide.[4a]

EPA consisting of ether, isopentane and ethanol in the volume proportions 5:5:2 at room temperature was used as solvent. Ether and ethanol were "Baker Analyzed" Reagent and U.S.I. Reagent, respectively, which were used without further purification. Isopentane, Phillips 99.5 mole %, was redistilled using a 50 cm. column with glass helices. The purity of the solvents was checked spectrophotometrically; no absorption due to impurities was observed over the ultraviolet and visible region of the spectrum.

Actinometry.—Both uranyl oxalate and ferric oxalate were used for the actinometry. Exposures were made using the cryostat at room temperature with actinometer solution in the cell.

(6) G. Wettermark, *Nature*, **194**, 677 (1962).

(7) G. Wettermark, *J. Phys. Chem.*, **66**, 2560 (1962).

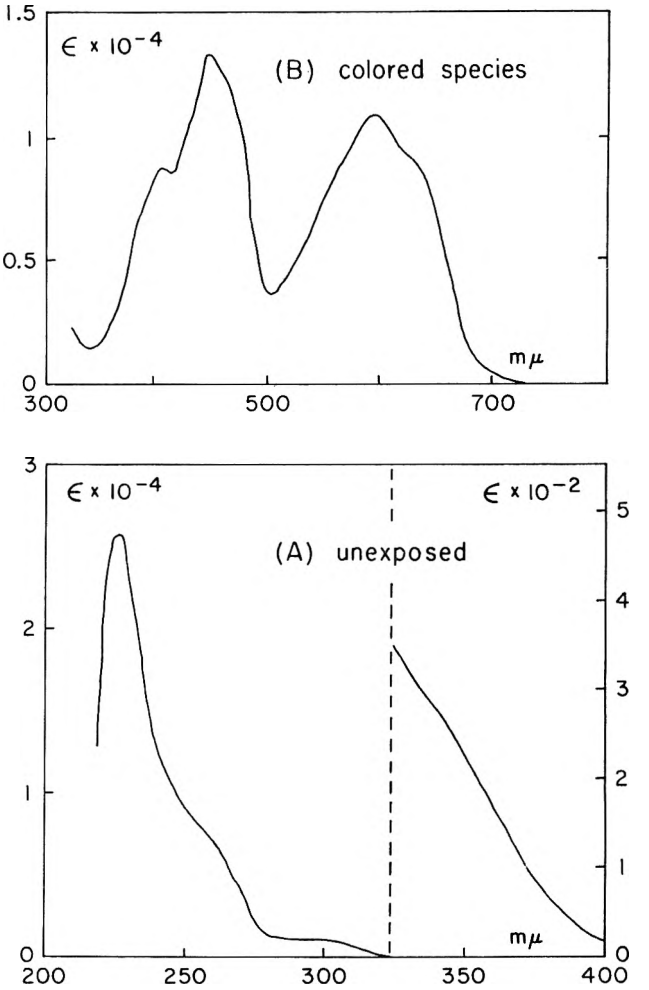

Fig. 1.—Molar absorptivity spectrum in EPA of 2-(2-nitro-4-cyanobenzyl)-pyridine: (A) before exposure to light; (B) after photoconversion.

For the uranyl oxalate the amount of decomposition was measured by treating the solution with ceric sulfate and measuring the excess ceric ion present in a spectrophotometer following essentially a procedure described by Pitts, *et al.*[8] In the calculations a quantum yield of 0.60 was assumed for the wave length 254 mμ.

Ferric oxalate was used exactly as described by Hatchard and Parker.[9] The quantum yields used were 1.25 and 1.21 for the wave lengths 254 and 365/366 mμ, respectively.

Results and Discussion

Using EPA as a solvent a perfectly clear glass could be obtained in the cryostat at liquid nitrogen temperatures. The molar absorptivity of 2-(2-nitro-4-cyanobenzyl)-pyridine dissolved in EPA in the dark at room temperature is shown in Fig. 1A. The molar absorptivity remained essentially the same at liquid nitrogen temperature; cooling solutions to this temperature gave an increase in optical density corresponding to the volume decrease.

In EPA glass the absorption spectrum of the colored species produced on exposure to light exhibits two characteristic maxima in the visible, at 450 and at 590 mμ. Once the colored species has been formed at liquid nitrogen temperature no change in optical density could be spectrophotometrically observed over several hours. The fading was accordingly assumed to be negligible in the present experiments.

(8) J. N. Pitts, Jr., J. D. Margerum, R. P. Taylor, and W. Brim, *J. Am. Chem. Soc.*, **77**, 5499 (1955).

(9) C. G. Hatchard and C. A. Parker, *Proc. Roy. Soc.* (London), **A235**, 518 (1956).

Molar Absorptivity of the Colored Species.—In order to obtain the molar absorptivity of the colored species an attempt was made to irradiate solutions of 2-(2-nitro-4-cyanobenzyl)-pyridine to complete conversion. When plotting the optical density as a function of time of irradiation it was found that the optical density increased to a maximum and was then followed by a linear decrease. The decrease is attributed to the slight irreversible decomposition of the sample. The magnitude of this decomposition depends strongly on the wave length of the light used to excite the sample. When using the mercury line at 254 mμ, no measurable decomposition occurred based on the observation that no decrease in optical density could be observed when irradiating the samples twice the time needed to obtain maximum optical density. For the samples which showed decomposition, the optical density of the totally converted solution was taken from a linear extrapolation of the decay curve to zero time. The molar concentration of the colored species was assumed to be equal to the concentration of the original compound (see the discussion of the mechanism). (The concentration measured at room temperature was corrected for the volume decrease.) Table I gives the molar absorptivity at the maxima, 450 and 590 mμ, obtained from different experiments.

TABLE I

DETERMINATION OF MOLAR ABSORPTIVITIES FOR THE COLORED SPECIES

Light	Concn. of 2-(2-nitro-4-cyano-benzyl)-pyridine (mole $l.^{-1}$)	Molar absorptivity ($l.\ mole^{-1}\ cm.^{-1}$) 450 mμ	590 mμ
Low pressure mercury lamp	6.57×10^{-6}	14,200	11,600
GE AH-6 (Filter) Corning 9863	1.32×10^{-5}	13,300	10,700
GE AH-6	5.32×10^{-6}	13,100	10,500
GE AH-6	2.63×10^{-5}	12,700	10,700
	Mean values	13,300	10,900

The high pressure mercury lamp was used to obtain light of wave lengths through the ultraviolet and visible. When Corning Filter 9863 was used, all visible light was absorbed in the filter. The low pressure mercury arc gave principally the 254 mμ line. It is seen that the molar absorptivities obtained for a particular wave length are essentially the same. From this we conclude that the sample has been essentially fully converted to the colored form and is not in a photochemical equilibrium with only partial conversion; it is quite unlikely that such a photochemical equilibrium should be independent of the wave length of the light to which the sample is exposed. Furthermore, experiments in the temperature interval −100° to +20° showed that the rate of fading was not affected by exposure to high intensity visible light. The absorption spectrum of the colored species normalized by the use of the mean values from Table I from 320 to 800 mμ appears in Fig. 1B in absolute units (liter $mole^{-1}$ $cm.^{-1}$).

Quantum Yields.—Exposure to ultraviolet light produces the colored species but even visible light is effective; crystals of the compound turn green in daylight. The ultraviolet absorption spectrum of the unexposed 2-(2-nitro-4-cyanobenzyl)-pyridine shows a strong peak at 227 mμ followed by a continually decreasing absorption at longer wave lengths which extends into the visible, compare Fig. 1A. It is thus of interest to compare the effectiveness of light absorbed in the middle of the absorption band around 230 mμ with that of light absorbed in the tail at longer wave lengths. In this investigation quantum yields for the production of the colored species were measured at 254 and 365/366 mμ using the mercury lines at these wave lengths.

The quantum yields were evaluated by exposing solutions and measuring the visible absorption spectrum of the solution for different times of exposure. Knowing the molar absorptivities (Fig. 1B) the amount of colored species formed was then easily calculated. The intensity of the incident light was obtained from chemical actinometry. In order to achieve closeness to homogeneous illumination, the optical density at the wave length of the actinic light was kept low so that only a fraction of the incident light was absorbed by the sample. This fraction was calculated using the molar absorptivities of unexposed 2-(2-nitro-4-cyanobenzyl)-pyridine at 254 and 365 mμ, respectively (Fig. 1A) and was then used to determine the light dose absorbed by the sample for a given exposure time.

For any specific solution a plot was made of amount of colored species formed as a function of the amount of light absorbed. Such a curve shows an initial linear increase and then the slope of the curve continually decreases as the concentration of the initial compound becomes significantly decreased. The slope of the initial linear increase was taken as the quantum yield and appears in Table II for different experiments.

TABLE II

QUANTUM YIELDS FOR THE PRODUCTION OF THE COLORED SPECIES

Light (mμ)	Intensity (einsteins $min.^{-1}\ cm.^{-2}$)	Concn. (mole $l.^{-1}$)	Quantum yield
253.7[a]	1.77×10^{-8}[d]	6.56×10^{-6}	0.032
253.7[b]	1.71×10^{-8}[e]	1.06×10^{-5}	.031
253.7[b]	1.56×10^{-8}[e]	6.56×10^{-5}	.033
365/366[c]	1.29×10^{-7}[e]	1.06×10^{-3}	.013
365/366[c]	1.08×10^{-7}[e]	2.64×10^{-4}	.015

[a] Low pressure mercury arc; filter: 5 cm. of solution containing 257 g. of $NiSO_4 \cdot 7H_2O$ and 45 g. of $CoSO_4 \cdot 7H_2O$/l. [b] Low pressure mercury arc; filter: Corning 9863. [c] GE AH-6; filter: Corning 7380 and 5860. [d] Uranyl oxalate actinometry. [e] Ferric oxalate actinometry.

In Table II, column one shows the wave length of the actinic light and in column two the intensity of the light incident on the sample is given as determined by chemical actinometry. The concentration of 2-(2-nitro-4-cyanobenzyl)-pyridine appears in column three.

The mean values for the quantum yields at 254 and 365/366 mμ are 0.032 and 0.014, respectively.

Nature of the Colored Species.—It seems that the absorption of light is accompanied by the formation of species (Q).

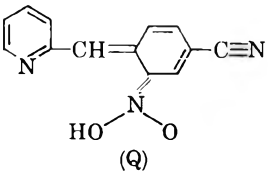

(Q)

Separate experiments[10] with 2,4-dinitrotoluene have

(10) G. Wettermark and R. Ricci, *J. Chem. Phys.*, in press.

shown species like (Q) to be very strongly acidic with a pK value of about 1. Consequently one would expect species (Q) to be rearranged because of the transfer of the proton to the nitrogen of the pyridine nucleus with the establishment of species shown in two extreme resonance forms as

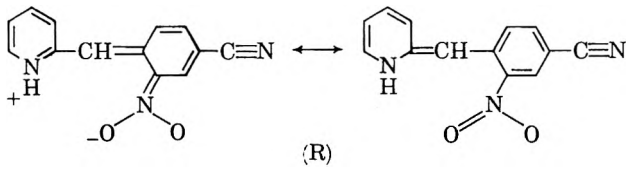

(R)

In an organic solvent with a low dielectric constant it is unlikely that the charge will be separated to any greater extent. The spectrum given in Fig. 1B is concluded to be the absorption spectrum of species (R).

From the quantum yields it is seen that in EPA glass at liquid nitrogen temperature only a small percentage of the light quanta absorbed is effective in accomplishing this chemical isomerization. It is interesting to note that the quantum yield seems to be of the same order of magnitude in liquid ethanol, EPA and ether, as comparable irradiation times were needed to obtain the same optical density in these solvents as in EPA glass.

THE SUBLIMATION PRESSURE OF CALCIUM(II) FLUORIDE AND THE DISSOCIATION ENERGY OF CALCIUM(I) FLUORIDE[1]

BY GARY D. BLUE, JOHN W. GREEN, RENATO G. BAUTISTA, AND JOHN L. MARGRAVE

Department of Chemistry, University of Wisconsin, Madison, Wisconsin

Received October 18, 1962

A vacuum microbalance and a mass spectrometer have been used to determine sublimation pressures and heats of sublimation for $CaF_2(s)$ over the range 1242–1669°K. The data are represented by $\log P_{atm} = -(95.46 \pm 0.49)/45.76 \times 10^4/T + 8.141 \pm 0.006$. The errors quoted are standard deviations of the least-squares fit. The heat of sublimation at 298°K. is 103.3 ± 2.0 kcal./mole. From studies of the reaction of CaF_2 with aluminum over the range 1271–1351°K., D^0_{298} for CaF(g) was determined to be 5.4 ± 0.2 e.v. from two independent equilibria. Close agreement with other investigators is found for the sublimation of $CaF_2(s)$ but the dissociation energy of CaF(g) is much greater than the previously accepted value.

I. Introduction

Reliable Knudsen or Langmuir vaporization and sublimation rates for alkaline earth halides have not been available, in spite of the fact that many of these compounds are easily procured as high-purity single crystals and that they find applications as refractories and reactants in high temperature systems. Brewer, Somayajulu, and Brackett[2] have reviewed the thermodynamic properties of the gaseous metal dihalides and present vaporization data for CaF_2 based on the early work of Ruff and LeBoucher.[3] More recently Schulz and Searcy[4] have investigated the vapor pressure of CaF_2 in the temperature range 1400 to 1850°K. by the torsion–effusion method. Finally, Pottie[5] has made a single Knudsen effusion measurement of the vapor pressure of liquid CaF_2 at 1823°K. In order to extend the temperature range of observations and identify the vapor species, we have measured the sublimation rate and heat of sublimation of CaF_2 by both the Langmuir and Knudsen techniques employing a vacuum microbalance and a mass spectrometer.

The dissociation energies of the alkaline earth monohalides are poorly known. The recent and extensive spectroscopic work on BeF,[6] BeCl,[7a] and thermochemical work on BeF,[7b] suggest that the stability of these molecules may be much greater than previously suspected. Gaydon[8] and Herzberg[9] have tabulated recommended values for the dissociation energies of a large number of diatomic molecules and both suggest a value of 3.15 e.v. or less for the CaF gaseous molecule, based on an apparent predissociation observed by Hellwege[10] and Harvey.[11] It is not possible to obtain a reliable value for the dissociation energy of this molecule by means of a Birge–Sponer extrapolation because the data reported depend on head measurements of bands of a weakly degraded system. In the work reported here, the dissociation energy of the CaF molecule was compared with that of the AlF molecule by utilizing the mass spectrometer to study the equilibrium $Ca(g) + AlF(g) = CaF(g) + Al(g)$ in a Knudsen cell. A second, independent value of D(CaF) was derived from the heat of the reaction $Ca(g) + CaF_2(s) = 2CaF(g)$.

II. Experimental Methods

The Langmuir studies were carried out with a microbalance built inside a vacuum system. The apparatus has been previously described in detail by Dreger and Margrave[12] and by Paule.[13] It consists basically of an inductively-heated graphite furnace, an electromagnetic beam balance, and an electrical circuit for the balance which permits changes in weight to be meas-

(1) Abstracted, in part, from the theses presented by G. D. Blue and J. W. Green in partial fulfillment of the requirements for the Ph.D. degree at the University of Wisconsin, 1963.

(2) L. Brewer, G. R. Somayajulu, and E. Brackett, Lawrence Radiation Laboratory Report UCRL-9840, September, 1961; *Chem. Rev.*, **63**, 111 (1963).

(3) O. Ruff and L. LeBoucher, *Z. anorg. allgem. Chem.*, **219**, 376 (1934).

(4) D. A. Schulz and A. W. Searcy, Lawrence Radiation Laboratory Report UCRL-10141, March, 1962; *J. Phys. Chem.*, **67**, 103 (1963).

(5) R. W. Pottie, E. I. du Pont Company, private communication.

(6) V. M. Tatevskii, L. N. Tunitskii, and M. M. Novikov, *Opt. Spectr.* (USSR), **5**, 521 (1958).

(7) (a) M. M. Novikov and L. N. Tunitskii, *ibid.*, **8**, 396 (1960); (b) Rocket Power, Inc., Fourth Quarterly Report, QR-7414-4, Contract AF 04(611)-7414, April, 1962, through June, 1962.

(8) A. G. Gaydon, "Dissociation Energies," Chapman and Hall, Ltd., London, 1950.

(9) G. Herzberg, "Molecular Spectra and Molecular Structure—I. Spectra of Diatomic Molecules," D. Van Nostrand Co., Inc., New York, N. Y., 1950.

(10) K. H. Hellwege, *Z. Physik*, **100**, 644 (1936).

(11) A. Harvey, *Proc. Roy. Soc.* (London), **133**, 336 (1931).

(12) L. H. Dreger and J. L. Margrave, *J. Phys. Chem.*, **64**, 1323 (1960).

(13) R. Paule, Ph.D. Thesis, University of Wisconsin, 1962.

ured in terms of a solenoid current. A single crystal of CaF_2 was suspended from a holder made of tungsten wire. No reaction was observed between the sample and the tungsten wire. A Pyro optical pyrometer was used for temperature measurements and the observed values were corrected for the effective transmission of a sighting window and a mirror.

The mass spectrometer employed in this work was a single focusing 60°, 12 in. radius of curvature instrument having differential pumping for the analyzer, ion source, and oven regions. The Knudsen cell assembly closely resembled that described by Chupka and Inghram[14] and consisted basically of a tantalum Knudsen cell heated by electron bombardment from a tungsten filament and surrounded by a series of six concentric tantalum radiation shields. The temperature of the cell was measured with a Leeds and Northrup optical pyrometer[15] which was sighted through a Pyrex window and a series of holes in the radiation shields onto a blackbody hole in the side of the cell. A magnetic shutter was employed to protect the window from evaporating materials and ensure that a constant transmission value could be used to correct the observed temperature.

A movable slit positioned just above the radiation shields and before the ion source served as a shutter for vapor effusing from the cell and provided a means of distinguishing between background and beam ions.

The effusing atoms and molecules passed through collimating slits to the ionization chamber where they were bombarded with electrons of controlled energy and ionized. The resulting ions were focused and collimated in the ion source and then mass analyzed by passing through the field of a 60° sector magnet.

A 16-stage electron multiplier employing 97% Ag–3% Mg alloy dynodes was used for ion detection. The output of this multiplier was measured with a Cary vibrating reed electrometer and recorded by a strip chart recording potentiometer. The multiplier made possible the measurement of ion currents as low as 10^{-19} amp. The instrument also was equipped with a simple collector which could be used to detect ions of intensity greater than 2×10^{-15} amp. and provided a means for direct measurement of the gain of the multiplier for high-intensity ion beams. The gain of the multiplier during most of the work reported here was approximately 2×10^5 for O_2^+ ions. Whenever direct measurement of the relative gains of ions was not possible due to low intensity, an estimate was made from the results of Inghram, Hayden, and Hess.[16]

The CaF_2 used for the mass spectrometer experiments was commercially available reagent grade powder which was outgassed extensively in the instrument before temperature dependence studies were begun. During the early part of this outgassing, extremely high-intensity peaks of H_2O^+ and $CaOH^+$ were observed, but these decreased rapidly to below background intensities. X-Ray diffraction powder patterns of the sample after completion of the experiment revealed only lines for CaF_2.

III. Sublimation Studies

The rate of weight loss was followed at a series of temperatures employing the vacuum microbalance and a pressure was calculated at each temperature from the Langmuir equation, taking the sublimation coefficient to be unity and assuming $CaF_2(g)$ to be the only important vapor species. Free energy functions for solid and gaseous CaF_2 were taken from Brewer, *et al.*,[2] who present molecular parameters and thermodynamic data necessary for the calculation of the thermodynamic properties of gaseous metal dihalides. The CaF_2 gaseous molecule was assumed to be linear with a Ca–F bond distance of 2.10 Å. and the frequencies were given as $\omega_1 = 484$ cm.$^{-1}$, $\omega_2(2) = 95$ cm.$^{-1}$, and $\omega_3 = 675$ cm.$^{-1}$. The free energy functions were combined with the pressure data to calculate an average heat of sublimation $\Delta H^0_{298} = 103.3$ kcal./mole. A least squares fit to a Clausius–Clapeyron plot of this same data gives a second law heat of sublimation $\Delta H^0_{1350} = 92.2 \pm 2.4$ kcal./mole which becomes 98.3 ± 2.4 kcal./mole when corrected to 298°K. The uncertainties given are the standard deviations of the least squares fit. The results of the Langmuir studies are summarized in Table I.

Table I

Microbalance Sublimation Data

T (°K.)	$10^4/T$	P_{atm}	$-\log P_{atm}$	$-\Delta\left(\frac{F^0_T - H^0_{298}}{T}\right)$	ΔH^0_{298}
1246.2	8.024	3.13×10^{-9}	8.504	43.43	102.6
1319.9	7.577	2.13×10^{-8}	7.672	43.14	103.3
1397.9	7.154	1.71×10^{-7}	6.767	42.77	103.1
1498.5	6.674	1.65×10^{-6}	5.781	42.53	103.4
1401.9	7.133	1.49×10^{-7}	6.827	42.86	103.9
1341.7	7.453	3.69×10^{-8}	7.433	43.06	103.4

Av. = 103.3 ± 0.4 kcal./mole

$$\log P_{atm} = -\frac{92.18 \pm 2.44}{45.76} \times \frac{10^4}{T} + 7.614 \pm 0.020$$

Schulz and Searcy[4] investigated the vapor pressure of CaF_2 in the temperature range of 1400 to 1850°K. by the torsion–effusion method. From their data in the range 1424–1691°K. they calculate the heat of sublimation at 298°K. to be 101.2 kcal./mole by the third law method and 101.4 kcal./mole by the second law method using Brewer's functions and frequencies. In a single Knudsen effusion experiment, Pottie[5] has determined the vapor pressure of liquid CaF_2 to be 0.27 torr at 1823°K. A third law treatment then indicates $\Delta H^0_{298} = 104$ kcal./mole. The earlier work of Ruff and LeBoucher[3] was reviewed by Brewer, *et al.*,[2] who recommended $\Delta H^0_{298} = 102.3$ kcal./mole for the heat of sublimation. The results of these various studies are shown in Fig. 1, together with the additional data obtained with the mass spectrometer.

To augment the weight-loss studies, the rate of sublimation was measured and vapor species identified between 1242 and 1669°K. by means of the mass spectrometric technique. The ionic species found to be due to molecules effusing from the tantalum Knudsen cell were $^{40}Ca^+$, $^{44}Ca^+$, $^{40}Ca^{19}F^+$, $^{44}Ca^{19}F^+$, and $^{19}F^+$. No CaF_2^+ or TaF_n^+ ions were observed. The absence of any CaF_2^+ ions is not unusual, since dissociative ionization is expected to be a highly probable process for metal halide molecules. The relative abundance of ions at mass 59 and mass 63 was checked and found to correlate with the isotopic abundance of ^{40}Ca and ^{44}Ca.

Ionization efficiency curves for the observed ions are presented in Fig. 2. In each case the measured ion intensity was corrected for background and photoionization effects.[14] Using the known value[17] of 6.1 e.v. for the ionization potential of calcium, we obtain $AP(CaF^+) = 5.8$ e.v. and $AP(F^+) = 17.4$ e.v. with an estimated uncertainty of ±0.3 e.v. The low energy tail of the CaF^+ ionization efficiency curve probably is due to simple ionization of the CaF(g) molecule while the break at *ca.* 12.5 e.v. is attributed to the onset of the process forming CaF^+ ions from $CaF_2(g)$ by dissociative ionization. The observation that $AP(CaF^+) < AP(Ca^+)$ requires that $D(CaF^+) > D(CaF)$ even though a bonding electron is removed.[9] The tempera-

(14) W. A. Chupka and M. G. Inghram, *J. Phys. Chem.*, **59**, 100 (1955).

(15) Calibrated by the National Bureau of Standards, Test No. G30772, May. 1962.

(16) M. G. Inghram, R. J. Hayden, and D. C. Hess, "Mass Spectroscopy in Physics Research," Natl. Bur. of Std. Circ. 522, 1953, p. 257.

(17) C. E. Moore, Natl. Bur. Std. Circ. 467, 1949.

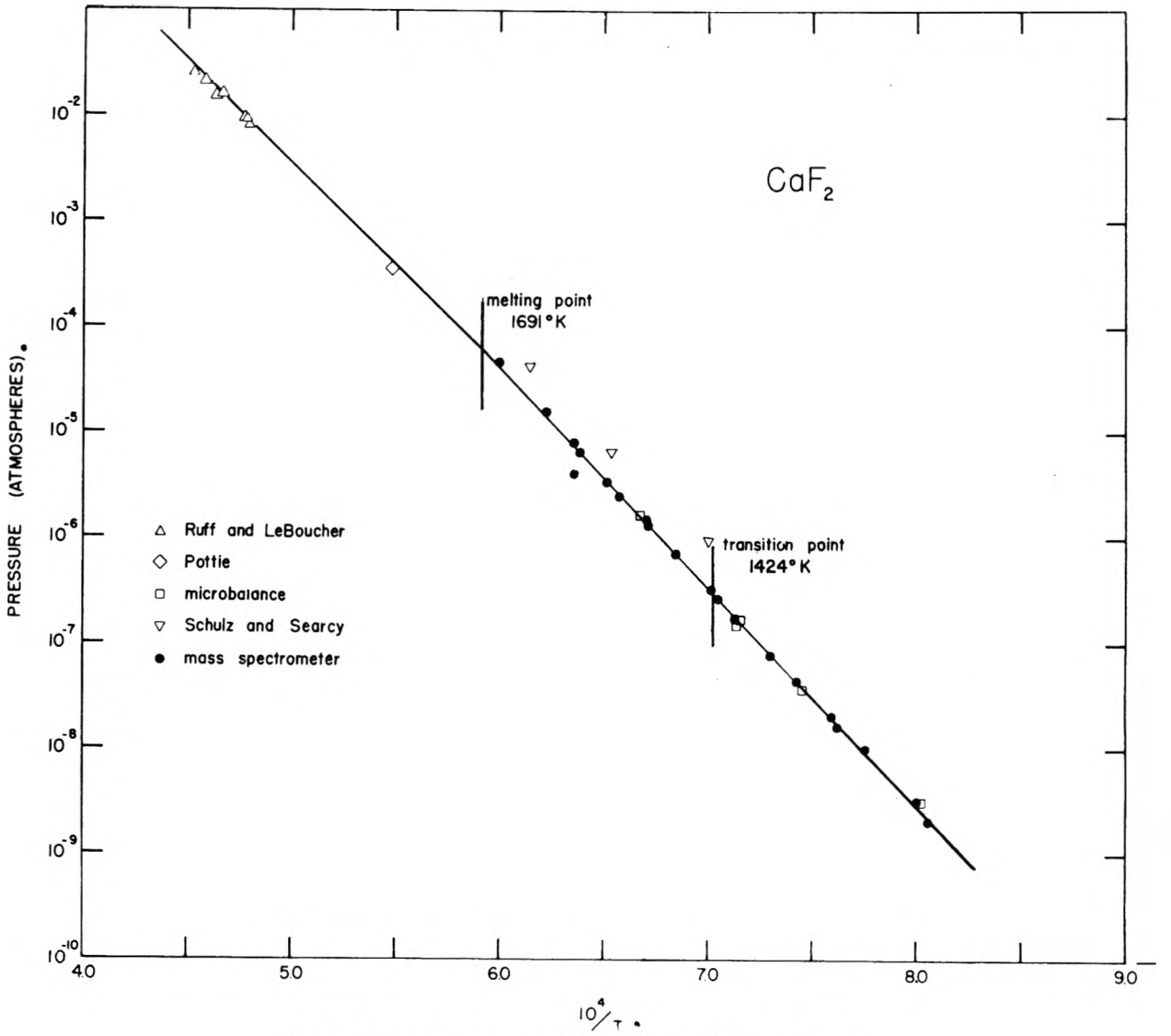

Fig. 1.—Vapor pressure data for CaF_2 by various investigators.

ture dependences of CaF^+ ions formed by bombardment with 10.5 and 75 volt electrons were found to be greatly different, demonstrating that the low energy tail is not due to fragmentation of $CaF_2(g)$. Further evidence, discussed in section IV, supporting CaF(g) as the precursor of the CaF^+ ions formed at low energy was found in the ionization efficiency curve for CaF^+ after aluminum was added to the calcium fluoride in the cell.

The observed intensity of Ca^+ and F^+ cannot be due to decomposition of CaF_2 to atoms since $P_{Ca} \approx 5.4 \times 10^{-11}$ atm. at 1600°K. It was not possible to follow the temperature dependence of low energy F^+ due to its high ionization potential and background, but the temperature dependence of F^+ from 75 volt electrons was very nearly equal to that of CaF^+ from 10.5 volt electrons, so it is conceivable that CaF(g) and F(g) may be formed in the same reaction which may possibly be with the tantalum cell.

Two independent methods were employed to determine the heat of sublimation of CaF_2 from the experimentally observed ion currents of CaF^+. The intensity of the $^{40}Ca^{19}F^+$ peak, using 75 volt electrons, was followed as a function of temperature, taking into account the CaF^+ due to CaF molecules. By making use of the ion current–pressure relationship[18] $P = kI^+T$

(18) W. A. Chupka and M. G. Inghram, *J. Chem. Phys.*, **21**, 371 (1953).

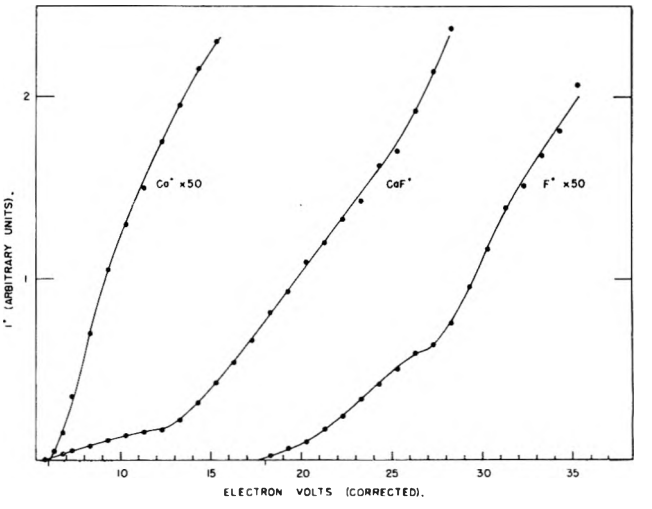

Fig. 2.—Ionization efficiency curves for species observed over CaF_2.

and the integrated form of the Clausius–Clapeyron equation, a value of ΔH_T which is independent of the proportionality constant k may be found from the slope of the curve obtained by plotting $\log (I^+T)$ *vs.* $1/T$. The slope of this plot yielded a heat of sublimation of $\Delta H^0_{1424} = 95.46 \pm 0.49$ kcal./mole where the uncertainty given is again the standard deviation of the least squares treat-

ment. The true uncertainty may be several times this figure due to such factors as temperature gradients in the cell. A heat of sublimation, $\Delta H^0_{298} = 103.6$ kcal./mole, was obtained from ΔH^0_{1424} by using Brewer's[2] molecular constants to calculate the enthalpy change of the gas and taking $H^0_{1424} - H^0_{298} = 24.3$ kcal./mole directly from Naylor's heat content measurements on $CaF_2(s)$.[19] There was no break in the vapor pressure curve at or near 1424°K. to suggest a phase change. From a review of Naylor's work, it appears that the designations α and β were simply used to describe the two different equations which fit the $H_T - H^0_{298}$ data above and below 1424°K. and that there is no real evidence for a phase change in $CaF_2(s)$ in this temperature range.

An alternative approach is to calculate ΔH^0_{298} at each temperature from the absolute pressure and the free energy function change for the reaction. In order to determine the instrument constant k, a weighed amount of silver was vaporized from the crucible and a pressure calibration made in the usual way.[14,20] When it was determined that the pressures from the microbalance studies were only *ca.* 20% higher than those calculated using the silver calibration, the constant k was calculated by normalizing the mass spectrometric data to the microbalance data by means of the least-squares equations.

The pressures then were used for a third law calculation of the heat of sublimation and yielded an average value of $\Delta H^0_{298} = 103.3$ kcal./mole. The results of the mass spectrometric runs are listed in Table II and plotted in Fig. 1.

Table II

Mass Spectrometric Sublimation Data

°K.	$10^4/T$	I (CaF^+),[a] arbitrary units	$-\log P_{atm}$	$-\Delta\left(\frac{F^0_T - H^0_{298}}{T}\right)$	ΔH^0_{298}
1573	6.357	4660	5.098	42.25	103.2
1521	6.575	1503	5.604	42.44	103.6
1461	6.845	442	6.154	42.65	103.3
1403	7.128	114	6.760	42.85	103.4
1347	7.424	30.7	7.348	43.05	103.3
1290	7.752	7.20	7.996	43.25	103.0
1250	8.000	2.36	8.494	43.40	102.8
1312	7.622	11.6	7.782	43.17	103.4
1370	7.299	51.9	7.112	42.97	103.5
1419	7.047	171	6.580	42.80	103.5
1490	6.711	810	5.881	42.55	103.5
1535	6.515	2040	5.468	42.38	103.5
1567	6.382	3800	5.190	42.27	103.5
1669	5.992	25400	4.339	41.86	103.0
1606	6.227	8950	4.806	42.12	103.0
1491	6.707	909	5.834	42.55	103.2
1426	7.013	211	6.484	42.78	103.2
1317	7.593	14.5	7.685	43.16	103.2
1242	8.052	1.53	8.685	43.43	103.3
				Av. =	103.3 ± 0.2 kcal./mole

[a] Second set of measurements corrected for change in emission and multiplier gain

$$\log P_{atm} = -\frac{95.46 \pm 0.49}{45.76} \times \frac{10^4}{T} + 8.141 \pm 0.006$$

While the small standard deviation of ±0.2 kcal./mole for the third law heat reflects the high reproducibility of the measurements, the true uncertainty must reflect errors in entropy estimates, primarily of $CaF_2(g)$. The quite low bending frequency of 95 cm.$^{-1}$ is particularly open to question. The third law heat of sublimation therefore was taken to be 103.3 ± 2.0 kcal./mole. In using the second law method to obtain the enthalpy of reaction the major inherent errors are those in temperature measurement. The enthalpy correction for the gas is very insensitive to the choice of molecular parameters. In practice, uncertainties of the order of ±3 kcal./mole are obtained in the temperature range covered by this investigation. The second law heat of sublimation then was taken to be 103.6 ± 3.0 kcal./mole.

IV. Stability of the CaF Gaseous Molecule

In order to achieve reducing conditions and enhance the amount of CaF(g) present, about 100 mg. of aluminum wire was added to the CaF_2 sample in the Knudsen cell. On heating to about 1330°K., ion peaks produced by 75 volt electrons were observed corresponding to Ca^+, CaF^+, Al^+, and AlF^+ in the relative amounts 41:1:100:850. Ionization efficiency curves for these ions are shown in Fig. 3. Using $IP(Ca) = 6.1$ e.v. as a standard,[17] one finds $AP(CaF^+) = 5.5$ e.v., $AP(AlF^+) = 9.7$ e.v. and $AP(Al^+) = 6.1$ e.v. The appearance potential of CaF^+ reproduces within the uncertainty (±0.3 e.v.) of the measurements, the appearance potential of AlF^+ agrees with work by Porter,[21] and the appearance potential of Al^+ agrees with the spectroscopic value[17] of 5.98 e.v. and the electron impact value of 6.1 ± 0.2 e.v. obtained by Porter, *et al.*[22] The fact that a new process was then responsible for the production of CaF(g) was established by the observations that the CaF^+ intensity was much greater than that due to $CaF_2(g)$ when observed at the same temperature and that the temperature dependence of the CaF^+ ion formed by 10.5 volt electrons differed greatly from that observed in the earlier sublimation experiments.

Fragmentation effects were minimized by working 5 v. above the appearance potential for Ca^+, CaF^+, and AlF^+ and only 2 v. above the appearance potential of Al^+ since there was a break in the Al^+ ionization efficiency curve about 3.1 e.v. above onset. The Al^+ formed by higher energy electrons was almost entirely due to fragmentation of AlF.[21] Temperature dependences of the individual ions formed at these voltages then established that Ca^+ and Al^+ were not produced by fragmentation of CaF and AlF. An important observation was that the activity of aluminum in the system was definitely much less than unity since the pressure of Al(g) was much less than, and the heat of formation from the condensed phase much greater than, that expected from the reaction Al(l) = Al(g). X-Ray diffraction powder patterns of the sample showed no lines due to Al even after long exposure though copious amounts of AlF(g) were still being produced at the completion of the experiment.

The equilibrium constant for the homogeneous reaction Ca(g) + AlF(g) = Al(g) + CaF(g) was determined at a series of temperatures using low energy ionizing electrons. The equilibrium constant, K_1, for this reaction is pressure independent so that instrument geometry and sensitivity factors cancel and it was

(19) B. F. Naylor, *J. Am. Chem. Soc.*, **67**, 150 (1945).

(20) M. G. Inghram, W. A. Chupka, and R. F. Porter, *J. Chem. Phys.*, **23**, 2161 (1955).

(21) R. F. Porter, *ibid.*, **33**, 951 (1960).

(22) R. F. Porter, P. Schissel, and M. G. Inghram, *ibid.*, **23**, 339 (1955).

only necessary to correct the ion current constant, $K_1' = (Al^+)(CaF^+)/(Ca^+)(AlF^+)$, for relative cross sections, differences in energy above threshold, and gains. The tabulated cross sections of Otvos and Stevenson,[23] an experimental value for the gain ratio of AlF^+ and CaF^+ and an estimate[16] of the relative gains of Al^+ and Ca^+ were used to calculate $K_1 = 2.3K_1'$. The values of log K_1 then were used together with free energy functions for Al and AlF from the JANAF Tables,[24] Ca from Stull and Sinke,[25] and CaF from Kelley[26] and Kelley and King[27] ($S^0_{298} = 54.9 \pm 0.2$ e.u.) to calculate third law heats of reaction at 298°K. The average value is $\Delta H^0_{298} = 32.7 \pm 0.2$ kcal./mole. The data and results are presented in Table III.

TABLE III

EQUILIBRIUM CONSTANT AND HEAT OF THE REACTION

$Ca(g) + AlF(g) = Al(g) + CaF(g)$

T, °K.	$10^4/T$	K_1'	$-\log K_1'$	$-\log K_1$	$-\Delta\left(\frac{F^0_T - H^0_{298}}{T}\right)$	ΔH^0_{298}
1289	7.758	3.891×10^{-5}	4.41	4.05	5.93	31.6
1311	7.628	2.554×10^{-5}	4.59	4.23	5.93	33.2
1335	7.491	4.042×10^{-5}	4.39	4.03	5.93	32.6
1323	7.559	3.252×10^{-5}	4.48	4.12	5.93	32.8
1292	7.740	2.716×10^{-5}	4.58	4.22	5.93	32.6
1276	7.837	2.472×10^{-5}	4.61	4.25	5.93	32.4
1349	7.413	4.821×10^{-5}	4.32	3.96	5.93	32.5
1281	7.806	2.03×10^{-5}	4.69	4.33	5.93	33.0
1334	7.496	3.79×10^{-5}	4.42	4.06	5.93	32.7
1271	7.868	2.06×10^{-5}	4.69	4.33	5.93	32.7
1351	7.402	4.69×10^{-5}	4.33	3.97	5.93	32.6

Av. = 32.7 ± 0.2 kcal./mole

The ion current constants, K_1', may be used as before to find an independent second law heat from the plot of log K_1' *vs.* $1/T$ shown in Fig. 4. A least squares treatment yields $\Delta H^0_{1310} = 34.8 \pm 2.7$ kcal./mole which when corrected gives $\Delta H^0_{298} = 34.6 \pm 2.7$ kcal./mole.

By combining the more reliable third law heat of this reaction with the known heat of dissociation[24,28] (157.7 kcal./mole) of AlF(g), one computes $D^0_{298}(CaF) = 125.0$ kcal./mole (5.44 e.v.). By combining this result with the heat of sublimation of calcium[25] and the dissociation energy of fluorine,[24] the heat of formation of CaF(g) from the elements in their reference states at 298°K. was computed to be $\Delta H^0_f = -63.9$ kcal./mole.

An independent value of the dissociation energy of CaF(g) was obtained by using the same ion intensity data to determine a third law heat for the heterogeneous reaction $Ca(g) + CaF_2(s) = 2CaF(g)$. The equilibrium constant, K_2, for this reaction was obtained from the ion current constant, $K_2' = (CaF^+)^2T/(Ca^+)$, by using the instrument sensitivity constant obtained in the sublimation studies and correcting for cross sections and gains as before. The calculation yielded $K_2 = 1.86 \times 10^{-12}K_2'$. The values of log K_2 were then combined with free energy functions to calculate third law heats of reaction at 298°K. The average value of

(23) J. W. Otvos and D. P. Stevenson, *J. Am. Chem. Soc.*, **78**, 546 (1956).
(24) JANAF Interim Thermochemical Tables, The Dow Chemical Company, Midland, Michigan, December 31, 1960.
(25) D. R. Stull and G. C. Sinke, "Thermodynamic Properties of the Elements," Advances in Chemistry Series, No. 18, 1956.
(26) K. K. Kelley, U. S. Bur. Mines Bull. 584, 1960.
(27) K. K. Kelley, and E. C. King, U. S. Bur. Mines Bull. 592, 1961.
(28) W. P. Witt and R. F. Barrow, *Trans. Faraday Soc.*, **55**, 730 (1959).

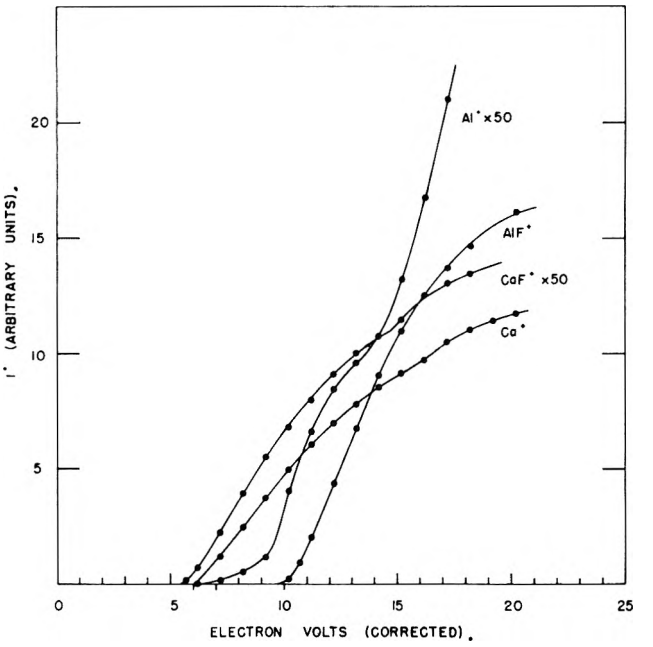

Fig. 3.—Ionization efficiency curves for species observed over Al–CaF_2.

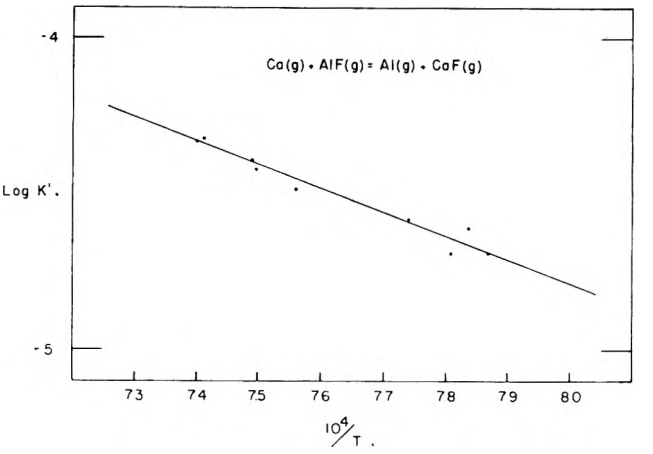

Fig. 4.—Temperature dependence of the equilibrium constant for $Ca(g) + AlF(g) = Al(g) + CaF(g)$.

the heat is $\Delta H^0_{298} = 120.7 \pm 0.8$ kcal./mole. The data and results are presented in Table IV.

TABLE IV

EQUILIBRIUM CONSTANT AND HEAT OF THE REACTION

$Ca(g) + CaF_2(s) = 2CaF(g)$

T, °K.	K_2'	log K_2'	$-\log K_2$	$-\Delta\left(\frac{F^0_T - H^0_{298}}{T}\right)$	ΔH^0_{298}
1335	2.089×10^3	3.320	8.411	51.47	120.1
1323	1.356×10^3	3.132	8.599	51.52	120.2
1292	2.928×10^2	2.467	9.264	51.67	121.5
1276	1.937×10^2	2.287	9.444	51.74	121.2
1349	2.368×10^3	3.374	8.357	51.40	120.9
1281	1.911×10^2	2.281	9.450	51.72	121.6
1334	2.709×10^3	3.433	8.298	51.47	119.3
1271	1.411×10^2	2.149	9.582	51.76	121.5
1351	3.647×10^3	3.562	8.169	51.40	119.9

Av. = 120.7 ± 0.8 kcal./mole

By combining the heat of this reaction with the heat of formation of $CaF_2(s)$,[2] the heat of sublimation of calcium,[25] and the dissociation energy of fluorine,[24] the dissociation energy of calcium monofluoride gas was com-

puted to be $D^0_{298}(CaF) = 124.8$ kcal./mole (5.41 e.v.), in excellent agreement with the value obtained from the homogeneous equilibrium. The value obtained from the heterogeneous equilibrium is considered less reliable than that from the homogeneous equilibrium because of the necessary use of the instrument pressure calibration and the uncertainty of the activity of CaF(s). Heats for various reactions in the Al–CaF_2 system are presented in Table V.

TABLE V

HEATS OF VARIOUS REACTIONS FOR THE Al–CaF_2 SYSTEM

Reaction	ΔH^0_{298} (kcal./mole)	D^0_{298} (e.v.)	Method
Ca(g) + AlF(g) = Al(g) + CaF(g)	34.6 ± 2.7		Second law
	32.7 ± 0.2		Third law
AlF(g) = Al(g) + F(g)	157.7 ± 2.0	6.85 ± 0.09	Available data
CaF(g) = Ca(g) + F(g)	123.1 ± 4.7	5.35 ± 0.20	Second law
	125.0 ± 2.2	5.44 ± 0.10	Third law
Ca(s) + $^1/_2F_2$(g) = Ca(g) + F(g)	61.1 ± 1.5		Available data
Ca(s) + $^1/_2F_2$(g) = CaF(g)	−62.0 ± 6.2		Second law
	−63.9 ± 3.7		Third law
Ca(g) + CaF_2(s) = 2CaF(g)	120.7 ± 0.8		Third law
CaF_2(s) = Ca(g) + 2F(g)	370.3 ± 2.0		Available data
CaF(g) = Ca(g) + F(g)	124.8 ± 2.8	5.41 ± 0.12	Third law

It is difficult to explain the difference in dissociation energies obtained from spectroscopic and mass spectrometric studies if a true predissociation at 3.15 e.v. was observed by Hellwege[10] and Harvey.[11] It may be, however, that what was observed was the formation of headless bands. Such a head for a sequence does not mean a dissociation or predissociation limit, but does explain the intensity distribution observed. The possibility that a perturbation was responsible for the observed intensity distribution cannot be excluded definitely either.

Since the difference between the ionization potential of calcium and the electron affinity of fluorine is only 2.6 e.v., it is certainly possible that CaF may be an ionic (rather than atomic) molecule.[9] The ions $Ca^+(^2S)$ + $F^-(^1S)$ may give the observed ground molecular state $^2\Sigma^+$. The non-crossing rule would then have this ionic state dissociate to the ground state atoms $Ca(^1S)$ + $F(^2P)$ and the atomic $^2\Sigma^+$ would correlate with the atomic ions.

Continuing work in this Laboratory[29] on the alkaline earth fluorides has yielded similar high values for the dissociation energies of SrF(g) and BaF(g), supporting 5.4 e.v. as the correct value for D(CaF).

Acknowledgments.—The authors are pleased to acknowledge the financial support of this work by the National Science Foundation, the United States Atomic Energy Commission, and the Wisconsin Alumni Research Foundation. In addition, the helpful suggestions and advice of Drs. W. A. Chupka and J. Berkowitz of the Argonne National Laboratory are gratefully recognized. Mr. I. Reithmeyer's careful workmanship in machining the inner parts of the instrument deserves our highest praise. Above all, we wish to thank Professor M. G. Inghram of the Department of Physics, University of Chicago, without whose assistance the construction of the mass spectrometer would not have been possible. During part of the time these investigations took place, G. D. Blue was a Shell Fellow.

(29) G. D. Blue, J. W. Green, T. C. Ehlert, and J. L. Margrave, *Bull. Am. Phys. Soc.*, **8**, 112 (1963).

INFRARED SPECTRA BY MATRIX ISOLATION OF LITHIUM FLUORIDE, LITHIUM CHLORIDE, AND SODIUM FLUORIDE

BY ALAN SNELSON AND KENNETH S. PITZER[1]

Department of Chemistry and Lawrence Radiation Laboratory, University of California, Berkeley, California

Received October 19, 1962

The matrix isolation method, which was adapted for infrared spectroscopy of molecular species existing at high temperatures by Linevsky, has been employed to examine the spectra of LiF, LiCl, and NaF. Rather complex spectra were found. Most of the features of these spectra must arise from polymeric alkali halide species. Spectra were taken for Ar, Kr, and Xe matrices and the effects of matrix material are considered. Isotope effects as well as spectral shifts after matrix diffusion assist in the interpretation of these data.

Introduction

At the present time there is much interest in the vapor species in equilibrium with materials at high temperature. Mass-spectrometric techniques have been widely used to determine vapor pressures and equilibrium data for a large number of gaseous–solid systems.

Unfortunately, this approach does not give any information concerning the structure or vibration frequencies of the gaseous species, which are of interest in their own right, and from which entropy data may be calculated. This latter quantity is often required to make full use of the mass-spectrometric approach, but usually has to be estimated through lack of experimental data.

One of the conventional methods for obtaining just this information is optical spectroscopy. However, there are experimental difficulties in observing the spectra of high-temperature species in the gas phase. These are due mainly to the chemical reactivity of the vapor species with the containing vessel, the complexity of the spectra because of highly excited vibration and rotation interactions, and the difficulty of obtaining a sufficiently high concentration of the required species for the spectra to be observed.

These difficulties are largely over-come, if the matrix isolation technique, as developed by Becker and Pimentel[2] and adapted to high temperature systems by Linevsky,[3] is used to observe the spectra. A Knudsen cell is used to produce a molecular beam of the gaseous

(1) Rice University, Houston, Texas.

(2) E. D. Becker and G. C. Pimentel, *J. Chem. Phys.*, **25**, 224 (1956).

(3) M. J. Linevsky, *ibid.*, **34**, 587 (1961).

species, which is simultaneously condensed with a stream of matrix gas on a window cooled to liquid hydrogen or helium temperature. The ratio of matrix to effusing species is kept sufficiently large to obtain effective isolation of the effusing species, and the spectrum is observed when a large enough amount of the active species has been deposited.

The matrix isolation technique is used in the present work to investigate the infrared spectra of lithium fluoride, lithium chloride, and sodium fluoride.

Experimental

Apparatus.—A molecular beam furnace and an optical system are combined with an all-metal cryostat of fairly conventional design. The cesium bromide window on which the matrix is formed, is housed in copper block, soldered into the bottom of a 2-in. diameter stainless steel tube, forming a hydrogen reservoir of about 1 l. capacity. Good thermal contact between the cesium bromide window and its housing is obtained by compressing thin strips of indium foil between the window and the copper block. The temperature of the window is measured by a copper–constantan thermocouple soldered to the housing. The e.m.f. is recorded on a Leeds and Northrop d.c. Microvolt amplifier. The hydrogen reservoir is surrounded by a closed copper cylinder, cooled to liquid nitrogen temperature to minimize radiative heat leak to the hydrogen pot, in which suitable holes are cut to allow the matrix to be deposited and the spectra observed. The entire low temperature assembly of the cryostat is supported on a ball-race, and can be rotated with respect to the vacuum housing; the vacuum at the rotating joint being retained by two rubber O-rings compressed radially. Two cesium bromide windows, sealed with O-rings to thev acuum jacket opposite the cooled window, permit spectral observations to be made on the matrix. The matrix gas enters the cryostat through a 2-mm. diameter jet and is directed at an angle of 45° on to the cooled window. The matrix gas flow is metered by a "Nupro" vacuum valve.

The molecular beam furnace is bolted to a flange on the cryostat. The Knudsen cell made of 0.020 in. platinum sheet is cylindrical, 0.75 in. in diameter, and 0.75 in. long, with flat ends. The effusion hole in one end of the cell is 0.025 in. in diameter and 0.25 in. off center.

The Knudsen cell is enclosed in a thick-walled tantalum receptor to minimize temperature gradients within the cell at elevated temperatures. The receptor is mounted on the end of a thin-walled tantalum tube. A small hole drilled in the base of the receptor enables the temperature of the Knudsen cell to be measured by an optical pyrometer, viewing the Knudsen cell through a window in the furnace housing, or by an iron–constantan thermocouple mounted in place of the window, the high temperature junction being trapped between the Knudsen cell and its housing. The Knudsen cell is heated electrically by two single-loop tungsten filaments. Resistance heating is used up to temperatures of 900°, the power being supplied by a low-voltage (8 v.) 800 watt transformer. Above 900° electron bombardment heating from a three kilowatt (3,000 v. at lamp.) d.c. power supply is used. A maximum temperature of about 2400° may be obtained. To minimize heat losses, the Knudsen cell is surrounded with tantalum radiation shields. The outer jacket of the furnace is water-cooled. The molecular beam is collimated by a single 5/16-in. diameter hole in a disk of sheet platinum located between the Knudsen cell and the cesium bromide window.

The evacuation of the cryostat and furnace is provided by an oil-diffusion pump and a mechanical pump. The pressure in the system is measured by an ion gage mounted in the furnace housing.

A Perkin–Elmer 421 double beam infrared spectrophotometer is used to record the spectra. The Dual Grating interchange is used for the region 4000–550 cm.$^{-1}$, and a cesium bromide interchange to cover the region from 550 to 260 cm.$^{-1}$. The calibration of the spectrophotometer is checked during each experiment against atmospheric H_2O and CO_2 bands.

General Procedure.—The experimental technique used for the matrix isolation of all the halides was essentially the same. The platinum Knudsen cell was filled with about 4 g. of sample, and the lid welded directly to the body of the cell. The Knudsen cell was placed in the furnace, evacuated and heated to a temperature such that about 0.03 g. of material effused from the cell per hour. (This was found by trial and error). The cell was then heated from 50–100° above this temperature until about 1 g. of material had effused out. In this way it was hoped that any volatile impurities in the sample were evaporated off. To prevent the sample from being deposited on the cesium bromide window during the above process, the window was turned to a position in which the molecular beam was cut-off by the surrounding copper heat shield. Care was always taken at this stage to keep atmospheric moisture out of the furnace and cryostat during any disassembly operation, and with this precaution a vacuum of about 1×10^{-5} mm. was obtained after three hours of pumping at room temperature.

Prior to performing a matrix isolation experiment, the cryostat was aligned in the sample beam of the spectrophotometer, the matrix gas line connected, and the whole system left evacuating overnight. At the same time atmospheric moisture was removed from the spectrophotometer by continual flushing with dry nitrogen obtained from the evaporation of liquid nitrogen in a 25-l. dewar.

The matrix gases, argon, krypton, and xenon, supplied by the Linde Company were all purified by passing over copper turnings at 600–700° to remove oxygen, Ascarite and magnesium perchlorate to remove CO_2 and H_2O, respectively, and finally activated charcoal cooled to solid carbon dioxide temperature to remove any remaining adsorbable impurities. The gases were collected at a rate of about 50 cc. per hour and stored in 10-liter reservoirs. The purity of the gases was checked spectroscopically by condensing about 200 cc. on the cooled window, and observing the spectra of the entire region 4000–260 cm.$^{-1}$.

For a matrix isolation experiment, the cryostat was cooled to a liquid hydrogen temperature (20–21°K.) and the spectra recorded the entire region from 4000 to 260 cm.$^{-1}$. The Knudsen cell was heated at the predetermined temperature until the pressure in the furnace was in the 10^{-5} mm. range (usually about 30 minutes). The matrix isolation was started by rotating the cooled window into a position perpendicular to the molecular beam and starting the matrix gas flow. The pressure in the furnace during isolation was of the order $2–3 \times 10^{-4}$ mm. The deposition of the matrix was interrupted periodically and the spectra of a particular absorption band recorded. When a suitable spectral absorption intensity has been obtained the deposition was terminated. After the spectrum had been observed over the entire region, the matrix was allowed to warm to a somewhat higher temperature to allow some diffusion of the trapped species within the matrix to occur, recooled to hydrogen temperature, and the entire spectrum again observed.

Materials.—Lithium fluoride was obtained from spectroscopic grade windows supplied by the Harshaw Chemical Company. Lithium chloride and sodium fluoride were reagent grade supplied by Baker and Adamson, specified purity of 98 and 99%, respectively.

Results and Discussion

In all matrix isolation experiments the mole ratio of matrix gas M to halide H condensed on the window is calculated. A nominal value of M is computed on the assumption that all the matrix gas entering the cryostat is condensed on the cooled window. Although this assumption is not realized experimentally, as evidenced by a 3–4-fold increase in pressure in the cryostat during the isolation experiment, a more reliable estimate does not seem possible. Since the same method of computation is used in all experiments, internal consistency is maintained. The value of H was computed from the weight loss of the Knudsen cell during the experiment and the geometry of the system. As a check on this method of calculating H, an experiment was made in which lithium fluoride alone was condensed on a cool polished metal plate in place of the cesium bromide window. The mass of lithium fluoride deposited on the plate was computed from the resulting diffraction pattern and was in good agreement with the value calculated from the weight loss of the Knudsen cell.

Preliminary experiments with lithium fluoride showed that isolation of the active species may be achieved with

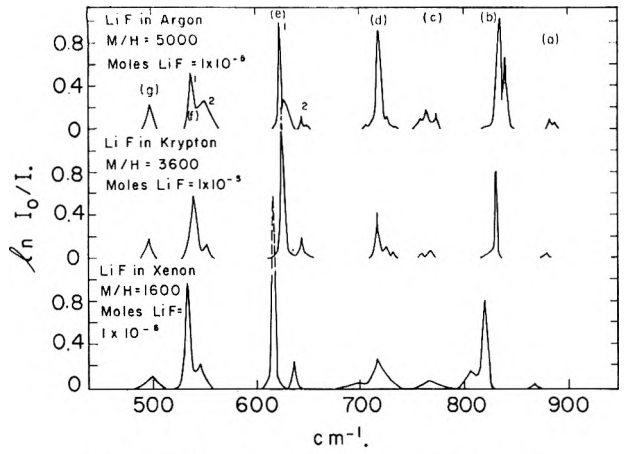

Fig. 1.—LiF spectra of matrices as deposited.

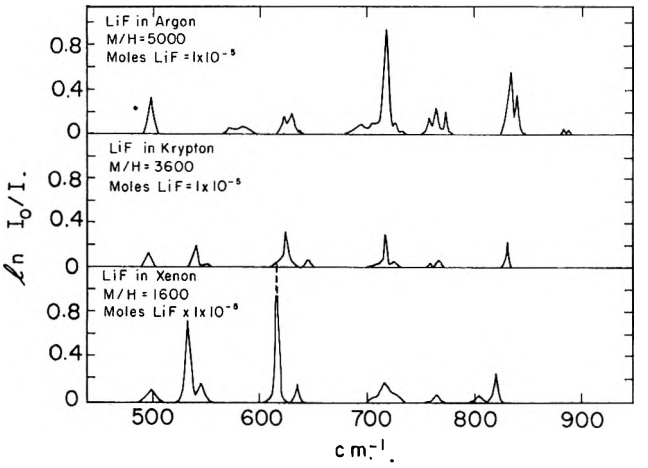

Fig. 2.—LiF spectra after allowing diffusion in the matrices.

M/H greater than 200. However, for a given value of H, values of M/H < 1000 resulted in a marked increase in the intensity of some absorption bands which previously at M/H > 2000 had been quite weak. To avoid complications due to poor isolation of the active species and to maintain consistency, M/H > 2000 has been used in most experiments. The effectiveness of the isolation achieved with the three matrix gases at M/H less than 1000 was found to decrease in the order xenon, krypton, argon; and with xenon the spectrum recorded with M/H = 700 was not noticeably different from that obtained with M/H = 2000. Presumably, xenon with the highest freezing point, forms a rigid matrix more rapidly at liquid hydrogen temperature than krypton, and similarly krypton more rapidly than argon.

Lithium Fluoride.—The lithium fluoride matrix isolation experiments were made with the Knudsen cell heated at 920 ± 20°. Isolation times of two or three hours were common. In warm-up experiments, the temperature of the window housing was raised 20, 30, and 45°K. above liquid hydrogen temperature for the argon, krypton, and xenon matrices, respectively. The higher the annealing temperature used, the greater the light scattering of the matrices became. Argon and krypton presented no problems in this respect, but with xenon it was difficult to raise the temperature sufficiently to obtain diffusion of the active species and yet still be able to record the spectrum. Effective isolation of the trapped species was destroyed at temperature approximately 15° higher than those stated above. This was shown by the absence of any absorption bands in the spectrum on recooling to liquid hydrogen temperature. The spectrum of pure lithium fluoride condensate was observed with negative results. Typical matrix isolation spectra of lithium fluoride in argon, krypton, and xenon before and after warm-up are shown in Fig. 1 and 2, respectively. The absorption frequencies are listed in Table I.

TABLE I

MATRIX ISOLATION SPECTRA OF LITHIUM FLUORIDE

Sec.	Frequencies, cm.⁻¹ Argon	Krypton	Xenon	Remarks
a	888	879	865	
	883			Monomer
b	840	830	820	
	835		805	
c	774	768		
	764	759	765	
	759			
	734			
	727	732		
d	719	726	716	
	706	717		
	649			
e	643	644	636	
	627	624	616	
	623			Dimer
f	550	552	545	
	537	540	533	
g	498	496	498	

The fundamental frequency of the lithium fluoride in the gas phase has been recorded by Vidale[4] at about 900 cm.$^{-3}$. Linevsky[3] has observed the spectra of lithium fluoride trapped in matrices of argon, krypton, and xenon, and reports values of 840 and 835, 830, and 823 cm.$^{-1}$ for the fundamental frequencies of the monomer in the respective matrices. The frequencies reported in Table I (sec. b), for the argon and krypton matrices are in agreement with the above values. However, in the present work, the monomer band in xenon is split, the major peak at 820 and a minor one at 805 cm.$^{-1}$, both at lower frequency than the single band observed by Linevsky. It is probable that even had the splitting been present in Linevsky's experiments, it would not have been observed since he worked at low spectral absorption intensities. The frequency shift between the gas and matrix bands of lithium fluoride in xenon is about 10% and it is conceivable that the small difference in frequency reported above, 3 cm.$^{-1}$, may be due to an impurity in the xenon sample used by Linevsky. In this work, the purity of xenon was >99.99% according to a mass-spectrometric analysis.

The absorption band occurring at a in Fig. 1 is due to the monomer of lithium fluoride containing the Li^6 isotope. The fundamental frequencies are listed in Table I (sec. a). The calculated value of ω^i/ω where ω^i and ω are the fundamental vibration frequencies of Li^6F and Li^7F, respectively, is 1.059. This agrees well with the average value of 1.057 found experimentally for the three matrices.

The remaining absorption bands shown in Fig. 1 (c, d, e, f, and g), are attributed to lithium fluoride polymers. It is well established[5] that the vapor of

(4) G. L. Vidale, *J. Phys. Chem.*, **64**, 314 (1960).

(5) R. F. Porter and R. C. Schoonmaker, *J. Chem. Phys.*, **29**, 1070 (1958).

lithium fluoride contains a large proportion of dimer, Li_2F_2, and also some trimer Li_3F_3. Recent electron diffraction studies[6] have shown that lithium chloride dimer has a planar rhombic structure. Three infrared active frequencies are expected for such a lithium halide dimer of D_{2h} symmetry. Two of the vibrations are in-plane stretching motions (B_{2u} and B_{3u}), and the third (B_{1u}), an out-of-plane bending. The structure of the trimer is not known, but assuming a plane hexagon of D_{3h} symmetry, there are seven infrared active frequencies (A_2 and 3E).

In Table II the abundances of the isotopic species of lithium fluoride dimer and trimer are listed.

TABLE II

RELATIVE ABUNDANCE OF DIMERIC AND TRIMERIC LITHIUM SPECIES

Li^7_2	85%	Li^7_3	79%
Li^6Li^7	14	$Li^6Li^7_2$	19
Li^6_2	1	$Li^6_2Li^7$	2
		Li^6_3	0

The frequency shift due to the mono-isotopic substitution of one Li^6 for Li^7 in the dimer cannot be calculated exactly, but a rough approximation may be made by applying the Redlich–Teller product rule to calculate the isotopic frequency shift for $Li^7_2F_2$ and $Li^6_2F_2$ and assuming half this shift for the mono-substituted dimer. This results in a value of $\omega^i/\omega = 1.03$ for each of the infrared active frequencies, where ω^i is the frequency of the mono-isotopically substituted dimer.

Comparison of Fig. 1 and 2 shows that the absorption bands e and f decrease noticeably in intensity after warm-up, while those at c, d, and g remain about the same. Also the intensity of the absorption bands at c, d, and g relative to those at e and f could be increased by working at low M/H values. Further examination of the absorption bands e and f in Fig. 1 shows that the stronger absorption ω^1 is always accompanied at higher frequencies by a weaker band, ω^2. The ratios ω^2/ω^1 for the absorption bands e and f are shown in Table III. These values may be compared with the approximate isotopic frequency shift calculated for the dimers $Li^7_2F_2$ and $Li^7Li^6F_2$ of 1.03.

TABLE III

	Absorption band	
Matrix	e	f
Argon	1.032	1.024
Krypton	1.032	1.023
Xenon	1.032	1.023

On the basis of the above results, the absorption bands e and f in Fig. 1 are assigned to the stretching frequencies of lithium fluoride dimer. No frequency unequivocably attributable to the dimer bending mode was observed. An absorption band consisting of a major and minor peak, not shown in Fig. 1, occurred in all three matrices at approximately 274 and 283 cm.$^{-1}$, respectively, in argon and at slightly lower frequencies in krypton and xenon, but always with a separation of about 9 cm.$^{-1}$ between the major and minor peaks. However it was not possible to show if this absorption band was due specifically to the dimer or higher polymeric species since the spectrometer was not very reproducible in this region. Theoretical calculation of the vibration frequencies of lithium fluoride dimer by

(6) S. H. Bauer, T. Ino, and R. F. Porter, *J. Chem. Phys.*, **33**, 685 (1960).

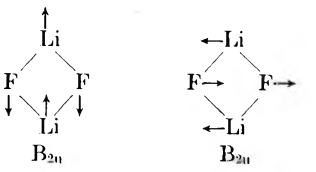

Figure 3.

Berkowitz[7] predicts the bending frequency at 385 cm.$^{-1}$.

The gas phase spectrum of lithium fluoride has been reported by Klemperer and Norris[8]; absorption bands at 640 and 460 cm.$^{-1}$ are attributed to the dimer stretching frequencies. This may be compared with the frequencies obtained in this work of approximately 620 and 537 cm.$^{-1}$. If the interpretations of the gas phase and matrix isolation spectra are correct, frequency shifts of −20 and +80 cm.$^{-1}$ occur in the matrix. Negative matrix frequency shifts are fairly common and may be interpreted in terms of attractive interactions between the isolated species and the surrounding matrix. The net effect is to reduce the effective value of the force constant between the vibrating atoms and thus lower the vibration frequency. Positive matrix shifts are less common and in the present case may be due to the matrix cage restricting the amplitude of the vibrational motion and hence increasing the frequency. The form of B_{2u} and B_{3u} vibrations is shown in Fig. 3.

In the lithium fluoride dimer, the amplitude of vibration of the lithium ion is greater than that of the fluoride ion. It is the lithium ion in the B_{2u} vibration moving perpendicularly to the walls of the matrix cavity which will suffer substantial restriction of movement, assuming the dimer is a "tight fit" in the cavity. The motion of the lithium ion in the B_{3u} vibration is unlikely to be restricted as it is directed tangentially to the walls of the cavity. On this qualitative basis, the matrix absorption bands at 620 and 537 cm.$^{-1}$ are tentatively assigned to the B_{3u} and B_{2u} modes, respectively. The assignment of the lower frequency to the B_{2u} mode is in agreement with the theoretical calculation of Berkowitz.[7]

Previously, it was noted that after annealing the matrix the absorption bands at e and f in Fig. 1 and 2 decreased in intensity. However, in argon the shapes of bands e and f also change and the absorption maxima are shifted to higher frequencies by 7 and 42 cm.$^{-1}$, respectively. A further anomaly present in the argon matrix spectrum is the splitting of the absorption band at e into two peaks, at 723 and 727 cm. It is difficult to interpret this behavior, but, since it only occurs in argon, it is perhaps connected with the trapped species occupying different types of sites in the argon matrix whereas in krypton and xenon matrices only one type of site is involved. It is possible the absorption bond at f is split in the same way as e noted above, but that the splitting is not observed due to the low resolving power of the cesium bromide optics. Certainly the splitting of the absorption band e, which was observed using the Dual Grating interchange, was not resolved when using the cesium bromide interchange.

Of the remaining absorption bands in Fig. 1 (c, d, and g) only g appears as a single peak in all three

(7) J. Berkowitz, *ibid.*, **29**, 1386 (1958); **32**, 1519 (1960).
(8) W. Klemperer and W. G. Norris, *ibid.*, **34**, 1071 (1961).

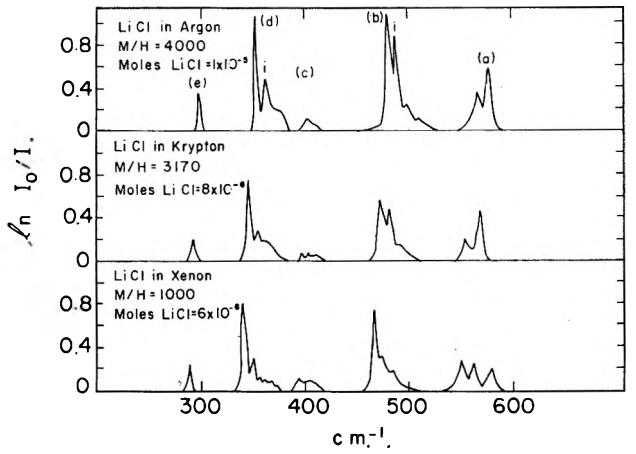

Fig. 4.—LiCl spectra of matrices as deposited.

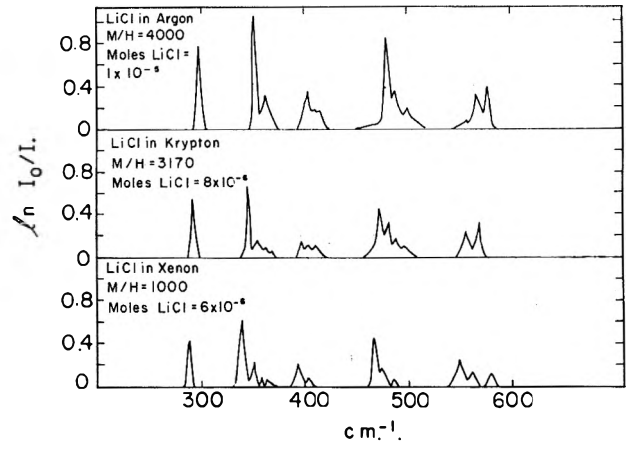

Fig. 5.—LiCl spectra after allowing diffusion in the matrices.

matrices. The absorptions at c and d have several maxima in argon and krypton, but only one in xenon. It seems likely that some of the maxima occurring in the argon and krypton matrices in bands c and d may be due to the trapped species occupying slightly different sites in the matrix. If all these absorption bands were due to lithium fluoride trimer, each major absorption at c, d, and g should be accompanied by a weaker band at higher frequencies of about one-quarter the intensity, due to the mono-isotopically substituted trimer. With the possible exception of the absorption at d in krypton, this is not observed. On the present evidence it is not possible to assign any of these frequencies specifically to the lithium fluoride trimer, and it may be that higher polymeric species are also present.

Lithium Chloride.—The lithium chloride matrix isolation experiments were made with the Knudsen cell heated at 710 ± 10°. Annealing temperatures, slightly higher than those used for lithium fluoride, were required to obtain diffusion of the trapped species in the matrix. No absorption bands were observed in the spectrum of pure lithium chloride condensate. Typical matrix isolation spectra of lithium chloride in argon, krypton, and xenon are shown in Fig. 4 and 5 before and after warm-up. The frequencies are listed in Table IV. As with lithium fluoride, lithium chloride[9,10] vapor contains a large proportion of dimer and some trimer. The abundance of the major isotopic species in the vapor phase is given in Table V. The relative abundance of the halogen dimer isotopes is not given in Table V, since shifts in frequency due to the substitution of Cl^{35} for Cl^{37} in the dimer are too small to be observed.

TABLE IV

MATRIX ISOLATION SPECTRA OF LITHIUM CHLORIDE

Sec.	Frequencies, cm.⁻¹ Argon	Krypton	Xenon	Remarks
a	578, 576, 567, 565	569, 567, 556, 554	563, 550	Monomer
b	510, 500, 488, 480	490, 482, 473	485, 474, 467	Dimer
c	403	410, 404, 397	404, 393	
d	362, 352	354, 344	350, 339	Dimer
e	298	292	288	

TABLE V

Monomer isotopes	Abundance, %	Dimer isotopes	Abundance, %
Li^7Cl^{35}	70	$Li^7_2Cl_2$	86
Li^7Cl^{37}	23	$Li^7Li^6Cl_2$	14

The absorption band at a in Fig. 4 is due to monomeric lithium chloride. The band has two maxima in argon and krypton, and three in xenon. Although not shown in Fig. 4, a shoulder was resolved on each of the two maxima at a in argon and krypton, about 2 cm. on the low-frequency side. This separation agrees with the isotopic shift expected for Li^7Cl^{37} and Li^7Cl^{35}. The frequencies in Table IV (sec. a) may be compared with the monomeric gas phase frequency of lithium chloride reported by Klemperer and Rice[11] at 641 cm.$^{-1}$.

Comparison of the relative intensities of the remaining absorption bands in Fig. 4 and 5 (b, c, d, and e) before and after warm-up, coupled with the results of isolation experiments at low M/H values, suggest that the absorption bands at b and d be assigned to lithium chloride dimer. Table VI gives the ratio ω^i/ω where ω^i and ω are the frequencies of the absorption bands at b and d in Fig. 4. These values may be compared with the approximate value of 1.033 expected for $Li^7_2Cl_2$

TABLE VI

Matrix	Absorption bands b	d
Argon	1.017	1.028
Krypton	1.021	1.027
Xenon	1.016	1.032

and $Li^7Li^6Cl_2$. The expected relative intensities of ω^i and ω in each of the absorptions at b and d, based on the natural abundance of the two isotopic species, is about 6:1. The discrepancy between the observed and predicted intensities of ω^i and ω might be justified if it is assumed that the dimer is trapped at two different sites in the matrix lattice, resulting in a separation of absorption maxima comparable in magnitude to the isotopic shift of the dimers $Li^7_2Cl_2$ and $Li^6Li^7Cl_2$. Presumably it is this type of site splitting which occurs with lithium fluoride dimer in argon (band e in Fig. 2),

(9) T. A. Milne and H. M. Kleine, *J. Chem. Phys.*, **33**, 1628 (1960).
(10) J. Berkowitz and W. A. Chupka, *ibid.*, **29**, 654 (1958).
(11) W. Klemperer, W. G. Norris, A. Büchler, and A. G. Emslie, *ibid.*, **33**, 1534 (1960).

but, in that case, the site splitting of 4 cm.$^{-1}$ is smaller than the isotope shift of about 20 cm.$^{-1}$, and no overlapping of the bands occur.

Since the discrepancy between the expected and observed relative intensities of ω^i and ω in the absorption bands at b is greater than that at d (Fig. 4), it is possible that an absorption band comparable to d, in the lithium fluoride spectra (Fig. 2), may be present in the lithium chloride spectrum and overlaps with the dimer absorption band at b (Fig. 4).

Klemperer and Norris[8] have reported the gas phase stretching frequencies of lithium chloride dimer at 460 and 335 cm.$^{-1}$. This may be compared with the average value for the absorption bands at b and d in the three matrices of 473 and 345 cm.$^{-1}$, corresponding to matrix shifts of the order +13 and +10 cm.$^{-1}$, respectively. The absorption bands at b and d are assigned to the B_{3u} and B_{2u} modes of the dimer, respectively.

Of the remaining absorption bands, c and e in Fig. 4, no definite assignment of the frequencies to the trimer (Li_3Cl_3) can be made for the same reasons as applied to the absorption bands at c, d, and g in the lithium fluoride spectra (Fig. 2). There is great similarity in the shape of the absorption bands c and e in Fig. 4 and c and g in Fig. 2. And, as mentioned above, it is possible that the absorption band at d in the lithium fluoride spectra (Fig. 2) may have a counter-part in the lithium chloride spectra which overlaps with the band at b (Fig. 4) attributed to the lithium chloride dimer.

Sodium Fluoride.—Mass-spectroscopic studies[10] indicate that the vapor of sodium fluoride consists mainly of monomer, a small proportion of dimer (<30%), and an almost negligible amount of trimer. In addition, sodium fluoride has no isotopes and this coupled with the virtual absence of trimer was expected to make the interpretation of the sodium fluoride spectrum rather simple.

The sodium fluoride matrix isolation experiments were made with the Knudsen cell heated at 1020 ± 20°. Annealing temperatures similar to those used for lithium fluoride were required to obtain diffusion of the trapped species in the matrices. No absorption bands were observed in the spectrum of pure sodium fluoride condensate. The results of the matrix isolation experiments with sodium fluoride are shown in Fig. 6 and 7 and the frequencies are listed in Table VII.

TABLE VII

MATRIX ISOLATION SPECTRA OF SODIUM FLUORIDE

	Frequencies, cm.$^{-1}$		
Sec.	Argon	Krypton	Xenon
a	495	486	475
	483		464
b	428	421	418
	418	414	408
		397	
c	404	387	386
	383	376	378
	370	365	
d	358	355	358
	350	347	347

The absorption band at a in Fig. 6 is assigned to sodium fluoride monomer, the band is split in argon and xenon and splitting also occurs in krypton after annealing. Comparison with the gas phase frequency is not possible since no experimental determination has been made. Berkowitz[7] estimates a frequency of 450 cm.$^{-1}$ for sodium fluoride in the gas phase. However if the frequency shift between the gas and matrix spectra of sodium fluoride is of the same order of magnitude as that found for lithium fluoride and lithium chloride then the present work would indicate a gas phase frequency of approximately 550 cm.$^{-1}$ for monomeric sodium fluoride.

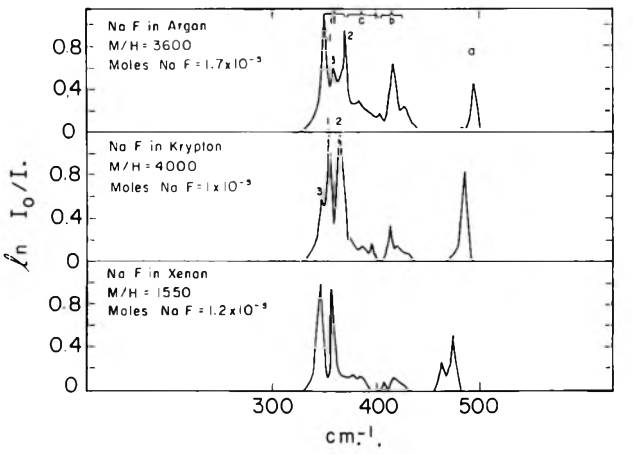

Fig. 6.—NaF spectra of matrices as deposited.

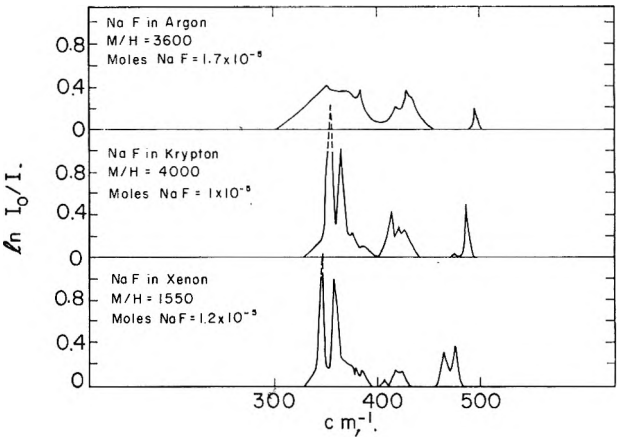

Fig. 7.—NaF spectra after allowing diffusion in the matrices.

The assignment of the absorption bands b, c, and d in Fig. 6 is difficult. If the mass-spectroscopic data concerning the relative abundance of the polymeric species present in sodium fluoride vapor are correct, the absorption bands d_1 and d_2 (Fig. 6) are attributable to the dimer stretching modes B_{2u} and B_{3u} since these are the two strongest bands. Although the absorption band in argon at b Fig. 6 is quite intense, the relative intensity of the band b to d in the three matrices decreases in the order xenon < krypton < argon.

As noted earlier xenon appears to have the best isolating properties of the three matrices, and it is conceivable that, since the spray-on temperature is higher for sodium fluoride than either lithium fluoride or lithium chloride, the isolating "power" of the matrix is of importance. On this basis the absorption band at b (Fig. 6) is assigned to some higher polymeric species. The absorption peak at d_3 (Fig. 6) in the argon and krypton matrices may be due either to site splitting of the dimer bands or to some higher polymeric species. The former alternative seems to be more likely in krypton since the band disappears after annealing. The behavior of the absorption band d in argon on

annealing does nothing to clarify the assignment, since the entire band d changes shape completely in sharp contrast to the behavior in krypton and xenon. This change on annealing of the band d in argon occurred even if only a small amount of diffusion of the trapped species was permitted as judged by the absorption intensity of the monomer band. No specific assignment of the absorption bands at b or c seems possible other than attributing them to higher polymeric species.

Summary

This work has demonstrated the feasibility of using the matrix isolation technique to obtain infrared spectral data for high temperature inorganic species. Certain precautions, however, must be noted.

(1) A given vibration of the trapped species may have more than one absorption maximum in a particular matrix environment. Spurious conclusions may result if this is not realized. In the present work this type of splitting was recognized from the different band shapes observed in the three matrices, but it is always possible that for other trapped species such differences may not occur. The splitting of an absorption band in a matrix spectrum is usually attributed to the trapped species occupying more than one type of site in the matrix,[3] the different environments causing changes in the interaction energy between the trapped species and the matrix cage. Since the different sites which the trapped species may occupy are presumably due to crystal imperfections in the lattice it would be interesting to try compressing the matrix to remove the imperfections and to observe if the splitting disappears.

(2) Large frequency shifts between gas and matrix phase spectra have been observed in the present work, and, if thermodynamic quantities are to be calculated, this limitation must be recognized. For the lithium halides investigated, frequency shifts in the matrix varying between the two extremes of +17 and −17% have been observed. Theoretical calculations of frequency shifts are usually hampered by lack of experimental information and by uncertainties concerning the actual environment of the trapped species in the matrix. Thus for lithium fluoride monomer Linevsky[3] was able to calculate from available experimental data the matrix frequency shift due to the dipole–induced dipole interaction, assuming the lithium fluoride monomer occupied a substitutional site in a perfect rare gas crystal lattice, but was unable to make any prediction as to the magnitude of the dispersion interaction.

Finally, although frequency shifts in the vibration spectra of trapped species are an obvious disadvantage of the technique, such large shifts as observed for lithium fluoride and lithium chloride may not be too common. Most of the reported rare gas matrix frequency shifts have been of the order of a few per cent for essentially non-polar trapped species, and this might indicate that perhaps large frequency shifts are likely only if highly polar molecules are involved. Some work in this Laboratory[12] in which the matrix isolation spectra of some group IIB chlorides were observed tends to support this view—the largest frequency shift being less than 4%. However, further work is required to clarify the situation before any firm prediction concerning matrix frequency shifts can be made.

Acknowledgment.—This research was carried out under the auspices of the U. S. Atomic Energy Commission.

(12) R. W. McNamee, Jr., Ph.D. Thesis, University of California, 1962.

THE VAPORIZATION BEHAVIOR OF BORON NITRIDE AND ALUMINUM NITRIDE[1]

BY D. L. HILDENBRAND AND W. F. HALL

Research Laboratory, Aeronutronic Division of Ford Motor Co., Newport Beach, California

Received October 20, 1962

The dissociation pressures of crystalline boron nitride and aluminum nitride have been measured by the torsion–effusion method over the ranges 1850 to 2160°K. and 1780 to 1970°K., respectively. Although the measured pressures for both substances showed a strong dependence on effusion orifice area, a simple expression relating equilibrium and observed pressures to effusion cell geometry was found to correlate the data quite satisfactorily. Equilibrium pressures evaluated by extrapolation of observed pressures to zero effective orifice area are in good agreement with dissociation pressures calculated from available thermodynamic data. The heats of formation of crystalline BN and AlN at 298°K. have been derived from the dissociation pressures as -59.8 ± 0.6 and -76.1 ± 2.1 kcal./mole, respectively. The magnitude of the hole-size dependence indicates that the gross condensation coefficient for BN is $<6 \times 10^{-3}$, while that for AlN is $<2 \times 10^{-3}$.

Because of the relatively low binding energies of gaseous metal nitrides and the very high stability of the nitrogen molecule, condensed nitrides vaporize primarily by decomposition to the elements. Substances such as the nitrides that decompose to diatomic gaseous molecules might be expected to have low condensation coefficients (fraction of the incident molecules which stick, or condense, on the vaporizing surface), presumably because of the difficulty in accommodating on the surface a gaseous molecule which does not exist as a structural unit in the condensed phase.[2] This is especially true for boron nitride and aluminum nitride, where the N–N internuclear distance, which is 1.1 Å. in the gaseous N_2 molecule, undergoes considerable change in the condensation process; the distance of closest approach of two nitrogen atoms is about 2.5 Å. in the BN lattice and 3.1 Å. in the AlN lattice.

(1) This work was supported by the Advanced Research Projects Agency and Bureau of Naval Weapons under Contracts NOrd 17980 and NOw 61-0905-C.

(2) L. Brewer and J. S. Kane, *J. Phys. Chem.*, **59**, 105 (1955).

In the research reported here, the effusion method has been used to study the vaporization of boron nitride and aluminum nitride in order to obtain information about the dissociation pressures and heats of dissociation of the two nitrides. Pressures determined by effusion methods, however, may be considerably lower than equilibrium values for substances with low condensation coefficients. From mass balance considerations, *i.e.*, the rate of vaporization equals the rate of condensation plus the rate of effusion, it can be shown qualitatively with the aid of elementary kinetic theory that equilibrium pressures (P_e) and observed effusion pressures (P_T) are related through the expression

$$P_e = P_T(1 + \beta Ca) \qquad (1)$$

where a is the effusion orifice area, C is the associated orifice Clausing factor, and β is a constant which is characteristic of a particular cell configuration and sample particle size. Under the very simplest conditions, β would be inversely proportional to the condensation coefficient, α. Therefore, for β approximately equal to or greater than $1/Ca$ (*i.e.*, for small α), observed pressures will fall significantly below equilibrium values. The application of eq. 1 in its simplified form where $\beta = 1/\alpha A$ (A is the effective vaporizing surface area) has been discussed by Speiser and Johnston[3a] and Stern and Gregory[3b]. A more complete analysis of the effusion process has been given by Whitman[4] and by Motzfeldt[5] in which the scattering of vapor molecules by the body of the effusion cell is taken into account. However, the derived relation between equilibrium and observed pressures is still of the form of eq. 1, with the constant β now being somewhat more complex. Even so, the more complete treatment[4,5] would indicate that $\beta \cong 1/\alpha A$ when α is small. In either case, one would expect from a rearrangement of eq. 1 into the form

$$\frac{1}{P_T} = \frac{1}{P_e} + \frac{\beta Ca}{P_e} \qquad (2)$$

that, if the analysis is valid, a plot of the reciprocal of observed pressure *vs.* the effective orifice area, Ca, should be linear with intercept $1/P_e$. Thus it should be possible in favorable cases to evaluate equilibrium pressures from effusion data, even when low condensation coefficients effect significant degrees of undersaturation.

Some caution must be exercised in applying eq. 1 to the interpretation of effusion measurements, however, since it is difficult to judge the validity of some of the assumptions involved in the derivation. In particular, objections can be raised to the assumption that vaporization and condensation coefficients are equal and independent of pressure. Also, there may be horizontal pressure gradients within the cell that should be accounted for. Unfortunately, there are few cases in the literature where the necessary equilibrium pressures and orifice-size data are available so that eq. 1 can be put to the test. Some very recent calorimetric measurements have put the thermodynamics of dissociation of BN and AlN on a rather firm basis, so that in these cases at least, one can compare calculated and extrapolated equilibrium pressures and thus check the validity of eq. 1.

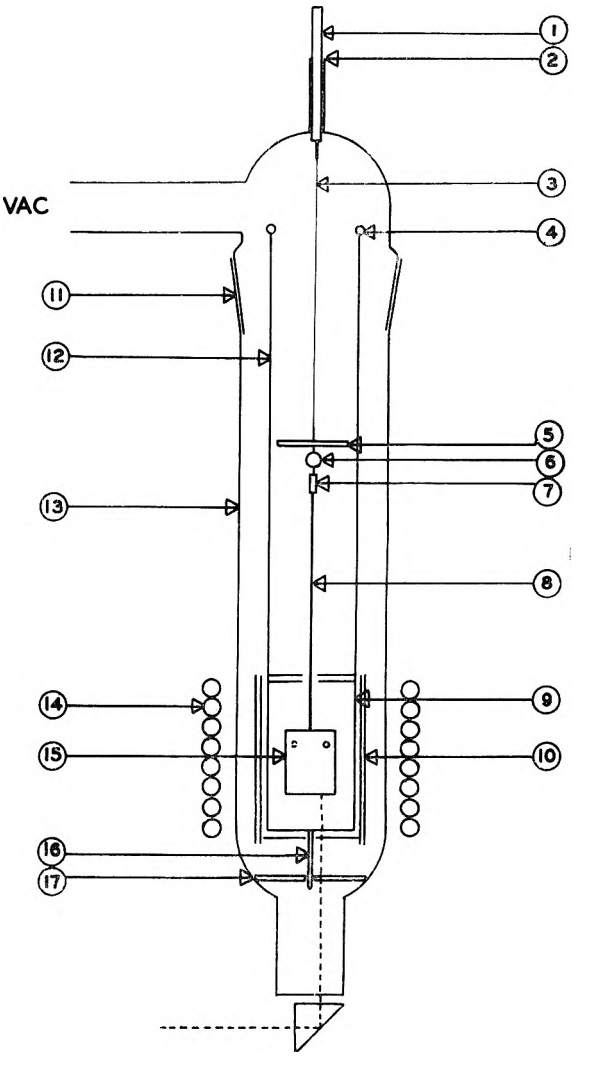

Fig. 1.—Torsion-effusion apparatus: 1, support rod for suspension system; 2, wax seal joint; 3, 2 mil tungsten torsion filament; 4, susceptor support hook; 5, aluminum damping disk; 6, galvanometer mirror; 7, aluminum connector link; 8, 50 mil tungsten rod; 9, tantalum susceptor; 10, radiation shields; 11, 55/50 standard taper joint; 12, 50 mil tantalum support wire; 13, 6 cm. o.d. quartz tube; 14, 8 turn copper induction coil; 15, effusion cell; 16, tantalum stud; 17, molybdenum centering plate.

Experimental

The dissociation pressures were measured by the torsion–effusion method[6-8] in which the substance to be studied is contained in an effusion vessel suspended from a torsion filament. Streaming of vapor from orifices offset from the center of suspension induces a rotation of the cell which is related directly to the pressure within. Under molecular flow conditions, the pressure, P_T, can be calculated from the relation

$$P_T = \frac{2k\theta}{\Sigma afq} \qquad (3)$$

where k is the torsion constant of the filament, θ is the angle through which the cell is rotated, and a, f, and q are the area, force factro,[9] and moment arm of each of the effusion orifices. Vapor composition does not enter the total pressure calculation, although the nature of the vapor must be ascertained before a thermodynamic analysis can be made.

A schematic diagram of the torsion–effusion apparatus is

(3) (a) R. Speiser and H. L. Johnston, *Trans. Am. Soc. Metals*, **42**, 283 (1950); (b) J. H. Stern and N. W. Gregory, *J. Phys. Chem.*, **61**, 1226 (1957).
(4) C. I. Whitman, *J. Chem. Phys.*, **20**, 161 (1952).
(5) K. Motzfeldt, *J. Phys. Chem.*, **59**, 139 (1955).
(6) M. Volmer, *Z. physik. Chem., Bodenstein Festb.*, 863 (1931).
(7) A. W. Searcy and R. D. Freeman, *J. Am. Chem. Soc.*, **76**, 5229 (1954).
(8) M. D. Scheer, *J. Phys. Chem.*, **61**, 1184 (1957).
(9) R. D. Freeman and A. W. Searcy, *J. Chem. Phys.*, **22**, 762 (1954).

given in Fig. 1. All measurements were made with effusion cells machined from graphite (National Carbon Co. Grade ATJ). The cells were 2 × 2 cm. in horizontal cross section and 3 cm. long, and contained four separate cylindrical sample chambers which were 0.7 cm. in diameter and 2.5 cm. deep. An effusion orifice was drilled in each of the four vertical faces at the point of minimum wall thickness, resulting in moment arms of about 0.55 cm. The orifices were located in opposite sides of opposite faces. A wide cut milled across the face of each hole reduced the orifice depths to about 0.04–0.05 cm. The tops of the sample chambers were sealed with tapered graphite plugs. The geometrical constants of the effusion cells, as measured with a traveling microscope, are given in Table I; constants for the individual orifices did not vary by more than a few per cent from the average values given. Because of a defect in one of the orifices, only three sample chambers were loaded with cell 5.

TABLE I

EFFUSION CELL GEOMETRICAL FACTORS[a]

Cell	$\bar{d}$, cm.	$\bar{a}$, cm.²	$\overline{Ca}$, cm.²	$\Sigma af/q$, cm.³
3	0.115	0.0105	0.00790	18.72×10^{-3}
4	.077	.0046	.00281	6.81×10^{-3}
5	.035	.0010	.00053	9.77×10^{-4}

[a] $\bar{d}$ = average orifice diameter; $\bar{a}$ = average orifice area; C = orifice Clausing factor; f = orifice force factor; q = orifice moment arm.

The effusion cell and associated tungsten supported rod were suspended from a 30 cm. length of 0.005 cm. diameter tungsten wire, the torsion filament. Oscillations were damped out through interaction of a permanent magnet with an aluminum disk attached to the rigid part of the suspension system. The torsion constant of the filament was determined from the period of oscillation of the system with and without a body of known moment of inertia attached; the values for k for a given filament never differed by more than a few per cent from run to run. Angular deflection of the cell was measured with a telescope and scale assembly by sighting on a galvanometer mirror cemented to the suspension system. The deflection could be determined to within 0.001 radian.

The high temperatures required were produced by radiofrequency induction heating. In order to avoid a troublesome interaction[7] between the suspension system and the induction field, however, the effusion cell was heated by radiation from a shielding susceptor which surrounded the cell. This indirect method of heating the cell, used also by Scheer,[8] proved to be entirely satisfactory as far as the torsion measurements were concerned. Blank experiments with empty effusion cells showed that extraneous deflections due to the induction field were quite negligible. A 10-cm. length of seamless tantalum tubing, 3.8 cm. in diameter and 0.05 cm. wall, served as the susceptor. Twelve holes of 0.2 cm. diameter in the side of the susceptor and 0.5 cm. diameter holes in the bottom and removable lid allowed for evacuation of the cell region. Thermal radiation shielding of the suseeptor was provided by several layers of tantalum sheet formed into cylindrical sectors and joined in such a way as to present a high resistance to eddy currents. Power input to the susceptor was supplied by a 25 kw., 450 kc. Westinghouse induction heating unit equipped with saturable reactor control.

The system was ordinarily evacuated to a pressure of 5×10^{-5} mm. or lower while measurements were in progress. At the highest temperatures encountered, the residual pressure was occasionally higher by a factor of five, but this was not high enough to create a significant back-pressure. A cylindrical black-body cavity in the cell bottom 1.0 cm. deep and 0.25 cm. in diameter, viewed through a prism and optical window, served as a radiation source for temperature measurement by optical pyrometry. The pyrometer calibration was checked frequently against a standard ribbon filament lamp. Corrections were applied for prism and window transmissivities.

The operation of the torsion-effusion apparatus was checked by measuring the vapor pressure of gold in the range 1650 to 1970°K.[10] Vapor pressures obtained with three different graphite cells were in close agreement with the most recently reported data for gold, indicating the technique to be reliable in respect to both the experimental arrangement and the method of determining absolute calibration constants for the cells and the torsion wires.

(10) D. L. Hildenbrand and W. F. Hall, *J. Phys. Chem.*, **66**, 754 (1962).

Boron nitride, stated to be of 99.5% purity, was obtained from the Carborundum Co., while the aluminum nitride sample, about 99% purity, was obtained through the courtesy of Dr. G. Long, Alcoa Research Labs. Both samples were in the form of finely divided powders. A brief microscopic examination indicated particle dimensions of 2 to 10 μ for the BN sample. The X-ray diffraction patterns of both starting materials showed only the peaks characteristic of the well crystallized nitrides. Prior to the measurements, both samples were outgassed under vacuum at temperatures slightly higher than the range of the torsion runs. X-Ray diffraction analyses of the samples after completion of the measurements showed that any reaction of the nitrides with the graphite cells was at most relatively minor. Aluminum carbide was never detected in the residual AlN powder, while only the thin surface layer of one of the BN samples gave evidence for some very weak boron carbide lines. Only if there were appreciable vaporization of boron would the graphite cell be expected to affect the dissociation pressures through reaction at the walls. However, under the experimental conditions the boron pressure is several orders of magnitude less than the nitrogen pressure, so that the boron can be considered essentially non-volatile.

Results and Discussion

(a) **Boron Nitride.**—The experimental pressure (P_T) data obtained for crystalline boron nitride are given in Table II. Several sets of reproducible results were obtained with each cell; only the results of a single series are given in Table II. There is, however, a marked trend in observed pressure with effusion hole size such that the highest pressures are obtained with the smallest orifices. Such an effect is predicted from eq. 1 as β approaches $1/Ca$ in magnitude, which signifies that the rate of effusion is becoming comparable to the rate of condensation. Observed pressures will then fall appreciably below the equilibrium values, the deviation being greater with the larger effective orifice areas. In order to relate equilibrium and observed pressures for BN, the smooth P_T values at 1950, 2000, and 2050°K. from each cell were plotted as $1/P_T$ *vs.* Ca. From the slopes and intercepts of the resulting linear plots at the three temperatures, values of β were derived as 470, 440, and 424. Selecting an average β of 440 and using the geometrical factors in Table I, one computes from eq. 1 the ratio P_e/P_T for cells 3, 4, and 5 as 4.40, 2.23, and 1.23, respectively. These ratios were used to convert the observed pressures for each cell to equilibrium (P_e) values, as shown in Table II. The hole-size correlation brings the pressure data of all three cells into close ngreement.

Schissel and Williams[11] have examined the mass spectrum of the molecular beam effusing from a Knudsen cell containing BN and detected no mixed gaseous species. It is reasonably certain, therefore, that vaporization proceeds according to the process

$$2BN(s) = 2B(s) + N_2(g) \qquad (4)$$

and that N_2 is the only significant gaseous species in the temperature range investigated. X-Ray diffraction analysis of the partially decomposed BN samples at the conclusion of the experiments gave no indication of the presence of crystalline boron or of a change in lattice parameters so that the vaporization process is assumed to produce amorphous boron. From the derived equilibrium pressures, heats of dissociation were calculated by the absolute pressure or third-law method using the relation

(11) P. O. Schissel and W. S. Williams, *Bull. Am. Phys. Soc.*, [II] **4**, 139 (1959).

$$\Delta H_{298} = -T\left[\Delta\left(\frac{F - H_{298}}{T}\right) + R \ln K\right] \quad (5)$$

where, for reaction 4, $K = P_{N_2}$. Values of $-\Delta(F - H_{298}/T)$ for reaction 4 were calculated as 41.99, 41.91, and 41.87 cal./mole deg at 1800, 2000, and 2200°K., respectively, using available free-energy functions for BN(s),[12] B(amorph),[13] and N_2(g).[14] The calculated third-law heats for reaction 4 are given in Table II. From the temperature dependence of pressure (second-law method) one obtains for reaction 4 by least-squares analysis $\Delta H_{298} = 119.8$ kcal., as compared to the average third-law value of 120.5 kcal. The third-law value is believed to be the more reliable and is assigned an uncertainty of ±1.0 kcal. based on an analysis of contributing errors. A possible error of 15° in temperature measurement contributes most of the uncertainty. An error analysis of the factors involved indicates that the pressure, exclusive of temperature errors, should be reliable to within 10%.

TABLE II

BORON NITRIDE DISSOCIATION PRESSURES AND HEAT OF THE REACTION

$$2BN(s) = 2B(s) + N_2(g)$$

T, °K.	$\theta \times 10^3$, rad.	$P_T \times 10^5$, atm.	$P_e \times 10^5$, atm.	ΔH_{298}, kcal.
	Cell 3 (k = 3.19 dyne cm./rad.)			
1945	30.2	1.01	4.44	120.3
1971	43.8	1.47	6.47	120.5
1978	48.8	1.64	7.22	120.5
2023	102.1	3.44	15.1	120.3
2042	123.8	4.16	18.3	120.7
2045	131.8	4.43	19.5	120.6
1998	70.6	2.37	10.4	120.2
1987	54.9	1.84	8.10	120.5
1936	24.5	0.82	3.61	120.5
1912	16.5	.55	2.43	120.7
	Cell 4 (k = 3.15)			
1860	6.2	0.57	1.27	119.7
1925	15.6	1.42	3.17	120.5
1978	34.0	3.10	6.92	120.7
2022	71.0	6.48	14.4	120.4
2043	94.3	8.60	19.2	120.5
1995	49.0	4.47	9.96	120.2
1957	26.0	2.37	5.28	120.5
1920	13.8	1.26	2.81	120.6
1893	8.5	0.78	1.74	120.7
	Cell 5 (k = 3.21)			
1941	5.4	3.5	4.30	120.2
1984	10.9	7.1	8.74	120.2
2022	19.5	12.6	15.5	120.2
2043	24.5	15.9	19.6	120.5
2076	37.2	24.1	29.6	120.5
2162	114.2	74.0	91.0	120.7
2114	65.0	42.1	51.8	120.5
2056	29.5	19.1	23.5	120.3
2001	12.7	8.2	10.1	120.4
1966	7.3	4.7	5.78	120.6
			Av.	120.5 ± 0.2

By combining the heat of reaction 4, $\Delta H_{298} = 120.5 \pm 1.0$ kcal, with the heat of formation of amorphous boron[12] at 298°K., 0.4 kcal./mole, one derives the heat of formation of crystalline boron nitride at 298°K. as −59.8 ± 0.6 kcal./mole. The stated uncertainty includes a possible error of 0.4 kcal./mole in the heat of formation of amorphous boron, in addition to that in the heat of dissociation. The value of ΔH^0_{f298} for BN derived in this way from the dissociation pressure measurements is in good agreement with calorimetric values determined by direct oxygen combustion (−60.3)[15] and by direct nitridation of boron (−60.7),[16] as well as with several unpublished determinations referred to by Dreger, Dadape, and Margrave[17] (−60 ± 1), and thus serves to confirm these values.

Although the agreement between the heat of dissociation obtained from this work and corresponding values obtained by calorimetry is good indication of the validity of eq. 1 in this case, a more direct appraisal can be made by comparing calculated dissociation pressures with values obtained by extrapolating observed pressures to zero effective orifice area. Free-energy functions from sources cited above were used along with $\Delta H^0_{f298} = -60 \pm 1$ for BN(s) to calculate the nitrogen pressure over boron nitride. At 2000°K., for example, the observed pressures with cells 3, 4, and 5 were 2.2×10^{-5}, 4.8×10^{-5}, and 8.1×10^{-5} atm., respectively, giving a linear extrapolation according to eq. 1 to an equilibrium pressure of 11.0×10^{-5} atm., as compared to the calculated pressure of $(9.1 \pm 3.0) \times 10^{-5}$ atm. Similar agreement was obtained at other temperatures. This would support the use of eq. 1 in interpreting orifice size effects in effusion experiments. Sizable errors will be introduced into third-law heats derived from the dissociation pressures if departures from equilibrium are not considered. Average third-law ΔH_{298} values for reaction 4, assuming $\beta = 1$, are derived as 126.3, 123.5, and 121.3 kcal. for cells 3, 4, and 5, respectively, while cognizance of the value $\beta = 440$ yields the corresponding heats 120.5, 120.4, and 120.4 kcal.

The magnitude of the condensation coefficient of N_2 on BN can be roughly assessed from the pressure–orifice area correlation since both the simple[3a,b] and more complete[4,5] treatments indicate that $\alpha \cong 1/\beta A$ and $\beta >> 1$. If the sample chamber cross-sectional area is taken as the lower limit to A, the effective vaporizing area, one obtains $\alpha < 6 \times 10^{-3}$. It is quite probable that α is very much smaller than this upper limit, since A is undoubtedly larger than the cross-sectional area. This difficulty in defining the effective vaporizing area constitutes one of the chief drawbacks to the estimation of condensation coefficients from effusion data. However, since the sample chamber cross-sectional area was the same for all cells and the cells were filled to approximately the same level in all cases, it is felt that A was essentially the same for all experiments, so that eq. 1 can be applied with confidence. Dreger, Dadape, and Margrave[17] have estimated α for BN to vary from 6×10^{-3} to 10×10^{-3} in the range 1400 to 2000°K. from a comparison of Langmuir free-evaporation rates with thermodynamically-predicted maximum evaporation rates. Although the agreement between the free-evaporation and effusion data as to the magnitude of α is good, the interpretation is in both cases

(12) National Bureau of Standards Report No. 7093, 1 January 1961.

(13) S. S. Wise, J. L. Margrave, and R. L. Altman, *J. Phys. Chem.*, **64**, 915 (1960).

(14) D. R. Stull and G. C. Sinke, "Thermodynamic Properties of the Elements," Advances in Chemistry Series, No. 18, Am. Chem. Soc., 1956.

(15) A. S. Dworkin, D. J. Sasmor, and E. R. Van Artsdalen, *J. Chem. Phys.*, **22**, 837 (1954).

(16) G. L. Galchenko, A. N. Kornilov, and S. M. Skuratov, *Zh. Neorg. Khim.*, **5**, 2651 (1960).

(17) L. H. Dreger, V. V. Dadape, and J. L. Margrave, *J. Phys. Chem.* **66** 1,556 (1962).

influenced by the surface area difficulty mentioned above. At best, only the product αA can be fixed with any assurance.

(b) **Aluminum Nitride.**—The vaporization of aluminum nitride was studied over the range 1780 to 1970°K. in the same three torsion cells; the observed pressure data are given in Table III. As with BN, there is a significant variation of pressure with orifice size, although the results obtained with each cell were in themselves consistent and reproducible. The observed increase in pressure with decreasing hole size again is indicative of a low condensation coefficient. A plot of $1/P_T$ *vs.* Ca, as suggested by eq. 2, yields a β value of 1200, significantly larger than that for BN. Although there was some indication that β decreases slightly with temperature, a constant value was used in analyzing the data, leading to P_e/P_T ratios of 10.45, 4.36, and 1.64 for cells 3, 4, and 5, respectively. It is worth emphasizing that the pressures obtained with cell 3, a cell with rather small (0.12 cm. diameter) orifices and otherwise normal geometry, are an order of magnitude lower than the equilibrium values. This points up the absolute necessity of establishing the relation between equilibrium and observed pressures in effusion experiments.

From the equilibrium to observed pressure ratios for each cell, P_e values were calculated as shown in Table III. Again, it is apparent that the hole size correlation brings the results from all three cells into good agreement. Schissel and Williams[11] have also studied the vaporization of AlN with the mass spectrometer and detected only the gaseous species Al and N_2, so that vaporization proceeds according to the reaction

$$2AlN(s) = 2Al(g) + N_2(g) \qquad (6)$$

Since the lattice constants did not appear to change with amount vaporized, the process must be essentially congruent. The equilibrium constant for reaction 6 can be expressed as

$$K = 0.148P_e^3 \qquad (7)$$

where P_e is the total equilibrium pressure. Because the masses of Al and N_2 are almost the same, the vapor within the cell will have the composition of the solid. Third-law heats for reaction 6 have been calculated from the absolute pressure data and are given in Table III. Available free-energy functions for Al(g)[14] and AlN(s)[18] were used in calculating $-\Delta(F - H_{298}/T)$ values for reaction 6 of 112.48, 112.27, and 112.06 cal./mole deg. at 1700, 1800, and 1900°K., respectively. A weighted least-squares analysis gave the second-law heat ΔH_{298} = 309.5 kcal., as compared with the average third-law value of 307.3 kcal. Since the free-energy functions are well known for all species involved, the third-law value is preferred. An uncertainty of ± 2.8 kcal. is assigned to this value, considering possible errors in experimental and auxiliary data.

The heat of formation of crystalline AlN at 298°K. is derived as −76.1 ± 2.1 kcal./mole from the third-law heat of dissociation and the heat of sublimation of aluminum[14] (ΔH_{298} = 77.5 ± 1.5 kcal./mole). The value thus derived from the dissociation pressures agrees with two recent calorimetric determinations of the heat of formation of AlN based on direct nitridation (−76.5)[19] and oxygen combustion (−75.6)[18]; other reported values ranging from −57 to −71 kcal./mole apparently can be ruled out.

(18) A. D. Mah, E. G. King, W. W. Weller, and A. U. Christensen, U. S Bur. of Mines Rept. of Invest. No. 5716 (1961).

TABLE III

ALUMINUM NITRIDE DISSOCIATION PRESSURES AND HEAT OF THE REACTION

$2AlN(s) = 2Al(g) + N_2(g)$

T, °K.	$\theta \times 10^3$, rad.	$P_T \times 10^5$, atm.	$P_e \times 10^5$, atm.	ΔH_{298}, kcal.
	Cell 3 (k = 3.18 dyne cm./rad.)			
1894	113.0	3.78	39.5	307.8
1917	175.8	5.88	61.2	306.5
1908	157.4	5.28	55.1	306.4
1883	101.2	3.39	35.4	307.4
1861	76.4	2.56	26.7	307.0
1894	116.3	3.90	40.8	307.6
1908	153.1	5.13	53.6	306.7
1898	128.9	4.32	45.1	307.2
	Cell 4 (k = 3.02)			
1818	38.9	3.40	14.8	306.5
1877	83.1	7.28	31.8	307.8
1899	143.9	12.6	55.0	305.0
1887	112.0	9.80	42.7	306.0
1840	53.3	4.66	20.3	306.6
1782	21.4	1.87	8.1	306.6
1795	21.4	1.87	8.1	309.1
1846	52.9	4.63	20.2	307.8
1887	99.2	8.70	38.0	307.3
1887	106.6	9.34	40.6	306.5
1901	135.5	11.9	51.9	306.1
1911	148.5	13.0	56.6	306.6
	Cell 5 (k = 3.17)			
1846	19.9	12.7	20.8	307.4
1899	40.6	26.0	42.6	307.9
1919	54.0	34.6	56.7	307.3
1880	31.2	20.0	32.8	307.7
1845	18.1	11.6	19.0	308.2
1803	9.5	6.1	10.0	308.2
1776	6.3	4.0	6.6	308.1
1972	106.8	68.3	112.0	308.1
1934	63.0	40.3	66.0	308.4
			Av.	307.3 ± 0.7

At 1900°K., the observed pressures with cells 3, 4, and 5 were 4.40×10^{-5}, 1.12×10^{-4}, and 2.66×10^{-4} atm., respectively. The intercept of a linear plot of $1/P_T$ *vs.* Ca yielded $P_e = 4.44 \times 10^{-4}$ atm., compared with the value $(4.6 \pm 1.5) \times 10^{-4}$ atm. calculated from the thermodynamic data. Much larger errors will be made in this case in third-law calculations if a large β is not considered. Assuming $\beta = 1$, one calculates for reaction 6 ΔH_{298} = 333.5, 323.1, and 313.5 kcal. from the data of cells 3, 4, and 5, while the proper value β = 1200 yields heats of 307.1, 306.8, and 307.9 kcal. The validity of the hole-size correlation again is apparent.

In the same fashion as described for BN, one estimates $\alpha < 2 \times 10^{-3}$ for AlN. Dreger, Dadape, and Margrave[17] estimate from free-evaporation studies on AlN α values ranging from 7×10^{-4} to 3×10^{-3} in the interval 1600 to 1900°K. Both results are subject to the surface area limitations discussed earlier.

(c) **Conclusions.**—It appears that the effusion method can be made to yield equilibrium data for sub-

(19) C. A. Neugebauer and J. L. Margrave, *Z. anorg. allgem. Chem.*, **290**, 82 (1957).

stances vaporizing by dissociation even when low condensation coefficients effect serious departures from saturation, provided that proper cognizance is made of the relation of equilibrium and observed pressures to effusion cell geometry. The over-all consistency of the derived results and the good general agreement suggest that the model upon which eq. 1 is based is essentially correct. As noted earlier, however, some caution should be used in interpreting the significance of the derived α values, particularly because of the surface area problem. In the AlN case, where two different gaseous species are involved, the resulting α must be a composite value and nothing can be said about the coefficients of the separate species.

The factors affecting the magnitude of α are as yet not well understood. In the BN case, the residual surface layer of non-volatile boron did not appear to affect the results, since the torsion pressures could be readily reproduced over a number of heating and cooling cycles. No lowering of the pressure with time was ever observed. AlN, however, which vaporizes so as to leave the composition of the solid unchanged, exhibits a larger hole-size effect than BN. Both the results of this work and of Dreger, Dadape, and Margrave[17] indicate α to increase slightly with temperature for BN and AlN, whereas the results of Stern and Gregory[3] show the reverse temperature dependence for iodine. More information is needed on a wider variety of substances before generalizations regarding α can be made with confidence.

ELECTRODE POTENTIALS IN FUSED SYSTEMS. VI. MEMBRANE POTENTIALS

BY KURT H. STERN

Electrochemistry Section, National Bureau of Standards, Washington, D. C.

Received October 22, 1962

Membrane potentials have been measured for the cells Ag|AgCl(X_1), NaCl ($1 - X_1$)|Vycor glass|AgCl(X_2), NaCl($1 - X_2$)|Ag. In contrast to the simple liquid junction whose potential is zero in this system, (the transport number equals the mole fraction), most of the current is carried through the glass by the sodium ion and $t_{Na^+} = 0.95$, independent of melt composition. Cells in which $X_1 \simeq 1$, *i.e.*, reagent grade AgCl, also operate as concentration cells with a Na^+ impurity ($X_{Na^+} \simeq 2 \times 10^{-4}$). The use of these cells for reference electrodes is discussed.

Introduction

Although systems consisting of two fused salts or salt mixtures separated by a porous barrier, *e.g.*, glass, are of interest in connection with reference electrodes as well as with the more general problem of ion transport through membranes, relatively little work in this field has been carried out.

In connection with the design of a reference electrode in halide melts Bockris, Hills, Inman, and Young[1] studied the cell Ag|AgCl(m_1), LiCl–KCl eutectic|glass|-AgCl(m_2), LiCl–KCl|Ag over the temperature range 330–550° using a thin glass diaphragm whose resistance was 2–5 kohms. They found that for small values of m_2/m_1 ($m_1 = 0.13$) or m_1 and m_2 the electromotive force of the cell was given by $E = RT/F \ln m_2/m_1$. However, at high values of m_2 they observed significant variations from this value which they attributed to differences in the alkali metal ion activity on either side of the glass. In modifying this electrode for use at higher temperatures Littlewood[2] used a Supremax glass tube of 1 mm. thickness filled with 0.271 mole fraction AgCl in NaCl–KCl eutectic in one half-cell while varying the AgCl composition in the other. He concluded that virtually all the current was carried through this glass by the alkali metal cations. In both of the above-cited studies all ions are present on both sides of the membrane. For the cell Ag|AgCl(X_1), NaCl($1 - X_1$)|-glass|(AgCl(X_2), NaCl($1 - X_2$)|Ag, using Vycor glass, for which results are reported in the present work $E_{cell} = RT/F[\ln a_2/a_1 - \int_{a_1}^{a_2} \Sigma t_i \, d \ln a_i]$. Assuming charge transport by cations only and concentration-independent transport number

$$E_{cell} = t_{Na^+} RT/F[\ln(X_2/X_1) + \ln (1 - X_1)/(1 - X_2)] = t_{Na^+} RT/F \ln [(X_2/X_1)(1 - X_1)/(1 - X_2)] \quad (1)$$

where t_{Na^+} is the transport number of Na^+ in the glass, and activities have been replaced by mole fractions since AgCl–NaCl solutions are nearly ideal.[3,4] Moreover, because the diffusion potential[5] in this system is nearly zero,[6,7] the potential of the above cell with a liquid junction instead of a glass membrane is just the Nernst value $E_N = RT/F \ln (a_2/a_1) = RT/F \ln X_2/X_1$. In that case, assuming current transport by cations only, $t_i = X_i$. A comparison of E_N with eq. 1 shows the effect of the membrane on the transport numbers.

A more difficult case arises when not all ions are present on both sides of the junction. In discussing the measurements of Tamman[8] and of Grube and Rau,[9] Laity[10] has shown that, if the membrane is not permeable to all the ions in the system, a knowledge of its properties is also required since the membrane constitutes a separate electrolyte system. For example, the

(1) J. O'M. Bockris, G. J. Hills, D. Inman, and L. Young, *J. Sci. Instr.*, **33**, 438 (1956).

(2) R. Littlewood, *Electrochim. Acta*, **3**, 270 (1961).

(3) K. H. Stern, *J. Phys. Chem.*, **62**, 385 (1958).

(4) M. B. Panish, R. F. Newton, N. R. Grimes, and F. F. Blankenship, *ibid.*, **62**, 1328 (1958).

(5) To distinguish between "liquid junction" or "diffusion" potentials on the one hand, and "membrane potentials" on the other, the former term is restricted to those cases in which the transport properties at any point in the junction are the same as those in a melt of the composition at that point. The latter term implies the existence of a substance in the junction which alters or prevents current transport across the junction by some of the ions present.

(6) I. G. Murgulescu and D. I. Marchidan, *Rev. Chim.*, Acad. de la Repub. Populaire Roumaine III, No. 1 (1958); these authors show that the diffusion-potential is zero in the AgCl–KCl system.

(7) K. H. Stern, *J. Phys. Chem.*, **63**, 741 (1959).

(8) G. Tamman, *Z. anorg. allgem. Chem.*, **133**, 267 (1924).

(9) G. Grube and E. A. Rau, *Z. Elektrochem.*, **40**, 352 (1934).

(10) R. W. Laity, in "Reference Electrodes," by D. J. G. Ives and G. J. Janz, Academic Press, New York, N.Y., 1961, Chapter 12.

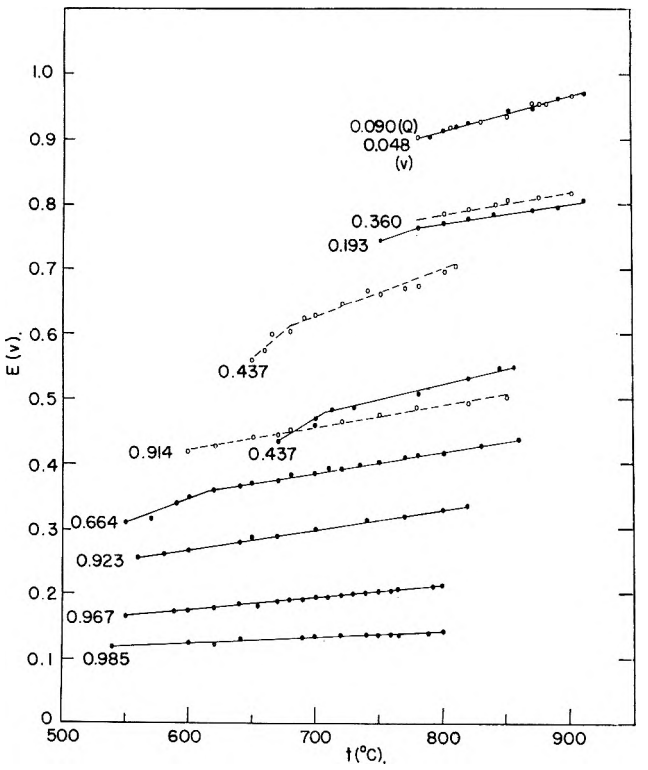

Fig. 1.—E.m.f. for the cell Ag|AgCl(X), NaCl|glass|AgCl|Ag: —●—●— Vycor, —O—O— fused silica. X values are shown to the left of the respective curves.

cell Ag|AgCl|glass|$PbCl_2$|Pb can be broken down into its series components Ag|AgCl|Na-glass|Na and Na|-Na-glass|$PbCl_2$|Pb. Laity argues that the properties of the cell will then depend on the properties of the glass and that the intermediate composition region must be prohibitively difficult to study. To begin an attack on this problem it seemed useful to study a slightly simpler system, *i.e.*, a concentration cell in which one salt is present on both sides of the membrane, while another is present only on one side. Reported here are measurements on the cells Ag|AgCl|glass|-AgCl(X), NaCl|Ag, using Vycor glass[11] and fused silica.

Experimental

In order to avoid changes in the glass which occur in the presence of moisture all experiments were carried out in the helium-filled dry-box described previously.[12,13]

Materials.—Reagent grade NaCl was dried by heating under continuous pumping for several days. Reagent grade AgCl was used without further purification. Reference electrodes were made by melting the appropriate salt composition to a depth of ~5 cm. into previously cleaned (with concd. HNO_3, distilled H_2O) and dried 9 mm. o.d., 20 cm. long Vycor or fused silica tubes, closed at one end; 25 mil Ag wires, cleaned with acetone, NH_4OH, distilled H_2O, and dried, were used for electrodes. The thinness of the wire minimizes heat transport out of the cell, mass transfer of silver, and concentration changes in the more dilute solutions due to silver oxidation.[13]

Furnace and Temperature Regulation.—The furnace and control have been described previously.[13]

Chemical Analysis.—All melts were analyzed gravimetrically as AgCl or by electrodeposition. Large samples (>1g.) were used for the more dilute solutions to minimize errors.

Procedure.—An AgCl–NaCl mixture (20–25 g.) of the desired composition was melted in 25 mm. o.d., 200 mm. long Vycor test tubes or alumina tubes of similar dimensions positioned with the melt close to the center of the furnace. Temperature gradients were additionally minimized by lining the entire furnace with a heavy graphite tube. The top of the furnace hole, except for the holes admitting the test tube and thermocouple, was closed with transite. The hot junction of the controlling chromel-alumel thermocouple was placed next to the melt (outside the container) and also used for temperature measurement. Temperatures reported are estimated to be accurate to within ±3°. Cell e.m.f. were followed continuously on a Sargent recording potentiometer with the temperature slowly increasing and decreasing. Values reported in this paper were reproducibly (±2 mv.) approached both from above and below. For the cell Ag|AgCl|glass|AgCl|Ag the e.m.f. was zero to ±2 mv. from 500 to 900°. Cell resistance varied with temperature but was typically in the range 1000–3000 ohms.

Results

Experimental results for the cells Ag|AgCl|Vycor|-AgCl(X), NaCl(1 − X)|Ag and Ag|AgCl|quartz|-AgCl(X), NaCl|Ag are shown in Fig. 1. Some of the more dilute (in AgCl) melts exhibit a higher temperature coefficient at the low-temperature end of the curve. The change in slope occurs well above the melting point in every case. No explanation is evident. For cells of equal composition the e.m.f. is higher for those with silica membranes.

For measurements on the cell Ag|AgCl(X_1), NaCl-(1 − X_1)|Vycor|AgCl(X_2), NaCl(1 − X_2)|Ag, X_1 was kept constant at the low value 0.038 in order to maximize the measured e.m.f.'s. Analysis of the melt before and after the experiment showed that concentration changes due to silver oxidation were negligible. X_2 was varied from 0.1 to 1.0. Since the dilute solutions freeze near 800°, measurements were made from just below this value to a little above 900°. The e.m.f. varied linearly with temperature for each of the melt compositions studied. Results are given in Table I.

TABLE I

E.M.F. VALUES FOR THE CELL Ag |AgCl(0.038), NaCl(0.962)| -Vycor |AgCl(X), NaCl(1 − X)| Ag

X	$E_{800°}$ (v.)	$E_{900°}$ (v.)	dE/dT(mv./deg.) × 10^2
1.00	0.765	0.830	65
0.985	.673	.733	60
.940	.518	.578	60
.840	.415	.475	60
.705	.340	.375	35
.485	.278	.298	20
.242	.166	.182	16
.132	.125	.137	12

Discussion

The data of Table I are simpler to interpret than those in Fig. 1 (since all ions are present on both sides of the membrane) and will be considered first. If the glass serves only to separate the solutions in the manner of a porous frit in which the hole size is large compared to ionic dimensions, the cell e.m.f. is just the Nernst value (since the diffusion potential is zero). If the glass is permeable to all ions, but the cation transport numbers are different in the membrane than in the bulk, eq. 1 applies. The comparison is shown in Table II.

t_{Na^+} can be obtained from equation 1 by plotting the log term against E_{exp}. The same straight line over the entire range of composition and passing through the origin results at both 800 and 900°, from whose slope $t_{Na^+} = 0.95$, in qualitative agreement with Littlewood's[2] results for Supremax glass.[14] Thus, 95% of the current

(11) Vycor is a 96% silica glass, containing 3% B_2O_3, some Al_2O_3, and a very small concentration of ionic impurities.

(12) J. M. Sherfey, *Ind. Eng. Chem.*, **46**, 435 (1954).

(13) K. H. Stern, *J. Phys. Chem.*, **66**, 1311 (1962).

(14) Evidently the great difference in composition between Supremax (53% SiO_2, 10% B_2O_3, 21% Al_2O_3, 5% CaO, 10% MgO) and Vycor has virtually no effect on transport numbers.

TABLE II

E.M.F. VALUES FOR THE CELLS OF TABLE I

X	$E_{\text{Nernst (800°)}}$	E^a (eq. 1)	E_{exp}
1.000	0.301	...	0.765
.985	.300	.685	.673
.940	.296	.551	.518
.840	.285	.450	.415
.705	.269	.378	.340
.485	.235	.293	.278
.242	.171	.193	.166
.132	.115	.125	.125

[a] Assuming $t_{Na^+} = 1$.

is carried across the glass by sodium ions, independent of melt composition. This is in striking contrast to the strongly concentration-dependent transport numbers in this system across a simple liquid junction. For this case since the liquid-junction potential is zero[6]

$$E_J = -RT/F \int_A^B (t_1 \, d \ln a_1 + t_2 \, d \ln a_2)$$

$$= -RT/F \int_A^B \frac{X_2 t_1 - X_1 t_2}{X_2} \, d \ln a_1 = 0$$

where the subscripts 1 and 2 here refer to Ag^+ and Na^+ ions and the integration is carried out between compositions A and B. Hence $X_1 t_1 - X_2 t_2 = 0$, from which, since $t_1 + t_2 = 1$, $t_1 = X_1$, $t_2 = X_2$. Thus, when the melt composition is very different on both sides of the junction no single transport number adequately describes the behavior of the system. Fairly good agreement is obtained, however, by taking t_{Na^+} as the average between the compositions on both sides of the junctions. This comparison is shown in Table III

TABLE III

LIQUID JUNCTION CALCULATION FOR CELL OF TABLE I (800°)

X	t_{Na^+}[a]	E_{cell} (eq. 1) (v.)	E_{Nernst}[b]
0.985	0.488	0.334	0.300
.940	.511	.281	.296
.840	.561	.252	.285
.705	.628	.237	.269
.485	.741	.217	.235
.242	.860	.166	.171
.132	.915	.115	.115

[a] $t_{Na^+} = [0.962 + (1 - X)]/2$. [b] $E_{\text{Nernst}} = [RT/F \ln (X/0.038)$.

for the cell in Table I. Thus, even when the melt compositions differ by a factor of ten, the arithmetic mean of X_{Na^+} is a good approximation for t_{Na^+}.

Although equation 1 cannot be applied when $X_2 = 1$, since then $1 - X_2 = 0$, it might be assumed that some Na^+ ions diffuse into the AgCl from the glass. Assuming that equation 1 can then be applied to the cell, with $t_{Na^+} = 0.95$, there results $1 - X_2 = X_{Na^+} = 2.0 \times 10^{-4}$ at 800° and 2.2×10^{-4} at 900°. This is then the sodium ion concentration necessary to account for the observed e.m.f. of 0.765 v. The same argument can also be applied to the cells of Fig. 1. Thus, by assuming that $t_{Na^+} = 0.95$ in these systems, one can calculate from the measured e.m.f.'s what value of X_{Na^+} on the AgCl-rich side is required to satisfy equation 1.

The results are shown for 800° in Table IV, but are essentially independent of temperature. For an experimental test of this hypothesis samples of the reagent grade AgCl used as starting material, and of the same AgCl heated to 820° for two hours in a Vycor tube

TABLE IV

X_{Na^+} VALUES FOR CELLS OF TABLE I CALCULATED FROM EQ. 1

(A) Vycor		(B) Quartz	
X_{Ag^+}	$X_{Na^+} \times 10^3$	X_{Ag^+}	$X_{Na^+} \times 10^4$
0.985	2.3	0.914	3.5
.967	3.3	.437	4.3
.923	1.9	.360	2.2
.664	4.3	.0895	2.9
.437	3.3		
.193	0.6		Av. (4.2 ± 1.0) $\times 10^{-4}$
.048	0.6		
	Av. (2.3 ± 1.1) $\times 10^{-3}$		

(while making e.m.f. measurements) were analyzed by flame photometry. For the former $X_{Na^+} = 2.8 \times 10^{-4}$; this increased to 3.2×10^{-4} in the latter. These results suggest that the scatter of values in Table IV results from variations in length of time and temperature to which individual cells were exposed. The lowest calculated value of X_{Na^+} in Table IV matches closely that for the AgCl used. Concentrations are lower by a factor of five for fused silica, presumably because that material contains less sodium ions to be extracted into the melt. Thus equation 1 is evidently applicable even to a concentration cell in which the concentration ratio is 10^4. Moreover, a single value of t_{Na^+} applies over the entire range of composition.

Cells of the type in Fig. 1 or Table I may be used for the measurement of silver ion activity in melts. Reference electrodes based on this principle have been described.[1,2] For an AgCl reference electrode in a dilute AgCl melt eq. 1 can be rearranged to

$$\log X_2 = \frac{E_{\text{cell}}}{2.303(RT/F)t_{Na^+}} - \log(1 - X_1) \quad (2)$$

since $X_1 \simeq 1$ and $(1 - X_2) \simeq 1$. The second term is nearly constant for a particular glass and can be calculated from data like those in Table IV. Alternatively, equation 2 can be rearranged to

$$2.303(RT/F)t_{Na^+} \log X_2 =$$

$$E_{\text{cell}} - 2.303(RT/F)t_{Na^+} \log (1 - X_1) = E_{\text{cell}} - E_M$$

or

$$\log X_2 = \frac{E_{\text{cell}} - E_M}{2.303(RT/F)t_{Na^+}} \quad (3)$$

t_{Na^+} can be determined in a separate experiment and will probably, for most glasses, be nearly unity. The application of eq. 3 to a study of the kinetics of silver oxidation in fused NaCl has been described.[15] E_M can be greatly reduced by using dilute solutions in the reference electrode. For that case, it is most convenient to write equation 1 in the form (for dilute solutions on the unknown side)

$$E_{\text{cell}} = 2.303t_{Na^+}(RT/F) \log X_2 + 2.303t_{Na^+}(RT/F) \log \left(\frac{1 - X_1}{X_1}\right) \quad (4)$$

where the last term is now E_M. For example, at 850° E_M decreases from 540 mv. in pure AgCl to 9 mv. in a 10 mole % AgCl in NaCl solution.

Acknowledgment.—The author wishes to thank Dr. Blanton Duncan for helpful discussions.

(15) K. H. Stern, paper presented at the American Chemical Society National Meeting, Atlantic City, N. J., September, 1962.

THE VAPOR PHASE DIFFUSION FLAME REACTION OF SODIUM WITH FLUORINATED CHLOROMETHANES[1]

BY E. D. KAUFMAN AND J. F. REED

Department of Chemistry, Loyola University, Chicago, Illinois

Received October 24, 1962

The rates of the gas phase reactions of CCl_4, $CFCl_3$, CF_2Cl_2, and CF_3Cl with sodium vapor have been measured by the diffusion flame method. Products were collected and analyzed. The specific rate constants for the primary processes were found to be 14.9×10^{11} cc./mole-sec., 6.2 to 9.1×10^{11} cc./mole-sec., 3.2 to 4.6×10^{11} cc./mole-sec., and 0.78×10^{11} cc./mole-sec., respectively, at 583°K. The energies of activation were calculated using a unit steric factor; the values obtained were 8.4, 8.7 to 9.2, 9.0 to 9.5, and 10.2 kcal./mole, respectively. Based on the known value of $D(CCl_3\text{–}Cl)$, values were deduced for $D(CF_2Cl\text{–}Cl)$ as 72 ± 4 kcal./mole, $D(CF_2\text{–}Cl)$ as 62 ± 14 kcal./mole, and $D(CFCl_2\text{–}Cl)$ as 71 ± 3 kcal./mole. The heats of formation of CF_2Cl and $CFCl_2$ were deduced as -69 ± 4 kcal./mole and -24 ± 6 kcal./mole, respectively. Chemiluminescence is observed in these reactions and based on limited measurements some discussion is presented.

Introduction

The "diffusion flame" method, first reported by v. Hartel and Polanyi,[2] has been applied to the investigation of many fast reactions.[3]

In particular, the method has been used extensively in the study of the reactions of sodium vapor with organic halides. A number of workers have reported on the reactions of sodium with polyhalides.[4-7] Chemiluminescence was reported by Heller and Polanyi[5] in the study of metal polyhalides, Haresnape, Stevels, and Warhurst[6] in the study of polybromides, and Bawn and co-workers[7] in the study of polychlorides. The latter workers furthermore reported that halogen atoms are successively abstracted from the parent halide by reaction with sodium.

The present work has been undertaken in an effort to gain further understanding of the reactions of fluorinated polyhalides with sodium and of the diffusion flame. The kinetics of the gas phase reactions of chlorotrifluoromethane, dichlorodifluoromethane, trichlorofluoromethane, and carbon tetrachloride with sodium vapor have been studied. These compounds were selected because their reactions with sodium would yield fluorinated and chlorinated radicals whose characteristics are not yet fully understood. Some of the compounds studied in this work have been studied earlier in much less detail. The reaction of carbon tetrachloride has been studied repeatedly. In their original work, v. Hartel and Polanyi[2] reported that the reaction proceeds essentially without activation energy. Heller and Polanyi[5] also investigated the behavior of this system, and found a somewhat lower specific rate constant and also expressly stated that this reaction is not accompanied by chemiluminescence. Haresnape, Stevels, and Warhurst[6] reported a specific rate constant virtually identical with that reported by Heller and Polanyi. Bawn and co-workers[7] reported complete abstraction of chlorine from carbon tetrachloride accompanied by intense luminescence. The reaction of chlorotrifluoromethane with sodium has been studied by Hodgins and Haines[8] and by Reed and Rabinovitch.[9] These workers reported the same products for the reaction, but they gave different mechanistic explanations for their occurrence. Neither report chemiluminescence.

The theory and range of applicability of the "diffusion flame" method have been examined by several authors.[8-12] The work of Heller[12] consisted of an extensive experimental study in which the original assumptions of v. Hartel and Polanyi were subjected to careful scrutiny, and the range of their applicability was laid down. One of the original assumptions sets the partial pressure of the halide reaction partner at an average value. Cvetanovic and LeRoy[10] and Smith[11] obtained solutions for the differential equations describing a diffusion model when the halide pressure may not be approximated by a constant value throughout the flame. Reed and Rabinovitch,[9] in a different extension, corrected for the integrated intensity of the sodium fluorescence at the boundary of the flame zone used as a measure of the reaction rate. These authors also took specific cognizance of secondary radical reactions of halogenated radicals in the flame.

Experimental

Materials.—Nitrogen, used as a carrier gas, was purified by passage through two sodium–potassium acetophenone traps, a cold trap, and a silica gel trap.[13] Sodium was purified by distillation *in vacuo*. Cutting of small pieces and filling of the carburetor were carried out under dry nitrogen. Chlorofluoromethane, dichlorofluoromethane, trichlorofluoromethane, obtained from the Matheson Company, Inc. as spectroscopically pure reagents, and carbon tetrachloride, obtained from the Eastman Chemical Company as a spectroscopically pure reagent, all were further purified by three further bulb to bulb distillations discarding the initial and final fractions.

Analytical reagents were obtained commercially and used without further purification. Silver nitrate, sodium fluoride, and sodium chromate were Baker and Adams Reagent Grade chemicals. Titanium trichloride solution was obtained in nominal 20% strength. Hydrogen peroxide, 30%, was obtained as a Certified Reagent Grade chemical from the Fisher Scientific Co. Sodium chloride was obtained with a National Bureau of Standards certification of 98.12% purity.

Apparatus.—The apparatus was modeled after the flow system of Reed and Rabinovitch.[9] The horizontal reactor had two

(1) Abstracted from the Ph.D. Thesis submitted to the faculty of Loyola University by E. D. Kaufman, 1962.

(2) H. v. Hartel and M. Polanyi, *Z. physik. Chem.*, **B11**, 97 (1930).

(3) E. W. R. Steacie, "Atomic and Free Radical Reactions," Reinhold Publ. Corp., New York, N. Y., 1954.

(4) H. v. Hartel, N. Meer, and M. Polanyi, *Z. physik. Chem.*, **B19**, 139 (1932).

(5) W. Heller and M. Polanyi, *Trans. Faraday Soc.*, **32**, 633 (1936).

(6) J. N. Haresnape, J. M. Stevels, and E. Warhurst, *ibid.*, **36**, 465 (1940).

(7) C. E. H. Bawn and E. F. Hunter, *ibid.*, **34**, 608 (1938); C. E. H. Bawn and W. L. Dunning, *ibid.*, **35**, 185 (1939).

(8) J. W. Hodgins and R. L. Haines, *Can. J. Chem.*, **30**, 473 (1952).

(9) J. F. Reed and B. S. Rabinovitch, *J. Phys. Chem.*, **59**, 261 (1955); **61**, 598 (1957).

(10) R. J. Cvetanovic and D. J. LeRoy, *Can. J. Chem.*, **29**, 597 (1951); R. J. Cvetanovic, *ibid.*, **34**, 54 (1956).

(11) F. Smith, *J. Chem. Phys.*, **22**, 1605 (1954).

(12) W. Heller, *Trans. Faraday Soc.*, **33**, 1556 (1937).

(13) L. Fieser, "Experiments in Organic Chemistry," 3rd Ed., D. C. Heath Co., New York, N. Y., 1957, p. 299.

plane windows. One of the windows was placed to permit head-on viewing of the nozzle. To facilitate observation, a prism was mounted in front of this window so that the nozzle could be seen from the side of the reactor. Temperatures were measured with calibrated thermocouples. Runs were made at a carburetor temperature of 228° (501°K.) and a reaction zone temperature of 246° (519°K.) and also at a carburetor temperature of 284° (557°K.) and 290° (563°K.) and a reaction zone temperature of 313° (583°K.). The temperature profile in the furnace was adjusted to maintain the temperature along the carburetor within ±0.5° and within ±1° in the reaction zone.

Procedure.—The system pressure was adjusted to the desired value after the reactor had attained thermal equilibrium. Circulation of the carrier gas was then started and the halide flow was initiated and adjusted to give a flame radius between 1.0 and 1.8 cm. as soon as the reaction chamber was filled with sodium. After a few minutes the flame reached its steady-state size. Runs were made over a range of v/D values of 0.9 to 16 $cm.^{-1}$. The flame size was measured on a reticule mounted in front of the viewing prism. The reticule was marked at one millimeter intervals on cross-hairs.

The limiting visible pressure of sodium was established by slowly heating the reactor and observing the lowest temperature at which sodium could be detected in the nozzle tube. The limiting visible flux of sodium was determined in a closed cell which was substituted for the nozzle tube in the reactor. This cell was equipped with two plane windows one centimeter apart which provided a convenient depth of field for the observations. A small sodium reservoir was attached to the bottom of the cell. The furnace was slowly heated and the temperature at which sodium could first be seen in the cell was recorded. A number of determinations were made over a total system nitrogen pressure range of 0.5 to 10.0 mm. A number of observations were made at each pressure by allowing the furnace to heat and cool alternately. The sodium vapor pressures at the temperatures recorded were obtained from the data of Sittig.[14]

To determine the nature and relative amounts of products, runs of approximately 40 hours duration at 583°K. were made. Gaseous products were condensed and collected in liquid nitrogen cooled traps. Solid products were collected on a Pyrex glass shovel placed under the reaction zone. The solid products collected on the nozzle tube itself were carefully removed and preserved separately.

Product Analysis.—The gaseous products were transferred to Pyrex glass bulbs for storage prior to analysis. The analysis of gaseous products was carried out on a Consolidated Model 21–103c mass spectrograph. The presence of the species listed in Table I was deduced. The ratio of concentrations of C_2F_4 to C_2F_6 for the CF_3Cl reaction was found to be 2.8 from peak heights.

TABLE I

ANALYSIS OF GASEOUS PRODUCTS

Halide	Product species
CF_3Cl	C_2F_4, C_2F_6, trace C_4F_6
CF_2Cl_2	C_2F_4, C_2F_4Cl, trace of C_3 compounds
$CFCl_3$	$C_2F_2Cl_2$, $C_2F_2Cl_4$
CCl_4	None

Solution of the solid products of all reactions left a flaky black deposit. This deposit did not undergo any changes on heatng to 300° in a Fisher–Johns melting point apparatus. From these results it was deduced that the black deposit was carbon. The presence of C_2Cl_6 in the solid products of the CCl_4 reaction was eliminated since the melting point of this substance is 187°.[15] Qualitative tests on the solutions obtained when the solid products were dissolved indicated the presence of both chloride and fluoride ions except in the case of the CCl_4 reaction. The total amount of sample collected on the nozzle was of the order of 0.5 g., while the total amount of sample collected on the plate was usually much less, being of the order of 20–30 mg.

The products collected on the shovel were washed into a suitable container, evaporated to dryness, and diluted to 10 cc. in a volumetric flask. The product collected from the nozzle tube was dried in an oven at 80° for three hours and weighed. Approximately 10 mg. of this product was reserved for carbon analysis, the remainder was reserved for chlorine and fluorine analysis.

Carbon, in the nozzle product, was determined by the Micro-Tech Laboratories of Skokie, Illinois, by measuring the amount of CO_2 evolved in a combustion train at 800°. Comparison of the weight loss on combustion and the amount of CO_2 trapped calculated as carbon showed that the combustible product was carbon.

Chlorine was determined by the Mohr method, calibrated with standard sodium chloride solutions. A one-cc. sample of filtered salt solution was titrated with standard $AgNO_3$ solution using 0.1 cc. of 4×10^{-2} M Na_2CrO_4 as an indicator. A yellow light was used to facilitate end-point detection.

Fluorine was determined by measurement of the bleaching of the $TiO_4^=$ ion in solution by F^-.[16] For the analysis, 5 cc. of the stock reagent, 0.2 cc. of fluoride solution and 0.5 cc. of H_2O_2 were mixed and the optical density of the resulting solution was determined with a Beckman DU spectrophotometer at 440 mμ. The method was calibrated using standard fluoride solutions.

The results of the quantitative analysis of the solid products are presented in Table II in the form of product ratios.

TABLE II

RESULTS OF ANALYSIS OF SOLID PRODUCTS

Halide	Source of sample	F/C	Cl/C	F/Cl
CF_2Cl	Nozzle	1.452	0.415	3.49
	Plate	...	...	0.75
CF_2Cl_2	Nozzle	1.098	0.788	1.390
	Plate	...	...	0.10
$CFCl_3$	Nozzle	0.869	1.315	0.653
	Plate	...	...	0.00
CCl_4	Nozzle	...	2.90	...

Measurement of the Luminescence Wave Length.—Luminescence was observed in all reactions carried out at 583°K. Carbon tetrachloride was the only compound that showed luminescence at 519°K. In general, it appeared that a high concentration of sodium and a relatively low concentration of halide are required to produce luminescence. In any one series of reactions it was observed that the visual light intensity is somewhat greater for reactions in which the halide pressure is lower. No luminescence is observed in the absence of halide flow. The wave length of the luminescence was first measured with interference filters with a 25 Å. band width.

These measurements established that the emission is virtually continuous from 450 to 580 mμ with an apparent visual maximum at 480 mμ. The luminescence was then observed with a Gaertner manual monochromator. Of the compounds studied the luminescence of only CCl_4 could be detected by this instrument, due to its low optical efficiency and the relative weakness of the observed emission, and indicated a strong line at 472 ± 5 mμ and a weaker line at 563 ± 5 mμ. Measurements were then made as follows.

A condensing lens system consisting of a 270-mm. focal length lens and a 35 mm. focal length lens was placed in front of the viewing prisms. The image thus obtained was focused on the 2 mm. slit of a Jarrell-Ash Model 8200 500 cm. grating scanning spectrometer. This instrument was equipped with a 1P21 RCA multiplier phototube powered by a John Fluke Model 405 DC power supply. The output of the phototube was amplified by a Minneapolis–Honeywell Acu-Ata III Model DISA-1003 wide band amplifier and recorded on a Brown recorder. The emission spectrum was scanned at a rate of 500 Å. per minute over the range 650–300 mμ. For calibration the emission of the sodium resonance lamp was used as an internal standard. Spectra of the luminescence were obtained both with and without irradiation of the reaction zone with sodium resonance light. These measurements gave a line at 467 mμ for the CCl_4 reaction and a line at 466 mμ for the $CFCl_3$ reaction.

The luminescence was also observed in a static reactor. Suitable pressures of halide gases were introduced into an evacuated 3-liter bulb in which a small sodium reservoir was heated with a bunsen burner. The resulting intense luminescence permitted clear visual color distinction. In the series CCl_4, $CFCl_3$, CF_2Cl_2, CF_3Cl all emissions appear blue, becoming a deeper blue in the series as written. For comparison the reaction of CH_2Cl_2 was also observed in the static experiments. Here it

(14) M. Sittig, "Sodium, Its Manufacture, Properties and Uses," Reinhold Publ. Corp., New York, N. Y., 1956, p. 476.

(15) R. L. Shriner and R. C. Fuson, "The Systematic Identification of Organic Compounds," John Wiley and Sons, New York, N. Y., 1948, p. 258.

(16) D. Monnier, R. Vaucher, and P. Wenger *Helv. Chim. Acta*, **31**, 929 (1948).

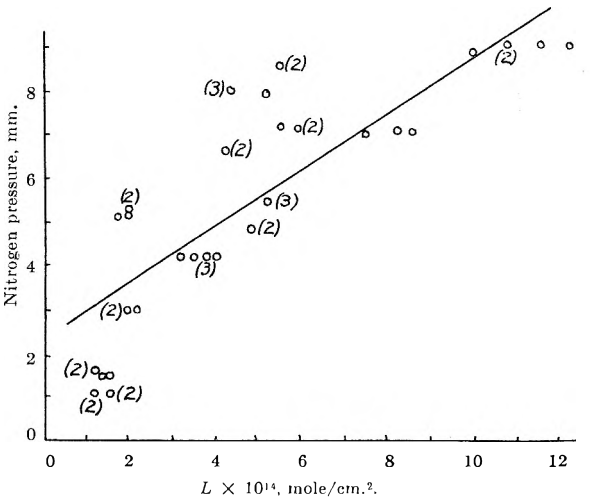

Fig. 1.—Behavior of the limiting visible flux as a function of the total pressure. The numbers in parentheses are the number of repetitions of the data point.

was noted that the appearance of the originally orange-yellow luminescence faded to a gray-blue glow as the reaction proceeded. Interference filters showed continuous emission in the range from 450 to 600 mμ in all cases.

Results

Limiting Visible Flux Determination.—The limiting visible flux was determined as a function of total system pressure and is plotted in Fig. 1. Although the actual data show poor precision, it is clearly shown that the numerical value of the limiting visible flux depends on the total pressure. For the calculation of the rate constants in this study, a value of $L = 6.13 \times 10^{-14}$ mole/cm.^{2} was adopted as representative of the value of the flux in the pressure region of interest. Numerically this value agrees satisfactorily with the values obtained by others.[9,17]

Calculation of the Specific Rate Constants.—The rate constant, $k^{(0)}$, was calculated from the relation

$$k^{(0)} = \left(\frac{\ln p^* r_0/p_1 R}{R - r_0}\right)^2 \frac{D}{p'} \qquad (1)$$

where p^* is the equilibrium vapor pressure of sodium at the temperature of the carburetor, p_1 is the least pressure of sodium the fluorescence of which can be detected visually by irradiation with the sodium-D line, R is the flame radius, r_0 is the nozzle radius, p' is the partial pressure of the halide in the reaction, zone, and D is the diffusion coefficient of sodium into the mixture of halide and nitrogen, taken to be the same as the diffusion coefficient of the sodium into nitrogen alone.

A more accurate value of the specific rate constant may be obtained by considering the limit of visibility of sodium to be the integrated intensity over the line of sight rather than a fixed value of the sodium pressure.[9,18] The value of the rate constant, $k^{(3)}$, thus obtained depends on the experimental measurement of the limiting visible flux by the relation

$$L = \int_S A \frac{\exp(-Cr)}{r} ds$$

where L is the limiting visible flux, A is a constant of integration obtained by setting the total amount of sodium streaming into the reaction zone equal to the total amount of reaction, r is the radial distance from the nozzle, S is the line of sight, and C^2 is given by the expression $k^{(3)}p'/D$.

Effect of Non-uniform Halide Pressure.—It has been pointed out by Heller[12] that the specific rate constant should be calculated using an effective halide pressure somewhat lower than that calculated from the flow of halide into the system and the total pressure. Mathematical treatments of a diffusion model for the calculation of the halide pressure in the flame have been proposed by Cvetanovic and LeRoy[10] and by Smith.[11]

The Cvetanovic and LeRoy treatment results in a differential equation of which numerical evaluations,[10] based on a zero halide pressure at the nozzle, permit the calculation of a correction factor for the rate constant which does not exceed 20% for the cases studied here. The calculations required are somewhat laborious and probably lead to overcorrection since the pressure of halide at the nozzle is surely not depleted to zero.[12]

The Smith treatment leads to solutions for the pressure of sodium and of halide using the halide pressure at the nozzle as a parameter. Unfortunately, it is not possible to obtain a simple correction to the rate constant from this treatment. Solution for the corrected rate constant must be accomplished by successive approximations. The magnitude of the correction here is also of the order of 20% for the cases studied, although it is usually smaller than that obtained from the Cvetanovic and LeRoy treatment. Neither of the above treatments appear to have a significant effect on the precision of the calculated rate constants.

In view of the relatively small magnitude of the correction, and the large amount of labor required, it is desirable to apply a simpler treatment which will give similar results. This might be done as follows. Let n be the total number of halogen atoms abstracted from the halide molecule by sodium. Then the quantity of the parent halide molecule consumed will be given by $1/n$th of the total amount of sodium reaction, *i.e.*, b_0/n. If F_{RX} is the flow of halide into the system, then the average flow of halide in the flame is given by

$$\bar{F}_{RX} = [F_{RX} + (F_{RX} - b_0/n)]/2 = \pi r_0^2 v_0 \bar{p}'/RT$$

substituting $\pi r_0^2 v_0 p'/RT$ for F_{RX} we have

$$\bar{p}' = p_\infty' - p^*/2n$$

where p_∞' is the halide pressure calculated from the flow of halide into the system and the total pressure.

As a test, this treatment was applied to the case of the reactions of CCl_4 at 583°K. where the effect of the halide depletion due to reaction is expected to be most marked. The correction was applied to a rate constant calculated using the total amount of reaction as boundary condition in order to determine the value of the sodium pressure at the nozzle. For comparison the constants obtained from the Cvetanovic and LeRoy and Smith treatments are also presented. The latter constants were calculated using the same lower boundary condition for the sodium pressure.

The results of these calculations for an uncorrected specific rate constant of $49.0 \pm 13.9 \times 10^{+11}$ cc./mole-sec. are as follows. The constant corrected by the Cvetanovic and LeRoy method is $61.8 \pm 17.1 \times 10^{+11}$

(17) E. M. Nemeth, Loyola University, Chicago, Ill., M.S. Thesis, 1960.
(18) E. M. Nemeth and J. F. Reed, to be submitted.

cc./mole-sec.; correction by the Smith method yields 54.4 ± 18.1 × 10^{+11} cc./mole-sec.; and correction by the simple technique gives 57.8 ± 16.8 × 10^{+11} cc./mole-sec. It is clearly shown that the magnitude of the simple correction gives results comparable with those of the more complete treatments, while saving considerable time and labor. For this reason, this treatment was used in the calculation of all rate constants reported in this work.

Specific Rate Constants.—The constants used in the calculation of the specific rate constants were obtained as follows. The diffusion coefficient of sodium into nitrogen was calculated from the values of v. Hartel and Polanyi[2] and Cvetanovic and LeRoy[10] using a 3/2 power dependence for the temperature. The halide diffusion coefficients were calculated from the kinetic theory[19] using collision cross sections calculated from viscosity data. The coefficients of viscosity of CF_3Cl, CF_2Cl_2, $CFCl_3$, and CCl_4 were taken to be 139.6 × 10^{-6},[20] 124.7 × 10^{-6},[21] 108.4 × 10^{-6},[21] and 195 × 10^{-6} [12] poise at 25°, respectively. The coefficient of viscosity of nitrogen was taken to be 176.5 × 10^{-6} [22] at 23°.

Average values for the calculated specific rate constants are presented in Table III for each of the compounds studied. The numbers in parentheses are average deviations from the mean. Detailed data and values for the various experimental parameters for each of the runs may be found elsewhere.[23]

TABLE III

CALCULATED SPECIFIC RATE CONSTANTS

Halide	Temp., °K.	No. of runs	$k^{(0)}$, cc./mole-sec. × 10^{-11}	$k^{(3)}$, cc./mole-sec. × 10^{-11}
CF_3Cl	519	21	5.40(1.75)	1.62(0.28)
	583	17	3.42(1.17)	1.14(0.13)
CF_3Cl_2	519	7	6.45(1.11)	2.77(0.31)
	583	25	25.4 (5.95)	10.6 (1.94)
$CFCl_3$	519	7	50.5 (16.7)	19.8 (5.10)
	583	14	47.6 (13.7)	20.2 (3.78)
CCl_4	519	7	206 (45.0)	57.6 (6.21)
	583	17	143 (51.8)	59.7 (13.0)

Discussion

The Mechanism of the Reactions.—The primary process for the reactions of sodium vapor with organic halides has been reported to be RX + Na → Na^+X^- + R. For the compounds under consideration here, the radical, R, produced is still halogenated and as such is still subject to further attack by sodium. The presence of carbon in the products indicates that abstraction of halogen atoms proceeds until there are none left on the carbon atom. Similar complete abstractions have been reported by Bawn and Dunning,[7] Haresnape, *et al.*,[6] and Reed and Rabinovitch.[9]

The mechanism proposed by the latter authors is as follows, for the case of CF_3Cl

$$CF_3Cl + Na \longrightarrow CF_3 + Na^+Cl^- \qquad (a)$$

$$CF_3 + Na \longrightarrow CF_2 + Na^+F^- \qquad (b)$$

$$CF_2 + Na \longrightarrow CF + Na^+F^- \qquad (c)$$

$$CF + Na \longrightarrow C + Na^+F^- \qquad (d)$$

$$2CF_3 \longrightarrow C_2F_6 \qquad (e)$$

$$2CF_2 \longrightarrow C_2F_4 \qquad (f)$$

The products found in this study in the reaction of CF_3Cl were NaCl, NaF, C, C_2F_4, and C_2F_6, in accord with this mechanism. C_4F_8 is ignored since it is present only in trace amount.

The mechanisms for the reactions of sodium with CF_2Cl_2 and $CFCl_3$ must be substantially the same, since the gaseous products found correspond to recombination products of halogenated methyl and methylene type species, and the solid products were NaCl, NaF, and carbon. In the CCl_4 reaction it appears that the halogen abstraction proceeds so rapidly that no gaseous products are formed, and that the mechanism for this reaction consists essentially of the four halogen abstractions only.

Calculation of the Individual Reaction Rates.—The over-all rate constants calculated thus far are based on the consideration that the total reaction may be represented by a single reaction term in the original differential equation, implying that there is only one reaction per halide molecule. The mechanism presented in the previous section clearly shows that sodium undergoes several reactions to bring about the observed products. In order to extract the specific rate constants for the individual reaction steps, the following procedure was used. For simplicity, again consider the reaction of CF_3Cl.

The total amount per second of the abstraction reactions, x_i, may be represented by integrals of the type $x_i = \int_V k_i p_i p_{Na}\, dV$, where k_i is the rate constant for the ith step, p_i is the pressure of the halide species reacting in the ith step, and dV is the element of volume in which the reaction occurs. The total amounts per second of the recombination reactions may be represented by integrals of the type $x_j = \int_V k_j p_j^2 dV$, where the symbols have the same meaning as above. Since sodium is completely consumed in the over-all reaction by the abstraction processes, one may write for the total flow rate of sodium into the reaction zone, b_0

$$x_a + x_b + x_c + x_d = b_0 \qquad (1)$$

where the subscripts refer to the individual steps in the mechanism. Since all the CF_3 generated in the primary step may be accounted for by the C_2F_6 found and the CF_3 consumed in the second abstraction, then

$$2x_e + x_b = x_a \qquad (2)$$

Similarly, for CF_2

$$2x_f + x_c = x_b \qquad (13)$$

The only significant reaction of CF is the production of C and NaF by reaction with sodium, therefore

$$x_c = x_d \qquad (4)$$

Since the F/Cl deposit ratio on the nozzle is not the same as that found on the collection plate, the ratio

(19) E. H. Kennard, "Kinetic Theory of Gases," McGraw-Hill Book Co., New York, N. Y., 1938. pp. 145, 194.

(20) J. F. Reed and B. S. Rabinovitch, *Chem. Eng. Data Ser.*, **2**, 75 (1957).

(21) A. F. Benning and W. H. Markwood, *Refrig. Eng.*, **37**, 243 (1939).

(22) "International Critical Tables," Vol. II, McGraw-Hill Book Co., New York, N. Y., 1928.

(23) E. D. Kaufman, Loyola University, Chicago, Illinois, Ph.D. Thesis, 1962.

of the concentrations of the different species in the flame must change with distance from the nozzle. Since virtually no carbon was found on the plate, it seems reasonable to say that reaction (d) does not contribute a significant amount of NaF to the plate salt mixture. We now assume that the ratio of the amounts of reactions (a) and (b) is constant throughout the reaction zone. Furthermore, a fraction, ϕ, of the amount of these reactions occurs in the outer flame region and contributes to the plate deposit, while a fraction, $1 - \phi$, occurs near the nozzle and contributes to the nozzle deposit. Similarly, a fraction, θ, of reaction (c) contributes to the nozzle deposit and a fraction, $1 - \theta$, contributes to the plate deposit. The amount of a solid product found in a deposit may then be obtained by summing the total amounts of the reactions giving rise to the species each multiplied by the appropriate fraction. We now define α as the fluoride to chloride ratio in the outer flame region, β as the chloride to carbon ratio on the nozzle, and γ as the fluoride to carbon ratio on the nozzle, and take for these the values found on the collection plate and the nozzle, respectively. Thus we have

$$\alpha = \frac{\phi x_b + (1 - \theta)x_e}{\phi x_a} \tag{5}$$

$$\beta = \frac{(1 - \phi)x_a}{x_d} \tag{6}$$

$$\gamma = \frac{(1 - \phi)x_b + \theta x_e + x_d}{x_d} \tag{7}$$

Calling the ratio of C_2F_4 to C_2F_6 found in the products δ

$$\delta = x_f/x_e \tag{8}$$

it is then possible to solve the set of simultaneous equations 1 through 8 for x_i, ϕ, and θ in terms of b_0. The solutions are presented in Table IV.

TABLE IV

TOTAL AMOUNTS OF INDIVIDUAL REACTIONS

x_a	x_b	x_c	x_d
$0.566b_0$	$0.418b_0$	$0.0066b_0$	$0.0066b_0$
x_e	x_f	ϕ	θ
$0.074b_0$	$0.0206b_0$	0.995	0.146

In order to calculate the specific rate constants of the individual steps, we proceed as follows. It is assumed that the partial pressure of the halide may be taken as an average pressure throughout the flame. Taking the value of the pressure used in the calculation of $k^{(3)}$, one may now calculate the value of the specific rate constant for the primary process from the relation

$$k_a = \frac{x_a}{\bar{p}_{CF_3Cl}\int_V \bar{p}_{Na}\,dV}$$

If one assumes that the partial pressure of the other halide species may also be represented by some average value throughout the flame, the remaining integrals may be solved in the following fashion. Using the value $k_c = 2.34 \times 10^{13}$ cc./mole-sec.[24,25] in the relation

$$x_c = \int_V k_c p_{CF_3}{}^2 dV = k_f \bar{p}_{CF_3}{}^2 V$$

a value of $\bar{p}_{CF_3}$ may be obtained. Substitution of this value into $x_b = k_b \bar{p}_{CF_3}\int_V p_{Na}dV$ will then yield a value of k_b.

In order to evaluate k_c by a similar process a value of k_f is needed. Unfortunately no value for this constant is available at this time. We therefore express our result in terms of the recombination constant, k_f. The result gives $k_c = 1.09 \times 10^5\ k_f{}^{1/2}$ cc./mole-sec. The value found by Reed and Rabinovitch[9] was $5 \times 10^6\ k_f{}^{1/2}$. The value of k_d cannot be established, since there is no reliable means available for evaluating $\bar{p}_{CF}$.[21,22]

A further check on the self-consistency of this treatment may be made. In the solution of the original differential equation the reaction term was taken to be kpp', and was considered to be of the form C^2p, where $C^2 = kp'/D$ = a constant. It is therefore essential that the total observed rate be related to the rates of the individual steps in such a fashion that the term C^2p adequately represents the reaction. The reaction term in the differential equation is properly written

$$k_a p_{CF_3Cl} p_{Na} + k_b p_{CF_3} p_{Na} + k_c p_{CF_2} p_{Na} + k_d p_{CF} p_{Na}$$

The assumption of constant average pressures for the halide species and the factoring of p_{Na}, the variable quantity, gives

$$\left(k_a + k_b \frac{\bar{p}_{CF_3}}{\bar{p}_{CF_3Cl}} + k_c \frac{\bar{p}_{CF_2}}{\bar{p}_{CF_3Cl}} + k_d \frac{\bar{p}_{CF}}{\bar{p}_{CF_3Cl}}\right)\bar{p}_{CF_3Cl} p_{Na}$$

Realizing that

$$x_a = k_a \bar{p}_{CF_3Cl}\int_{r_0}^{\infty} p_{Na}\,dV \text{ and } x_b = k_b \bar{p}_{CF_3}\int_{r_0}^{\infty} p_{Na}\,dV, \text{ etc.}$$

the term $k_b\bar{p}_{CF_3}/\bar{p}_{CF_3Cl}$ may be shown to be $(x_b/x_a)k_a$ and the over-all rate constant

$$k^{(3)} = k_a + \frac{x_b}{x_a}k_a + \frac{x_c}{x_a}k_a + \frac{x_d}{x_a}k_a$$

from which it is seen that $k^{(3)} = k(b_0/x_a) = k_a/0.566$. Substitution of the appropriate data into these relations shows that the value of k_a thus calculated agrees with the observed value within 5%.

The specific rate constants for the elementary reactions in the other cases, CF_2Cl_2, $CFCl_3$, and CCl_4, cannot be obtained in this way since insufficient data are available. However for the reaction of sodium with CCl_4 only carbon and NaCl were found in the products; no gaseous products were obtained. For complete reaction the primary process must necessarily consume $0.25b_0$. From this, a value for the rate constant of the primary process may be calculated. The primary processes of the reactions of CF_2Cl_2 and $CFCl_3$ must consume at least $0.25b_0$. It appears that the reactions of the radicals with sodium become more important in the series CF_3, CF_2Cl, $CFCl_2$, CCl_3 as one proceeds from CF_3 to CCl_3. It is reasonable therefore to expect that the primary processes of the reactions of CF_2Cl_2 and $CFCl_3$ will consume a fraction of the total amount of sodium streaming into the reaction zone which lies between $0.25b_0$, the rate for CCl_4, and

(24) P. B. Ayscough, *J. Chem. Phys.*, **24**, 939 (1956).
(25) G. O. Pritchard and J. R. Dacey, *Can. J. Chem.*, **38**, 182 (1960).

$0.566b_0$, the rate for CF_3Cl. It is then possible to calculate limits for the rate constants for these reactions. The values obtained in this fashion are presented in Table V.

TABLE V

SPECIFIC RATE CONSTANTS[a] FOR Na + RX → NaX + R AT 583°K.

Species	k_i	Other values (ref.)	Schwartz lower limit
CF_3Cl	0.78	1.98 (9)	...
CF_3	926	672 (9)	205
CF_2	$1.1 \times 10^{-6} k_f^{1/2}$	$45 \times 10^{-6} k_f^{1/2}$ (9)	$0.5 \times 10^{-6} k_f^{1/2}$
CF_2Cl_2	3.2–4.6	...	...
$CFCl_3$	6.2–9.1	...	...
CCl_4	14.9	70–300 (4,5)	...

[a] Units are 10^{11} cc./mole-sec.

A check on the reliability of the rate constants thus obtained may be made through the application of the Schwartz inequality. Treatment by the method of Reed and Rabinovitch[9] gives the results listed in Table V.

Calculation of Bond Energies and Heats of Formation.—It has been shown by Ogg and Polanyi[26] that for a series of reactions RX + Na → NaX + R where R is varied, the activation energy changes in the series may be related to the changes in RX bond energy by the relation $(\Delta E) = \alpha'(\Delta D)$ where α' is a simple constant of proportionality. This relation will be expected to hold as long as there are no significant changes in the magnitude of the polarizabilities of the radicals, R, produced in the reactions, as long as the equilibrium internuclear separation C–X is constant, and as long as there is no appreciable change in the resonance stabilization of the transition state.[27]

In order to apply this treatment to the present problem, it is necessary to assess the validity of the relation $(\Delta E) = \alpha'(\Delta D)$ for the series studied. Since specific values for the polarizability of the radicals are not available at this time, it is necessary to proceed with an inductive argument.

It would appear on the basis of a molecular volume treatment that the polarizabilities of the radicals CCl_3, $CFCl_2$, and CF_2Cl will not differ greatly. However, the polarizability of CF_3 may be significantly different. Numerically, it is estimated that doubling the value of α from 2 to 4 $\times 10^{-24}$ cm.^{3} results in an increase of the activation energy of approximately 1.5 kcal./mole. Thus in comparing the reaction of CF_3Cl with that of CCl_4 one would expect a decrease in activation energy as a result of the change in the radical polarizability.

The carbon–chlorine equilibrium separation in the stable R–Cl molecules is constant in the series CCl_3–Cl, $CFCl_2$–Cl, CF_2Cl–Cl[28,29] at 1.77 Å. The equilibrium separation in the CF_3–Cl molecule is somewhat lower[29] at 1.75 Å. On the basis of a simple geometric argument involving the appropriate cut through the energy surface for the reaction, it may be shown that the activation energy will increase by approximately 0.3 kcal./mole when the equilibrium separation increases by 0.02 Å. This change will tend to offset partially the decrease in activation energy resulting from the polarizability effect.

(26) R. A. Ogg and M. Polanyi, *Trans. Faraday Soc.*, **31**, 1375 (1935).
(27) M. G. Evans and E. Warhurst, *ibid.*, **53**, 593 (1939).
(28) R. L. Livingston and D. H. Lyon, *J. Chem. Phys.*, **24**, 1285 (1956); Q. L. Karle, *ibid.*, **17**, 1052 (1949).
(29) L. S. Bartell and L. O. Brockway, *ibid.*, **23**, 1860 (1955).

A decrease in resonance stabilization of the transition state in the series CCl_4, $CFCl_3$, CF_2Cl_2, CF_3Cl would result in a further increase in activation energy. On the basis of the number of resonance structures that may be written,[30] CCl_4 and $CFCl_3$ will not show any variation due to this effect, while CF_2Cl_2 and CF_3Cl would be expected to show somewhat higher activation energies. The magnitude of the change in activation energy will probably not exceed 1.0 kcal./mole.

The forgoing arguments indicate that the application of the relation $\Delta E = \alpha'\Delta D$ to the data for the reaction of CF_3Cl with sodium is not warranted in view of the variations in activation energy resulting from changes in the polarizability and the radical stabilization. The application of the relation to the data in the series CCl_4, $CFCl_3$, CF_2Cl_2, in which the constancy of the C–X bond length and the estimated constancy of the radical polarizabilities are satisfactory, is reasonable.

In view of the fact that the values obtained for the specific rate constants at 519 and 583°K. are substantially the same within experimental error, a plot of ln k *vs.* $1/T$ cannot be expected to give satisfactory results for the activation energy.

The energies of activation corresponding to the specific rate constants found in this study may be obtained from a simple Arrhenius treatment using the usual value 5×10^{14} for the pre-exponential factor. The values of the rate constants reported must however be corrected by a statistical factor reflecting the number of identical reacting atoms in the molecule.

The value of the constant, α', is usually taken to be between 0.20 and 0.25.[31] These values are adopted as limits in the calculations of the bond strengths. The calculated bond strengths are reported in Table VI, where the value $D(CCl_3\text{–}Cl) = 67.9$ kcal./mole has been taken as the reference value.[32]

TABLE VI

BOND DISSOCIATION ENERGIES

Species	E, kcal./mole	D, kcal./mole
CF_3–Cl	10.2	...
CF_2Cl–Cl	9.0–9.5	72 ± 4
$CFCl_2$–Cl	8.7–9.2	71 ± 3
	...	(75.6 ± 2)[33]
CCl_3–Cl	8.4	(67.9 ± 2)[32]
CF_2–F	3.2	...
CF_2–Cl	...	62 ± 14

Taking the values for the heats of formation[34–36] of the halide molecules, the heats of formation of the radicals produced in the primary steps of the CF_2Cl_2 and $CFCl_3$ reactions may be calculated. These values were found to be $\Delta H_f(CF_2Cl) = -69 \pm 4$ kcal./mole and $\Delta H_f(CFCl_2) = -24 \pm 6$ kcal./mole.

Considerations of the Observed Luminescence.—The appearance of the maximum intensity of emission at

(30) E. Warhurst, *Quart. Rev.* (London), **5**, 44 (1951).
(31) N. N. Semenov, "Some Problems of Chemical Kinetics and Reactivity," Pergamon Press, London, 1958, p. 27; J. R. Dacey and R. Young, *J. Chem. Phys.*, **23**, 1302 (1955); R. N. Haszeldine and B. R. Steele, *Chem. and Ind.* (London), 684 (1951).
(32) J. B. Farmer, L. H. S. Henderson, F. H. Lossing, and D. G. H. Marsden, *J. Chem. Phys.*, **24**, 348 (1956).
(33) R. K. Curran, *ibid.*, **34**, 2007 (1961).
(34) F. W. Kirkbride and F. G. Davidson, *Nature*, **174**, 79 (1954).
(35) D. R. Stull, "Janaf Thermochemical Data," Dow Chem. Co., Midland, Mich., 1961.
(36) F. D. Rossini, *et al.*, "Selected Values of Chemical Thermodynamic Constants," Circular 500, National Bureau of Standards, Washington, D. C., 1952.

466 mμ for the CCl_4 reaction indicates a process that is exothermic to the extent of at least 61 kcal./mole. The apparent shift toward the ultraviolet observed in the static experiments indicates that the corresponding processes in the reactions of $CFCl_3$, CF_2Cl_2, and CF_3Cl may be more energetic.

Ogg and Polanyi[26] explained the luminescence observed in the reactions of metal tetrahalides with sodium by a process involving radical disproportionation. Since no evidence for disproportionation was found in these reactions, the mechanism must also be discounted. Evans and Walsh[37] have suggested that the luminescence of the CH_2Cl_2 reaction arises from the collisional deactivation by sodium of excited C_2H_4 formed by recombination of two CH_2 radicals. Such a mechanism would not explain the luminescence observed in the series under consideration here, since the CCl_4 reaction does not lead to gaseous products. Bawn and Dunning[7] have suggested that the observed luminescence in the CH_2Cl_2 reaction arises from the rearrangement of the CH_2 radicals produced after the second halogen abstraction. The radicals are presumably produced in an excited state and are collisionally deactivated by sodium.

Parmetier and Gaydon[38] observed a strong C–H line at 431 mμ in an oxygen flame of CH_3Cl. A further greenish blue coloration of the flame was attributed to CCl fragments. Durie[39] found some weak lines in CCl_4 flames in the region from 450 to 500 mμ. Andrews and Barrow[40] observed a band spectrum with lines to 480 mμ in electric discharge experiments with CF_4, which they attributed to the presence of CF. Unfortunately, these workers did not examine the spectrum in the visible region in any detail.

It was qualitatively observed that the reaction of CCl_4 gave a very intense luminescence zone, the reaction of $CFCl_3$ gave a zone somewhat less intense, that of CF_2Cl_2 gave still less and the reaction of CF_3Cl gave a relatively very weak luminescence intensity. The variation of the reaction rates for these species is in the same order, *i.e.*, CCl_4 gives the fastest over-all reaction rate and CF_3Cl gives the slowest rate. It would be expected that the flame zone in CCl_4 reaction would contain more CX_2 and CX radicals than those of the other reactions, and that the concentration of these radicals in the steady state would perhaps decrease with decreasing over-all reaction rate. The observed luminescence intensity variation is consistent with the conception that the phenomenon is due to one or both of the radicals CX_2 or CX. In view of the emissions attributed to CX species by previous workers, and in view of the fact that the observed radiation appears to be confined to the region in the vicinity of the nozzle where CX radicals are present, it seems reasonable to attribute the observed luminescence to the CX species produced in the third halogen abstraction.

Since carbon is one of the reaction products, it is possible that the observed luminescence arises from carbon–carbon rearrangements such as were reported by Gaydon[41] in the study of CH_4 flames. The observed blue color of the luminescence is at least in qualitative agreement with Gaydon's conclusions.

Furthermore, it is entirely possible that the observed effect is due to several processes occurring simultaneously. Unfortunately the data are not sufficiently accurate to draw a definitive conclusion.

Acknowledgments.—The authors gratefully acknowledge the coöperation of S. Meyerson of the American Oil Company, who provided the mass spectra, and G. Swenson of Loyola University, whose assistance was invaluable in making the measurements of the luminescence. E. D. K. also wishes to thank the National Science Foundation for a fellowship during the summer of 1961.

(37) M. G. Evans, *Trans. Faraday Soc.*, **35**, 193 (1939); A. D. Walsh, *Discussions Faraday Soc.*, **2**, 144 (1947).
(38) G. Parmetier and A. G. Gaydon, *Compt. rend.*, **225**, 1139 (1947).
(39) R. A. Durie, *Proc. Phys. Soc.* (London), **A211**, 110 (1952).
(40) E. B. Andrews and R. F. Barrow, *Nature*, **165**, 890 (1950).
(41) A. G. Gaydon, *Quart. Rev.* (London), **4**, 1 (1950).

A THERMOCHEMICAL STUDY OF SOLUTIONS OF CALCIUM AND CADMIUM NITRATES IN LIQUID LITHIUM, SILVER, AND THALLIUM NITRATES

BY O. J. KLEPPA AND S. V. MESCHEL

Department of Chemistry and Institute for the Study of Metals, University of Chicago, Chicago 37, Illinois

Received October 26, 1962

Some new calorimetric data are reported for the solutions of calcium and cadmium nitrates in liquid lithium, silver and thallium nitrates. The limiting enthalpies of solution of the undercooled, liquid divalent nitrates in the silver and thallium salts are about 2 kcal. more positive than one would have predicted from available information on solutions of calcium nitrate in the alkali nitrates. This is attributed to the significant van der Waals contributions to cohesion in the silver and thallium salts. By extrapolation of the new enthalpy data for the liquid solutions, the heat of fusion of cadmium nitrate was found to be 4.35 kcal./mole at 300°. The entropy of fusion of this salt is comparable in magnitude to that of calcium nitrate, but much smaller than that of the corresponding strontium and barium salts. An interpretation in terms of the rotational freedom of the NO_3^- ions in the melt is suggested.

Introduction

Recently one of the authors reported some new thermochemical data for the liquid solutions of the alkaline earth nitrates in the alkali nitrates.[1] In the present work our study of charge-unsymmetrical fused salt mixtures is extended to the solutions of calcium nitrate in silver and thallium nitrates, and to cadmium nitrate in lithium, silver, and thallium nitrates. We have already stressed that the thermal instability of the divalent nitrates imposes very definite restrictions on the temperature of measurement, and consequently also

(1) O. J. Kleppa, *J. Phys. Chem.*, **66**, 1668 (1962).

on the range of liquid concentrations which can be studied effectively. For this reason we have not studied calcium nitrate solutions above 350° nor cadmium nitrate systems above 300°. At these temperatures the considered liquid mixtures contain a maximum of from 30 to 50 mole % of the divalent nitrates. Since lithium nitrate is the only alkali nitrate which is liquid at 300°, it is particularly regrettable that our study of the cadmium nitrate solutions could not be carried out at higher temperatures.

Experimental and Chemicals

The calorimetric equipment and the experimental procedures used have been described elsewhere.[2] The only significant modification in procedure consisted in our adoption of the electrical calibration method instead of the "gold drop" technique. In separate experiments we found agreement between these two methods to about ±1%.

The lithium, calcium, and cadmium nitrates were all Mallinckrodt Analytical Reagents. The silver nitrate similarly was of reagent grade, purchased from Goldsmith Bros. These salts were used without further purification after appropriate drying. The thallium nitrate was purchased from Millmaster Chemical Corporation as "99.9% pure" and was recrystallized twice from distilled water before use.

Results

All heat data obtained in the course of the present study are given in graphical form in Fig. 1 and 2. The type of plot used in these figures has been discussed previously.[3] In Fig. 1, which gives the results for the calcium nitrate systems, we have included also corresponding data for the solutions of this salt in lithium, sodium, and potassium nitrates taken from earlier work.[3] Note that ΔH^M is the molar change in enthalpy associated with formation of a liquid solution of mole fraction X (of divalent nitrate) from liquid monovalent plus solid divalent nitrate. The (extrapolated) value of $\Delta H^M/X$ at $X = 1$ represents the heat of fusion of the solid nitrate at the considered temperature. For calcium nitrate we previously obtained a heat of fusion of 5.7 kcal./mole at 350°.[3] The new results for solutions containing this salt are consistent with this value. For cadmium nitrate we find in this way a heat of fusion of 4.35 kcal./mole at 300°. In arriving at this value we have attached most weight to the data for silver nitrate–cadmium nitrate, for which system the dilution data indicate that the energetic asymmetry is small. The thermal decomposition of cadmium nitrate becomes quite rapid above 300°, so that the heat of fusion at the normal melting point of 350° cannot be measured. However, if we neglect the probably small change in enthalpy between 300 and 350°, we estimate the molar entropy of fusion to be 7.0 cal./degree. The corresponding value for calcium nitrate is 6.8 cal./degree. It should be noted that for strontium and barium nitrates the entropies of fusion are about 11.5 cal./degree. One of the authors has suggested elsewhere[4] that the very low entropy of fusion for calcium nitrate, compared to strontium and barium nitrates, may be due to lack of rotational freedom for the nitrate ions in liquid calcium nitrate. Our new value for the entropy of fusion of cadmium nitrate suggests that this probably holds also for this salt in the liquid state.

The limiting value of $\Delta H^M/X$ at $X = 0$ represents the partial molal heat of solution of the *solid* divalent nitrate in the pure liquid monovalent nitrate. When we subtract from this the heat of fusion at the same temperature, we obtain the partial molal heat of solution referred to the undercooled *liquid* divalent nitrate. A summary of the limiting heats of solution obtained in the course of the present work is given in Table I.

(2) O. J. Kleppa, *J. Phys. Chem.*, **64**, 1937 (1960).
(3) O. J. Kleppa and L. S. Hersh, *Trans. Faraday Soc.*, **32**, 99 (1961).
(4) O. J. Kleppa, *J. Phys. Chem. Solids*, **23**, 819 (1962).

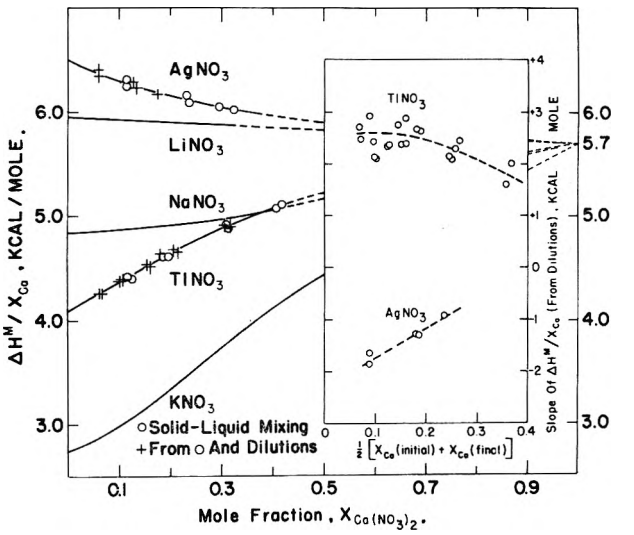

Fig. 1.—Heat data, at 350°, for solutions of calcium nitrate in liquid silver and thallium nitrates. For comparison corresponding curves are given for calcium nitrate in lithium, sodium, and potassium nitrates taken from Kleppa and Hersh.[3]

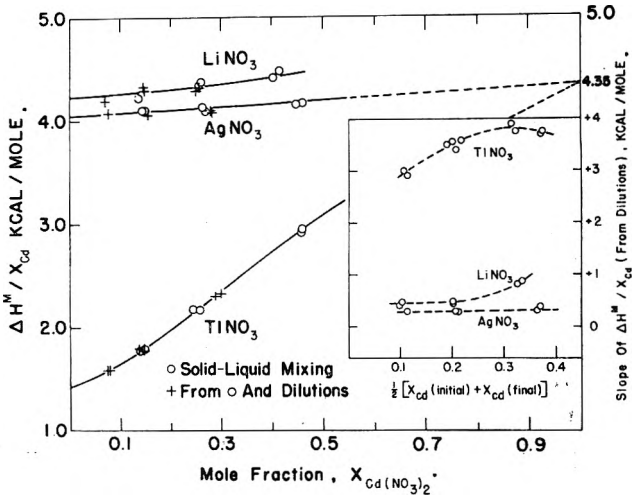

Fig. 2.—Heat data, at 300°, for solutions of cadmium nitrate in liquid lithium, silver, and thallium nitrates.

TABLE I

LIMITING HEATS OF SOLUTION OF CALCIUM AND CADMIUM NITRATES IN SOME MONOVALENT NITRATES

Solute	Temp., °C.	Solvent	$\Delta\bar{H}_{solute\ (s)}$, kcal./mole	$\Delta\bar{H}_{solute\ (l)}$, kcal./mole
$Ca(NO_3)_2$	350°	$AgNO_3$	+6.49	+0.8
		$TlNO_3$	+4.08	−1.6
$Cd(NO_3)_2$	300°	$LiNO_3$	+4.23	−0.1
		$AgNO_3$	+4.05	−0.3
		$TlNO_3$	−1.42	−2.9

It finally is pointed out that Fig. 1 and 2, in addition to the results derived from solid + liquid mixing experiments, also contain enthalpy of dilution data. These were obtained from calorimetric experiments in which more concentrated salt melts were mixed with the pure solvents. Dilution data are particularly useful in the derivation of partial molal heat quantities for the considered solutions.[3]

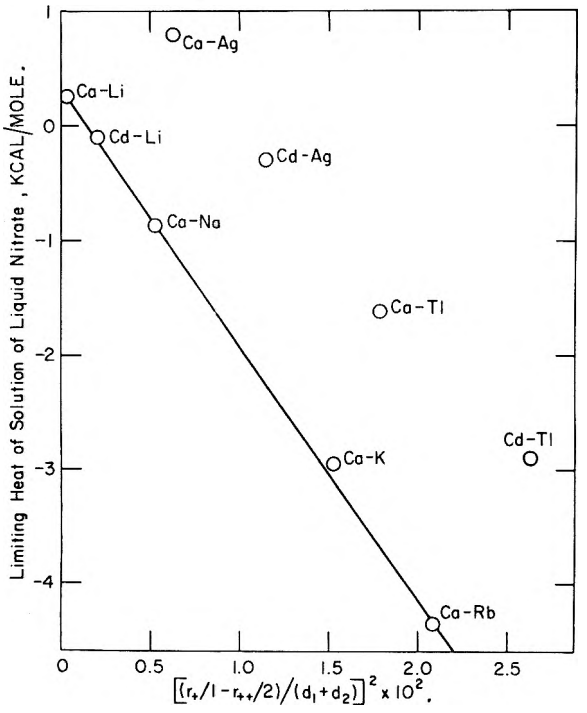

Fig. 3.—The dependence of the limiting heat of solution of undercooled, liquid cadmium and calcium nitrates on the parameter $(r_+/1 - r_{+2}/2)/(d_1 + d_2)$.

Discussion

We noted in our earlier work that the limiting heats of solution of the alkaline earth nitrates in the alkali nitrates could be represented by semi-empirical relations of the form

$$\Delta\bar{H}_{M(NO_3)_2} = A - 225\delta'^2 \text{ kcal./mole} \qquad (1)$$

Here A is a constant which for each salt depends on the chosen reference state, and which was found to vary somewhat from one solute to another. The parameter

$$\delta' = [(r_+/1 - r_{++}/2)/(d_1 + d_2)]$$

where r_+ and r_{++} are the ionic radii of the two cations; $d_1 = r_+ + r_{NO_3^-}$ and $d_2 = r_{+2} + r_{NO_3^-}$.

For liquid, undercooled calcium nitrate in the alkali nitrates at 350° the constant A was found to be +0.3 kcal. The corresponding values for liquid strontium and barium nitrates at 450° were slightly larger, +0.6 and +0.8 kcal., respectively.

Except in cases where δ' is quite small the limiting heat of solution of liquid nitrate given by (1) is dominated by the second term on the right-hand side, and is negative. In a qualitative sense we explained these results in the following way.

In any fused salt mixture where the two solution partners have different charge structures, the mixing process must be associated with a certain structural reorganization, in which coulombic energy presumably is released. This reorganization is believed to be centered on the cation which has the larger ionic potential (Z/r), while it is resisted by the cation with the weaker potential. Hence, the dependence of $\Delta\bar{H}$ on the parameter δ', which is simply related to the difference in ionic potential between the two cations.

It is of interest to explore to what extent our new heat data can be represented by equation 1. At this point we unfortunately encounter a rather fundamental difficulty. This arises from the fact that the ionic radii of non-octet ions such as Ag^+, Tl^+, and Cd^{+2} appear to vary significantly from one medium to another. For example, for Ag^+ Pauling[5] lists a radius of 1.26 Å. However, Blander[6] has noted that the molar volume of silver nitrate actually is only slightly larger than that of sodium nitrate. This suggests that the effective ionic radius of Ag^+ in a nitrate medium should not be much larger than that of Na^+, for which Pauling lists 0.95 Å. In the present work we have adopted the value 1.0 Å. A similar uncertainty exists in the case of Cd^{+2}. Here Pauling gives 0.97 Å., which is comparable to that of Ca^{+2} (0.99 Å.). However, density data for $Cd(NO_3)_2$[7] and $Ca(NO_3)_2$[8] indicated that Cd^{+2} in this salt is much smaller than Ca^{+2}. Based on the density data and on the contraction usually associated with going from a monovalent ion to a divalent ion with the same core (*i.e.*, in this case from Ag^+ to Cd^{+2}), we have tentatively adopted 0.7 Å. as the ionic radius of Cd^{+2} in cadmium nitrate. We have found Pauling's empirical radius for Tl^+, 1.40 Å., to be reasonably consistent with the molar volume of $TlNO_3$.[8]

In Fig. 3 we have plotted the limiting heats of solution observed in the present work against δ'^2 as calculated from the quoted radii. We have included in this figure the corresponding data for calcium nitrate in the alkali nitrates taken from Kleppa and Hersh.[3] For the calcium ion and for the alkali metal ions we have used Pauling's radii; for NO_3^- we have adopted the value 2.19 Å.

The graph given in Fig. 3 is of considerable interest. Note first that the point for cadmium nitrate in lithium nitrate (Cd–Li) falls on the straight line for calcium nitrate in the alkali nitrates. It is very unfortunate that the thermal instability of cadmium nitrate has prevented us from getting data for the liquid solutions of this salt in the other alkali nitrates. However, our single result for cadmium–lithium nitrate, and a very rough value for cadmium–sodium nitrate (about -1.5 ± 0.5 kcal.; not included in Fig. 2 and 3) suggest that cadmium nitrate as a *solute* in the alkali nitrates does not differ significantly from the nitrates of the simple octet ions calcium, strontium, and barium. On the other hand, the dilution data indicate that this analogy is lost if these salts were to act as *solvents* for the alkali nitrates. Thus we find in Fig. 2 that $\Delta H^M/X$ *vs.* X for cadmium–lithium nitrate increases significantly with increasing cadmium content. This points toward an energetic *asymmetry* not detected in the corresponding calcium–lithium and calcium–sodium nitrate systems.

In our previous investigations of the charge-symmetrical silver–alkali nitrate and thallium–alkali nitrate systems, the energetic asymmetries were found to be relatively small, and on the whole comparable in magnitude to those observed in the binary alkali nitrates.[9,10] However, our new results for the solutions of calcium and cadmium nitrates in the silver and

(5) L. Pauling, "Nature of Chemical Bond," 3rd Ed., Cornell University Press, Ithaca, N. Y., 1960.
(6) M. Blander, *J. Chem. Phys.*, **36**, 1092 (1962).
(7) N. P. Popovskaya and P. I. Protsenko, *Zh. Fiz. Khim.* **29**, 225 (1955).
(8) "Handbook of Chemistry and Physics," 38th Ed., Chemical Rubber Publishing Co., Cleveland, Ohio, 1956.
(9) O. J. Kleppa and L. S. Hersh, *J. Chem. Phys.*, **34**, 315 (1961); **36**, 544 (1962).
(10) O. J. Kleppa, R. B. Clarke, and L. S. Hersh, *ibid.*, **35**, 175 (1961).

thallium salts demonstrate in a striking manner the special position of salts of non-octet ions when they act as *solvents* in charge-unsymmetrical fused salt mixtures. Thus, we note from Fig. 3 that all the limiting heats in these solutions are much more positive than in the corresponding alkali nitrate systems. For all four systems the positive deviation is of the order of 2 kcal. In view of the uncertainty in the accepted ionic radii it may be fortuitous that the four values lie on or near a straight line which is roughly parallel to that for the alkali nitrate solutions.

In our earlier discussion of the alkaline earth–alkali nitrate systems we noted that the small variations in the term A in eq. 1 might be related to the polarizability of the divalent solute cations. However, the results obtained in the course of the present research seem to indicate that the principal contributions to the positive terms A, or more generally to the observed positive "shifts" in the limiting heats of solution, must be sought less in the properties of the *solutes* than in the properties of the *solvent* salts. The more positive enthalpies of solution in liquid silver and thallium nitrates compared to those observed in the corresponding alkali nitrates undoubtedly result from a combination of several factors. Prominent among these presumably is the very significant van der Waals contribution to the cohesive energy in the solvent salts. It is worth noting that these positive contributions to the enthalpy of solution are significantly larger in the presently explored charge-unsymmetrical mixtures than in the simpler silver–alkali nitrate and thallium–alkali nitrate systems. For these solutions Blander[6] was able to show that the magnitude of the observed positive shifts (compared to the binary alkali nitrates) is consistent with the change in the van der Waals interaction between second nearest neighbors. It is possible that the larger positive shifts observed for solutions of divalent nitrates in the silver and thallium salts may be related to the local structural adjustment. This adjustment may, for example, involve both the population of ions in the various coördination shells and changes in interionic distances. In either case the van der Waals energy might be significantly changed.

Acknowledgments—This work has been supported by The National Science Foundation (Grant G 19513) and by the Office of Naval Research under Contract Number Nonr-2121 (11) with The University of Chicago.

HYDROLYSIS OF BIS-(ACETYLACETONATO)-BERYLLIUM(II)

BY R. W. GREEN AND P. W. ALEXANDER

School of Chemistry, Sydney University, Sydney, Australia

Received October 29, 1962

Distribution of ^7Be between water and cyclohexane in the presence of excess acetylacetone at 25° has been used to study the formation and hydrolysis of complexes between pH 4 and pH 11. At zero ionic strength, stability constants are $\log \beta_1$ 7.96 and $\log \beta_2$ 14.67. The mono-complex, $BeL(H_2O)_2$, undergoes two stages of acid dissociation with $pk_1 = 6.4$ and $pk_2 = 9.8$.

Bis-(acetylacetonato)-beryllium(II), first prepared by Combes,[1] has attracted attention through its high stability and ready solubility in non-polar solvents. Step formation constants in water and in dioxane–water mixtures have been measured,[2,3] and complete extraction of the bis complex into an organic from an aqueous phase at pH 5–10 has been reported.[4] However, the last authors observed that the efficiency of extraction into chloroform fell sharply at pH values greater than 10.

The present paper describes the use of distribution measurements to investigate the nature and stability of the products formed at high pH.

Experimental

Cyclohexane, special grade for spectroscopy, supplied by British Drug Houses, was used without further purification. Acetylacetone was purified by fractional distillation (b.p. 139°). Acidic aqueous solutions of acetylacetone were found to absorb only weakly in the near-ultraviolet, but in alkaline solution a very strong absorption peak developed at 294 mμ. From measurements on a number of alkaline solutions, the molar extinction coefficient at 25° was determined as 2.40×10^4, with a standard error of 0.01×10^4. This value was then used for measurement of the acetylacetone concentration of experimental solutions. Aqueous solutions were suitably diluted and made alkaline and their optical densities at 294 mμ were determined. Solutions in cyclohexane were completely extracted into aqueous alkali and treated similarly. In neither instance did the presence of small amounts of beryllium mar the precision of the determination.

Beryllium perchlorate solution was prepared from Analar beryllium sulfate and barium perchlorate. After filtration, the solution was evaporated to crystallization on a steam-bath. Crystals of beryllium perchlorate were filtered and redissolved in water as an approximately 0.2 M solution. This was standardized by the chromazurol S method[5] and then appropriately diluted for distribution experiments. Beryllium solutions were labeled with ^7Be, supplied in carrier-free solution by the United Kingdom Atomic Energy Authority. The beryllium content of experimental solutions was related to known standards by counting the γ-ray emission of ^7Be with a thallium-activated sodium iodide well crystal coupled to a scintillation counter, Ekco Type N664A.

pH measurements were made at 25° with a Radiometer 4 pH meter with saturated calomel and glass electrodes, standardized against 0.05 M potassium tetroxalate (pH 1.681), 0.05 M potassium hydrogen phthalate (pH 4.005), or 0.01 M sodium borate (pH 9.177).[6] For spectrophotometric measurements, a Hilger Uvispek instrument was used with 1-cm. quartz cells thermostated at 25°. Distribution of solutes between water and cyclohexane was effected by gentle agitation in rotating glass cells immersed in a thermostat at 25°.

Results

As a preliminary to examining the equilibria involving

(1) A. Combes, *Compt. rend.*, **119**, 1222 (1894).

(2) R. M. Izatt, W. C. Fernelius, and B. P. Block, *J. Phys. Chem.*, **59**, 80 (1955).

(3) R. M. Izatt, W. C. Fernelius, C. G. Haas, and B. P. Block, *ibid.*, **59**, 170 (1955).

(4) J. A. Adam, E. Booth, J. D. H. Strickland, *Anal. Chim. Acta*, **6**, 462 (1952).

(5) L. O. Matveev and I. S. Mustafin, *Trudy Komiss. Anal. Khim. Akad. Nauk SSSR*, **11**, 217 (1960).

(6) V. E. Bower and R. G. Bates, *J. Res. Natl. Bur. Std.*, **59**, 261 (1957).

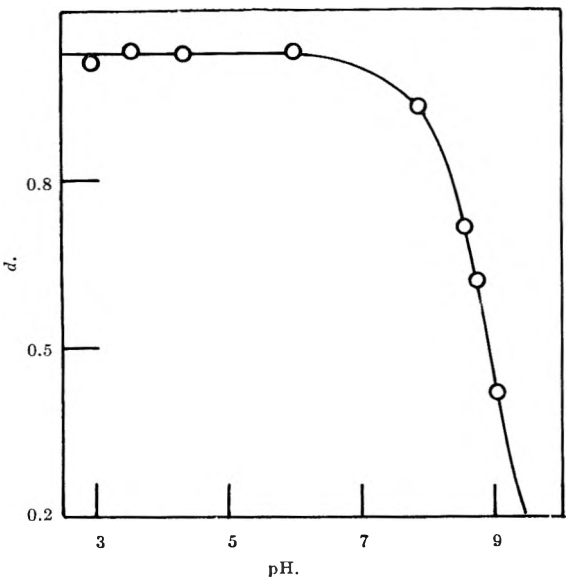

Fig. 1.—Distribution of acetylacetone between water and cyclohexane. The curve is calculated from pk = 9.03 and d = 1.02.

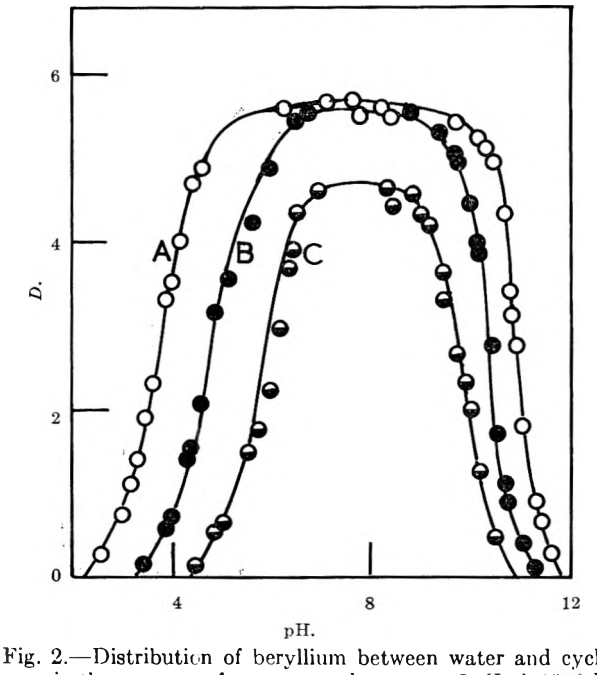

Fig. 2.—Distribution of beryllium between water and cyclohexane in the presence of excess acetylacetone: ○, [L_T], 10^{-1} M; [Be_T] range, 6×10^{-5} to 3×10^{-2} M. ●, [L_T], 10^{-2} M; [Be_T], 6×10^{-4} to 6×10^{-3} M. ◒, [L_T], 10^{-3} M; [Be_T], 6×10^{-5} M.

beryllium, the pk of acetylacetone at 25° was determined. The conventional pH titration method with a 10^{-3} M solution, after the application of an approximate activity correction of log γ = −0.01,[7] gave pk = 9.05 with a standard error of 0.006. This was confirmed by a series of spectrophotometric determinations at 3.5×10^{-5} M, yielding pk 9.03 with a standard error of 0.008. In 1 M $NaClO_4$ solution the spectrophotometric method gave pk = 8.71.

The distribution of acetylacetone between water and cyclohexane reached equilibrium in less than 5 hr., but equilibration was usually allowed to continue overnight. From acid solutions, the distribution coefficient, d = (concentration in cyclohexane)/(concentration in water), was found to be very nearly unity, but fell sharply near pH 8. Figure 1 shows experimental points, together with a distribution curve calculated from pk = 9.03 on the assumption that only the acid form (HL) is soluble in cyclohexane, with a distribution coefficient of 1.02. From 1 M $NaClO_4$ the distribution coefficient was 0.79.

Distribution of beryllium between water and cyclohexane was established in less than 24 hr. at all pH values. Some of the experimental points are shown in Fig. 2, where the distribution coefficient, D = (total Be concn. in organic phase)/(total Be concn. in aqueous phase), is plotted against pH. In these experiments total ligand concentrations in each phase were also measured. Figure 3 shows distribution of beryllium from 1 M $NaClO_4$ into cyclohexane in the presence of excess acetylacetone.

Discussion

The curves of Fig. 2 show that, in the presence of a sufficiently large excess of acetylacetone, D is almost constant in the pH range 5–10 and is independent of the total Be concentration. It is evident that polynuclear complexes are of no importance here. Since the system is clearly not saturated with beryllium, the constant distribution coefficient indicates a constant maximum value for the concentration of distributable species, which, considering the non-polar character of cyclohexane, can only be the bis complex, BeL_2. In this pH and concentration region, then, the beryllium must be virtually all converted to this complex and D must now be identical with $D_2 = [BeL_2]_{organic}/[BeL_2]_{aqueous}$. Its value is 5.6, or 7.9 from 1 M $NaClO_4$ solutions.

From solutions more acid than those represented by the plateau region of the curve, distribution is a function of acetylacetonate ion concentration [L^-], and hence of pH. In the absence of polynuclear complexes it is easily shown that

$$(D - D_2)\beta_2\gamma^2 [L^-]^2 + D\beta_1\gamma [L^-] + D = 0 \quad (1)$$

where β_1, β_2 are the thermodynamic step stability constants and γ is an approximation to the activity coefficient of a singly charged ion calculated from Güntelberg's formula.[7] Equation 1 is most easily applied to experimental points, like those of set A (Fig. 2), where the total ligand concentration, [L_T], is at least ten times as great as the total Be concentration, [Be_T], and the plateau region of the curve is fairly extensive. As a first approximation, the concentration of free ligand, [L_F], can then be equated to [L_T], and [L^-] can be found from pH and pk, with appropriate correction for activity. Any of the usual curve-fitting techniques applied to eq. 1 then yields β_1 and β_2. From these and the above estimate of [L^-], estimates of [BeL] and [BeL_2] can be formed and subtracted from [L_T] to give a second approximation to [L_F]. This in turn leads to refined values of β_1 and β_2. It was found in practice that one such repetition was sufficient for convergence to constant values of β_1 and β_2. Table I reports two sets of results: those for solutions of ionic strength < 0.02, corrected for activity; and those for 1 M $NaClO_4$, which are stoichiometric constants. Agreement with the results of pH titration methods used by previous authors[2,3] is satisfactory.

Above pH 10 nearly all the free ligand is in the anionic form, insoluble in cyclohexane. Analysis of the cyclohexane phase in equilibrium with these alkaline

(7) E. Güntelberg, *Z. physik. Chem.*, **123**, 199 (1926).

TABLE I
EQUILIBRIUM CONSTANTS

Equilibrium	Constant	Thermodynamic	Stoichiometric (1 M $NaClO_4$)
Dissociation of HL	pk	9.03	8.71
Formation of $BeL(H_2O)_2$	$\log \beta_1$	7.96	7.55
Formation of BeL_2	$\log \beta_2$	14.67	14.35
Acid dissociation	pk_1	6.4	
of $BeL(H_2O)_2$	pk_2	9.8	

solutions showed it to contain beryllium and acetylacetone in the exact proportion of 1:2, indicating that the only distributable species is still BeL_2. The fall in D in this high pH region thus points to a fall in $[BeL_2]$ in the aqueous phase, suggesting the formation of hydroxy-complexes insoluble in the organic phase. Within the limits of the distribution technique, D is independent of $[Be_T]$, so that polynuclear complexes can be neglected, and the most probable hydroxy-complexes can be formulated $BeL(OH)H_2O$ and $BeL(OH)_2$. These two complexes appear as hydrolysis products of BeL_2, but formally it is more convenient to treat them as products of the first and second acid dissociations of the mono complex, $BeL(H_2O)_2$, with equilibrium constants

$$k_1 = \frac{[BeL(OH)H_2O][H^+]}{[BeL(H_2O)_2^+]}$$

$$k_2 = \frac{[BeL(OH)_2^-][H^+]}{[BeL(OH)H_2O]}$$

If, as seems justified below pH 11 in the presence of excess ligand, we now neglect water-soluble species containing no acetylacetone, it is possible to write for the aqueous phase

$$[Be_T] = [BeL(H_2O)_2^+] + [BeL(OH)H_2O] + [BeL(OH)_2^-] + [BeL_2]$$

and an expression for the distribution coefficient

$$D = \frac{D_2\beta_2[L^-]}{\beta_1\{1 + k_1/[H^+] + k_1k_2[H^+]^2\} + \beta_2[L^-]}$$

or

$$\left\{\frac{(D_2 - D)\beta_2[L^-]}{D\beta_1} - 1\right\}[H^+] = k_1 + \frac{k_1k_2}{[H^+]} \quad (2)$$

In the presence of excess ligand, the left-hand side of eq. 2 can be estimated and plotted against $1/[H^+]$ to give values for k_1 and k_2, which can then be refined by successive approximations. The numerical values of pk_1 and pk_2 shown in Table I were derived in this way.

It should now be possible to use the two formation constants, β_1 and β_2, and the two acid dissociation constants, k_1 and k_2, together with d and D_2, to calculate

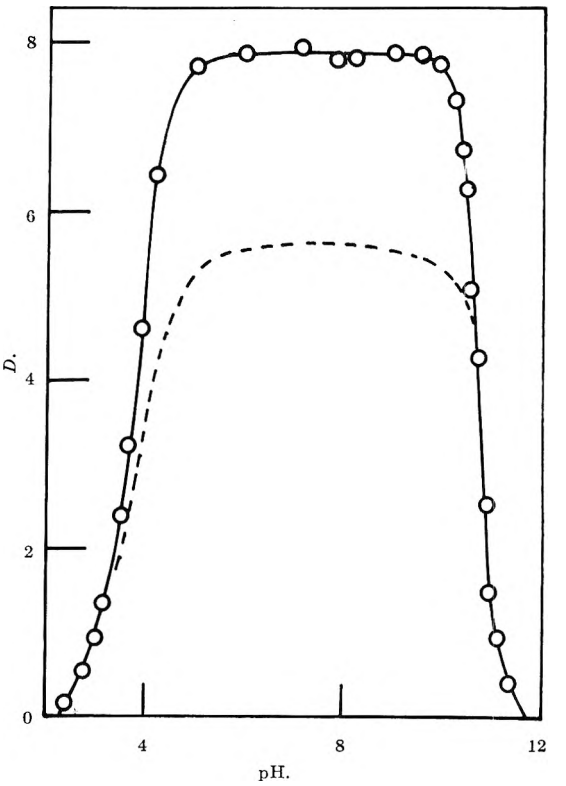

Fig. 3.—Distribution of beryllium between 1 M $NaClO_4$ and cyclohexane in the presence of excess acetylacetone: $[L_T]$, 10^{-1} M; $[Be_T]$, 6×10^{-3} M. Broken curve reproduces results for water from curve A, Fig. 2.

D for any set of conditions. Successive approximations are again necessary but, with the fairly large excess of ligand used here, present no serious computational problem, and two cycles are sufficient. The results of these calculations are represented by the continuous curves of Fig. 2. The equilibrium constants were derived from the experimental points of set A, but calculation shows good agreement with observation within a hundredfold range of both $[Be_T]$ and $[L_T]$. Only for the most dilute solutions at low pH is there any noticeable discrepancy. This divergence does not arise from hydrolysis of Be^{2+}, as can be shown by a more extensive calculation in which the hydrolysis constants of Kakihana and Sillén[8] are incorporated in the above treatment. It is possible that, under these extreme experimental conditions, our assumption of the constancy of D_2 is not wholly justified. Otherwise the wide range of experimental results are satisfactorily accounted for by the interpretation adopted above.

Acknowledgments.—The authors gratefully acknowledge a research grant from the Australian Atomic Energy Commission, and also the assistance of the Analytical Chemistry Section of the A.A.E.C., who standardized the beryllium solutions.

(8) H. Kakihana and L. G. Sillén, *Acta Chem. Scand.*, **10**, 985 (1956).

EFFECTS OF THE NATURE OF THE SUBSTRATE UPON THE PICKUP OF ALKALINE EARTH STEARATE LAYERS[1]

BY FREDERICK P. MERTENS AND ROBERT C. PLUMB

Department of Chemical Engineering and Chemistry, Worcester Polytechnic Institute, Worcester, Massachusetts

Received October 30, 1962

The mode of deposition of barium and calcium stearate films and the orientation of molecules within the first few layers is shown to be significantly different for gold and oxidized metal surfaces such as aluminum and copper. Some films may have the hydrocarbon function pointing outward, whereas others may have the carboxyl function pointing outward. Films deposited on oxidized surfaces follow a 1,3,5-sequence of pickup, whereas films deposited on gold follow a 1,2,4,6-sequence of pickup. The mode of pickup is explained in terms of specific interactions between the barium stearate molecules and the substrate surfaces.

Introduction

It is well known from the work of Blodgett[2] and others that monomolecular films of alkaline earth salts of certain fatty acids can be formed on top of aqueous solutions containing the metal ions when a very dilute benzene solution of the fatty acid is spread on the surface. These salt films may be transferred to solid substrates such as glass or metal by dipping the substrate through the film when the film is under compression. Three types of films have been observed. X type films are deposited during a down trip through the spread film, Y type films are deposited during both the down and up trips through a spread film, and Z type films are deposited during the up trip only. According to Blodgett[2] the tendency to form X or Y films depends upon the pH of the solution, the temperature, and to some extent on the previous number of barium stearate monolayers which have been deposited on the surface. Monomolecular films on water are oriented with the metal-carboxyl function pointing toward the water. The films deposited on glass, and presumably all other metals studied to date, have the carboxyl heads pointed toward the substrate; the outer surface, in the first layer and in multilayer films, consists of closely packed CH_3 groups. In Y type films the layers alternate in direction. In X type films the layers are oriented in the same direction.

Attempts have been made to explain the factors promoting the formation of X, Y, and Z type films. Bikerman[3] proposed that the type of deposition depends upon the hydrophobic character of the surface. He proposed that the difference between receding and advancing contact angles and the value of the contact angle was important. Thus, depending upon the hydrophobic character of the surface, both the advancing and receding angle may be less than 90°, the advancing angle may be less than 90° and the receding angle greater than 90°, or both angles may be greater than 90°. One might assume that a monolayer on a water surface could only touch and attach itself to the solid surface if the direction of movement of the slide and that of the water surface near the slide forms an obtuse angle so that the monolayer on water and the metal can approach one another. Then one would expect the tendency for pickup to increase with decreasing hydrophobic character (decrease in contact angles) and one might find sufficient difference between advancing and receding contact angles to produce pickup on the down trip only. In a more detailed analysis one should take account of the fact that the opposite sides of monolayers have different hydrophobic characters and the orientation of the monolayer deposited on the previous trip through the interface will have a pronounced effect upon the pickup of a film.

One can envision composite multilayer film pickup where the simple classification as X, Y, or Z would not be valid because of specific orienting effects of the substrate and subsequent effects of the first film upon the pickup of succeeding films. Apparently specific effects of the substrate and the behavior of the first few layers of a multilayer film have not been the subject of much investigation.

One might anticipate that there would be a definite relationship between the orientation of a deposited film and the orientation of the salt upon the surface of the water. The early investigation of Langmuir and Schaefer[4] on enzyme films leads to the conclusion that the relative orientation of the hydrophilic and hydrophobic functions of the molecules in the deposited films cannot necessarily be predicted from their relative orientations on the aqueous surface by simply assuming that the substrate picked up the film by attaching to it the portion of the molecule in closest proximity but, rather, depends upon the hydrophilic or hydrophobic character of the substrate surface itself.

Other work indicates that the attractively simple picture of a uniform monolayer is probably not correct. Epstein[5] studied fatty acid monolayers by electron microscopy and electron diffraction and proposed the existence of groups of molecules or micelles to explain some of the varying results concerning film thickness and molecular orientation as obtained by previous workers.

By and large, the majority of the significant work on barium stearate films has dealt with multilayers, rather than with the first few monolayers close to the substrate. In the course of investigations underway in this Laboratory on the oxidation of metals, it was desired to make step wedges in the range of 0 to 50 Å. units of thickness to test the methods which are being used for the determination of thickness of films. Several significant observations on the pickup of the first few layers were made and, in particular, effects of the nature of the substrates which had not been noted previously were encountered. This report will describe these observations and point out certain generalities about the mode of pickup which are indicated by our work.

(1) Based upon a portion of a dissertation submitted by F. P. Mertens in partial fulfillment of the requirements for the Ph.D. degree in Chemistry.

(2) K. B. Blodgett, *J. Am. Chem. Soc.*, **57**, 1007 (1935).

(3) J. J. Bikerman, *Proc. Roy. Soc.* (London), **A170**, 130 (1939).

(4) I. Langmuir and V. J. Schaefer, *J. Am. Chem. Soc.*, **60**, 1351 (1938).

(5) H. T. Epstein, *J. Phys. Colloid Chem.*, **54**, 1053 (1950).

Experimental

Preparation of Metal Substrates.—Three different metals, aluminum, copper, and gold, were used as substrates. Clean films of these metals were prepared by evaporation *in vacuo* at approximately 3×10^{-6} mm. pressure onto clean glass plates ($10 \times 70 \times 1$ mm.) cut from microscope slides. The plates were cleaned and vapor phase degreased with benzene before they were introduced into the vacuum system. They were ion bombarded with argon gas before the evaporation. A magnetically controlled movable shield in the vacuum chamber shielded the slides from the volatile contaminants present in the early stages of filament heating.[6] The metal coated slides were examined with monochromatic light (5461 Å.) linearly polarized at an angle of 135° to the plane of incidence and impinging at an angle of incidence of about 70° to establish that they were optically uniform over the entire slide surface. The conditions of evaporation were adjusted to produce uniform films.

Deposition of Stearate Layers.—The films of barium and calcium stearate were deposited by the conventional Blodgett technique. A dilute stearic acid solution in benzene was spread on the surface of the clean aqueous solution containing barium or calcium ions at the proper pH. The stearic acid solution was enclosed by a waxed nylon thread and the film was compressed by oleic acid. The films were stabilized and step wedges were prepared by successive dips. The slides were perpendicular to the solution surface during dipping. The first monolayer usually required 15 to 25 minutes to dry before successive dips were made. As was observed by Blodgett, the samples retracted completely dry from the solution after two or three films had been deposited.

Film Thickness Determinations.—The film thicknesses were measured by determining the characteristics of the elliptically polarized light generated by reflecting linearly polarized light from the surfaces of the step wedges. The details of this technique will not be discussed since the general procedures are already well known. Special procedures and techniques which we have developed are being described elsewhere.[7] The film thicknesses were calculated by the Drude linear approximation for thin dielectric films on metal substrates.[8] The Drude linear approximation equations are valid for thin films such as were studied in this work[9] and their accuracy may be extended to a few per cent at 100 Å. by a modification in the calculation procedures which we are describing elsewhere.[7] The explicit solution of the equations for the thickness and index of refraction of any particular film was used. Computations were performed on an IBM 1620 computer.

Sequence of Film Pickup by Different Metal Surfaces.—A significant reproducible dependence of the sequence of film pickup upon the nature of the metal surface was found. The sequence of film pickup may be readily established from experimental observations of the film thickness as a function of the number of dips by plotting the film thickness *vs.* the number of monolayers for an assumed sequence of pickup and seeing which assumed sequence of pickup gives the most linear plot. Figure 1 shows such a plot for barium stearate on gold. It is apparent that the films of barium stearate are picked up by gold in a 1,2,4-sequence. Similar determinations for barium stearate on copper and calcium stearate on aluminum indicate a 1,3,5-sequence of pickup in both cases. (We have also noted, under some experimental conditions, a 2,4,6-sequence on gold, but we have not studied it in detail and will not discuss it in this paper.)

Hydration of the oxide film on the surface of copper during the first dip was found to be significant. It was found, on dipping an oxidized copper film through a clean water–air interface, that a step about 14 Å. thick was produced. It was assumed that this step

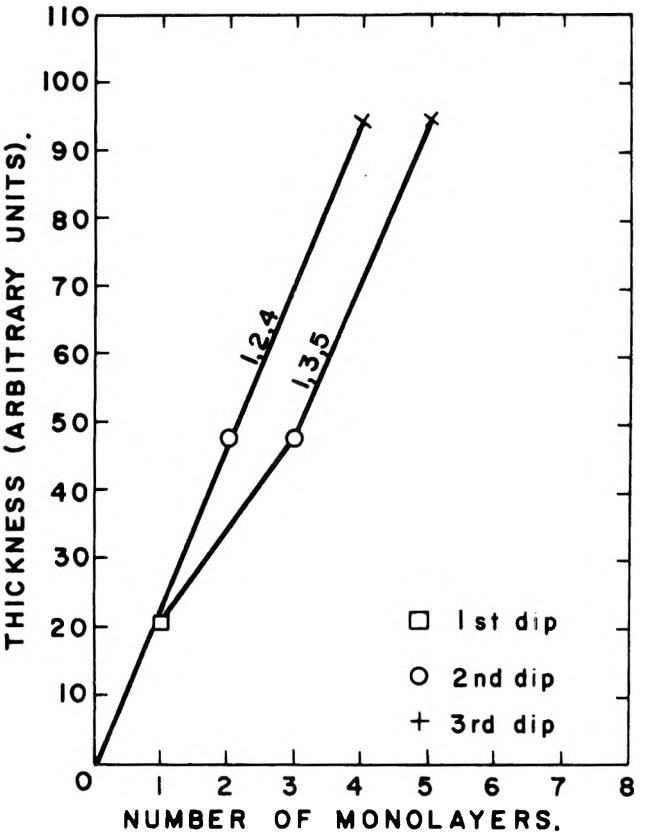

Fig. 1.—Observed thicknesses of barium stearate films on a gold substrate plotted for a 1,2,4- and a 1,3,5-sequence of pickup.

was the boundary between hydrated copper oxide and the unhydrated oxide. The observed film thicknesses on copper were corrected for the hydration of the oxide.

The film thickness, plotted as the ordinates in Fig. 1, is in arbitrary units. Absolute values for the film thicknesses are being published elsewhere along with a more comprehensive discussion of the problem of thin film thickness determination.[7]

From the work of Blodgett and others it is well established that, under these conditions, no film is picked up on the first down dip, one film is picked up on the first up dip, and a film is picked up on each of the subsequent down and up dips producing a 1,3,5-sequence of film deposition. The sequence of film pickup could be observed on copper and aluminum by observing the motion of the thread boundary during the down and up trips. An unsuccessful attempt was made to decide if the films deposited in the first two dips on gold were deposited on the down trip or the up trip. Glass microscope slides were coated with gold by two evaporations, one on each side. The changes in area of the spread barium stearate monolayer on water during dipping were measured by photographing the thread. A confusing pattern of results emerged which did not clearly indicate deposition on either the down trip or the up trip. It was found when the two sides of the gold coated slide were examined with elliptically polarized light that film deposition was different on the two sides. One side gave a deposition characteristic of gold, whereas the other side gave a deposition in a 1,3,5-sequence, characteristic of other metals. It is believed that the surface of the gold which gave the non-gold like behavior was, in fact, contaminated with a foreign metal as a result of its having deposited first in the vacuum system. Two possible mechanisms by

(6) H. L. Rook and R. C. Plumb, *Appl. Phys. Letters*, **1**, 11 (1962).
(7) F. P. Mertens and R. C. Plumb, to be published.
(8) A. Vasicek, "Optics of Thin Films," North Holland Publishing Co., 1959.
(9) A. B. Winterbottom, *Norske Videnskabers Selskab*, **45**, 1 (1955).

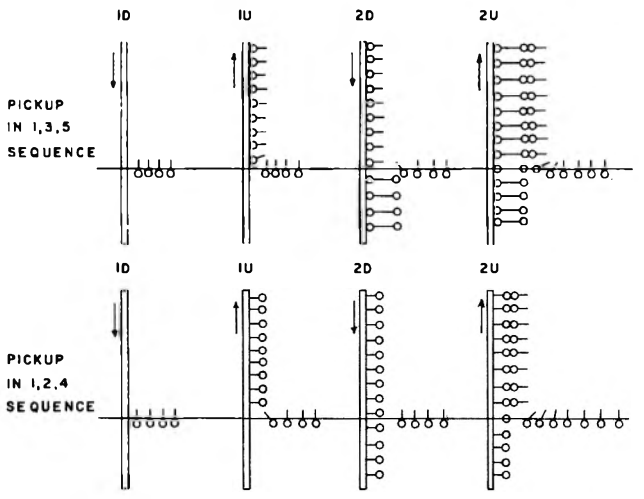

Fig. 2.—Schematic representation of process of film pickup in 1,3,5-sequence and 1,2,4-sequence.

which it may have become contaminated are diffusion of impurities to the surface (which would be enhanced by the ion bombardment used to clean the glass on the other side of the slide prior to evaporation) and sputtering of aluminum from the aluminum ion bombardment electrodes.

Orientation of Molecules within the Deposited Films.—It is to be expected from the work of others that, in the 1,3,5-sequence of film formation, the hydrocarbon function points outward in the first, third, and fifth layers. By forming step wedges consisting of 1,3,5 and 7 layer steps and observing the flow characteristics of drops of benzene placed upon these steps, it was established that all of the outer surfaces had approximately the same hydrophobic character. The contact angle to benzene and the tendency of benzene drops to flow when placed at one end of an incline step wedge showed no differences between successive steps.

A variety of orientations are conceivable in the 1,2,4,6-sequence of film pickup observed on gold. On the 2, 4, and 6 layer steps benzene behaved the same as on the 1,3,5-steps observed on other metals. The benzene behaved markedly different on the 1 layer step adjacent to the metal surface. The benzene wet this layer readily and flowed up to the second step where there was a pronounced barrier. Thus, in the 1,2,4,6-sequence the first layer has the hydrocarbon function pointed toward the gold surface and the carboxylate group pointed outward, the second layer has the carboxyl group pointed toward the carboxyl group of the first layer and the hydrocarbon group outward, and succeeding layers are in the same orientation as that observed on aluminum and copper.

Discussion

The essential differences between gold and aluminum and copper seem to be caused by the fact that both aluminum and copper are coated with oxides, whereas the gold is, to a great extent, oxide-free. It has been demonstrated that the unexpected observation of oxidation of gold by some investigators really results from diffusion of impurities in gold to the surface forming an impurity oxide film.[10] Apparently a pure gold surface is essentially oxide-free.

It has been shown by Langmuir and Schaefer that the orientation of layers in a multi-layer film is not necessarily that which one would predict from the direction of traverse when the film is being picked up. There is no fundamental reason to expect that molecules at the air–substrate–film interface cannot rotate as they are being absorbed. The explanation of the mode of pickup and the orientation of molecules which are picked up must lie in specific interactions between the various substances involved.

We will assume, as seems reasonable, that carboxyl functions may interact with each other, if in the right orientation, by dipole–dipole forces. The principal interaction between hydrocarbon groups will be by Heitler–London Dispersion forces. The interactions between carboxyl groups and hydrocarbon groups will be of a mixed Heitler–London Dispersion and dipole–induced dipole character. The attractive energy between two carboxyl groups or between two hydrocarbon groups will be assumed to be stronger than the energy of interaction between a carboxyl group and a hydrocarbon group. The process by which layers are deposited and specific orientations of the molecules produced, as we envision it, is shown schematically in Fig. 2. We believe that pickup of the first layer in a 1,2,4-sequence takes place when the slide is being withdrawn from the solution, but we are not completely certain about this point. This pickup would involve a reorientation of molecules at the three-phase interface. The second down trip of the slide may or may not pick up a film depending upon the orientation of the first layer which has already been deposited. If the hydrocarbon function of the first layer is pointed outward, then it will be energetically favorable to deposit a second layer because, by so doing, the molecules avoid generating a high energy hydrocarbon–solution interface. The second down dip in a 1,2,4-sequence will not produce pickup because of the weak attractive forces between the hydrocarbon function and the carboxyl group. Pickup of a second layer at this stage by attraction of the carboxyl group of one molecule to the carboxyl group of another would require generation of a hydrocarbon–water interface which would be unstable. After the second down trip the outer surfaces of either a 1,3,5-sequence or a 1,2,4-sequence are identical and the films will be picked up in the usual way.

Apparently the carboxyl groups are strongly attracted to oxides, whereas the hydrocarbon function is attracted to a bare metal surface. Thus, one would classify a bare metal as more hydrophobic than an oxide coated metal. According to this picture then the orientation of the first layer is determined by the specific interactions between the barium stearate film and the metal surface. The orientation of the second layer is determined by specific interaction between the molecules in the second layer and molecules in the first layer.

Acknowledgment.—This research was supported by United States Atomic Energy Commission Basic Research Contract AT(30-1)2479.

(10) L. D. Carpenter, D. Clark, W. H. Main, and T. Dickinson, *Trans. Faraday Soc.*, **55**, 1924 (1959).

CONDUCTANCE OF THE ALKALI HALIDES. V. SODIUM CHLORIDE IN DIOXANE–WATER MIXTURES[1,2]

BY ROBERT W. KUNZE AND RAYMOND M. FUOSS

Contribution No. 1721 from the Sterling Chemistry Laboratory of Yale University, New Haven, Connecticut

Received October 31, 1962

The conductance of sodium chloride at 25° was measured in dioxane–water mixtures covering the range of dielectric constant $12.24 \leq D \leq 78.54$. The Fuoss conductance equation reproduces the conductance as a function of concentration within the experimental error of 0.01–0.05% for concentrations where κa does not exceed 0.2. The contact distance $\mathring{a}_J$ is 3.38 for aqueous solutions; it increases to 5.33 at $D = 12.24$. The distance a_K from the association constant also increases with decreasing dielectric constant.

In this paper are presented the conductances of dilute solutions of sodium chloride in dioxane–water mixtures. As for potassium chloride,[3] cesium iodide,[4] and rubidium bromide,[5] the observed equivalent conductances Λ are accurately reproduced as a function of the concentration c by the equation[6]

$$\Lambda = \Lambda_0 - Sc^{1/2}\gamma^{1/2} + Ec\gamma \log c\gamma + Jc\gamma + J_2(c\gamma)^{3/2} - K_A c\gamma f^2\Lambda \quad (1)$$

This equation contains three arbitrary constants, Λ_0, a_J and K_A, where a_J is an implicit function of the coefficient J in the present formulation of the theory. In principle, it is also possible to derive values of the center-to-center contact distance from the limiting conductance[7] Λ_0 and from the association constant[8] K_A. Denoting these distances by a_Λ and a_K, we would expect a_J, a_Λ, and a_K as derived from the data *via* eq. 1 to be equal to each other and to be independent of solvent composition for systems which conform to the sphere-in-continuum model on which the present theory is based. As will be shown below, sodium chloride, like the other alkali halides so far investigated, gives a_J and a_K values which increase with increasing dioxane content and which are considerably larger than the hydrodynamic value a_Λ. It is evident that a more realistic model will be required for this and similar systems, where the ions and (part of) the solvent molecules have about the same size.

Experimental

Sodium chloride was purified by precipitation from saturated solution by hydrogen chloride, as recommended by Shedlovsky.[9] After washing with ice-water, the salt was redissolved and reprecipitated. After washing, it was dried for 3 hours at 100°, 3 days at 110° *in vacuo*, and finally for 51 hours under nitrogen at 400°. The product was neutral.[9] A flame analysis showed less than 0.005% potassium. Sulfate and iron were absent (less than 0.0005%). Dioxane was purified as described by Lind and Fuoss[3]; b.p. 101.3 = 0.2°; density 1.0274–1.0280. Equipment and technique were essentially the same as those described in the first paper of this series.[3] The properties of the dioxane–water mixtures used as solvents are summarized in Table I, where w = wt. % dioxane, ρ_0 = density, D = dielectric constant, η = viscosity (poise), and κ_0 = solvent conductance. Four cells were used, with constants equal to 0.073389 ± 0.000013, 0.14318 ± 0.00002, 0.39121 ± 0.00005, and 1.0109 ± 0.0002. The fourth cell was calibrated by the method of Lind, Zwolenik, and Fuoss[10] and rechecked frequently during the work. The other cells were calibrated by comparison with the directly calibrated cell or with each other, using dilute aqueous solutions of sodium bicarbonate or solutions of tributylammonium picrate in isopropyl alcohol. The concentrations were chosen to give a resistance of at least 500 ohms for the cell with the smaller constant and less than 5000 ohms for the cell with the higher constant of the pair being compared.

TABLE I

PROPERTIES OF SOLVENTS

No.	w	ρ_0	D	$100\,\eta$	$10^6\kappa_0$
1	79.9	1.03542	12.12	1.721	0.025
2	77.7	1.03571	13.51	1.778	.018
3	73.5	1.03635	16.67	1.871	.051
4	70.6	1.03670	18.74	1.917	.060
5	60.5	1.03584	26.85	1.992	.189
6	53.7	1.03433	32.77	1.953	.213
7	34.2	1.02461	49.54	1.598	.417
8	0.0	0.99707	78.54	0.8903	1.35

All solutions were made up by weight, and concentrations c in moles/l. were calculated from the molal concentration m moles/kg. solvent by the equation $c/m = \rho_0 + km$ where ρ_0 is the density of the solvent mixture and k is determined experimentally. For sodium chloride in dioxane–water mixtures, $k = -0.017 \pm 0.002$, based on the following data: 80.0% dioxane, $\rho_0 = 1.03540$, $m = 0.0089$, $\rho = 1.03574$, $k = -0.014$; 70.6% dioxane, $\rho_0 = 1.03670$, $m = 0.0205$, $\rho = 1.03756$, $k = -0.015$; 53.7% dioxane, $\rho_0 = 1.03433$, $m = 0.0149$, $\rho = 1.03490$, $k = -0.017$. For sodium chloride in water,[11] $k = -0.018$.

The conductance data are summarized in Table II, where Λ is equivalent conductance at concentration c, and $\Delta\Lambda = [\Lambda_{obsd} - \Lambda_{calcd}]$. The calculated value of Λ is that obtained from eq. 1 on substituting the given concentration and the values of the three constants which were obtained from the IBM analysis of the data. When association is negligible, eq. 1 is simplified by setting K_A equal to zero and γ equal to unity.

Discussion

When the conductance decrease due to pairs of ions in contact is negligible, Λ', defined by the equation

$$\Lambda' = \Lambda + Sc^{1/2} - Ec \log c \quad (2)$$

is a linear function of concentration

$$\Lambda' = \Lambda_0 + Jc \quad (3)$$

Reliable values of Λ_0 and J are then readily obtained as intercept and slope of a Λ'–c plot, as shown by curves 1

(1) This paper is based on part of a thesis which will be presented by Robert W. Kunze to the Graduate School of Yale University in partial fulfillment of the requirements for the degree of Doctor of Philosophy.

(2) Grateful acknowledgment is made to the donors of The Petroleum Research Fund, administered by the American Chemical Society, for support of this research.

(3) J. E. Lind, Jr., and R. M. Fuoss, *J. Phys. Chem.*, **65**, 999 (1961).

(4) J. E. Lind, Jr., and R. M. Fuoss, *ibid.*, **65**, 1414 (1961).

(5) J. E. Lind, Jr., and R. M. Fuoss, *ibid.*, **66**, 1727 (1962).

(6) R. M. Fuoss and F. Accascina, "Electrolytic Conductance," Interscience Publishers, Inc., New York, N. Y., 1959. Symbols used in this paper are defined in Chapters 15 and 17.

(7) R. M. Fuoss, *Proc. Natl. Acad. Sci. U. S.*, **45**, 807 (1959).

(8) R. M. Fuoss, *J. Am. Chem. Soc.*, **80**, 5059 (1958).

(9) T. Shedlovsky, *ibid.*, **54**, 1411 (1932).

(10) J. E. Lind, Jr., J. J. Zwolenik, and R. M. Fuoss, *ibid.*, **81**, 1557 (1959).

(11) H. S. Harned and B. B. Owen, "The Physical Chemistry of Electrolytic Solutions," 3rd. edition, Reinhold Publ. Corp., New York, N. Y., 1958, p. 725.

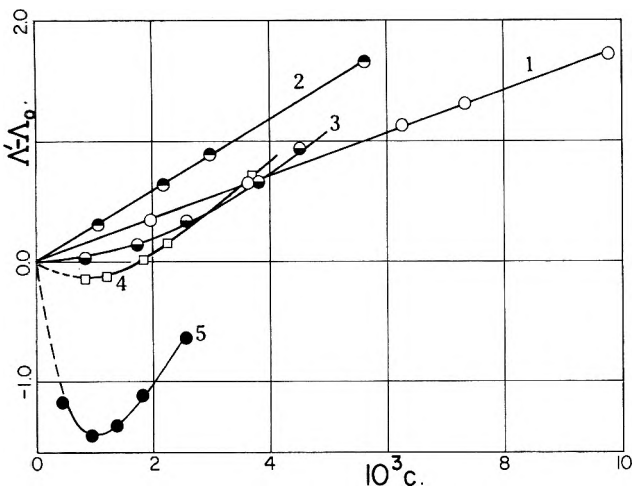

Fig. 1.—Function defined by eq. 3. Curve 1, D = 78.54 (water); 2, D = 49.54; 3, D = 32.77; 4, D = 26.85; 5, D = 18.74.

TABLE II

CONDUCTANCE OF SODIUM CHLORIDE IN DIOXANE–WATER MIXTURES AT 25°

10^4c	Λ	$10^3\Delta\Lambda$	10^4c	Λ	$10^3\Delta\Lambda$
	D = 12.12			D = 26.85	
17.868	17.053	−11	36.581	40.671	− 2
15.977	17.558	− 1	22.373	42.286	7
14.423	18.041	+21	18.335	42.872	− 1
12.615	18.674	+14	12.068	43.968	−14
10.840	19.409	+ 3	8.624	44.752	9
9.043	20.306	−10		D = 32.77	
7.091	21.536	−17	44.931	46.345	− 5
5.223	23.110	+14	37.782	46.872	6
	D = 13.51		25.527	47.948	4
20.616	20.443	−13	17.099	48.890	− 9
15.701	21.754	26	8.424	50.234	3
11.723	23.187	− 1		D = 49.54	
8.227	24.958	−19	55.711	65.756	− 6
4.590	27.803	7	29.365	67.138	12
	D = 16.67		21.457	67.692	6
24.211	27.074	0	10.639	68.689	−11
15.063	29.252	2		D = 78.54	
9.982	31.122	− 2	97.379	118.603	− 5
5.923	33.305	1	72.999	119.558	− 6
	D = 18.74		62.258	120.051	19
24.568	31.020	− 9	36.228	121.459	−12
18.225	32.351	21	19.659	122.738	5
13.951	33.469	− 1			
9.613	34.934	−18			
4.799	37.272	7			

and 2 of Fig. 1 for water and 34.2% dioxane as solvents. (To make the figure compact, $\Lambda' - \Lambda_0$ is plotted here instead of Λ' itself.) If the data for these two systems are analyzed on the basis of eq. 1, the computer delivers small negative values of K_A (−1.3 ± 0.6 and −2.6 ± 0.1, respectively); clearly, association is negligible in these two cases. Curve 3 is for 53.7% dioxane (D = 32.77); the association constant is only 7 ± 2, but this is enough to destroy the linearity of Λ', although the Λ'–c curve is still useful for obtaining a preliminary value of Λ_0. At dielectric constants of 26.85 and 18.74 (association constants 20 ± 4 and 127 ± 9, respectively), the Λ'–c curves go through minima, because the negative $K_A c\gamma f^2\Lambda$ term now becomes comparable to and then exceeds the positive Jc term in the conductance. When K_A is greater than about ten, the Λ'–c curve no longer can be used to estimate Λ_0, but the curve still is useful as a test plot to examine the data for self-consistency, and serves to detect gross errors. (The data should always be controlled graphically before being fed to the computer, of course. The conventional Λ–$c^{1/2}$ plot is not sensitive enough for this purpose for data of high precision.)

The derived constants Λ_0 (limiting conductance), K_A (association constant), and a_J are summarized in Table III, which also gives σ, the standard deviation between calculated and observed values of conductance; the coefficients S, E, J, and J_2 of eq. 1 are given in Table IV.

TABLE III

CONSTANTS FOR SODIUM CHLORIDE IN DIOXANE–WATER MIXTURES AT 25°

D	Λ_0	$\mathring{a}_J$	K_A	$10^3\sigma$
12.12	35.87 ± 0.19	5.35 ± 0.10	1475 ± 50	17
13.51	37.51 ± .17	5.09 ± .14	753 ± 34	26
16.67	40.85 ± .02	5.26 ± .03	278 ± 2	2
18.74	42.45 ± .08	4.59 ± .22	127 ± 9	21
26.85	48.67 ± .05	4.06 ± .30	20 ± 4	13
32.77	53.25 ± .03	3.68 ± .28	7 ± 2	9
49.54	71.21 ± .01	3.42 ± .05	...	13
78.54	126.60 ± .02	3.38 ± .04	...	15

TABLE IV

COEFFICIENTS OF CONDUCTANCE EQUATION

D	S	E	J	J_2
12.12	219.2	4860	12,600	11,060
13.51	193.4	3542	8480	6680
16.67	158.2	2039	4990	2960
18.74	140.9	1482	3380	1785
26.85	102.1	564	1250	344
32.77	87.92	333.2	720	118
49.54	75.00	121.1	302	−35
78.54	89.52	46.31	189	−79

In order to obtain an estimate of the association constant for the systems at high dielectric constant, where the computer cannot separate the J and K_A terms, arbitrary values of $\mathring{a}$ where chosen and then Λ_K was computed where

$$\Lambda_K = \Lambda + Sc^{1/2}\gamma^{1/2} - Ec\gamma \log c\gamma - J(a)\, c\gamma - J_2(c\gamma)^{3/2} = \Lambda_0 - K_A c\gamma f^2\Lambda \quad (3)$$

Assuming Λ_K to be a linear function of $c\gamma f^2\Lambda$, the association constant can then be evaluated. The resulting values of K_A depend, of course, on the choice of $\mathring{a}$; for D = 49.54, $\mathring{a}$ 3.5, 4.0, and 4.5 give K_A = 0.1, 0.9, and 1.7, respectively; for water, the same set of $\mathring{a}$ values give K_A = 0.06, 0.33, and 0.57. In Fig. 2, the logarithm of the association constant is plotted against the reciprocal of the dielectric constant. The solid black point was obtained by Purlee and Grunwald[12] for sodium chloride in 70% dioxane, using a potentiometric method and the Bjerrum definition of ion pairs; agreement is satisfactory. Simple theory[8] predicts a straight line, but the values for sodium chloride, like those for the other alkali halides so far investigated, show curvature, especially in the range of higher dielectric constants. The sharp curvature in the range of high dielectric constants could be avoided by appropriate choice of the $\mathring{a}$-value used in computing Λ_K, but the values needed (4.5–5.0) to linearize the curve seem unrealistically large. Based on

(12) Private communication from Dr. E. Grunwald.

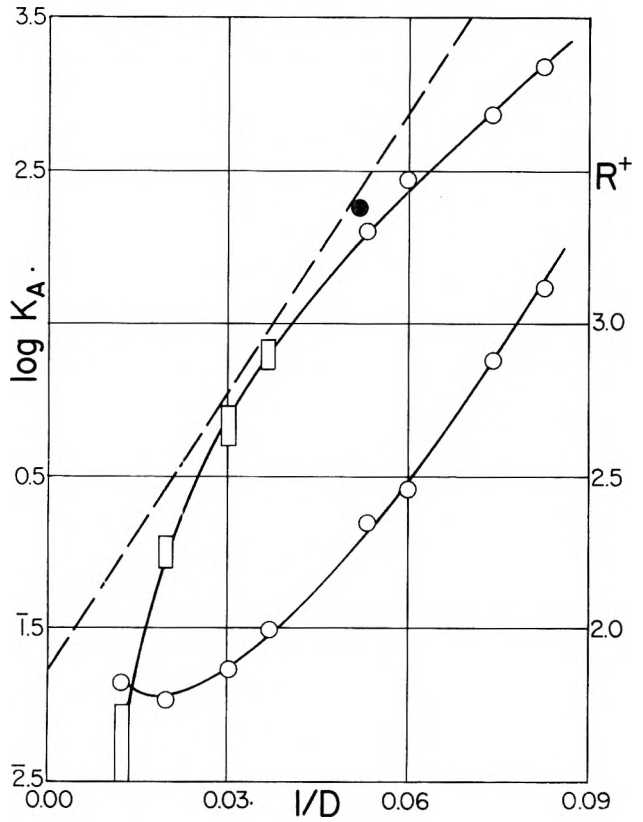

Fig. 2.—Upper curve: log K_A *vs.* D^{-1}, ordinates left. Lower curve, Stokes radius *vs.* D^{-1}, ordinates right.

unpublished theoretical work, we ascribe the curvature to approximations made in deriving eq. 1, which cause the coefficient J to absorb part of the conductance variation which should be in K_A. The systematic increase of a_J with decreasing dielectric constants shown in Table III also probably has the same origin. The log K_A–D^{-1} curve does approach linearity as the dielectric constant decreases, but the slope leads to a value a_K = 5.8 which also seems unreasonably large.

The Stokes radius of the sodium ion (lower curve of Fig. 2) shows a much more complicated behavior than that due to simple ion–dipole interaction.[7,13] Assuming that the curve approaches linearity at low dielectric constants, a linear extrapolation to $D = \infty$ from the middle part of the range gives R_∞ (Na^+); the value is found to be 1.3 Å. which gives $\mathring{a}_\Lambda$ = 2.1 using Lind's value[3] R_∞ (Cl') = 0.8. If the Sutherland factor of 1.5 is applied, a value of $\mathring{a}_\Lambda$ of about 3.1 results. This at least is nearer the expected value than was found for the other alkali halides, although less than the sum of the lattice radii.

Finally in Fig. 3 is shown a comparison of our results with those obtained by other workers for sodium chloride in water. The data were all treated by the Λ'–c method in order to obtain a self-consistent set of con-

(13) R. H. Boyd, *J. Chem. Phys.*, **35**, 1281 (1961).

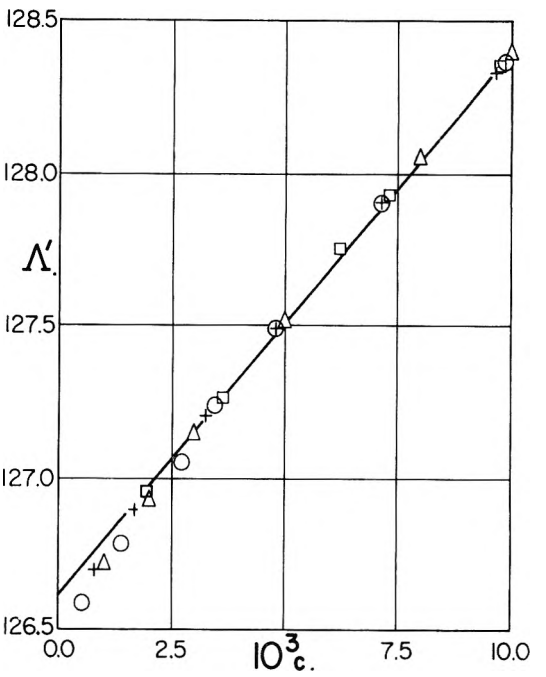

Fig. 3.—Comparison of data for sodium chloride: □, this work; +, Tober[13]; ○, Gordon[14]; Δ, Shedlovsky.[15]

stants. The results are: Λ_0 = 126.60 ± 0.02 (this work); 126.58 ± 0.01 (Tober)[14]; 126.58 ± 0.04 (Gordon,[15] neglecting the point at c = 0.0014301); 126.59 ± 0.02 (Shedlovsky).[16] The different limiting conductances agree with each other well within the probable error. The data below 0.002 N from the several laboratories have one interesting feature in common; the points *all* fall below the theoretical straight line which fits the data perfectly in the range $0.002 \leqslant c \leqslant 0.01$ At c = 0.001, a solvent conductance $\kappa_0 = 1.0 \times 10^{-6}$ gives a correction of nearly 1%. The 0.05% discrepancy between theoretical and observed conductance at 0.001 N could be easily accounted for if conductances of solute and solvent failed to be additive by only 5%. We are inclined to disregard the data for $c \leqslant 2 \times 10^{-3}$. Before the theoretical value of the coefficient E was known, the experimenter tried to measure to as low concentrations as possible in order to reduce the uncertainty on extrapolation for Λ_0 by means of foreknowledge only of S, and using an empirical extrapolation function. But given theoretical values of both S and E, the experimenter can now work in a range of concentration where errors due to solvent correction become negligible, and use a theoretically justified linear scale for extrapolating Λ' to Λ_0 for solvents of high dielectric constant.

(14) F. W. Tober, Dissertation, Yale University, 1948.

(15) H. E. Gunning and A. R. Gordon, *J. Chem. Phys.*, **10**, 126 (1942). Data corrected by $\Delta\Lambda = -0.02$; *cf.* G. C. Benson and A. R. Gordon, *ibid.*, **13**, 473 (1945).

(16) T. Shedlovsky, A. S. Brown, and D. A. MacInnes, *Trans. Electrochem. Soc.*, **66**, 165 (1934).

CONDUCTANCE OF THE ALKALI HALIDES. VI. RUBIDIUM CHLORIDE IN DIOXANE–WATER MIXTURES[1,2]

BY ROBERT W. KUNZE AND RAYMOND M. FUOSS

Contribution No. 1722 from the Sterling Chemistry Laboratory of Yale University, New Haven, Connecticut

Received November 2, 1962

The conductance of rubidium chloride at 25° has been measured in dioxane–water mixtures covering the range of dielectric constant $11.88 \leqslant D \leqslant 78.54$. The limiting conductance of the salt in water is 153.57 ± 0.02 which gives 77.20 for the single ion conductance of rubidium. The contact distance $\mathring{a}_J$ in water is 3.02; it increases to 7.56 at $D = 11.88$. Like the other alkali halides in dioxane–water mixtures, a_K and a_Λ also vary with dielectric constant. The sequence of association constants at a given dielectric constant is K_A (RbCl) > K_A (KCl) > K_A (NaCl).

We present in this paper conductance data for dilute solutions of rubidium chloride in dioxane–water mixtures, covering the range $11.88 \leqslant D \leqslant 78.54$ in dielectric constant. All symbols are defined in the previous paper[3] of this series.

Experimental

Rubidium chloride (99.9% pure) was used as received from A. D. MacKay, Inc. (198 Broadway, New York, 38, N. Y.). Analysis by the flame photometer showed the presence of the following trace impurities: 0.092% potassium chloride, 0.030% cesium chloride, and 0.030% sodium chloride. One sample was dried by heating at 550° for two days under nitrogen; a second sample was fused under nitrogen (m.p. 715°). Conductances on the two samples agreed within 0.01 Λ-unit, as shown in Fig. 1.

Conductances were measured at 25.000 ± 0.003°, using the same cells as were used with sodium chloride. All details of technique were as for sodium chloride. Volume concentrations c were obtained from molality m by the equation $c/m = (\rho_0 + km)$ with $k = -0.035 \pm 0.003$. The value of k is based on the following data: 80.1% dioxane, $\rho_0 = 1.03523$, $m = 0.0075$, $\rho = 1.03590$, $k = -0.032$; 70.5% dioxane, $\rho_0 = 1.03675$, $m = 0.0086$, $\rho = 1.03750$, $k = -0.039$; water,[4] $k = -0.033$. The properties of the solvent mixtures are summarized in Table I and the conductance data are given in Table II.

TABLE I

PROPERTIES OF SOLVENTS

No.	w	ρ_0	D	100η	$10^6\kappa_0$
1	80.1	1.03523	11.88	1.720	0.011
2	77.5	1.03590	13.73	1.786	.019
3	70.5	1.03675	18.93	1.920	.049
4	61.9	1.03642	25.80	1.987	.065
5	36.2	1.02618	48.02	1.636	.372
6	0.0	0.99707	78.54	0.8903	1.28

Discussion

Plots of Λ′ against concentration were linear for solutions in water and in the 36.2% dioxane mixture ($D = 48.02$). At 61.9% dioxane ($D = 25.80$), the Λ′-c curve becomes concave-up and for lower dielectric constants, goes through a minimum, just as the curves for sodium chloride. The derived constants and the coefficients of the conductance equation (ref. 3, eq. 1) are summarized in Tables III and IV.

Three runs (6, 7, 8) were made in water, one using fused salt and two using salt dried at 550°. The agreement is excellent, as shown in Fig. 1. The average of J for runs 6, 7, and 8 was 194. We define Λ″ by the equation

$$\Lambda'' = \Lambda(\text{obs.}) + Sc^{1/2} - Ec \log c - Jc \quad (1)$$

TABLE II

CONDUCTANCE OF RUBIDIUM CHLORIDE IN DIOXANE–WATER MIXTURES AT 25°

10^4c	Λ	$10^3\Delta\Lambda$	10^4c	Λ	$10^3\Delta\Lambda$
$D = 11.88$			$D = 48.02$		
10.694	17.689	− 7	69.664	72.693	1
8.272	19.000	11	47.680	73.830	− 6
6.228	20.512	3	36.109	74.587	5
4.322	22.531	−11	25.918	75.371	0
2.3945	25.858	4	14.453	76.507	− 1
$D = 13.73$			$D = 78.54$		
16.871	21.278	− 8	85.060	145.369	−11
12.762	22.778	11	62.499	146.460	9
9.377	24.483	6	52.857	146.984	1
6.714	26.342	−17	34.969	148.165	11
3.6716	29.629	5	17.764	149.665	−12
$D = 18.93$					
20.390	33.329	− 5	109.116	144.393	−17
15.088	34.864	9	85.482	145.377	24
11.644	36.125	3	65.112	146.293	−15
8.147	37.744	−12	43.588	147.570	20
4.569	40.031	5	21.709	149.256	−15
$D = 25.80$					
25.605	44.045	− 4	104.703	144.595	1
20.754	44.880	16	83.738	145.440	1
16.265	45.747	−14	61.142	146.513	−10
9.777	47.407	6	41.783	147.676	4
5.567	48.846	− 1	20.823	149.358	1

TABLE III

CONSTANTS FOR RUBIDIUM CHLORIDE IN DIOXANE–WATER MIXTURES AT 25°

D	Λ_0	a_J	K_A	$10^3\sigma$
11.88	38.94 ± 0.11	7.56 ± 0.20	3280 ± 50	13
13.73	40.54 ± .11	5.71 ± .15	1200 ± 25	16
18.93	46.21 ± .05	5.24 ± .20	217 ± 7	12
25.80	52.77 ± .06	5.32 ± .63	53 ± 6	16
48.02	79.85 ± .02	3.45 ± .26	1.9 ± 0.5	5
78.54	153.67 ± .02	3.02 ± .04	...	16

TABLE IV

COEFFICIENTS OF CONDUCTANCE EQUATION

D	S	E	J	J_2
11.88	232.2	5474	15800	13740
13.73	199.2	3673	9270	7130
18.93	146.6	1578	3860	1893
25.80	111.8	705	1830	340
48.02	80.38	154.6	363	−23
78.54	95.74	60.7	194	−58

(1) This paper is based on part of a thesis which will be presented by Robert W. Kunze to the Graduate School of Yale University in partial fulfillment of the requirements for the degree of Doctor of Philosophy.

(2) Grateful acknowledgment is made to the donors of the Petroleum Research Fund, administered by the American Chemical Society, for support of this research.

(3) R. W. Kunze and R. M. Fuoss, *J. Phys. Chem.*, **67**, 911 (1963).

(4) H. S. Harned and B. B. Owen, "The Physical Chemistry of Electrolytic Solutions," 3rd. Ed., Reinhold Publ. Corp., New York, N. Y., 1958, p. 725.

where $S = 95.74$, $E = 60.7$, and $J = 194$. If the current theory correctly predicts the conductance through terms of order c, then a plot of Λ'' against $c^{3/2}$ should be linear (neglecting the relatively small change in log c in the $c^{3/2}$ log c term theoretically expected also). Figure 1 (note the very open ordinate scale where one ordinate unit as drawn is only 0.05 Λ-units; $\Lambda_0 = 153.67$) shows Λ'' as a function of $c^{3/2}$; it changes by only 0.059 Λ-units over the working range of concentration ($0.002 \leqslant c \leqslant 0.01$) but within the experimental error of about ± 0.015 Λ-unit, the Λ''-$c^{3/2}$ curve is linear, showing that the $c^{3/2}$ terms, while small at 0.01 N in water, are not negligible in precision work. The value of J_2, the coefficient of the $c^{3/2}$ term, from Fig. 1 is −60, which agrees with the theoretical value,[5] as it should if the functional form of the conductance equation $\Lambda = \Lambda(c)$ and the functional form of $J_2 = J_2(a)$ are correct. If the former were not correct, the deviations from the average computed straight line would be systematic; they appear to be random. The theoretical $c^{3/2}$ term includes one from the $(1 + \kappa a)$ term in electrophoresis[6] and the one from third term in the expansion of the exponential integrals in the relaxation field[7]; all others, which derive from higher terms of the equation of continuity than those which were retained by Fuoss and Onsager,[8] were neglected.

The $J_2 c^{3/2}$ term is, of course, of the same order in c as the second term in the expansion of the ion pair term, $K_A c\gamma f^2\Lambda$, where on series expansion

$$K_A c\gamma f^2\Lambda = K_A\Lambda_0 c[1 - 2\beta' c^{1/2} + O(c)] \quad (2)$$

The interaction between the J_2 terms and this term is shown by the following calculations; using the data at $D = 18.93$, $K_A = 224$, $\Lambda_0 = 46.23$, $J = 4060$ if J_2 is neglected and activities are calculated by the usual equation

$$-\ln f = \beta\kappa/2(1 + \kappa a) \quad (3)$$

where

$$\beta = \epsilon^2/DkT \quad (4)$$

If the J_2 term is retained, the values of the constants are found to be 216, 46.21, and 3860, respectively. If activities are calculated by the limiting law, $-\ln f = \beta\kappa/2$, the values 207, 46.21 and 3530 result. If activities are calculated by the equation[9]

$$-\ln f = \beta\kappa/(1 + \beta\kappa/2) \quad (5)$$

the values 245, 46.24, and 4800 result. While the limiting conductance fortunately is not sensitive to J_2 nor to the choice of the activity function, we must conclude that absolute values of association constants are uncertain to at least 10%, even in the range where the term is large enough to be precisely calculated from the data. Of course, comparisons of K_A for different salts are valid, provided the values have been computed in the same way. Pending completion of some current theoretical work which bears on this problem, we suggest that for the time being, conductance data be analyzed using eq. 1 of the previous paper with J_2 neglected and with activity coefficients calculated by the limiting law.

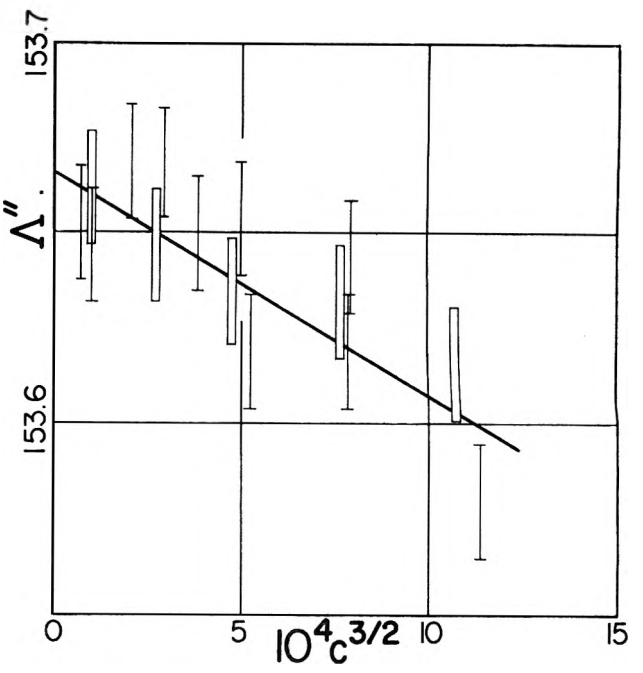

Fig. 1.—Higher terms in the conductance function.

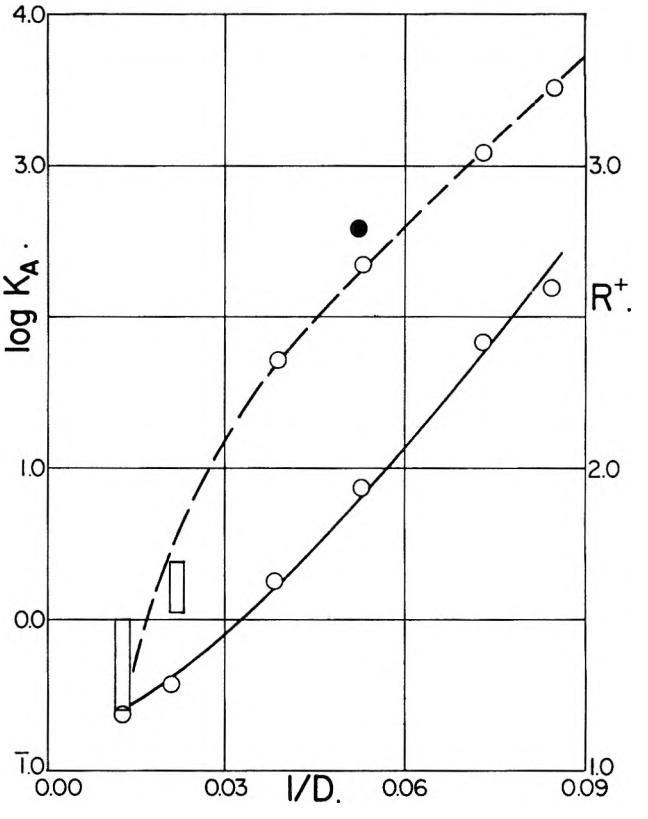

Fig. 2.—Association constants (ordinates left) and Stokes radii (ordinates right) for rubidium chloride in dioxane–water mixtures.

The value of Λ_0 obtained in water for our sample of rubidium chloride requires correction for the 0.152% impurity (see Experimental section). If w g. of impure salt are dissolved to make W g. of solution, and x_j is the weight fraction of component j ($x_1 \approx 1$), the sample contains $w\,\Sigma(x_j/M_j)$ moles of salts, where M_j is molecular weight. The molar concentration c_j of each component is given by

(5) R. M. Fuoss and F. Accascina, "Electrolytic Conductance," Interscience Publishers, New York, N. Y., 1959; eq. 14.102, 14.104. Several misprints in these equations were corrected by eq. 2 and 3 in D. S. Berns and R. M. Fuoss, *J. Am. Chem. Soc.*, **82**, 5585 (1960).

(6) Reference 5, eq. 13.49.

(7) Reference 5, eq. 13.19.

(8) R. M. Fuoss and L. Onsager, *J. Phys. Chem.*, **61**, 668 (1957).

(9) R. M. Fuoss and L. Onsager, *Proc. Natl. Acad. Sci. U. S.*, **47**, 818 (1961).

$$c_j = x_j w\rho \times 10^3/M_j W \quad (6)$$

where ρ is density. At low concentrations of strong electrolytes, we may assume approximate additivity of specific conductances, so that

$$\kappa(\text{obs.}) = (w\rho/W)\Sigma(x_j\Lambda_j/M_j) \quad (7)$$

If c_a is $10^3 w\rho/M_1 W$, the apparent concentration obtained by assuming the sample to be pure, the apparent equivalent conductance

$$\Lambda_a = 10^3\kappa_{\text{obsd}}/c_a \quad (8)$$

is found to be

$$\Lambda_a = x_1\Lambda_1 + \Sigma x_j\Lambda_j M_1/M_j \quad (9)$$

Using

$$x_1 = 1 - \Sigma x_j \quad (10)$$

and going to the limit of zero concentration (where the additivity approximations made above become rigorously valid)

$$\Lambda_{0\text{cor.}} = \Lambda_{0\text{app.}} + \Lambda_0\Sigma_2 x_j - \Sigma_2(x_j\Lambda_j{}^0 M_1/M_j) \quad (11)$$

For our material, the correction reckons to -0.102 Λ-units, which gives $\Lambda_0(\text{RbCl}) = 153.57 \pm 0.02$. This is lower than Voisinet's value[10] of 154.53 by considerably more than the experimental error of either work. No explanation of the discrepancy can be suggested. Using Λ_0 (Cl′) = 76.37, based on Lind's value[11] of 149.89 for Λ_0 (KCl) and Longsworth's values[12] of transference numbers, our value of 153.57 gives Λ_0 (Rb^+) = 77.20 which agrees very well with the value 77.25 found by Lind[13] from his measurements on rubidium bromide.

The association constants are shown in Fig. 2; as with the other alkali halides, log K_A approximates linearity in reciprocal dielectric constant in the range of low dielectric constants, but the value of $\mathring{a}_K = 6.25$ calculated from the slope seems too large. The solid point was obtained by Purlee and Grunwald[14] in 70% dioxane–water by a potentiometric method, and using the Bjerrum definition of ion pairs. Also, the Stokes radius approximates linearity in D^{-1}, but here the extrapolated value R_∞ (Rb^+) = 1.19×10^{-8} cm. seems too small. If the Sutherland[15] correction of 1.5 for slipping is made, the more reasonable value of 1.78 Å. results. As might be expected from the previous results on the other alkali halides in this solvent system, we must conclude that the sphere-in-continuum model is inadequate. At a given value of dielectric constant, rubidium chloride is more associated than the bromide[13] but for fixed anion (chloride), association increases in the sequence $K_A(\text{RbCl}) > K_A(\text{KCl})$[11] $> K_A(\text{NaCl})$,[3] that is, the largest lattice ion gives the highest amount of ion pairs at a given value of D. Similar reversals of the sequence expected on the basis of simple electrostatics, and lattice radii are reported: Fratielli[16] finds $K_A(\text{CsCl}) > K_A(\text{KCl})$ in ethanol–water mixtures, and Gordon's data[17] for salts in ethanol give $K_A(\text{KCl}) = 85$, $K_A(\text{NaCl}) = 34$, and $K_A(\text{LiCl}) = 16$.

(10) W. E. Voisinet, Thesis, Yale University, 1951.
(11) J. E. Lind, Jr., and R. M. Fuoss, *J. Phys. Chem.*, **65**, 999 (1961).
(12) L. G. Longsworth, *J. Am. Chem. Soc.*, **54**, 2741 (1932).
(13) J. E. Lind, Jr., and R. M. Fuoss, *J. Phys. Chem.*, **66**, 1727 (1962).
(14) E. Grunwald, private communication.
(15) W. Sutherland, *Phil. Mag.*, **9**, 781 (1905).
(16) A. Fratielli, Thesis, Brown University, 1962.
(17) J. R. Graham, G. S. Kell, and A. R. Gordon, *J. Am. Chem. Soc.*, **79**, 2352 (1957).

SOLUBILITY RELATIONS OF THE ISOMERIC TRICHLOROTRIFLUOROETHANES

BY H. HIRAOKA AND J. H. HILDEBRAND

Department of Chemistry, University of California, Berkeley, California

Received November 24, 1962

Solvent properties of $CCl_2F{\cdot}CClF_2$ (A) and $CCl_3{\cdot}CF_3$ (B) have been determined and compared, with the following results: Vapor pressures at 25° are: A, 361.1 mm.; B, 363.6 mm. Their variations with temperature yield the molal heats of vaporization: A, 6.86 kcal., B, 7.24 kcal., and the solubility parameters: A, 7.25; B, 7.46. Their partial vapor pressures over mixtures with $(C_4F_9)_3N$ correlate closely with the respective solubility parameters. The solubility of iodine in B is 0.283 mole % at 25°. This and the previously found solubility in A likewise agree closely with solubility parameters. A graphic representation of all available solubilities of iodine in violet solutions, paraffin solvents excepted, shows excellent correlation with the equation, $\ln a_2^s = \ln x_2 + v_2\phi_1{}^2(\delta_2 - \delta_1)^2/RT$ with the activity of solid iodine, $a_2^s = 0.256$, $v_2 = 58.5$ cc., and $\delta_2 = 14.1$. ϕ_1 is the volume fraction of the solvent.

Smith, Walkley, and Hildebrand[1] found the partial molal volume of bromine in c-$C_4Cl_2F_6$ to be 64.3 cc., but that in a mixture containing 0.6 mole % CCl_4 it had fallen to 54 cc., its value in pure CCl_4. This suggested that in the "freon" $CCl_3{\cdot}CF_3$ not only iodine but also a non-polar fluoride might find the environment more friendly than in its isomer, $CCl_2F{\cdot}CClF_2$. In any event, a comparison of these two solvents seemed well worth making.

Experimental

The $CCl_3{\cdot}CF_3$ was supplied by du Pont through the kindness of Dr. C. L. Hobbs. It was used without further purification, since its only significant impurity was claimed to be about 1% of the other isomer. The $CCl_2F{\cdot}CClF_2$ was a product of Allied Chemical and Dye Co.; the $(C_4F_9)_3N$ was from Minnesota Mining and Manufacturing Co. The two latter compounds were distilled. The two freons were degassed by repeated freezing and melting under vacuum.

Vapor pressures were measured in a simple isoteniscopic apparatus. In the case of the mixtures with the perfluoroamine, compositions were determined by the weights of the components, correcting for the weight of freon in the vapor phase.

The solubility of iodine in $CCl_3{\cdot}CF_3$ was determined from the extinction coefficient of the visible band, standardized by the extinction of solutions of known composition.

Results

Table I gives the observed vapor pressures of the two compounds. Plots of log p *vs.* $1/T$, show straight lines

(1) E. B. Smith, J. Walkley, and J. H. Hildebrand, *J. Phys. Chem.*, **63**, 703 (1959).

TABLE I

OBSERVED VAPOR PRESSURES

$CCl_3 \cdot CF_3$		$CCl_2F \cdot CClF_2$	
T, °K.	p^0 (mm.)	T, °K.	p^0 (mm.)
287.2	230.1	273.35	129.4
288.2	240.1	278.15	159.6
290.7	265.1	283.45	200.5
293.2	295.0	283.60	201.7
295.7	325.0	288.25	244.5
298.2	361.1	293.15	299.8
300.7	405.2	298.20	363.6
303.2	444.8	303.25	439.0
305.2	478.2	308.25	524.2
307.2	511.0	313.25	617.2
309.2	544.0	318.10	726.8

whose slopes give for the molal heats of vaporization, $CCl_2F \cdot CClF_2$ 6.86 kcal.; $CCl_3 \cdot CF_3$ 7.24 kcal., at 25°. We have no values of the heat capacities of liquid and vapor. We found the densities of the two liquids at 25° to be 1.5635 and 1.5654, respectively. The corresponding solubility parameters, $\delta = (\Delta E^V/v)^{1/2}$, are 7.25 and 7.46, respectively.

Table II gives vapor pressures of the two liquids

TABLE II

VAPOR PRESSURE OF TRICHLOROTRIFLUOROETHANES FROM SOLUTIONS WITH PERFLUOROTRIBUTYLAMINE AT 25°

$CCl_3 \cdot CF_3$		$CCl_2F \cdot CClF_2$	
x_2	p_2 (mm.)	x_2	p_2 (mm.)
0.277	150.5	0.452	206.9
.412	208.5	.586	250.0
.474	226.8	.587	258.3
.684	289.3	.607	258.0
.684	294.9	.712	286.7
.863	332.0	.851	314.3
.914	343.0	.918	334.0

over their mixtures with perfluorotributylamine, $(C_4F_9)_3N$ at 25°. The vapor pressure of the amine at this temperature is negligible. These pressures correspond to positive deviations from Raoult's law. When plotted as log γ_2 *vs.* ϕ_1^2 where $\gamma_2 = p_2/p_2^0 x_2$, and ϕ_1 is the volume fraction of the amine, both sets of values give straight lines with intercepts at $\phi_1^2 = 1.00$ of 0.170 for $CCl_2F \cdot CClF_2$ and 0.215 for $CCl_3 \cdot CF_3$.[2] The data thus conform to the simple solubility equation

$$\ln\gamma_2 = v_2\phi_1^2(\delta_2 - \delta_1)^2/RT \qquad (1)$$

where v_2 is the molal volume of the volatile components, 119.6 cc. in both cases. The above intercepts yield the data in Table III.

TABLE III

SOLUBILITY PARAMETERS

		$CCl_2F \cdot CClF_2$	$CCl_3 \cdot CF_3$
$\delta_2 - \delta_1$	(vap. pres.)	1.38	1.56
δ_2	(freon)	7.25	7.46
δ_1	(amine)	5.87	5.90

We see that both solutions yield the same value of δ_1 for $(C_4F_9)_3N$ well within the limit of error. Moreover, this is exactly the value obtained from its own heat of vaporization and its solvent power for iodine and various gases.[3]

(2) This method for treating the activity coefficients of volatile binary mixtures is exemplified in "Regular Solutions," by J. H. Hildebrand and R. L. Scott, Prentice-Hall, Engelwood Cliffs, N. J., 1962, pp. 149-150.

(3) Reference 2, pp. 47, 162, 172.

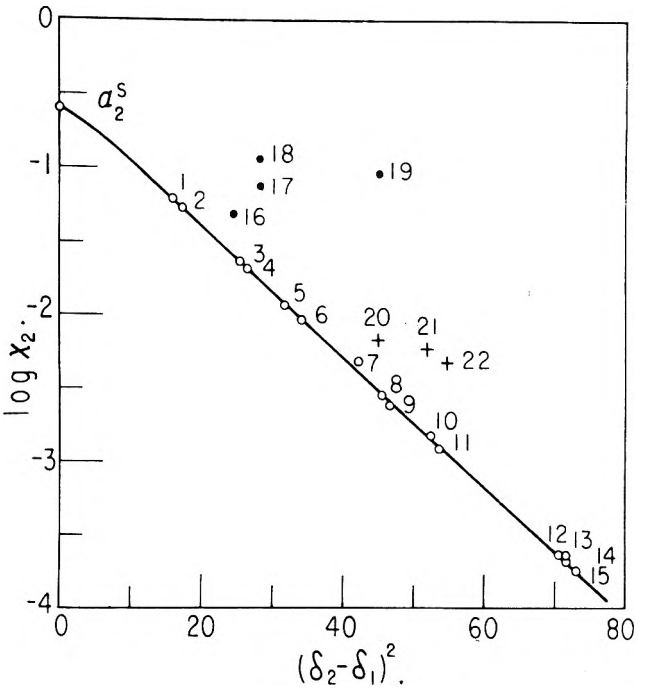

Fig. 1.—Correlation of the solubility of iodine at 25° with solubility parameters of solvents: 1, $CHBr_3$; 2, CS_2; 3, $CHCl_3$; 4, $TiCl_4$; 5, CCl_4; 6, *c*-C_6H_{12}; 7, $SiCl_4$; 8, $CCl_3.CF_3$; 9, $CCl_2F.CClF_2$; 10, 2,2,3-$C_4Cl_3F_7$; 11, *c*-$C_4Cl_2F_6$; 12, $(C_4F_9)_3N$; 13, *c*-$C_6F_{11}CF_3$; 14, *c*-$C_8F_{16}O$; 15, C_7F_{16}; 16, C_6H_6; 17, *p*-$C_6H_4(CH_3)_2$; 18, 1,3,5-$C_6H_3(CH_3)_3$; 19, $(C_2H_5)_2O$; 20, *n*-C_7H_{16}; 21, *i*-C_8H_{18}; 22, $(CH_3)_3$-CC_2H_5.

We turn next to the results of the solubility of iodine in these two freons.

Three determinations of the solubility of iodine in $CCl_3 \cdot CF_3$ at 25° yielded 0.289, 0.278, and 0.283, mean, 0.283 mole %. This is to be compared with the figure 0.245 mole % in $CCl_2F \cdot CClF_2$ obtained by Shinoda and Hildebrand.[4] Using the value 0.258 for the activity of solid iodine, the standard value heretofore used in treating all iodine solubilities, we obtain $\gamma_2 = 105$ from its solubility in the 1,1,2–1,2,2 freon and 91 in the 1,1,1–2,2,2 isomer. These figures give the parameters in Table IV.

TABLE IV

SOLUBILITY PARAMETERS FROM IODINE SOLUTIONS

	$CCl_2F \cdot CClF_2$	$CCl_3 \cdot CF_3$
$\delta_2 - \delta_1$	6.83	6.72
δ_1 (freon)	7.25	7.46
δ_2 (I_2)	14.08	14.18

The solubility parameter of iodine corresponding to its solubility in $SiCl_4$, CCl_4, $TiCl_4$, and CS_2, covering an 11-fold range in x-values, is 14.1. The solubility parameters of these two freons calculated from their heats of vaporization serve to account amazingly well for their respective solvent powers for $(C_4F_9)_3N$ on the one hand, and for I_2 on the other. This gives a clear negative answer to the question whether the more unsymmetrical freon might be a slightly better solvent for both iodine and the amine as a result of favorable orientations.

It is appropriate at this stage to give a graphic summary of all available, pertinent iodine solubilities.[5] Figure 1 shows values of log x_2 plotted against $(\delta_2 - \delta_1)^2$, with the parameter of iodine, $\delta_2 = 14.1$. The solid

(4) K. Shinoda and J. H. Hildebrand, *J. Phys. Chem.*, **62**, 292 (1958).

(5) The data are from ref. 2, pp. 164, 171 ff.

circles are for the violet solutions. The line to which they closely conform is the graph of the simple equation

$$\log a_2^s = \log x_2 + v_2\phi_1^2(14.1 - \delta_1)^2/1360 \quad (2)$$

The best fit was obtained with $a_2^s = 0.256$ and $v_2 = 58.5$ cc. These are only slightly different from the values heretofore used: 0.258 and 59.0, respectively, obtained by extrapolation to 25° of the properties of liquid iodine.

Among the aliphatic hydrocarbons, the compact molecule, cyclohexane, conforms well with the violet solvents, but the three far from compact species, heptane, 2,2,4-trimethylpentane, and 2,2-dimethylbutane, fall far off the line.

The complexing solvents, benzene, *p*-xylene, and mesitylene, deviate in order of increasing donor strength from the region on the line where they would fall if there were no complexing. The still stronger donor, ether, departs even more widely.

Acknowledgment.—We express our thanks to Dr. C. L. Hobbs and the du Pont Company for the sample of $CCl_3 \cdot CF_3$, and to the Atomic Energy Commission for its support of the project.

NOTES

THERMODYNAMICS OF LIQUID SURFACES: THE SURFACE TENSION OF DIMETHYL SULFOXIDE AND SOME DIMETHYL SULFOXIDE–ACETONE MIXTURES

By H. Lawrence Clever and C. C. Snead

Department of Chemistry, Emory University, Atlanta 22, Georgia

Received September 13, 1962

Theories of surface tension of binary mixtures succeed best when applied to symmetrical, non-polar, non-electrolytes that differ in surface tension by only a few dynes/cm. This report gives data on a polar system whose pure components differ in surface tension by about 20 dynes/cm., but involves molecules of similar size, shape, and polarity so that they may fit into each others liquid structure with a minimum of interaction.

Surface tension, density, and one heat of mixing were measured for dimethyl sulfoxide–acetone mixtures at 30°. The surface tension and density of dimethyl sulfoxide were measured at several temperatures between 20 and 60°.

Experimental

Materials.—The dimethyl sulfoxide was a sample furnished and purified by the Crown Zellerbach Corporation Research Laboratory. They heated the dimethyl sulfoxide 1.5 hr. at 120° with 1 weight % KOH, then distilled it through a packed column at reduced pressure. We fractionally crystallized the material twice just before use. Reagent grade acetone was dried over anhydrous K_2CO_3 and distilled through a packed column just before use.

Density.—Densities were determined in a 25-ml. pycnometer that had been calibrated at each temperature with distilled water.

Surface Tension.—Surface tensions were measured by the maximum bubble pressure technique on apparatus built and described by Quayle.[1] The bubbler was calibrated with highly purified samples of benzene and *n*-heptane. The dimethyl sulfoxide–acetone mixtures were prepared by volume. The surface tension bubbler air was presaturated with vapor from the liquid mixtures to prevent evaporation losses during the measurement.

Heat of Mixing.—One, relatively crude, heat of mixing was measured. The temperature increase on mixing 0.5 mole of acetone with 0.5 mole of dimethyl sulfoxide in a dewar flask was measured. The heat capacity of the resulting mixture was assumed to be the mean of the two pure liquid heat capacities. The dewar heat capacity was determined from a heat of neutralization experiment.

(1) O. R. Quayle, *Chem. Rev.*, **53**, 439 (1953).

Results and Discussion

The surface tension, density, and parachor of dimethyl sulfoxide as a function of temperature are given in Table I. The least squares line $\gamma = 45.78 - 0.1145t$, where γ is surface tension in dynes/cm. and t, centigrade temperature between 20 and 60°, reproduces the experimental surface tensions with an average deviation of 0.05 dyne/cm. Another sample of dimethyl sulfoxide fractionally distilled under reduced pressure and twice fractionally crystallized gave a surface tension 0.3 dyne/cm. higher than the results in Table I. Freezing point and other tests lead us to believe that sample might have been contaminated with as much as 1.5 mole % water. The densities check well with some reported by Schlafer and Schaffernicht.[2]

Table I

Surface Tension, Density, and Parachor of Dimethyl Sulfoxide

Temp., °C.	Density, g./cm.[3]	Surface tension, dynes/cm.	Parachor
20	1.098	43.54	182.7
25	...	42.86	182.7
30	1.0913	42.41	182.7
35	...	41.73	182.8
40	1.0816	41.17	183.0
50	1.0721	40.05	183.4
60	1.0616	38.94	183.8

Table II gives the free energy, heat content, entropy, and latent heat for forming 1 cm.[2] of new surface. The values were calculated from the surface tension and temperature dependence of surface tension[3] for both acetone and dimethyl sulfoxide. The acetone surface tensions were taken from Prucino.[4] The thermodynamic values can be converted to molar values by multiplying by the molar surface area. The molar volumes and molar surface areas, calculated assuming spherical molecules, are, respectively, 71.6 cm.[3] and 146×10^7 cm.[2] for acetone; 74.5 cm.[3] and 150×10^7 cm.[2] for dimethyl sulfoxide.

(2) H. L. Schlafer and W. Schaffernicht, *Angew. Chem.*, **72**, 618 (1960).

(3) W. D. Harkins and A. E. Alexander, Chapter XIV, "Physical Methods of Organic Chemistry," Part I, A. Weissberger, Ed., Interscience, New York, N. Y., 1959.

(4) L. J. Prucino, Ph.D. Thesis, Emory University, 1951.

TABLE II

THERMODYNAMICS OF NEW SURFACE FORMATION: COMPARISON OF ACETONE AND DIMETHYL SULFOXIDE AT 30°

	Surface free energy, ergs/cm.²	Entropy, ergs/deg./cm.²	Heat content, ergs/cm.²	Latent heat, ergs/cm.²
Acetone	22.42	0.169	73.6	51.2
Dimethyl sulfoxide	42.41	0.115	77.1	34.7

The surface tension and density of five acetone–dimethyl sulfoxide mixtures are given in Table III. The surface tensions of the mixtures indicate considerable enrichment of the surface in acetone. Excess volumes of mixing, calculated from the densities, are large, positive, and unsymmetrical, with a maximum between 0.75 and 0.50 mole fraction of acetone.

TABLE III

SURFACE TENSIONS, DENSITIES, EXCESS VOLUMES OF MIXING, AND EXCESS HEAT OF MIXING OF SOME ACETONE–DIMETHYL SULFOXIDE MIXTURES AT 30°

Dimethyl sulfoxide, mole fraction	Density, g./cm.³	Surface tension, dynes/cm.	Excess volume, cm.³/mole	Excess heat, cal./mole
0.0	0.7793	22.42	0.0	...
.10	.8003	23.02	0.8	...
.25	.8356	24.10	1.7	...
.50	.9160	26.36	1.3	−80 ± 10
.75	.9968	32.64	1.0	...
.90	1.056	36.74	0.2	...
1.00	1.091	42.41	0.0	...

Guggenheim[5,6] suggests that the surface tension of an ideal mixture obeys the single parameter symmetrical equation

$$e^{-\gamma a/kT} = x_1 e^{-\gamma_1 a/kT} + x_2 e^{-\gamma_2 a/kT}$$

where

γ_1, γ_2	are the pure component surface tensions
γ	the surface tension of the mixture
x_1, x_2	the bulk mole fraction
k	the Boltzmann constant
T	absolute temperature
a	average surface area per molecule, which for a spherical molecule is $(V/N)^{2/3}$

Figure 1 shows the results of several efforts to fit this equation to the data. Values of a tried were 24.5×10^{-16} cm.²/molecule, the average area calculated from the molar volumes; 43.5×10^{-16}, calculated from the parachor as a corresponding state molar volume at unit surface tension; 55.0×10^{-16}; and 69.6×10^{-16} cm.²/molecule. The last value forced a fit at 0.5 mole fraction. No one value fits the data well over the entire composition range. The last value fits the data within experimental error between 0 and 0.5 mole fraction of dimethyl sulfoxide, but gives too low a value of surface tension at high concentrations of dimethyl sulfoxide.

Acetone and dimethyl sulfoxide are near enough alike in size, shape, and polarity that they meet the requirements of a regular solution. The interaction energy between an acetone–dimethyl sulfoxide molecular pair

(5) E. A. Guggenheim, *Trans. Faraday Soc.*, **41**, 150 (1945).

(6) E. A. Guggenheim, "Mixtures," Clarendon Press, Oxford, 1952, Chapter IX.

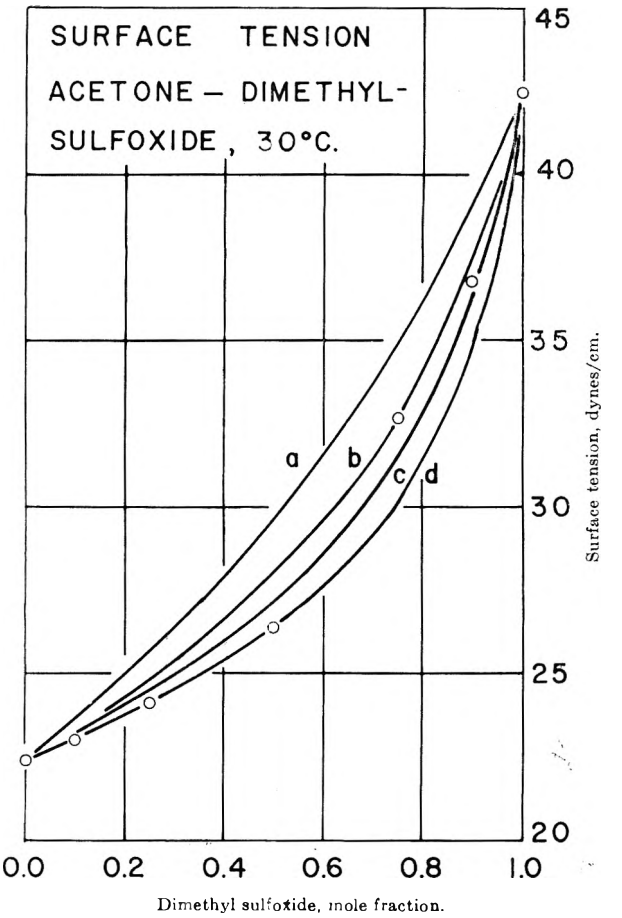

Fig. 1.—Surface tension *vs.* mole fraction dimethyl sulfoxide. The curves show the fit of the ideal solution equation with various values of surface area: curve a, 24.5×10^{-16}; curve b, 43.5×10^{-16}; curve c, 55.0×10^{-16}; and curve d, 69.6×10^{-16} cm.² per molecule.

can be calculated from the heat of mixing at 0.5 mole fraction and is 55×10^{-16} ergs. Curves aa′ of Fig. 2 show the fit when the Guggenheim[5,6] regular solution equations

$$\gamma = \gamma_1 + \frac{kT}{a} \ln \frac{x_1'}{x_1} + (x_2'^2 - x_2^2) \frac{lw}{a} - mx_2^2 \frac{w}{a}$$

and

$$\gamma = \gamma_2 + \frac{kT}{a} \ln \frac{x_2'}{x_2} + (x_1'^2 - x_1^2) \frac{lw}{a} - mx_1^2 \frac{w}{a}$$

are solved simultaneously for, γ, the mixture surface tension, and x', the surface layer mole fractions, assuming a close packed lattice with $l = 1/2$ and $m = 1/4$ and an a of 24.5×10^{-16} cm.²/molecule and w of 55×10^{-16} ergs/molecular pair. Curve a′ gives the surface composition and curve a the surface tension. Obviously the calculated surface tensions are too high. The fit is improved only several tenths of a dyne over the fit of the ideal equation with the same surface area. The fit is no better if the simple cube model is used.

The equation can be forced to fit the experimental surface tension at 0.5 mole fraction if w is increased about 13-fold to 730×10^{-16} ergs/molecular pair (1050 cal./mole). Curves bb′ of Fig. 2 show calculated values of surface tension and surface composition with the larger interaction energy. The fit to the experimental points is reasonably good over the entire composition range.

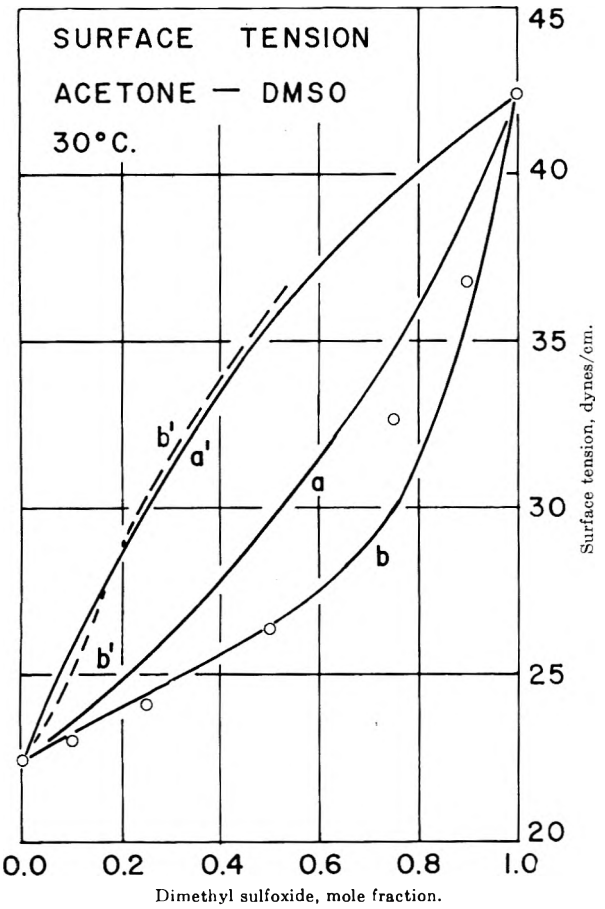

Fig. 2.—Surface tension *vs.* mole fraction dimethyl sulfoxide. The curves show the fit of the regular solution equations: curves aa′ are for an a of 24.5×10^{-16} and a w of 55×10^{-16}; curves bb′ are for an a of 24.5×10^{-16} and a w of 730×10^{-16}; curves a and b refer to bulk composition; curves a′ and b′ refer to surface composition.

Acknowledgment.—We thank Mr. William Chase for checking several of the dimethyl sulfoxide surface tensions. We thank Mr. E. M. Seidel and the Crown Zellerbach Corporation for a purified sample of dimethyl sulfoxide.

This work was supported in part by National Science Foundation Grant 7357.

DETERMINATION OF THE SEPARATION FACTOR FOR THE VAPORIZATION OF MIXTURES OF PROTIUM AND TRITIUM OXIDES

By Hilton A. Smith and Karl R. Fitch

Department of Chemistry, University of Tennessee, Knoxville, Tennessee

Received September 20, 1962

An apparatus for the determination of the separation factor accompanying the vaporization of mixtures of protium oxide and deuterium oxide has been described previously.[1] Analytical procedures by the falling drop method allowed precise determinations when appreciable fractions of the heavier hydrogen isotope were present.[2] While this transpiration apparatus is quite satisfactory for use in determining the separation factor for protium oxide–tritium oxide with tracer quantities of tritium oxide added to ordinary water, the analytical procedures previously employed are quite unsatisfactory; however, methods depending on the radiochemical nature of the tritium molecule may be used. This article describes the results of separation factor determinations using the transpiration apparatus previously described and radiochemical analyses of the equilibrium phases.

Experimental

The general method and apparatus used for saturating the nitrogen carrier gas passing over a mixture of protium and tritium oxides was identical with that already described.[1] This equipment involves four efficient equilibration units in series, with virtually no pressure drop across the saturator. As in earlier work, most of the water picked up by the nitrogen carrier gas passing through the saturator at flow rates of 15 to 25 l./hr. was condensed in a trap at 0°, with the remaining moisture removed by a chemical drying agent. The time required for collection of a liquid sample varying in volume between 0.5 and 1 ml. was from 0.5 to 3 hr., depending on the temperature of the run. The minimum quantity required for accurate analysis was 0.5 ml. It was found that best results were obtained when runs were made one after another with minimum interruption of the nitrogen flow. In fact, the first run of a series always gave a value of the separation factor which was high, and was excluded from consideration.

The apparatus used in analyzing the tritium samples was patterned after that in common use in the determination of the tritium content of urine.[3] The water sample to be analyzed was decomposed by reaction with calcium metal in an all-glass system and the tritium gas collected in a 250-ml. capacity Borkowski type ionization chamber. The chamber then was placed on a Cary Model 31 vibrating reed electrometer, and the tritium activity was measured by the rate of charge counting procedure.

The analytical apparatus was calibrated with a tritium oxide–protium oxide sample, portions of which were placed in the analytical apparatus. Various pressures of gas evolved by reaction with the calcium metal were allowed to enter the ionization chamber, and the rate of charge of the electrometer determined. A plot of the reciprocal of the time for reaching a given charge *vs.* the pressure of gas in the chamber was linear over the fourfold change in pressure studied (13 to 52 mm.). Since the separation factors to be calculated involved ratios of activities, no absolute determination of the tritium activity in a sample was necessary.

The actual procedure involved the passage of dry nitrogen through the four-stage separator and condensation of the moisture in the drying trap. Attempts to remove the moisture content of the chemical absorbers as well as the cold trap and combine the two led to erratic results, while use of the water samples collected in the cold traps only gave no difficulty as long as 0.5 ml. or more of liquid was obtained. A liquid sample corresponding to each condensed vapor sample was removed from the final stage of the saturator after each run, and was analyzed. Because of the very efficient operation of each cell of the saturator, the composition of the fourth stage was constant within experimental error throughout the run.

Experimental Calculations and Results

The separation factor, α, to be determined is given by the equation

$$\alpha = \frac{(H/T)_g}{(H/T)_l}$$

where H/T represents the atomic ratio of protium and tritium in a sample, g refers to the gaseous phase, and l to the liquid phase. Since the tritium was present in tracer quantities only, the fraction of the hydrogen in the form of protium was essentially unity in both phases, and the expression for the separation factor may be written as

(1) H. A. Smith, R. L. Combs, and J. M. Googin, *J. Phys. Chem.*, **58**, 997 (1954).

(2) R. L. Combs, J. M. Googin, and H. A. Smith, *ibid.*, **58**, 1000 (1954).

(3) J. McClelland, M. F. Milligan, B. P. Bayhurst, B. C. Eutsler, W. W. Foreman, B. M. Head, R. D. Hiebert, R. J. Watts, and W. E. Wilson, Report No. LA-1645 (Decl.), Los Alamos Scientific Laboratories, Los Alamos, New Mexico, March, 1954.

$$\alpha = \frac{(T)_l}{(T)_g}$$

In view of the fact that a plot of the reciprocal of the time of the accumulation of a given charge in the electrometer *vs.* the tritium activity of the gas in the hydrogen sample in the ionization chamber is linear, the expression for the separation factor becomes simply

$$\alpha = \frac{(t)_g}{(t)_l}$$

where t represents the time necessary to cover a set range on the electrometer scale with a constant pressure of hydrogen in the ionization chamber.

The calculated values of the separation factor at various temperatures are given in Table I.

TABLE I

SEPARATION FACTORS FOR VAPORIZATION OF MIXTURES OF PROTIUM OXIDE–TRITIUM OXIDE AT VARIOUS TEMPERATURES

t, °C.		20.03	30.01	40.02	50.00	60.01
$\alpha = \frac{(H/T)_g}{(H/T)_l}$		1.1130	1.0966	1.0760	1.0632	1.0519
		1.1136	1.0961	1.0764	1.0636	1.0521
		1.1167[a]	1.1037[a]	1.0761	1.0635	1.0521
		1.1130	1.0962	1.0761	1.0634	1.0523
		1.1132	1.0963	1.0762	1.0635	1.0521
		1.1134	1.0961	1.0761	1.0636	1.0523
		1.1151[a]	1.1054[a]			
		1.1132	1.0963			
Av. α		1.113	1.096	1.076	1.064	1.052
Stand. dev.		0.00022	0.00017	0.00014	0.00014	0.00014
Calcd.[b] α		1.108	1.095	1.075	1.065	1.055

[a] These values are not included in calculating the average or the standard deviation. [b] Calculated from the approximate equation $\alpha = \sqrt{P^0_{H_2O}/P^0_{T_2O}}$.

Discussion

It has been shown[2] that the separation factor for deuterium oxide–protium oxide mixtures is given approximately by the relationship

$$\alpha = \sqrt{\frac{P^0_{H_2O}}{P^0_{D_2O}}}$$

This expression may be derived if one assumes random distribution of the isotopic hydrogen atoms among the oxygen atoms, and hence an equilibrium constant of 4 for the reaction

$$H_2O + T_2O \rightleftarrows 2HTO$$

It is also necessary to assume that the mole fraction in the gas phase is directly proportional to the partial pressure of each component, and that Raoult's law applies to each component in the liquid–vapor equilibrium.[4] Using the same assumptions, it can be shown that for protium oxide–tritium oxide mixtures, the separation factor accompanying vaporization is approximated by the equation

$$\alpha = \sqrt{\frac{P^0_{H_2O}}{P^0_{T_2O}}}$$

The vapor pressure of tritium oxide of 98.1 mole % purity has been reported[5] over the temperature range included in the experiments reported here. The values calculated from this approximate equation are shown in the last line of Table I, and are in reasonable agreement with the experimental values, particularly considering the fact that the vapor pressure of 98.1% tritium oxide is used for that of the pure component.

It will be noted that the standard deviation of the experimental values of the separation factors would indicate a precision of approximately 0.02%, while the tabulated values suggest an accuracy of only 0.1%. This is due to the fact that the vapor samples taken for analysis were removed from the cold trap (0°) without recovery of the water from the chemical traps. Additional fractionation could occur in the cold trap, and this would lead to low values of the separation factor, the error being greater at the lower temperatures. One can calculate that the error from this source would have a maximum value of a few tenths of one per cent, and could be negligible. Furthermore, the trend in the differences between the observed values and those calculated from the approximate relationship would be in the opposite direction.

Acknowledgment.—This work was performed with funds supplied by the United States Atomic Energy Commission. The authors are grateful for this support.

(4) G. N. Lewis and R. E. Cornish, *J. Am. Chem. Soc.*, **55**, 2616 (1933).
(5) M. M. Popov and F. I. Tazedinov, *At. Energ.*, **8**, 420 (1960).

RADIOLYSIS PRODUCTS OF C_8 AND GREATER CARBON CONTENT FROM 2,2,4-TRIMETHYLPENTANE

BY J. A. KNIGHT, R. L. MCDANIEL, AND FRED SICILIO

Nuclear Sciences Division, Engineering Experiment Station, Georgia Institute of Technology, Atlanta, Georgia

Received September 25, 1962

Work current in this Laboratory is concerned with a detailed study of the radiation chemistry of branched hydrocarbons. Radiolysis products, hydrogen and hydrocarbons through C_7, from the X-irradiation (50 kvp.) of 2,2,4-trimethylpentane have been reported.[1] In addition to hydrogen, $G = 2.2$, there were 17 radiolysis products in the C_1–C_7 range, total $G \sim 5.6$. Radiolysis products C_8 and greater from the X-irradiation of 2,2,4-trimethylpentane have been investigated mainly with gas chromatographic techniques, and the results are reported in this paper.

Experimental

Materials.—The 2,2,4-trimethylpentane, Eastman, used in this work was percolated through activated alumina. The infrared spectra of the "treated" 2,2,4-trimethylpentane and of a sample of Phillips research grade material were identical. Authentic hydrocarbon samples for identification purposes were obtained mainly from Phillips, Eastman, and National Bureau of Standards. The 2,2,4,4,6,8,8-heptamethylnonane was obtained from Humphrey–Wilkinson, Inc.

X-Ray Apparatus and Irradiation Cell.—The X-ray apparatus and irradiation cell have been previously described.[1] All investigations were performed at 50 kvp. and 50 ma., at a dose rate of 8.2×10^{17} e.v./g./min. for the volumes of samples studied.

Irradiation Technique.—During the irradiations, the sample was stirred and helium gas at a known flow rate in the range of 5 to 10 ml. per min. was bubbled continuously through the hydrocarbon. This served to remove volatile radiolysis products constantly after buildup to steady-state conditions.

Hydrocarbon Radiolysis Products in the C_8 and Greater Range.—Samples of the irradiated 2,2,4-trimethylpentane were fractionally distilled with a 1.2 by 33 cm. column packed with

(1) J. A. Knight, R. L. McDaniel, R. C. Palmer, and F. Sicilio, *J. Phys. Chem.*, **65**, 2109 (1961).

Podbielniak Heli-Pak 3013 stainless steel packing. The distillations were performed very slowly in order to concentrate the radiolysis products of carbon content C_8 and greater in the final fraction.

Gas Chromatographic Analysis.—The hydrocarbon radiolysis products in the C_8–C_{10} range were analyzed with two columns, one a 28-ft. column of 25% (by weight) tri-*m*-cresyl phosphate and the other a 32-ft. column of 15% di-2-ethylhexyl sebacate. The support was 50–60 mesh Chromosorb in both cases. The gas chromatographic unit was calibrated for thermal response for each of the products identified, except as noted in Table I. Qualitative identification was made by use of retention times and enrichment techniques.

The hydrocarbon radiolysis products in the C_{11}–C_{16} range were analyzed with two columns, one a 20-ft. column of 15% Apiezon L and the other a 23-ft. column of 15% Ucon oil LB-550-X, both with 50–60 mesh Chromosorb as the solid support. The gas chromatographic unit was calibrated for thermal response to 2,2,4,6,6-pentamethylheptane, which was used in determining *G*-values for products in the C_{12} range, and 2,2,4,4,6,8,8-heptamethylnonane for products in the C_{16} range. All peak areas were measured with a planimeter.

Molecular Weight Determinations.—The higher molecular weight radiolysis product was isolated by removing the parent hydrocarbon, 2,2,4-trimethylpentane, under vacuum. Molecular weight determinations were made on this material with benzene as a solvent on a semimicro scale with a thermistor thermometer.[2] The quantity of the higher molecular weight product isolated was determined by the pressure (15 to 30 mm.) and the length of time (6–24 hr.) employed for isolation. Most of the molecular weight determinations of the radiolysis products isolated in this manner were in the range of 200–210.

Unsaturation.—Unsaturation was determined by measuring volumetrically the amount of hydrogen absorbed by a known amount of the irradiated material. Glacial acetic acid was used as the solvent, and 5% Pt on carbon was used as a catalyst. The apparatus employed was very similar to that of Ogg and Cooper.[3] It was necessary to use fairly large samples for analysis, and the most successful technique employed for introducing a large sample was the use of a sample holder similar to a separatory funnel with a pressure-equalizing tube.

Measurements were made on: (1) irradiated 2,2,4-trimethylpentane after removal of radiolysis products of carbon content less than C_8; and (2) irradiated 2,2,4-trimethylpentane after removal of radiolysis products of carbon content less than C_8 and greater than C_{12}. The difference between the two gave a measure of the unsaturation in the products of C_{12} and greater. The radiolysis products of carbon content less than C_8 were removed by slowly distilling about 1/3 of a sample through the distillation column described above. Samples from which products of less than C_8 and greater than C_{12} were removed were obtained by first removing the products of less than C_8 by thermal distillation. Then, the material remaining in the flask was vacuum distilled at 15 mm. for about 14 hr. This separated the 2,2,4-trimethylpentane along with radiolysis products in the C_8–C_{11} range from the major portion of the products of C_{12} carbon content and greater. Qualitative infrared evidence for unsaturation in the C_{12} to C_{16} range products was obtained with a Perkin–Elmer 221 spectrophotometer with a NaCl prism.

Dosimetry.—The method of dose determination has been described previously.[1]

Results and Discussion

The radiolysis products of C_8 and C_9 carbon content are listed in Tables I and II.

Radiolysis Products in the C_8–C_{10} Range.—The radiolytic saturated hydrocarbon products in the C_8–C_{10} range could form by a combination of two appropriate intermediate fragments which are derived from the parent hydrocarbon by either carbon–carbon or carbon–hydrogen bond fission. It is also possible that some C_8 products could form from 2,2,4-trimethylpentane by rearrangement processes involving a methyl group. Of the six C_8 products listed in Table I, all can be accounted for by one or the other of these modes of formation except 2,3-dimethylhexane. With the gas chromatographic conditions used, the 2,3,4-trimethylpentane and 2,3-dimethylhexane were not resolved. All five C_9 products can be accounted for by a combination of the two appropriate fragments except 2,3,5-trimethylhexane. With the gas chromatographic conditions used, the 2,4,4- and 2,3,5-trimethylpentane were not resolved. No C_{10} products were identified. One C_{10} compound, 2,2,5,5-tetramethylhexane, that might be expected as a product from a combination of two neopentyl radicals, was not detected as a radiolytic product. It could have been detected if its *G*-value had been at least 0.005. There are two possible unsaturates, 2,4,4-trimethylpentene-1 and -2, which can be formed by loss of hydrogen from the parent hydrocarbon. The *G*-values, Table II, for these unsaturates decrease with increasing dose which indicates that they are acting as scavengers.

Table I

Radiolysis Products C_8–C_9 from 2,2,4-Trimethylpentane

Product[a]	G[b]
2,2-Dimethylhexane	0.05
2,4-Dimethylhexane	.01
2,5-Dimethylhexane	.13
2,2,3,3-Tetramethylbutane[c]	.03
2,3,4-Trimethylpentane and/or 2,3-dimethylhexane	.03
2,2,3-Trimethylpentane[d]	< .005
2,2,3,4-Tetramethylpentane	.05
2,2,4,4-Tetramethylpentane	.04
2,2,5-Trimethylhexane	.025
2,2,4-Trimethylhexane	.07
2,4,4- and/or 2,3,5-Trimethylhexane	.06
Total (including 2 unknowns) =	0.53

[a] In addition there were two unidentified peaks on the chromatograms, one just before and one just after 2,2,4-trimethylhexane. These had *G*-values of 0.01 and 0.02, respectively. [b] In molecules/100 e.v.; total dose of 2.5×10^{22} e.v. for 75-ml. samples. [c] Calibration for 2,2,3,4-tetramethylpentane used for this component. [d] Tentative identification on di-2-ethylhexyl sebacate column only.

Table II

C_8 Unsaturates from 2,2,4-Trimethylpentane

	G			
	Dose[a] in e.v. $\times 10^{-22}$			
Product	1.25	2.5	5.0	7.5
2,4,4-Trimethylpentene-1	0.7	0.6	0.43	0.34
2,4,4-Trimethylpentene-2[b]	0.13	0.08	0.06	0.043

[a] Total dose for 75-ml. samples. [b] *G*-values for this compound were calculated with the calibration of 2,4,4-trimethylpentene-1.

Radiolysis Products in C_{11}–C_{16} Range.—There are at least 24 products in this range with a total *G* of 1.15 and *G*-values varying from ~0.001 to 0.36. It was possible to identify tentatively only a few of these products since authentic hydrocarbons in this range, of the types expected from the radiolysis of 2,2,4-trimethylpentane, are not available. The products identified and the *G*-values are: 2,2,4,4,6-pentamethylheptane, 0.36; 2,2,4,6,6-pentamethylheptane, 0.05; 2,2,4,4,6,8,8-heptamethylnonane, 0.03; triisobutylene, 0.05; and tetraisobutylene, 0.09.

Molecular Weight of Residual Radiolysis Product.—Molecular weight determinations were made on the radiolytic material remaining after removal of parent hydrocarbon and material volatile at 15 mm. of Hg. The values of 200–210 are in the range of C_{12} to C_{16}

(2) J. A. Knight, B. Wilkins, Jr., D. K. Davis, and F. Sicilio, *Anal. Chim. Acta*, **25**, 317 (1961).

(3) C. L. Ogg and F. J. Cooper, *Anal. Chem.*, **21**, 1400 (1949).

saturated hydrocarbons which have molecular weights of 176 and 226, respectively. These values along with the gas chromatographic analyses indicate very strongly that the highest molecular weight products, at least in the earlier stages of radiolysis, are those of C_{16} carbon content.

Unsaturation.—In addition to the identification of the two unsaturates that can be formed by loss of hydrogen from the parent hydrocarbon (Table II) and gas chromatographic evidence for triisobutylene and tetraisobutylene as radiolytic products, evidence for unsaturation in the C_8–C_{16} radiolysis products has been found by catalytic hydrogenation and infrared measurements. G-values for carbon–carbon double bond formation, respectively, for total doses of 1.5×10^{22} e.v. and 8×10^{22} e.v. were: (1) irradiated 2,2,4-trimethylpentane after removal of radiolysis products of less than C_8 content, 1.16 and 0.86; (2) irradiated 2,2,4-trimethylpentane after removal of radiolysis products of less than C_8 and greater than C_{12}, 0.83 and 0.62; and (3) C_{12}–C_{16} products (obtained by difference), 0.33 and 0.24. A comparison of these G-values with those of Table II for 2,4,4-trimethylpentene-1 and -2 shows that a major portion of the unsaturation in the C_8–C_{16} products is due to the C_8 unsaturates.

Infrared spectra of the radiolytic product of the C_{12}–C_{16} range showed that the most likely carbon–carbon double bonds present are those of the *trans* double bond, the $R_1R_2C{=}CH_2$ group and the $R_1R_2C{=}CHR_3$ group.

There are at least 40 radiolysis products in the C_8–C_{16} range from irradiated 2,2,4-trimethylpentane. Since very few authentic hydrocarbons above C_{10} of the types expected from the radiolysis of 2,2,4-trimethylpentane are available, identification of most products above C_{10} cannot be made. Comparison of the total G-values for C_8–C_{16} products, $G \sim 2.4$, with the total G-values for C_1–C_7 products, $G \sim 5.6$, shows that the processes leading to the lower molecular weight products predominate. In addition to the identification of 2,4,4-trimethylpentene-1 and -2, evidence for unsaturation in the C_8–C_{16} range was obtained from H_2-uptake measurements and infrared spectra. Molecular weight measurements on the higher molecular weight product showed that it is in the C_{12} to C_{16} range. These measurements along with the gas chromatographic analyses indicate that the largest molecular products are those due to dimerization of two C_8 components, at least in the earlier stages of irradiation.

Acknowledgment.—This work was supported in part by the United States Atomic Energy Commission, Division of Research, Contract No. AT (40-1)-2490.

RADIATION DAMAGE IN SOLID TETRAMETHYLAMMONIUM HALIDES. FREE RADICALS STABLE AT LOW TEMPERATURES[1]

BY A. J. TENCH

Department of Chemistry, Brookhaven National Laboratory, Upton, Long Island, New York

Received September 26, 1962

The electron spin resonance (e.s.r.) spectra of irradiated tetra-*n*-butylammonium iodide and bromide have been reported by Burrell.[2] The spectra consist of seven lines and have been interpreted as arising from the interaction of an odd electron with six protons. Burrell assumed that the radicals remained attached to the central, positively charged nitrogen. The e.s.r. spectra of the iodide and bromide salts were found to be very similar, in contrast to the work reported below on irradiated tetramethylammonium halides.

Experimental

Dry, powdered samples and in some cases single crystals of the recrystallized tetramethylammonium halides were sealed in silica tubes under vacuum. The halides were irradiated at 298 and 77°K. with γ-rays from a Co^{60} source. After irradiation, one end of the silica tube was thermally annealed to remove radiation defects and the sample transferred to the annealed end. The sample was maintained at 77°K. throughout this operation. The spectra were measured at either 298 or 77°K. on a Varian Model V-4501 100-kc. e.s.r. spectrometer and recorded as the first derivative. The samples were thermally annealed in a liquid bath at 148°K. for various lengths of time; the annealing processes were quenched by rapid cooling to 77°K. and the spectra then were measured at this temperature.

Results and Discussion

The e.s.r. spectra of the iodide and bromide irradiated and observed at room temperature consisted of a single line, width 30 to 40 gauss.[3] A polycrystalline sample of the chloride gave a weak complex pattern.[4] However when the halides were irradiated and examined at 77°K. considerable fine structure was observed. All the spectra observed were found to be centered about $g = 2.003 \pm 0.001$ by comparison with DPPH. The spectrum of the irradiated iodide (Fig. 1A) at 77°K. is a well resolved quartet of line width 3.5 gauss and relative peak heights of 1:2.9:2.8:1, superimposed on a low intensity broad line similar to that observed for the room temperature irradiations. The relative peak heights and the coupling constant of 21.5 gauss indicate that the quartet can be identified as a methyl radical.[5,6] When the irradiated iodide was thermally annealed at 148°K., the shape of the spectrum remained unchanged while the absorption decreased to 10% of its original value. Moreover, the spectra of an irradiated single crystal of the iodide recorded at various orientations in the magnetic field showed no differences from the spectra of the powdered samples.

The e.s.r. spectrum of the bromide (Fig. 1B) at 77°K. is very different. After thermal annealing at 148°K. the spectrum reduces to a triplet (Fig. 1C) of line width 16 gauss and a coupling constant of 23 gauss. Further annealing to 298°K. gives a single broad line. The complex spectrum in Fig. 1B can be synthesized by superimposing a quartet (a,b,c,d), corresponding to a methyl radical, on the triplet. The poor resolution of the triplet makes identification difficult. However, the relative peak heights indicate that the triplet probably results from the interaction of an unpaired electron with two protons.[7,8] The radical could be free $CH_2{\cdot}^+$, but the thermal annealing data show that the triplet is much more stable than the quar-

(1) Research performed under the auspices of the U. S. Atomic Energy Commission.

(2) E. J. Burrell, *J. Chem. Phys.*, **32**, 955 (1960).

(3) All line widths quoted correspond to the distance between the points of maximum slope of the absorption curve.

(4) A. J. Tench, *J. Chem. Phys.*, in press.

(5) B. Smaller and M. S. Matheson, *Ibid.*, **28**, 1169 (1958).

(6) C. K. Jen, S. N. Foner, E. L. Cochran, and V. A. Bowers, *Phys. Rev.*, **112**, 1169 (1958).

(7) I. Miyagawa and W. Gordy, *J. Am. Chem. Soc.*, **83**, 1036 (1961).

(8) J. F. Gibson, D. J. E. Ingram, M. C. R. Symons, and M. G. Townsend, *Trans. Faraday Soc.*, **53**, 914 (1957).

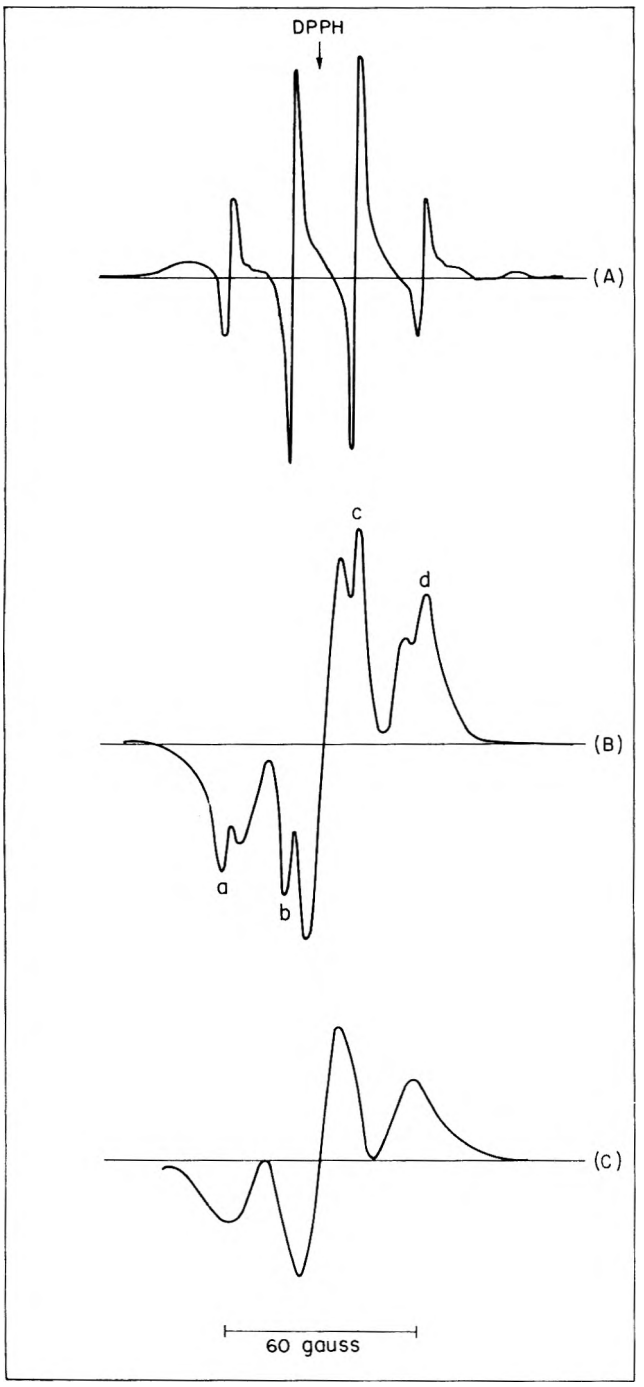

Fig. 1.—(A): The e.s.r. spectrum of $Me_4N^+I^-$ γ-irradiated and observed at 77°K.; (B) the e.s.r. spectrum of $Me_4N^+Br^-$ γ-irradiated and observed at 77°K; (C) the e.s.r. spectrum of $Me_4N^+Br^-$ γ-irradiated at 77°K. then thermally annealed at 148°K. and the spectrum observed at 77°K. All the e.s.r. spectra are first derivative curves.

tet, and this would indicate that a species such as $(CH_3)_3\overset{+}{N}CH_2\cdot$ is observed and not $CH_2\cdot^+$. Spectra taken using a single crystal of the chloride did not give an increased resolution. The microwave power was reduced to the lowest possible levels but no further fine structure could be observed in the triplet.[9] The variation of signal intensity with microwave power showed that saturation was not occurring at the low power levels used. The lines may be broadened by an unequal coupling of the unpaired electron with the two protons of CH_2 if this group is not rotating[10]—further broadening may be caused by an unresolved hyperfine interaction with the nitrogen atom. The chloride behaves very similarly to the bromide except that the methyl radical signal is only just observable and slowly anneals at 77°K. The spectra of the irradiated iodide and bromide did not change significantly after several weeks at 77°K.

The difference between the behavior of the iodide and that of the bromide and chloride is interesting. Since the crystal structures are the same and the dimensions of the unit cell are very similar,[11] the difference may be related directly to the chemical properties of the halides. The methyl radical observed in all three irradiated salts probably is formed by decomposition of an excited tetramethylammonium species. The species tentatively identified as $(CH_3)_3\overset{+}{N}CH_2\cdot$ could be formed as a result of hydrogen abstraction from the tetramethylammonium cation by bromine or chlorine atoms. Photochemical evidence[12] shows that the iodine atom cannot undergo such a reaction. No e.s.r. signal was observed from halogen atoms, and it is assumed that matrix interaction broadens the peaks beyond detection.[6]

Acknowledgment.—The author is indebted to Dr. N. Sutin for helpful discussion and comment.

(9) J. A. Simmons, *J. Chem. Phys.*, **36**, 469 (1962).

(10) E. L. Cochran, F. J. Adrian, and V. A. Bowers, *ibid.*, **34**, 1161 (1961).

(11) R. W. G. Wyckoff, *Z. Krist.*, **67**, 91 (1928).

(12) E. W. R. Steacie, "Atomic and Free Radical Reactions," Vol. II, Reinhold Publ. Corp., New York, N. Y., 1954, p. 701.

THE DENSITY OF LIQUID ARSENIC AND THE DENSITY OF ITS SATURATED VAPOR[1]

BY P. J. MCGONIGAL[2] AND A. V. GROSSE

Research Institute of Temple University, Philadelphia 44, Pa.

Received September 26, 1962

The density of liquid arsenic is difficult to measure in spite of its comparatively low melting point (1090°K.) due to the fact that the vapor pressure of arsenic at its melting point is already 35.8 atm.[3] In the present work the density of liquid arsenic and the density of its saturated vapor were measured over a range extending from the m.p. to 1323°K.

The density of liquid arsenic was determined by cathetometric measurement of the liquid level in calibrated, sealed Vycor tubes of known volume which contained a known mass of arsenic. The mass of the liquid was obtained by subtracting from the total the mass present as vapor. A total of 49 points was obtained from eight series of experiments. Least squares treatment of the data yielded the equation

$$D \text{ g./cm.}^3 = 5.80 - 5.35 \times 10^{-4}T \text{ (°K.)}$$

The probable error is ±0.02 g./cm.^{3}.

Vapor densities were determined by observing the temperature at which a known mass of arsenic vaporized completely in a sealed Vycor tube of known volume. Determinations were made at seven different tempera-

(1) This work was supported in part by the National Science Foundation under Grant 18829.

(2) A report of this work will constitute a portion of a dissertation to be submitted by P. J. McGonigal to the Graduate Board of Temple University in partial fulfillment of the requirements for the degree of Doctor of Philosophy.

(3) S. Horiba, *Z. physik. Chem.*, **105**, 295 (1922).

tures in the range of interest. The experimental vapor densities fall on a smooth curve which is best represented by the equation obtained by the method of least squares

$$D \text{ g./cm.}^3 = 0.2072 - 6.182 \times 10^{-4}T + 5.043 \times 10^{-7}T^2 \text{ (°K.)}$$

The probable error is ±0.0007 g./cm.^{3}.

A summary of the smoothed results, together with several derived quantities, is shown in Table I. The vapor pressures were calculated from Horiba's experimental data,[3] extrapolated as necessary.

TABLE I

DENSITY, ATOMIC VOLUME, AND COEFFICIENT OF CUBICAL EXPANSION OF LIQUID ARSENIC; VAPOR DENSITY AND VAPOR PRESSURE

	Liquid				
T, °K.	D, g./cm.^{3}	At. vol., cm.^{3}	Coeff. of cubical exp., $T^{-1} \times 10^6$	Vapor density, g./cm.^{3}	Vapor pressure, atm.
1090 m.p.	5.22	14.35	102.5	0.1326	35.8
1150	5.19	14.44	103.1	.1632	46.8
1200	5.16	14.52	103.7	.1916	57.6
1250	5.13	14.59	104.2	.2224	69.2
1300	5.10	14.67	104.8	.2558	83.2
1320	5.09	14.70	105.0	.2699	87.1

The experiments were carried out in a specially constructed furnace equipped with observation ports and three separate resistance windings. Temperature measurement was accomplished by three Chromel–Alumel thermocouples. The arsenic used was supplied by Penn Rare Metals, Inc., and had a purity of 99.99%. The major impurities were 0.001% Cu, 0.001% Fe, 0.004% Sb, and 0.002% Si. No detectable reaction occurred between the arsenic and the Vycor glass.

However, several tubes burst due to the high vapor pressures (about 90 atm. at 1323°K.) and extension of the measurements to higher temperatures was not considered feasible with Vycor tubes. The design of the furnace incorporated several features to minimize the danger from bursting tubes.

Arsenic is a very interesting element from the standpoint of allotropy. It exists in several solid modifications of which the gray, or metallic, form is stable at ordinary temperatures. On the basis of its physical properties Klemm[4] has termed it a "Halbmetall." Liquid arsenic is opaque but the vapor in equilibrium with it is yellow. Brewer and Kane[5] examined arsenic vapor from a Langmuir type experiment with a mass spectrometer and found it to be predominantly As_4. Stull and Sinke[6] state that according to the data of Brewer and Kane[5] there is no appreciable concentration of the As_2 species below 1000°K. The vapor densities obtained in this work are higher than those calculated from the ideal gas law assuming 100% As_4 molecules. This corroborates the predominance of the As_4 species up to 1323°K. Jolibois,[7] who determined that liquid arsenic is opaque at 1100°K., has suggested that liquid arsenic may change into a yellow transparent form (As_4) at some higher temperature. Rassow[8] has determined by direct observation that the critical temperature of arsenic is greater than 1400° and presumably the liquid is still opaque at this temperature since no information to the contrary is reported. At temperatures above 1700°K. at atmospheric pressure, the As_2 species predominates[6] in the vapor but the pressure effect on the equilibrium is unknown. Dissociation to the monatomic species appears to be unfavorable even at 3000°K. In view of the fact that arsenic is a "Halbmetall," it is not excluded that it may become nonmetallic at higher temperatures. The critical temperature of arsenic is obviously higher than that of phosphorus, 993.8°K.,[9] and probably less than that of antimony.

The density of liquid antimony recently has been measured over a wide temperature range[10] and, in contrast to typical metals (whose density *vs.* temperature behavior is in general linear up to the normal boiling point) shows significant curvature downward with increasing temperature. It is most likely that this deviation from linearity is due to structure changes in the liquid. In view of their positions in the periodic table, it is reasonable to assume that arsenic will behave in a manner similar to that of antimony. That is, at higher temperatures the usual rectilinear diameter line will begin to curve downward and significant structure changes may be expected.

NOTE ADDED IN PROOF.—We have only recently become aware of previous measurements of the density of liquid arsenic. W. Klemm, H. Spitzer, and H. Niermann, *Angew. Chem.*, **72**, 985 (1960), report five points between 830 and 850°. These points show considerable scatter and it is not possible to establish a slope from them. H. Niermann, Dissertation, Münster, 1961, reports six points between 771° (subcooled) and 960° which fall approximately on a straight line. Both sets of measurements are about 4% lower than our values.

(4) W. Klemm, *Angew. Chem.*, **62**, 133 (1950).

(5) L. Brewer and J. S. Kane, *J. Phys. Chem.*, **59**, 105 (1955).

(6) D. R. Stull and G. C. Sinke, "Thermodynamic Properties of the Elements," Advances in Chemistry Series, No. 18, American Chemical Society, Washington, D. C., 1956.

(7) P. Jolibois, *Compt. rend.*, **152**, 1767 (1911).

(8) H. Rassow, *Z. anorg. allgem. Chem.*, **114**, 117 (1920).

(9) W. Marckwald and K. Helmholtz, *ibid.* **124**, 81 (1922).

(10) A. D. Kirshenbaum and J. A. Cahill, *Am. Soc. Metals. Trans. Quart.*, **55**, 849 (1962).

GASEOUS FLUORIDES OF XENON[1]

BY MARTIN H. STUDIER AND ERIC N. SLOTH

Chemistry Division, Argonne National Laboratory, Argonne, Illinois

Received September 28, 1962

The existence of xenon tetrafluoride, first reported by Claassen, Selig, and Malm of this Laboratory,[2] has been verified further by observation of gaseous XeF_4 in the Bendix Time-of-Flight mass spectrometer.[3] Their suggestion of the existence of a lower fluoride of xenon has been confirmed by the observation of the difluoride of xenon as an independent species. In addition, a number of oxyfluorides of xenon were seen. The masses of the observed ions correspond to the formulas

Xe^+	Xe^{++}	XeO^+
XeF^+	XeF^{++}	$XeOF^+$
XeF_2^+	XeF_2^{++}	$XeOF_2^+$

(1) Based on work performed under the auspices of the U. S. Atomic Energy Commission.

(2) H. H. Claassen, H. Selig, and J. G. Malm, *J. Am. Chem. Soc.*, **84**, 3593 (1962).

(3) D. B. Harrington, "Encyclopedia of Spectroscopy," Reinhold Publ. Corp., New York, N. Y., 1960, pp. 628–647.

XeF_3^+ XeF_3^{++} $XeOF_3^+$

XeF_4^+ $XeOF_4^+$

The underlined ions probably arise from independent neutral species whereas the others are primarily fragmentation products.

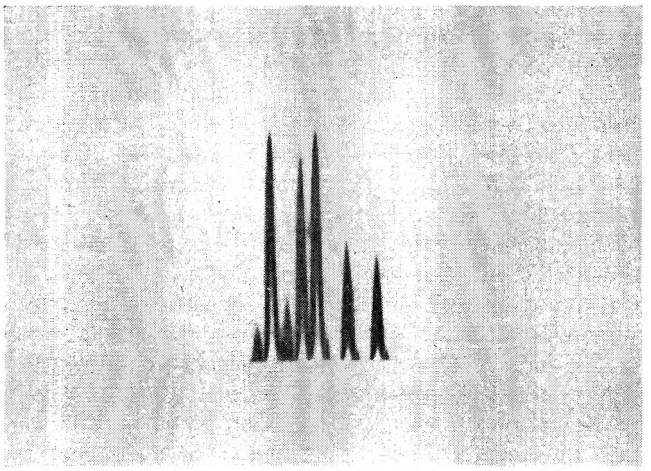

Fig. 1.—Mass spectrum of xenon.

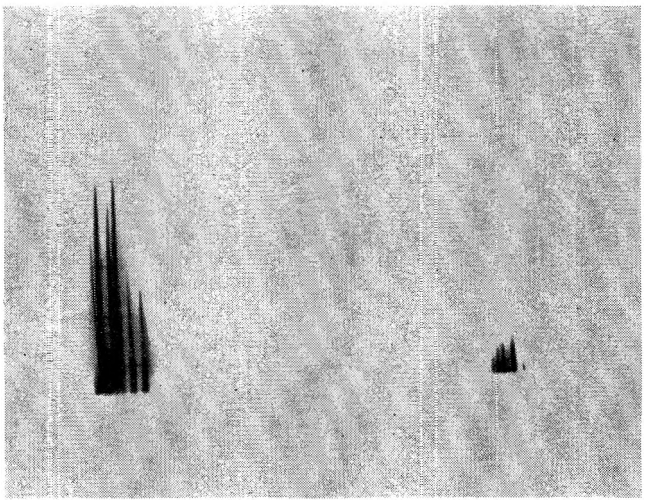

Fig. 2.—Mass spectra of xenon and mercury.

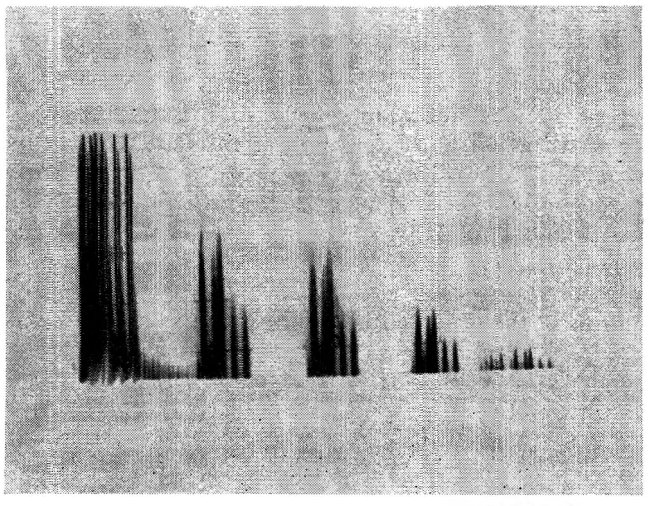

Fig. 3.—Mass spectra of xenon fluorides. Xe^+ spectra distorted because of its very large size.

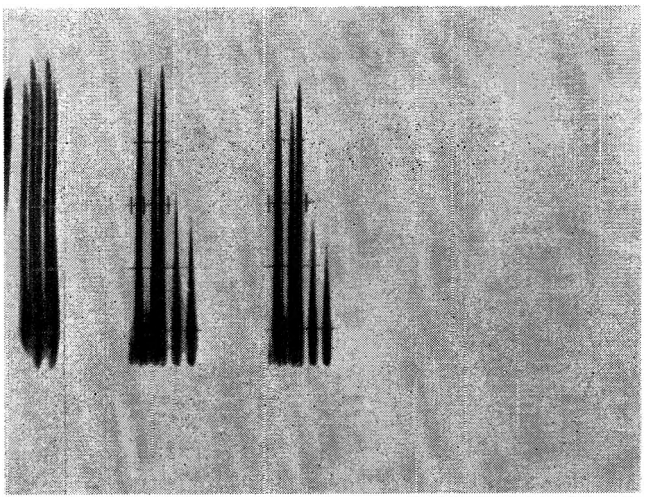

Fig. 4.—Mass spectra of XeF and XeF_2.

A 300-mg. sample of solid xenon tetrafluoride in a nickel weighing can was attached to the gas inlet system of the spectrometer. Ions produced by electron bombardment of the vapors were identified by their masses and the characteristic xenon isotopic abundance pattern (Fig. 1). Since fluorine has only one stable isotope, this pattern is preserved in fluorides of xenon. The isotopes of xenon and mercury (Fig. 2) as well as hydrocarbon peaks (which occur at every mass from impurities in the spectrometer) were used to determine precise masses. The mass spectrum of gaseous xenon fluoride ions from the sample at room temperature is given in Fig. 3. It will be noted from Fig. 3 that the abundant $Xe^{129}F_4$ (mass 205) peak occurs one mass unit higher than that of Hg^{204}, the highest stable isotope of that element. With the nickel weighing can at a temperature slightly above $-80°$ only the species XeF^+ and XeF_2^+ were observed (Fig. 4).

We conclude that XeF_2 exists as an independent species of *greater* volatility than XeF_4. The XeF_4 is probably a primary gaseous product since it has the highest mass of any fluoride observed. In addition, variation of intensity ratios with electron energy indicates that XeF^+ and XeF_3^+ were observed primarily as fragmentation products.

The residue from which the bulk of a XeF_4 sample had been removed by vacuum distillation was analyzed in a similar manner with variations in temperature, vapor pressure, and electron energy. In addition to the fluorides observed in the first sample a number of oxyfluorides were present in the spectrum. All of the species listed above were observed. Although XeO^+, $XeOF^+$, and $XeOF_2^+$ are formed by fragmentation of the higher oxyfluorides, some fractionation of $XeOF_3^+$ and $XeOF_4^+$ with respect to each other suggests that both $XeOF_3$ and $XeOF_4$ may have an independent existence. The presence of $XeOF_4$ suggests the existence of XeF_6.

Acknowledgment.—We gratefully acknowledge the coöperation of C. L. Chernick, H. H. Claassen, H. H. Hyman, J. G. Malm, and H. Selig, who supplied all samples.

THE FERROUS CHLORIDE–FERROUS BROMIDE SYSTEM AT 400°

By N. W. Gregory and Theodore Wydeven

Department of Chemistry, University of Washington, Seattle, Washington

Received September 28, 1962

It has been shown recently that $FeBr_2$ undergoes a transition in the vicinity of 360°.[1] We find evidence from X-ray powder patterns that $FeBr_2$ above the transition temperature has the same structure as $FeCl_2$, a $CdCl_2$ type ($R\bar{3}m$) with halogen ions in a cubic close-packed arrangement.[2] At room temperature, well formed crystals of $FeBr_2$ have the CdI_2 structure ($C\bar{3}m$) in which the halogen ions are hexagonally close-packed.[2] High temperature powder patterns (450 ± 20°) were taken with the rotating sample sealed in a Pyrex capillary and heated in a small furnace (with a small opening for the X-ray beam); the diffraction lines were recorded on a rotating flat photographic plate *ca.* 4 cm. from the sample. The apparatus was not designed to give cell dimensions with high precision (estimated uncertainty of 1% in d-spacings) but provided strong evidence for the structural form (Table I).

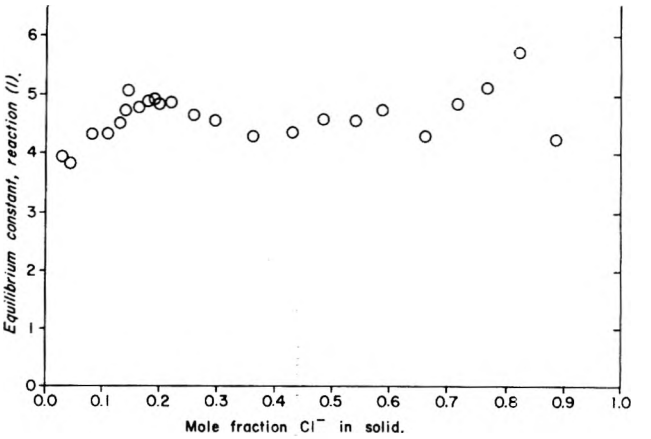

Fig. 1.—Apparent values of the equilibrium constant at various compositions of the solid phase.

$$Cl^-(\text{in solid soln. with } Fe^{+2} \text{ and } Br^-) + HBr(g) = HCl(g) + Br^-(\text{in solid soln. with } Fe^{+2} \text{ and } Cl^-) \quad (I)$$

If ionic activities are taken as mole fractions ($X_{Cl^-} + X_{Br^-} = 1$), the ratio (equilibrium constant)

Table I

Powder Pattern Data (Mo Kα Radiation) for $FeBr_2$

Indices (and cell dimensions) in parentheses are for a non-primitive hexagonal cell, comparable for the two structures

Room temperature $C\bar{3}m$ $a = 3.78$ $c = 6.20$ (18.61)					450 ± 20° $R\bar{3}m$ $a = 6.71$ (3.85) $\alpha = 33°\ 18'$ ($c = 19.0$)				
hkl	d_{obsd}	d_{calcd}	I_0	I_c (rel)	*hkl*	d_{obsd}	d_{calcd}	I_0	I_c (rel.)
002 (006)	3.16	3.10	W	20	222 (006)	3.18	3.16	M	11
					110 (012)		3.14		31
101 (103)	2.93	2.90	VS	100	211 (104)	2.76	2.74	VS	100
102 (106)	2.26	2.25	S	64	221 (015)	2.51	2.51	W	6
110 (110)	1.88	1.89	S	49	322 (107)	2.10	2.10	W	3
103 (109)	1.76	1.75	M	38	332 (018)	1.93	1.94	S	38
					$10\bar{1}$ (110)		1.93		37
201 (203)	1.57	1.58	M	47	210 (113)	1.83	1.84	VW	5
004 (0012)		1.55		13					
202 (206)	1.44	1.45	W	16	321 (116)	1.65	1.64	W	10
203 (209)	1.27	1.28	VW	12	220 (024)	1.57	1.57	M	20
					444 (0012)		1.58		7
114 (1112)	1.20	1.20	S	28	422 (208)	1.35	1.36	W	13
211 (213)		1.21		8					
212 (216)	1.15	1.15	W	14	$20\bar{1}$ (211)	1.25	1.26	VW	1
105 (1015)		1.16		11					
300 (300)	1.08	1.09	VW	20	543 (1112)	1.21	1.22	M	19
213 (219)	1.06	1.06	VW	15	431 (128)	1.10	1.11	W	12

Interatomic distances, as indicated by the non-primitive hexagonal cell parameters, do not appear to have changed significantly as a result of the transition from hexagonal to cubic close packing. A linear thermal expansion of *ca.* 2% has been assumed.

Heat capacity data for $FeCl_2$ show no evidence of a transition between room temperature and 400°.[3] Hydrogen halide exchange equilibrium data[4] provide evidence that $FeCl_2$ and $FeBr_2$ form a continuous series of solid solutions at 400°; this behavior is now easier to understand in view of the apparent isostructural character of these substances at this temperature. The equilibrium data reported earlier[4] have been re-interpreted in terms of a reaction of the form

$P_{HCl}a_{Br^-}/P_{HBr}a_{Cl^-}$ decreases from a value around 8.3 where $X_{Cl^-} = 0.05$ to 3.0 where $X_{Cl^-} = 0.9$. A much better correlation results if ionic activity coefficients of the form

$$\ln \gamma_{Br^-} = \beta X^2_{Cl^-} \text{ and } \ln \gamma_{Cl^-} = \beta X^2_{Br^-}$$

are assumed. $\beta = 0.8$ gives an average equilibrium constant of 4.6; the spread of values, calculated from each experimental measurement, is shown in Fig. 1. In simple regular solution theory, this value of β corresponds to a non-ideal interaction energy of 1150 cal. mole^{-1}. ΔF^0 for the exchange reaction agrees well with the value calculated from standard thermodynamic properties (predicted $K = 4.5$).[4] Since the temperature at which the equilibrium was studied is close to the transition temperature for $FeBr_2$, thermodynamic properties of the low temperature form were used for this comparison (ΔH_{tr} is very small).

(1) N. W. Gregory and H. E. O'Neal, *J. Am. Chem. Soc.*, **81**, 2649 (1959).
(2) A. Ferrari, A. Celeri, and F. Giorgi, *Atti accad. nazl. Lincei*, **9**, 782, 1134 (1929).
(3) F. L. Oetting and N. W. Gregory, *J. Phys. Chem.*, **65**, 138 (1961).
(4) R. O. MacLaren and N. W. Gregory, *J. Am. Chem. Soc.*, **76**, 5874 (1954).

Acknowledgment.—Financial support for this work was received from the U. S. Army Research Office.

FLUORINE N.M.R. SPECTROSCOPY. XI. CCl_2F–CCl_2F; PROOF OF OPPOSITE SIGNS FOR $J(C^{13}F)$ AND $J(C^{13}CF)$ BY SPIN DECOUPLING

By George Van Dyke Tiers

Contribution No. 243 from the Central Research Department of the Minnesota Mining and Manufacturing Co., St. Paul 19, Minnesota

Received September 28, 1962

In a study of C^{13} satellites in the n.m.r. spectra of the *cis* and *trans* isomers of dichlorodifluoroethylene[1] it was found that the "direct" and "distant" spin couplings, $J(C^{13}F)$ and $J(C^{13}{=}CF)$ were of opposite sign. In that case the relative intensities of the satellite lines varied substantially owing to the relatively large magnitudes (37.5 and 129.6 c./sec., respectively) of the fluorine–fluorine coupling constants, $J(FC{=}CF)$.

It would be of interest to make similar observations upon simple saturated fluorine compounds, for example 1,2-difluorotetrachloroethane, the chlorine addition product of the aforementioned olefin. The coupling constant, $J(FCCF)$ = 15.4 c./sec., is relatively large for fluorine atoms on adjacent saturated carbon atoms,[2–5] yet does not produce sufficient intensity differences in the weak C^{13} satellite spectrum to yield the desired information. Fortunately, as has been shown recently,[6–8] the technique of "spin decoupling" (double resonance) may be used to determine relative signs in cases that cannot be analyzed by intensity measurements. In the present case the large direct and indirect fluorine couplings to C^{13} permit a spin decoupling approach similar to that used for thallium alkyls.[8] However, owing to the low abundance of C^{13}, some additional experimental difficulties are encountered.

Experimental

A purified sample of CCl_2F–CCl_2F, furnished by the Du Pont Co., was used; from the n.m.r. spectrum it was found to contain only about 1% of the unsymmetrical isomer. A low percentage is required since the peak for CCl_3CF_2Cl lies within the region of interest. As it proved difficult to work with the supercooled neat liquid, some of the C^{13} satellite measurements were taken on 9:1 (by volume) mixtures with CCl_3F.

The n.m.r. equipment and techniques were as previously described[1,2] except that sidebands for measurement of ϕ-values were generated by amplitude modulation (AM) of the radiofrequency[9] as well as by the older frequency modulation technique.[1,2] No difference (within experimental error) was observed in ϕ-values measured by the two techniques.

The wide range of sideband frequencies accessible *via* AM includes all those required for ϕ-value measurements.[9] The virtual constancy of sideband intensity over this range is particularly noteworthy.

For the spin decoupling experiment according to the general method of Kaiser,[10] AM sidebands[9] were used, and the phase detector in a Varian-type n.m.r. integrator was employed in a circuit very similar to one recently described.[11] On the V-4300-2 instrument the probe "paddles" provide the only phasing control, and it was found that the normal leakage adjustment was unusable at the high radiofrequency power levels required for decoupling. Reasonably symmetrical absorption-mode C^{13} satellites were obtained by cautious introduction of leakage by means of the v-mode paddles, at the particular radiofrequency level used.

The radiofrequency field intensity for the decoupling experiments, H_2 = 4.06 milligauss, was chosen to be numerically approximately equal to $J/4$ (in c./sec.). As has been shown by Freeman and Whiffen,[6] when $H_2 = 2\pi J/\gamma$ (which for fluorine is $H_2 = J/4$) is employed to collapse a doublet, the "extra component" which is produced by the irradiation does not acquire substantial intensity (*i.e.*, <20%) at any stage during the approach to the correct decoupling frequency. This was important, as no diminution in the height of the exceedingly weak peaks due to C^{13} could be tolerated. The normal "field-sweeping" technique was used, and the doublet separation, s, was measured for each choice of decoupling frequency ν. For determination of the optimal decoupling frequency, ν_0, a plot of s *vs.* ν was made in which s was taken as negative when $\nu < \nu_0$. Values of ν were measured to ±1 c./sec. by a frequency counter.

The experimental points, together with several theoretical ones taken from the plot of Freeman and Whiffen,[6] lay on a smooth "S-shaped" curve for each of the readily observable outer C^{13} satellites. With good precision, the values of ν_0 were obtained from the points at which the two curves crossed their horizontal axes (*i.e.*, $s = 0$). Since the choice of $H_2 = J/4$ yields $d\nu/ds \cong 1$ within the region $\nu_0 \pm J/4$, the error (standard deviation) in each value of ν_0 is estimated as ±1.0 c./sec. In Table I are given the decoupling frequencies, and also the spectral positions of the doublet centers relative to normal CCl_2F–CCl_2F. The center separation for the inner pair of doublets could be measured with good accuracy as 35.6 ± 0.3 c./sec., but separate values for m_H and m_L were not, for instrumental reasons, obtained directly. A roundabout procedure, explained in Table I, footnote *b*, therefore was employed; it was gratifying to find 35.4 ± 1.4 c./sec for the calculated separation, in excellent agreement with the measured value.

Table I

N.M.R. Spectral Data for $C^{13}Cl_2F$–CCl_2F

Low-field C^{13} satellite	High-field C^{13} satellite
M_L[a] = −147.68 ± 0.06	M_H[a] = +160.27 ± 0.24
ν_0(L) = −165.0 ± 1.0	ν_0(H) = −177.0 ± 1.0
m_L[b] = +18.0 ± 1.0[c]	m_H[b] = −17.4 ± 1.0[c]

[a] Positions are measured relative to the strong central line for CCl_2F–CCl_2F, and refer to the neat liquid at 24.5° (supercooled). [b] Obtained by the relation $m_X = \nu_0(X) + M_X + J(FF')^2/2\nu_0(X)$. [c] By direct measurement, $|m_H - m_L| = 35.6 \pm 0.3$ c./sec., in excellent agreement with these values.

From direct measurements, together with the data of Table I, the spectral parameters reported in Table II have been calculated. As previously has been noted,[12] the apparent separation, $M_H - M_L$, requires a small correction to give $J(C^{13}F)$. For the present case, in which there is also a "distant" coupling, the "direct" carbon-13 coupling constant, in c./sec., is obtained by the formula

$$-(\text{or }+)\,J(C^{13}F) = (M_H - M_L) - J(FF')/(M_H - m_H - M_L + m_L)$$

and the "distant" coupling constant by the analogous equation

$$-(\text{or }+)\,J(C^{13}CF) = (m_H - m_L) + J(FF')/(M_H - m_H - M_L + m_L)$$

the prefixed signs being alike. The choice of sign cannot be made until the absolute sign of some coupling constant, *e.g.*, $J(C^{13}H)$, has been established. The second-order corrections tend to cancel in the calculation of the isotope shifts, and accordingly are omitted in the relations which give (in p.p.m.)

$$\Delta\phi(C^{13}F\text{–}C^{12}F) = (M_H + M_L)/80$$

$$\Delta\phi(C^{13}CF\text{–}C^{12}CF) = (m_H + m_L)/80$$

(1) G. V. D. Tiers and P. C. Lauterbur, *J. Chem. Phys.*, **36**, 1110 (1962).
(2) G. V. D. Tiers, *J. Phys. Chem.*, **66**, 945 (1962).
(3) E. Pitcher, A. D. Buckingham, and F. G. A. Stone, *J. Chem. Phys.*, **36**, 124 (1962).
(4) L. M. Crapo and C. H. Sederholm, *ibid.*, **33**, 1583 (1960).
(5) C. A. Reilly, *ibid.*, **25**, 604 (1956).
(6) R. Freeman and D. H. Whiffen, *Proc. Phys. Soc.*, **79**, 794 (1962).
(7) R. Freeman and D. H. Whiffen, *Mol. Phys.*, **4**, 321 (1961).
(8) J. P. Maher and D. F. Evans, *Proc. Chem. Soc.*, 208 (1961).
(9) L. G. Alexakos and C. D. Cornwell, private communication.
(10) R. Kaiser, *Rev. Sci. Instr.*, **31**, 963 (1960).
(11) D. D. Elleman and S. L. Manatt, *ibid.*, in press.
(12) G. V. D. Tiers, *J. Chem. Phys.*, **35**, 2263 (1961).

TABLE II

N.M.R. SPECTRAL PARAMETERS FOR CCl_2F–CCl_2F AND $C^{13}Cl_2F$–CCl_2F

Parameter	90 vol. % in CCl_3F, 21.0°	Neat, 24.5°
ϕ^*, CCl_2F–CCl_2F	$+67.842 \pm 0.007$[a]	.....
$\Delta\phi$ for impurity, CCl_3–$CClF_2$	-2.755 ± 0.010[b]	-2.819 ± 0.005[b]
$\Delta\phi$ ($C^{13}F$–$C^{12}F$)	.....	$+0.157 \pm 0.003$[b]
$\Delta\phi$ ($C^{13}CF$–$C^{12}CF$)	$+0.008 \pm 0.018$[b]	.....
$J(C^{13}F)$, c./sec.	.....	-307.26 ± 0.24[c,d]
$J(C^{13}CF)$, c./sec.	$+34.9 \pm 0.3$[c]	.....
$J(FF')$, c./sec.	15.6 ± 0.3[e]	15.40 ± 0.08[e]

[a] $\phi^*(20\%) = +67.806 \pm 0.004$ and $\phi^*(5\%) = +67.802 \pm 0.004$, from which (at inf. diln. and 21.0°), $\phi = +67.798 \pm 0.003$. [b] In p.p.m., relative to the strong line due to CCl_2F–CCl_2F. [c] Corrected for AB analysis as described in the text. [d] Sign of $J(C^{13}F)$ arbitrarily taken as negative, to emphasize reversal of sign for $J(C^{13}CF)$. [e] Sign not determined.

Discussion

It is seen from the spin-decoupling frequencies of Table I that for the saturated molecule, CCl_2F–CCl_2F, the "direct" and "distant" couplings of carbon-13 to fluorine are opposite in sign, just as had been found for its dechlorinated derivative.[1] One may predict that this reversal of sign will be found to be quite general for fluorine compounds, as is the closely related alternation of sign recently reported for fluorine–fluorine coupling constants.[13–15] The relative signs of $J(C^{13}F)$ and $J(FF')$ cannot be decided from the present evidence, but such information would be accessible by a rather similar spin decoupling technique which has been described recently.[16]

The "direct" isotope shift, $\Delta\phi(C^{13}F–C^{12}F)$, is slightly larger for the $-CCl_2F$ group than for those previously reported,[1,2,12,17] but further studies will be required to establish the generality of such structural correlations. A similar situation exists with regard to $J(C^{13}CF)$, the "distant" coupling constant, while for the "direct" one, $J(C^{13}F)$, Harris[18] has demonstrated that useful correlations can be found.

Acknowledgment.—The author wishes to thank Richard B. Calkins for the development of the spin decoupler and the associated instrumental techniques, and for the careful spectral work.

(13) S. L. Manatt and D. D. Elleman, *J. Chem. Phys.*, in press.
(14) S. L. Manatt and D. D. Elleman, *J. Am. Chem. Soc.*, **84**, 1305 (1962).
(15) D. F. Evans, *Mol. Phys.*, **5**, 183 (1962).
(16) P. C. Lauterbur and R. J. Kurland, *J. Am. Chem. Soc.*, **84**, 3405 (1962).
(17) G. V. D. Tiers, *J. Phys. Soc. Japan*, **16**, 354 (1960).
(18) R. K. Harris, *J. Phys. Chem.*, **66**, 768 (1962).

THE PARTIAL SPECIFIC VOLUME OF PROTEINS BY A MAGNETIC BALANCE TECHNIQUE[1]

BY A. M. CLARKE, D. W. KUPKE, AND J. W. BEAMS

Department of Physics and the Department of Biochemistry, School of Medicine, University of Virginia, Charlottesville, Virginia

Received October 5, 1962

Two ways of determining the density of solutions by the magnetic balance principle have been described recently.[2] Because the determinations are more rapid and the volumes of solution are much smaller than those by conventional pycnometric methods, a study of the partial specific volume, $\bar{v}$, of a number of proteins has been initiated. The possibility of achieving greater over-all accuracy by magnetic means was a further incentive, because values of $\bar{v}$ in the literature for given proteins often are so different that the corresponding molecular weights by ultracentrifugation are 10% apart or more. This report concerns data obtained with two well known proteins, ribonuclease and tobacco mosaic virus (TMV), which are near the extremes of the molecular weight spectrum for proteins. The first apparatus described in the original report was used throughout.

Experimental

Two samples of ribonuclease were measured, the Sigma Chemical Co. Type II, Lot R101B-67 (52 Kunitz units per mg.) and Type III, Lot R111B-51 (56 Kunitz units per mg.). The protein was dissolved in 0.15 *M* KCl–0.00625 *M* K_2HPO_4–0.00075 *M* KH_2PO_4, pH 7.7,[3] and the resulting solution was dialyzed against this solvent overnight before use. The molecular weight of the Type III sample has been compared in this solvent in two types of equilibrium ultracentrifuges and essentially linear plots of the logarithm of the concentration *vs.* the square of the distance to the axis of rotation were obtained.[4]

Four samples of TMV were used. These were grown by Dr. R. L. Steere of the U. S. Department of Agriculture, Beltsville, Md., and purified by the method of Boedtker and Simmons.[5] For the determination of $\bar{v}$, the virus solutions were dialyzed against 0.01 *M* ethylenedinitrilotetraacetate (Na), pH 7.5. Velocity sedimentation studies showed that dimers and higher aggregates formed with time if the virus was stored in dilute phosphate buffer or in water. The aggregates dispersed completely to yield a clean monomer boundary (181 S at 0.12 g./100 ml.) when the virus was transferred to the sequestering medium even after several weeks storage.

The concentration of the proteins was estimated at 20° in a differential refractometer at 546 mμ with the dialysate as reference solution. The refractometer was calibrated regularly before use with a sample of sucrose obtained from the National Bureau of Standards. The refractive increment for the Type III ribonuclease was obtained by determining the dry weight of equal volumes of protein solution and of dialysate after the refractometric measurements. Two separate experiments each gave a value for the increment, in this solvent, of 0.1850 ml./g.; the last digit probably is of little significance. This value was assumed for the Type II sample. For TMV, the increment of 0.194 ml./g. was used as determined by Boedtker and Simmons. Excellent agreement was obtained from the absorbancy at 265 mμ using their optical density value of 3.06 for 1 mg. of virus per ml.

For the estimation of $\bar{v}$, the densities of 0.2-ml. samples of each solution were determined several times and the averages were plotted against concentration. The precision of the readings was within a range of ±0.0002 g./ml. All observations were made at 25 ± 0.01°. The solutions were enclosed in a tightly covered, thermostated chamber containing the small permalloy float (0.042 g.) which was raised magnetically to a preselected level when viewed through a permanently mounted telescope. The support current values were translated into densities from calibration curves on liquids of known density (glass-distilled water and solutions of sucrose, NaCl and KCl) all of which were internally consistent. These currents were measured with a Leeds and Northrup Type K potentiometer with readings accurate to within 20 μv.

Results and Discussion

The densities of the ribonuclease solutions *vs.* concentration are shown in Fig. 1. The value at zero concentration is that of the dialysate; the undialyzed solvent gave the same readings within experimental error. Since the data from the two samples of ribonuclease appeared to be indistinguishable, a straight

(1) This work was supported in part by Grant No. A-3118 of the U. S. Public Health Service.
(2) J. W. Beams and A. M. Clarke, *Rev. Sci. Instr.*, **33**, 750 (1962).
(3) K. E. Van Holde and R. L. Baldwin, *J. Phys. Chem.*, **62**, 734 (1958).
(4) R. F. Bunting and P. E. Hexner, unpublished results.
(5) H. Boedtker and N. S. Simmons, *J. Am. Chem. Soc.*, **80**, 2550 (1958).

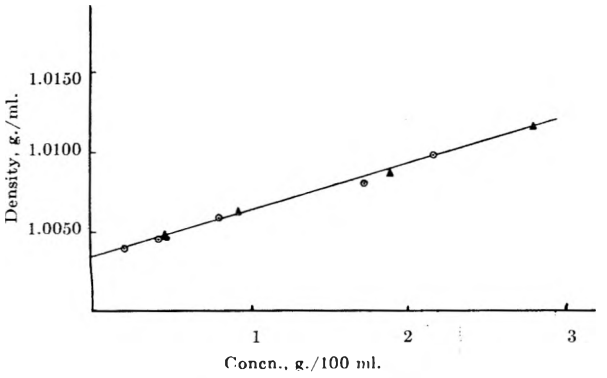

Fig. 1.—Density of ribonuclease solutions *vs.* protein concentration in 0.15 *M* KCl–0.007 *M* (K)PO_4, pH 7.7, at 25°: △, Type II sample; ⊙, Type III sample (see text).

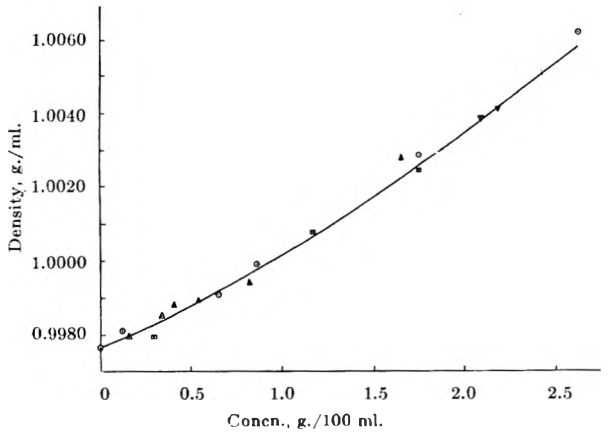

Fig. 2.—Density of TMV solutions *vs.* protein concentration in 0.01 *M* (Na)EDTA, pH 7.5, at 25°. Each symbol refers to a different preparation. A fit of data to a cubic expression is shown by the solid line.

line was fitted by the method of least squares to all the points. From the calculated slope (22.8), the value of $\bar{v}$ by the equation

$$\bar{v} = 1/\rho - 1/\rho^2 d\rho/dc$$

is 0.709 ± 0.002 ml./g. In this equation ρ is the density at $c = 0$, where c is grams of protein per 100 ml. A least squares fit to the data from the two separate samples gave values within 0.001 ml./g. of one another. This value is identical with that of Rothen[6] determined pycnometrically and with that of Brunish and Högberg[7] determined in density gradient tubes. Other values of $\bar{v}$ recorded for this protein vary from 0.693 to 0.728 ml./g.[8–10] McMeekin has suggested that this large difference in values may not reflect experimental error so much as real differences in the respective preparations.[11]

The densities for different concentrations of TMV are shown in Fig. 2. The entire curve best follows a cubic equation, both quadratic and fourth power expressions showing greater deviation. The least squares fit to the points below $c = 1.17\%$ gives a line of slope 24.5 which intercepts the observed density of the dialysate. The value of $\bar{v}$ at this limiting slope is 0.738 ± 0.002 ml./g. The slope from the least squares fit above $c = 1.2\%$ yields a value for $\bar{v}$ at the latter concentration of 0.66 ml./g. Because of the paucity of data at the higher concentrations, no limits have been assessed. Several attempts were made to obtain readings on solutions at the highest concentration indicated, but, except for the one experiment shown, the densities decreased with time; probably the TMV rods were forming an ordered lower phase as they are known to do in dilute salt solutions at these virus concentrations.[12] Values in the literature for TMV range from 0.646 to 0.77 ml./g.[13,14] Our value from the limiting slope agrees best with the average value of 0.73 ml./g. obtained by Lauffer[15] and by Bawden and Pirie.[16] It is quite possible that a dependence on concentration in the various solvents used, or the state of aggregation of the TMV, is reflected in the wide range of reported values. An abbreviated series of determinations in 0.005 *M* ethylenedinitrilotetraacetate exhibited curvature somewhat more marked than that shown in Fig. 2, whereas a series at 0.05 *M* showed no obvious curvature. Both series were carried out over the same protein concentration range as that shown in the figure. Whether the lower values of $\bar{v}$ reflect association of virus with exclusion of hydration water in solutions where the chelating agent is in limited supply must be left open. Polydispersity at the high virus concentrations could not be demonstrated clearly by velocity sedimentation. Other means are required to give a more definitive answer.

Acknowledgments.—We are indebted to Dr. R. L. Steere for the samples of purified TMV and to Mr. T. E. Dorrier for special assistance.

(6) A. Rothen, *J. Gen. Physiol.*, **24**, 203 (1940).
(7) R. Brunish and B. Högberg, *Compt. rend. trav. Lab. Carlsberg*, **32**, 35 (1960).
(8) T. L. McMeekin, M. Wilensky, and M. L. Groves, *Biochem. Biophys. Res. Comm.*, **7**, 151 (1962).
(9) W. F. Harrington and J. A. Schellman, *Compt. rend. trav. Lab. Carlsberg*, **30**, 21 (1956).
(10) J. G. Buzzell and C. Tanford, *J. Phys. Chem.*, **60**, 1204 (1956).
(11) T. L. McMeekin, personal communication.
(12) G. Oster, *J. Gen. Physiol.*, **33**, 445 (1950).
(13) I. Eriksson-Quensel and T. Svedberg, *J. Am. Chem. Soc.*, **58**, 1863 (1936).
(14) W. M. Stanley, *J. Phys. Chem.*, **42**, 55 (1938).
(15) M. A. Lauffer, *J. Am. Chem. Soc.*, **66**, 1188 (1944).
(16) F. C. Bawden and N. W. Pirie, *Proc. Roy. Soc.* (London), **B125**, 274 (1937).

SPECIFIC RATE CONSTANT FOR URETHAN CLEAVAGE

BY A. V. TOBOLSKY AND E. PETERSON

Department of Chemistry, Princeton University, Princeton, N. J.

Received October 9, 1962

In a recent study of the stress relaxation of urethan rubbers, Colodny and Tobolsky[1] found that stress decay at constant extension in the temperature range 100–140° could be expressed by the formula

$$f(t)/f(0) = \exp(-t/\tau_{ch}) \qquad (1)$$

In eq. 1 $f(t)$ is the stress measured at time t, $f(0)$ is the stress measured initially, and τ_{ch} is a constant of the system which depends on temperature. It was deduced that in the rubber network obtained by treating a hydroxy terminated ethylene–propylene adipate polyester with methyl triphenyl triisocyanate (sample II of ref. 1) the stress decay in the temperature range 100–140° was due to a cleavage of urethan linkages.[1,2]

From the data in ref. 1, it can be shown that for sample II

(1) P. C. Colodny and A. V. Tobolsky, *J. Am. Chem. Soc.*, **79**, 4320 (1957).
(2) A. V. Tobolsky, "Structure and Properties of Polymers," John Wiley and Sons, Inc., New York, N. Y., 1960, pp. 262–264.

$$\tau_{ch}\ (\text{sec.}) = 2 \times 10^{-11} \exp(-27{,}700/RT) \quad (2)$$

It will be shown that it is easy to deduce the specific rate constant for the cleavage of the urethan linkages in sample II.

The following relation is clear[3]

$$f(t)/f(0) = N(t)/N(0) \quad (3)$$

In eq. 3, $N(0)$ is the number of network chains per cc. originally present in the sample and $N(t)$ is the number of network chains per cc. which have not undergone *any* cleavage up to time t. Whether or not the urethan linkages re-form is immaterial in discussion of stress decay at constant extension.

Each network chain of sample II contains *two* urethan linkages. The rate law for $N(t)$ is

$$\frac{dN}{dt} = 2k_1N(t) \quad (4)$$

where k_1 is the specific rate constant for cleavage of the urethan linkage. (We assume all urethan linkages in sample II to be equivalent.)

Integrating eq. 3 one obtains

$$N(t) = N(0) \exp(-2k_1t) \quad (5)$$

Inserting eq. 5 into eq. 3 there results

$$f(t)/f(0) = \exp(-2k_1t) \quad (6)$$

Comparing with eq. 1 and 2, we obtain an expression for the specific rate constant for urethan cleavage

$$k_1 = 1/2\tau_{ch} = 2.5 \times 10^{10} \exp[-27{,}700/RT] \quad (7)$$

It is to be noted from this expression that τ_{ch} is independent of the actual concentration of network chains and hence independent of the molecular weight of the original polyester. Of course, expression 7 is valid only for the urethan linkages of sample II, *i.e.*, those produced by treating aliphatic primary hydroxyl with methyl triphenyl trisiocyanate. Also, eq. 7 is written as if the cleavage of the urethan linkage is unimolecular. It may be that the cleavage is actually a bimolecular reaction involving the urethan linkage and an unknown concentration of catalyst (*e.g.*, amine). If this is so k_1 is to be regarded as a pseudo first order constant.

Another urethan rubber (sample IV) was discussed in ref. 1. This was obtained by treating the same ethylene–propylene polyester with excess 2,4-toluene diisocyanate to form isocyanate terminated "prepolymer." This prepolymer was cured to a three-dimensional network by reaction with 1,2,6-hexanetriol.

In this network (sample IV) each network chain contains *four* urethan linkages.

If the urethan linkages of sample IV were identical with those of sample II, it is clear from equations analogous to (5), (6), and (7) that $\tau_{ch}(II)/\tau_{ch}(IV)$ should equal 2.3.

In actual fact, the ratios of $\tau_{ch}(II)/\tau_{ch}(IV)$ at 100, 120, and 140° were 1.32, 1.44, and 1.44, respectively. We have no right to expect that the cleavage rates of the slightly different urethan linkages formed in sample II and sample IV are exactly identical, but the fact that $\tau_{ch}(II)/\tau_{ch}(IV)$ is so close to the ideal value of 2.0 is very gratifying.

(3) A. V. Tobolsky, ref. 2, pp. 208–209, 233.

Acknowledgment.—We appreciate valuable discussions with Drs. R. Gobran and M. Berenbaum. The partial support of the Office of Naval Research is gratefully acknowledged.

PHOTOLYSIS OF ALKYL NITRITES. THE PRIMARY PROCESS IN *t*-BUTYL NITRITE AT 3660 Å.

BY G. R. MCMILLAN[1]

Celanese Chemical Co., a Division of Celanese Corporation of America, Clarkwood, Texas

Received October 13, 1962

Recent interpretations of photolysis of alkyl nitrites include decomposition to alkoxy radicals and nitric oxide as an important primary process.[2–6]

In the supposedly continuous region of absorption (strong below 3000 Å.), the primary process in *t*-butyl nitrite is best written

$$(CH_3)_3CONO + h\nu \longrightarrow \alpha_0(CH_3)_3CO^* + [1 - \alpha_0](CH_3)_3CO + NO$$

with a probable primary quantum yield, φ, of unity.[6] The excited *t*-butoxy radicals decompose rapidly to acetone and methyl.

The primary quantum yield of alkyl nitrite photodecomposition following absorption of light in the banded region (3200–4000 Å.) is less certain, but is known to be high.[2,5] Gray and Style[2] estimated a primary quantum yield of 0.32 for methyl nitrite but it was not possible to take into account recombination of methoxy radicals and nitric oxide.

Excited molecule mechanisms have not been considered, possibly because the bands were described by Thompson and Purkis[7] as diffuse. However, the appearance of the spectrum of a polyatomic molecule is no sure guide to photochemical behavior, and it seemed possible to obtain a direct estimate of the primary yield by measuring the photochemical exchange between *t*-butyl nitrite and nitric oxide.

Experimental

t-Butyl nitrite was prepared as before.[6] Nitric oxide containing 96% $N^{15}O$ was obtained from Isomet Corporation, Palisades Park, New Jersey.

The volume of the quartz photolysis cell was 210 ml. The volume of cell plus connecting tubing was 252 ml.

A 5-mm. thickness of Corning Glass 5860 isolated the mercury lines near 3660 Å. Light of 2537 Å. was obtained with the filter used before.[6] The light intensity at 3660 Å. was measured with the potassium ferrioxalate actinometer,[8] taking $\Phi = 1.21$. The intensity absorbed by the nitrite was calculated by the usual methods.[9] The light beam was monitored with a GE 935 phototube and a pen recorder.

Isotopic analysis was based on the 88/89 peak ratio in the mass spectrum of the nitrite.

(1) Evans Chemical Laboratory, The Ohio State University, Columbus 10, Ohio.

(2) J. A. Gray and D. W. G. Style, *Trans. Faraday Soc.*, **48**, 1137 (1952).

(3) P. Tarte, *Bull. soc. roy. sci. Liege*, **22**, 226 (1953).

(4) P. L. Hanst and J. G. Calvert, *J. Phys. Chem.*, **63**, 2071 (1959).

(5) P. Kabasakalian and E. R. Townley, *J. Am. Chem. Soc.*, **84**, 2711 (1962).

(6) G. R. McMillan, *ibid.*, **84**, 4007 (1962).

(7) H. W. Thompson and C. H. Purkis, *Trans. Faraday Soc.*, **32**, 1466 (1936).

(8) C. G. Hatchard and C. A. Parker, *Proc. Roy. Soc.* (London), **A235**, 518 (1956).

(9) A. Farkas and H. W. Melville, "Experimental Methods in Gas Reactions," Macmillan and Co., London, 1939, p. 247; R. E. Hunt and T. L. Hill, *J. Chem. Phys.*, **15**, 111 (1947).

At low pressures of *t*-butyl nitrite and nitric oxide, no exchange of nitrite was observed in blank experiments carried out in a darkened room. The nitric oxide did show dark exchange, yet the N^{15} did not appear in the nitrite. Evidently the nitrite contains an impurity (0.5 to 2%) which undergoes fast dark exchange with nitric oxide but not with *t*-butyl nitrite. The impurity could not be removed by distillation and was not detected by gas chromatography. In the experiments at 2537 Å., a small correction was necessary for exchange due to the small amount of λ 4047 Å. light transmitted by the filter.

Results

A few experiments were carried out at 25° and 2537 Å., using pressures of nitrite and nitric oxide of 14.5 mm. The quantum yield of combination of *t*-butoxy radicals and nitric oxide should be 0.16 under these conditions if the proposed mechanism[6] is correct. The observed quantum yields of exchange were 0.3, 0.7, and 0.7. The excess may be due to dark exchange between *t*-butyl nitrite and some reaction product, nitrosomethane, for example, derived from methyl radicals formed by decomposition of excited *t*-butoxy.

The quantum yield of acetone at 3660 Å. (temperature, 25°; nitric oxide, 14.5 mm.; nitrite, 14.5 mm.) was found to be 0.03, 0.04, and 0.04. This may be compared with 0.84 at 2537 Å. under these conditions.[6] Dark exchange with reaction products may thus be a small effect at 3660 Å. The observed photochemical exchange under different conditions at 3660 Å. is included in Table I.

TABLE I

PHOTOLYSIS OF $(CH_3)_3CONO$ IN THE PRESENCE OF $N^{15}O$

λ, 3660 Å.; *T*, 25°; incident light intensity, ~5 × 10^{15} quanta/sec.

P_{NO}, mm.	$P_{Nitrite}$, mm.	Time, sec.	% Exch. found	% Exch. theoret./φ	φ
14.5	14.5	540	1.68	1.72	0.98
14.5	15.5	600	1.65	1.85	.89
14.5	17.5	900	2.44	2.44	1.00
14.5	32.5	1200	2.07	2.15	0.96
14.5	33.5	1200	2.14	2.09	1.02
40.5	14.5	540	1.65	1.66	0.99
44.0	16.5	900	2.58	2.61	.99

Discussion

Ignoring for the present the small amount of acetone formed, the main reactions in the system at 3660 Å. are

$$(CH_3)_3CONO + h\nu \longrightarrow (CH_3)_3CO + NO \quad (1)$$

$$(CH_3)_3CO + NO \longrightarrow (CH_3)_3CONO \quad (2)$$

Re-formation of nitrite accounts for the observation that prolonged illumination of *t*-butyl nitrite with 3660 Å. radiation led to no net decomposition.[10] Decomposition of primary and secondary nitrites did occur,[10] presumably because disproportionation is possible between primary or secondary alkoxy radicals and nitric oxide.

Based on reactions 1 and 2, the quotient % exchanged (theoretical)/φ may be calculated and divided into the observed % exchange to give the primary quantum yield. The mean value of φ is 0.98 with an uncertainty not easily estimable. Possibly the acetone quantum yield, 0.04, should be added to the photo-exchange quantum yield. But if the view is correct that rapid dark exchange takes place between *t*-butyl nitrite and nitrosomethane (or derivatives thereof), the small portion of the primary process ultimately yielding acetone may already be counted in the photo-exchange.

No firm conclusions can be drawn about the source of the small amount of acetone. In consistency with the low wave length results,[6] the acetone may be ascribed to decomposition of excited *t*-butoxy radicals. This does not require that excited radicals be formed by absorption of light in the bands; the few excited radicals may be formed by absorption in the weak continuum underlying the bands.

The results on *t*-butyl nitrite might be summarized by noting that the primary process following light absorption in the bands or in the "continuum" is dissociation to a *t*-butoxy radical and nitric oxide, with a probable primary quantum yield of unity. The net photochemistry is different in the two regions because of the increased importance of decomposition of excited *t*-butoxy radicals at lower wave lengths.

(10) H. W. Thompson and F. S. Dainton, *Trans. Faraday Soc.*, **33**, 1546 (1937).

DIFFUSION OF TRITIATED WATER ($H^3H^1O^{16}$) IN AGAR GEL AND WATER

BY F. S. NAKAYAMA AND R. D. JACKSON

U. S. Water Conservation Laboratory, Tempe, Arizona

Received October 26, 1962

The "self-diffusion" coefficients of liquid water are of interest in that they may be used to ascertain the structural properties of liquid water.[1] These coefficients are by necessity determined by isotopic tracer techniques. Wang, *et al.*,[2] by use of a diffusion capillary technique, determined the diffusion coefficient of tritiated water ($H^3H^1O^{16}$) in ordinary water at 25°. Their value of 2.44 ± 0.057 × 10^{-5} cm.^{2} sec.$^{-1}$ is widely accepted, although it is the only reported value known to the authors. We have determined the coefficient using a different technique and obtained a value of 2.41 ± 0.055 × 10^{-5} cm.^{2} sec.$^{-1}$, which agrees with Wang's value within the error of the experiment.

Experimental

The method consisted of determining the diffusion coefficient of tritiated water in low concentrations of gel and getting the coefficient in liquid water by extrapolating to infinite dilution of gel. Working with gel material minimized error caused by non-diffusional movement of the liquid resulting from mechanical shock and vibrations.

Four low concentrations (0.3, 0.5, 0.75, and 1.0% by weight) of steam-sterilized agar-agar solutions in duplicate were allowed to set in cylinders 1.9 cm. i.d. by 12 cm. long. The cylinders were constructed so that incremental 1-cm. sections could be separated easily at the end of a diffusion run. A 1.9-cm. filter-paper disk was placed in contact with one end of the sample and treated with 0.01 ml. of a 100 μc./ml. tritiated water solution. The sample was sealed and stored at 25 ± 1° for 48 hr., and then sectioned. Water was extracted from the gel by vacuum dehydration, and the activity of the $H^3H^1O^{16}$ in the extracted water was determined by the liquid scintillation technique.[3] The diffusion coefficient was calculated by obtaining the ratio of the activity (A_x) in the column from $x = 0$ to $x = x$ to the total activity (A_T) in the column. Assuming a semi-infinite column, this ratio is equal to the integral of the instantaneous plane source solution of the general diffusion equation. That is

$$A_x/A_T = \text{erf}\, x(4Dt)^{-1/2}$$

(1) J. H. Wang, *J. Am. Chem. Soc.*, **73**, 510 (1951).

(2) J. H. Wang, C. V. Robinson, and I. S. Edelman, *ibid.*, **75**, 466 (1953).

(3) F. E. Kinard, "A Liquid Scintillator for the Analysis of Tritium in Water," Atomic Energy Comm. Rept. DP-190, 1956.

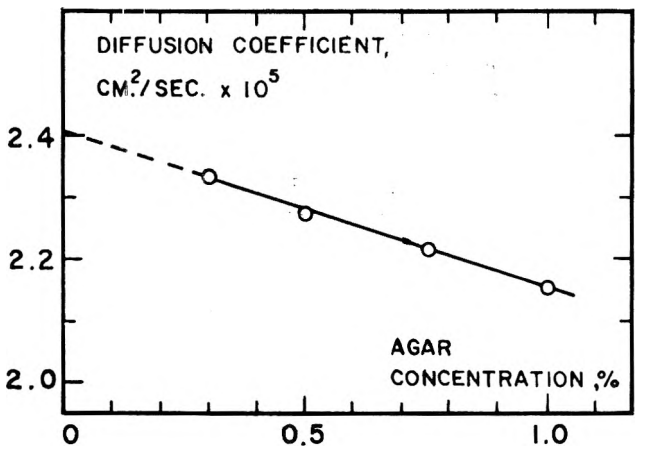

Fig. 1.—Diffusion coefficient of tritiated water in agar gel at different concentrations.

The assumption of a semi-infinite column was validated in that tracer activity was not present in the untreated end within the 48-hr. exposure period. An average diffusion coefficient was taken from the calculation for the first five 1-cm. sections of each column.

Results

The diffusion coefficients of $H^3H^1O^{16}$ measured at four agar gel concentrations are presented in Fig. 1. A linear regression equation was calculated for this relation from which a value $D = 2.41 \pm 0.055 \times 10^{-5}$ cm.² sec.$^{-1}$ was determined for the diffusion coefficient of tritiated water in ordinary water. This value compares favorably with the results of Wang, *et al.*[2]

THERMODYNAMIC PROPERTIES OF THE ATMOSPHERIC GASES IN AQUEOUS SOLUTIONS[1]

BY CORNELIUS E. KLOTS AND BRUCE B. BENSON

Department of Physics, Amherst College, Amherst, Massachusetts

Received April 18, 1962

Recent precision determinations of the solubility coefficients of nitrogen, oxygen, and argon in distilled water[2] permit straightforward evaluations of certain thermodynamic properties of these solutions. Their magnitudes are of interest as an indication of the "iceberg" structures surrounding the solute molecules in water.[3] A previously unreported relationship among these properties has now been obtained which supports previous ideas and offers a means of testing detailed models of these structures.

Experimental

The solubility measurements covered the temperature range 2–27°. Both manometric determinations of the absolute solubilities and mass spectrometric measurements of solubility ratios for a pair of gases were made, the two techniques giving identical results. These methods and the solubility coefficients are reported elsewhere.[2]

Results

The derived partial molal enthalpies and entropies of solution and the partial molal heat capacities in solution are given in Table I. They are in good agreement with previously reported values based upon more qualitative solubility data.[4] A precision of 0.1% in the solubility measurements permitted the graphical evaluation of these data with an estimated error of 1% for the enthalpies and entropies and 10% for the heat capacities. Relative values for different solutes are, however, considerably more accurate. Thus, for example, the identical values of the partial molal heat capacities reflect a relationship revealed in this work and exhibited in Fig. 1 and 2. Plots of $\ln[K(N_2)/K(Ar,O_2)] = \ln[\alpha(Ar,O_2)/\alpha(N_2)]$ *vs.* $1/T$, where the K's are the Henry's law constants and the α's are the Bunsen solubility coefficients, give excellent straight lines. The standard deviations are 0.16% in the case of oxygen and 0.10% for argon. The nitrogen solubility coefficients employed for this purpose were the result of thirty-two absolute measurements throughout the full temperature range.

Discussion

The observed entropies of solution and the enormous partial molal heat capacities give substance to the iceberg picture of aqueous solutions[3] which envisages this heat capacity as arising largely from the melting of an ice-like structure surrounding each solute molecule. This view has proved a useful one[5] and has been extended to larger molecules of biological importance.[6,7] Recent N.m.r. investigations reveal, however, that the situation is not so simple.[8,9] The present results therefore are of interest as they suggest an approach to this intriguing and important problem of the structural modifications in aqueous solution.

The slopes of Fig. 1 and 2 are related to $\Delta(\Delta H) = \Delta H(N_2)_{soln.} - \Delta H(O_2,Ar)_{soln.}$ and imply that these quantities are constant throughout the temperature range studied despite the fact that the individual enthalpies of solution display a pronounced temperature dependence. This suggests that the "icebergs"

TABLE I

HEATS AND ENTROPIES OF SOLUTION AS FUNCTIONS OF TEMPERATURE (BASED ON A HYPOTHETICAL STANDARD STATE IN SOLUTION OF UNIT MOLE FRACTION)

$\Delta C_p = C_p(M)soln. - C_p(M)gas$

T, °C.		2	5	10	15	20	25
$-\Delta H$ (cal./mole)	N_2	4190	3650	3260	2950	2695	2520
	O_2	4560	4020	3630	3320	3065	2890
	Ar	4510	3970	3580	3270	3015	2840
$-\Delta S$ (cal./mole-deg.)	N_2	36.9	34.9	33.5	32.5	31.6	31.0
	O_2	36.8	34.8	33.4	32.4	31.5	30.9
	Ar	36.4	34.4	33.0	32.0	31.1	30.5
ΔC_p (cal./mole-deg.)	N_2, O_2, Ar	161	120	76	59	46	33

for these solutes are virtually identical at any given temperature. Small differences in the enthalpies (and entropies) of solution are then due solely to the process of introducing the solute molecule into its ice-like cage. Thus one may write: $\Delta H(M)_{soln.} = \Delta H(\text{iceberg}) + \Delta H(M)_{cavity}$. Here the first term on the right represents the heat of formation of the iceberg and is strongly temperature dependent; the second term arises from the introduction of the solute molecule (M)

(1) This work was supported by the National Science Foundation under Grant NSF-G9437.

(2) C. E. Klots and B. B. Benson, *J. Marine Res.*, **21**, 48 (1963).

(3) (a) H. S. Frank and M. W. Evans, *J. Chem. Phys.*, **13**, 507 (1945); (b) W. F. Claussen and M. F. Polglase, *J. Am. Chem. Soc.*, **74**, 4817 (1952).

(4) D. M. Himmelblau, *J. Phys. Chem.*, **63**, 1803 (1959).

(5) (a) H. S. Frank and W. Y. Wen, *Discussions Faraday Soc.*, **24**, 133 (1957); (b) H. S. Frank, *Proc. Roy. Soc.* (London), **A247**, 481 (1958).

(6) I. M. Klotz, *Science*, **128**, 875 (1958).

(7) I. M. Klotz and S. W. Luborsky, *J. Am. Chem. Soc.*, **81**, 5119 (1959).

(8) E. A. Balazs, A. A. Bothner-By, and J. Gergely, *J. Mol. Biol.*, **1**, 147 (1959).

(9) F. A. Bovey, *Nature*, **192**, 324 (1961).

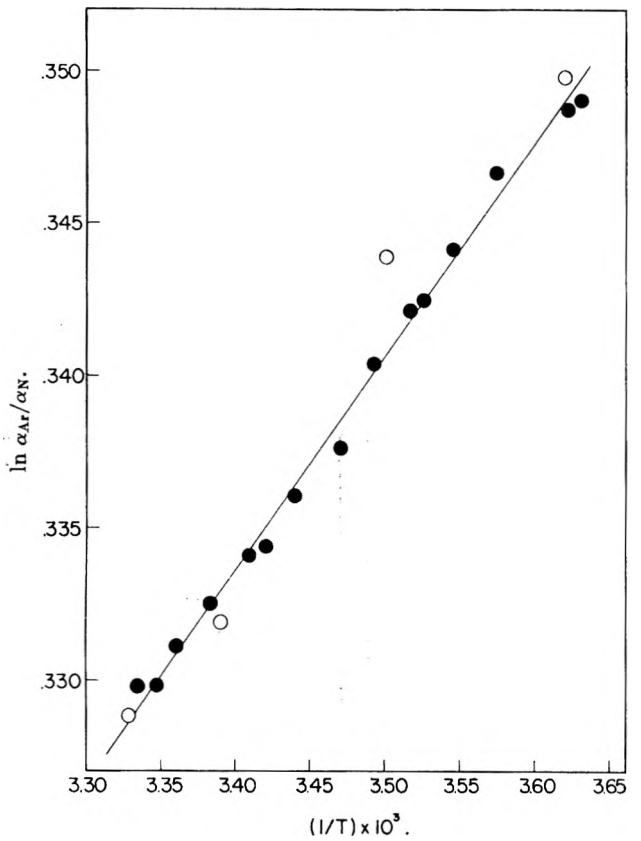

Fig. 1.—Experimental determinations of the ratio of the solubility coefficients of argon and nitrogen as a function of temperature: open circles, mass spectrometric ratio measurements; closed circles, manometric measurements.

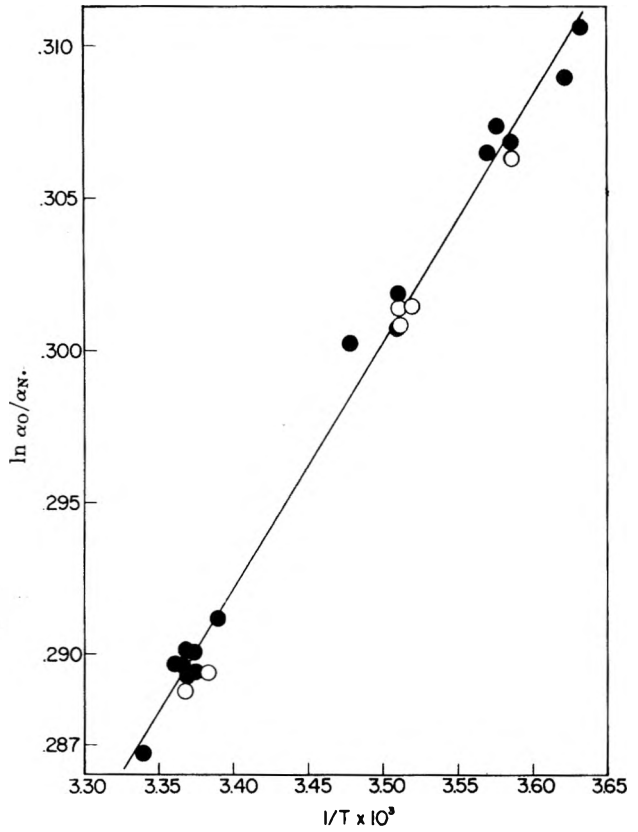

Fig. 2.—Experimental determinations of the ratio of the solubility coefficients of oxygen and nitrogen as a function of temperature: open circles, mass spectrometric ratio measurements; closed circles, manometric measurements.

into its cavity and is probably relatively insensitive to temperature.

A detailed iceberg model should permit evaluation of these terms independently. The small differences in the solute-dependent term will then serve as a sensitive test of the model. It has been suggested[10] that a cell theory approach should be useful for this purpose. Solubility isotope effects with oxygen and nitrogen, for example, indicate a slightly larger free volume for the oxygen molecule, properly reflecting its smaller "hard-sphere" diameter and consistent with the entropies of solution reported here. A further correlation between solute force constants and thermodynamic data of the present type has been noted previously.[4]

The present data also illustrate unambiguously that a previous notion[11] of a *unique* water–oxygen complex is untenable. A recent communication[12] suggesting a more general interaction of the contact charge transfer type is reasonable. The existence of a shifting equilibrium among more than one "kind" of iceberg is, however, not excluded and may be indicated by the temperature-dependent absorption spectrum.[11]

(10) C. E. Klots and B. B. Benson, *J. Chem. Phys.*, in press.
(11) L. J. Heidt and A. M. Johnson, *J. Am. Chem. Soc.*, **79**, 5587 (1957).
(12) J. Jortner and U. Sokolov, *J. Phys. Chem.*, **65**, 1633 (1961).

SOLUTION STRUCTURE IN CONCENTRATED NON-IONIC SURFACTANT SYSTEMS

By J. M. Corkill

Basic Research Dept., Procter & Gamble Ltd., Newcastle-upon-Tyne, England

and K. W. Herrmann

Miami Valley Laboratories, The Procter & Gamble Company, Cincinnati, Ohio

Received August 31, 1962

The X-ray diffraction patterns obtained from moderately concentrated anionic surfactant solutions led Mattoon, Stearns, and Harkins[1] to suggest that in addition to micelle formation, a second structural transition took place in these solutions. The existence of this change has also been demonstrated by other techniques, notably viscosity and diffusion coefficient[2,3] measurements. The interpretation of the X-ray patterns is still a matter of discussion[4]; however, it is generally agreed that an increase in order in the solution takes place above the second transition region.

In this paper, the results of light scattering and X-ray measurements on aqueous solutions of the dimethyloctyl and dimethyldodecylamine oxides (C_8AO and $C_{12}AO$) are described. These results are discussed in terms of the structural changes that occur above the critical micelle concentration (c.m.c.), but below the concentration at which a mesomorphic (middle) phase separates. Although the amine oxides can show cationic character below pH 7, the surfactant is completely non-ionic under the conditions employed.[5]

Experimental

Light Scattering Measurements.—Turbidities were determined with a commercial apparatus (Phoenix Precision Instrument Company) similar to that described by Brice, *et al.*[6] The narrow

(1) R. W. Mattoon, R. S. Stearns, and W. D. Harkins, *J. Chem. Phys.*, **15**, 209 (1947).
(2) R. J. Vetter, *J. Phys. Chem.*, **61**, 262 (1947).
(3) K. Tyuzyo, *Koll. Z.*, **175**, 40 (1961).
(4) G. W. Brady, *J. Chem. Phys.*, **12**, 1547 (1951).
(5) K. W. Herrmann, *J. Phys. Chem.*, **66**, 295 (1962).
(6) B. A. Brice, M. Halwer, and R. Speiser, *J. Opt. Soc. Am.*, **40**, 768 (1950).

slits provided with this instrument were used along with a cylindrical cell which was painted black except for the window. Measurements were made at room temperature (27°) using the blue line of mercury (λ 4358 Å.). It was found that in these systems, the turbidities were practically independent of temperature in the 25–35° range.

The N,N-dimethylalkylamine oxide solutions were prepared using doubly distilled water. All solutions were clarified by nitrogen pressure filtration through a 0.45 μ pore size Millipore filter. The cell and the bottles in which the solutions were kept were made dust free using the technique described by Thurmond.[7]

Scattering measurements were made at $\theta = 90°$ and also as a function of angle over the range 30–135°. No turbidity corrections were made for dissymmetry and depolarization effects.

X-Ray Data.—The X-ray diffraction patterns were obtained from solutions sealed in 1/2 mm. internal diameter capillary tubes. A General Electric XRD-1 diffraction unit was used for these measurements. Nickel filtered copper radiation was used, generated at 45 kv. and 19 ma. The films (Kodak No-Screen) were conventionally processed and optical density measurements were made with a Jocyl-Lobel microdensitometer.

Materials.—The dimethylalkylamine oxides [alkyl $N(CH_3)_2O$] were prepared by the hydrogen peroxide oxidation of the corresponding dimethylalkylamines. After the oxidation was complete, the excess hydrogen peroxide was catalytically decomposed by the addition of platinium black. Unreacted amine was removed by repeated extraction with petroleum ether. The solution was then freeze-dried and the residue repeatedly recrystallized from dried $CaSO_4$ and redistilled acetone.

The dimethylalkylamines were prepared by treating the *n*-alkyl bromides with dimethylamine. Vapor phase chromatography showed that after fractional distillation the dimethylalkylamines contained less than 0.5% of homologous contaminants.

Solutions.—All solutions were prepared on a weight basis in doubly distilled water. The concentration units employed in this paper are g. of solute per 100 g. of solution, unless otherwise noted. All solutions were of greater than pH 7, thus, only non-ionic surfactant was present.[5]

Results

Light Scattering Data.—The turbidity–concentration results for C_8AO and $C_{12}AO$ are given in Fig. 1. The $C_{12}AO$ results show a clear maximum in the region of 9 g./100 g. of solution; the C_8AO, in addition to the c.m.c. break at 3.23 g./100 g., shows a plateau beginning at 12 g./100 g. The dissymmetries observed for the C_8AO solutions remained below 1.1 over the concentration range studied; however, for $C_{12}AO$, both dissymmetry and depolarization began to rise in the region of the turbidity maximum (Fig. 2). The micellar properties for C_8AO and $C_{12}AO$ in the concentration region of their c.m.c.'s have already been reported.[5] These results are summarized in Table I and are not inconsistent with the view that the micelles are small and sphere-like near the c.m.c.

TABLE I

SUMMARY OF MICELLAR PROPERTIES

Surfactant	c.m.c. (g./100 ml.)	MMW	Monomers per micelle
C_8AO	3.23	2,600	15
$C_{12}AO$	0.048	17,300	76

Estimates of a particle size parameter at concentrations above the second transition region were made from low angle scattering data shown in Fig. 3. The radii of gyration of the micellar aggregates, estimated from the extrapolated intercepts, the approximate slopes at low angles, and Zimm's equation,[8] ranged from 880 to 1040 Å. in the more concentrated solutions. Calculations were not made for concentrations below

(7) C. D. Thurmond, *J. Polymer Sci.*, **8**, 607 (1952).
(8) B. H. Zimm, *J. Chem. Phys.*, **16**, 1099 (1948).

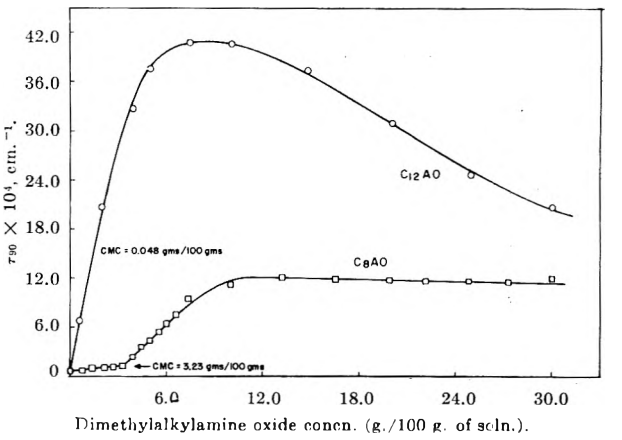

Fig. 1.—Turbidity–concentration data for C_8AO and $C_{12}AO$

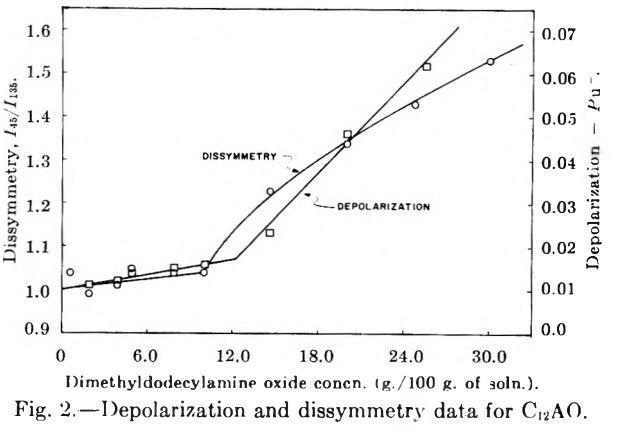

Fig. 2.—Depolarization and dissymmetry data for $C_{12}AO$.

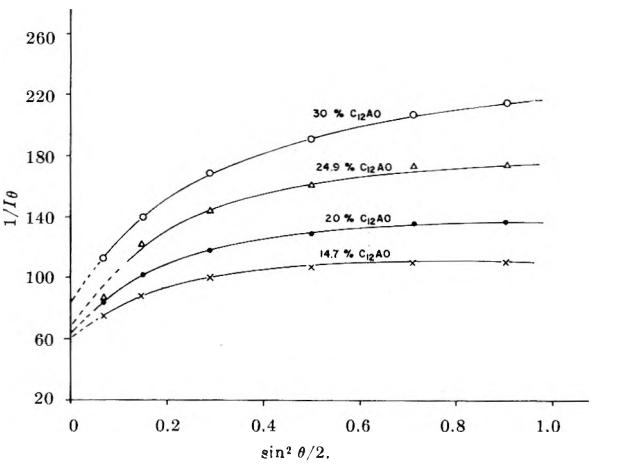

Fig. 3.—Angular scattering data for $C_{12}AO$ solutions.

the concentration at which the turbidity, dissymmetry, and depolarization breaks occur because of the low dissymmetries and the greater inaccuracies involved.

X-Ray Data.—Some evidence for the existence of a long spacing in the $C_{12}AO$ solutions has been obtained as low as 5 g./100 g. from densitometer tracings. These diffraction rings are diffuse and do not become very distinct until solution concentrations of 10–12 g./100 g. are reached. Furthermore, the minimum concentration at which these rings can be detected depends somewhat on the experimental conditions employed, particularly exposure time. As the concentration is further increased, the rings become more intense and the spacings decrease (Table II).

The spacings given in Table II were calculated from the relationship $d = \lambda/2 \sin \theta$. Middle phase can first be detected at room temperature at 34% $C_{12}AO$ by

TABLE II

X-RAY DIFFRACTION DATA FOR $C_{12}AO$ SOLUTIONS

Concn. (g./100 g. soln.)	d Spacing
5.0	No definite band
10.0	54 Å. weak, diffuse
15.0	53 Å. strong, diffuse
20.0	51 Å. strong, diffuse
25.0	47 Å. strong, less diffuse
30.0	44 Å. strong, less diffuse
41.0	40 Å. } middle phase;
	23 Å. } strong, sharp

polarized light microscopy methods. The detailed interpretation of the X-ray results is still uncertain.

As in the case of $C_{12}AO$, distinct diffraction bands are observed with C_8AO solutions from the middle phase boundary (53% C_8AO) down to the 20% C_8AO concentration region. Below this concentration there is less certainty as to the origin of the density differences observed on the X-ray films.

Discussion

The light scattering results for $C_{12}AO$ indicate a considerable growth in micelle size, relative to the species at the c.m.c., by the time the concentration region has been reached where the turbidity maximum and the breaks in the dissymmetry and depolarization curves occur. The appearance of definite X-ray bands in the same concentration region suggests that the same structural change in solution is responsible for all these phenomena. In view of the absence of ionic forces in this system, the turbidity decrease may well result from steric interference between the micelles. The crowding together of these large micelles could lead to regions of order in the solution, and the appearance of the X-ray long spacings would be a consequence of the existence of these ordered regions. The word "order" as used here must remain somewhat ambiguous because existing theory does not allow a precise interpretation of the experimental data. The authors prefer to think of "increased order" as meaning an increase in the alignment of rod-like micellar aggregates within localized regions of solution and an increase in the size of these regions. Some specific points supporting this general concept, which at present must be considered as being a hypothesis, are given below.

(1) The first mesomorphic phase formed by the $C_{12}AO$–water system as the surfactant concentration is increased (34% w.w., 27°) has the microscopic appearance of a typical middle phase.[9] Middle phase, in surfactant–water systems, has been shown by Luzzati, Mustacchi, and Skoulios[10] to be formed by the hexagonal arrangement of cylinders of indefinite length, the diameters of these cylinders being of the order of 30 Å. for the C_{12} soaps. The cylinders themselves are thought to be similar in structure to micelles, with a hydrocarbon chain interior and a surface composed of the hydrated hydrophilic groups. We consider that steric interference and ordering between rods, similar to those found in the middle phase, might account for our results.

(2) The existence of a maximum in the turbidity *vs.* concentration plot has not previously been reported for surfactant systems but has been observed for polymer systems. Debye and Bueche[11,12] have attempted a theoretical treatment of the maxima in polymer systems where the particle molecular weight is large and fixed, and where the configuration of the polymer is taken to be similar to a flexible string. The theoretical considerations used in the derivation of these expressions are not applicable to surfactant systems. Zimm[13] has considered the effect of steric interference on the colligative properties of certain solutions. The use of Zimm's expression for the second virial coefficient in a system of rods leads to the conclusion that an elongating rod system will exhibit an experimental turbidity maximum. For rods of fixed length, the turbidity will approach a limit asymptotically. It should be recognized that these treatments include rough approximations (*e.g.*, neglect of higher virial coefficients), however, they do indicate that increased aggregation with increased concentration can lead, theoretically, to the turbidity maxima observed.

(3) Onsager[14] has proposed that there exists a region of instability of isotropic phase relative to nematic phase (a mesomorphic phase). If rod-like micellar aggregates are assumed and if the rod-length (l) is much greater than rod-diameter (d), then according to Onsager

$$\phi_i = 3.34 \frac{d}{l}$$

where ϕ_i is the concentration of instability in terms of volume fraction. The experimental data suggest that the volume fraction where marked deviations in turbidity, dissymmetry, and depolarization occur, *i.e.*, $C_{12}AO$ volume fraction $\cong$ 0.09, may be taken as ϕ_i. In the case of aggregates having rod-diameters of 30 Å., the particle length according to this interpretation of Onsager's ϕ_i term would be about 1000 Å. This value is consistent with the large dimensions calculated for the micellar aggregates in the more concentrated solutions using the low angle scattering data.

(4) Some further support is given to the concept of increased micellar aggregation and increased particle ordering by preliminary measurements of the relative vapor pressure of both the C_8AO and $C_{12}AO$ solutions using a thermistor technique. The degree of vapor pressure lowering ($\Delta p/p_0$) remains relatively constant from

$$\frac{\Delta p}{p_0} = \frac{p_{solvent} - p_{solution}}{p_{solvent}}$$

the c.m.c. to the second transition region but increases with increased surfactant concentration from this point on. Increases in $\Delta p/p_0$ of $12 \pm 0.5 \times 10^{-3}$ and $3.5 \pm 0.5 \times 10^{-3}$ were observed on increasing the surfactant concentration from 14 to 30 g. of C_8AO/100 g. and 12 to 30 g. of $C_{12}AO$/100 g., respectively. This behavior is indicative of a large departure from solution ideality and deserves further study. It is known that water forms an integral part of the ordered structure in the mesomorphic phase. The vapor pressure depressions above the second transition point may, therefore, be a consequence of the incorporation of water into the ordered arrangement of micellar aggregates.

X-Ray and light scattering methods indicate that the

(9) F. B. Rosevear, *J. Am. Oil. Chem. Soc.*, **31**, 628 (1954).

(10) V. Luzzati, H. Mustacchi, and A. Skoulios, *Trans. Faraday Soc.*, **25**, 43 (1958).

(11) P. Debye *J. Chem. Phys.*, **31**, 680 (1959).

(12) P. Debye and A. M. Bueche, *ibid.*, **18**, 1423 (1950).

(13) B. H. Zimm, *ibid.*, **14**, 164 (1946).

(14) L. Onsager, *Ann. N. Y. Acad. Sci.*, **51**, 627 (1949).

second transition region is less distinct in the case of C_8AO. The low dissymmetry in the transition region is evidence for a reduced particle size (relative to $C_{12}AO$), and the weakness of the long spacing diffraction bands suggests that the micelles are less ordered than in the $C_{12}AO$ system of the same concentration.

Conclusions

Although it is difficult to interpret the results individually in terms of changes in micellar structure with increasing surfactant concentration, the combined results have led us to propose the following hypothesis in explanation of the observed behavior. Somewhere above the c.m.c. but below the turbidity maximum the initially spherical micelles begin to elongate. In the transition region, steric interference is accompanied by increasing alignment of the elongated micelles. As the concentration further increases, the degree of orientation increases until, finally, a well-ordered phase (mesomorphic) appears.

The assignment of a definite second transition concentration for these systems does not seem possible. It would appear that the structural changes in these solutions are gradual rather than sharp transitions. It is hoped that these observations will stimulate further work in this relatively neglected region of surfactant–water systems and will encourage theoretical treatments of the structural changes that occur with increased surfactant concentration.

TEMPERATURE COEFFICIENT OF THE MERCUROUS ACETATE ELECTRODE

By W. D. Larson

Department of Chemistry, College of St. Thomas, St. Paul 1, Minn.

Received September 15, 1962

The e.m.f.'s of the cells

$$H_2 \mid HOAc(m), Hg_2(OAc)_2(s) \mid Hg \qquad (I)$$

were measured over a temperature range from 5 to 37.5° and a concentration range of 0.4 to 1.0 molal. Previous work[1,2] gave the standard e.m.f. of the mercury, mercurous acetate electrode at 25° only. The e.m.f. of cells I is given by the equation

$$E = E^0 - RT/F_y \ln a_H a_{OAc} =$$

$$E - RT/F_y \ln mK(1 - \alpha)\gamma_u \qquad (1)$$

where m is the molality of the acetic acid, K is its thermodynamic dissociation constant, α is its degree of ionization, and γ_u is its activity coefficient for undissociated molecules. Values of K and of α may be obtained from the work of Harned and Ehlers.[3]

Experimental methods and materials used were substantially the same as in the earlier work. Agreement between replicate cells was within 0.2 mv.

Table I shows the average values of the e.m.f. of the cells at various molalities and temperatures. At least four cells were measured at each concentration; since cells were measured only in the range 5–25° or 25–37.5°, each figure at 25° represents the average of at least eight cells while the figures for the other temperatures

(1) W. D. Larson and F. H. MacDougall, *J. Phys. Chem.*, **41**, 493 (1937).
(2) W. D. Larson and W. J. Tomsicek, *J. Am. Chem. Soc.*, **61**, 65 (1939).
(3) H. S. Harned and R. W. Ehlers, *J. Am. Chem. Soc.*, **54**, 1350 (1932).

Table I

Electromotive Forces of Cells I at Various Temperatures

m	$E_{obs.}$	$E_{calc.}$	Δ(mv.)
	5°		
0.4057	0.80745	0.80749	−0.04
0.5217	.80139	.80130	+ .09
0.7736	.79190	.79186	+ .04
1.039	.78484	.78488	− .04
	12.5°		
0.4057	0.81093	0.81095	−0.02
0.5217	.80470	.80481	− .11
0.7736	.79501	.79501	.00
1.039	.78772	.78774	− .02
	20°		
0.4057	0.81391	0.81412	−0.21
0.5217	.80753	.80778	− .25
0.7736	.79756	.79777	− .19
1.039	.79010	.79026	− .16
	25°		
0.4057	0.81625	0.81602	+0.23
0.5217	.81013	.81011	+ .02
0.7736	.79962	.79940	+ .22
1.039	.79203	.79207	− .04
	30°		
0.4057	0.81786	0.81777	+0.09
0.5217	.81127	.81128	− .01
0.7736	.80095	.80087	+ .08
1.039	.79323	.79314	+ .09
	37.5°		
0.4057	0.81998	0.82009	−0.11
0.5217	.81323	.81332	− .09
0.7736	.80268	.80276	− .08
1.039	.79476	.79492	− .16

are the average of at least four cells. The electromotive forces at various temperatures were fitted by the method of least squares to an equation of the form

$$E = a + bt + ct^2 \qquad (2)$$

Values of the constants of this equation are given in Table II. The fourth column in Table I gives the

Table II

Constants of Equations 2 and 3

m	a	10^4b	10^6c
0.4057	0.80488	5.259	−3.209
0.5217	0.79872	5.361	−3.912
0.7736	0.78955	4.781	−3.354
1.039	0.78281	4.295	−2.846
	a_0	10^4b_0	10^6c_0
E^0	0.52441	−3.754	−5.859

difference in mv. between the e.m.f. calculated from equation 2 and the average of the experimental values. Table II gives also the constants for equation 3

$$E^0 = a_0 + b_0t + c_0t^2 \qquad (3)$$

This latter equation gives the values of the standard e.m.f., E^0, of the mercury, mercurous acetate electrode from 5 to 37.5°. Values of E^0 computed at each temperature from measurements at the various concentrations and from equation 3 are given in Table III. The fourth column of Table III gives the difference in mv. between these E^0 values and those calculated from equation 3.

The constants of equation 1 were computed with the values of Bearden and Watts.[4] Recalculation

TABLE III

VALUES OF E^0 AT VARIOUS TEMPERATURES

t (°C.)	$E^0_{obsd.}$	$E^0_{calcd.}$	Δ(mv.)
5.00	0.52244	0.52238	+0.06
12.50	.51882	.51881	+ .01
20.00	.51432	.51456	− .24
25.00	.51156	.51147	+ .09
30.00	.50800	.50788	+ .12
37.50	.50199	.50209	− .10

of the Harned and Ehlers[3] dissociation constants using absolute volts in all cases did not affect their magnitudes enough to be significant in this work.

The standard free energy change for the cell reaction was computed from equation 4

$$\Delta F^0 = E^0 n F_y \qquad (4)$$

The standard change in heat content was calculated from the Gibbs–Helmholtz equation in the form

$$\Delta H^0 = nF_y\left(E^0 - T\frac{\partial E^0}{\partial T}\right) \qquad (5)$$

and the standard entropy change for the cell reaction was computed from equation 6

$$\Delta S^0 = nF_y\frac{\partial E^0}{\partial T} \qquad (6)$$

It was found that for the cell reaction

$$\Delta F^0 = -23600 \text{ cal.}$$

$$\Delta H^0 = -32800 \text{ cal.}$$

$$\Delta S^0 = 30.8 \text{ e.u.}$$

at 25°.

Using this value of ΔH^0 at 25° and standard heat of formation for acetate ion given by Latimer,[5] the standard heat of formation of mercurous acetate is computed to be −200.9 kcal./mole. This may be compared with −201.1 kcal./mole given by Rossini, *et al.*[6] No value of S^0 for acetate ion is available, so S^0 for mercurous acetate cannot be computed from these data.[7]

The partial molal heat content (the heat of transfer) relative to an infinitely dilute solution of acetic acid was computed from the temperature coefficients of electromotive force by the Gibbs–Helmholtz equation

$$\overline{L_2} = \overline{H_2} - \overline{H_2^0} = \Delta H - \Delta H^0 = -nF_y \times \left[E - E^0 - T\frac{\partial E}{\partial T} + T\frac{\partial E^0}{\partial T}\right] \qquad (7)$$

Into equations 2 and 3 were substituted $(T - 273.16)$ for t; this gives the equations

$$E = A + BT + CT^2 \qquad (8)$$

$$E^0 = A_0 + B_0T + C_0T^2 \qquad (9)$$

Substitution of equations 8 and 9 into 7 gives

$$\overline{L_2} = -F_y(A - A_0) + F_y(C - C_0)T^2 \qquad (10)$$

In Table IV are given A, A_0, B, B_0, C, C_0, and the values of $\overline{L_2}$ for the four solutions studied.

TABLE IV

m	A	10^3B	10^5C	$\overline{(L_2)}_{298}$	$\overline{(C_p - C^0_p)}_{298}$
0.4057	0.42169	2.279	−3.209	84	36
0.5217	0.36028	2.674	−3.912	58	27
0.7736	0.40848	2.311	−3.354	91	35
1.039	0.43505	1.985	−2.846	105	41
	A_0	10^3B_0	10^5C_0		
E^0	0.18967	2.826	−5.859		

The relative partial molal specific heat

$$\overline{C_p} - \overline{C_p^0} = \left(\frac{\partial \overline{L_2}}{\partial T}\right)_p = 2F_y(C - C_0)T \qquad (11)$$

was also computed, and the values for the solutions are given in Table IV. The heat content and specific heat values are in calories.

Acknowledgment of a grant from the National Science Foundation (grant number G2380) in support of this work is made.

(4) J. A. Bearden and H. M. Watts, *Phys. Rev.*, **81**, 73 (1951).

(5) W. M. Latimer, "Oxidation Potentials," 2nd Ed., Prentice-Hall, New York, N. Y., 1952, p. 128.

(6) F. D. Rossini, *et al.*, "Selected Values of Chemical Thermodynamic Properties," Circular 500, National Bureau of Standards.

(7) NOTE ADDED IN PROOF.—K. S. Pitzer and L. Brewer in their revision of G. N. Lewis and M. Randall, "Thermodynamics," McGraw-Hill Book Company, New York, N. Y., 1961, p. 400, give a value for the entropy of acetate ion of 20.8 e.u. Using this value and the entropies of Hg(l) and H_2(g) given by Latimer, "Oxidation Potentials," Prentice-Hall, New York, N. Y., 1952, 2nd Ed., and the value of 30.8 e.u. found in this study, leads to a value of 16.6 e.u. for $Hg_2(OAc)_2$.

THE EFFECT OF OXIDES OF NITROGEN ON METHANE OXIDATION IN REACTORS COATED WITH LEAD OXIDE[1]

BY ELLINGTON M. MAGEE

Central Basic Research Laboratory of the Esso Research and Engineering Company, Linden, New Jersey

Received September 21, 1962

Two very interesting effects in the slow oxidation of methane are the inhibition of the reaction by lead oxide surfaces[2,3] and the sometimes conflicting reports on the catalysis of the reaction by oxides of nitrogen.[4-7] It was the purpose of the present investigation to study the net result of oxidizing methane in the simultaneous presence of the two oxides. It was hoped that the results of such a study would furnish information as to what parts of the reaction sequence were being influenced by the individual oxides.

Experimental

The experiments reported here were carried out in a flow system similar to that described previously.[8] A number of quartz reactors were employed; all of them having preheat, reactor, and quench sections. In one group of experiments a stainless steel reactor was used.

The surface-to-volume ratio was varied by changing the diameter of the reactor section while keeping the volume approximately constant at 15 ml. One reactor was filled with quartz cylinders that had been fire-polished.

A coating of PbO was obtained by rinsing a reactor with a 10% solution of lead nitrate in water. The solution was allowed

(1) This work was begun at the Research Division, Humble Oil and Refining Company, Baytown, Texas.

(2) D. E. Hoare and A. D. Walsh, "Fifth Symposium (International) on Combustion," Reinhold Publishing Corp., New York, N. Y., 1955, p. 467.

(3) A. C. Egerton, G. J. Minkoff, and K. C. Salooja, *Combust. Flame*, **1**, 25 (1957).

(4) C. H. Bibb and H. J. Lucas, *Ind. Eng. Chem.*, **21**, 633 (1929).

(5) C. H. Bibb, *ibid.*, **24**, 10 (1932).

(6) D. F. Smith and R. T. Milner, *ibid.*, **23**, 357 (1931).

(7) R. G. W. Norrish and J. Wallace, *Proc. Roy. Soc.* (London), **A145**, 307 (1934).

(8) E. M. Magee, *J. Am. Chem. Soc.*, **81**, 278 (1959); **82**, 3553 (1960).

to drain out and the remaining moisture was removed by drawing air through the reactor. The $Pb(NO_3)_2$ was decomposed to PbO by heating to 600–800° while a stream of N_2 flowed through the reactor.

Similar results were found when the coating was applied by adding small amounts of lead tetraethyl or lead tetramethyl to the stream of CH_4 and O_2 during reaction.

Additions of oxides of nitrogen to the reaction mixtures were made in two ways. In one method NO_2 was added directly through a capillary tube and its rate of addition followed by readings on a silicone oil manometer. In the second method, either the CH_4 or O_2–N_2 stream or both were allowed to bubble through a nitric acid solution in an ice bath. The amount of HNO_3 added could be regulated by varying the concentration of the acid solution. Measurement of the amount added was carried out in blank experiments in which the HNO_3 was collected in a basic solution that was then back titrated.

In the present experiments the concentrations of products were determined as a function of temperature. The analyses were carried out as described previously.[8] The reaction time and the initial partial pressures of the reactants were held constant. The residence time was 0.7 second; the concentration of reactants was: CH_4, 33.3%; O_2, 13.3%; and N_2, balance (except that small amounts of oxides of nitrogen were added). All experiments were carried out at atmospheric pressure. The methane was Phillips Research Grade and was better than 99.5% pure.

Results

Figure 1 is an example of the results from these experiments when a PbO coating was used. As the temperature was increased the concentration of formaldehyde passed through a maximum and the carbon monoxide began increasing rapidly in this region. Little carbon dioxide was formed.

Data from curves such as those in Fig. 1 show that the amount of CH_4 converted to CH_2O increases as the concentration of nitric acid increases. This is illustrated by Table I.

TABLE I

EFFECT OF HNO_3 CONCENTRATION ON YIELD OF CH_2O IN PbO COATED REACTOR

% HNO_3	% CH_4 converted to CH_2O	Moles CH_2O / Moles HNO_3
0.077	1.0	4.3
.135	2.2	5.4
.23	2.6	3.7
.47	3.1	2.2

Table I also shows that the ratio of CH_2O produced to HNO_3 introduced into the reactor is always greater than unity.

The effect of surface-to-volume ratio on the yield of CH_2O is shown in Table II.

TABLE II

EFFECT OF SURFACE-TO-VOLUME RATIO ON MAXIMUM YIELD OF CH_2O

Initial NO_2 = 0.3%; PbO coating

S/V ratio, cm.$^{-1}$	% CH_4 converted to CH_2O
2.5	2.6
4.0	3.0
8.0	3.25
37.0	3.15

The maximum yield of CH_2O begins to decrease as the surface-to-volume ratio falls below about 8 cm.$^{-1}$.

In Fig. 2 the yield of CH_2O in the stainless-steel reactor is shown as a function of temperature for several conditions. The large increase in yield with the use of the combination of PbO coating and HNO_3 is quite interesting. The experiments with HNO_3 in the clean reactor were not extended to higher temperatures,

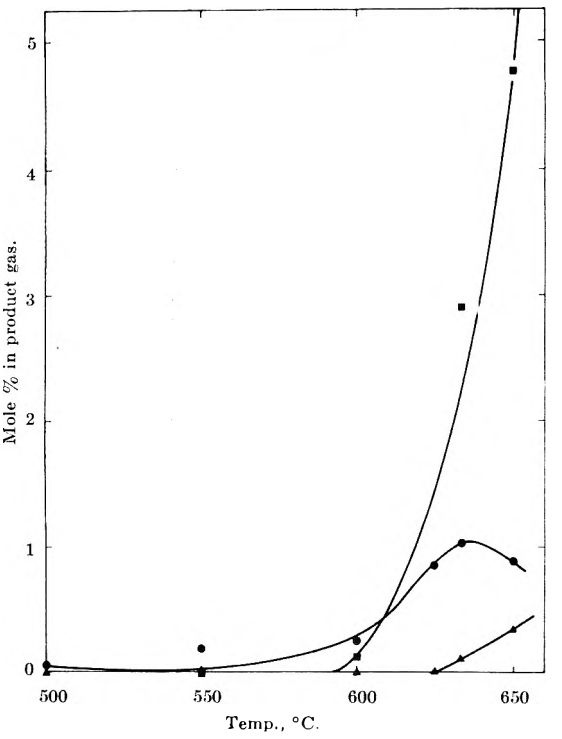

Fig. 1.—Concentration of products in exit gas. Quartz reactor with PbO coating. ●, CH_2O; ■, CO; ▲, CO_2; initial CH_4, 33.3%; initial O_2, 13.3%; initial NO_2, 0.3%; initial N_2, remainder.

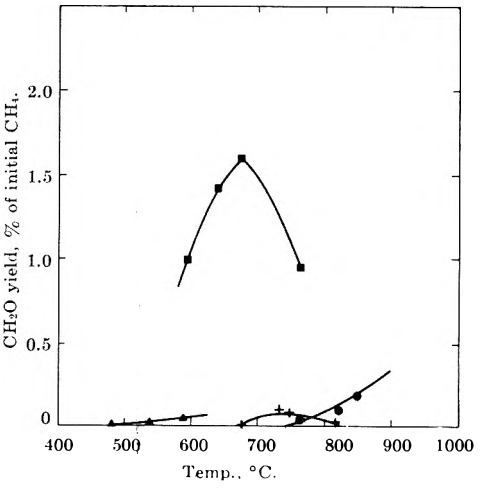

Fig. 2.—CH_2O yield in stainless-steel reactor: +, no coating, no HNO_3; ▲, no coating, 0.1% HNO_3; ●, PbO coating, no HNO_3; ■, PbO coating, 0.3% HNO_3.

because at 600° the oxygen was essentially completely consumed.

Discussion

The quantity of CH_2O produced when nitrogen oxides and PbO are used in the oxidation of pure CH_4 can be as large as that previously reported for CH_4–C_2H_6 mixtures.[4,5] Furthermore, when a PbO-coated reactor is used, the ratio of CH_2O produced to HNO_3 introduced into the reactor can be larger than 1 or 2, indicating that the HNO_3 is acting catalytically. This is contrary to previous findings when no PbO was used.[6]

Perhaps the most significant finding in the present work is that the inhibiting action of the PbO coatings is removed by traces of oxides of nitrogen. The resulting temperature at which the formaldehyde peaks is over 100° below that in an uncoated quartz reactor when no nitrogen oxides are present.[8]

Another significant effect is the increase of CH_2O concentration when nitrogen oxides are present. According to the mechanism proposed by Enikolopyan[9] to explain his studies of methane oxidation, the maximum CH_2O concentration should be independent of the surface. It has been shown, however, that PbO coatings alone reduce the concentration of CH_2O.

Results similar to these have been found in the oxidation of methane over potassium tetraborate surfaces using oxides of nitrogen as homogeneous catalysts (see for example ref. 10). These workers observed that in quartz and steel vessels without the coating the reaction is not reproducible when oxides of nitrogen are present. Furthermore, they find that the amount of formaldehyde produced is increased by coating the surfaces with $K_2B_4O_7$.

The increase of CH_2O when nitrogen oxides and PbO are present can be explained in at least two ways. (1) The PbO alone allows CH_2O to decompose or to be oxidized without chain branching. The nitrogen oxides then simply increase the rate of formation of CH_2O. (2) The PbO, as has been suggested previously,[11] removes species such as HO_2 or H_2O_2 which lead to chain branching. The nitrogen oxides then furnish a route for the oxidation of methane without the usual necessary destruction of CH_2O.

The latter possibility seems very probable. As pointed out above, the CH_2O yield begins to drop when the surface-to-volume ratio becomes less than about 8. A previous report[3] indicates that marked differences in the rate of reaction appear when the surface-to-volume ratio is increased to 8 $cm.^{-1}$ in uncoated vessels. The fact that the same critical ratio appears in the present work indicates that the same radical species is involved.

It is felt that studies of the methane oxidation using PbO coatings and nitrogen oxides offer a valuable tool for obtaining further insight into the role played by surfaces.

Acknowledgment.—The author is grateful to Mr. G. C. McCollum and Mr. R. W. Thomas for assistance in carrying out these experiments.

(9) N. S. Enikolopyan, "Seventh Symposium (International) on Combustion." Butterworths Scientific Publications, London, 1959, p. 157.
(10) N. S. Enikolopyan, *et al.*, *Zh. Priklad. Khim.*, **32**, 913 (1959).
(11) D. E. Cheaney, *et al.*, "Seventh Symposium (International) on Combustion," Butterworths Scientific Publications, London, 1959, p. 183.

LONG RANGE SPIN–SPIN SPLITTINGS IN 4-VINYLIDENECYCLOPENTENE

By Melvin W. Hanna and J. Kenneth Harrington

Department of Chemistry, University of Colorado, Boulder, Colorado

Received September 24, 1962

Recent experimental work by Snyder and Roberts has shown that in a large number of allenes and acetylenes the spin–spin splittings between protons separated by four carbons (J_{14}) are between 2 and 3 c.p.s.[1] These experimental results can be nicely correlated by Karplus' theory of π-electron coupling of nuclear spins.[2] In this theory the π-electron contribution to the spin–spin splitting, $A_{HH}'(\pi)$, is given approximately by

$$A_{HH}'(\pi) = 2.1 \times 10^{-15} \sum_T \frac{a_H(T)a_H'(T)}{\Delta\pi(T)} \quad (1)$$

where a_H and a_H' are the hyperfine coupling constants of protons H and H', respectively, and $\Delta\pi(T)$ is the π-electron singlet-triplet transition energy. For the methyl-substituted allenes studied by Snyder and Roberts eq. 1 predicts $J_{14} = 2.9$ c.p.s.

4-Vinylidenecyclopentene (I) has recently been isolated in these Laboratories,[3] and its n.m.r. spectrum is of

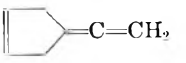

I

interest in checking a more general application of eq. 1. The proton resonance peaks of interest are a triplet due to the allylic protons at 6.87τ and a quintet due to the vinylic protons at 5.40τ. The spin–spin splitting if 4.58 ± 0.08 c.p.s., substantially larger than the long range splitting in the methyl allenes.[1] This larger splitting is of interest because of the basic structural difference between allene I and the allenes studied by Snyder and Roberts. In the latter case the methyl groups are freely rotating and the average value of $a_H' = 75 \times 10^6$ c.p.s. was used in eq. 1 to calculate A_{HH}'. In allene I the methylene protons have a fixed spatial orientation with respect to the 2-p orbital on the adjacent carbon. This allows a test of the more general equation for the hyperfine coupling of an H–C–Ċ fragment. In this case

$$a_H' = (+155 \cos^2 \phi) \times 10^6 \text{ c.p.s.} \quad (2)$$

where ϕ is the angle between the H–C–Ċ plane and the Ċπ-orbital axis.[2,4] Assuming an HCH bond angle of 109°, a_H' is 99.4×10^6 c.p.s. Using this value in eq. 1 gives $A_{HH}'(\pi) = +5.4$ c.p.s., in good agreement with the observed value of 4.6 c.p.s. The important thing is that a larger splitting is predicted for allene I than for methylallene.

Acknowledgment.—Acknowledgment is made to the donors of the Petroleum Research Fund administered by the American Chemical Society and to the National Institutes of Health for partial support of this research.

(1) E. I. Snyder and J. D. Roberts, *J. Am. Chem. Soc.*, **84**, 1582 (1962).
(2) M. Karplus, *J. Chem. Phys.*, **33**, 1846 (1960).
(3) S. J. Cristol and J. K. Harrington, to be published.
(4) C. Heller and H. M. McConnell, *J. Chem. Phys.*, **32**, 1535 (1960); D. Pooley and D. H. Whiffen, *Mol. Phys.*, **4**, 81 (1961).

THERMODYNAMICS OF SILVER BROMATE SOLUBILITY IN PROTIUM AND DEUTERIUM OXIDES[1]

By Richard W. Ramette and Edward A. Dratz

Department of Chemistry, Carleton College, Northfield, Minnesota

Received October 4, 1962

Except for studies of weak acid dissociation, very little attention has been given to ionic equilibria in deuterium oxide. One recent paper deals with oxalato-complexes of cadmium and copper.[2]

Almost as soon as deuterium oxide was isolated it was discovered[3] that sodium and barium chlorides are less soluble in this solvent than in ordinary water, and since that time a number of solubilities have been determined

(1) From the Senior Thesis submitted by E. A. Dratz, Carleton College, 1961.
(2) D. L. McMasters, *et al.*, *J. Phys. Chem.*, **66**, 249 (1962).
(3) H. Taylor, E. Caley, and H. Eyring, *J. Am. Chem. Soc.*, **55**, 4334 (1933).

by Menzies and co-workers,[4] Noonan,[5] Chang and co-workers,[6] and a few others.[7]

However, these studies have been concerned with rather soluble salts for the purposes of straight comparison of solubilities, observation of temperature effects, and the use of solvent mixtures. In an intensive series of investigations Lange and co-workers[8] contributed a body of knowledge on the integral heats of solution and dilution of a large number of salts in both waters, but otherwise the literature lacks thermodynamic data, and it remains to apply equilibrium theory and activity coefficient considerations to electrolyte solubility in heavy water.

Silver bromate was chosen for the present and initial study because it can be prepared in pure form without water of crystallization, is soluble enough to permit accurate determination of concentration of the saturated solutions which nevertheless are sufficiently dilute to permit application of the Debye–Hückel theory, and in general seems to be an excellent representative of 1:1 completely dissociated electrolytes.[9]

Experimental

Crystalline silver bromate was prepared by slow and simultaneous addition of solutions of silver nitrate and potassium bromate to mechanically-stirred distilled water at room temperature, over a five-hour period. Gravimetric analysis of the washed and dried product (as silver bromide) gave 99.8% purity, while iodometric titration with thiosulfate using ammonium molybdate as catalyst gave 99.7% purity. Recrystallization caused no improvement in purity. It has been shown that the use of sodium bromate in the precipitation of silver bromate leads to an impure product because of solid solution formation,[10] but that this is not a problem when potassium bromate is used.[11]

Deuterium oxide was obtained from the Liquid Carbonic Division of General Dynamics Corporation, with their specification of greater than 99.5% purity. All other chemicals were of analytical reagent grade.

Lithium perchlorate was used as the inert electrolyte for the purpose of ionic strength variation, and each solution also contained 1×10^{-4} M perchloric acid to repress any tendency for silver to form hydroxy species. A large excess of silver bromate was added, and the solutions were rotated in borosilicate glass bottles for two days in a thermostated air-bath at 38°, and were then transferred to a water-bath controlled at 35.0° where they stood for three days with occasional manual shaking. The water-bath was equipped with an electrically-heated cover to keep air above the bottles slightly above 35°, thus preventing distillation of water into the tops. With the aid of an apparatus described elsewhere[12] the saturated solutions were filtered through fine porous glass by pressure, and five-ml. samples were pipetted into titration flasks. The entire sampling apparatus, including pipet, was maintained at 35°.

The dissolved bromate was determined by iodometric titration using sodium thiosulfate, after adding 25 ml. of water, 3 ml. of 6 M sulfuric acid, about 1.5 g. of potassium iodide (sufficient to redissolve silver iodide), and allowing to stand in the dark for ten minutes. The bottles and remaining solutions were then equilibrated in a similar manner at 25.0° and finally at 14.7°, and samples were taken at each temperature.

Results

Table I shows the average values (from two closely agreeing results in each case) obtained for solubility (moles/liter).

TABLE I

SILVER BROMATE SOLUBILITIES

		H_2O solutions	D_2O solutions
	$LiClO_4$, M	$S \times 10^3$	$S \times 10^3$
14.7°	0.000	5.56	4.54
	.025	5.99	4.94
	.050	6.26	5.16
	.075	6.43	5.30
	.100	6.55	5.42
25.0°	.000	8.09[a]	6.76
	.025	8.73	7.33
	.050	9.09	7.65
	.075	9.35	7.89
	.100	9.52	8.02
35.0°	.000	11.22	9.57
	.025	12.03	10.26
	.050	12.48	10.62
	.075	12.84	10.92
	.100	13.09	11.12

[a] This value is identical with that reported by C. B. Monk, *Trans. Faraday Soc.*, **47**, 292 (1951), and is consistent with the range of other values. See ref. 10 and 11, and I. Tananaev, *et. al.*, *Zhur. Obschei Khim.*, **19**, 1207 (1949).

Discussion

If the solubility process is represented by the reaction

$$AgBrO_3(c) + nH_2O \text{ (or } mD_2O) \rightleftharpoons Ag^+(aq.) + BrO_3^-(aq.) \quad (1)$$

where the ions are solvated, then application of the solubility product principle gives

$$K = Qf^2 \quad (2)$$

where K is the equilibrium product of the ion activities, Q is the product of the equilibrium molarities, and f is the mean activity coefficient. In logarithmic form, with the introduction of the Debye–Hückel equation for a 1:1 electrolyte

$$pQ = pK - \frac{2A\mu^{1/2}}{1 + Ba\mu^{1/2}} \quad (3)$$

The parameter A varies only with the temperature and the dielectric constant. Values of the latter for protium oxide were taken from Harned and Owen[13] while the equation proposed by Malmberg[14] was used to calculate the values for deuterium oxide. At the temperatures of 14.7, 25.0, and 35.0° the corresponding

(4) F. Miles, R. Shearman, and A. Menzies, *Nature*, **138**, 121 (1936); R. Shearman and A. Menzies, *J. Am. Chem. Soc.*, **59**, 185 (1937); F. Miles and A. Menzies, *ibid.*, **59**, 2392 (1937); R. Eddy and A. Menzies, *J. Phys. Chem.*, **44**, 207 (1940); R. Eddy, P. Machemer, and A. Menzies, *ibid.*, **45**, 908 (1941).

(5) E. C. Noonan, *J. Am. Chem. Soc.*, **70**, 2915 (1948).

(6) T. Chang and T. Chu, *Z. physik. Chem.*, **A184**, 411 (1939); T. Chang and Y. Hsieh, *Sci. Repl. Natl. Tsing Hua Univ.*, **A5**, 252 (1948), *J. Chinese Chem. Soc.*, **16**, 10, 65 (1949); T. Chang and E. Tseng, *Sci. Rec.*, **3**, 101 (1950); T. Chang and K. Wang, *Hua Hsueh Hsueh Pao*, **22**, 414 (1956); T. Chang and Y. Chang, *Sci. Sinica*, **4**, 555 (1955).

(7) R. Kingerly and V. LaMer, *J. Am. Chem. Soc.*, **63**, 3256 (1941); L. Brickwedde, *J. Res. Natl. Bur. Std.*, **36**, 377 (1946); H. E. Vermillion, B. Werbel, J. Saylor, and P. Gross, *J. Am. Chem. Soc.*, **63**, 1346 (1941); J. Curry and C. Hazelton, *ibid.*, **60**, 2771 (1938); F. Hein and G. Bähr, *Z. physik. Chem.*, **B38**, 270 (1937).

(8) E. Lange, W. Martin, and H. Sattler, *Z. ges. Naturw.*, **1**, 441 (1936); *Chem. Zentr.*, *I*, 4882 (1936); E. Lange and W. Martin, *Z. Elektrochem.*, **42**, 662 (1936), *Z. physik. Chem.*, **A178**, 214 (1937); **A180**, 233 (1937); E. Lange and H. Sattler, *ibid.*, **A179**, 427 (1937); W. Birnthaler and E. Lange, *Z. Elektrochem.*, **43**, 643 (1937); **44**, 679 (1938).

(9) It has been proposed, by analogy to other salts, that silver bromate might be very slightly associated in solution (P. B. Davies and C. B. Monk, *J. Chem. Soc.*, 71, 2718 (1951)). This idea has not been applied in the present model because it is uncertain; the effect would be very small in any case, and if the evidence ever becomes definite corrections can then be applied to our calculations.

(10) J. Ricci and J. Aleshnick, *J. Am. Chem. Soc.*, **66**, 980 (1944).

(11) J. Ricci and J. Offenbach, *ibid.*, **73**, 1597 (1951).

(12) R. W. Ramette, E. A. Dratz, and P. W. Kelly, *J. Phys. Chem.*, **66**, 527 (1962).

(13) H. S. Harned and B. B. Owen, "The Physical Chemistry of Electrolytic Solutions," Reinhold Publ. Corp., New York, N. Y., 3rd Ed., 1958, p. 161.

(14) C. G. Malmberg, *J. Res. Natl. Bur. Std.*, **60**, 609 (1958).

values of the quantity $2A$ are, for deuterium oxide; 1.014, 1.030, and 1.050; and for protium oxide; 1.002, 1.018, and 1.038.

It is seen from equation 3 that a plot of the experimental quantity, pQ, *vs.* the ionic strength function $\mu^{1/2}/(1 + Ba\mu^{1/2})$ should be linear with a slope equal to $-2A$ and an intercept equal to the logarithmic thermodynamic value of the solubility product, pK. A difficulty arises in the choice of a proper value for the ion-size parameter Ba. This was treated as an empirical constant for each solvent at each temperature, and with the help of an IBM 610 computer successive values for Ba were tried, each time fitting the line by the method of least squares, until the straight line had the predicted value for the slope. Table II summarizes the values of Ba used and the values of pK found. The uncertainties in the pK values, estimated for 90% confidence, are of the order of 0.006 log unit.

TABLE II

THERMODYNAMIC VALUES FOR SILVER BROMATE SOLUBILITY PRODUCT IN PROTIUM AND DEUTERIUM OXIDES

	H_2O		D_2O	
t, °C.	pK	Ba	pK	Ba
14.7	4.577	1.71	4.749	1.55
25.0	4.265	1.50	4.414	1.56
35.0	3.994	1.57	4.126	1.82

A more regular progression of Ba values might be expected, but it should be pointed out that at the low ionic strengths used the pK values are not particularly sensitive to the choice of the value for Ba. Thus, the extrapolated value of pK varies about 0.002 log unit for each 0.1 unit change in Ba.

The standard free energy changes for the processes of equation 1 were calculated from the relationship $\Delta F_0 = -RT \ln K$, while the standard enthalpy changes were determined by means of plots of pK (K expressed in molarity units) *vs.* $1/T$, fitted by least squares. Standard entropy changes followed directly from the free energy and enthalpy changes. These thermodynamic quantities are listed for the temperature of 25.0° in Table III. The uncertainties shown are estimated for 90% confidence. Probable (50% confidence) errors are only one-third as large.

TABLE III

THERMODYNAMIC FUNCTIONS FOR SILVER BROMATE SOLUBILITY AT 25°

	ΔF^0, kcal./mole	ΔH^0, kcal./mole	ΔS^0, cal./deg. mole
H_2O	5.83 ± 0.02	11.7 ± 0.3	19.7 ± 1.2
D_2O	6.02 ± 0.01	12.5 ± 0.4	21.8 ± 1.3

From these results it is seen that the lower solubility of silver bromate in deuterium oxide (*i.e.*, the more positive free energy change) is due to an enthalpy effect which is larger and thus overcomes an entropy effect which would favor higher solubility in deuterium oxide. This would indicate that the hydration energy is larger in protium oxide, although the water structure is broken down to a larger extent in deuterium oxide. This is consistent with the theoretical results of Swain and Bader[15] for alkali halides, but further discussion awaits a larger body of data.

Kelley and King[16] adopt 17.54 ± 0.15 cal./deg.mole for the standard entropy at 25° of the aqueous silver ion, and 38.5 ± 1.0 for that of the aqueous bromate ion. The present results for the entropy of solution in protium oxide can be subtracted from the sum of these ion entropies to give 36.3 ± 1.5 for the entropy of crystalline silver bromate, which agrees with a calculated value of 37.3 ± 0.6 reported by Kireev.[17]

Acknowledgment.—This work was supported by a National Science Foundation grant for scientific research. We are grateful to Robert F. Broman for performing the computer calculations, and to John B. Spencer for the initial experimental work.

(15) C. G. Swain and R. F. W. Bader, *Tetrahedron*, **10**, 182 (1960).

(16) K. K. Kelley and E. G. King, U. S. Bureau of Mines, Bull. 591, 1962.

(17) V. A. Kireev, *Zhur. Obschei Khim.*, **16**, 1199 (1946).

THERMODYNAMICS OF COPPER(II) IODATE SOLUBILITY IN PROTIUM AND DEUTERIUM OXIDES[1]

BY RICHARD W. RAMETTE AND ROBERT F. BROMAN

Department of Chemistry, Carleton College, Northfield, Minnesota

Received October 5, 1962

The lack of information on ionic equilibria in deuterium oxide solution and a bibliography of previous solubility studies have been reported in an earlier paper[2] dealing with the thermodynamics of silver bromate solubility. The present work differs from the latter in two respects: a 2:1 charge type electrolyte is used, and the crystalline form includes water of solvation. For the latter reason the isotope effects, as characterized by the differences in the thermodynamic functions, are not merely dependent upon the state of the ions in the infinitely dilute solution. A more thorough comparison could be made if the thermodynamics of the reaction

$$Cu(IO_3)_2 \cdot H_2O(c) + D_2O \rightleftharpoons Cu(IO_3)_2 \cdot D_2O(c) + H_2O \quad (1)$$

were known, but such information is not yet available.

Experimental

The copper(II) iodate monohydrate was prepared[3] by adding 0.6 mole of iodic acid in 200 ml. of water and slightly over 0.3 mole of copper sulfate in 300 ml. of water simultaneously and dropwise into 400 ml. of hot water with constant mechanical stirring. The product was washed thoroughly with a total of about 2 liters of hot water, using a repetitive process of partial sedimentation and decantation to remove smaller particles. After drying, the assay according to iodometric titration with thiosulfate gave 99.9% for the purity.

A monodeutrate form of the salt was prepared in a similar manner but on a smaller scale: 125 ml. of 0.3 M potassium iodate in D_2O and 125 ml. of 0.15 M copper sulfate in D_2O were added dropwise to about 30 ml. of D_2O at 60° with constant stirring. The precipitate was digested at this temperature for an hour, was collected on a glass filter, and dried at 100°. Titrimetric assay with EDTA indicated a purity of 99.9%.

The D_2O was specified as greater than 99.5% pure (from General Dynamics Corp.) and all chemicals were of reagent grade.

The lithium perchlorate solutions, which also contained 10^{-4} M perchloric acid to repress the formation of hydroxy-copper species, were equilibrated with solid copper iodate and sampled as previously described[2] at 14.7, 25.0, and 35.0°. Analysis for dissolved copper was made by adding, to each 5-ml. sample of saturated solution, 2 ml. of 0.1 M acetic acid, 0.1 M sodium

(1) From the Senior Thesis submitted by Robert F. Broman, Carleton College, 1961.

(2) R. W. Ramette and E. A. Dratz, *J. Phys. Chem.*, **67**, 940 (1963).

(3) J. L. Sudmeier, Senior Thesis, Carleton College, 1959.

acetate buffer, and 1 drop of Snazoxs indicator[4] (saturated solution in dimethylformamide), followed by titration with standard EDTA solution. The latter was standardized by the same titration *vs.* a weighed quantity of pure electrolytic copper. Duplicate titrations usually gave results checking to within 0.2%.

Results

As expected, the solubility in D_2O is markedly less than in H_2O. The results for solubility, S, in moles/liter are given in Table I.

TABLE I

COPPER(II) IODATE SOLUBILITIES

		H_2O solutions	D_2O solutions
	$LiClO_4$, M	$S \times 10^3$	$S \times 10^3$
	0.000	2.76	2.03
	.025	3.30	2.36
14.7°	.050	3.52	2.55
	.075	3.78	2.71
	.100	3.89	2.79
	.000	3.24[a]	2.35
	.0025	3.29	
	.0060	3.38	
25.0°	.025	3.78	2.74
	.050	4.00	2.94
	.075	4.18	3.09
	.100	4.37	3.21
	.000	3.69	2.73
	.025	4.16	3.09
35.0°	.050	4.44	3.36
	.075	4.69	3.52
	.100	4.86	3.66

[a] This value agrees with that (0.003245) reported by R. M. Keefer, *J. Am. Chem. Soc.*, **70**, 476 (1948).

Discussion

In making the various calculations we have assumed copper(II) iodate to be completely dissociated[5] in aqueous solution, so that the solubility process would be

$$Cu(IO_3)_2 \cdot H_2O(c) + nH_2O \rightleftharpoons Cu^{++}(aq.) + 2IO_3^-(aq.) \quad (2)$$

or

$$Cu(IO_3)_2 \cdot D_2O(c) + mD_2O \rightleftharpoons Cu^{++}(aq.) + 2IO_3^-(aq.) \quad (3)$$

At the low ionic strengths used the solvent activities are considered to be constant, so application of the solubility product principle yields

$$K = [Cu^{++}][IO_3^-]^2 f^3 = Qf^3 \quad (4)$$

where K is the thermodynamic value of the solubility product in terms of activities, Q is the experimentally observed value in terms of molarities, and f is the mean activity coefficient for copper(II) iodate. The values of Q are calculated from the measured solubilities by the relationship $Q = 4S^3$. When the Debye–Hückel equation for $\log f$ (using $Z_+ = 2$, $Z_- = 1$) is combined with equation 4 in logarithmic form, we find

$$pQ = pK - \frac{6A\mu^{1/2}}{1 + Ba\mu^{1/2}} \quad (5)$$

(4) Snazoxs (Mary's dye) is 7-(4-sulfo-1-naphthylazo)-8-hydroxyquinoline-5-sulfonic acid. See G. Guerrin, M. V. Sheldon, and C. N. Reilley, *Chemist-Analyst*, **49**, 36 (1960).

(5) C. B. Monk, *Trans. Faraday Soc.*, **47**, 285 (1951), suggests that the ion pair $CuIO_3^+$ may be present in slight amount, by analogy to other salts. However, in the absence of direct evidence for this species it seems best to ignore this possibility on the principle that no correction is better than a very small, highly uncertain one.

The values of the parameter A for the three temperatures used were calculated using the dielectric constants of both waters,[2] and with the aid of an IBM 610 computer those values of the ion size parameter, Ba, were found which resulted in linear plots with slopes of precisely $-6A$ when the experimental values of pQ were plotted *vs.* the function $\mu^{1/2}/(1 + Ba\mu^{1/2})$. The final plots were extrapolated by the method of least squares in order to determine the values of pK. Table II summarizes the values of Ba used and the pK values. The uncertainties in the pK values correspond to 90% confidence, and as with the uncertainties in the thermodynamic functions shown later, are about three times as large as the probable (50% confidence) error.

TABLE II

THERMODYNAMIC VALUES FOR COPPER(II) IODATE SOLUBILITY PRODUCT IN PROTIUM AND DEUTERIUM OXIDES

	H_2O solutions		D_2O solutions	
t, °C.	pK	Ba	pK	Ba
14.7	7.31 ± 0.04	1.33	7.69 ± 0.02	1.79
25.0	7.13 ± .03	1.72	7.51 ± .01	1.85
35.0	6.97 ± .02	1.97	7.34 ± .03	2.02

The values of Ba used in this and in the previous silver bromate study do not seem precisely meaningful. Probably this is because the plots were forced to have the theoretical slope, and with the small number of points this did not always correspond to the straight line with the smallest sum of the squares of the deviations. However, a plot of the sum of the squares *vs.* the successive values of Ba showed a broad minimum. For example, in Table II at 25° the H_2O pK value is given as 7.13. This was obtained by using Ba equal to 1.72, which gave the theoretical slope of −3.053 while the sum of the squares was 0.00059. The "best fit" for this case, however, was obtained using a value of 3.2 for Ba, when the sum of the squares was 0.00039, and extrapolation indicated pK to be 7.21. But the slope of this plot was −4.51! In spite of the somewhat better precision of the latter fit, we presumed that the procedure of using the theoretical slope was based on sounder principles.

The standard free energy changes for equations 2 and 3 were calculated from the usual relationship, $\Delta F^0 = -RT \ln K$, and standard enthalpy changes were determined by plots of pK *vs.* $1/T$, fitted by the method of least squares using the IBM 610 computer to obtain the large number of significant figures necessary in the intermediate steps of the calculations. Standard entropy changes follow from the relationship $\Delta S^0 = (\Delta H^0 - \Delta F^0)/298.2$. These thermodynamic quantities are given for 25.0° in Table III, with 90% confidence limits.

TABLE III

THERMODYNAMIC FUNCTIONS FOR COPPER(II) IODATE SOLUBILITY AT 25.0°

	ΔF^0, kcal./mole	ΔH^0, kcal./mole	ΔS^0, cal./deg. mole
H_2O	9.73 ± 0.03	6.77 ± 0.42	−9.9 ± 1.5
D_2O	10.25 ± 0.01	7.00 ± 0.30	−10.9 ± 0.9

Thus the lower solubility of copper iodate in D_2O can be attributed to an unfavorable entropy effect as well as an unfavorable enthalpy effect. The confidence limits are large enough to cause overlapping of the values for ΔH^0 and ΔS^0, but the precision of the

ΔF^0 values is such that the direction of the enthalpy and entropy effects would seem to be correct.

The compilation by Kelley and King[6] gives -26.5 ± 1 cal./deg. mole for the standard entropy of the copper ion in H_2O, and 28.0 ± 1.0 for that of the iodate ion. Therefore we calculate $(-26.5 + 56.0) - (-9.9)$ or 39.4 ± 2 cal./deg. mole for the entropy of crystalline copper(II) iodate monohydrate. No data are yet available to permit calculation of entropies in deuterium oxide.

Acknowledgment.—This work was supported by a National Science Foundation grant for scientific research. We are grateful to Kenneth Caulton and to John B. Spencer for their help in the early experimental work.

(6) K. K. Kelley and E. G. King, U. S. Bureau of Mines, Bull. 592, 1961.

ELECTROLYTE EFFECTS ON SILVER BROMATE SOLUBILITY IN PROTIUM AND DEUTERIUM OXIDE SOLUTIONS AT 25°. EVIDENCE FOR ASSOCIATION OF SILVER AND NITRATE IONS

By Richard W. Ramette and John B. Spencer

Department of Chemistry, Carleton College, Northfield, Minnesota

Received October 11, 1962

Electrolytes which are traditionally considered to be chemically "inert" nevertheless show individual effects on ionic equilibrium systems, particularly at higher ionic strengths. In some cases this would seem to be a matter of atmospheric effects as reflected by activity coefficient variation. For example see the dependence of the mean activity coefficient of hydrochloric acid[1] or the extent of water dissociation[2] on the particular cation used in alkali metal chloride solutions of constant ionic strength.

In some other systems individual effects are much better explained by ion-association reactions, especially when there is independent evidence for the existence of previously unsuspected species. A good example is the study of the formation of the aqueous $PbNO_3^+$ ion,[3] which shows that the nitrate ion can serve as a ligand.

The present work deals with relative electrolyte effects on solubility. The effects are not large, and there are no Raman lines or other spectra to give support to the proposed existence of ion pairs. Redlich[4] has reviewed the evolution of ideas about electrolytic dissociation, and has warned of the inherent difficulty of demonstrating complex formation in this kind of system. Nevertheless, we shall proceed to calculate association quotients because the data seem sufficiently precise and the effects seem large enough to permit this. If later work should prove that the assumptions are not valid, then the calculations will at least serve for illustrative purposes.

Experimental

The silver bromate was prepared as described in another paper.[5] The lithium salt solutions also contained 10^{-4} M perchloric acid to repress the formation of hydroxy-silver species. The deuterium oxide was specified as greater than 99.5% pure (General Dynamics Corp.). Although equilibrium was reached in 2–3 hours, solutions were rotated in an air-bath at 25.0° for at least 24 hours, and were transferred to a water-bath for sampling by pressure filtration.[5] Dissolved bromate was determined by duplicate iodometric titrations with sodium thiosulfate.

Results

The observed solubilities are given in Table I.

Table I

Solubility (Millimoles/L.) of Silver Bromate in Electrolyte Solutions at 25°

Electrolyte, M	H_2O solutions of			D_2O solutions of	
	$HClO_4$	$LiClO_4$	$LiNO_3$	$LiClO_4$	$LiNO_3$
0.00	8.03 (pure solvent)			6.78 (pure solvent)	
.02	8.54	8.55	8.62		
.03				7.46	
.05	8.95	8.97	9.17		
.075				7.86	8.20[a]
.10	9.37	9.39	9.73		
.15	9.61	9.70	10.14	8.32	8.68
.20	9.79	9.94	10.51		
.225				8.60	9.15
.30				8.84	9.54

[a] Judging from the constancy of the D_2O/H_2O solubility ratios, this value is about 1% too high and leads to an inconsistent value for the silver nitrate formation quotient (see Table II).

Previously reported[5] solubilities of silver bromate in lithium perchlorate solutions in protium oxide are slightly higher and yield 4.265 for the value (pK) of the solubility product at zero ionic strength. The present data give 4.271 for pK, in satisfactory agreement, when processed in the same way. For D_2O the present data give pK equal to 4.412, compared to the previous 4.414. For the sake of internal consistency we have not taken account of these other results in the calculations which follow.

Discussion

We assume that all perchlorates and silver bromate are completely dissociated in the solutions used. We also assume this for lithium nitrate, although there is some suggestion[6] that very weak association may occur.

It has been shown[1,7] that there is reason to expect lithium ion to affect activity coefficients in the same way as hydronium ion. With the presumption that this can be applied to the mean activity coefficient of silver bromate, we compare the solubility of the latter in lithium perchlorate and perchloric acid solutions. If the acid solubility were greater, this would be evidence for the formation of undissociated bromic acid. However it is seen (Fig. 1) that the opposite occurs, and although this does not rule out the possibility of a slight formation of bromic acid, let it be assumed that bromic acid is "strong" and that the higher solubility observed when hydronium ion is replaced by lithium ion is due to the formation of a small concentration of undissociated lithium bromate. The literature contains some evidence for bromate ion pairs with sodium and potassium ions.[8]

Then, at a given ionic strength

$$Q_{sp} = [Ag^+][BrO_3^-] = S_H^2 \qquad (1)$$

$$S_L = [Ag^+] = [BrO_3^-] + [LiBrO_3] \qquad (2)$$

(1) H. S. Harned and B. B. Owen, "Physical Chemistry of Electrolytic Solutions," Reinhold Publ. Corp., 3rd. Ed., New York, N. Y., 1958, p. 598.
(2) Reference 1, p. 641.
(3) H. M. Hershenson, M. E. Smith, and D. N. Hume, *J. Am. Chem. Soc.*, **75**, 507 (1953).
(4) O. Redlich, *Chem. Rev.*, **39**, 333 (1946); O. Redlich and G. Hood, *Discussions Faraday Soc.*, **24**, 87 (1957).
(5) R. W. Ramette and E. A. Dratz, *J. Phys. Chem.*, **67**, 940 (1963).
(6) J. Bjerrum, G. Schwarzenbach, and L. Sillén, "Stability Constants, Part II, Inorganic Ligands," The Chemical Society, London, 1958, p. 54.
(7) R. W. Ramette and R. F. Stewart, *J. Phys. Chem.*, **65**, 243 (1961).
(8) Reference 6, p. 118.

$$Q_{LiBrO_3} = [LiBrO_3]/[Li^+][BrO_3^-] \quad (3)$$

where the molarities refer to those in the lithium perchlorate solution, Q_{sp} is the solubility product for silver bromate, S_H is the solubility in perchloric acid solution, S_L is the solubility in lithium perchlorate solution, and Q_{LiBrO_3} is the proposed formation quotient.

From these equations the following relationship can be derived

$$Q_{LiBrO_3} = \frac{S_L^2 - S_H^2}{[Li^+]S_H^2} \quad (4)$$

Because so little lithium ion would be consumed in the formation of the ion pair, its concentration may be taken simply as the stoichiometric concentration of lithium perchlorate. Then, using the data of Table I we calculate: $Q_{LiBrO_3} = 0.17$ and 0.15 at ionic strengths 0.15 and 0.20, respectively. Below this the solubility differences are too small to permit estimation. But consideration of activity coefficients, assuming that of the ion pair to be unity, results in an estimate of Q_{LiBrO_3} equal to about 0.3 at zero ionic strength. According to Fuoss and Kraus[9] the Q value for sodium bromate as determined by precise conductance measurements is 0.50.

Now, when silver bromate solubility in lithium nitrate solutions is compared to that in lithium perchlorate solutions the differences are more striking. Unlike the lithium ion–hydronium ion situation there is no reason to expect nitrate and perchlorate ions to have identical effects on activity coefficients, but the enhancement of solubility by nitrate is not only marked but persists to low ionic strengths. Therefore, the calculations are presented on the presumption that specific activity coefficient effects are small compared to the effect of formation of undissociated silver nitrate.

The solubility, S_N, in lithium nitrate solutions is, then

$$S_N = [Ag^+] + [AgNO_3] = [BrO_3^-] + [LiBrO_3] \quad (5)$$

Because the extent of $LiBrO_3$ formation would be small and nearly identical in the lithium nitrate and lithium perchlorate solutions of equal concentrations, this effect is negligible, and analogous to equation 4 we may derive

$$Q_{AgNO_3} = \frac{S_N^2 - S_L^2}{[NO_3^-]S_L^2} \quad (6)$$

For the molarity of nitrate ion we may use the stoichiometric concentration of lithium nitrate, since the concentration of undissociated silver nitrate does not exceed a few tenths of a per cent of total nitrate. The values of Q_{AgNO_3} calculated using equation 6 are summarized in Table II.

TABLE II

VALUES OF SILVER NITRATE FORMATION QUOTIENT

Ionic strength	0.02	0.05	0.075	0.10	0.15	0.20	0.225	0.30
Q_{AgNO_3} in H_2O	0.82	0.90		0.74	0.62	0.59		
Q_{AgNO_3} in D_2O			(1.20)		0.59		0.59	0.55

It is judged from Fig. 2 that there is no significant difference between the Q values in the two waters within the experimental errors. The dashed line in Fig. 2 shows the behavior which would be expected if: the thermodynamic value of the formation constant is 1.1, the activity coefficient of undissociated silver nitrate is unity, and the mean activity coefficient of the ions can be represented by Davies[10] modification of the Debye–Hückel equation, that is

$$\log f = -0.5\mu^{1/2}/(1 + \mu^{1/2}) + 0.1\mu \quad (7)$$

Because the solubility differences become so small at lower ionic strengths, it is not surprising that the points scatter badly. For example, the highest point in Fig. 2

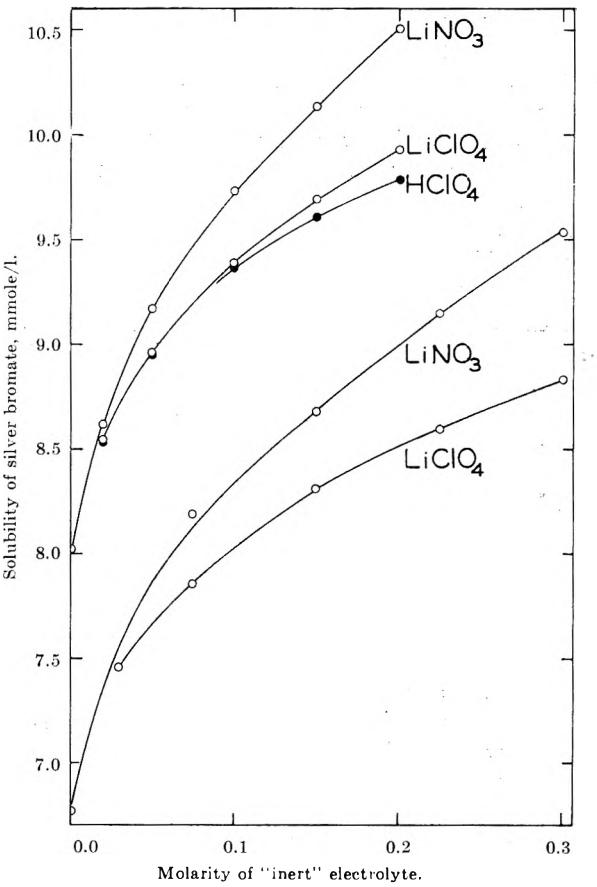

Fig. 1.—Solubility of silver bromate in electrolyte solutions. Top curves refer to protium oxide solutions, bottom curves to deuterium oxide solutions.

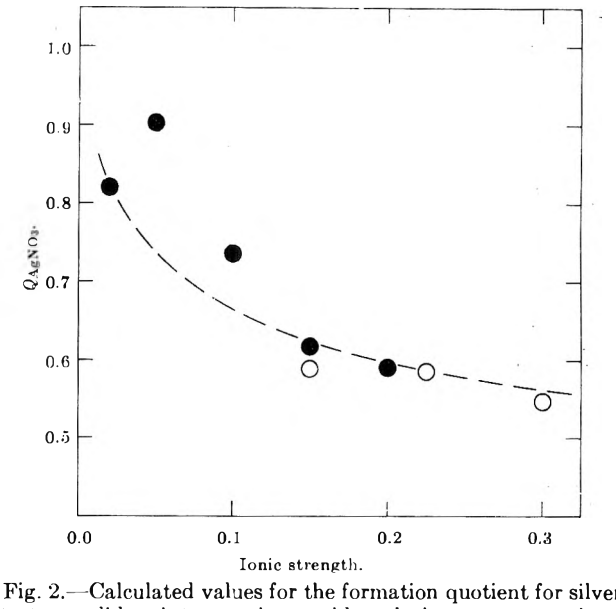

Fig. 2.—Calculated values for the formation quotient for silver nitrate: solid points, protium oxide solutions; open points, deuterium oxide solutions; dashed line, type of variation expected with ionic strength (see text).

(9) R. M. Fuoss and C. A. Kraus, *J. Am. Chem. Soc.*, **79**, 3304 (1957).

(10) C. W. Davies, *J. Chem. Soc.*, 2093 (1938).

at ionic strength 0.05 would have fallen on the dashed line if the solubility had been observed as 9.14 instead 9.17 mmoles/l. Thus, the deviations cannot be taken as significant. According to these results, a one-tenth molar solution of silver nitrate is 94% dissociated, while a one molar solution would be about 75% dissociated.

These values of Q may be compared with the calculations by Monk,[11] based on conductivity data, which indicate a formation constant of 0.58 ± 0.01.

Acknowledgment.—This work was supported by a National Science Foundation grant for scientific research.

(11) C. B. Monk, "Electrolytic Dissociation," Academic Press, New York, N. Y., 1961, p. 140.

THERMAL DIFFUSION OF POLYSTYRENE IN SOLUTION[1]

BY B. RAUCH AND G. MEYERHOFF

Institute of Physical Chemistry, University of Mainz, Germany

Received October 5, 1962

Introduction and Basic Equations.—With a convection-free thermodiffusion cell, applying continuous optical observation of the concentration gradient, it is possible to measure simultaneously the Ludwig–Soret coefficient D'/D and the regular (isothermal) diffusion coefficient D of polymers in solution.[2a] From the knowledge of these coefficients the thermal diffusion coefficient D' results.

In a one-dimensional two-component system with concentrations c_1 and c_2 and movement of the particles in the x-direction there are mean relative velocities v_1 of material flux, due to the concentration difference alone

$$v_1 = -D' \frac{\partial \ln c_1/c_2}{\partial x} \qquad (1)$$

due to the thermal gradient alone

$$v_1' = -D' \frac{\partial T}{\partial x} \qquad (2)$$

and for combined effects as observed during thermo diffusion.

$$v_1 + v_1' = -D\left[\frac{\partial \ln c_1/c_2}{\partial x} + \frac{D'}{D}\frac{\partial T}{\partial x}\right] \qquad (3)$$

Former Experimental Work.—Determinations of the thermal diffusion coefficient were performed by Debye–Bueche,[2b] who used a diffusion cell with convection, by Hoffman–Zimm,[3] Whitmore,[4] Nachtigall–Meyerhoff[5] and Herren–Ham,[6] working under convection-free conditions, but applying different experimental techniques. Since all the authors tested polystyrene in toluene a comparison of the results is possible. This is done in Fig. 3 for the experiments with non-convectional diffusion. The data of Whitmore,[4] which were discussed recently, see Fig. 11 of ref. 2a, are omitted to avoid a too complicated drawing. The indirect determination of D' from D'/D and D delivered a thermal diffusion coefficient D' which is nearly independent of both the concentration, $c > 10^{-2}$ g./ml., and the molecular weight ranging from 44,000 to 2,850,000. Hoffman–Zimm[3] and Herren–Ham[6] measured the migration velocity of a solution–solvent boundary formed in a thermal gradient (70°/cm. with the former authors). The observation was performed by a cathetometer telescope or by a triangle path interferometer, which could only be used after taking off the temperature gradient, which produced too high a refraction. An observation of the boundary was not possible.

Hoffman–Zimm[3] observed a pronounced concentration dependence, but nearly no effect of the molecular weight. Herren–Ham[6] operating at one concentration only measured from M 267,000–1000,000 a $D' \sim 1.5\ 10^{-7}$, but for M 82,000, $D' = 0.6\ 10^{-7}$, a value appreciably lower than found by the other authors.

Experimental Details and Results.—Since the behavior of $D' = f(M, c)$ was rather unclear, on the other hand D' being a very important factor in the understanding of the thermofractionation of polymers, it seemed interesting to determine D' as done by Hoffman–Zimm[3] but using a refined optical technique. This technique, recently[7] described, is able to reproduce by the Philipot–Svensson–Schlieren method the shape of the moving boundary continuously. The optical observation also at very high temperature gradients, *e.g.*, 70°/cm., was possible by placing two cells, one filled with the solution–solvent, the other with pure solvent on the optical path. The thermal refraction gradient of the solvent was eliminated by a reversal prism, which resulted in an optical inversion of one of the cells, such that at the image the cold side was up and the hot side down. Further details on the cells applied are reported elsewhere.[7]

We tested two good fractions of polystyrene, M_w = 70,000 and 950,000, at a mean temperature of 20°.

Figure 1 shows a typical photograph of the concentration gradient at increasing times after putting on the temperature difference. The curves show a pronounced skewness with a steep descent at the side of the boundary, with the higher temperature and the lower concentration. Therefore the skewness is probably a result of the temperature and concentration dependence of D and (for small c) of D'. Observation of such a curve by a cathetometer telescope means practically measuring the maximum. It is rather unlikely that the migration of this maximum is a good representation of the mean relative velocity v_1' demanded by eq. 2.

Being aware of this hitherto unknown skewness we calculated for each curve the center of gravity abscissa. The migration of this point away from the hot plate of the cell is demonstrated for the experiment of Fig. 1 in Fig. 2. There is a good straight line to be found during this 5-hr. test. For comparison we applied also the cathetometer telescope technique and received for $M = 9.5 \times 10^5$ and $c = 2 \times 10^{-2}$ g./ml. a $D' = 0.6 \times 10^{-7}$ which is practically the same as reported by Hoffman–Zimm[3] for the similar molecular weight sample with $M = 1.1 \times 10^6$. [Also for the low concentration $c = 5 \times 10^{-3}$ g./ml. we observed with $D' = 1.5 \times 10^{-7}$ nearly the same result as Hoffman–Zimm.[3]]

The application of the more reliable center of gravity migration resulted in D' values which were nearly independent of both the concentration and the molecular weight, as shown in Fig. 3. The behavior is nearly the same as measured indirectly by Nachtigall–Meyerhoff.[5] The indirect D' obtained by a technique which means a homogeneous concentration throughout

(1) Presented on September 13, 1962, before the Polymer Division at the fall meeting of the American Chemical Society, Atlantic City, N. J.

(2) (a) G. Meyerhoff and K. Nachtigall, *J. Polymer Sci.*, **57**, 227 (1962); (b) P. Debye and A. M. Bueche in H. A. Robinson, Ed., "High Polymer Physics."

(3) J. D. Hoffman and B. H. Zimm, *J. Polymer Sci.*, **15**, 405 (1955).

(4) F. C. Whitmore, *J. Appl. Phys.*, **31**, 1858 (1960).

(5) K. Nachtigall and G. Meyerhoff, *Z. physik. Chem.* (Frankfurt), **30**, 35 (1961).

(6) C. L. Herren and J. S. Ham, *J. Chem. Phys.*, **35**, 1479 (1961).

(7) G. Meyerhoff, H. Lütje, and B. Rauch, *Makromol. Chem.*, **44–46**, 489 (1961).

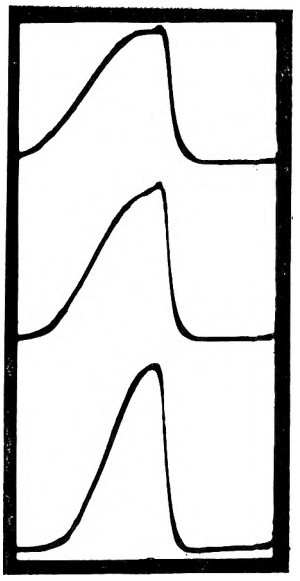

Fig. 1.—Concentration gradient of the migrating boundary at 60, 120, 180 min.: $M = 9.5 \times 10^5$; $c \doteq 2 \times 10^{-2}$ g./ml.

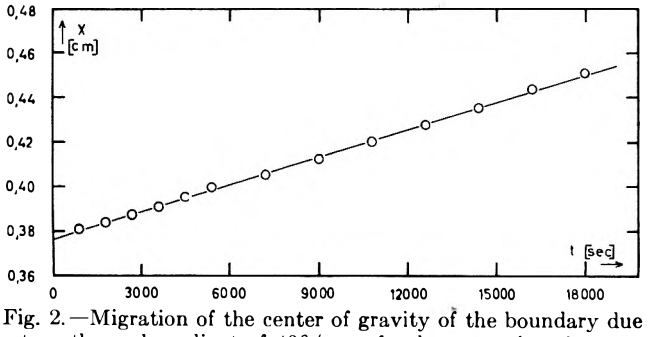

Fig. 2.—Migration of the center of gravity of the boundary due to a thermal gradient of 40°/cm. of polystyrene in toluene.

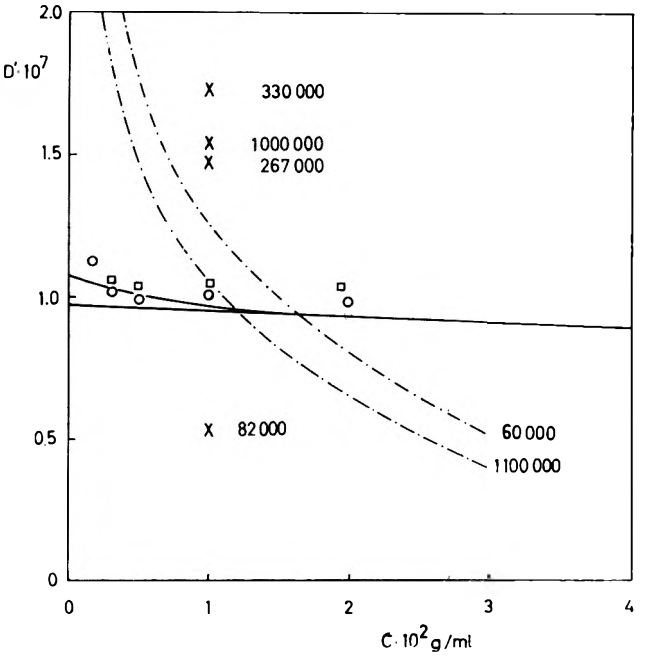

Fig. 3.—Thermal diffusion coefficients of polystyrene in toluene *vs.* concentration; the numbers are the molecular weights of the samples: -·-·-, Hoffman and Zimm[3]; ×××, Herren and Ham[6]; ———, Nachtigall and Meyerhoff[2a,5] 44,000–2,850,000; this work: □, 70,000; O, 950,000.

the cell are a few per cent smaller. This little difference can easily be explained by the different thermal difference, which were $\Delta T = 1$–$2°$/cm. as compared with $\Delta T = 40$–$70°$/cm. here. Also the different averaging of both techniques may cause a slight difference though our polymers were of good uniformity.

Discussion

Our results on polystyrene in toluene demonstrate that the thermal diffusion coefficient D', nearly independent of M and c, cannot be responsible for the thermofractionation effect on polymers, except perhaps for very low concentrations. So the regular diffusion coefficient D, the pronounced molecular weight and concentration dependence of which is well known, seems to be the governing factor with this fractionation, proven to be effective, *e.g.*, by Debye–Bueche,[2b] Langhammer,[8] and Kössler–Kresja.[9]

(8) G. Langhammer, H. Pfenning, and K. Quitzsch, *Z. Elektrochem.*, **62**, 458 (1958).

(9) I. Kössler and J. Kresja, *J. Polymer Sci.*, **57**, 509 (1962).

EFFECT OF ALKALI AND ALKALINE EARTH PROMOTERS ON IRON OXIDE CATALYSTS FOR DEHYDROGENATION OF ETHYLBENZENE IN THE PRESENCE OF STEAM

By Emerson H. Lee and Lawrence H. Holmes, Jr.

Hydrocarbons Division, Monsanto Chemical Company, Texas City, Texas

Received October 6, 1962

The literature[1] describes the use of alkali (group I) and alkaline earth (group II) promoters on iron oxide catalysts for dehydrogenation of ethylbenzene to styrene, but this literature does not clarify the functions of these additives, except that they are known water gas and structural promoters. We have measured the intrinsic activities of promoted iron oxide catalysts for dehydrogenation of ethylbenzene, using a differential reactor. The group I and group II promoters increased the intrinsic activity of iron oxide in a regular trend for each group; an apparent relation between electronic and catalytic properties was observed and investigated.

Experimental

A. Catalyst Preparation and Activity Measurements.—Catalysts were prepared from reagent grade materials. A paste of iron oxide powder and distilled water was mixed with the proper concentration of nitrates of the group I or II metals. The paste was oven dried and broken into granules, then calcined at 800–900° in an electric furnace for two hours. 20 × 30 mesh granules of this material were used for activity measurements. For contact potential measurements, a finely ground paste was packed into each sample hole (described below), smoothed, dried, and calcined at 800–900°. The specific surface areas of all of these catalysts were about 2 m.²/g. as determined by nitrogen absorption isotherms and the B.E.T. equation, utilizing a flow system previously described.[2]

The catalyst activities were measured with a differential reactor, keeping conversions of ethylbenzene to styrene below 10%. The water used for the feed was distilled and de-ionized; the ethylbenzene was of 99.7% purity.

Ethylbenzene and a 13/1 mole ratio of steam were metered and fed in the gas phase into a 20 mm. o.d. horizontal Vycor reactor at 1 atm.; 20 × 30 mesh (U. S. series) catalyst pellets were supported on a stainless steel screen in an open-ended quartz boat. Temperatures were measured by three thermocouples in a 6 mm. Vycor tube just above the catalyst bed. The temperature was 600 ± 2° above the 4 × 0.5 in. catalyst bed; temperature control was better than ±0.5°. Tests were made for mass

(1) K. K. Kearby, from P. H. Emmett, Ed., "Catalysis," Vol. III, Reinhold Publ. Corp., New York, N. Y., 1955, p. 453.

(2) K. V. Wise and E. H. Lee, *Anal. Chem.*, **34**, 301 (1962).

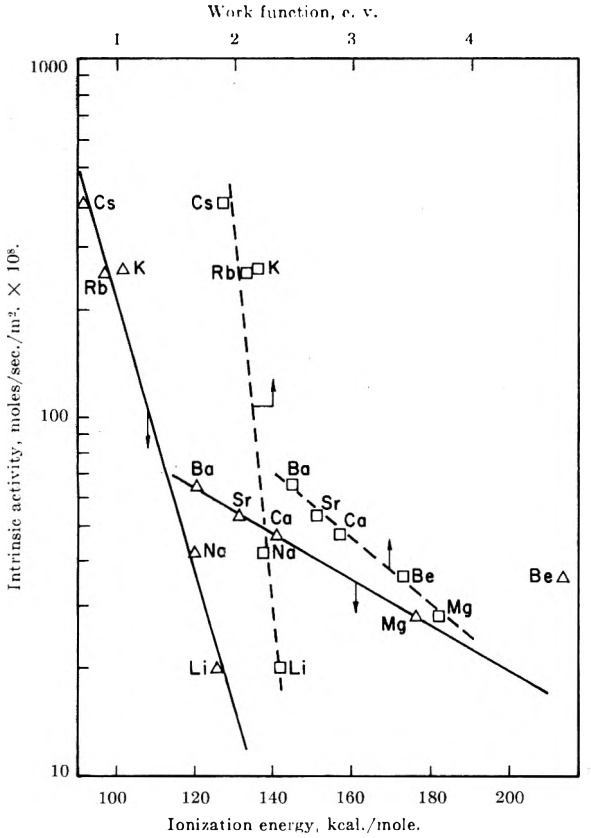

Fig. 1.—Ln intrinsic activity of iron oxide catalysts *vs.* first ionization energy of the promoter atom on lower scale (solid lines) and *vs.* electronic work function of the promoter metal on upper scale (broken lines).

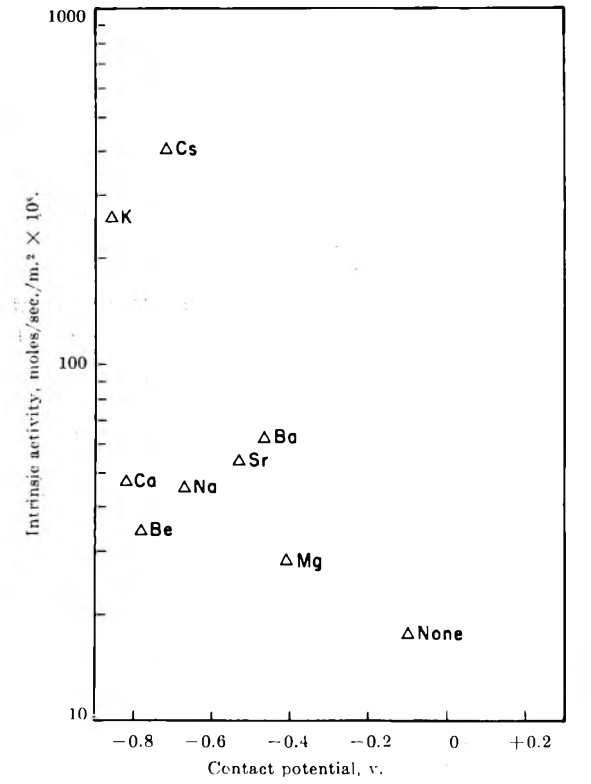

Fig. 2.—Ln intrinsic catalyst activity *vs.* contact potential of iron oxide catalysts quenched in argon at 600°, promoted with group I and group II metal oxides as indicated. The negative sign corresponds to a work function lower than that of the S.S. reference, and the contact potential differences correspond to effective differences in the work function of the catalysts.

transfer limitations as previously described.[3] The styrene made from gas phase reactions in the empty reactor were subtracted from total conversions to give net catalytic conversion to styrene. Thus the reported data are intrinsic catalyst activities, unmodified by mass transfer effects or gas phase reactions. The styrene concentration in the organic layer of the reactor effluent was determined by gas chromatography.

B. **Contact Potentials.**—Contact potentials were measured by the vibrating condenser method introduced by Zisman.[4] The reactor was a high temperature adaptation of the apparatus used by one of us to measure contact potentials in an evacuated system[5]; a vertical 2.25 × 25 in. Vycor reactor tube was used with a conventional tube furnace for heating. The tube was flanged and sealed on the ends with metal flange plates and Teflon gaskets. The preheater coil in the top of the reactor and the reference surface, sample holder, and thermocouple well in the center of the reactor were of stainless steel. The sample holder was a circular disk supported by a threaded rod through the bottom flange. The disk contained four circular depressions in the top face for catalyst samples. The potential of each sample with respect to the stainless steel reference was measured under steady state conditions of operation by aligning each sample in turn with the reference. Thus the differences of work function between catalysts were determined under reaction conditions and subsequently in an argon atmosphere. The feed, catalyst materials, and operating conditions (1 atm., 600°) were the same as those used in the differential reactor for activity measurements. Commercial grade argon was used for the inert gas feed.

Results and Discussion

All promoter concentrations used were in the range of 5 to 10% metal oxide by weight; the activities of the catalysts were insensitive to promoter concentration in this range.

The intrinsic activity of the iron oxide catalyst increased by a factor of ten and reached a plateau with about 1% K_2O. The plateau was reached with a calculated 1–2 monolayers of potassium ions; it was also noted that the cesium-promoted catalyst was the most active. These facts suggested that the dehydrogenation reaction is promoted by bases at the catalyst surface, and the solid that is the strongest electron donor is the most active catalyst. Figure 1 illustrates two possible correlations of the data, one with the first ionization potential of the promoter atom, the other with the electronic work function of the promoter metal. The latter correlation between ln rate *vs.* work function occurred to us through analogy to the equation for electron emission from a solid, where

$$I = AT^2e^{-W/kT} \qquad (1)$$

and

$$\ln I/AT^2 = -W/kT \qquad (2)$$

Here

I = thermionic current
A = constant
T = temperature
W = electronic work function

The increased reaction rate caused by the surface alkali ions is analogous to the well known increase in thermionic emission caused by the same. Thus the broken lines in Fig. 1 are a plot of equation 2 if ln reaction rate is substituted for ln emission rate (T is constant).

To test this apparent correlation between work function and activity, contact potential differences between a stainless steel reference and various catalysts were measured in order to obtain effective differences of work function among the catalysts, as described in the Ex-

(3) E. H. Lee, *Ind. Eng. Chem.*, **53**, 205 (1961).
(4) W. A. Zisman, *Rev. Sci. Instr.*, **3**, 367 (1932).
(5) N. Hackerman and E. H. Lee, *J. Phys. Chem.*, **59**, 900 (1955).

perimental section. The differences of work function under steady state conditions of reaction or subsequently in argon did not correlate with catalyst activity as shown by data in Fig. 2 on measurements in argon (contact potential measurements on rubidium and lithium promoted catalysts were not made). The values plotted are averages of two or more sample preparations for each point; deviations from the average were normally no more than a few hundredths of a volt. Contact potentials under reaction conditions were randomly displaced from those shown in Fig. 2. No significance could be given to potential changes caused by different gases, because this changes the work function of both the catalyst and reference in an unknown way. The work function at 600° of the argon-quenched samples should be similar to those *in vacuo*, since no argon is adsorbed at this temperature.

The results with contact potential measurements indicated that the group I or II promoters lowered the effective work function of the catalysts as expected. However, the lack of a monotonic trend in this direction indicates that different concentrations of promoter existed at the surface in various cases. On the other hand, Fig. 1 indicates a correlation between atomic properties (ionization energies) of the promoters and catalyst activity. It is concluded that in this case, only a fraction of the catalyst surface was responsible for its catalytic activity, and thus the electronic work function, in this case integrated over the whole surface, could not be related to catalytic properties. This illustrates the conclusion of Thompson and Wishlade[6] that gross physical measurements on solids may not be related to catalyst properties in some cases because only parts of the surface are catalytically active. On the other hand, Roginskii[7] has demonstrated in some cases a direct relation between electronic work function and catalytic activity of solids.

Acknowledgments.—We wish to thank H. C. Tucker for assistance on electronic gear, and Professors Herman Pines, W. H. Urry, and Norman Hackerman for helpful discussions.

(6) S. J. Thompson and J. L. Wishlade, *Trans. Faraday Soc.*, **58**, 1170 (1962).

(7) S. Z. Roginskii. *Kinetika i Kataliz.* **1**, 15 (1960) (English translation).

SURFACE CONCENTRATION BUILD-UP DURING DIFFUSION IN POROUS MEDIA WITH DEAD-END PORE VOLUME

By Richard C. Goodknight

California Research Corporation, La Habra, California

and Irving Fatt

Miller Institute for Basic Research in Science and Department of Mineral Technology, University of California, Berkeley, California

Received October 10, 1962

Recent treatments[1-3] of non-steady state diffusion through porous media which contain dead-end pores did not include the case of surface concentration build-up when a linear system at steady state was suddenly closed off at the exit end.[4] This case is presented here.

(1) R. C. Goodknight, W. A. Klikoff, Jr., and I. Fatt, *J. Phys. Chem.*, **64**, 1162 (1960).

(2) R. C. Goodknight and I. Fatt, *ibid.*, **65**, 1709 (1961).

(3) I. Fatt, *ibid.*, **66**, 760 (1962).

(4) The equivalence of the equations describing non-steady state diffusion to those for flow of a slightly compressible fluid in a porous medium has been discussed in references 1 and 2.

When a linear porous body of length L and containing dead-end pores is discharging matter by diffusion from the outflow end at steady state the initial conditions are

$$C(x, 0) = (C_L - C_0)\left(1 - \frac{x}{L}\right) \text{ and } C_2(x, 0) = (C_L - C_0)\left(1 - \frac{x}{L}\right) \quad (1)$$

Definition of terms is given in the section labeled "Nomenclature." If the outflow end is suddenly closed while the inflow end is maintained at constant concentration the boundary conditions are

$$\frac{\partial C}{\partial x}(L, t) = 0 \text{ and } C(0, t) = C_L \quad (2)$$

The concentration at any point and time can be obtained[1-3] by solving equations 3 and 4 subject to the conditions given by equations 1 and 2.

$$\frac{\partial C}{\partial t} = \frac{D}{\theta^2}\frac{\partial^2 C}{\partial x^2} - \frac{V_2}{V_1}\frac{\partial C_2}{\partial t} \quad (3)$$

$$\frac{\partial C_2}{\partial t} = \frac{DA_0}{l_0 V_c}(C - C_2) \quad (4)$$

The solution, by methods described previously,[1-3] is

$$C(x, t) = C_0 + (C_L - C_0) \times \sum_{n=1}^{\infty} \frac{(-1)^{n+1} (\sin \beta_n x) \exp(S_n t)}{\beta_n L^2 S_n \left(\frac{\partial \beta}{\partial S}\right)_n} \quad (5)$$

where

$$\beta_n = (2n - 1)\frac{\pi}{2L} \quad (6)$$

and S_n are all roots of

$$\beta_n^2 - = \frac{1}{\alpha}\left[S_n + \frac{V_2 H}{V_1}\left(\frac{S_n}{S_n + H}\right)\right] \quad (7)$$

That is

$$2S_n = -\left[H\left(1 + \frac{V_2}{V_1}\right) + \alpha\beta_n^2\right] \pm \sqrt{\left[H\left(1 + \frac{V_2}{V_1}\right) + \alpha\beta_n^2\right] - 4\alpha\beta_n^2 H} \quad (8)$$

and

$$\left(\frac{\partial \beta}{\partial S}\right)_n = -\frac{1}{2\alpha\beta_n}\left[1 + \frac{V_2}{V_1}\left(\frac{H}{S_n + H}\right)^2\right] \quad (9)$$

Equation 5 was evaluated by use of a Fortran program on an IBM 704 computer for several laboratory systems of interest.

Nomenclature

A_0 cross-sectional area of neck of dead-end pore
C concn. in flow channels (variable)
C_L concn. at downstream end
C_0 concn. at upstream end
C_2 concn. in dead-end pore

D diffusion coefficient
H a system parameter, DA_0/l_0V_c
l_0 length of neck of dead-end pore
L length of porous medium
S parameter of the Laplace transform
t time
V_1 pore volume of flow channels
V_2 total volume of dead-end pores
V_c volume of a single dead-end pore
x distance coördinate
α a system parameter, D/θ^2
β a constant defined by equation 6
θ tortuosity, diffusion path length/L
ϕ porosity

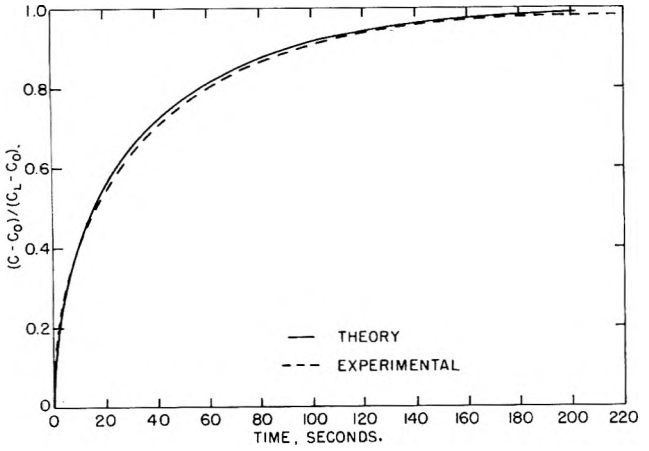

Fig. 1.—Comparison of solution of equations 3 and 4 with experimental data from fluid flow model with initial and boundary conditions of equations 1 and 2: $X/L = 1.0$; $V_1 = 926$ cc.; $V_2 = 450$ cc.; $H = 0.04540$ sec.$^{-1}$; $\alpha = 341$ cm.^{2} sec.$^{-1}$.

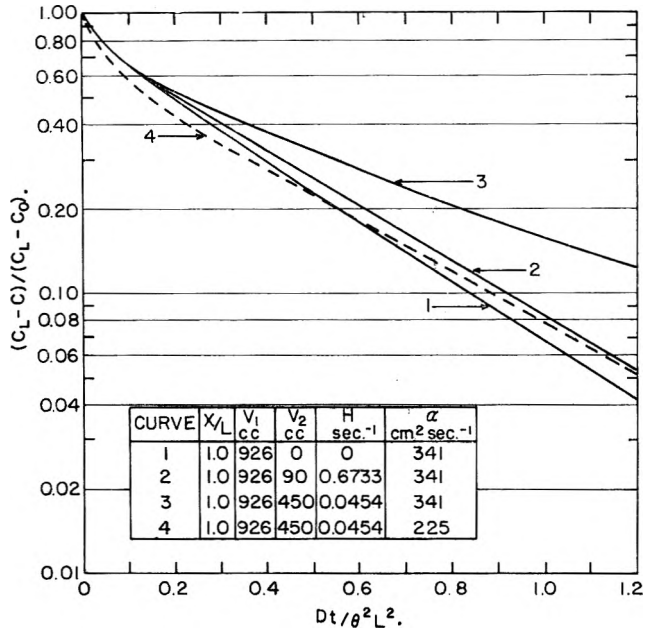

CURVE	X/L	V1 cc	V2 cc	H sec.-1	α cm2 sec.-1
1	1.0	926	0	0	341
2	1.0	926	90	0.6733	341
3	1.0	926	450	0.0454	341
4	1.0	926	450	0.0454	225

Fig. 2.—Dimensionless concentration parameter at $X = L$ as a function of dimensionless time. System parameters used in equations 3 and 4 are shown in the insert table.

Experimental

The solution to equations 3 and 4 as given in equation 6 was checked experimentally by using the mathematically equivalent fluid flow system. This method of studying solutions of the diffusion equation has been described in detail previously.[1-3] Briefly, it is a method in which pressure transients during non-steady state flow of a slightly compressible fluid in a porous medium are measured for initial and boundary conditions equivalent to the diffusion problem of interest. Air, at a mean pressure near atmospheric and a one per cent pressure gradient, is a satisfactory slightly compressible fluid. The porous medium is a plastic coated sandstone bar, five feet long and of cross-section 2 in. by 2 in. Parameters used in both the experiment and equation 5 are shown in the caption of Fig. 1.

Figure 1 shows a typical comparison of experimental and theoretical curves. The experimental curve was obtained as a continuous recording from an electronic pressure transducer.[1-3] The maximum difference between theory and experiment is one per cent.

Discussion

Problems in non-steady state diffusion are usually treated graphically by plotting the solution of the governing differential equation in dimensionless form. For a porous system without dead-end pores equations 3 and 4 reduce to the dimensionless form

$$\frac{\partial(C/C_0)}{\partial\left(\frac{Dt}{\theta^2L^2}\right)} = \frac{\partial^2(C/C_0)}{\partial(x/L)^2} \qquad (10)$$

If the terms accounting for dead-end pore space are included then equations 3 and 4 cannot be reduced to a convenient dimensionless form. In the dimensionless form equation 3 will still have the ratio V_2/V_1. This prevents solutions of equation 3 from being independent of system parameters. For each V_2/V_1 there will be a separate solution.

Figure 2 shows a semilogarithmic plot of the dimensionless concentration parameter $(C_L - C)/(C_L - C_0)$, measured at the outflow end when this end is closed after being at steady-state flow, as a function of the dimensionless time parameter Dt/θ^2L^2. Concentration as a function of time can be read from this curve because all other terms are constants for a given system. The curve labeled 1 is for a porous body without dead-end pores. This curve is independent of the system parameters and therefore applicable to all linear diffusing systems with the conditions given by equations 1 and 2 and with known D and θ. D must be measured independently by the methods conventionally used for measuring molecular diffusion coefficients. θ may be calculated from a steady state diffusion or an electrical resistivity measurement.[5]

A measurement of tortuosity by steady-state diffusion or electrical resistivity always gives ϕ/θ^2. If the porous material has no dead-end pores then ϕ is unambiguous and θ is easily calculated. However, if there are dead-end pores then a gravimetric or volumetric measurement of ϕ will normally include these pores. If, for a system with dead-end pores, ϕ from total pore volume is used to calculate θ from the measured ϕ/θ^2 and then this θ is used in the term Dt/θ^2L^2, the solution of equations 3 and 4 will give the curve labeled 4 in Fig. 2. This curve is for a system of the same total pore volume as for curve 1 but some of the volume is in dead-end pores.

Curves 2 and 3 in Fig. 2 are for systems in which the dead-end pore volume is known and only the connected pore volume was used to calculate ϕ. Unfortunately, there is no method at present whereby the dead-end pore volume can be measured. If experimental diffusion data together with an experimental θ^2 term are plotted on Fig. 2 then any deviation from curve 1 is an indication of the presence of dead-end pores. Thomas[6] has reported deviations of this kind in sandstone for which other evidence also points to the presence of dead-end pore space.

(5) I. Fatt, *J. Phys. Chem.*, **63**, 751 (1959).
(6) G. H. Thomas, M. S. Thesis, University of California, Berkeley, June, 1962.

Acknowledgment.—The authors wish to thank the donors of the Petroleum Research Fund, administered by the American Chemical Society, for their support of the research which led to this paper.

ON THE CONFORMATION OF THE D-GLUCOPYRANOSE RING IN MALTOSE AND IN HIGHER POLYMERS OF D-GLUCOSE

BY V. S. R. RAO AND JOSEPH F. FOSTER

Department of Chemistry, Purdue University, Lafayette, Indiana

Received October 12, 1962

In considerations of the configuration in solution of amylose and other polysaccharides the question of ring conformation of the monomer units is of utmost importance.[1,2] Thus Hollo and Szejdli[1] have pointed out that if the D-glucose residues in amylose exist in the Cl conformation the chain should be relatively rigid and possess an essentially helical configuration. Of the two possible chair forms and innumerable boat forms it has been suggested from stability considerations that either the Cl, Bl, or 3B conformations are most probable.[2] While it seems to have been generally accepted that D-glucose (in common with most monosaccharides), simple D-glucosides, and the glucose units of cellobiose and cellulose exist exclusively in the Cl conformation, there have been several suggestions that the same is not true for maltose and higher polysaccharides of the amylose series. Reeves[3] called attention to the difficulty of forming α-1,4-glucosidic bonds between two glucose residues both of which are in the Cl conformation. He further suggested, on the basis of the incomplete reaction of amylose with cuprammonium reagent and as an explanation for the decrease in optical rotation in alkaline solution, that approximately half of the glucose residues of amylose exist in a boat conformation. This conclusion has been questioned by Greenwood and Rossotti,[2] who favored the Cl conformation. Since methyl β-maltoside also shows a decrease in rotation of alkali Reeves further suggested that the non-reducing residue of maltose exists in a boat conformation.[3] Bentley,[4] on the basis of comparative studies of the rates of oxidative bromination and hydrolysis, also concluded that the non-reducing unit of maltose possesses a boat conformation, while the reducing unit of maltose and both units of cellobiose have the usual Cl conformation.

It would appear that clear answers to such questions should be attainable through nuclear magnetic resonance (n.m.r.) spectroscopy. It has been shown that in sugars[5] and in acetylated sugars[6] the signal due to the anomeric proton appears at lower field than that of any of the other carbon-bonded hydrogen atoms. Furthermore, it seems clear from those same studies that the signal for an equatorial anomeric proton (H_{1e}) occurs at a somewhat lower field by about 0.5–0.7 p.p.m. than for an axial anomeric proton (H_{1a}). In addition, the dihedral angle between the anomeric proton and the hydrogen on the adjacent carbon atom may be obtained from the magnitude of the splitting of the corresponding absorption peak through application of the Karplus equation.[5,7]

The n.m.r. spectra of maltose and a number of related compounds have been determined at 60 Mc./sec. with a Varian A-60 n.m.r. spectrometer employing 10–20% by weight solutions of the carbohydrates in D_2O. The assignment of τ values was made by taking the water peak (5.2 τ) as an internal standard. Results are shown in Table I.

In the case of cellobiose two peaks have been observed in the lower field region at 4.70 and 5.38 τ. From intensity considerations it seems clear that the peak at 5.38 is due to the anomeric proton of the non-reducing unit plus the anomeric proton at the reducing end when it is in the axial position (β-anomer). The peak at 4.70 is due to the anomeric proton at the reducing end when it is in the equatorial position (α-anomer). These two peak positions approximately coincide with those of the β- and α-anomers, respectively, of D-glucose and the methyl D-glucosides. The dihedral angles deduced using the modified Karplus equation, namely, 54 and 160° for the peaks at 4.70 and 5.38 τ, respectively, while not in agreement with the expected angles for the Cl conformation (60 and 180°) do agree well with the corresponding values deduced in the same way for α- and β-glucose and the methylglucosides. Hence these results are in agreement with Bentley's conclusion and with the recent demonstration by Jacobson, Wunderlich and Lipscomb[8] that both glucose units in cellobiose exist in the Cl conformation.

In the case of maltose three peaks are seen in the lower field range at 4.58, 4.74, and 5.30. From the intensity of these peaks it can be concluded that the peak at 4.58 is due to the anomeric proton (H_1) of the non-reducing unit. Because of mutarotation the signal due to the protons H_1 of the reducing glucose units appears at two places, 4.74 and 5.30. The dihedral angles obtained from the splitting of these peaks are 54 and 154°, respectively. From the dihedral angles and the peak locations, it may be concluded that the reducing glucose unit in maltose is in the Cl conformation. The dihedral angle obtained from the splitting of the peak at 4.58 is about 55°, in accord with either the Cl or Bl but not the 3B conformation. The τ value of this peak is slightly lower than that of α-glucose (4.78). If this unit were in the Bl conformation this proton should be in an essentially axial position and it might be expected that its signal would appear at a much higher τ value (above 5.0). However, this cannot be stated with certainty in the absence of suitable test compounds known to exist in a boat conformation. It is, nevertheless, very unlikely that the glucose ring would occur in a perfect Bl conformation due to repulsion between the protons at C_1 and C_4, which would be very close in this conformation. Any twisting to relieve this repulsion would lead to a considerable change in dihedral angle. Bentley[4] has suggested that the conformation is between that of the idealized Bl and 3B, which seems very unlikely from the observed dihedral splitting. Furthermore, due to the ready interconvertability of the boat forms it would be

(1) J. Hollo and J. Szejdli, *Die Starke*, **13**, 222 (1961).
(2) C. T. Greenwood and H. Rossotti, *J. Polymer Sci.*, **27**, 481 (1958).
(3) R. E. Reeves, *J. Am. Chem. Soc.*, **76**, 4595 (1954); *Ann. Rev. Biochem.*, **27**, 15 (1958).
(4) R. Bentley, *J. Am. Chem. Soc.*, **81**, 1952 (1959).
(5) R. W. Lenz and I. P. Heeschen, *J. Polymer. Sci.*, **51**, 247 (1961).
(6) R. U. Lemieux, R. K. Kullnig, H. J. Bernstein, and W. G. Schneider, *J. Am. Chem. Soc.*, **79**, 1005 (1957); **80**, 6098 (1958).
(7) M. Karplus, *J. Chem. Phys.*, **30**, 11 (1959).
(8) R. A. Jacobson, J. A. Wunderlich, and W. N. Lipscomb, *Acta Cryst.*, **14**, 598 (1961).

TABLE I

SUMMARY OF N.M.R. RESULTS

Sample	Coupling, const. $J_{H_1H_2}$, cycles/sec.	Dihedral angle (degrees)	Chemical shifts (τ values)				
			Anomeric protons[a]		Other protons		
			H_{1e}	H_{1a}			
α-D-Glucose[b]	2.4	58	4.78		6.25	6.41	
β-D-Glucose[b]	7.5	151		5.36	6.25		6.57
α-Methyl-D-glucoside[c]					6.23	6.42	6.60 (methyl)
β-Methyl-D-glucoside	7.7	152		5.54	6.13	6.43 (methyl)	6.58
Cellobiose	8.8	160		5.38 (4)	6.03	6.32	6.46
	2.9	54	4.70 (1)				
Maltose	2.8	55	4.58 (5)				
	3.0	53	4.74 (2)		6.13	6.32	
	8.0	154		5.30 (3)			
Schardinger γ-dextrin	2.7	56	4.79		6.08	6.18	6.33

[a] The numbers in the parentheses indicate relative peak intensities. [b] Data for α- and β-D-glucose are from Lenz and Heeschen.[5] [c] Peak corresponding to the anomeric proton was not resolved from the water peak.

expected in that case that the protons would be changing continuously from equatorial to axial positions and *vice versa*, with a continuous fluctuation in the dihedral angle. The sharp dihedral splitting strongly suggests that this is not the case, as does the existence of the two peaks at 6.13 and 6.32, which approximately coincide with the corresponding peaks in α-D-glucose. Hence the most probable conformation of the non-reducing glucose unit in maltose is also Cl, possibly with some distortion.

In the case of the Schardinger γ-dextrin a single peak appears at lower field, namely at 4.8 τ. This immediately demonstrates the near-identity or identity of all the anomeric protons in this cyclic octasaccharide. It is probable that in this compound all the glucose units are in the same conformation. The dihedral angle obtained from the peak splitting is about 55° and the peak position is in good agreement with that of the α-anomer of D-glucose.

It thus seems highly probable that both rings in maltose and all eight rings in the Schardinger-γ-dextrin exist in the Cl conformation or a conformation very closely related thereto. It is suggested that in all probability the same will be found to hold true for the higher polymers of D-glucose including amylose.

Acknowledgment.—We are indebted to the Corn Industries Research Foundation for financial support of this work, to Mr. W. E. Baitinger for technical assistance, and to Professor Norbert Muller for helpful discussions. We also wish to express our appreciation to Dr. Nelson K. Richtmeyer of the National Institute of Arthritis and Metabolic Diseases for supplying highly purified samples of the methyl-D-glucosides and to Professor Dexter French of Iowa State University for supplying the crystalline Schardinger-γ-dextrin.

THE DECOMPOSITION PRESSURE AND MELTING POINT OF URANIUM MONONITRIDE[1]

BY W. M. OLSON AND R. N. R. MULFORD

University of California, Los Alamos Scientific Laboratory, Los Alamos, New Mexico

Received November 5, 1962

The decomposition pressure of uranium mononitride has been determined in the temperature range 2500–2850° by observing the apparent melting point as a function of nitrogen pressure. At pressures below that necessary to observe congruent melting of UN, the following reaction occurs

$$UN(s) \longrightarrow U(l, \text{sat. with N}) + {}^1/_2\ N_2(g)$$

This decomposition proceeds very rapidly whenever the decomposition pressure exceeds the nitrogen pressure in the system, and the solid liquefies. When the nitrogen pressure is 2.5 atm. or greater, congruent melting of UN occurs. This melting point has been determined to be 2850 ± 30°.

Previous workers[2] have reported a lower melting point, but undoubtedly the decomposition of the nitride was actually observed.

Experimental

Apparatus.—The melting point or decomposition temperature was determined with an optical pyrometer by observing a few granules of UN placed on a tungsten strip heated by resistance. These strips were 5 mils thick and had a vee with an included angle of 30° formed in the center. The strips were $^5/_{16}$ in. wide and $2^1/_4$ in. long, and the vee was about $^5/_{16}$ in. along each side. The strip was mounted between two water-cooled copper electrodes. The pyrometer was sighted into the vee from above, and the granules of UN which were placed in the apex of the vee could be observed at the same time the temperature was determined. Although a small amount of tungsten nitride formed near the electrodes during heating, this formation caused no difficulties.

The copper electrodes were fitted into the bottom of a water-cooled stainless steel can. A quartz window was mounted in the lid of the can. This enclosure and all attendant parts were designed to operate either with vacuum or up to 200 p.s.i. pressure.

Temperature Determination.—Mendenhall[3] first suggested the use of a vee shaped metal strip heated by resistance to obtain blackbody radiation for the determination of the emissivity of metals. His method consisted of bending a strip of metal longitudinally into a vee with an enclosed angle of 10°. Under such conditions blackbody radiation is essentially obtained if the reflectivity of the metal is 0.75 or less.[4] Theoretically, if a powder were placed in the apex of such a vee it could not be seen because of the blackbody conditions existing. When the enclosed angle is considerably greater than 10°, blackbody conditions are not obtained, and a material placed in the vee can be observed. It is possible to correct for the deviation from blackbody radiation if the emissivity of the metal and the angle of the vee are known.[4] In the work reported here the emissivity of

(1) Work done under the auspices of the United States Atomic Energy Commission.

(2) J. J. Katz and E. Rabinowitch "The Chemistry of Uranium," NNES VIII-5, McGraw-Hill, New York, N. Y., 1951, p. 234.

(3) C. F. Mendenhall, *Astrophysical J.*, **33**, 91 (1911).

(4) A. G. Worthing, in "Temperature," Rheinhold Publ. Corp., New York, N. Y., 1941, p. 1164ff.

tungsten determined by De Vos[5] was used. The formula for the 30° vee used is

$$\frac{{}_{w}B_{\lambda}}{{}_{b}B_{\lambda}} = \epsilon(1 + r_{\lambda} + r_{\lambda}^{2} + r_{\lambda}^{3} + r_{\lambda}^{4} + r_{\lambda}^{5})$$

where ${}_{w}B_{\lambda}$ is the spectral brightness of the 30° vee, ${}_{b}B_{\lambda}$ is the blackbody brightness, ϵ is the emissivity, and r is the reflectivity of the vee material. Six terms are included in the equation because a light beam originating in a 30° vee will have six reinforcements from reflections. The ratio ${}_{w}B_{\lambda}/{}_{b}B_{\lambda}$ is the effective emissivity of the vee and for a 30° tungsten vee in the temperature region 2500–3000° is 0.96. This corresponds to a difference between the observed brightness temperature and the true temperature of 12° at 2500° and 17° at 3000°.

There are several errors which are immediately discernible in the method used. As De Vos has observed,[5] the emissivity of tungsten is quite dependent upon its surface condition, and therefore the emissivity which we used may be in error. Also, when the vee itself was melted, melting occurred about one mm. up the side from the apex and therefore the sample was not located at the hottest point in the vee. This happened because the apex of the vee was radiating entirely toward a cold wall whereas the side of the vee radiated partially to the other side of the vee. Also, in our modified form of the Mendenhall wedge there is a temperature gradient in the vee because the apex of the vee is at the center of the strip which is heated by resistance and cooled at the ends. Thus the vee must have temperature gradients and the temperature reading is a composite of several different temperatures, rather than the composite of six sources each at the same temperature assumed in the derivation of the formula.

Because of these possibilities for error, the technique was tested using melting points of known materials. In the first method thirty degree vees were made of Pt, Rh, Ta, and W and the melting points determined. A melting point of 1770 ± 5° was obtained for Pt (1948 Int. Temp. Scale.: 1769.3°), 1961 ± 5° was obtained for Rh (NBS value 1960°[6]), 3001 ± 5° was obtained for electron beam melted Ta (Stull and Sinke report 2997 ± 10°[7]), and 3356 ± 5° was obtained for tungsten (1948 Int. Temp. Scale: 3380°). In each case the effective emissivity of the vee was determined from the emissivity of the metal. The second method was to melt filings of Ta, Mo, and Ir in a 30° tungsten vee in the same way that the UN melting points were measured. Electron beam refined Ta gave a melting point of 2980 ± 5°, filings of electron beam melted Mo melted at 2632 ± 5° (accepted value[7] is 2617 ± 10°) and filings of iridium (99.89% pure) melted at 2425 ± 5° (NBS value[6] 2443° and Baird[8] reports 2410 ± 10°). It would appear from the results of the two methods that the accuracy of the technique is well within the ±30° limit assigned.

Calibration of the disappearing filament Pyro optical pyrometer up to 1900° was done with a ribbon filament lamp calibrated by NBS, and up to 3300° by the use of rotating sectors. The absorption of the windows and prism was determined with the NBS certified bulb and the pyrometer.

Preparation of UN.—Uranium nitrides can be prepared by reaction of UH_3 with flowing nitrogen at 350°. This method gave a finely divided product which ignited spontaneously upon exposure to air. Direct reaction of massive uranium with nitrogen at temperatures between 1000 and 2000° was also tried. Only partial conversion of the uranium to nitride occurred in six hours. The method which was finally adopted was the direct reaction of uranium foil with nitrogen gas. Uranium foil about 2 mils thick was cleaned with emery paper and placed in a 30° tungsten vee. The foil was heated to about 900° and then 1 atm. of spectroscopically pure nitrogen was put in. Heating at 900° continued for several hours, and then the temperature was increased to approximately 1600°. After heating at 1600° for approximately one hour, the nitrogen was pumped off, and the product was heated at 1600° for about one half hour *in vacuo* to decompose higher nitrides. The UN prepared in this manner was face centered cubic with a cell constant of 4.8891 ± 0.0002 Å.

(5) J. C. De Vos, *Physica*, **20**, 669 (1954).

(6) F. D. Rossini, *et al.*, "Selected Values of Chemical Thermodynamic Properties," NBS Circular 500, U. S. Government Printing Office, Washington, D. C., 1952.

(7) D. R. Stull and G. C. Sinke, "Thermodynamic Properties of the Elements," American Chemical Society, 1956.

(8) J. D. Baird, Report A 843, Associated Electrical Industries Ltd., Aldermaston, England.

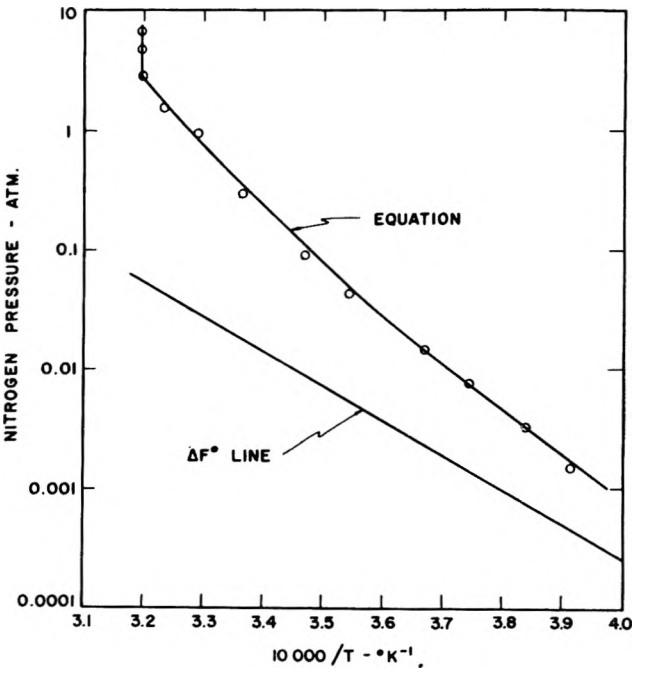

Fig. 1.—Decomposition pressure of UN.

No deviations from this value were noted in this work, although the stoichiometry of UN was not studied. This product proved to be very stable to oxidation. One sample was stored for three months in air without any oxidation detectable by X-ray diffraction.

Metallographic examination of UN which had been melted congruently in a tungsten vee did not reveal a reaction product at the tungsten-UN interface. Erosion of the tungsten did occur, however, as evidenced by globules of tungsten in the melt. There was very little intergranular penetration of the tungsten by the UN.

It was found that UN which was contaminated with oxygen, either from oxidation of the starting material or from an impure nitrogen atmosphere, gave substantially higher decomposition temperatures than pure UN.

Procedure.—To determine a melting point, or decomposition temperature, a few granules of UN were placed in the bottom of the vee, the apparatus was evacuated, and the tungsten ribbon was heated to about 1600° *in vacuo* to ensure decomposition of any nitrides higher than UN. Spectroscopically pure nitrogen was then admitted to the desired pressure. The temperature was increased rapidly until the expected melting point was almost reached, and then very slowly until melting or decomposition was observed. A temperature and pressure reading was taken before and after melting, and the melting point and decomposition pressure were assumed to be half way between these readings. By careful power adjustment this range could be reduced to 10° at 3000°.

Results and Discussion

The decomposition pressure–temperature data plotted as log p *vs.* 10,000/T are shown in Fig. 1. The vertical portion above 2.5 atmospheres corresponds to the true congruent melting point of UN, 2850 ± 30°. Below 2.5 atmospheres the data are fitted by a gentle curve. It is not possible to determine the standard heat of formation of UN from these data, because the liquid uranium present after decomposition is saturated with nitrogen and therefore is at some unknown activity less than unity.

It is, however, desirable to somehow compare our results with the available thermodynamic information on UN. Rand and Kubaschewski[9] give heat and entropy values for the formation of UN at 298°K. The

(9) M. H. Rand and O. Kubaschewski, Document AERE-T-3487, "Thermochemical Properties of Uranium Compounds," United Kingdom Atomic Energy Authority, 1960.

entropy is estimated, and the heat is obtained from calorimetric measurements by Gross, *et al.*[10] The values are $\Delta S_{f\,298}^{0} = -21.9$ cal. deg.$^{-1}$ mole^{-1} and $\Delta H_{f\,298}^{0} = -70.4$ kcal. mole^{-1} The standard free energy of formation in the temperature range of our measurements may be calculated by using estimated heat capacities: $\Delta C_{p_f}^{0} = +1.5$ cal. deg.$^{-1}$ mole^{-1} (298–1406°K.) and $\Delta C_{p_f}^{0} = +1.8$ (1406–3125°K.). The line representing the ΔF^0 thus calculated is shown in Fig. 1. This line gives the nitrogen pressure expected if UN decomposed to pure liquid uranium and N_2 gas. But the liquid uranium phase actually produced is saturated with nitrogen and the observed nitrogen pressure deviates from the ΔF^0 line because of this. As the temperature increases, the solubility of nitrogen in the liquid also increases and the deviation becomes larger as seen in Fig. 1. At lower temperatures the experimental curve should approach the ΔF^0 curve quite closely. In order to extend the range of usefulness of our P–T data, an empirical equation has been fitted to the data such that the curve represented by the equation not only fits the observed points but also has the property of asymptotically approaching the ΔF^0 line as the temperature decreases. The equation is: $\log p$ (atm.) $= 8.193 - (29.54 \times 10^3)1/T + (5.57 \times 10^{-18})T$.[5] This fits the data quite well and comes very close to the ΔF^0 line at the melting point of uranium. The choice of this equation implies that the solubility of nitrogen in liquid uranium at its melting point is very small. We believe this to be the case, although experimental confirmation is lacking. It is suggested that the above empirical equation is suitable for calculation of the nitrogen pressure in equilibrium with nitrogen-saturated liquid uranium and UN in the temperature range from 1406 to 3125°K.

Acknowledgment.—We wish to thank F. H. Ellinger for the X-ray work reported herein.

(10) P. M. Gross, *et al.*, Paper SM-26/7 at Symposium on the Thermodynamics of Nuclear Materials, Vienna, 1962. To be published by the International Atomic Energy Agency, Vienna.

CONDUCTANCE STUDIES OF TETRA-*n*-BUTYL-AMMONIUM IODIDE IN 1-BUTANOL[1-3]

BY H. V. VENKATASETTY[4] AND GLENN H. BROWN[5]

Department of Chemistry, University of Cincinnati, Cincinnati, Ohio

Received October 3, 1962

The investigation of the properties of ionophores[6] in non-aqueous systems has received considerable attention in recent years. A number of 1:1 electrolytes have been investigated in a variety of solvents.[7] There appear to be only two studies of the conductance of electrolytes in 1-butanol at different temperatures. Seward[8] measured the conductances and viscosities of solutions of tetra-*n*-butylammonium picrate in 1-butanol over the entire concentration range from dilute solution to fused salt at 91°. Venkatasetty and Brown[9] have studied the conductance of lithium iodide and ammonium iodide in 1-butanol at 0, 25, and 50°.

Experimental

Apparatus and Materials.—The apparatus used for this study has been described previously.[9] Tetra-*n*-butylammonium iodide of "extra pure" quality from Eastman Organic Chemicals was recrystallized three times from pure ethyl acetate and dried to constant weight in a vacuum oven at 70°. The melting point of 144–145° checked well with the literature value.[10]

The method for purification of the 1-butanol used in this study has been described in a previous paper.[9]

Preparation of Solutions and Procedure for Measurements.—All solutions were prepared in a drybox by transferring to a container a known weight of the salt and dissolving it in an exact volume of the solvent. Dilute solutions were prepared by further dilutions, using calibrated pipets and burets. Concentrations were established by analysis. These solutions were preserved in bottles which had been coated on the outside with black paint and were sealed with serum caps. 1-Butanol is found to have no effect on these serum caps. Transfers of solutions were always made using the proper-sized hypodermic syringe. All weighings were corrected for the buoyancy effect of air. The procedure for making the conductance measurements is described in a previous paper.[9]

Results and Discussion

The data for the equivalent conductance of tetra-*n*-butylammonium iodide at various concentrations in gram equivalents per liter corresponding to each temperature are recorded in Table I. The maximum experimental error inherent in these data is 0.1%.

TABLE I

EQUIVALENT CONDUCTANCE OF TETRA-*n*-BUTYLAMMONIUM IODIDE IN 1-BUTANOL

Temp. 0.00°		Temp. 25 ± 0.02°		Temp. 50 ± 0.02°	
$c \times 10^4$, N	Λ_{obsd}	$c \times 10^4$, N	Λ_{obsd}	$c \times 10^4$, N	Λ_{obsd}
7.64	5.60	7.46	10.91	7.29	18.45
15.28	4.74	14.93	9.29	14.59	15.27
19.04	4.50	18.60	8.74	18.20	14.11
22.93	4.21	22.40	8.27	21.89	13.53
38.20	3.54	37.30	7.02	36.50	11.49
57.30	2.98	56.00	6.09	54.70	10.10
76.40	2.57	74.70	5.38	72.99	9.21
95.50	2.37	93.30	4.97	91.20	8.59
114.60	2.20	112.00	4.69	109.50	8.12
133.70	2.09	130.70	4.44	127.70	7.74
152.80	2.06	149.30	4.39	145.90	7.43

The plots of equivalent conductance *vs.* the square root of concentration for Bu_4NI at all the temperatures studied show marked deviation from linearity. These deviations indicate that Bu_4NI behaves as a weak electrolyte in 1-butanol with definite ion-pair formation.

The limiting equivalent conductance (Λ_0) and the ion-pair dissociation constant (K) were evaluated by the Shedlovsky method.[11,12] The values of Λ_0 and K, along with related data, are summarized in Table II.

Tetra-*n*-butylammonium iodide is an interesting salt for conductance studies because its cation combines large size and symmetrical shape with low charge den-

(1) Presented at the 139th National Meeting of the American Chemical Society, St. Louis, Missouri, March, 1961.

(2) This paper is abstracted in part from a dissertation submitted by H. V. Venkatasetty to the Graduate School of the University of Cincinnati in partial fulfillment of the requirements for the Degree of Doctor of Philosophy, 1961.

(3) The conductance equipment used in this research was made available through a grant from the Research Corporation.

(4) Radiochemistry and Isotope Division, Indian Atomic Energy Commission, Bombay, India.

(5) Department of Chemistry, Kent State University, Kent, Ohio.

(6) R. M. Fuoss, *J. Chem. Educ.*, **32**, 527 (1955).

(7) H. S. Harned and B. B. Owen, "The Physical Chemistry of Electrolyte Solutions," 3rd Ed., Reinhold Publ. Corp., New York, N. Y., 1958, Chapter 6.

(8) R. P. Seward, *J. Am. Chem. Soc.*, **73**, 515 (1951).

(9) H. V. Venkatasetty and G. H. Brown, *J. Phys. Chem.*, **66**, 2075 (1962).

(10) "Dictionary of Organic Compounds," Vol. 4, edited by I. Heilbron and H. M. Bunbury, Eyre and Spottiswodde, London, 1953, p. 554.

(11) T. Shedlovsky, *J. Franklin Inst.*, **225**, 739 (1938).

(12) R. M. Fuoss and T. Shedlovsky, *J. Am. Chem. Soc.*, **71**, 1496 (1949).

TABLE II

CONSTANTS FROM SHEDLOVSKY TREATMENT AND RELATED DATA FOR TETRA-*n*-BUTYLAMMONIUM IODIDE IN 1-BUTANOL

Temp., °C.	Λ_0, exptl.	$K \times 10^4$	Λ_0, Stokes	λ_0^+	$\Lambda_0\eta_0$
0.0	8.85	7.75	9.94	2.63	0.458
25.0	17.54	6.863	20.95	5.54	0.432
50.0	37.73	2.70	36.54	9.66	0.532

sity. The experimental values (Table II) of the limiting equivalent conductances for Bu_4NI at the three temperatures studied are low compared with those of aqueous[13] and of most non-aqueous solutions[14] of most salts, considering the size and structure of the conducting ions and the viscosity of the different solvents. The low value of the limiting equivalent conductance for the Bu_4NI may be attributed to the large size of the cation as well as ion–solvent interaction.

One would predict the cation cannot exert a sufficiently strong attractive force on the solvent molecules to draw them to its surface and, therefore, the ion will move with few, if any, solvent molecules attached to it. However, the pronounced inconstancy observed in the values of the Walden product (Table II) at the three temperatures studied indicates that there must be factors other than the viscosity of the solvent which also affect the mobility of the ions. Walden's rule is at best an approximation. Nevertheless, the deviations in the values of the Walden product show that there may be specific interactions between the charge on the Bu_4N^+ ion and the solvent dipoles. Inconstancy in the Walden product has been observed by Mercier and Kraus[15] and by Fuoss and co-workers[16–18] for several tetraalkylammonium salts in several solvent mixtures. This inconstancy was attributed to interactions between the ions and the solvent.

A modification of Stokes' law[19] may be used to calculate Λ_0. This law may be written as

$$\Lambda_0\eta_0 = 0.8147 \times 10^{-8} \sum_{j=1}^{p} \frac{z_j}{a_j} \qquad (1)$$

where Λ_0 is the limiting equivalent conductance of an electrolyte dissociating into p kinds of ions, a_j is the radius of the large spherical ion, z is the valence, and η_0 is the viscosity of the solvent.

On substitution of the radius of 2.16 Å.[20] for the iodide ion and the radius of 6.0 Å. for the Bu_4N^+ ion (estimated from a Fisher–Hirschfelder–Taylor model[21] corresponding to the most compressed conformation) into equation 1, one obtains limiting equivalent conductances in rough agreement with the experimental values. In addition to affording a test of Stokes' law, approximate values of limiting ion conductances (λ_0^+) in 1-butanol (Table II) can be readily calculated from a modification of Stokes' law.

Of the factors which affect the ion-pair dissociation constants for Bu_4NI, the dielectric constant seems to be the most influential while the viscosity and the structure of the solvent molecule determine the mobility of the ions.

(13) M. Azzarri and C. A. Kraus, *Proc. Natl. Acad. Sci.*, **42**, 590 (1956).
(14) For example see ref. 7 pp. 698 and 703.
(15) P. L. Mercier and C. A. Kraus, *Proc. Natl. Acad. Sci.*, **41**, 1033 (1955).
(16) H. Sadek and R. M. Fuoss, *J. Am. Chem. Soc.*, **76**, 5905 (1954).
(17) H. Sadek and R. M. Fuoss, *ibid.*, **76**, 5897 (1954).
(18) F. Accasina, A. D'Aprano, and R. M. Fuoss, *ibid.*, **81**, 1058 (1959).
(19) Reference 7, p. 284.
(20) L. Pauling, "Nature of the Chemical Bond," Cornell University Press, Ithaca, New York, 1960, p. 518.
(21) N. N. Lichtin and H. P. Leftin, *J. Phys. Chem.*, **60**, 1960 (1956).

POSSIBLE EXISTENCE OF JUMPS IN ACTIVATION ENERGY OF FLOW IN SOME MOLTEN METALS WITHIN 150° OF THE FREEZING POINT

BY M. M. QURASHI[1]

Division of Pure Physics, National Research Council, Ottawa, Canada

Received October 31, 1962

The viscous behavior of melts and other liquids has been the subject of considerable study because it shows promise of important information regarding pre-freezing aggregation and clustering in the form of "miscelles,"[2] and recently McLaughlin and Ubbelohde[3] have shown that the marked upward curvature of the ln η *vs.* $1/T$ plots for molten tin and zinc near the melting point is capable of interpretation in terms of the increasing concentration of aggregates or "clusters" of 20 to 50 atoms formed as much as 50° above the freezing point. It is the purpose of the present communication to extend their ideas by examining further the character of the increase in activation energy of viscous flow, $E\eta$, from the freezing point to 150° above it in tin, zinc, and aluminum.

Graphs of log η *vs.* $1/T$ for Super-pure Tin and Zinc. —The experimental data of Yao and Kondic[4] have a high degree of reproducibility for tin and (to a lesser degree) for zinc and aluminum, as shown by the small differences between their repeated measurements at each temperature, giving a root-mean-square deviation of ±0.025 centipoise about their mean values of η for tin, which corresponds to an uncertainty of 0.004 to 0.006 in the values of log η for tin. The corresponding estimates of uncertainty (in log η) for zinc and aluminum come to about ±0.008 and ±0.007, respectively, corresponding to 0.006 and 0.005 for means of readings at successive temperatures. Figure 1 shows a re-plot of the experimental data of Yao and Kondic[4] on super-pure tin and crown zinc, with the two modifications that (i) the means of successive points above 440° have been plotted as crosses in the case of zinc and (ii) three linear segments (with an average of six points per segment) are drawn in place of the smooth curves previously envisaged.[3,4] The arms of the crosses and the radii of the solid circles in Fig. 1 indicate the standard deviation of the experimental data, and it can be seen that the full straight lines in Fig. 1 give a closer fit (r.m.s. deviation = 0.0035) with the experimental data than would a smooth curve, *cf.* those in Fig. 1 and 2 of ref. 3 (r.m.s. deviation of about 0.008), thus providing evidence for the presence of fairly sharp bends at "A" and "B" in the log η *vs.* $1/T$ plots, and indicating sharp jumps in activation energy, $E\eta$.

It is to be noted that, for the elucidation of these phenomena, *relative* accuracy or reproducibility is

(1) Physics Division, Central Laboratories of the Pakistan Council of Scientific and Industrial Research, 35, P.N.H. Lines, Karachi, Pakistan.
(2) (a) J. W. H. Oldham and A. R. Ubbelohde, *Proc. Roy. Soc.* (London), **A176**, 50 (1940); (b) A. R. Ubbelohde, *Quart. Rev.* (London), **4**, 356 (1950).
(3) E. McLaughlin and A. R. Ubbelohde, *Trans. Faraday Soc.*, **56**, 988 (1960).
(4) T. P. Yao and V. Kondic, *J. Inst. Metals*, **81**, 17 (1952).

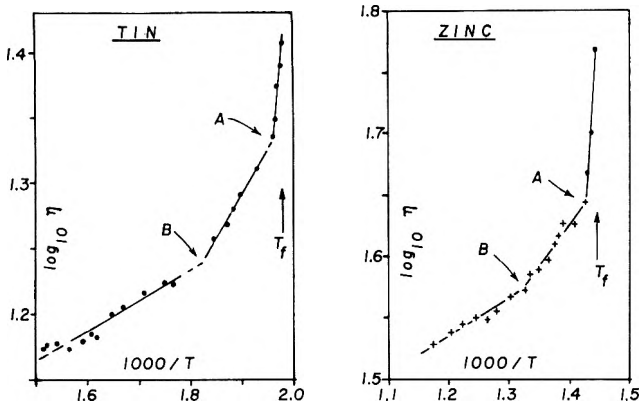

Fig. 1.—log η *vs.* $1000/T$ plots of Yao and Kondic's data for super-pure tin and crown zinc, with means of successive pairs of measurements for zinc (above 440°) shown as crosses, and straight linear segments drawn in place of the smooth curves envisaged by McLaughlin and Ubbelohde.

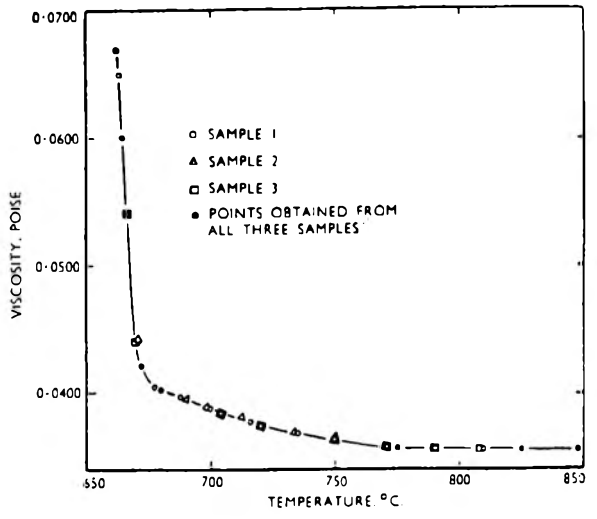

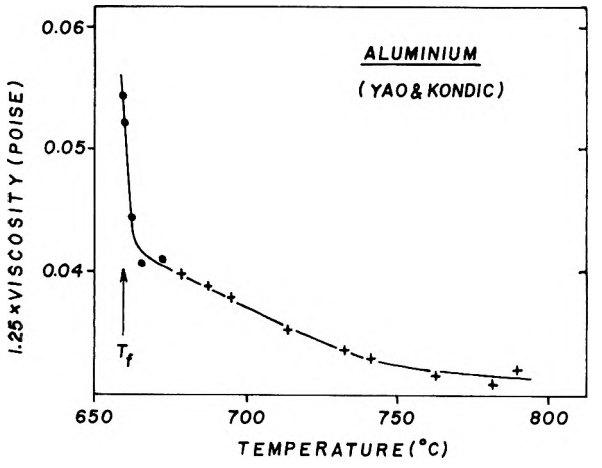

Fig. 2.—Comparative graphs of viscosity data obtained by two groups of workers on super-pure aluminum: top, Jones and Bartlett; bottom, Yao and Kondic. In spite of the disagreements between the absolute values of viscosity, the graphs show the correspondence between the well defined inflections occurring near 670 and 760° in both these viscosity–temperature plots.

rather more important than absolute accuracy. Because the *slope* of the ln η *vs.* $1/T$ graph gives $E\eta/R$, therefore the consistent errors in a given series of measurements, due for example to an error in calibration of the viscometer or thermocouple, will not affect $E\eta$ significantly, whereas these would put the absolute values of η very much out when compared with another series. A case in point is the data on aluminum (Fig. 2).

Comparison of Different Measurements on Aluminum.—Very definite sharp inflections, corresponding to the two bends in Fig. 1, have previously been noticed in the viscosity of pure aluminum by several experimenters, and are seen particularly well in the careful rotating cylinder measurements of Jones and Bartlett,[5] which are believed accurate to about 0.2%. The η *vs.* temperature graph in their paper is reproduced photographically in the top half of Fig. 2, while the lower half shows a corresponding plot of Yao and Kondic's[4] measurements on aluminum. Although the actual viscosities do not agree at all well, both these graphs show clearly the sharp bend near 670°, only a few degrees above the freezing point, and the rather less sharp one at about 760°. In the upper plot, a third possible inflection at about 720° is just discernable.

Magnitude of Jumps in $E\eta/R$.—It thus appears probable that such sharp bends or inflections in the ln η *vs.* $1/T$ (or η–T) graphs occur in more than one pure metal, and may conceivably correspond to a succession of aggregates or clusters of more or less definite sizes. This suggestion stems from the results of accurate measurements of activation energy of flow in water,[6,7] ethylene glycol,[8] ethyl alcohol,[9] water–alcohol,[7] and other systems, made by the author at a series of temperatures with a differential technique, which brought out several sharp steps of depth about 100 cal./mole at intervals of 5–10°.

The values of $E\eta/R$ corresponding to the three linear segments observed in Fig. 1 and 2 can be estimated from the slopes, $\Delta \ln \eta/\Delta(1/T)$, to be as

	(1)	(2)	(3)
Tin	12×10^3	1.6×10^5	0.54×10^3
Zinc	20×10^3	1.5×10^3	0.72×10^3
Aluminum	60×10^3	3.5×10^3	0.9×10^3

While the estimates corresponding to the third segment are of course very close to the high-temperature values used in ref. 3, the values of the energy jump between the first and second segments are in each case unexpectedly large, being ten to twenty times the latent heat of fusion, thus suggesting the presence of some unusually large clusters. Further work on the interpretation of these energy values is being undertaken.

(5) W. R. D. Jones and W. L. Bartlett, *J. Inst. Metals*, **81**, 145 (1952). These authors do not give a table of the actual data in the paper, which could otherwise be used to calculate ln η and $E\eta/R$.

(6) M. M. Qurashi and A. K. M. Ahsanullah, *British J. Appl. Phys.*, **12**, 65 (1961).

(7) A. K. M. Ahsanullah, S. R. Ali, and M. M. Qurashi, *Pakistan J. Sci. Ind. Res.*, **5**, 110 (1962).

(8) A. K. M. Ahsanullah and M. M. Qurashi, *British J. Appl. Phys.*, **13**, 334 (1962). Also, A. Rauf and M. M. Qurashi, *Pakistan J. Sci. Ind. Res.*, **2**, 30 (1959).

(9) A. M. Chowdhry, H. Ahmad, and M. M. Qurashi, *ibid.*, **3**, 101 (1960).

COMMUNICATION TO THE EDITOR

A NEW SERIES OF "HEXAGONAL FERRITE" STRUCTURES

Sir:

During a morphological and X-ray study of melt-grown, single-crystal "hexagonal ferrites," four new structures have been found. These are closely related to the Zn"Y" phase, $Ba_2Zn_2Fe_{12}O_{22}$. For purposes of brevity in this preliminary report, the reader is referred to Braun[1] and to Smit and Wijn[2] for detailed crystallographic discussions of the six previously identified structural members of the hexagonal ferrite group. Suffice it to say at present that structures in this ferrimagnetic family consist of a *c*-axis interlayering of three distinct building blocks: S, having two close-packed oxygen layers and a spinel arrangement; R, with three oxygen layers, the middle one containing a substitutional barium; T, having four layers of oxygen, the middle two each having a substitutional barium. The "Y" phase consists of an alternate stacking of T and S blocks, TSTSTS---, or $(TS)_\infty$. The rhombohedral six-layered TS block leads to a triply-primitive hexagonal unit cell having 18 oxygen layers along *c*, designated $(TS)_3$.

tures are, respectively, 84-layered rhombohedral (84R), 102-layered rhombohedral (102R), 40-layered hexagonal (40H), and 138-layered rhombohedral (138R). These are listed in Table I, along with other members of the series, some of which are to be expected after further studies. On the basis of these findings, it is reasonable to anticipate other arrangements involving relatively simple stacking sequences from which various blocks are "missing." The latter might entail one or more S blocks, T blocks, or combinations of blocks. In general, since there are three basic building blocks available for variable stacking in the hexagonal ferrite group, it is probable that new structures and series of structures remain to be encountered.

Crystals studied are black, lustrous, hexagonal tabular, with excellent basal faces and fairly well developed pyramid zones; maximum dimension is 3 mm. Identification of the structures was accomplished on zero-level *a*-axis Weissenberg X-ray films. The latter showed excellent *h0l* series of discrete reflections. Row-line streaking was essentially absent, indicating little or no stacking randomness. Most specimens show syntactic intergrowth of the new structures

TABLE I

COMPOSITE DATA FOR $(TS)_nT$ STRUCTURAL SERIES

n in $(TS)_nT$	Layers in smallest cell	Unit cell[a] (referred to hexagonal axes)	Hexagonal c_0, Å.	Space group	Stoichiometry of smallest cell
0	4	4H	9.69	$P\bar{3}ml$	$Ba_2Fe_8O_{14}$
1	10	30R	72.6	$R\bar{3}m$	$Ba_4Zn_2Fe_{20}O_{36}$
2	16	48R	116.2	$R\bar{3}m$	$Ba_6Zn_4Fe_{32}O_{58}$
3	22	22H	53.3	$P\bar{3}ml$	$Ba_8Zn_6Fe_{44}O_{80}$
[4[b]	28	84R	203.	$R\bar{3}m$	$Ba_{10}Zn_8Fe_{56}O_{102}$
5	34	102R	247.	$R\bar{3}m$	$Ba_{12}Zn_{10}Fe_{68}O_{124}$
6	40	40H	96.8	$P\bar{3}ml$	$Ba_{14}Zn_{12}Fe_{80}O_{146}$
7]	46	138R	334.	$R\bar{3}m$	$Ba_{16}Zn_{14}Fe_{92}O_{168}$]
8	52	156R	378.	$R\bar{3}m$	$Ba_{18}Zn_{16}Fe_{104}O_{190}$
⋮	⋮	⋮	⋮	⋮	⋮
∞	6	18R	43.56	$R\bar{3}m$	$Ba_2Zn_2Fe_{12}O_{22}$ (Y)

[a] Lattice is either hexagonal (H) or rhombohedral (R). [b] Brackets indicate newly identified structures.

The new structures entail "missing" S blocks on a strictly periodic basis, denoted by $(TS)_nT$. Specifically, structures have been identified with one S block "missing" after every fourth, fifth, sixth, or seventh TS block, *i.e.*, $n = 4$, 5, 6, or 7. Thus the structures are denoted, respectively, $[(TS)_4T]_3$, $[(TS)_5T]_3$, $(TS)_6T$, and $[(TS)_7T]_3$. The subscript "3" denotes a tripling of the rhombohedral unit for reference to hexagonal axes. In the case of $(TS)_6T$, the latter unit is non-rhombohedral, and tripling is unnecessary. Such is the case with every third member of the series (Table I). Referred to hexagonal axes, unit cells of the new structures with each other or with a known hexagonal ferrite. At least six examples of each type have been found, with 40H and 138R apparently more common. Triply primitive hexagonal unit cells (Table I) range up to 334 Å. along *c* in the structures which have been identified. The *a* dimension is essentially the same (5.88 Å.) for all structures, as is the case with other members of the hexagonal ferrite series.

Since the stoichiometry of a T block is $Ba_2Fe_8O_{14}$ and that of an S block is $M_2^{2+}Fe_4O_8^{2}$ (in the present case M^{2+} is Zn), it is possible to derive stoichiometries for the structures on the basis of observed stacking sequences. These are shown in Table I. Compositional complexity is indeed striking.

Magnetically, the structures appear to be neither

(1) P. B. Braun, *Philips Res. Rept.*, **12**, 491 (1957).

(2) J. Smit and H. P. J. Wijn, "Ferrites," John Wiley and Sons, New York, N. Y., 1959, Chapter IX.

strongly planar nor strongly axial. Each specimen assumed either a horizontal or vertical position with equal readiness on the pole face of a magnet. Since the structures are syntactically intergrown, no definitive conclusions can yet be drawn as to their true anisotropy or other magnetic behavior.

Further studies are in progress, and a detailed paper describing these and other related findings will be forthcoming. The structures reported herein were detected in reaction products prepared by Arthur Tauber and R. O. Savage of this Laboratory during the course of their comprehensive crystal chemistry study of the hexagonal ferrites.[3,4]

Acknowledgment.—We are most grateful to these co-workers for making their material available for crystallographic study.

(3) A. Tauber, R. O. Savage, R. J. Gambino, and C. G. Whinfrey, *J. Appl. Phys.*, **33**, 1379S (1962).

(4) A. Tauber and R. O. Savage, submitted to *J. Am. Ceram. Soc.*

INSTITUTE FOR EXPLORATORY RESEARCH J. A. KOHN
U. S. ARMY ELECTRONICS RESEARCH D. W. ECKART
AND DEVELOPMENT LABORATORY
FORT MONMOUTH, NEW JERSEY

RECEIVED JANUARY 17, 1963